DYNAMIC BEHAVIOR OF MULTIPLE-ANCHOR CONNECTIONS IN CRACKED CONCRETE

by

Yonggang Zhang, B.S.

DISSERTATION

Presented to the Faculty of the Graduate School of

The University of Texas at Austin

in Partial Fulfillment

of the Requirements

for the Degree of

DOCTOR OF PHILOSOPHY

THE UNIVERSITY OF TEXAS AT AUSTIN

August 1997

DYNAMIC BEHAVIOR OF MULTIPLE-ANCHOR CONNECTIONS IN CRACKED CONCRETE

APPROVED BY

DISSERTATION COMMITTEE:

Richard E. Klingner

John E. Breen

Karl H. Frank

Stelios Kyriakides

Jose M. Roesset

To my wife, Qing Yang;

and to my family,

for their support, love and understanding.

ACKNOWLEDGMENTS

The author would also like to express his deep, sincere gratitude and appreciation to Dr. Richard E. Klingner. Without his constant guidance, sustained encouragement, patient and unfailing support through this research project, the author would not been able to successfully complete this research project and his graduate education. It has been a privilege to work with him.

The author wishes to express his gratitude to his other dissertation committee members, Dr. John E. Breen, Dr. Karl H. Frank, Dr. Stelios Kyriakides and Dr. Jose M. Roesset for their valuable time and suggestions in this study. Special thanks are due to Dr. John Tassoulas, for providing his finite element solver that the author used as a platform to conduct his numerical modeling.

The author is very grateful to Milton Rodriguez, Dieter Lotze, and Jennifer M. Hallowell, who contributed their energy and effort to fulfill this research project. The help from the undergraduate assistant, Palinda DeSilva, for this physically-demanding program is gratefully acknowledged.

Tests could not have been conducted without enormous help from the staff of Ferguson Structural Engineering Laboratory, particularly Blake Stasney, Wayne Fontenot, Pat Ball, Wayne Little, Ray Madonna, Ryan Green, and Mike Bell. In addition, the author wishes to thank the laboratory administrative staff, April Jekins, Laurie Goldling, and Sharon Cunningham, for their assistance and advice throughout the entire program.

Finally, the author would like to dedicate this dissertation to Qing Yang, and to his family for their support, love and understanding.

The anchor acknowledges the U.S. Nuclear Regulatory Commission (NRC) and its Technical Contact Herman L. Graves III, for their support for this research program.

Austin, Texas
April, 1997

Yonggang Zhang

DISCLAIMER

This dissertation presents partial results of a research program supported by U.S. Nuclear Regulatory Commission (NRC) under Contract No. NRC-03-92-05 ("Anchor Bolt Behavior and Strength during Earthquakes"). The technical contact is Herman L. Graves III. Any conclusions expressed in this dissertation are those of the author. They are not to be considered NRC policy or recommendations.

DYNAMIC BEHAVIOR OF MULTIPLE-ANCHOR CONNECTIONS IN CRACKED CONCRETE

Publication No. _____

Yonggang Zhang, B.S.
The University of Texas at Austin, 1997

Supervisor: Richard E. Klingner

Anchors are widely used to attach structural and non-structural elements to concrete structures in nuclear, highway, and building constructions. However, the behavior of anchors and anchor connections is still not well understood, especially for anchors in cracked concrete under dynamic loading.

In an experimental research program conducted at Ferguson Structural Engineering Laboratory in The University of Texas at Austin, various configurations of anchor connections were tested. The behavior of single anchors was examined in cracked concrete, under static and dynamic loading. The behavior of near-edge, two-anchor connections under both static and dynamic loading was observed, the effect of hairpins (transverse reinforcement on the front anchor) was also assessed. Finally, the behavior of multiple-anchor connections was evaluated under earthquake-type loading in two combinations of moment and shear, with different conditions of concrete specimens, such as cracks, edges, and hairpins. Based on these test results, the behavior and design of anchor connections in cracked concrete and under dynamic loading are addressed.

In the analytic research, the tensile behavior of single anchor in concrete was modeled with axisymmetric finite elements. It was accomplished with the fixed smeared-cracking concept, using a progressive approach, which predicts the crack propagation and assigns the tensile cracking properties of concrete only to elements along the crack path. Predicted capacity and crack path were similar to those observed experimentally. The

concrete plastic deformation around anchor head was not considered; therefore, the displacement behavior of anchor was not correctly predicted. A macro-model program (BDA5) provided by the University of Stuttgart was also used to predict the load-displacement behavior of multiple-anchor connections, based on single-anchor load-displacement behavior under oblique loading obtained in the earlier stage of this testing program. Its predictions compared reasonably well with the corresponding test results.

Table of Contents

List of Tables

List of Figures

CHAPTER 1

INTRODUCTION

1.1 General

In various types of construction, it is common to attach mechanical and structural components to structures. This is accomplished using embedded anchors, through which tension and shear forces are transferred into the base concrete .

To safely and reasonably design such connections, it is very important to clearly understand their behavior under various combinations of loading and conditions, and the effects on that behavior caused by different conditions of the base concrete.

Very little test data are available regarding the behavior and strength of anchor connections under dynamic loading in cracked concrete. However, many mechanical and structural components are constantly subjected to cyclic loading, and possibly to seismic loading. Moreover, concrete structures may have cracks due to various reasons, such as restrained thermal movements or shrinkage. This issue becomes very critical to designing safe connections .

In recognition of these issues in the design of anchor connections under dynamic conditions, the US Nuclear Regulatory Commission (NRC) sponsored this testing program, to assess the behavior and strength of anchor connections under dynamic loading in cracked concrete.

1.2 Scope

1.2.1 Scope of Overall Program

The US Nuclear Regulatory Commission sponsored a multi-year research program ("Behavior of anchor bolts under earthquake loading") at The University of Texas at Austin, to investigate the behavior of different types of anchors in cracked and uncracked concrete subjected to static and dynamic loading. To systematically investigate and understand the effects of these various factors, the overall research program consists of four tasks:

Task 1: Tensile behavior of single anchors under static and dynamic loading in uncracked and cracked concrete;

Task 2: Behavior of two-anchor connections under dynamic tensile loading and static eccentric shear, and behavior of single anchors under loading at various angles;

Task 3: Shear behavior of near-edge, single and double-anchor connections under static and dynamic loading in cracked and uncracked concrete, and the effects of hairpins on these near-edge connections; and

Task 4: Behavior of four-anchor connections under simulated seismic loads (eccentric shear loading) applied dynamically in repeated reversed cycles.

1.2.2 Scope of This Study

The study reported here consists of two phases, tests and finite element modeling. The test phase conducted by the author here is a portion of the overall research program, consisting of:

1) Tests on single anchors in cracked concrete under static and dynamic loading, which is a part of Task 1. These test results are evaluated together with the results of Rodriguez (1995) and Hallowell (1996).

2) Tests on near-edge, two-anchor connections in cracked and uncracked concrete under static and dynamic loading, which is a part of Task 3. The effectiveness of hairpins on the capacity of near-edge anchor connections is also determined.

3) Behavior of four-anchor connections under eccentric shear (Task 4). Variables include eccentricities of shear loading, edge distance, loading type (static and reversed cyclic loading), hairpins, and cracked versus uncracked concrete.

In the finite element modeling phase, the behavior of single tensile anchors is predicted with a smeared-crack approach. A scheme which predicts the crack path and consequently confines the crack elements along this path is developed to reduce computational time. The analytical results are compared with test results.

In addition, a macro-model program (BDA5) provided by the University of Stuttgart was extensively used to predict load-displacement behavior of multiple-anchor connections, and its predictions were compared to test results.

1.3 Objectives

1.3.1 Objective of Overall Program

The objective of this project is to obtain specialized technical assistance to verify, by testing, the adequacy of the assumption used in the US nuclear power plant designs that the behavior and strength of anchor bolts (cast-in-place, expansion, and bearing-type (undercut)) and their supporting concrete under seismic loads do not differ significantly from those for static conditions (Klingner 1991).

1.3.2 Objectives of This Dissertation

As a portion of the overall test program, the objectives of this dissertation are:

1) To investigate the effect of cracks on the behaviors of single anchors under static and impact loading;

2) To investigate the behavior of near-edge, two-anchor connections under the influence of concrete cracking and impact loading, and the effect of hairpins;

3) To investigate the effects of dynamic loading, cracks, hairpins, anchor types, and stiffness of the baseplate on the behavior of multiple-anchor connections;

4) To verify the suitability of a macro-level program (BDA5) developed at the University of Stuttgart, for analysis of load-displacement behavior of multiple-anchor connections; and

5) To develop a feasible finite element method to model the behavior of a single anchor in concrete under tension load.

CHAPTER 2

BACKGROUND: BEHAVIOR OF CONNECTIONS TO CONCRETE

2.1 Introduction

Depending on the concrete strength, the connection geometry, the embedment depth, the edge distance and the steel strength of the anchor itself, an anchor exhibits different failure modes, such as steel failure, concrete failure, and some failure modes related only to particular types of anchors. To fully understand the behavior of various types of anchors, a great amount of research has been conducted in the past years and is extensively summarized in CEB (1991).

Most tests on connections have been conducted under quasi-static monotonic loading to determine ultimate capacities. A few studies have investigated the effects on connections of different types of loading, such as impact loading, seismic loading and reversed loading (Malik 1980, Cannon 1981, Copley et al. 1985, Collins et al. 1989). In most of those tests, the loading patterns involved a particular dynamic loading pattern at a magnitude much smaller than the anchor's ultimate capacity, followed by a monotonic load to failure to investigate the effects of dynamic loading on ultimate load-displacement behavior (Copley et al. 1985, Collins et al. 1989). Few data were available on the dynamic behavior of anchors with small embedment. Only a few investigations (Eibl and Keintzel 1989) existed regarding the influence of loading rate on the entire load-displacement behavior of anchors, including earlier tests in this project by Rodriguez (1995) and Lotze (1997).

In addition, most connections had been tested in uncracked concrete. Some tests had been conducted in cracked concrete or in high-moment regions (Cannon 1981, Copley et al. 1985, Eligehausen et al. 1987, Eibl and Keintzel 1989, and Eligehausen and Balogh 1995). However, some of those tests focused only on load-displacement behavior of anchors under service or factored loads (Cannon 1981, Copley et al. 1985).

In this chapter, the basic types of anchor systems are first explained. The static behavior of connections in uncracked concrete, observed in previous research, is then discussed. Also, the effect of hairpins, concrete cracking, and dynamic loading on the behavior of anchors are briefly explained, with some review of the earlier tests of this project.

2.2 Connection Terminology

2.2.1 Definition and Classifications of Anchors

Attachments (structural or mechanical elements) that are attached into concrete (or masonry) structures using anchors can be subject to various types of loading. Loads on the attachments are transferred into the base concrete through anchors as concentrated loads, by friction, mechanical interlock, bond, or a combination of these mechanisms. Many types of anchors are currently used. The load-transfer mechanisms of anchors determine their performance characteristics.

Anchors may be broadly classified as cast-in-place anchors or post-installed anchors. They may be further classified according to their principal load-transfer mechanisms:

1) Cast-in-place anchors

Cast-in-place anchors are placed in position before concrete is cast.

A cast-in-place anchor can be a headed bolt of standard structural steel, placed with its head in the concrete. It can also be a standard threaded rod and a hexagonal nut, with the nut end embedded in concrete. Finally, it can be a bar bent at one end and threaded at the other end, with the bent end placed in concrete. Figure 2.1 shows these variations.

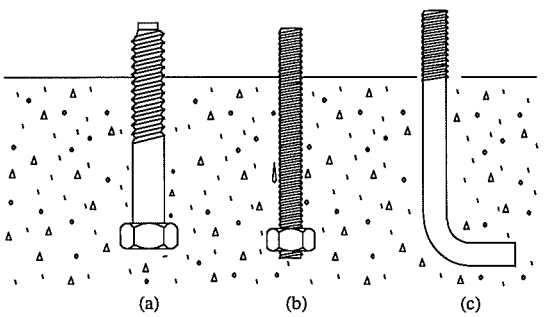

Figure 2.1 Typical Cast-in-Place Anchors

A headed cast-in-place anchor depends on mechanical interlock at the bolt head for load transfer. Some bond may also exist between the anchor shank and surrounding concrete.

Other types of cast-in-place anchors, (such as inserts) are not discussed here. In this study, all cast-in-place anchors were headed bolts.

2) Post-installed anchors

Post-installed anchors are installed in existing concrete or masonry structures. They are widely used in repair and strengthening work, as well as in new construction, due to advances in drilling technology, and to the flexibility of installation that they offer.

There are many different types of post-installed anchors, classified according to their load-transfer mechanisms. In the following sections, the types of the anchors tested in this program and their load-transfer mechanisms are explained.

a) Expansion anchors

An expansion anchor consists of an anchor shank with a conical wedge and expansion element at the bottom end (Figure 2.2). The spreading element is expanded by the conical wedge during installation and throughout the life of the anchor. The spreading element is forced against the concrete wall of the hole as the wedge is pulled by tension on the anchor shank. The external load is transferred by the frictional resistance from the conical wedge to the spreading element, and from the spreading element to the surrounding concrete.

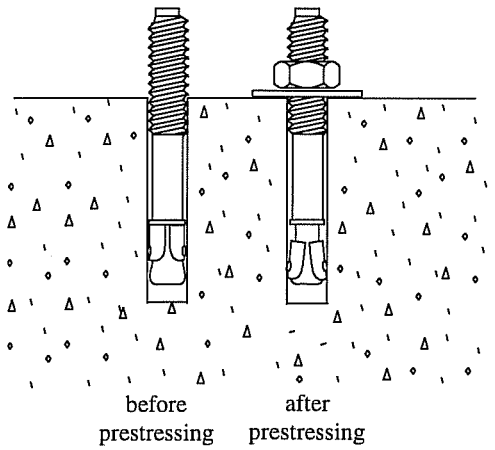

Figure 2.2 Expansion Anchors

Depending on the relative diameters of the bolt and the drilled hole, expansion anchors are classified as either bolt-type or sleeve-type anchors. For a bolt-type anchor, the nominal diameter of the drilled hole equals that of the anchor bolt. For a sleeve-type anchor, the nominal diameter of hole equals that of the sleeve encasing the bolt. A wedge anchor is the most common bolt-type anchor.

Both a typical wedge-type anchor (referred as Expansion Anchor II, or EAII for short) and a typical sleeve-type (referred to as Sleeve) anchor were tested in this study. Their dimensions are given here and elsewhere (Rodriguez 1995, Hallowell 1996).

b) Undercut anchors

An undercut anchor is installed in a hole in the base material that is locally widened (undercut). The undercut hole accommodates the expansion elements of the anchor, expanded during installation. Undercut anchors mainly rely on bearing to transfer tension load.

Different undercut geometries are used for various undercut anchor systems. Figure 2.3 shows the two different geometries of undercut anchors tested in this project: Undercut Anchor 1 and Undercut Anchor 2, designated as UC1 and UC2 respectively. It can be seen from this figure that Anchor UC2 has a much smaller bearing area on the surrounding concrete than Anchor UC1.

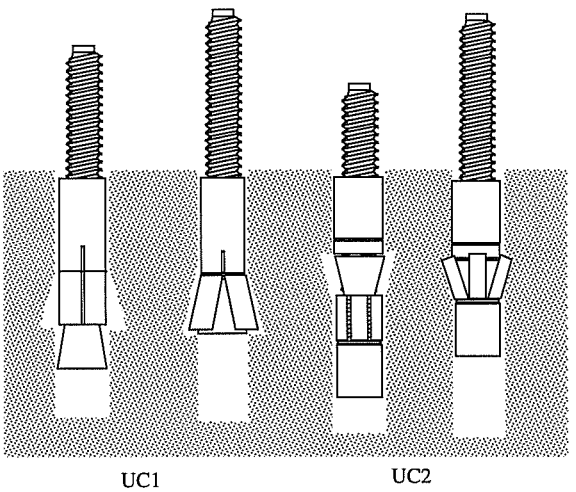

Figure 2.3 Undercut Anchors

c) Grouted anchors

A grouted anchor may be a headed bolt or a threaded rod with a nut at the embedded end, placed in a drilled hole filled with a pre-mixed grout or a Portland cement-sand grout (Figure 2.4). This type of anchor transfers load to the surrounding concrete primarily by friction at the interface between the grout and the concrete. The hole can be keyed or belled to increase the friction, or a deformed bar can be used instead of a threaded bolt.

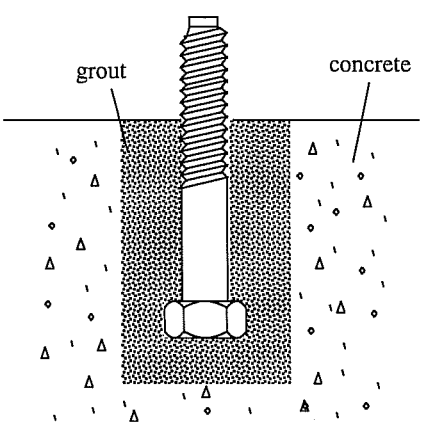

Figure 2.4 Grouted Anchor

2.2.2 Definition of Embedment Depth

Anchors are commonly identified by a nominal embedment depth, used primarily to indictate the required hole depth. For most of the anchors studied here, that nominal embedment depth was the length of the anchor (Sleeve, most UC). For CIP anchors, it is the depth to the bearing surface. Nominal embedment depths are defined in Figure 2.5a.

The effective embedment depth of an anchor is the distance between the concrete surface and the bearing portion of the anchor head. For most anchors studied here, the effective and nominal embedment depths were equal. An exception was the Expansion Anchor, whose contact point (a dimple on the clip) is considerably above the end of the anchor. Effective embedment depths are defined as shown in Figure 2.5b.

For the anchors tested here, nominal embedment depths are given in the text and tables describing each test series. Effective embedment depths are given in Appendix B,

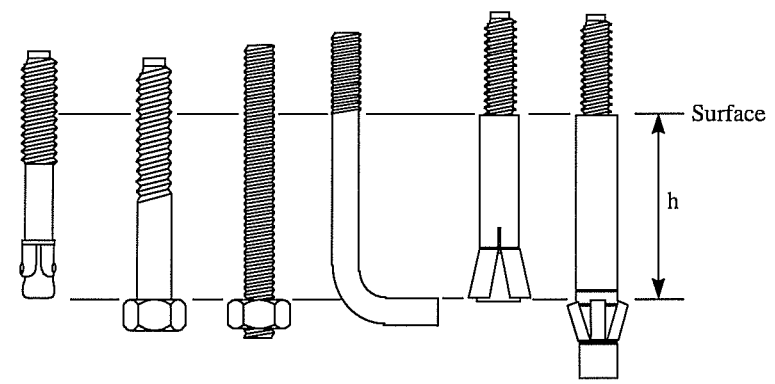

Nominal Embedment Depth

(a)

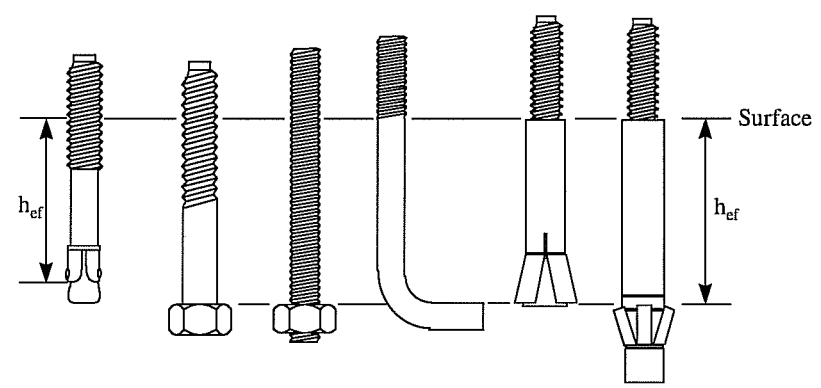

Effective Embedment Depth

(b)

Figure 2.5 Demonstration of Anchor Embedment Depths Defined in This Study

along with the test results.

2.3 Behavior of Single-Anchor Connections to Concrete

2.3.1 Tensile Load-Displacement Behavior

Depending on the type of anchor, the strength of the anchor steel, the strength of the surrounding concrete embedment, and sometimes also on the condition of the drilled hole during installation, an anchor can exhibit different failure modes, each with a corresponding failure capacity. The following section explains all the failure modes of anchors in tension and the corresponding calculation procedures, if available.

2.3.1.1 Tensile Failure Modes and Failure Loads

a) Steel failure in tension

Steel failure occurs by yield and fracture of the steel shank of the anchor as shown in Figure 2.6. The maximum fracture capacity of the anchor shank can be simply calculated from the effective tensile stress area of the anchor and the tensile strength of the anchor steel:

$$T_{nt} = A_s F_{ut} \qquad (2\text{-}1)$$

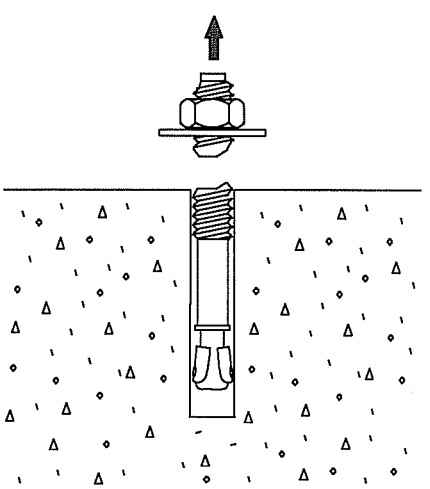

Figure 2.6 Anchor Steel Failure under Tensile Load

where: T_{nt} = tensile strength of the anchor shaft;

A_s = effective tensile stress area of the anchor;

F_{ut} = tensile strength of anchor steel.

When a threaded connection is involved, the effective tensile stress area should include the effect of the threads:

$$A_s = 0.7854\left[D - \frac{0.9743}{n}\right]^2 \qquad (2\text{-}2)$$

where: D = the major diameter of the threaded part, inch; and

n = the number of threads per inch.

Steel failure can also occur by thread stripping. In tests, this usually happened at almost the ultimate capacity.

b) Concrete cone breakout in tension

Concrete breakout failure occurs by the propagation of a roughly conical fracture surface from the bearing edge of the anchor head of a cast-in-place anchor, or from the tip of the expansion mechanism of an expansion or an undercut anchor. The angle of the cone (α in Figure 2.7), as measured from the concrete surface, increases from around 35° at shallow embedments, to about 45° at deep embedments.

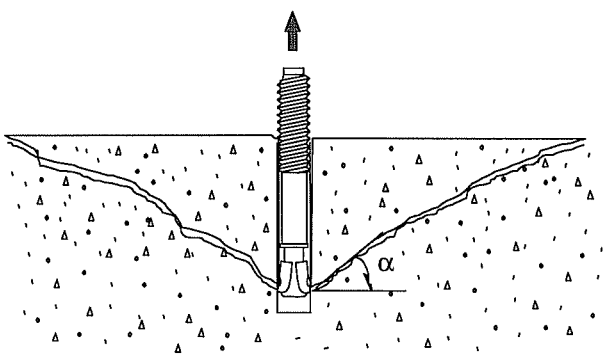

Figure 2.7 Concrete Breakout Failure

The primary factors determining the concrete breakout capacity are the anchor embedment depth and the concrete strength. Many empirical formulas have been proposed to calculate this capacity. These formulas have been compared with available databases of test results (Klingner and Mendonca 1982a, CEB 1991, Sutton and Meinheit 1991, Frigui 1992, Farrow 1992, Fuchs et al. 1995). A 45-degree breakout cone model has traditionally been used, and is used by ACI 349 Appendix B (1990) and *PCI Design Handbook* (1992). More recently, the Concrete Capacity Method (Fuchs et al. 1995) has been proposed as a derivative of the so-called Kappa Method (CEB 1991). The 45-degree cone method and the CCD Method has been compared against a large database of test results (Frigui 1992,

Farrow 1992, Fuchs et al. 1995). The CCD method has been shown to be an more accurate predictor of anchor capacity. It is also somewhat more designer-friendly for dealing with breakout cones involving edge effects or multiple anchors (Fuchs et al. 1995). In the following, only the 45-Degree Cone Method used in ACI 349 and the CCD Method are presented.

45-Degree Cone Method

The 45-Degree Cone Method assumes that a constant tensile stress of $4\sqrt{f_c'}$ acts on the projected area of a 45-degree cone radiating towards the free surface from the bearing edge of the anchor (Figure 2.8). Therefore, for a single tensile anchor far from edges, the cone breakout capacity is determined by:

$$T_o = 4\sqrt{f_c'}\pi h_{ef}^2\left(1 + d_h/h_{ef}\right) \quad \text{lb} \qquad (2\text{-}3a)$$

$$T_o = 0.96\sqrt{f_c'}\pi h_{ef}^2\left(1 + d_h/h_{ef}\right) \quad \text{N} \qquad (2\text{-}3b)$$

where: f_c' = specified concrete compressive cylinder strength (psi in US units, MPa in SI units);

d_h = diameter of anchor head (inch in US units, mm in SI units); and

h_{ef} = effective embedment (inch in US units, mm in SI units).

If the cone is affected by edges ($c < h_{ef}$) or by an adjacent concrete breakout cone, the breakout capacity is:

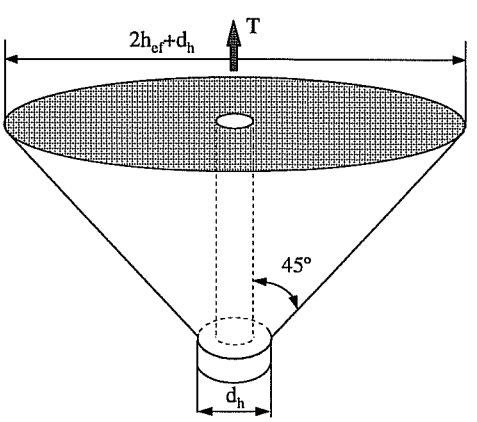

Figure 2.8 Concrete Tensile Breakout Cone as Idealized in ACI 349 Appendix B

$$T_n = \frac{A_N}{A_{No}} T_o \tag{2-4}$$

where: A_N = actual projected area of failure cone or cones;

A_{No} = projected area of a single cone unaffected by edges;

= $\pi h_{ef}^2 \left(1 + d_h / h_{ef}\right)$.

Concrete Capacity Method (CC Method)

The CC Method, based on a large amount of test results and to some extent on fracture mechanics (Eligehausen and Sawade 1989), computes the concrete breakout capacity of a single tensile anchor far from edges as:

$$T_o = k\sqrt{f_c'} h_{ef}^{1.5} \tag{2-5}$$

where: T_o = tension cone breakout capacity;

k = constant; for anchors in uncracked concrete the mean values originally proposed based on previous tests are: 35 for expansion and undercut anchors, 40 for headed anchors, in US units; or 15.5 for expansion and undercut anchors, 17 for headed anchors, in SI units;

f_c' = specified concrete compressive strength (6 × 12 cylinder) (inch in US units, MPa in SI units.);

h_{ef} = effective embedment depth (inch in US unit, MPa in SI unit).

In design codes, different values for k based on 5% fractile may be used.

In the CC Method, the breakout body is idealized as a pyramid with an inclination of about 35 degrees between the failure surface and the concrete member surface (Figure 2.9). As a result, the base of the pyramid measures $3h_{ef}$ by $3h_{ef}$.

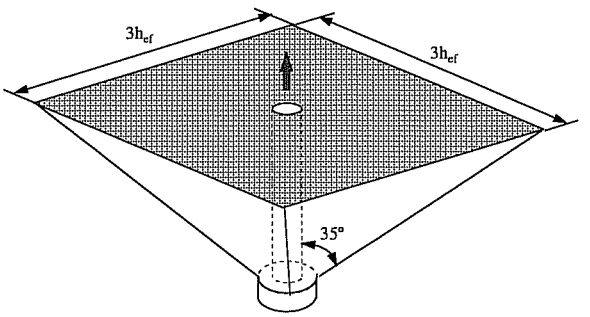

Figure 2.9 Tensile Concrete Breakout Cone for Single Anchor as Idealized in CC-Method

If the failure pyramid is affected by edges or by other concrete pyramids, the concrete capacity is calculated according the following equation:

$$T_n = \frac{A_N}{A_{No}} \psi_2 \, T_{no} \qquad (2\text{-}6)$$

where: A_{No} = projected area of a single anchor at the concrete surface without edge influences or adjacent-anchor effects, idealizing the failure cone as a pyramid with a base length of $s_{cr} = 3h_{ef}$ ($A_{no} = 9\ h_{ef}^2$);

A_N = actual projected area at the concrete surface;

ψ_2 = tuning factor to consider disturbance of the radially symmetric stress distribution caused by an edge,

= 1, if $c_1 \geq 1.5h_{ef}$;

= $0.7 + 0.3\frac{c_1}{1.5h_{ef}}$, if $c_1 \leq 1.5h_{ef}$;

where:

c_1 = edge distance to the nearest edge.

c) Pullout failure in tension

Pullout failure (Figure 2.10) occurs when the anchor pulls completely out of the hole. It is usually accompanied by crushing of the concrete above the head of the anchor. Sometimes, the anchor pulls out part way, and then re-engage the concrete at a smaller embedment, and subsequently fails by concrete cone breakout. Currently, there is no theoretical formula to predict this type of failure load.

This kind of failure is most likely to occur with expansion anchors.

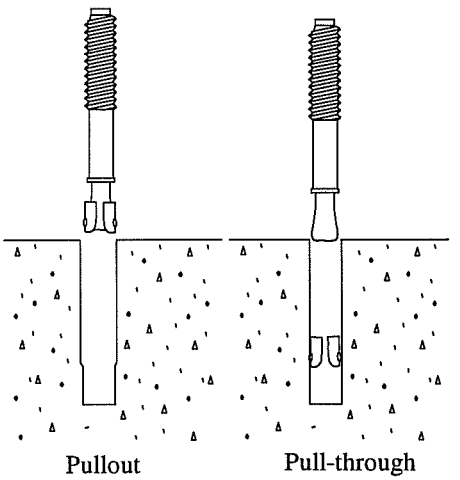

Figure 2.10 Pullout and Pull-through Failure

d) Pull-through failure in tension

Pull-through failure occurs when the cone of the anchor shank slides through the expansion clip or sleeve (Figure 2.10), leaving the clip or sleeve inside the hole. This usually happens with expansion anchors with large embedment depths, when the tensile force exceeds the frictional resistance between the expansion sleeve and the cone. Several factors affect the pull-through failure of an anchor, such as the surface condition of the cone and the clip or sleeve, the inclination of the cone, and the relative diameters of the hole and the anchor.

The capacity associated with this type of failure depends on the expansion mechanism, the condition of the hole, and the concrete strength and stiffness. Currently, there is no theoretical method to calculate this capacity.

e) Lateral blowout failure in tension

If an anchor is placed too close to a free edge and has a relatively large embedment depth (compared to the edge distance), the high bearing stresses generated by the anchor head can cause the concrete between the anchor head and the adjacent free surface to spall off in the form of a conical body (Figure 2.11).

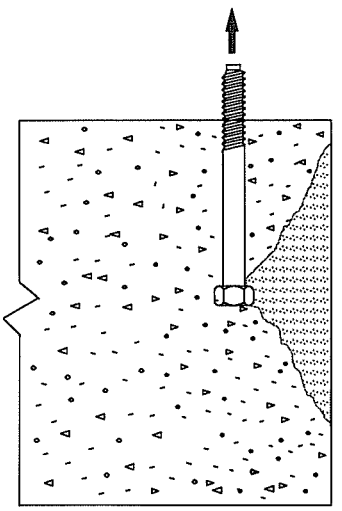

Figure 2.11 Concrete Lateral Blowout

In ACI 349 Appendix B, a 45-degree cone model is again assumed to calculate the lateral blowout capacity. The lateral blowout force is taken as 40% of the tension in the anchor.

Recent research by Furche and Eligehausen (1991) suggests that the ACI 349 approach overestimates lateral blowout capacity for large edge distances. It indicates that lateral blowout capacity is a function of concrete strength, anchor bearing area, and edge distance, as shown in Equation 2-7. However, since those tests were conducted on specimens with only one concrete strength, the effect of concrete strength needs to be investigated further. Furthermore, the effect of different geometry of various types of anchors also needs to be examined. They suggest:

$$F_n = 200\, m\sqrt{A_b\ f_c'} \qquad \text{lb} \qquad (2\text{-}7a)$$

$$F_n = 16.8\, m\sqrt{A_b\ f_c'} \qquad \text{N} \qquad (2\text{-}7b)$$

where: F_n = average lateral blowout capacity;

m = edge distance (inch in US units, mm in SI units);

A_b = bearing area of anchor head (si in US units, mm^2 in SI units); and

f_c' = specified concrete compressive strength (psi in US units, MPa in SI units).

Based on test results on T-headed reinforcing bars, Bashandy (1996) proposed a pyramid model similar to the tension model of the CC Method, but with a base dimension

of 6 times the edge distance, to estimate the lateral blowout capacity of a group of anchors. However, those bars were placed very close to concrete member edges. Therefore, the value of 6 might underestimate the ultimate strength for anchors with a larger edge distance.

f) Splitting failure in tension

Splitting failure is characterized by the propagation of a crack in a plane containing the anchor. This happens when an anchor is installed in a thin member, or close to an member edge (Figure 2.12). This phenomenon generally is limited to anchors with very large expansion force, such as expansion or some undercut anchors. Currently, there is no theoretical formula for predicting capacity as governed by this type of failure.

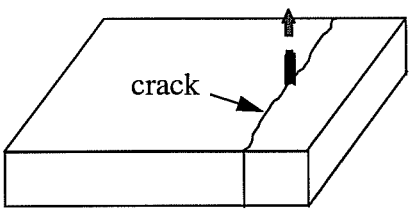

Figure 2.12 Splitting Failure

2.3.1.2 Load-Displacement Behavior of Anchors in Tension

The total displacement of an anchor in tension is the summation of the steel elongation of the anchor shank, the concrete deformation, and the relative slip of the anchor head due to local crushing of the concrete. If the anchor fails by cone breakout, the concrete deformation consists of local concrete plastic crushing, concrete crack opening, and elastic deformation of the cracked concrete body. Figure 2-13 shows some typical load-displacement curves associated with different failure modes.

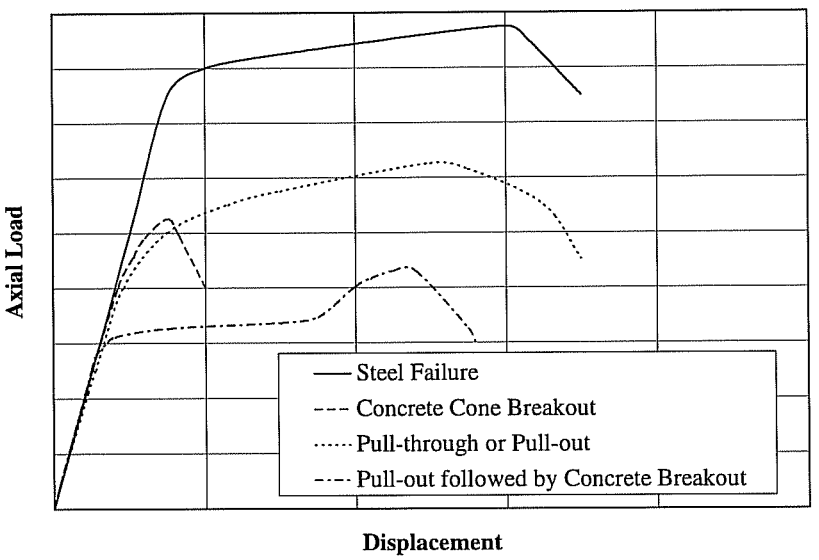

Figure 2.13 Typical Load-Displacement Curves of Different Failure Modes in Tension

2.3.2 Shear Load-Displacement Behavior

The anchor in plain concrete loaded in shear exhibits various failure modes, depending on the shear strength of the steel, the strength of surrounding concrete, the edge distance and the presence of adjacent anchors. These various shear failure modes and their corresponding capacities are discussed below.

2.3.2.1 Failure Modes and Failure Loads in Shear

a) Anchor steel failure in shear

Steel failure in shear occurs with bending, eventually leading to yield and rupture of the anchor shank. Due to the high local pressure in front of the anchor, a shell-shaped concrete spall may occur at the surface of the concrete before maximum load is obtained (Figure 2.14). This increases the deformation at failure of the anchor.

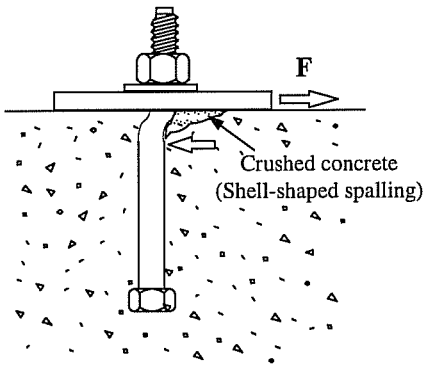

Figure 2.14 An Anchor Loaded in Shear

The shear capacity is a function of steel strength and cross-sectional area. It can be predicted by Equation 2-8:

$$V_n = \alpha T_{nt} = \alpha A_s F_{ut} \tag{2-8}$$

where: V_n = shear strength of the anchor shank;

A_s = cross-sectional area of the anchor;

F_{ut} = minimum specified tensile strength of the anchor steel;

α = reduction factor.

If the threads are in the shear plane, the effective stress area of Equation 2-2 should also be used.

In ACI 349 Appendix B (1990), shear transfer is ascribed to shear friction. It is assumed that bolt shear is transmitted from the bolt to the concrete through bearing of the bolt at the concrete surface, forming a concrete wedge. The wedge is assumed to be pushed upward against the steel plate by the bolt, which produces a clamping force between the wedge and the baseplate, leading to a friction. This friction is assumed to increase in proportion to the clamping force and therefore to the shear on the anchor, as long as the anchor remains elastic.

In ACI 349, the coefficient α in Equation 2-8 is treated as a friction coefficient, whose value varies with different plate position on the concrete surface (inset, surface, or

grout pad). Even though the shear-friction mechanism is not consistent with tests in which the loading plate rotates away from the concrete surface, capacity can be correctly predicted by shear friction theory.

Alternately, the coefficient α can be regarded as the ratio between the ultimate strength of the anchor in shear and in tension. The reduction factor α varies with the type of anchor. Cook (1989) excluded the effect of friction between the steel baseplate and the concrete surface, and determined that for an anchor whose sleeve is flush with the surface of the concrete, a value of 0.6 can be used. This is about $1/\sqrt{3}$, the theoretical ratio of shear to tensile yield according to the van Mises model. For anchors without sleeves, the average value was determined to be 0.5.

b) Concrete cone breakout in shear

Concrete breakout usually occurs when the anchor is located close to the free edge of a member and is loaded in shear towards the edge. The angle α (Figure 2.15) varies from small angles with small edge distances to large angles with large edge distances.

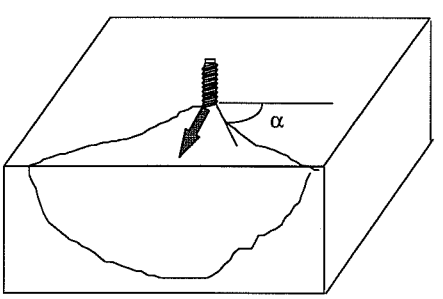

Figure 2.15 Lateral Concrete Cone Failure under Shear

Many procedures have been proposed to predict the concrete shear capacity. Some of them were compared against test results (Klingner and Mendonca 1982b, CEB 1991, Fuchs et al. 1995). The most widely used are the 45-Degree Cone Method and the CC Method In the following, these two methods are described.

45-Degree Cone Method

Using an analogous assumption as for tension anchors, that a tensile stress of $4\sqrt{f_c'}$ acts on a 45-degree concrete half-cone, leads to Equation 2-9:

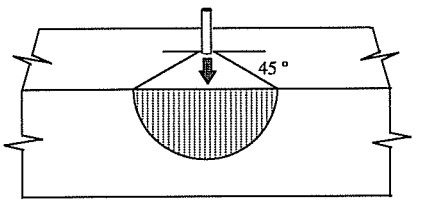

Figure 2.16 Idealized Shape of Shear Breakout Cone of a Single Anchor (45-Degree Cone Method)

$$V_{no} = 2\pi\sqrt{f_c'}c_1^2 \qquad \text{lb} \qquad (2\text{-}9a)$$

$$V_{no} = 0.48\sqrt{f_c'}c_1^2 \qquad \text{N} \qquad (2\text{-}9b)$$

where: c_1 = edge distance in loading direction.

If the depth of the concrete member is smaller than the edge distance, or the spacing of anchors is smaller than $2c_1$, or the width of the concrete member is smaller than $2c_1$, or any combination of these, the capacity is modified as follows:

$$V_n = \frac{A_v}{A_{vo}} V_{no} \qquad (2\text{-}10)$$

where: A_v = actual projected area of semi-cone on the side of concrete member;

A_{vo} = projected area of one fastener in thick member without influence of spacing and;member width, idealizing the shape of projected fracture cone as a half-cone with a diameter of c_1, ($A_{Vo} = (\pi/2)\, c_1^2$).

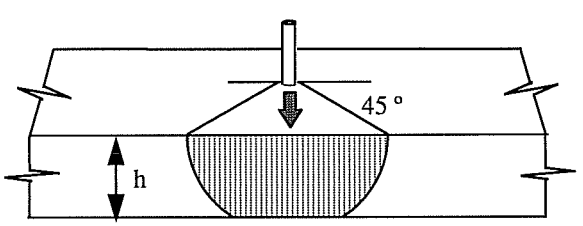

$$A_V = \left(\pi - \frac{\pi\theta}{180} + \sin\theta\right)\frac{c_1^2}{2}$$

$$\theta = 2\cos^{-1}\left(\frac{h}{c_1}\right)$$

Figure 2.17 Projected Areas for Shear Anchors According to 45-Degree Cone Method

Concrete Capacity Method (CC Method)

Based on regression analyses of a large number of tests with headed, expansion, and adhesive anchors, the following equation was proposed for the calculation of shear breakout capacity (Fuchs et al. 1995):

$$V_{no} = 13\left(d_o f_c'\right)^{0.5}\left(l/d_o\right)^{0.2} c_1^{1.5} \quad \text{lb} \qquad (2\text{-}11a)$$

$$V_{no} = \left(d_o f_c'\right)^{0.5}\left(l/d_o\right)^{0.2} c_1^{1.5} \quad \text{N} \qquad (2\text{-}11b)$$

where: d_o = the outside diameter of the anchor (inch in US units, mm in SI units);

l = activated load-bearing length of fasteners, $\leq 8d_o$;

= h_{ef}, for fasteners with a constant overall stiffness;

= $2d_o$ for torque-controlled expansion anchors with spacing sleeve separated from the expansion sleeve;

f_c' = compressive strength of concrete; and

c_1 = edge distance in the direction of load.

This formula is valid for a member with a thickness of at least $1.4h_{ef}$. For anchors in a thin structural member or affected by the width of the member, by adjacent anchors, or both, a reduction must be made based on the idealized model of a half-pyramid measuring $1.5c_1$ by $3c_1$.

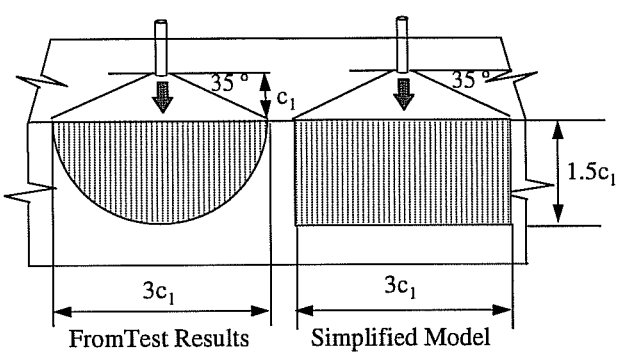

Figure 2.18 Idealized Design Model for a Single Anchor Under Shear in CC Method

$$V_n = \frac{A_v}{A_{vo}} \psi_5 V_{no} \qquad (2\text{-}12)$$

where: A_v = actual projected area at the side of concrete member;

A_{vo} = projected area of one fastener in thick member without influence of

spacing and member width, idealizing the shape of the projected fracture cone as a half-pyramid with side length of $1.5c_1$ and $3c_1$;

ψ_5 = reduction factor considering the disturbance of symmetric stress distribution caused by a corner;

= 1, if $c_2 \geq 1.5\ c_1$

$0.7+0.3\frac{c_2}{1.5c_1}$, if $c_2 \leq 1.5\ c_1$;

where c_1 = edge distance in loading direction,

= max ($c_{2,max}$/1.5, h/1.5) for anchors in a thin and narrow member with $c_{2,max} < 1.5c_1$ and $h < 1.5c_1$;

where: h = thickness of concrete member;

c_2 = edge distance perpendicular to loading direction.

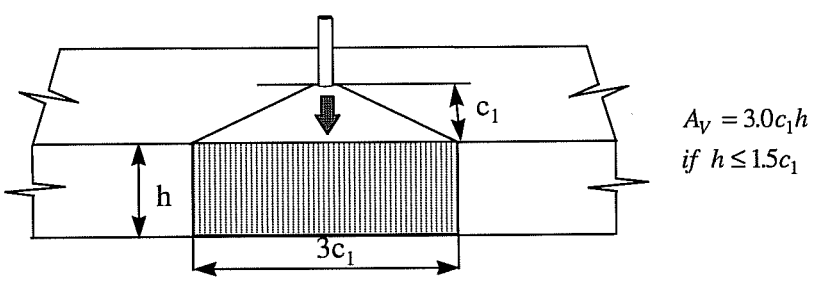

Figure 2.19 Projected Areas for Shear Anchors in Thin Members According to CC Method

c) Anchor pryout

Anchor pryout is characterized by crushing of concrete in front of the anchor, combined with breakout of the concrete behind the anchor, leading to anchor pullout, as shown in Figure 2.20. It generally happens to anchors with small embedment depths. Prediction formulas for this kind of failure are not currently available.

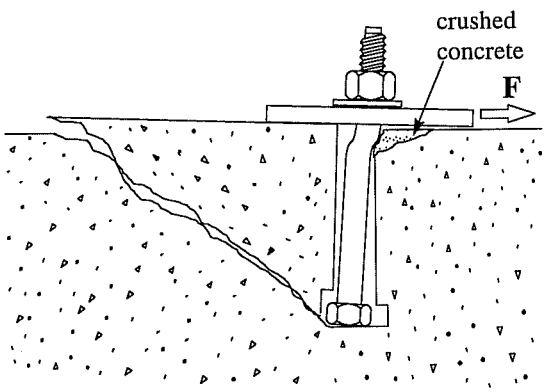

Figure 2.20 Pryout Cone Failure

2.3.2.2 Load-Displacement Curves of Anchors in Shear

The shear load-shearing displacement history of an anchor failing by steel rupture, comprises the steel shear deformation, and the steel flexural deformation as a result of concrete spalling in front of the anchor. In case of concrete breakout failure, the total deformation consists mainly of concrete deformation, with little steel deformation, and

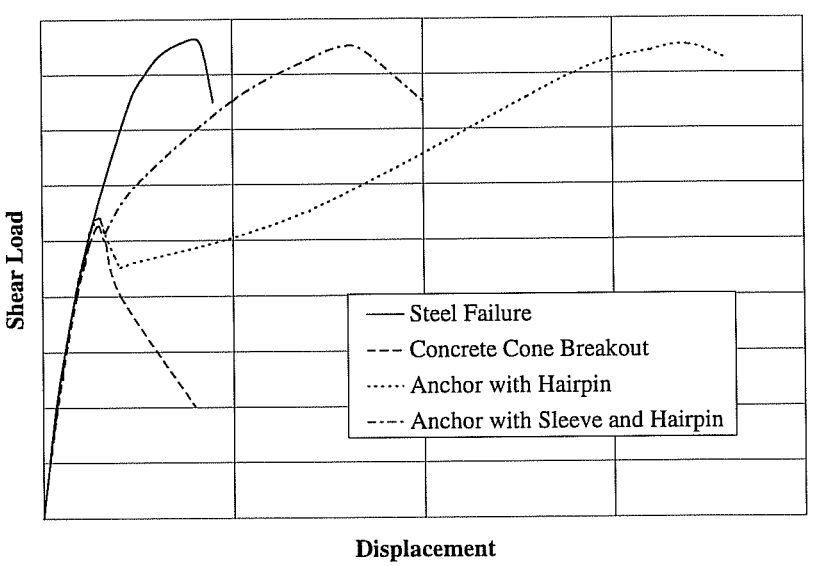

Figure 2.21 Typical Load-Displacement Curves of Anchors in Shear

shell-shaped concrete spalling is usually not observed, due to the smaller failure load. Figure 2.21 shows typical load-displacement curves of anchors in shear, associated with various failure modes.

2.3.3 Oblique Tension Loading

Anchors loaded under oblique tension can have any combination of tension and shear failure, depending on the strength of the anchor system, the strength of the concrete member, and the edge distance.

The steel failure mechanism is yielding and fracture of the anchor shank due to tension, bending and shear. Several interaction relations are available for pure steel failure.

a) Linear interaction formula

According to ACI 349 Appendix B (1990), the shear strength of an anchor with full embedment is calculated by shear-friction theory, using Equation 2-13:

$$P + V/\mu = A_s f_{ut} \tag{2-13}$$

This equation results in a straight-line interaction diagram, sometimes expressed in the following form:

$$\frac{P}{P_n} + \frac{V}{V_n} = 1 \tag{2-14}$$

where: P, V = applied anchor tensile and shear loads;

P_n = capacity in pure tension; and

V_n = capacity in pure shear.

b) Tri-linear interaction formula

A tri-linear interaction formula was proposed by Bode and Roik (1987) as follows:

$$\begin{aligned} &P/P_n \le 1 \\ &V/V_n \le 1 \\ &P/P_n + V/V_n \le 1.2 \end{aligned} \qquad (2\text{-}15)$$

where: P, V = applied tension and shear loads, respectively; and

P_n, V_n = capacity in pure tension and pure shear, respectively.

c) Elliptical interaction formula

An elliptical interaction formula for tension and shear is expressed in the following form:

$$\left(\frac{P}{P_n}\right)^{p_1} + \left(\frac{V}{V_n}\right)^{p_2} = 1 \qquad (2\text{-}16)$$

where: P, V = External tension and shear loads on the anchor, respectively;

P_n, V_n = pure tension and shear capacities, respectively; and

p_1, p_2 = constant (equal or different).

The constants p_1 and p_2 vary with different proposed relationships. In the *PCI Design Handbook* (1992), $p_1 = p_2 = 2$ is used for steel-to-concrete connections. However, the value of 5/3 founded by McMackin et al. (1973) was recommend in the report by the Task Group on Steel Embedment (1984) and in CEB (1991).

Cook (1989) used tests on two-anchor connections on a rigid baseplate under eccentric shear with both anchors on the tension side to determine the interaction relation. The test results justified an elliptical interaction relationship with n = 5/3. In Task 2 of this project, Lotze (1997) tested several types of anchors under oblique loading at different angles from 0° to 90° at 15° intervals to determine the interaction equation. It was found

that an elliptical interaction equation with an exponent of 1.67-1.8 can describe the failure load appropriately.

All three interaction formulas are shown in Figure 2.22.

Lotze (1997) also notes that an elliptical interaction equation with a smaller exponent (1.2-1.5) can also be used to describe the ultimate concrete breakout strength of an anchor in oblique tension.

If anchors are installed close to an edge or at a small embedment depth, a transition of failure mode between concrete failure and steel failure can occur (if other failure modes are precluded). In this case, different elliptical formulas can be used for each failure mode, and the intersection of those two curves indicates the angle at which the transition occurs (Lotze 1997).

Lotze (1997) observed the bulbous form shown in Figure 2.23 in the interaction curve for displacements of anchors under oblique tension. Due to shell-shaped concrete spalling in front of the anchor, and also due to the extraction of the anchor under tensile load, the anchor is more flexible under small-angle oblique tension, and has a relatively

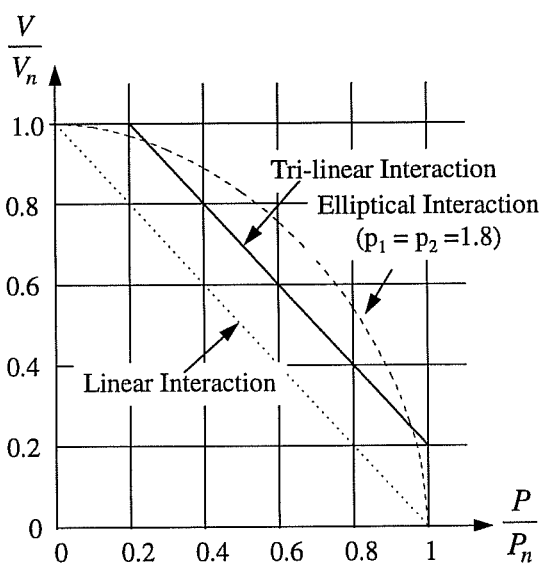

Figure 2.22 Tension-Shear Interaction for Single Anchors

larger horizontal (shear) displacement. For anchors under shear and large-angle oblique load, the concrete in front of the anchor is confined by the loading plate, so that the shell-shaped concrete spalling is much smaller or does not even occur. As a result, the transverse displacement is reduced.

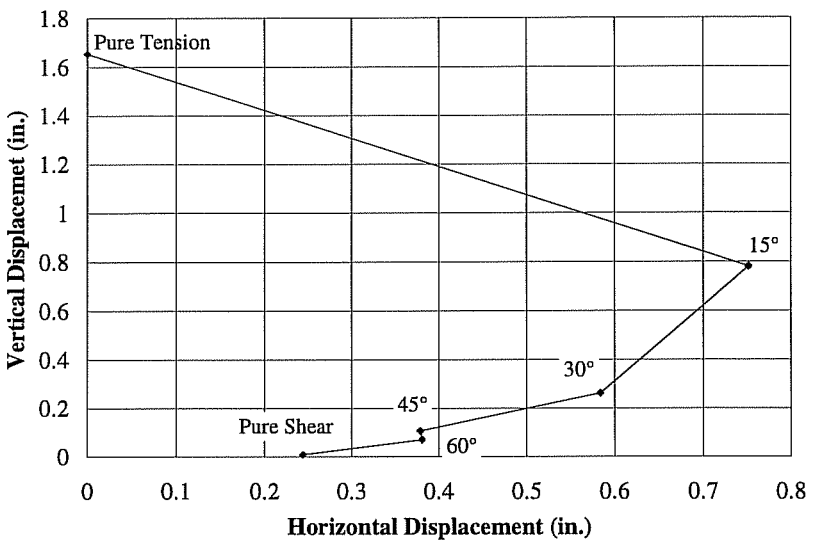

Figure 2.23 Typical Horizontal/Vertical Displacement Interaction Diagram (Lotze 1997)

2.4 Effect of Dynamic Tensile Loading on Anchor Behavior

In both Task 1 and Task 2, dynamic tension tests were conducted on single-anchor and two-anchor connections (Rodriguez 1995, Lotze 1997). The conclusions from those tests are as follows:

1) For undercut and grouted anchors, the capacity generally increased with the loading rate. In those tests, the capacity increased by 10% to 20%.

2) For clip-type expansion anchors, the tendency for pull-through failure increased with the loading rate, probably due to the smaller dynamic friction coefficient (Rabinowicz

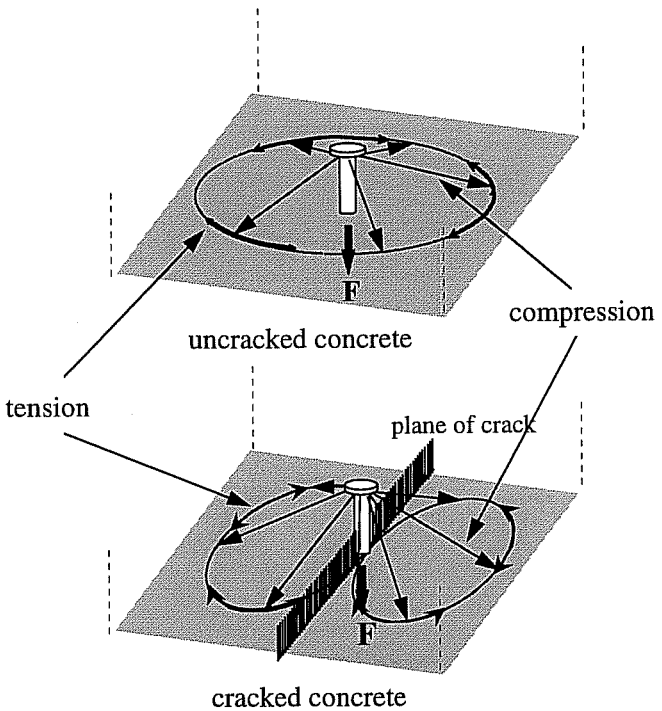

Figure 2.24 Effect of Cracking on Load-Transfer Mechanism of Headed Anchors in Tension (Eligehausen and Fuchs 1987)

1995). It also varies with each anchor, due to individual design of expansion mechanisms.

3) In the tests without pullout failure, the loading rate did not affect the cone breakout shape.

2.5 Effect of Cracks on Anchor Capacity

In general, cracks decrease anchor capacity as governed by concrete breakout. This effect could be explained by the hypothesis of Eligehausen and Fuchs (1987), shown in Figure 2.24. The crack interrupts the tensile stress field in the concrete surrounding the anchor, thereby altering the stresses distribution in the concrete.

Although the scatter of the test results is rather large, the reduction of ultimate load of concrete breakout generally increases with initial crack width. An effort was also made by Eligehausen and Ozbolt (1992) to determine the effect of cracks numerically with a finite element method. Previous test results (Eligehausen et al. 1987, CEB 1991, Eligehausen and Balogh 1995, Takiguchi and Hotta 1995) and numerical modeling show that concrete breakout capacity decreases with an increasing crack width up to 0.15 mm, to approximately 70% of the breakout capacity in uncracked concrete for undercut and cast-in-place anchors. The crack results in a significant reduction of the expansion force of an expansion anchor. The effect of crack width on the ultimate load of an expansion anchor is greater than for undercut or cast-in-place anchors. Figure 2.25 shows the average reduction of the ultimate capacity of pullout tests of headed anchors (Eligehausen and Balogh 1995). These tests compared large numbers of anchors of all kinds in particular uncracked concrete, with large numbers of anchors of all kind, in different concrete.

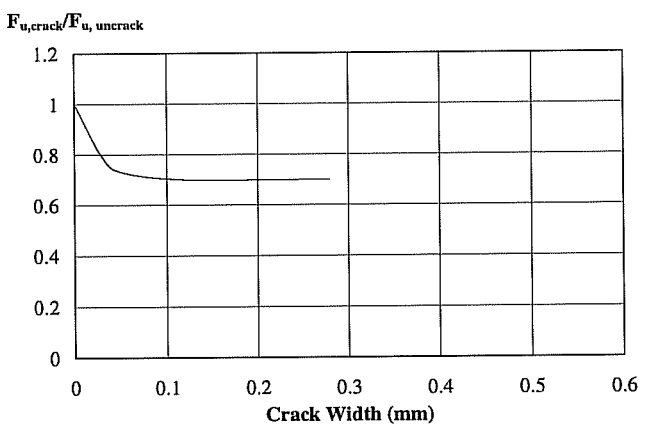

Figure 2.25 Influence of Crack Width on Concrete Cone Breakout Capacity (Eligehausen and Balogh 1995)

For anchors in shear failing by lateral concrete breakout, the cracks reduce the ultimate load capacity of concrete breakout in the same manner as in tension (CEB 1991).

2.6 Effect of Hairpins on Load-Displacement Behavior of Shear-Loaded Anchors

Hairpins reinforcement encloses near-edge shear anchors to increase their shear capacity. U-loops and V-loops are two configurations widely used currently, as shown in Figure 2.26.

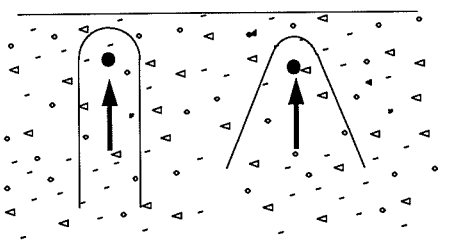

Figure 2.26 Reinforcement for Near-Edge Anchors in Shear

In the tests conducted by Malik (1980), the effect of hairpins with combinations of different concrete cover and different distances to the anchors was investigated. It was found out that the hairpins can increase the load capacity and the stiffness of anchors in two ways. One way is by confining the concrete around the anchor. The other is by increasing the flexural stiffness of the anchor shank by reducing its unsupported length, as shown in Figure 2.27. Although in all tests the shear strength of the anchors was completely developed, the displacement at maximum load was much greater than that for anchors placed far from an edge. In all combinations, far hairpins with the smallest concrete cover increased the stiffness and strength of the anchor most effectively.

Also, some anchors were tested under reversed shear loading. Anchors with close hairpins had higher stiffness than those with far hairpins (Malik 1980).

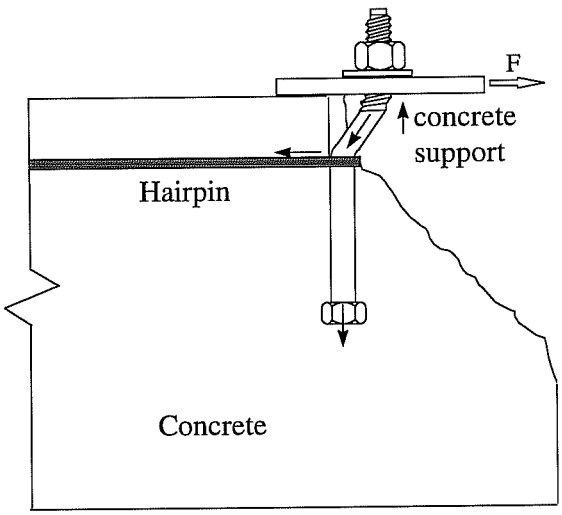

Figure 2.27 Action of a Close Hairpin on an Anchor in Shear (Malik 1980)

In Task 3 of this project, some tests were conducted on anchors with hairpins with different distances to the anchors with concrete cover of 1-1/2 inches (38 mm) (Hallowell 1996). Results showed that the close hairpins had a better effect on the load-displacement behavior of anchors; they increased the capacity when the concrete in front of the anchor failed, and also increased the stiffness of the load-displacement curve, more than far hairpins did. The reason is that a hairpin with 1-1/2-inch (38-mm) concrete cover may not confine the concrete above it very well, and after the concrete spalls off, the stiffness of the concrete between the hairpin and the anchor is much smaller than that of a hairpin that directly contacts the anchor shank. In those tests, several types of anchors were tested, including an undercut anchor with a sleeve, which increases the stiffness of the anchor shank. Test results show that the displacement at the ultimate load of the Undercut Anchor with hairpins is only about half that of the CIP anchor under the same conditions.

Figure 2.21 shows a typical load-displacement curve for a shear-loaded anchor, including the effect of hairpins.

2.7 Load-Displacement Behavior of Multiple-Anchor Connections

Loading conditions on a multiple-anchor connections can be very complex. The external load can usually be categorized into pure tension, pure shear, eccentric shear, or combined eccentric shear and tension.

2.7.1 Tension Loading

If a group of equally loaded tensile anchors fails in steel, the capacity of the connection is the summation of the tensile steel capacity of each individual anchor. In case of an eccentric tension load, the anchor with the greatest load determines the failure load of the group.

If the embedment depth of anchors is small enough for anchors to fail by concrete breakout, the methods explained in previously can be used to estimate the ultimate load. Appendix A has a comparison of the 45-Degree Cone Method and the CC Method for several typical configurations.

2.7.2 Shear Loading

If a group of equally loaded shear anchors fails in steel, the strength of the connection can be the summation of the shear steel capacity of each individual. However, if load distribution to the anchor is not uniform, special attention may be required. Large gaps between anchors and baseplate holes of two-anchor connections reduce the ultimate capacity (Eligehausen and Fuchs 1988).

When concrete breakout failure is expected, the prediction method explained in Section 2.3.2.1 and Appendix A should be used. The 45-Degree Cone Method (used in ACI 349) and the CC Method are compared in Appendix A for several typical configurations of shear anchors.

In Task 3 of this project, tests were conducted on two-anchor connections under pure shear (Hallowell 1996), in which only one of the anchors was placed near an edge.

Test results show that without hairpins, the front anchor does not contribute to the ultimate load capacity of the anchor group. Some tests also were performed using hairpins for the front anchor. These test results show that the ultimate capacity is the summation of ultimate load capacity of the back anchor, and that of the front anchor at an equal displacement.

2.7.3 Connections with Eccentric Shear

Methods for calculating the capacity of a connection loaded by eccentric shear can be divided into the Elastic Method and the Plastic Method.

The Elastic Method is based on the assumption that all materials behave elastically up to failure. It assumes that elastic anchors are connected to a rigid baseplate, and that the shear force is distributed uniformly among all anchors (McGuire 1986). This method was mainly based on the working stress method, proved to be too conservative by DeWolf and Sarisley (1980).

The Plastic Method recognizes that the connection is not rigid, and that considerable plastic redistribution of anchor forces can occur. However, assumptions varies regarding the distribution of compressive stress under the baseplate. One assumption is a linear compressive stress distribution with the maximum compressive stress at the toe of the baseplate (Maitra 1978). This assumption also yields conservative results (Hawkins et al. 1980). Another assumption is a linear compressive stress distribution with the compressive reaction at the centroid of the compression element of the attached member (Shipp and Haninger 1983). A procedure similar to the compressive stress block used in ultimate reinforced concrete beam was proposed by DeWolf and Sarisley (1980). In some cases, a maximum stress greater than $0.85 f_c'$ was used because of the confinement of base concrete (Salmon et al. 1955, Picard and Beaulieu 1985). Test results also show that this assumption produces conservative results. In the above assumptions, the flexibility of the baseplate and the consequent interaction between the baseplate and the concrete were not considered. Based on test observations, TVA DS-C1.7.1 (1984) suggests

that the compressive reaction is located at two times the plate thickness from the edge of the compression element of the attached member.

Cook (1989) proposed a method based on plastic behavior of anchors, which is an extension of the above procedures. This model assumes that anchors transfer shear by bearing on the anchor, and that tensile and shear forces in the anchors redistribute prior to failure.

According to test results by Cook (1989), the location of the compression reaction can be assumed at the edge of a rigid baseplate, or at the edge of the attached member for a flexible baseplate. However, in those tests the compression force was much smaller than some of the above tests, where the connection was loaded with axial compression as well.

According to the plastic design method proposed by Cook, the behavior of a ductile multiple-anchor connection can be separated into three distinct ranges:

1) Strength dominated by moment: The strength of the connection is controlled by the tensile strength of the anchor in the tension zone. All shear is transferred through friction ($e > e_1$).

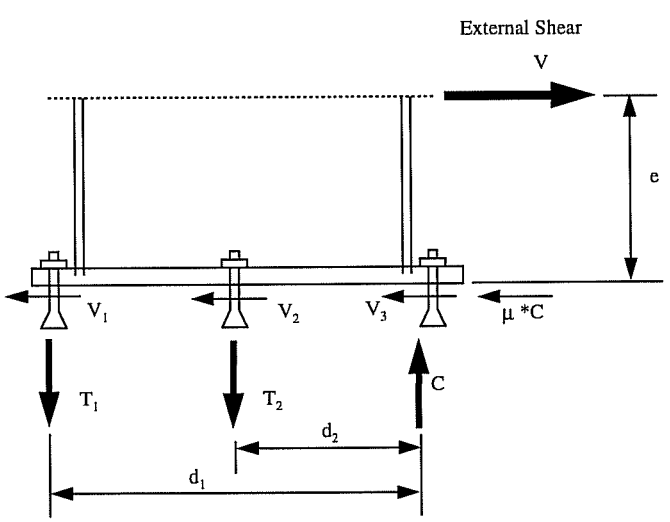

Figure 2.28 Distribution of Forces on a Multiple-Anchor Connection

2) The tension anchors develop their full tensile strength for moment resistance, while the shear resistance is provided by the friction force and the anchors in the compression zone ($e_1 < e < e_2$).

3) The anchors in the compression zone and the friction force provide a portion of shear resistance. The anchors in the tension zone must transfer tension and the remaining shear ($e < e_2$).

The transitions between these three ranges can be determined by two critical shear load eccentricities, e:

$$e_1 = \frac{d}{\mu} \tag{2-17}$$

and

$$e_2 = \frac{nd}{n\mu + m\gamma} \tag{2-18}$$

where: e_1 = the minimum eccentricity for multiple-anchor connections without shear anchors;

e_2 = the minimum eccentricity for multiple-anchor connection without combined tension and shear in the anchors;

n = the number of rows of anchors in the tension zone;

m = the number of rows of anchors in the compression zone;

μ = the coefficient of friction between steel and concrete;

γ = the ratio of the shear strength to the tensile strength of the anchor; and

d = the distance from the compressive reaction to the centroid of the tension anchors.

To ensure that the inner row of anchors develops the minimum specified tensile strength, the distance between the inner row of anchors and the compression reaction, d_1 in Figure 2.28, should not be less than 10% of the distance from the outer row of anchors to the compression reaction, d_2.

If an elliptical interaction curve ($p_1 = p_2 = 2$) is used for the strength of a single anchor in combined shear and tension, then:

$$V_n = \gamma\sqrt{T_o^2 - T_n^2} \tag{2-19}$$

where: V_n = the shear strength of a single anchor under combined tension and shear.

Therefore, for $e > e_2$,

$$V_{nt} = \frac{nT_o d}{e} \tag{2-20}$$

and for $e < e_2$,

$$V_{nt} = \gamma T_o \frac{ma + \sqrt{n^2(a^2 + b^2) - m^2 b^2}}{a^2 + b^2} \tag{2-21}$$

where: V_{nt} = the maximum predicted strength of the connection;

n = the number of rows of anchors in the tension zone;

T_o = the pure tensile strength of a row of anchors in the tension zone;

d = the distance from the compressive reaction to the centroid of the tension anchors;

m = the number of rows of anchors in the compression zone;

$a = 1 - \frac{\mu e}{d}$;

$b = \frac{\mu e}{d}$; and

μ = the coefficient of friction between steel and concrete.

Lotze (1997) conducted extensive tests in Task 2 of this project to determine the distribution of forces in a connection. It was found that at smaller loading eccentricities, the Plastic Method overestimates the capacity of a connection by more than 10% because it ignores the fact that the shear capacity on the tension anchor can not be fully developed due

to the small horizontal displacement capacity of the shear anchors. Lotze proposed a modification of the Plastic Method. By assuming the shear load to be evenly distributed among all anchors, the overestimation was eliminated. However, this contradicts the fact that the shear force on the shear anchors is much greater than that on the tension anchors.

2.8 Design Requirements for Baseplates Used in Tests on Multiple-Anchor Connections

Cook (1989) outlines the design criteria for the baseplate of a multiple-anchor connection, which are based on the *AISC LRFD Specifications* (1986) for bolted connections. The criteria used for designing the baseplate of the multiple-anchor attachment are reviewed here.

1. The anchor holes should meet the following requirements:
    a) Anchor hole oversize should not exceed 3/16 inch (4.8 mm) for anchors 7/8 inch (22 mm) and less in diameter, 1/4 inch (6.4 mm) for 1 inch (25.4 mm) anchors, and 5/16 inch (7.9 mm) for larger anchors.
    b) The minimum edge distance from the centerline of an anchor hole to the edge of the baseplate should not be less than 1.75 times the anchor diameter for a baseplate with sheared edges, and 1.25 times for other baseplates.
    c) The center-to-center distance between anchor holes should not be less than 3 times the anchor diameter.
2. To prevent prying action of the baseplate under load, the plastic moment capacity of the baseplate should meet certain requirements.

Prying is far less serious in steel-to-concrete connections than in steel-to-steel ones, because of the relatively greater tensile displacement of anchors to concrete. Depending on the relative stiffnesses of the baseplate and the anchors, the effects of prying completely dissipate at the ultimate state; however, it affects the loads on the anchors at the early load

stages (Metha et al. 1984). In any event, excessively flexible baseplates should be avoided (Carrato 1991).

By requiring that the minimum yield moment at the edge of the attached member exceed the moment induced by the tension force of the tension anchors (PCI 1992), prying effects can be prevented. This is equivalent to requiring:

$$\phi m_p \geq m_{ut}$$

where: ϕ = strength reduction factor for baseplate steel in flexure (0.90);

m_p = nominal flexural capacity of a baseplate, based on the plastic section modulus; and

m_{ut} = maximum moment induced in a baseplate by the tension anchors.

3. The design bearing strength of an anchor hole in the baseplate should exceed the average shear strength of an anchor.

4. The shear capacity of a baseplate should also exceed the shear induced in the baseplate by the tension anchors.

CHAPTER 3

DEVELOPMENT OF EXPERIMENTAL PROGRAM

3.1 Objectives of Experimental Program

In order to design an anchor connection safely and economically, the behavior of the anchors and the baseplate of the attachment should be clearly understood. A great amount of research has been conducted on the behavior of anchor connections. However, some factors affecting the behavior of connections need to be investigated further:

- the effect of loading type;
- the effect of concrete cracking; and
- the contribution of hairpins to the load-displacement behavior of near-edge connections loaded in shear.

The purpose of this experimental study was to assess the effects of earthquake-type loading and concrete cracking on the behavior of single- and multiple-anchor connections. In the context of the entire test program, the objectives of this experimental program were:

1) to determine the effect of dynamic loading on the ultimate capacity of anchors failing by concrete breakout;
2) to determine the effect of cracks on the ultimate capacity of anchors failing by concrete breakout;
3) to determine the effect of hairpins on the load-displacement behavior and the ultimate capacity of near-edge, multiple-anchor connections; and

4) to determine the behavior of multiple-anchor connections under effect of dynamic reversed loading.

3.2 Scope

The tests described here correspond to three different phases of the testing program:

1) single anchors in cracked concrete under static and dynamic tensile loading;
2) near-edge, two-anchor connections under static and dynamic eccentric shear loading in cracked and uncracked concrete; and
3) multiple-anchor connections under reversed, dynamic, eccentric-shear loading.

3.3 Development of Testing Programs

3.3.1 Single-Anchor Tension Tests in Cracked Concrete of Task 1

As a part of Task 1, the purpose of these tests was to determine the effect of cracking in concrete members on various types of anchors under static and dynamic loading. The other tests of Task 1 are reported by Rodriguez (1995) and Hallowell (1996).

The goal of Task 1 tests on single anchors was to investigate the behavior of different types of anchors under dynamic tensile loading. Several factors were studied in this task, such as types of anchors, types of aggregates, concrete strengths, reinforcement, types of loading, and concrete cracking. Most of these tests are reported in Rodriguez (1995).

Initially, to compare the effect of different properties of concrete, specimens for Task 1 tests were made of using concrete of two types of aggregates, river gravel and limestone. The specimens made with limestone aggregate had two strengths, 3000 psi (20.7 MPa) and 4700 psi (32.4 MPa). Those test results showed that concrete strength and aggregate type had little effect on anchor capacity. In the tests of this study, a reduced

number of anchor types, typical of those most in use in nuclear power plants, were selected for test, using concrete specimens with limestone aggregate at 4700 psi (32.4 MPa). Some tests with different anchors in concrete specimens with granite aggregates were later conducted (Hallowell 1996).

For one type of expansion anchor and one type of undercut anchor, two anchor diameters [3/8 inch (10 mm) and 3/4 inch (19 mm)] were tested to evaluate the effect of cracks. To eliminate other factors and thereby enable a direct comparison, the nominal embedment depths were kept the same throughout all Task 1 tests, at 4 inches (102 mm) for anchors of 3/4-inch (19-mm) diameter, and 2.25 inches (57 mm) for anchors of 3/8-inch (10-mm) diameter.

The serviceability provisions of ACI 318-95 are consistent with permissible crack widths of 0.016 inch (0.41 mm) and 0.013 inch (0.33 mm) in interior and exterior flexural members respectively. Based on these implicit considerations and on prior tests with that width, a crack with of 0.3 mm was selected for this study.

3.3.2 Tests on Near-Edge Two-Anchor Connections under Eccentric Shear of Task 3

The purposes of Task 3 tests were to assess the effects of cracks and the effect of hairpins on anchors loaded in shear. Most of Task 3 tests are reported by Hallowell (1996). In those tests, three types of anchors (cast-in-place, expansion, and undercut) were tested under both static and dynamic pure shear in uncracked concrete. The cast-in-place anchors, with and without hairpins, were also tested in cracked concrete. The results showed that anchors with hairpins behave similarly in both cracked and uncracked concrete under static loading; that hairpins far from anchors give higher concrete breakout loads; and that hairpins close to anchors increase ultimate capacity more effectively. Two-anchor connections with cast-in-place anchors, oriented perpendicular to the member edges, were also tested under pure shear, with and without hairpins. In these tests, the back anchor was expected to fail by steel fracture. The tests showed that without hairpins, the capacity of connections is controlled solely by the steel capacity of the back anchor; with hairpins,

however, the behavior of a double-anchor connection can be determined by superimposing the load-displacement behaviors of each anchor, and the maximum capacity of the connection is the summation of the maximum capacity of the back anchor and the capacity of the front anchor at the equal displacement.

Completing Task 3, the tests reported in this study were intended to determine the effect of edges on two-anchor connections in shear at a moderate eccentricity with steel fracture, and also the effect of hairpins, under both static and dynamic loading. Because a near-edge anchor with a close hairpin has a slightly lower concrete breakout capacity but a much higher ultimate capacity, and because the front anchor in cracked concrete without hairpins will have a smaller concrete breakout capacity, only six different configurations were tested: dynamic and static tests in uncracked concrete without hairpins, and dynamic and static tests in cracked concrete with and without hairpins.

To ensure shear redistribution between the anchors, the anchor embedment was chosen large enough so that the back anchor would fail by steel fracture. The loading eccentricity of the connection was chosen small enough so that the back anchor would be subjected to both tension and shear, which requires that the eccentricity of the external shear be less than the critical eccentricity, e_2. The spacing of the anchors was controlled at 10 inches (254 mm) by the loading plate used in Task 2 tests. The friction coefficient between the steel and the Teflon sheet, determined in Task 2, was 0.15 (Lotze 1997). According to Equation 2-18, the critical eccentricity is:

$$e_2 = \frac{10}{0.15 + 1 \times 0.5} = 15.5\ inches = 394\ mm \qquad (3\text{-}1)$$

with a shear strength ratio of 0.5 for cast-in-place anchors. Therefore, 12 inches (305 mm) was chosen as the loading eccentricity.

Meanwhile, to ensure that the front anchor would fail by concrete breakout under shear, the edge distance was chosen as 5 inches (127 mm), corresponding to a concrete

breakout capacity of 13.1 kips (58.2 kN), according to Equation 2-11 for 4700-psi (32.4-MPa) concrete.

3.3.3 Tests on Multiple-Anchor Connections under Dynamic Reversed Eccentric Shear of Task 4

Task 4 tests were intended to assess the effect of earthquake-type loading on the behavior of multiple-anchor connections under various conditions.

In Task 2, single-anchor connections with Undercut Anchor 1 were tested under various loading angles to determine the load and the displacement interaction curves. In order to use this information to calculate the theoretical load-displacement behavior of multiple-anchor connections, the same type of anchor was used in this study, with the same diameter and the same embedment depth. Two-anchor connections were also tested far from edges in Task 2, to determine the redistribution of shear and tension forces between anchors, and to evaluate the validity of the Plastic Method of design. Those tests derived the following conclusions (Lotze 1997):

1) Gaps between the anchors and the baseplate could significantly affect the ultimate capacity of connections depending on anchor diameters. The smaller the diameter, the greater the effect.

2) Due to shearing displacement at the ultimate capacity of the shear anchor, the shear capacity of the tension anchors cannot reach the levels given by the load interaction curves. This results in an overestimation of capacity of connections loaded in shear at small eccentricities.

3) Friction plays an essential role in the transfer of shear in multiple-anchor connections, and its effect can be accurately predicted given the coefficient of friction.

Based on this information, two different loading eccentricities were chosen for Task 4 tests.

- A small eccentricity of the external shear load was chosen so that the back row of anchors would always be loaded in combined tension and shear. Those test results could be used to evaluate the effect of reversed loading on the load capacity of connections loaded in shear at moderate eccentricities.
- A large eccentricity was chosen simply for the back anchors to fail under tension.

The dynamic loading capacity was restricted by the maximum flow rate of the closed-loop loading system (the capacity of the servo-valve and the line tamer used in tests). To fully utilize the loading system while achieving the highest possible loading rate, only a two-row connection configuration was tested; the spacing of the tension and shear anchors was chosen as 10 inches (254 mm), with a baseplate length of 14 inches (356 mm).

Assuming the baseplate to be rigid, using a value of 0.15 for the friction coefficient between the Teflon sheet and the steel, and using a value of 0.6 for the shear strength ratio of undercut anchors, Equation 2-18 gives the critical eccentricity as:

$$e_2 = \frac{1 \times 12}{1 \times 0.15 + 1 \times 0.6} = 16.0\ inches\ \ (406\ mm) \qquad (3\text{-}2)$$

Therefore, 12 inches (305 mm) was chosen for the small eccentricity, and 18 inches (457 mm) for the large eccentricity.

3.4 Development of Test Specimens

To fulfill these different test objectives and to meet the various requirements of each group of tests, different specimens and loading setups were used throughout the entire study. In the following sections, they are described in detail.

All concrete test specimens were designed to meet the requirements of ACI 318 (1989), and all steel members were designed according to *AISC LRFD Specifications* (1992).

3.4.1 Specimens for single-anchor tests

Tension tests on single anchors were conducted on concrete slabs 54 inches (1372 mm) wide by 74 inches (1880 mm) long by 10 inches (254 mm) thick. The configurations of reinforcing bars in specimens were designed differently for tests on the two sizes of anchors, to achieve the most efficient utilization of specimens.

For tests on 3/4-inch (19-mm) diameter anchors, the specimens were longitudinally reinforced with six #4 bars top and bottom with 1-1/2-inch (38-mm) concrete cover. They were designed to withstand the expansion force produced by the anchors under tension

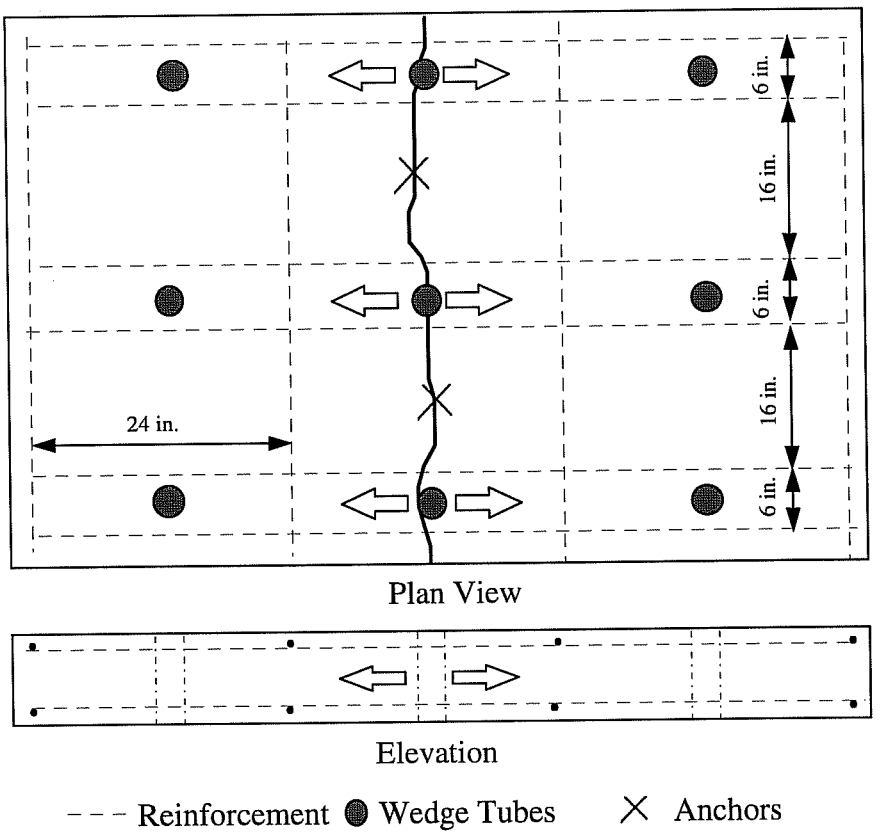

Note: 1 inch = 25.4 mm

Figure 3.1 Concrete Specimens for Tension Tests on Single Anchors of 3/4-inch (19-mm) Diameter

load, to keep the crack width constant during tests. A total of eight #4 transverse bars were also used to meet minimum reinforcement requirement in the specimens to prevent unwanted cracking. The placement of reinforcing bars is shown in Figure 3.1. To avoid interference of the bars with the potential breakout cones, the reinforcing bars were placed at least 8 inches (200 mm) from anchors (twice the embedment depth).

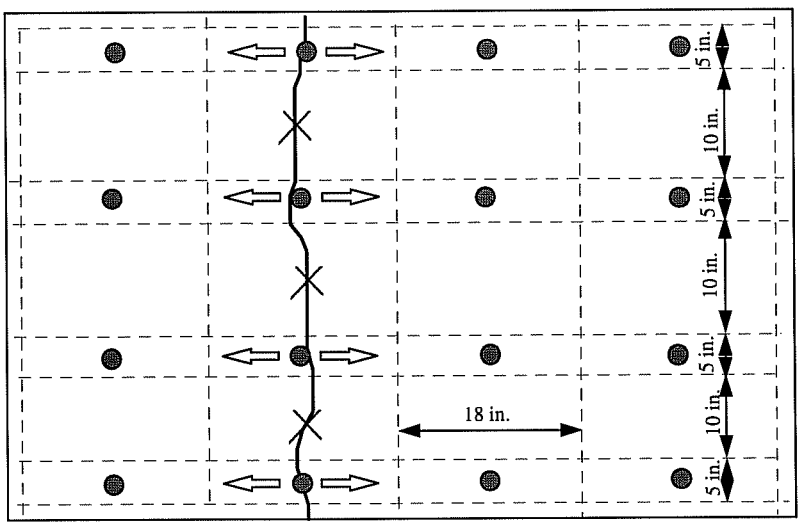

Note: 1 inch = 25.4 mm.

Figure 3.2 Plan of Specimens for Tension Tests on Single Anchors of 3/8-inch (10-mm) Diameter

In the tests on 3/8-inch (10-mm) diameter anchors, the embedment depth of anchors was smaller, and the area of concrete breakout cone was consequently smaller. Therefore, more tests could be done on a single specimen. The specimens of the same size were modified to accommodate 12 tests on a single slab. There were ten transverse reinforcing bars and sixteen longitudinal bars. The distance of the anchors to the nearest bar was 5 inches (127 mm). Figure 3.2 shows the plan view of these specimens.

3.4.2 Specimens for Tests on Two-Anchor Connections under Eccentric Shear

3.4.2.1 Concrete Specimens

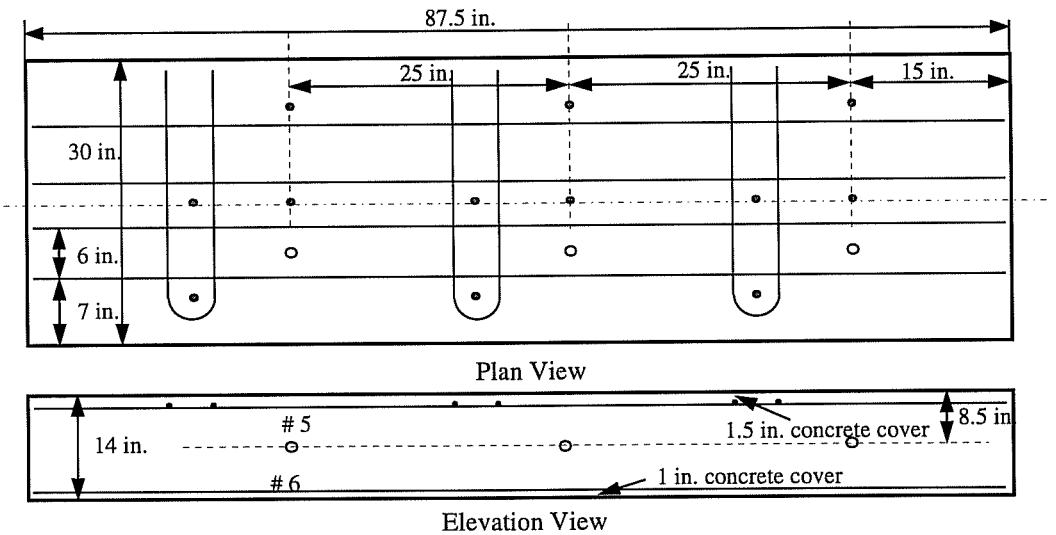

Note: 1 inch = 25.4 mm

Figure 3.3 Specimen for Eccentric Shear Tests on Two-Anchor Connections

The concrete specimens for eccentric shear tests on two-anchor connections were 30 inches (762 mm) wide by 87.5 inches (2223 mm) long by 14 inches (356 mm) thick. The formwork was previously used for the specimens of the other tests of this task. The minimum required embedment depth for steel failure of anchors was 7 inches (178 mm). To avoid any interference with the concrete breakout cone at the free edge, while achieving an uniform crack width along the crack, for each test in cracked concrete one splitting wedge was placed vertically just at the back of the loading plate, and the other was placed horizontally near the mid-depth of the specimen. Due to the constraint imposed by the embedment depth of the anchors, the splitting wedges could only be located at 8.5 inches (216 mm) from the top, away from the center of the specimens. In order to have a constant crack width through the thickness of the slab, four #5 reinforcing bars were placed on the

top with 2-1/4 inch (57 mm) cover (1-1/2 inch (38 mm) concrete cover for hairpins), and four #6 bars on the bottom with 1-inch (25-mm) cover to achieve balance of moment.

Each specimen was designed to permit three tests in uncracked concrete on one side, and three tests in cracked concrete on the other side. The specimens would be cracked with the Cast-in-Place Anchors already in position; to ensure that the cracks would pass through the anchor locations, thin steel sheets were placed between the two anchors of each group on one side of the specimen, to serve as crack initiators. The metal sheets were cut with several holes to allow concrete to flow freely during casting, to prevent them from being pushed out of position by the fresh concrete (Figure 3.4).

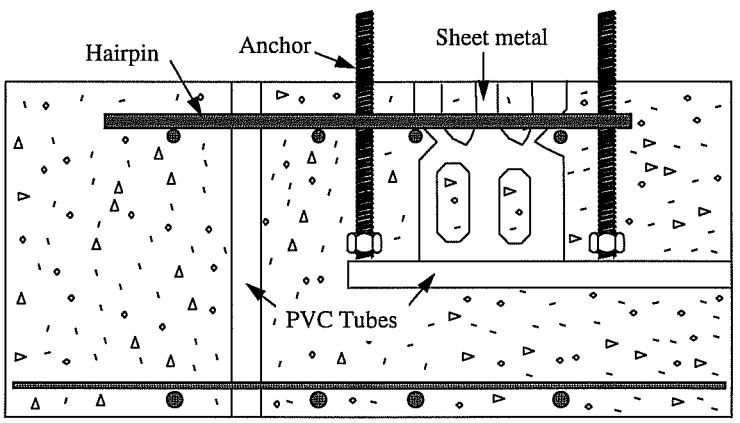

Figure 3.4 Sheet-Metal Crack Initiators Used with Cast-in-Place Anchors in Cracked Specimen

To eliminate the procedure of drilling holes in concrete specimens for the splitting tubes, especially the horizontal holes, 1-inch (25-mm) PVC tubes, sliced in half, were placed in the formwork at where the splitting wedges would be, sealed at both ends.

Hairpins like those used in the previous pure shear tests were again used here, and were placed above the top reinforcing bars.

3.4.2.2 Loading Plates

The loading plate was the same as that used previously in Task 2 of this program. The loading apparatus consists of a baseplate with two high-strength steel inserts, two tension rods, and two compression bars, as shown in Figure 3.5.

To reduce the deformations of the baseplate holes due to local bearing stresses under the anchors, two high-strength steel inserts were used, as shown in Figure 3.5. The inside thickness of these inserts was counterbored to 3/4 inch (19 mm), the same as the diameter of the anchor bolts. The diameter of the baseplate holes was 13/16 inch (20.6 mm).

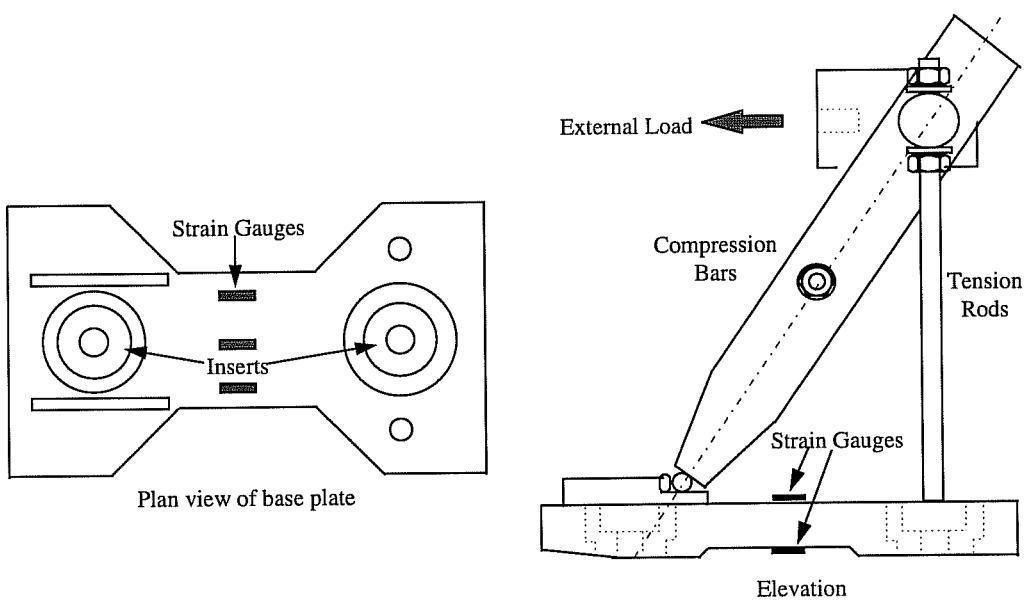

Figure 3.5 Loading Apparatus for Tests on Two-Anchor Connections under Shear

The tension rods and compression bars were bolt-connected at the top with a loading rod to transmit the external shear load. The center section of the base plate was machined narrower and thinner than the rest of the plate, to achieve uniform stress distribution and to avoid direct contact with the concrete surface. The other ends of the

compression bars rested on a circular steel bar, located so that the extension of the center line of the compression bars would pass through the point of contact between the front insert and the anchor shank. The compression end of the loading plate was beveled at 5 degrees from the front edge of the front hole to eliminate prying action on the compression anchors during testing, and also to reduce the bending moment in the baseplate caused by the force in the compression bars. The tension rods were placed at the same distance from the compression edge as the tension anchor, to eliminate any moment caused by the forces in them. Three strain gauges were evenly spaced on the top center section of the loading plate, and three on the bottom. However, due to a lack of data acquisition capacity, only the outside two pairs were used.

Using this loading apparatus, the horizontal load is transferred through the compression bars to the front end of the baseplate. The force measured by the strain gauges equals the shear force acting on the back anchor. As a result, the shear distribution between the two anchors can be determined experimentally, and the computed tension force on the back anchor can also be modified using the moment at the center of the baseplate.

Based on the geometry of the loading apparatus, the force in the tension rods is 1.2 times the external shear load. Therefore, as shown in Figure 3.6, the tension force on the back anchor can be calculated by equilibrium of moments about the center of the baseplate:

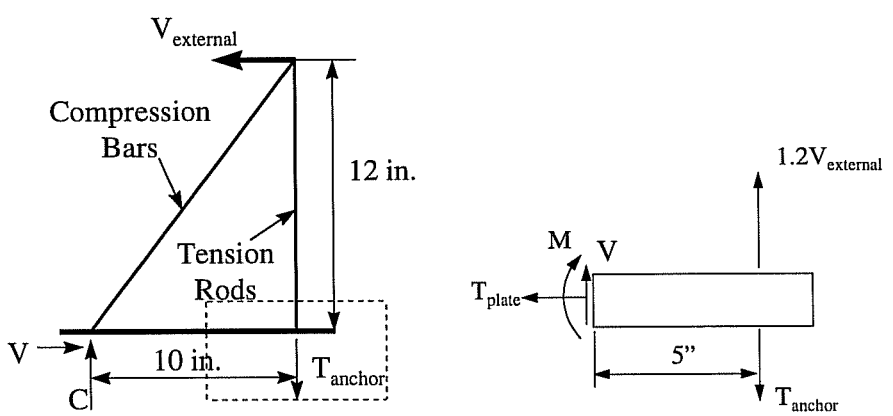

Figure 3.6 Free Body Diagram for Calculating Forces on Back Anchors

$$(1.2 \cdot V_{external} - T_{anchor}) \cdot (5) + V(0) = M \quad (3\text{-}3)$$

$$T_{anchor} = 1.2 \cdot V_{external} - M/5 \quad (3\text{-}4)$$

As mentioned before, the shear force on the back anchor equals the measured tension force on the baseplate, T_{plate}.

3.4.3 Specimens for Tests on Multiple-Anchor Connections under Eccentric Shear

3.4.3.1 Concrete Specimens

These tests on multiple-anchor connections were performed on both top and bottom sides of specimens measuring 50 inches (1270 mm) wide by 50 inches (1270 mm) long by 18 inches (457 mm) thick (Figure 3.7). Reinforcement was placed on both the top and the bottom of the specimens, with at least 1-1/2 in. (38 mm) concrete cover. In two specimens

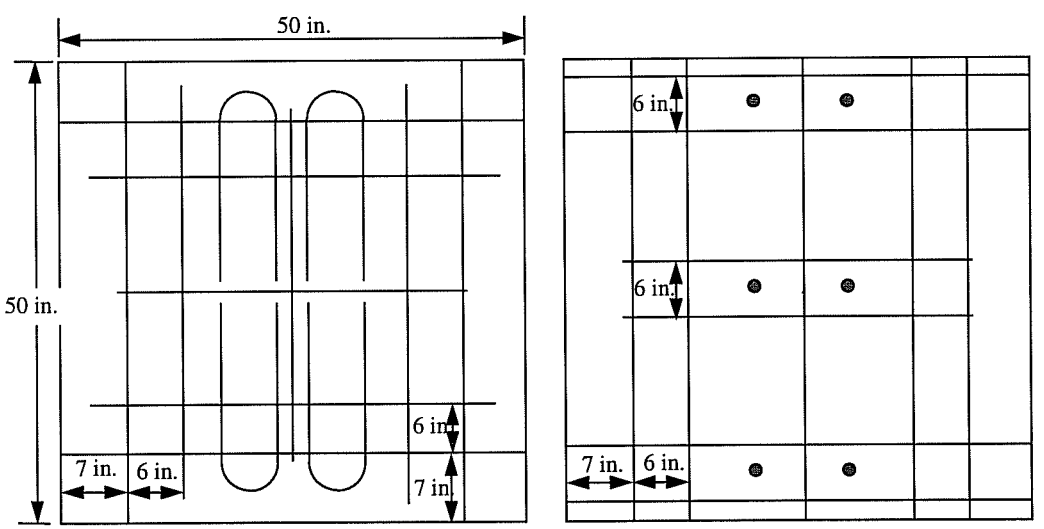

Specimen for Tests with Hairpins

Specimen for Tests in Cracked Concrete

● Holes for Splitting Wedges

Note: 1 inch = 25.4 mm

Figure 3.7 Specimens for Tests of Task 4

for the tests in cracked concrete, PVC tubes for splitting wedges were also pre-placed to eliminate the drilling procedure. As shown in Figure 3.7, the horizontal reinforcing bars in the middle of specimens were cut short and placed away from edges to avoid any interference with the concrete breakout cone of near-edge anchors.

3.4.3.2 Loading Plates

One Task 4 test was conducted using a flexible baseplate, to assess the effect of the baseplate flexibility on the behavior of connections. The flexible baseplate was designed to yield on its compression side, and to be at or just above yielding on its tension side at anchor failure.

The plate thickness was determined to avoid the formation of a plastic hinge at the edge of tension flange of the attached member, assuming that the baseplate would act as a tip-loaded cantilever (Figure 3.8), and that A36 steel has yield strength of 36 ksi (248 MPa). The effective width of the cantilever was taken as the plate width. Required thickness of the baseplate was determined as follows:

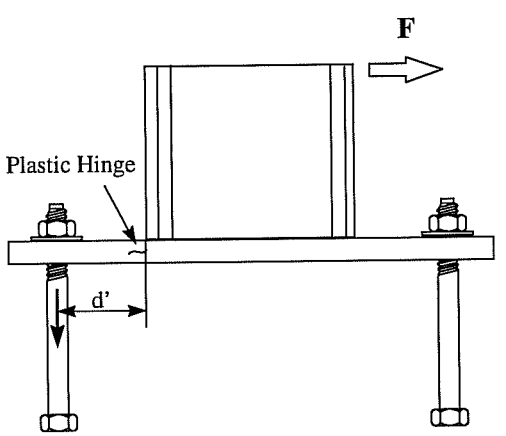

Figure 3.8 Avoiding Plastic Hinge of Baseplate at Tension Flange of Attached Member

$$M_p \geq 2A_s F_{ut,anchor} d' \tag{3-5}$$

$$F_y\left(\frac{bt^2}{4}\right) \geq 2A_s F_{ut,anchor} d'$$

$$(36)\left(\frac{12t^2}{4}\right) \geq 2(0.226)(125)(2)$$

$$t \geq 1.05 \text{ (inches). (26.7 mm)} \tag{3-6}$$

Therefore, the thickness of the baseplate was chosen as 1.0 inch (25.4 mm).

Since the compressive resultant force in the four-anchor tests would equal the load in the two tension anchors, the 4-inch (102-mm) portion of the baseplate projecting from the compression flange of the attachment was expected to yield.

Figure 3.9 shows the configuration of the loading attachment. The steel beams were designed according to *AISC LRFD specifications* (1994). High-strength steel inserts were again used at each anchor to reduce the bearing deformation of holes during tests. Since most tests would be done with a rigid baseplate, four triangular steel stiffeners were

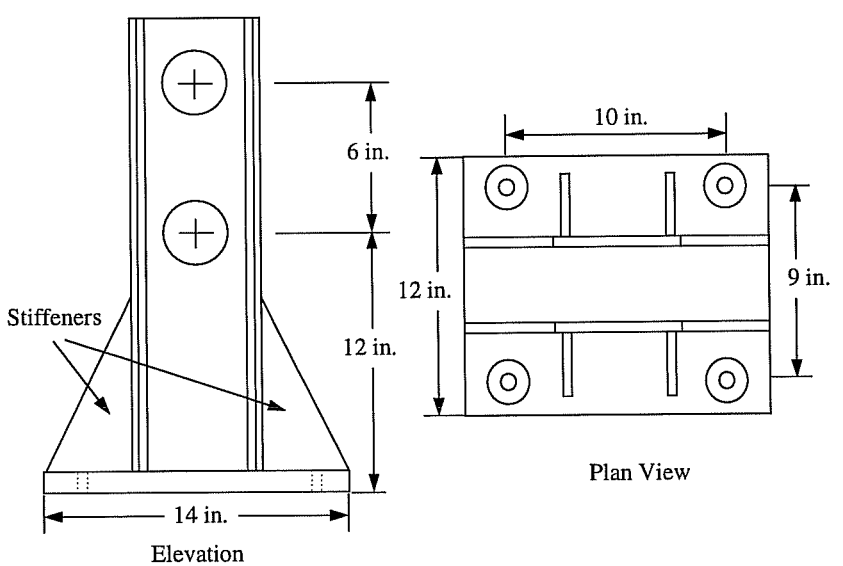

Note: 1 inch =25.4 mm

Figure 3.9 Steel Attachment for Task 4 Tests

welded to prevent the baseplate from flexural deformation by the reaction force of the concrete surface on the compression edge. For the test with a flexible baseplate, the stiffeners were completely removed.

3.5 Development of Test Setups

3.5.1 Single-Anchor Tension Tests

In the single-anchor tests, the loading setup shown in Figure 3.10 was used. The diameter of the reaction ring of this setup is 26 inches (660 mm). This is about six times the embedment depth of the tested anchors, large enough to avoid interfering with the breakout cone. The anchor and the tension rod were connected with an internally threaded coupler (right, Figure 3.10). The hydraulic ram was placed on top of two back-to-back channels, welded to the top of the reaction ring.

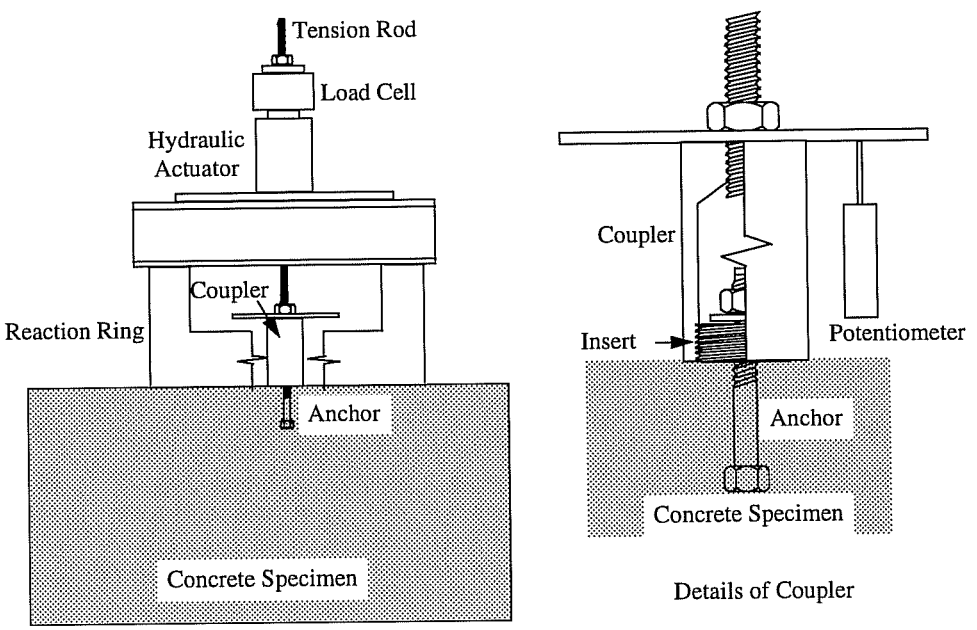

Figure 3.10 Testing Setup for Static Tension Tests on Single Anchors

3.5.2 Multiple-Anchor Connection Shear Tests

A large load is required to fail multiple-anchor connections loaded in eccentric shear. In addition, the seismic-type loading requires that the test specimens be held firmly during tests, and that the test setup be stiff. Using the existing tie-down holes on the lab floor to hold the testing specimens might have resulted in larger specimens and poor efficiency of utilization of those specimens. As an alternative, a tie-down frame made of W12 sections was used, as shown in Figure 3.11, to shift the tie-down positions. These sections were tied town on the lab floor and were joined using slip-critical (friction) connections.

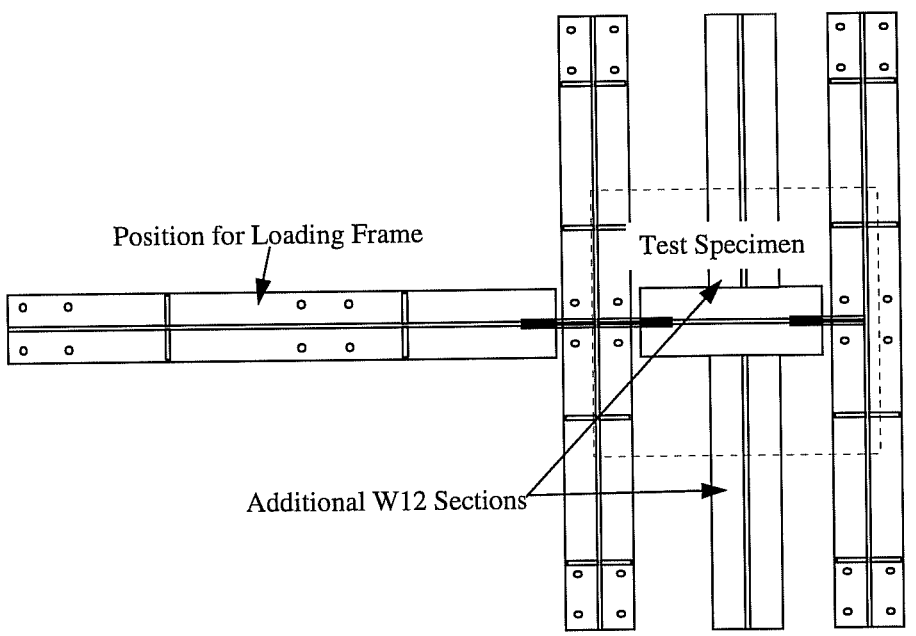

Figure 3.11 Plan of Tie-Down Frame

For the two-anchor connection tests, the specimen was set on top of four steel rollers in order to allow positioning without any crane operations during tests. These rollers were placed on the W12 sections and aligned with them. Since the specimens are narrower than the spacing of the W12 tie-down beams, two additional W12 sections were placed between the platforms (Figure 3.12). Two 3-inch (76-mm) steel structural tubes

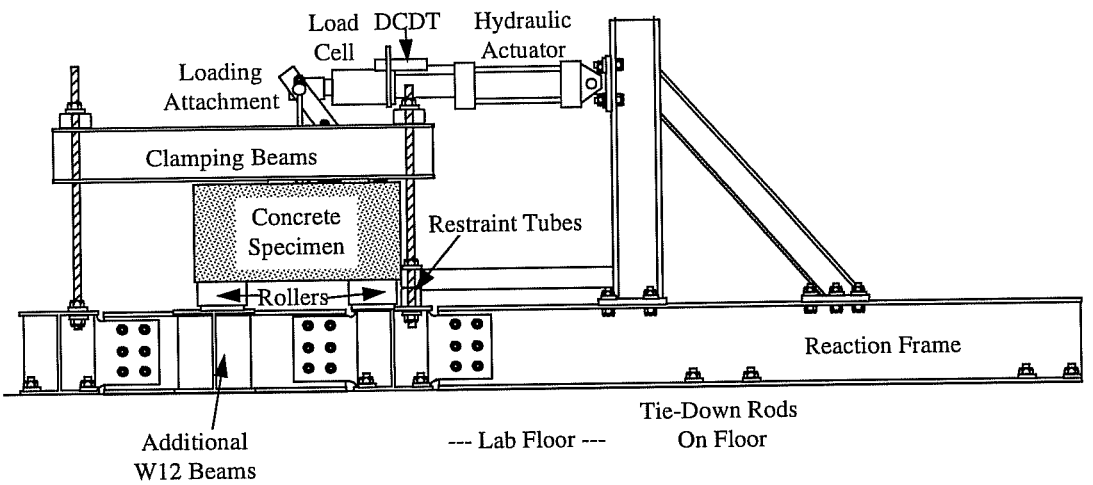

Figure 3.13 Setup for Tests on Two-Anchor Connections under Eccentric Shear

were bolted together at the front of the specimen to prevent it from moving horizontally during tests. Finally two small beams were clamped using threaded rods on the top of the specimen on each side of the loading baseplate, to prevent the specimen from rotating under external load.

For the multiple-anchor connection tests, the specimens were set directly on the tie-down beans, and also clamped to the tie-down frame by two beams on each side of the loading plate, using threaded rods. A 3-inch (76-mm) tube was bolted at each end of the

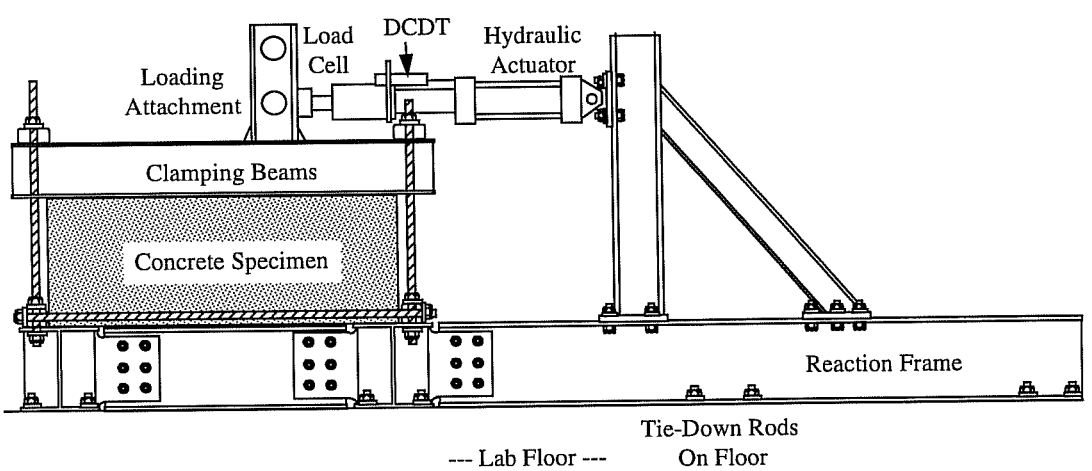

Figure 3.12 Test Setup for Multiple-Anchor Tests

specimens; gaps between the specimen and the tube were filled with hydrostone to keep the specimen from moving horizontally. This is shown in Figure 3.12.

3.6 Development of Loading Pattern for Dynamic Tests

3.6.1 Dynamic Tests on Single Anchors

In Task 1 and Task 2 of this project, to investigate how dynamic loading affects the ultimate load capacity of anchor, the load was applied in a very short time period.

Earthquake spectra typically have significant energy in the frequency range of 3-4 Hz. This frequency corresponds to a time from zero to maximum load of about 0.08 seconds. Therefore, these tests were conducted using a ramp load with a rise time of 0.1 second. Information from those tests was used to develop expression for dynamic capacity of anchors as governed by concrete breakout.

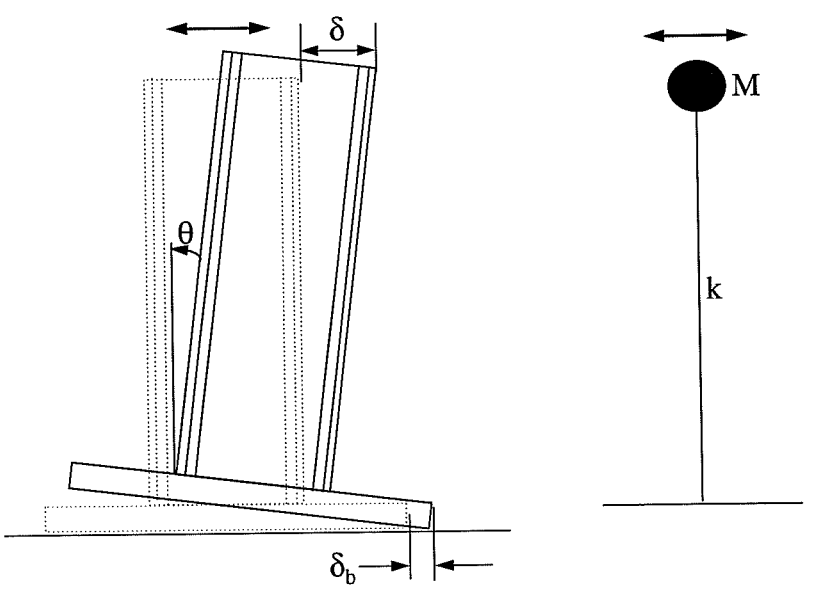

Figure 3.14 Simplified Model of Multiple-Anchor Connection

3.6.2 Estimated Response of an Attachment under Earthquake Loading

To simulate earthquake loading on the multiple-anchor attachments of Task 4 of this study, the displacement response of a typical attachment was estimated using the following procedure:

1) The attachment was assumed to be a single-degree-of-freedom system with a concentrated mass at 12 inches (305 mm) above the concrete surface (Figure 3.14).

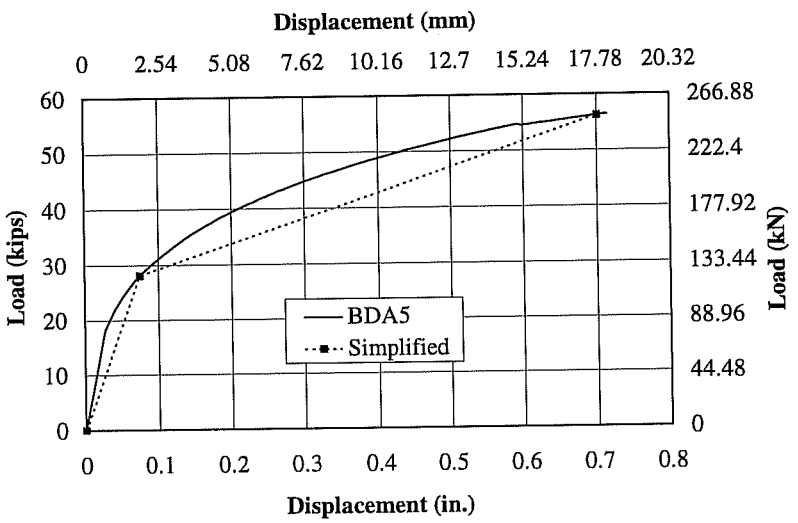

Figure 3.15 Simplified Load-Displacement Curve of Attachment

2) Using the BDA5 program (Chapter 7), and the load-displacement curves from Task 2 of this research program (Lotze 1997), the horizontal displacement and the rotation of the baseplate were estimated as functions of load. The resulting curves are shown in Figure 3.15.

3) This load-displacement curve of the attachment was simplified as bilinear. The displacement at 12 inches (305 mm) from the concrete surface was calculated using the horizontal displacement and the baseplate rotation of the attachment. The yield load of the elastic range is 28 kips (125 kN), at a total displacement

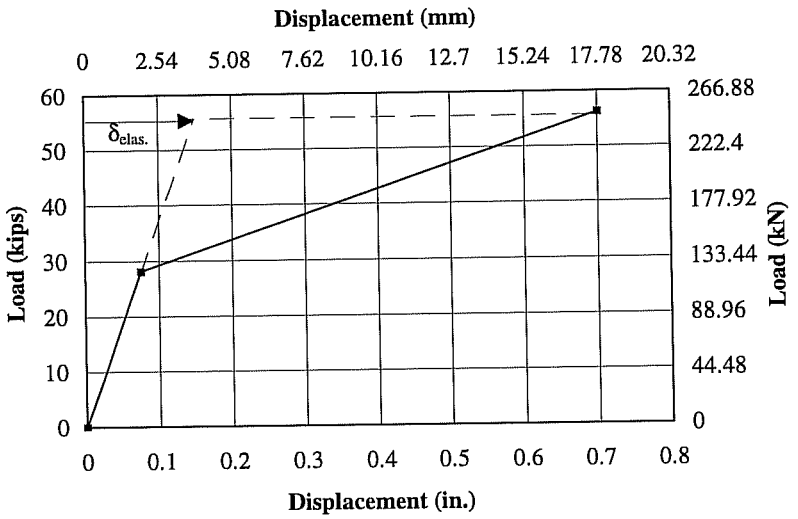

Figure 3.16 Calculation of Displacement Ductility Factor

of 0.074 inch (1.9 mm). The deformation of the beam at the maximum static load of 56 kips (249 kN) as calculated from Step 2, was estimated at 0.7 inch (17.8 mm).

4) To simplify the calculation, the response of the attachment was further simplified as linearly elastic, with a stiffness equal to the average of the secant stiffness at the maximum load and the elastic stiffness, which is about 230 kips/inch (40300 kN/m).

5) The displacement ductility factor, used for the reduction of the maximum acceleration, was estimated as shown in Figure 3.16: $\mu = 0.70/\delta_{ela} = 0.70/(2\times 0.074) = 4.73$. Assuming the acceleration of the earthquake load as 0.4g and the soil damping as 5%, and considering the displacement ductility, the maximum acceleration on the attachment is:

$$\ddot{u}_{\max} = \frac{0.4g\times 2.6}{\sqrt{2\mu - 1}} = \frac{0.4g\times 0.6}{\sqrt{2\times 4.73 - 1}} = 0.36g \approx 0.4g = \ddot{u}_{\max}. \qquad (3\text{-}7)$$

The mass was estimated according to the strength of the attachment (the

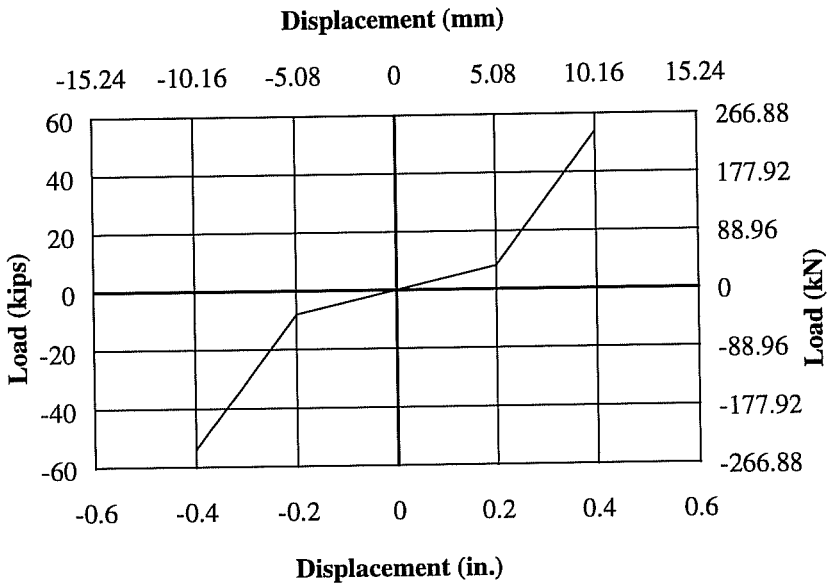

Figure 3.17 Idealized Load-Displacement Curves for Multiple-Anchor Attachment

smaller of the moment capacity of the beam and the capacity of the anchor group) to be 250 kN / 0.4g = 637100 kg = 140 k-sec^2/inch.

6) In a trial test, significant displacement occurred without much load, due to the gaps between the baseplate holes and the anchor shanks and between the anchor shanks and the surrounding concrete. Therefore, the stiffness of the attachment was idealized as bilinear, as shown in Figure 3.17. The lower-stiffness portion (40 kips/inch (7000 kN/m)), representing the effect of gaps on the baseplate was estimated from the trial test. The higher-stiffness portion was obtained from Step 4 above.

7) Using idealized bilinear load-displacement curves and the estimated mass of the attachment, the relative displacement response of the attachment at 12 inches (305 mm) was calculated numerically using the linear-acceleration method with the earthquake history of El Centro 1940 (NS component).

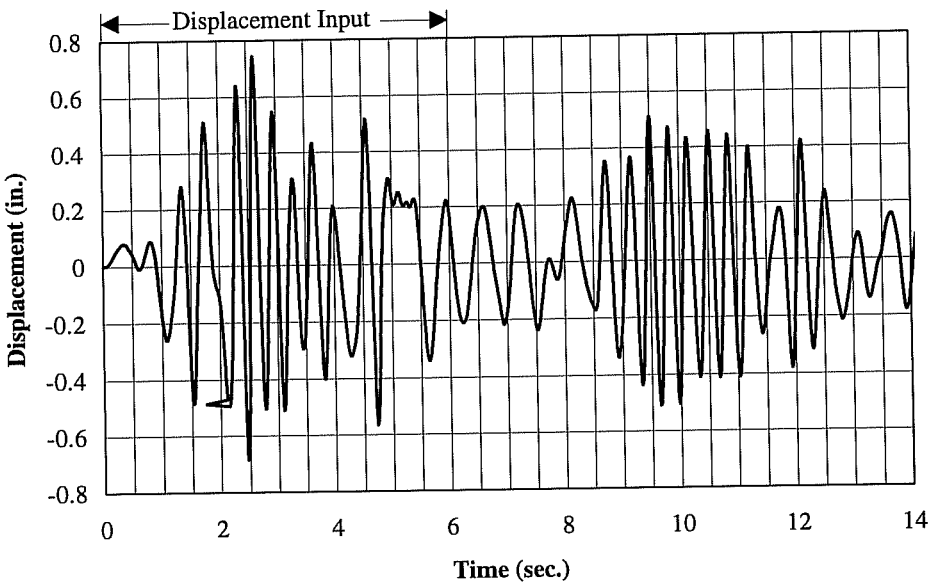

Figure 3.18 Time History of Estimated Attachment Displacement

8) The calculated displacement history of the attachment is shown in Figure 3.18. The most active portion, consisting of the first 6.0 seconds of that record, was used as the command signal. Each specimen was loaded repeatedly by that displacement input. As each test progressed, the input was scaled by larger and larger factors, until failure occurred.

3.7 Development of Test Instrumentation

3.7.1 Single-Anchor Tension Tests

Anchor load and displacement were essential test information, and were measured directly with a load cell and a linear potentiometer (Figure 3.10) respectively.

3.7.2 Eccentric Shear Tests on Two-Anchor Connections

The external load on the connections was measured with a load cell. The horizontal displacement and rotation of the baseplate are critical to understanding the behavior of the connections. The slip of the baseplate, δ_h, was measured with a linear potentiometer placed behind the baseplate. The baseplate rotation was measured indirectly using the upward displacement of baseplate at the back anchor, δ_v, which is an approximation to the displacement of that anchor (Figure 3.19).

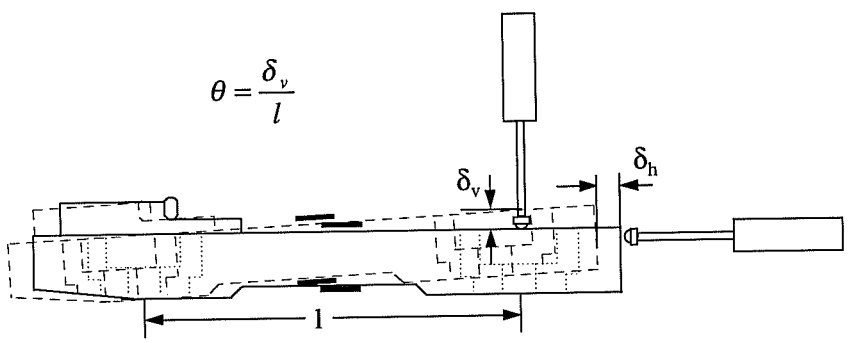

Figure 3.19 Instrumentation for Displacement Measurement in Two-Anchor Connection Tests

3.7.3 Eccentric shear tests on multiple-anchor connections

The external load on the connections was measured with a load cell. The tension forces on each anchor were measured with force washers placed between the normal washers and the baseplate.

The displacements of the attachment include slip and rotation of the baseplate. The slip of the baseplate, δ_{h1}, was measured with a potentiometer placed against the back of the baseplate. The displacement of the vertical beam at 12 inches (305 mm) from the surface, δ_{h2}, was also measured (Figure 3.20). The rotation was calculated as the difference between these two horizontal displacement, assuming the beam to be infinitely stiff. The

vertical displacement of the baseplate, δ_v, was measured at the center line of the baseplate as well. However, it may not be a precise indicator of the rotation of the baseplate, due to the uneven concrete surface and the flexibility of the baseplate.

The rotation of the attachment can be calculated from Equation 3-8:

$$\theta = \arctan\left(\frac{\delta_{h2} - \delta_{h1}}{12}\right) \tag{3-8a}$$

where: θ = rotation of attachment;

δ_{h1} = transverse displacements measured at the baseplate; and

δ_{h2} = transverse displacements measured at 12 inch (305 mm) above concrete surface.

or according to the vertical displacement of the center of the baseplate:

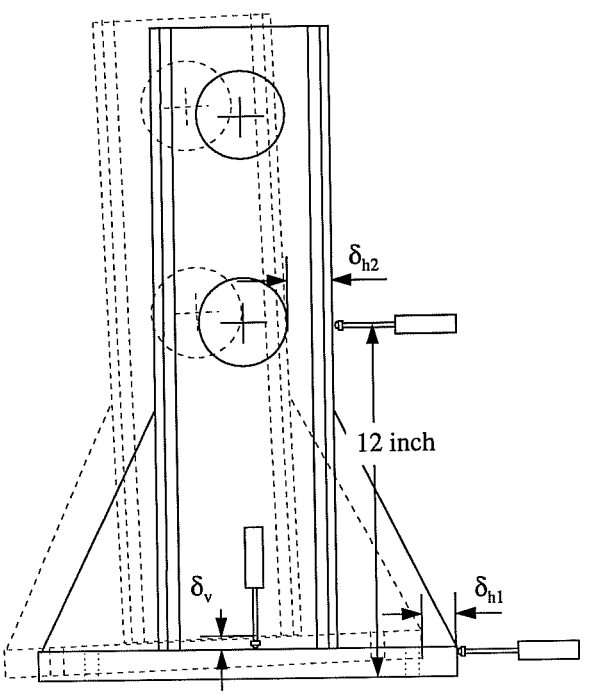

Figure 3.20 Displacement Instrumentation for Multiple-Anchor Connection Tests

$$\theta = \arctan(\delta_v / 7) \tag{3-8b}$$

where: δ_{h1} = vertical displacement measured at the center of the baseplate.

CHAPTER 4

IMPLEMENTATION OF EXPERIMENTAL PROGRAM

4.1 Introduction

All tests were conducted in the Ferguson Structural Engineering Laboratory at the J. J. Pickle Research Center of The University of Texas at Austin. This chapter contains a discussion of test matrices and test designations, test materials, test equipment, and testing procedures.

4.2 Test Matrices and Test Designations

4.2.1 Test Matrices

4.2.1.1 Series 1-7 and Series 1-8: Tests on Single Tensile Anchors in Cracked Concrete

These tests were designed to investigate the effect of concrete cracking on different anchors under both static and dynamic tensile loading. Five typical anchor types were chosen, two of which involved tests with two different diameters, as shown in Table 4.1. The Sleeve anchors were available only in SI diameters of 20 mm and 10 mm, which are approximately equivalent to 3/4 inch and 3/8 inch respectively.

Table 4.1 Test Matrix for Series 1-7 and Series 1-8

Series	Description	Concrete	Anchor Tested (5 Replicates)
1-7	Static tensile tests on single anchors in cracked concrete	4700 psi (32.4 MPa) limestone	Expansion Anchor II, 3/4 in. (19 mm) Undercut Anchor 1, 3/8 in. (10 mm) Undercut Anchor 1, 3/4 in. (19 mm) Undercut Anchor 2, 3/4 in. (19 mm) Sleeve Anchor, 3/8 in. (10 mm) Sleeve Anchor, 3/4 in. (19 mm) Grouted Anchor, 3/4 in. (19 mm)
1-8	Dynamic tensile tests on single anchors in cracked concrete	4700 psi (32.4 MPa) limestone	Expansion Anchor II, 3/4 in. (19 mm) Undercut Anchor 1, 3/8 in. (19 mm) Undercut Anchor 1, 3/4 in. (19 mm) Undercut Anchor 2, 3/4 in. (19 mm) Sleeve Anchor, 3/8 in. (10 mm) Sleeve Anchor, 3/4 in. (19 mm) Grouted Anchor, 3/4 in. (19 mm)

4.2.1.2 Series 3-9 to Series 3-12: Two-Anchor Connections under Eccentric Shear

As a part of Task 3, these tests were designated to continue the study on the effect of near-edge conditions and hairpins on the behavior of two-anchor connections under moderately eccentric shear loading. The shear load was applied both statically and dynamically. Table 4.2 is the test matrix for these tests.

Table 4.2 Test Matrix for Series 3-9 through 3-12

Series	Description	Concrete	Anchor Tested (5 Replicates)
3-9	Static eccentric shear tests on 2 near-edge anchors in uncracked concrete without hairpins	4700 psi (32.4 MPa) river gravel	Cast-in-Place, 3/4 in. (19 mm)
3-10	Dynamic eccentric shear tests on 2 near-edge anchors in uncracked concrete without hairpins	4700 psi (32.4 MPa) river gravel	Cast-in-Place, 3/4 in. (19 mm)
3-11	Static eccentric shear tests on 2 near-edge anchors in cracked concrete without hairpins	4700 psi (32.4 MPa) river gravel	Cast-in-Place, 3/4 in. (19 mm)
	Static eccentric shear tests on 2 near-edge anchors in cracked concrete with hairpins	4700 psi (32.4 MPa) river gravel	Cast-in-Place, 3/4 in. (19 mm)
3-12	Dynamic eccentric shear tests on 2 near-edge anchors in cracked concrete without hairpins	4700 psi (32.4 MPa) river gravel	Cast-in-Place, 3/4 in. (19 mm)
	Dynamic eccentric shear tests on 2 near-edge anchors in cracked concrete with hairpins	4700 psi (32.4 MPa) river gravel	Cast-in-Place, 3/4 in. (19 mm)

Note: edge distance for front anchors = 5 in. (127 mm), anchor spacing = 10 in. (254 mm), embedment = 7 in. (178 mm).

4.2.1.3 Multiple-Anchor Connections under Eccentric Shear

The purpose of these tests was to assess the behavior of multiple-anchor connections under dynamic reversed loading in various conditions, such as cracked concrete, proximity to member edges, hairpins, baseplate stiffness and eccentricity. Some static tests were also performed as baseline tests. Most tests used Undercut Anchor 1; some Expansion Anchors II were also tested.

Table 4.3 Test Matrix for Tests of Task 4

Series	Description	Concrete	Anchors Tested
4-1	Static tests on a 4-anchor group with a rigid baseplate in uncracked concrete under small eccentric loading	4700 psi (32.4 MPa) river gravel	Undercut Anchor 1, 5/8 in. (16 mm)
	Static tests on a 4-anchor group with a rigid baseplate in uncracked concrete under large eccentric loading	4700 psi (32.4 MPa) river gravel	Undercut Anchor 1, 5/8 in. (16 mm)"
4-2	Dynamic tests on a 4-anchor group with a flexible baseplate in uncracked concrete under small eccentric loading	4700 psi (32.4 MPa) river gravel	Undercut Anchor 1, 5/8 in. (16 mm)
	Dynamic tests on a 4-anchor group with a rigid baseplate in uncracked concrete under small eccentric loading	4700 psi (32.4 MPa) river gravel	Expansion Anchor II, 5/8 in. (16 mm)
	Dynamic tests on a 4-anchor group with a rigid baseplate in uncracked concrete under small eccentric loading	4700 psi (32.4 MPa) river gravel	Undercut Anchor 1, 5/8 in. (16 mm)
	Dynamic tests on a 4-anchor group with a rigid baseplate in uncracked concrete under large eccentric loading	4700 psi (32.4 MPa) river gravel	Undercut Anchor 1, 5/8 in. (16 mm)
4-3	Dynamic tests on a 4-anchor group with a rigid baseplate in cracked concrete under small eccentric loading	4700 psi (32.4 MPa) river gravel	Expansion Anchor II, 5/8 in. (16 mm)
	Dynamic tests on a 4-anchor group with a rigid baseplate in cracked concrete under small eccentric loading	4700 psi (32.4 MPa) river gravel	Undercut Anchor 1, 5/8 in. (16 mm)
	Dynamic tests on a 4-anchor group with a rigid baseplate in cracked concrete under large eccentric loading	4700 psi (32.4 MPa) river gravel	Undercut Anchor 1, 5/8 in. (16 mm)

Table 4.3 (continued)

4-4	Static tests on a near-edge 4-anchor group with a rigid baseplate in uncracked concrete without hairpins under small eccentric loading	4700 psi (32.4 MPa) river gravel	Undercut Anchor 1, 5/8 in. (16 mm)
	Static tests on a near-edge 4-anchor group with a rigid baseplate in uncracked concrete without hairpins under large eccentric loading	4700 psi (32.4 MPa) river gravel	Undercut Anchor 1, 5/8 in. (16 mm)
4-5	Dynamic tests on a near-edge 4-anchor group with a rigid baseplate in uncracked concrete without hairpins under small eccentric loading	4700 psi (32.4 MPa) river gravel	Undercut Anchor 1, 5/8 in. (16 mm)
	Dynamic tests on a near-edge 4-anchor group with a rigid baseplate in uncracked concrete without hairpins under large eccentric loading	4700 psi (32.4 MPa) river gravel	Undercut Anchor 1, 5/8 in. (16 mm)
4-6	Static tests on a near-edge 4-anchor group with a rigid baseplate in uncracked concrete with hairpins under small eccentric loading	4700 psi (32.4 MPa) river gravel	Undercut Anchor 1, 5/8 in. (16 mm)
	Dynamic tests on a near-edge 4-anchor group with a rigid baseplate in uncracked concrete with hairpins under small eccentric loading	4700 psi (32.4 MPa) river gravel	Undercut Anchor 1, 5/8 in. (16 mm)
	Dynamic tests on a near-edge 4-anchor group with a rigid baseplate in uncracked concrete with hairpins under large eccentric loading	4700 psi (32.4 MPa) river gravel	Undercut Anchor 1, 5/8 in. (16 mm)

Note: edge distance = 5 in. (127 mm), embedment = 7 in. (178 mm).

4.2.2 Test Designations

4.2.2.1 Single-Anchor Tension Tests

A consistent designation was used for all single-anchor tests of Task 1. That designation consists of an eight-character combination of letters and numbers. Figure 4.1 explains the meaning behind the test designation 7SKL5712. The first character specifies the series number of the test (7 and 8). The second character states the type of the loading: "S" stands for static loading, and "D" for dynamic loading. The third character refers to the type of the anchor tested: "K" represents Expansion Anchor II, "M" represents Undercut Anchor 1, "S" represents Undercut Anchor 2, "H" represents Sleeve Anchor, and "G" represents Grouted Anchor. The fourth character represents the type of the aggregate used in the specimen: "L" stands for limestone. The strength of the test specimen is represented by the fifth character: 4700 psi (32.4 MPa) was designated by "5." The sixth character is for the diameter of the anchor tested: A diameter of 0.375 inch (10 mm) was represented by "4," and a diameter of 0.75 inch (19 mm) by "7." The last two characters signify the test number in each series.

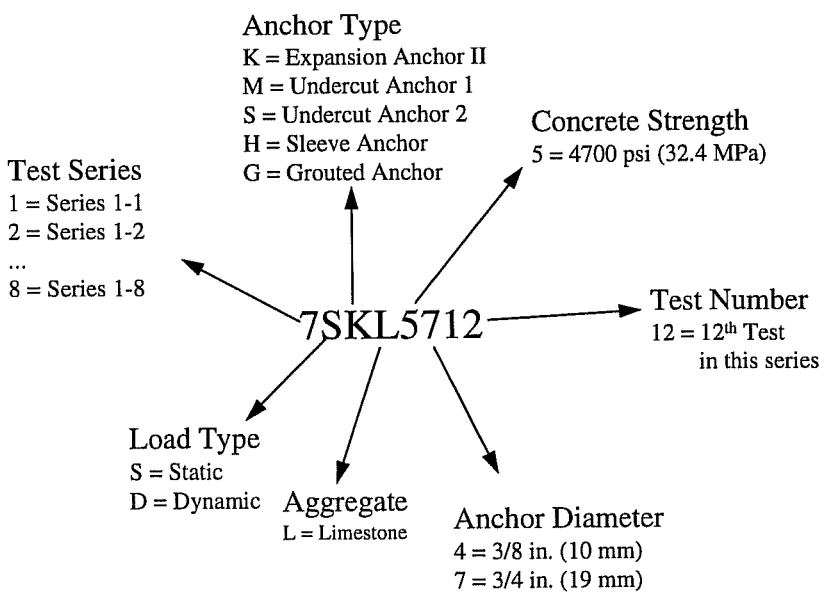

Figure 4.1 Test Designation of Task 1

4.2.2.2 Eccentric Shear Tests on Two-Anchor Connections

The designation of the tests in this series consists of three parts. Figure 4.2 explains the meaning behind the test designation 12SH23. The first specifies the series number of the test in Task 3 (9 through 12). The second part states the type of loading and if there is a hairpin in the concrete specimen: "S" stands for static loading; "D" represents dynamic loading; and "H" represents hairpins. The last part is a number from 01 to 30, which is the test number in this test section of Task 3. The condition of the concrete specimen (cracked or uncracked) is not represented in this test designation.

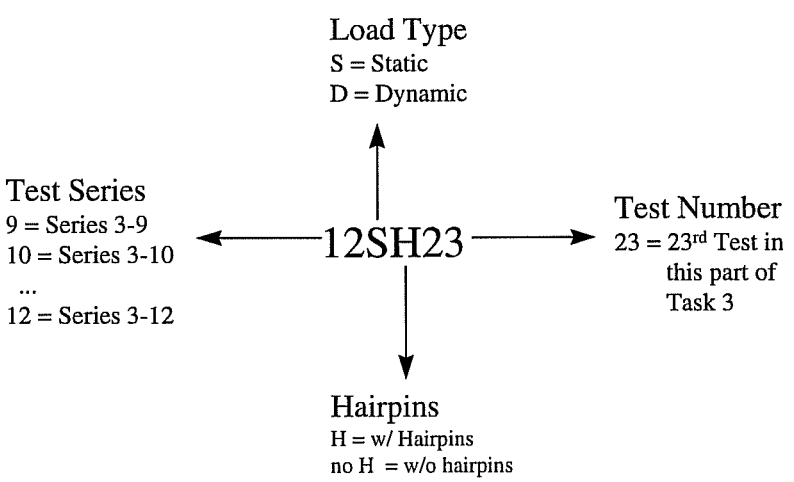

Figure 4.2 Test Designation of Task 3

4.2.2.3 Eccentric Shear Tests on Multiple-Anchor Connections

The designation of these tests is relatively simple. It consists of four-digit numbers. The first two-digit number specifies the series of the test, while the last two-digit number is the test number counted in the entire task according to the test matrix of Task 3.

4.3 Material

4.3.1 Concrete

The target concrete compressive strength for this testing program was 4700 psi (32.4 MPa) with a permissible tolerance of ±500 psi (±3.45 MPa) at the time of testing. This target value was selected because it is representative of concrete strengths in existing nuclear power plants. The mixture design is shown in Table 5.6. The mixture was proportioned to have a 6-inch (152-mm) slump. However, in earlier tests of this program, it was found out that concrete mixture with a 6-inch slump often had lower strength than 4200 psi (29.0 MPa) at 28 days. For that reason, all specimens described here were cast with a 4-inch (101-mm) slump. Limestone was used as coarse aggregate in the specimens of Task 1. The limestone aggregate used in these tests is very porous. Depending on its moisture content, the water-cement ratio in the concrete mixture can vary widely. To control the water content, the limestone aggregate had to be sprinkled several days before casting. In contrast, the river gravel did not need to be pre-sprinkled. Because comparison tests had shown no significant effects due to aggregate type (Rodriguez 1994), and because compressive strength was more difficult to control with the limestone aggregate, river gravel aggregate was used in the specimens of Tasks 3 and 4.

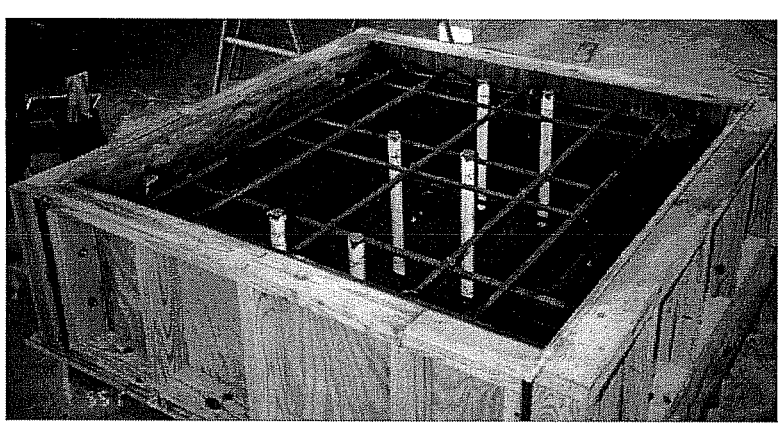

Figure 4.3 Formwork of Specimens for Task 4 Tests

All test specimens were cast inside the Ferguson Structural Engineering Laboratory using ready-mix concrete, consolidated with mechanical vibrators, screeded, trowelled, and covered with polythylene sheets. Formwork was usually stripped 5 days after casting, and specimens were stored indoors if space was available. Eighteen 6-inch (152 mm) diameter by 12-inch (305 mm) cylinders were usually cast with the test specimens. They were always cured beside the specimens during the first five days after casting. The specimens were not tested until at least 28 days after casting, and until the desired strength had been reached.

Table 4.4 Concrete Mixture Proportions for Test Specimens

Target Strength (psi)	Coarse Aggregate (lb/yd^3)	Type I Portland Cement (lb/yd^3)	Sand (lb/yd^3)	Rheobuild 1000 Superplasticizer (oz/yd^3)
4700	1867	390	1432	48

The cylinders were tested with neoprene pad caps at the medium loading rate specified by ASTM C39-86 (1986). Three cylinders were usually tested at 7 or 14 days, and the average values were used to predict the concrete strength. If the specimen was expected to reach the target window at close to 28 days, three more cylinders were tested at 28 days. Otherwise, more time was allowed until the concrete specimens were strong enough. Three cylinders were always tested before and just after testing, to determine the concrete strength. Since the tests on the specimens cast at the same took a certain time period, the strength of the specimens for a certain test was usually linearly interpolated within the testing window according to their testing dates. The cylinder compressive strengths of tested concrete specimens were listed in Table 4.5.

Table 4.5 Concrete Strength of All Specimens Used in Tests

Specimen Number	Casting Date	Strength at 28 days		Strength before Tests (psi)/date			Strength after Tests (psi)/date		
		psi	MPa	psi	MPa	date	psi	MPa	date
S1/2/3	5/6/94	4787	33.0	4787	33.0	6/3/94	4801	33.1	6/8/96
S4/5/6	5/23/94	N/A	N/A	4229	29.2	6/20/94	4269	39.4	6/29/94
S13/14/15	8/4/94	N/A	N/A	4303	29.7	9/6/94	4565	31.5	9/29/94
S19/20/21[1]	11/15/94	N/A	N/A	4090	28.2	12/16/94	4483	30.9	12/20/94
B1/2/3	5/20/96	N/A	N/A	4134	28.5	8/19/96	4425	30.5	9/10/96
B4/5/6	6/3/96	4110	28.3	4389	30.3	7/12/96	4524	31.2	7/31/96
B7/8/9	7/24/96	N/A	N/A	4735	32.6	9/10/96	4883	33.7	10/11/96
SS2	N/A	N/A	N/A	4559	31.4	9/10/96	4558	31.4	10/11/96

Note: 1) The strength of these specimens was lower than 4200 psi (29.0 MPa) before tests; however, the average of strengths before and after tests at 4288 psi (29.6 MPa) was used.

4.3.2 Anchors

A325 hex-head bolts, 3/4-inch (19 mm) diameter by 6 inches (152 mm) long, were used as grouted anchors in single-anchor tension tests. No washers were placed at the heads since the bearing area already meets the minimum requirement of ACI 349 Appendix B.

Cast-in-Place anchors tested in Task 4 were made of ASTM A193-B7 threaded rods 5/8 inch (16 mm) in diameter. Heavy-duty hexagonal nuts were used at the ends of the rods embedded in concrete. No washers were used at the embedded ends. Based on test data of Cook (1989), the average tensile capacity of 5/8-inch (16-mm) ASTM A197-B7 threaded rod is 31.0 kips (137.8 kN), or 137 ksi (944 MPa) based on the effective tensile stress area.

The other anchors were directly ordered from their respective manufacturers. They are shown from Figure 4.4 through Figure 4.7, with some measured critical dimensions listed from Table 4.6 through Table 4.9.

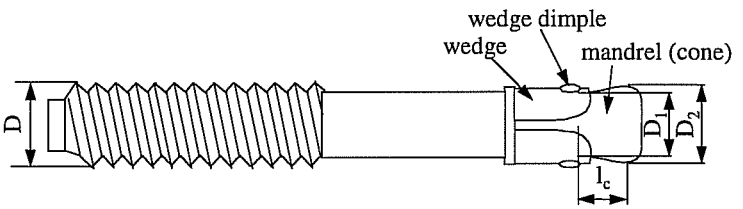

Figure 4.4 Key Dimensions of Expansion Anchor II

Table 4.6 Key Dimensions of Expansion Anchor II

Anchor Diameter (D)		D_1		D_2		l_c	
inch	**mm**	**inch**	**mm**	**inch**	**mm**	**inch**	**mm**
3/4	19.1	0.565	14.4	3/4	19.1	0.70	17.8

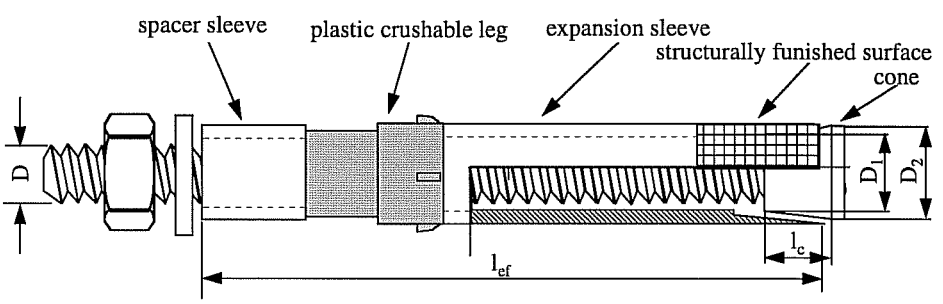

Figure 4.5 Key Dimensions of Sleeve Anchor

The anchor shown in Figure 4.5 has a step inside the expansion sleeves. The step exists in the tested anchors of 20-mm diameter. However, there is no step in the tested anchors of 10-mm diameter.

Table 4.7 Key Dimensions of Sleeve Anchor

Anchor Diameter (D)		Sleeve Diameter		l_{ef}		D_1		D_2		l_c	
mm	inch	mm	inch	inch	mm	inch	mm	inch	mm	inch	mm
10	3/8	14.3	0.563	2.25	57.2	0.48	12.2	0.58	14.7	0.43	10.9
20	3/4	27.3	1.07	4.0	102	0.92	23.4	1.09	27.7	0.55	14.0

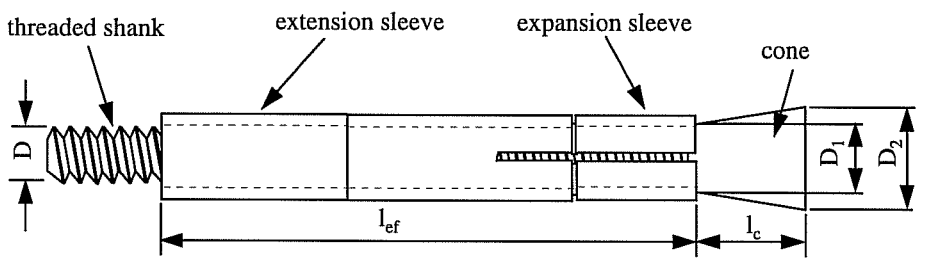

Figure 4.6 Key Dimensions of Undercut Anchor 1

Using a universal testing machine, Lotze (1997) performed three tension tests in Task 2 of this program on three anchor shafts of Undercut Anchor 1 of 5/8-inch (16-mm) diameter. The average ultimate strength was 912 N/mm^2 (132 kips/in^2).

Table 4.8 Key Dimensions of Undercut Anchor 1

Anchor Dia. (D)		Sleeve Diameter		l_{ef}		D_1		D_2		l_c	
inch	mm	inch	mm	inch	mm	inch	mm	inch	mm	inch	mm
3/8	10	0.625	15.9	2.25	57.2	0.440	11.2	0.625	15.9	0.600	15.2
5/8	16	0.910	23.1	7.0	178	0.720	18.3	0.940	23.9	0.800	20.3
3/4	19	1.105	28.1	4.0	102	0.815	20.7	1.140	29.0	0.915	23.2

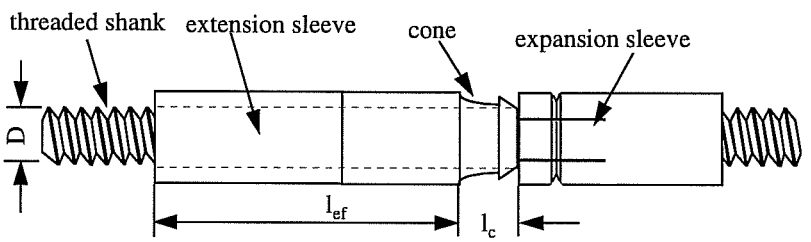

Figure 4.7 Key Dimensions of Undercut Anchor 2

Table 4.9 Key Dimensions of Undercut Anchor 2

Anchor Diameter (D)		Sleeve Diameter		l_c	
inch	**mm**	**inch**	**mm**	**inch**	**mm**
3/4	19	1.13	28.7	0.70	17.8

The actual bearing area of UC1 anchors (the surface area of the undercut portion of the sleeve) is 3.25 in^2 (2097 mm^2) for 3/4-in. (19-mm) diameter anchors, 1.79 in^2 (1153 mm^2) for 5/8-in. (16-mm) diameter anchors, and 1.23 in^2 (794 mm^2) for 3/8-in. (10-mm) diameter anchors. The bearing area of UC2 anchors is actually the cross-sectional area of expansion sleeves, which is 0.56 in^2 (362 mm^2) for 3/4-in. (19-mm) diameter anchors. The bearing area of UC2 is much lower than that of UC1.

4.3.3 Hairpins

The hairpins were designed to withstand the maximum possible shear load on the 3/4-inch (19 mm) anchors tested in Task 3. They were U-loops made of #6 ASTM 615 Gr60 deformed reinforcing bars with dimensions shown in Figure 4.8.

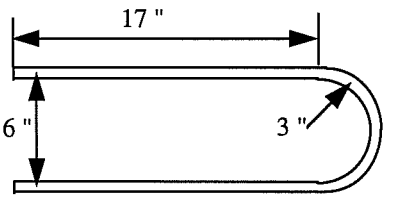

Figure 4.8 Size of Hairpins

4.3.4 Grout

The grout used in the installation of Grouted Anchors was a commercial, non-expansive, pre-mixed, sanded, cementitious grout, combined with the amount of water recommended by the manufacturer. When anchors were installed, six 2-inch (51-mm) cubes were also cast. Before and after tests, these cubes were tested to check the compressive strength of grout. Table 4.10 shows the average strength of cubes before and after tests.

Table 4.10 Average Strength of Cubes of Grout before and after Tests

Casting Date	Strength before Tests /date			Strength after Tests /date		
	psi	MPa	Date	psi	MPa	Date
5/23/94	5942	41.0	6/20/94	7161	49.4	6/29/94

4.4 Anchor Installation

4.4.1 Cast-in-Place Anchors

During setting up of the formwork, the Cast-in-Place Anchors were held in position with wooden templates, which were kept in position until the concrete was hardened. As shown in Figure 4.9, the anchors were secured with threaded rods on 2x4s crossing over

the formwork. The sheet-steel crack initiator discussed in Section 3.4.2 can also be seen in that figure, held by a spliced PVC tube and a 2×4.

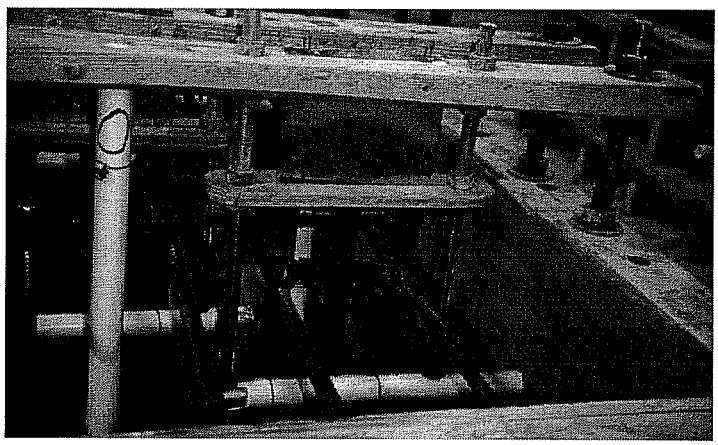

Figure 4.9 Cast-in-Place Anchors and the Steel Sheet in Between before Casting

4.4.2 Grouted Anchors

The Grouted anchors in tension tests were installed in 10-inch (254-mm) thick slabs. Holes 3 inches (76 mm) in diameter were cored with a hollow-core diamond bit deep enough to accommodate anchors at a 4-inch (102-mm) embedment. The holes were not roughened. Before grout was poured, excess water in the holes was dried with towels. Grout was then poured into the holes, and the bolts were immediately inserted head-down. They were held in the centers of the holes at the intended embedment depth with small pieces of plywood, and were covered with polythylene sheets until the grout had cured.

4.4.3 Undercut Anchors

Two types of undercut anchor were tested in this project. Their installation procedures only differ in the final procedure of sleeve expansion.

Undercut anchors were installed with the tools and devices provided by the manufacturers. Using a rotary hammer drill and a carbide bit, holes were drilled slightly

larger than the sleeve diameter. The dust in the holes was vacuumed using a small tube inserted into the holes. The holes were then undercut with special undercutting tools driven by a rotary hammer drill, with a little water in the holes to cool the undercutting bits.

For Undercut Anchor 1, a special setting tool was screwed on the anchor bolt to expand the expansion sleeve inside the hole. The setting tool has a small collar extending out 1/8 inch (3.2 mm) on the bottom to prevent the sleeve from sticking out of the concrete surface after installation. After the desired expansion had been achieved, the setting tool was removed.

For Undercut Anchor 2, after the anchor was inserted into the hole, a hydraulic actuator was used to load it up to 90% of its minimum specified capacity. This forced the expansion sleeve into the undercut. The hydraulic actuator was then removed.

4.4.4 Expansion Anchors

The holes for expansion anchors were drilled using a rotary hammer drill and carbide bits. The dust in the holes was vacuumed with a small tube inserted into the holes. The anchor was then simply tapped into the hole to the desired embedment depth.

4.5 Test Equipment

4.5.1 Splitting Tubes

Wedge-type splitting tubes made of high-strength steel were used to crack the concrete specimens and to widen the crack to the desired width. Each set consists of a wedge, and a pair of split bearing tubes, as shown in Figure 4.10. By tapping the splitting wedge, a large expansion force is exerted on the concrete specimen.

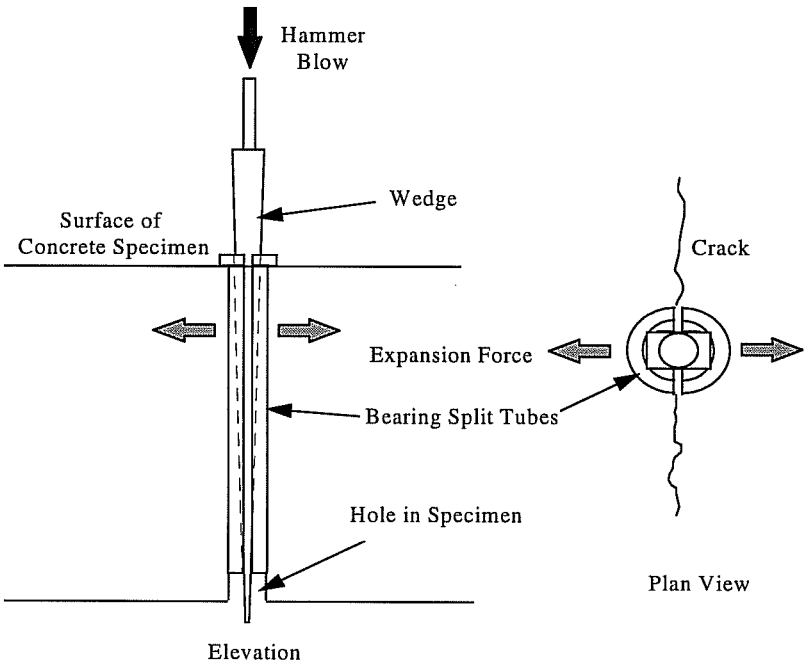

Figure 4.10 Splitting Tube for Concrete Cracking

4.5.2 Test Setups

Figure 4.11 shows the test setup for single-anchor tension tests. Figure 4.12 shows the test setup for eccentric shear tests.

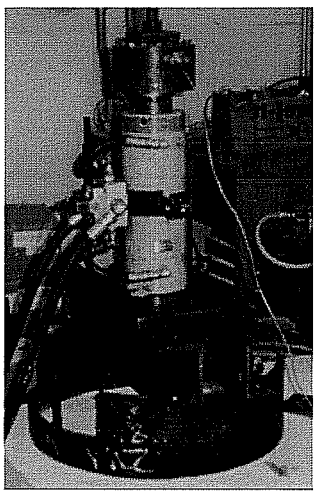

Figure 4.11 Test Setup for Single-Anchor Tension Tests

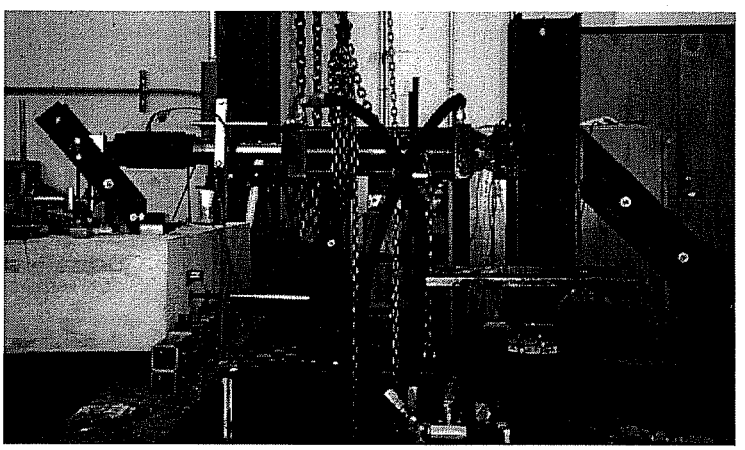

Figure 4.12 Test Setup for Eccentric Shear Tests

4.5.2.1 Static Tension Tests

A 60-ton, single-action, center-hole actuator, powered by an electric pump, was used to load the anchors. It was placed on the top of the setup shown in Figure 4.11. The loading rate was controlled manually by adjusting the flow rate of the hydraulic fluid with a needle valve.

4.5.2.2 Dynamic Tension Tests

For dynamic tension tests, the same loading setup of Figure 4.11 was used. Dynamic tension load was applied with a 60-ton, double-action, center-hole actuator. It was powered by a closed-loop hydraulic pumping system, which consisted of a 60-gpm pump, a 40-gpm line tamer, a 60-gpm servo-valve, and a Materials Test Systems (MTS) 458.10 MicroConsole controller (Figure 4.13). The loading command signals were programmed with a MTS 458.91 MicroProfiler attached on the servo-controller. The signal from a 100-kip (445-kN) load cell, which measured the load on the anchor, was used as the feedback to control the loading.

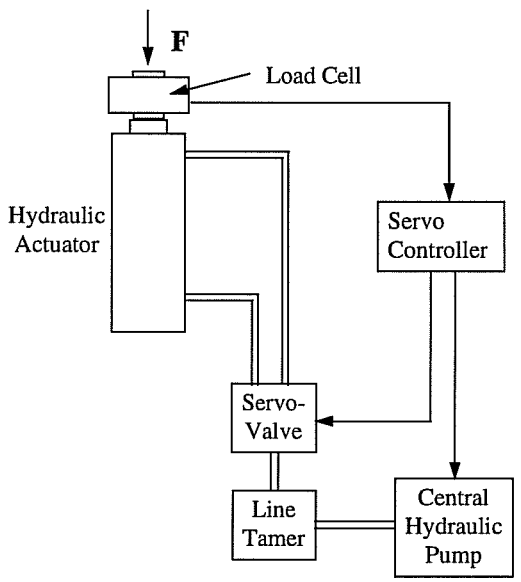

Figure 4.13 Schematic Diagram of Loading System for Dynamic Tension Tests

4.5.2.3 Static and Dynamic Eccentric Shear Tests

The static and dynamic eccentric shear tests used a closed-loop hydraulic system similar to that of the dynamic tension tests. The load was applied by a 100-ton, double-action actuator, and the servo-valve capacity was kept the same (60 gpm), but with a 120-gpm line tamer. The MTS 407 servo-controller was used to control the entire loading

system. The MTS 458 servo-controller with a MTS 458.91 MicroProfiler was used as a programmable profiler to export the command signals to the MTS 407 servo-controller. The loading system was configured for displacement control, using a 4-inch (102-mm) DCDT attached to the actuator, as shown in Figure 4.14.

In the static tests, the load was applied by manually adjusting the setpoint on the MTS 407 servo-controller. In dynamic tests, the command signals were exported from the MTS 458.91 MicroProfiler to the MTS 458.10 servo-controller.

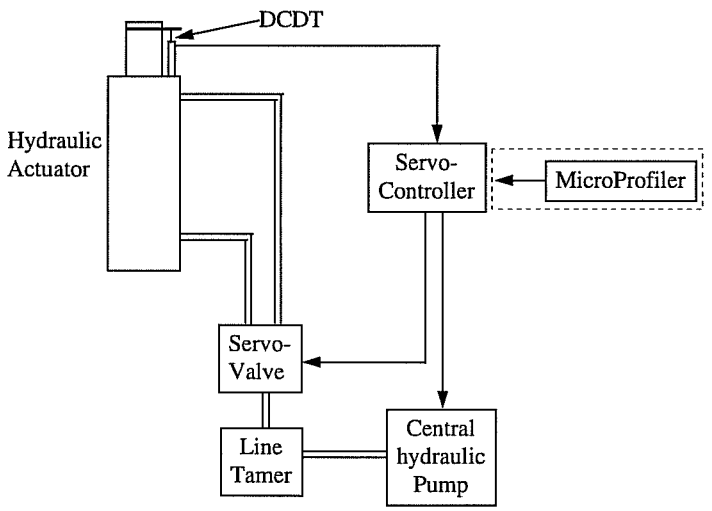

Figure 4.14 Schematic Diagram of Loading System for Eccentric Shear Tests

4.5.3 Instrumentation

4.5.3.1 Tension Tests

The tension load was measured with an Interface 100-kip (445-kN) load cell, placed on the top of the actuator, clamped by the tension rod during tests. The displacement of the anchor was measured by a 2-inch (51-mm) linear potentiometer oriented upwards against the plate which was tightened on the loading rod right above the coupler.

During tests in cracked concrete, two 0.5-inch (12.7-mm) DCDTs were used to monitor the crack opening on each side of the anchor. They were placed a few inches away from the coupler. Along with them, two digital displacement indicators were used to monitor crack opening to the initial width of 0.3 mm. The indicators were removed before testing.

4.5.3.2 Eccentric Shear Tests on Two-Anchor Connections

Instrumentation for eccentric shear tests on two-anchor connections is shown in Figure 4.15.

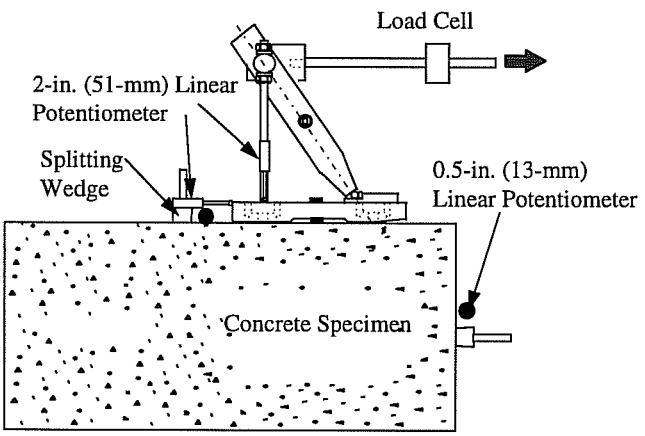

Figure 4.15 Instrumentation For Two-Anchor Connection Shear Tests

The eccentric shear load was measured directly with a 150-ton load cell, installed at the center of the horizontal loading arm.

Six strain gauges were placed symmetrically at the middle section of the baseplate with three on each side to measure the bending moment and tension force in the plate during tests.

Horizontal slip of the baseplate was measured with a 2-inch (51-mm) linear potentiometer, placed directly against the side of the baseplate away from the loading direction, as shown in Figure 4.16.

To prevent any damage to the potentiometers, two potentiometers measuring the vertical displacement were placed at the edges of the baseplate on two glass plates (Figure 4.17). The average value was used for the displacement of the back anchor to eliminate the influence of baseplate rotation.

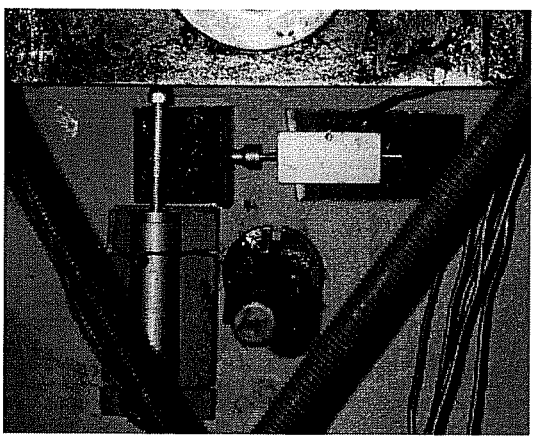

Figure 4.16 Potentiometers Measuring Horizontal Movement of Baseplate and Opening of Cracks in Two-Anchor Tests

Two 0.5-inch (12.7-mm) linear potentiometer were used to measure the crack opening and to monitor the crack during tests. One was placed at the back of the baseplate between the splitting wedge and the baseplate (Figure 4.15), the other on the front edge just above the splitting tube.

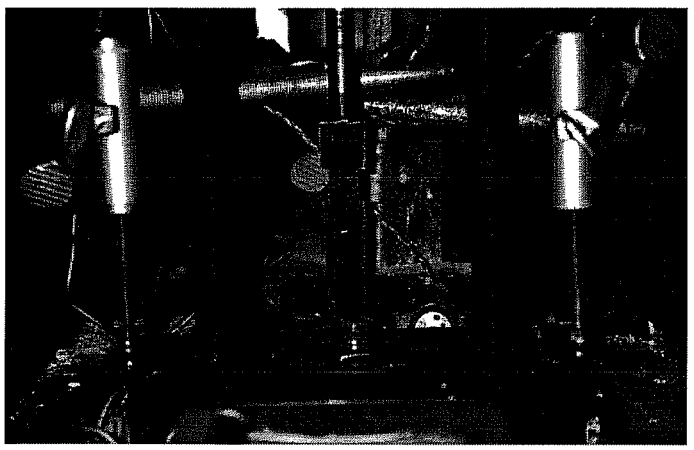

Figure 4.17 Potentiometers Measuring Vertical Displacement of Baseplate in Two-Anchor Tests

4.5.3.3 Eccentric Shear Tests on Multiple-Anchor Connections

Instrumentation for eccentric shear tests on multiple-anchor connections is shown in Figure 4.18.

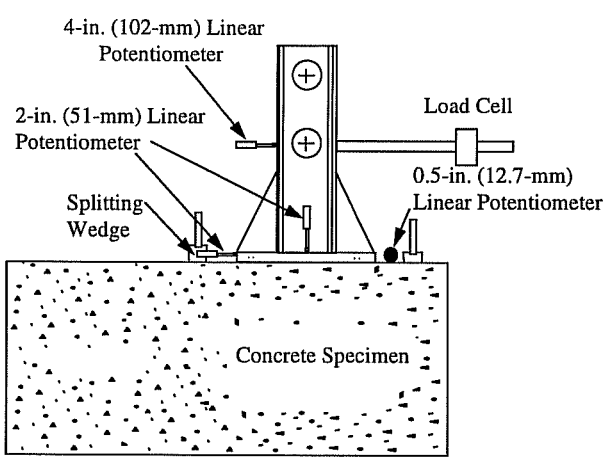

Figure 4.18 Instrumentation for Multiple-Anchor Connection Shear Tests

The eccentric shear load was directly measured with a 150-ton (667-kN) load cell, installed at the center of the horizontal loading arm.

The tension load on each anchor was measured with force washers, calibrated on a 600-kip universal testing machine before and after the test program.

A 4-inch (102-mm) stroke linear potentiometer was used to measure the horizontal displacement of the attachment at 12 inches (305 mm) above the concrete surface. Slip of the baseplate was measured with a 2-inch (51-mm) linear potentiometer. Two other 2-inch (51-mm) linear potentiometers were placed at the center of the baseplate on either side, to measure the vertical displacement of the baseplate. To prevent damage to the potentiometers, they were placed against two glued glass plates.

In tests in cracked concrete, four 0.5-inch (12.7-mm) linear potentiometers were used to measure the crack opening; two of them were kept on to monitor the cracks during tests. They were placed at the front of the baseplate on each crack, between the splitting tubes and the plate.

4.5.4 Data Acquisition and Reduction

All test data were electronically recorded with HP digital plotters and a Daqware system implemented on an IBM PC-AT. The HP plotter scans three channels simultaneously. The Daqware system scans eight channels one by one. Data files were copied, reduced, and converted into engineering units using spreadsheet programs on Pentium-based PCs.

4.5.4.1 Tension Tests

All test data were recorded with HP plotters, then transferred to and saved on an IBM PC-AT. In tests in uncracked concrete only one plotter was used; in tests in cracked concrete, another plotter was used to record two more channels for crack opening.

4.5.4.2 Eccentric Shear Tests

To record all the test data, two HP plotters and the Daqware system were used in the eccentric shear tests (Task 3 and Task 4). Test data recorded with the Daqware software were saved on the same computer. Test data recorded by the HP plotters were transferred to and saved on another IBM PC-AT.

4.6 Test Procedures

4.6.1 General

During installation, all anchors were tightened to the torque specified by the manufacturer. To simulate the reduction of prestressing force in anchors in service due to concrete relaxation, all anchors were first fully torqued, then released after about 5 minutes to allow the relaxation to take place, and finally torqued again, but up to only 50% of the specified values.

4.6.2 Crack Initiating and Opening

4.6.2.1 Single-Anchor Tension Tests

In tension tests on all types of single anchors reported here, cracks were initiated and opened using the following steps:

1) Drill 1-inch (25-mm) diameter holes along the potential crack plane at the middle of two adjacent longitudinal reinforcing bars (Figure 3.1).
2) Place splitting tubes into the holes.
3) Tap wedges one by one to initiate the crack, and extract them once the hairline crack was visible.
4) Drill holes at the crack for anchor installation, and install all anchors.

5) Pre-torque the anchors, wait for at least five minutes, then release and re-torque anchors.

6) Place crack-measuring equipment across the crack (two on each side of anchor).

7) Tap wedges again, one by one, to increase the crack width to 0.3 mm.

8) Set up loading and measuring apparatus to conduct tests.

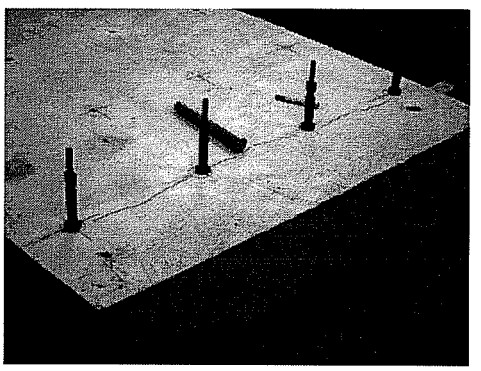

Figure 4.19 Cracked Concrete Specimen

The crack widths were monitored during tests, but not controlled. Figure 4.19 shows a concrete specimen for tension tests right after being cracked.

4.6.2.2 Eccentric Shear Tests on Two-Anchor Connections

These tests used cast-in-place anchors. Since anchors had to be placed in position before casting, a piece of thin steel sheet was placed directly in the plane of the expected crack, to force the crack through the anchors (Figure 4.9). Moreover, to facilitate drilling horizontal holes for splitting wedges, 1.0-inch (25-mm) diameter PVC tubes, sliced in half, were already placed where the wedges would be. The testing procedure for these anchors was as follows:

1) Torque the anchors, wait for at least five minutes, then release and re-torque.

2) Place crack-measuring equipment in position.

3) Insert splitting wedges into PVC tubes, and tap wedges until the crack opens uniformly to 0.3 mm.

4) Set up the loading and data acquisition equipment.

Crack widths were monitored but not controlled during tests.

4.6.2.3 Eccentric Shear Tests on Multiple-Anchor Connections

Two separate cracks were initiated for multiple-anchor tests parallel to the loading direction. The crack initiating and opening procedures were more complicated. Because the baseplate was already fabricated, it was desired to control the crack initiation so that as many anchors as possible could be installed directly in the cracks. The following steps were used:

1) Drill four holes in the positions where the undercut anchors were to be installed, using a smaller drill bit than that required for the installation of anchors.

2) Place splitting tubes into PVC pipes and the drilled holes. Then tap the wedges one by one until a crack was visible. Remove splitting tubes.

3) Initiate another crack.

4) Drill the four holes again with a regular drill bit, then undercut them. Install anchors and the baseplate. Torque anchors, release and re-torque after about 5 minutes.

5) Place crack-measuring equipment on the cracks.

6) Place splitting tubes into PVC pipes. Tap wedges one by one to open the cracks to 0.3 mm.

7) Set up the loading and data acquisition equipment

The crack widths were monitored during tests, but not controlled.

Tests on Expansion Anchors II in cracked concrete were conducted on the opposite side of the specimens, from where the cracks had been already started during previous tests on undercut anchors. Therefore, the procedure for initiating cracks was eliminated. However, the baseplate was carefully placed so that as many anchors as possible would be in or close to the cracks.

4.6.3 Single-Anchor Tension Tests

A typical single-anchor tension test involved the following steps:

1) Install anchor and set up loading reaction frame.
2) If the test required crack opening, set up crack-measuring equipment and open the crack.
3) Position the hydraulic actuator and the load cell. Place the coupler and the loading rod, then finger-tighten the nut on the top of the load cell. Finally, install the displacement potentiometer.
4) Conducted the test.
5) After anchor failure, remove all the equipment. Transfer data to the computer and save.

The loading patterns in the static and dynamic tests were different. They are explained below.

4.6.3.1 Static Tests

In static tests, the loading rate was controlled manually by adjusting the needle valve connected on the hydraulic hose while monitoring the pressure on the hydraulic actuator with a mechanical pressure gauge, to achieve a constant load increase up to failure during the entire loading period of about two minutes.

4.6.3.2 Dynamic Tests

Dynamic tests on single anchors were conducted under force control. In the MTS MicroProfiler, a linearly increasing ramp load was set as the command signal. Since the actual capacity of each anchor was unknown in advance, the maximum load of the command signal was set at one-and-one-half times the estimated load capacity of the anchors, with a rise time of 0.15 second. In this way, if the anchor failed just at the

estimated load, the loading time period would be 0.10 second, as shown in Figure 4.18. When the anchor failed, the error between the command and feedback signals stopped the test.

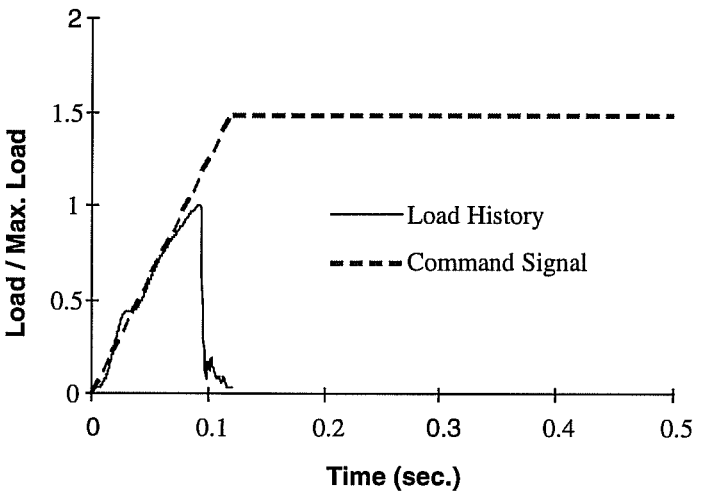

Figure 4.20 Typical Command Signal in Dynamic Tension Tests

4.6.4 Eccentric Shear Tests on Two-Anchor Connections

A typical eccentric shear test on a two-anchor connection involved the following steps:

1) Position baseplate so anchors contact sides of the anchor hole away from the load, then tighten all anchors.

2) If cracking was involved, set up the crack measuring equipment, and widen the crack.

3) Connect loading plate to horizontal loading rod, install clamping beams, and position all displacement potentiometers.

4) Conducted the test.

5) After connection failure, removed all equipment. Transfer data to computer and save.

The loading patterns in the static and dynamic tests were different. They are explained below.

4.6.4.1 Static Tests

The static load was applied by slowly adjusting the setpoint of the servo-controller to control the displacement of the hydraulic actuator, while monitoring the reading of the load cell to avoid any sudden increase of the load, until the connection failed.

4.6.4.2 Dynamic Tests

Since the loading system was controlled by the displacement of the hydraulic actuator, the loading rate was controlled indirectly by the velocity of the actuator. The maximum displacement was limited at 1.2 inches (30.5 mm) by the span on the servo-controller, which was set to twice the displacement at the failure load measured in static tests, while a ramp-type displacement increase was programmed in the profiler at a rate such that the maximum displacement would be reached in 0.2 seconds. In this way, the entire loading time would be about 0.15 seconds to failure. Loading was started manually, and stopped by an out-of-limits error signal.

4.6.5 Eccentric Shear Tests on Multiple-Anchor Connections

The testing procedure involved here were exactly the same as for tests on two-anchor connections. The loading patterns in the static and dynamic tests were different. They are explained below:

4.6.5.1 Static tests

The static load was applied by slowly and monotonically adjusting the setpoint of the servo-controller to control the displacement of the hydraulic actuator, while monitoring the reading of the load cell to avoid any sudden increase of load.

4.6.5.2 Dynamic tests

The loading pattern was dynamic reversed cyclic loading (Figure 3.17), applied with displacement control as discussed in Section 3.6.

During tests, the first load was applied with a smaller span [0.6 inch (15.2 mm)], that is, a smaller maximum displacement. If the connection had not yet failed, another sequence of loading with a larger maximum displacement was applied, by increasing the span on the servo-controller. The values of the span were set successively at 0.6, 1.0, and 1.5 inches (15, 25, and 38 mm). After the span reached 1.5 inch (38 mm), the loading sequence was repeated with the same span until the connection failed. Before each loading sequence, all the anchors were finger-tightened to reduce the displacement required to reach the desired load.

CHAPTER 5

TEST RESULTS

5.1 Introduction

In this chapter, test results are summarized in tabular form, and typical load-displacement curves are shown for each set of tests. The observations of all tests are described along with typical failure photos. Detailed test results, such as load history, failure loads, failure modes, displacements at maximum load, load-displacement displacement curves for each test, and curves of additional crack opening versus load, are all given in appendices.

To compare test results among specimens with different concrete strengths, all results of single-anchor tests failing by concrete breakout are normalized by $\sqrt{f_c}$ to 4700 psi (32.4 MPa) concrete, based on Equation 2-5. However, the results of tests with steel failure are presented directly, without any normalization.

5.2 Tension Tests on Single Anchors in Cracked Concrete

The tension tests on single anchors were designed to investigate the effects of cracks and the combined effect of cracks and dynamic loading on the behavior of various types of anchors failing by concrete breakout. Therefore, the nominal embedment depth of the anchors was chosen consistently at 4 inches (102 mm) for all anchors of 3/4-inch (19-mm) diameter, and at 2.25 inches (57 mm) for all anchors of 3/8-inch (10-mm) diameter,

through the entire Task 1. All discussions on the test results of single anchors are based on the average of 5 replicates.

5.2.1 Result of Series 1-7

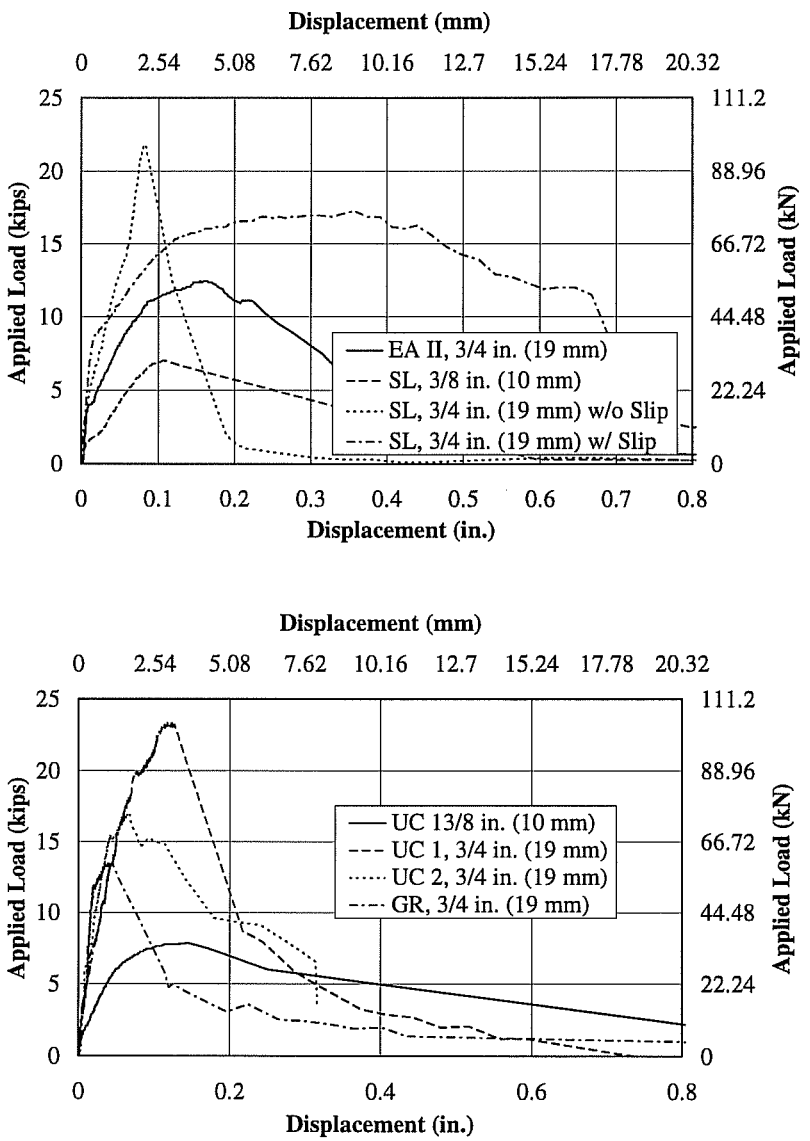

Figure 5.1 Typical Load-Displacement Curves of Series 1-7 Tests

The anchors of Series 1-7 were all loaded statically to determine the effect of concrete cracking. Figure 5.1 presents typical load-displacement curves for each type of anchor tested in Series 1-7. Table 5.1 displays the average maximum load and average displacement at maximum load for each type of anchor. In the following, results of each set of tests are described in detail.

Table 5.1 Average Results for Anchors under Static Tensile Loading in Cracked Concrete with Limestone Aggregate

Anchor	Average Maximum Load		COV	Average Displacement at Maximum Load		COV
	Kips	(kN)	%	inches	(mm)	%
EA II, 3/4 in. (19 mm)	12.97	57.7	5.8	0.158	4.01	39.8
UC1, 3/8 in. (10 mm)	8.23	36.6	38	0.145	3.68	30.3
UC1, 3/4 in. (19 mm)	22.85	101.6	2.8	0.125	3.18	23.8
UC2, 3/4 in. (19 mm)	15.61	69.4	7.0	0.039	0.99	50.1
SL, 3/8 in. (10 mm)	6.91	30.7	5.5	0.111	2.82	16.2
SL, 3/4 in. (19 mm)	19.36	86.1	12.0	0.146	3.71	83.4
GR, 3/4 in. (19 mm)	13.42	59.7	26.1	0.032	0.81	19.6

All tests on Expansion Anchor II failed by concrete breakout. All cones were completely developed. The cracks disrupted the cone surface along the cracks, but did not change the overall cone shape very much.

Undercut Anchor 1 in 3/8-inch (10-mm) diameter embedded at 2.25 inches (57 mm) showed a significant influence cracks on the breakout cone shape. In most tests, the breakout cones formed on one side only of the crack (Figure 5.2). For Undercut Anchor 1 in 3/4-inch (19-mm) diameter embedded at 4 inches (102 mm), the breakout cone was more fully developed. However, in one test, the concrete broke out on one side only of the crack.

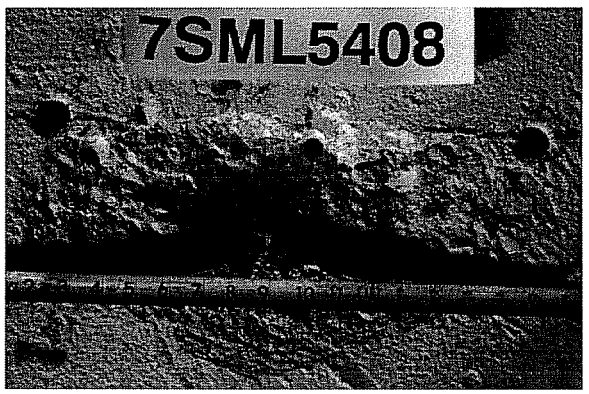

Figure 5.2 Typical Half-Cone Breakout of UC1 in 3/8-inch (10-mm) Diameter in Cracked Concrete

Undercut Anchors 2 were all tested at a 4-inch (102 mm) embedment. In all five tests, no particular effect of cracks on the cone shape was observed.

The Sleeve Anchor, embedded at 2.25 inches (57 mm), showed breakout cones similar to those of Undercut Anchor 1 embedded at 2.25 inches (57 mm), for which two out of five tests had only half-cones. Although for Sleeve Anchors embedded at 4 inches (102 mm) the breakout cones became more regular, there was still one exception with a half-cone. From the load-displacement curves, two tests showed significant displacements characteristic of pullout failure. The other three did not exhibit any sign of pullout in tests; nevertheless, their load-displacement curves showed increasing stiffness before reaching the maximum load.

Grouted anchors were installed after pre-cracking of concrete specimens. During crack opening, the cracks propagated cleanly through the interface between the grout and surrounding concrete. Virtually no crack through grout was observed. However, for most Grouted Anchors embedded at 4 inches (102 mm), the crack had no discernible effect on overall cone shape. In only one test, the grout body was partially pulled out from the cored hole.

Typical crack openings measured in tests are shown in Figure 5.3 for each type of anchor.

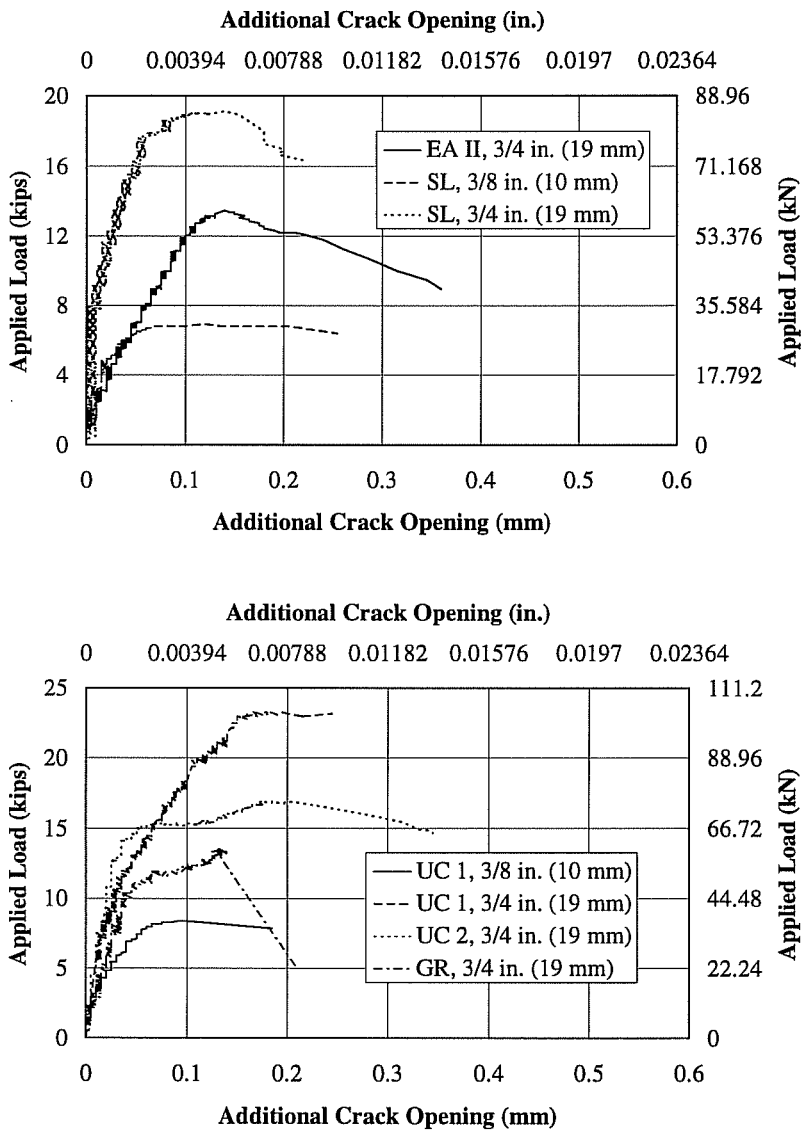

Figure 5.3 Typical Measured Additional Crack Opening During Tests of Series 1-7

5.2.2 Results of Series 1-8

The tests of Series 1-8 were conducted to determine the effect of dynamic loading on selected anchors installed in cracked concrete. Figure 5.4 displays typical load-displacement curves for each type of anchor tested in Series 1-8. Table 5.2 presents the

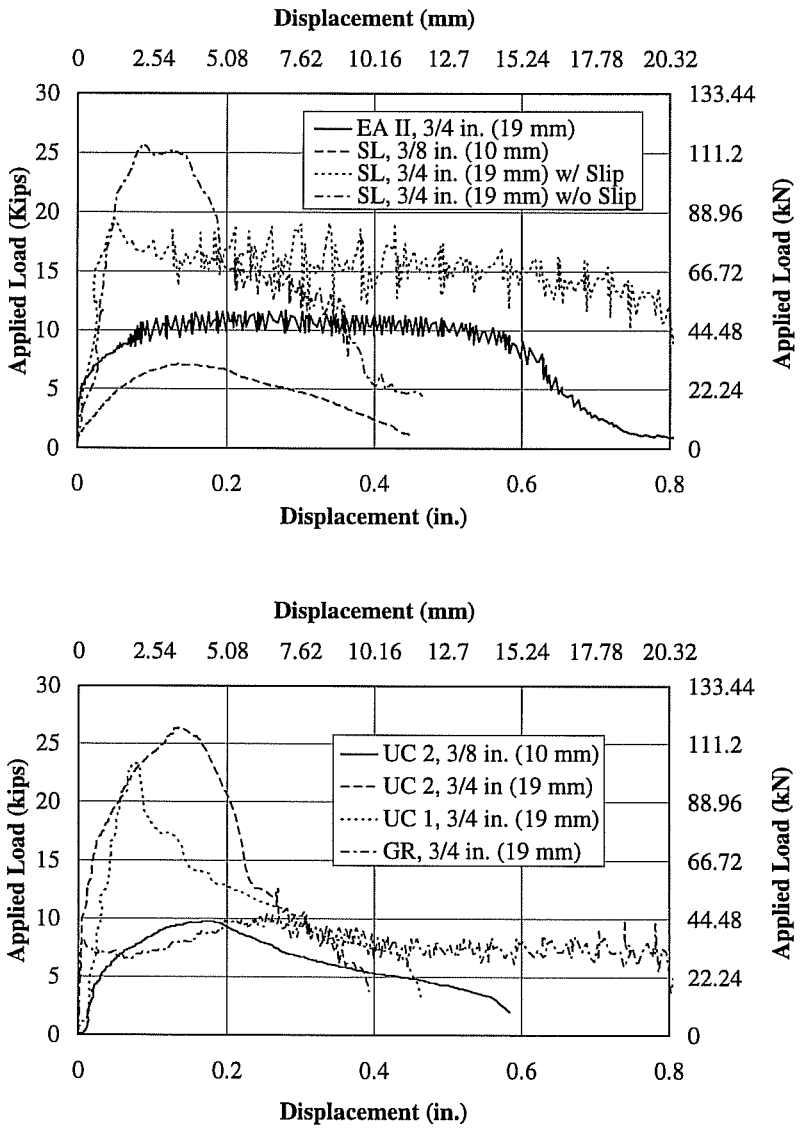

Figure 5.4 Typical Load-Displacement Curves of Series 1-8

average maximum loads and average displacements at maximum load for each type of anchor. Results of each set of tests are described in detail below.

Table 5.2 Average Results for Anchors under Dynamic Tensile Loading in Cracked Concrete with Limestone Aggregate

Anchor	Average Maximum Load		COV	Average Displacement at Maximum Load		COV
	Kips	(kN)	%	inches	(mm)	%
EA II, 3/4 in. (19 mm)	12.2	54.3	12.0	0.462	11.7	57.8
UC1, 3/8 in. (10 mm)	9.51	42.3	10.3	0.137	3.48	13.5
UC1, 3/4 in. (19 mm)	25.3	113	8.2	0.171	4.34	23.5
UC2, 3/4 in. (19 mm)	24.8	110	13.2	0.061	1.55	41.9
SL, 3/8 in. (10 mm)	6.87	30.6	6.6	0.138	3.51	50.0
SL, 3/4 in. (19 mm)	21.5	95.6	19.8	0.062	1.57	61.3
GR, 3/4 in. (19 mm)	8.52	37.9	33.1	0.124	3.15	96.0

The breakout cones of Expansion Anchor II, embedded at 4 inches (102 mm) and loaded dynamically, were considerable smaller on average at 13 inches (330 mm), compared to those under static loading with an average of 19 inches (483 mm). However, they were fully developed.

For Undercut Anchor 1 embedded at 2.25 inches (57 mm), the cone shapes, like those of static tests, were rough and uneven. Anchors embedded at 4 inches (102 mm) had much more regular cones. However, one test exhibited a half-cone.

The cones in the tests on Undercut Anchor 2 were quite normal.

For two of five Sleeve Anchors embedded at 2.25 inches (57 mm), tests showed half-cones, similar in the size to those of the static tests. Sleeve Anchors embedded at 4

inches (102 mm) had slightly smaller cones, averaging 19 inches (483 mm) in diameter compared to 21 inches (533 mm) in static tests.

The presence of cracks had the worst effect on Grouted Anchor under dynamic loading. In 4 of 5 tests, the breakout body took the form of a truncated cylinder pulled out of the cored holes (Figure 5.5) Correspondingly, the load-displacement curves show a very small load over a considerable range of displacement.

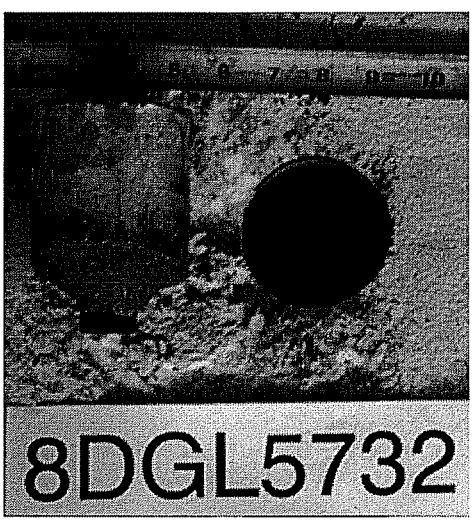

Figure 5.5 Typical Breakout Body in Dynamic Tests of Grouted Anchors

Typical crack openings measured in tests for each type of anchor are shown in Figure 5.6.

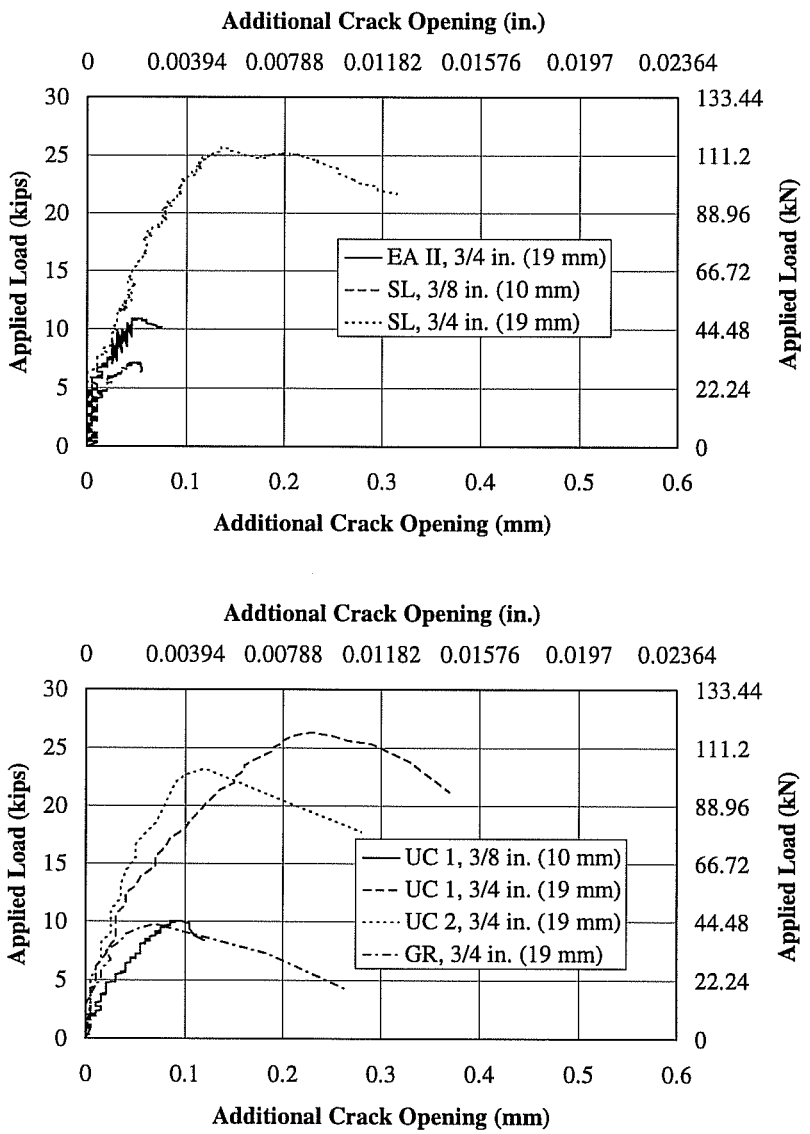

Figure 5.6 Typical Crack Opening During Tests of Series 1-8

5.3 Eccentric Shear Tests on Two-Anchor Connections

This section describes the tests of near-edge, two-anchor connections under both static and dynamic eccentric monotonic loading. To investigate the shear force distribution between anchors, each group of two anchors was installed perpendicular to the edge, with the front anchor placed close enough to the edge to fail by concrete breakout under shear. A 7-inch (178-mm) embedment was chosen to ensure steel failure of the back anchors. The same configuration of close hairpins as in previous Task 3 tests by Hallowell (1996), were used in some of the tests, to evaluate their effect on the load-displacement behavior of connections. All discussions on the test results are based on the average of five replicates.

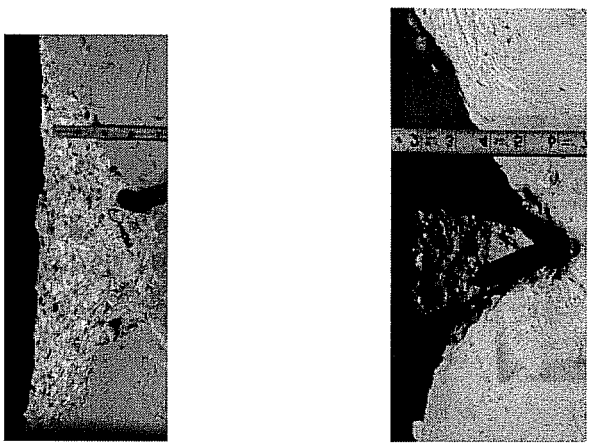

Figure 5.7 Left: Fractured Concrete Edge Affected by Forces of Baseplate. Right: Concrete Edge without Effect of Force of Baseplate.

In some tests, the concrete edge broke off under the combined effect of the shear force of the front anchor and the compression and friction forces of the compression side of the baseplate. As a result, the fractured concrete volume was much wider and deeper than would have been due just to shear on the front anchor. Figure 5.7 shows the cracked concrete volume with and without this effect.

Using the strain gauges on the center of the baseplate, the tension force and bending moment in each test were calculated and plotted in Appendix C.

5.3.1 Interaction of Tension and Shear Force on Anchors

Owing to the special design of the baseplate and the measurement of the stresses at its center portion, the shear and tension forces on the back anchors of the two-anchor connections were calculated as explained in Section 3.4.2.2.

The calculated shear and tension forces are then inserted into the left side of the elliptical interaction equation (Equation 2-15), using an exponent of 1.8, to compare the capacities of the back anchors under various loading conditions. All results are tabulated in the Appendix D. The average values for each set of tests are listed in Table 5.3.

Table 5.3 Average Values of Calculations According to Left Side of Elliptical Interaction Equation with an Exponent of 1.8

	Static Uncracked	Dynamic Uncracked	Static Cracked	Dynamic Cracked	Static Cracked Hairpins	Dynamic Cracked Hairpins
Ave.	1.00	1.11	0.99	1.05	1.01	1.03
COV.	6.0%	7.5%	6.8%	6.8%	11.0%	8.5%

5.3.2 Results of Series 3-9

Tests of Series 3-9 were conducted under static load in uncracked concrete without hairpins, to serve as baseline tests. Results of these tests are summarized in Table 5.4. The results are characterized by two distinctive load peaks, as shown in Figure 5.8. The first peak occurred when the concrete edge broke out; the second one, when the back anchor fractured. In three of the five tests, the maximum load occurred when the concrete edge broke out.

Table 5.4 Average Results for Near-Edge Two-Anchor Connections under Static Eccentric Shear Loading in Uncracked Concrete without Hairpins

	Load		COV	Horizontal Displacement		COV	Vertical Displacement		COV
	kips	kN	%	inch	mm	%	inch	mm	%
First Peak	24.9	111	9.6	0.149	3.78	25.8	0.058	1.48	37.0
Second Peak	24.9	111	3.3	0.399	10.1	26.3	0.116	2.95	18.4
Maximum	25.6	114	5.5						

The concrete edge was broken out mainly by the shear force on the front anchor. However, in two tests, the concrete fractured in front of the edge of the baseplate due to combined compression and friction forces, plus the shear force of the front anchor.

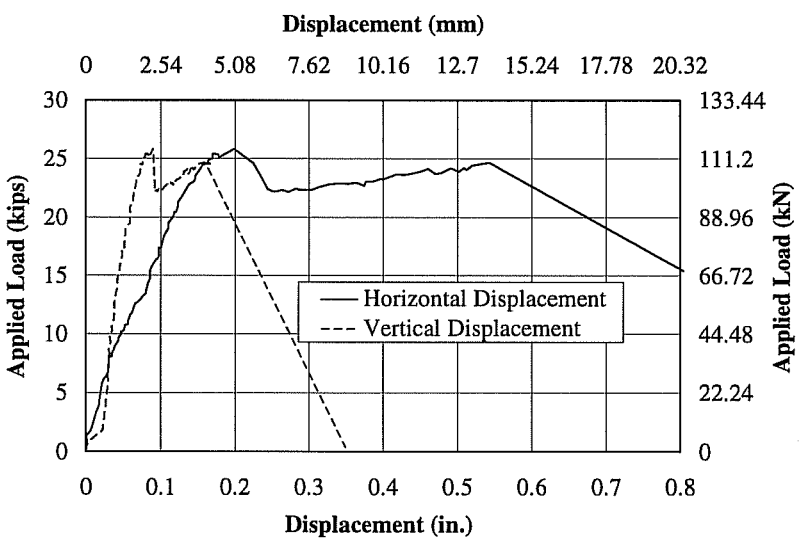

Figure 5.8 Typical Load-Displacement Curves of Test Series 3-9

5.3.3 Results of Series 3-10

Tests of Series 3-10 were conducted under dynamic load in uncracked concrete without hairpins, to assess the effect of dynamic loading. Table 5.5 shows the average values of five replicates.

Table 5.5 Average Results for Near-Edge Two-Anchor Connections under Dynamic Eccentric Shear Loading in Uncracked Concrete without Hairpins

	Load		COV	Horizontal Displacement		COV	Vertical Displacement		COV
	kips	kN	%	inch	mm	%	inch	mm	%
First Peak	27.7	123	8.1	0.153	3.88	20.8	0.051	1.29	27.2
Second Peak	29.5	131	4.0	0.530	13.5	14.1	0.138	3.52	18.4
Maximum	29.7	132	3.7						

In four of five tests, the concrete edge was broken out by both the force on the anchor and the forces on the compression side of the baseplate.

Like the test results of Series 3-9, the load-displacement curves of these tests also show a two-peak pattern. Figure 5.9 is a typical load-displacement curve from this series.

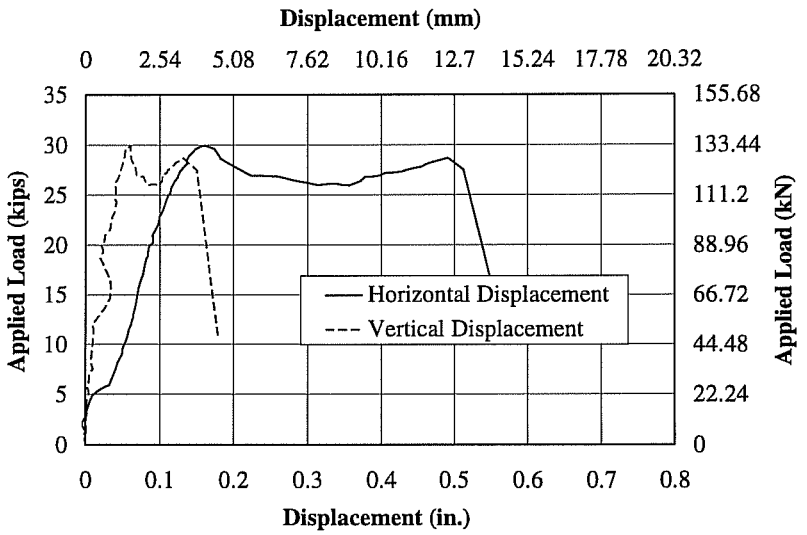

Figure 5.9 Typical Load-Displacement Curves of Test Series 3-10

5.3.4 Results of Series 3-11

This series was designed to assess the effect of cracks in concrete member and the effect of hairpins in front the edge anchor under static loading. Table 5.6 contains summaries of test results.

One test without hairpins failed by fracture of the concrete specimen. Only one test without hairpins exhibited the effect of the combination of anchor shear force and the forces on the compression side of the baseplate. In the tests with hairpins, however, two tests showed the results of combined forces.

For most of the tests, no obvious two-peak pattern was observed in the load-displacement curves. Figure 5.10 shows a typical load-displacement curve from each test, with and without hairpins. However, the term of "first peak load" is still retained to identify the load corresponding to concrete edge breakout. This load was read from the curves of the tension in the baseplate versus the external loading, corresponding to a

sudden change in tension on the center of the baseplate, signifying a rapid redistribution of shear force from the front to the back anchor.

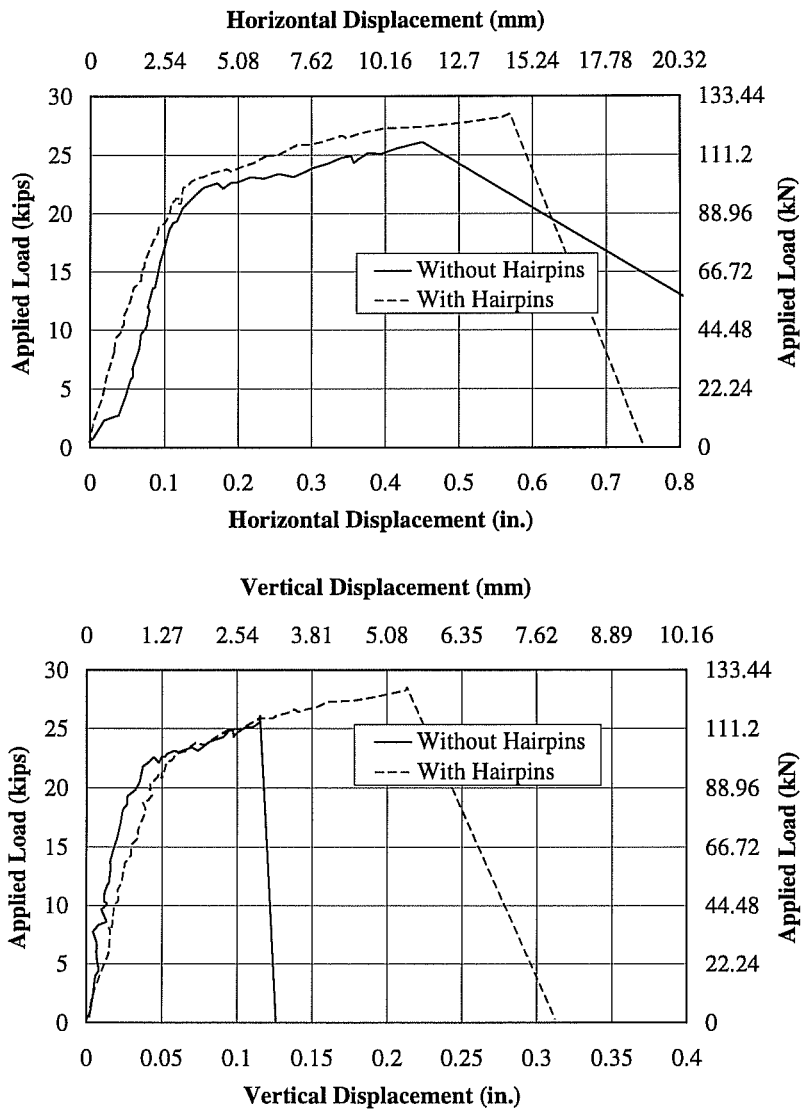

Figure 5.10 Typical Load-Displacement Curves of Series 3-11

Table 5.6 Average Results for Near-Edge Two-Anchor Connections under Static Eccentric Shear Loading in Cracked Concrete

without Hairpins	Load		COV	Horizontal Displacement		COV	Vertical Displacement		COV
	kips	kN	%	inch	mm	%	inch	mm	%
First Peak	20.9	92.8	10.0	0.146	3.71	10.7	0.036	0.92	19.7
Second Peak	24.3	108	8.2	0.443	11.3	12.0	1.109	2.78	11.1
Maximum	24.3	108	8.2						

with Hairpins	Load		COV	Horizontal Displacement		COV	Vertical Displacement		COV
	kips	kN	%	inch	mm	%	inch	mm	%
First Peak	22.7	101	6.7	0.138	3.51	19.4	0.046	1.16	16.3
Second Peak	29.0	129	6.8	0.486	12.3	15.8	0.164	4.17	17.9
Maximum	29.0	129	6.5						

5.3.5 Results of Series 3-12

As a continuation of Series 3-11, the tests of Series 3-12 were conducted under dynamic loading. Table 5.7 shows summaries of test results.

Table 5.7 Average Results for Near-Edge Two-Anchor Connections under Dynamic Eccentric Shear Loading in Cracked Concrete

without Hairpins	Load		COV	Horizontal Displacement		COV	Vertical Displacement		COV
	kips	kN	%	inch	mm	%	inch	mm	%
First Peak	26.1	116	14.2	0.186	4.73	27.9	0.063	1.60	44.8
Second Peak	27.8	124	4.5	0.610	15.5	12.6	0.168	4.26	12.6
Maximum	28.7	128	6.5						

with Hairpins	Load		COV	Horizontal Displacement		COV	Vertical Displacement		COV
	kips	kN	%	inch	mm	%	inch	mm	%
First Peak	27.7	123	15.8	0.199	5.05	29.2	0.065	1.66	30.8
Second Peak	31.1	138	4.6	0.457	11.6	41.9	0.167	4.25	44.4
Maximum	31.8	138	4.6						

In two of the five tests without hairpins, the fracture of the concrete edge showed combined effects from the shear force of the front anchor and also from the forces on the compression side of the baseplate. In all five tests with hairpins, the concrete edge was affected by both forces.

In the tests without hairpins, the pattern of two-peak load-displacement curves was again evident. However, in tests with hairpins, the load-displacement curves were very smooth (Figure 5.11).

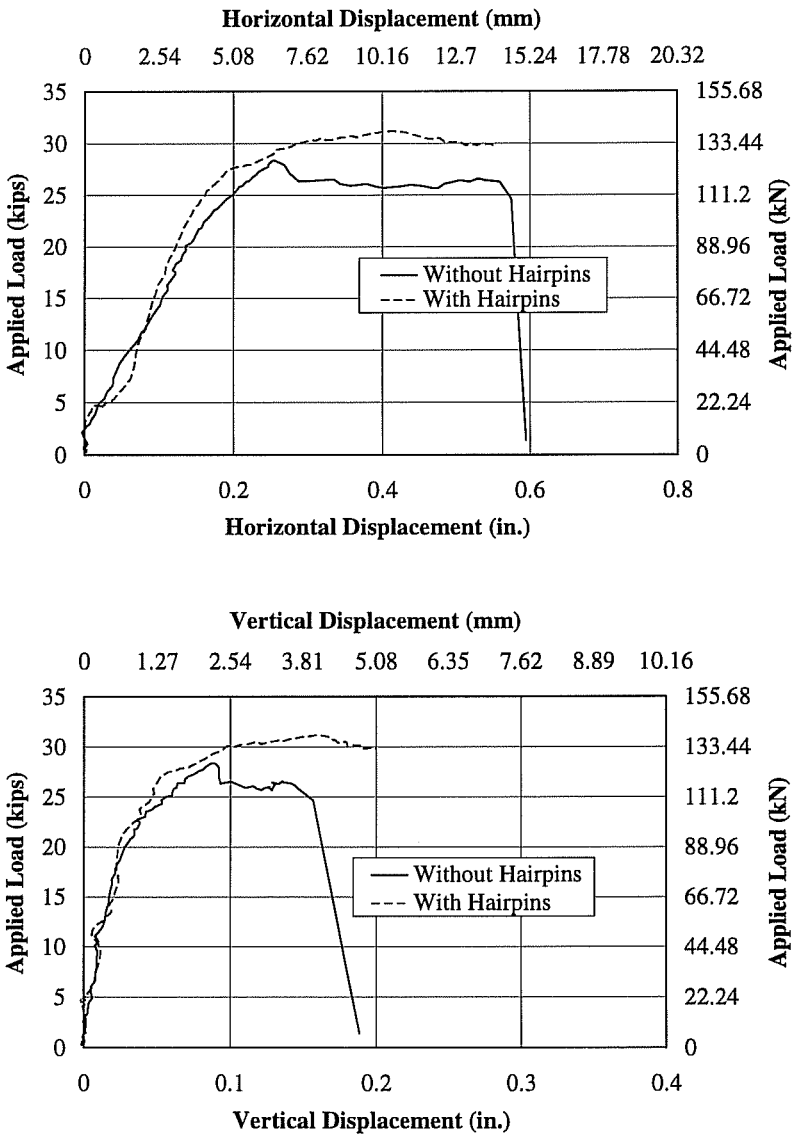

Figure 5.11 Typical Load-Displacement Curves of Test Series 3-12

5.4 Eccentric Shear Tests on Multiple-Anchor Connections

These tests were designed to assess the effects of dynamic reversed loading on anchor connections. Several static tests were also conducted as baseline tests. All test results are presented graphically in Appendix D, as curves of horizontal displacement versus external shear, time histories of displacement at 12 inches (305 mm) from the concrete surface, time histories of external load, curves of the tension force on each anchor versus external load, and curves of vertical displacement at the center of the baseplate versus external load.

The numbering of the four anchors, used in the presentation of test results, is shown in Figure 5.12.

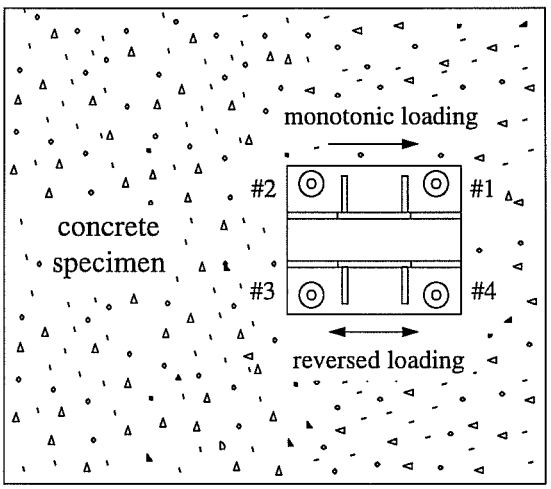

Figure 5.12 Numbering of anchors

For tests involving several phases of dynamic reversed loading cycles, in which the anchors were re-tightened by hand after each loading phase, the reduction in displacement of the attachment due to anchor tightening was added back when the load-displacement curves were plotted. Since the deflection of each anchor was difficult to measure, it was estimated from the load-displacement curve of the previous loading phase, and was adjusted visually according to the continuity and shape of the curves. To distinguish the

curves of vertical displacement of the baseplate of each loading sequence in the same test set, these curves were plotted separately from each other.

During the installation of the baseplates, the locations and magnitude of the gaps between the baseplate and each anchor varied from anchor to anchor. However, no attempt was made to record any gaps.

The following sections describe in detail the test results of each series.

5.4.1 Results of Series 4-1

In Series 4-1, intended as baseline tests, the connection was loaded statically. The test with a 12-inch (305-mm) eccentricity exhibited steel failure under shear of one of the front anchors. The test with an 18-inch (457-mm) eccentricity resulted in steel failure under tension of one of the back anchors. Table 5.8 summarizes the test results. Figure 5.13 shows typical load-displacement curves, and Figure 5.14 illustrates typical curves of tension forces on anchors versus the external load.

Table 5.8 Test Results of Multiple-Anchor Connections under Static Loading

Test	Maximum Load		Hor. Displ. at Baseplate		Hor. Displ. at 12 inches (305 mm)		Tension on Failed Anchor	
	kips	kN	inch	mm	inch	mm	kips	kN
4101	49.2	219	0.275	7.01	0.556	14.1	N/A	N/A
4102	41.9	186	0.318	8.08	0.924	23.5	28.9	129

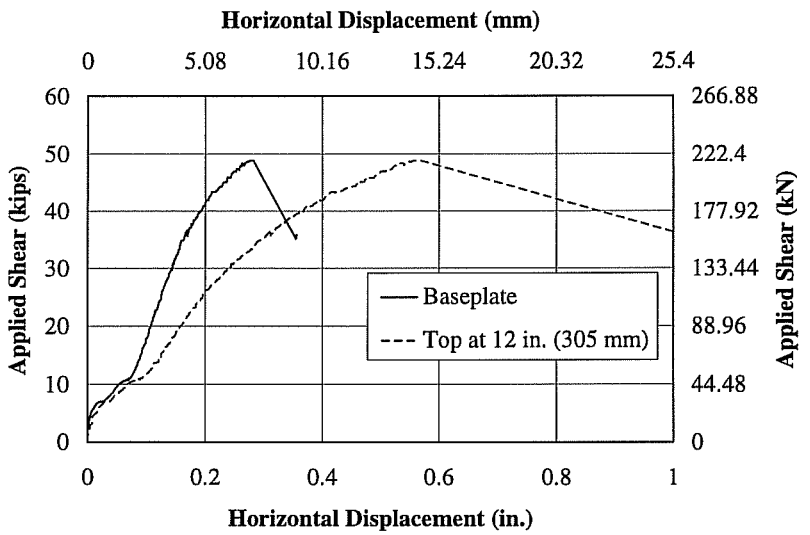

Figure 5.13 Typical Load-Displacement Curves for Multiple-Anchor Connections under Static Loading

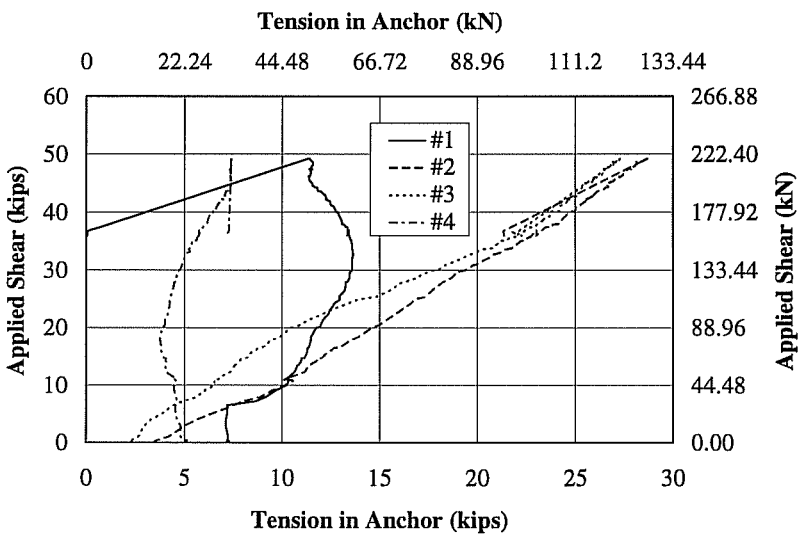

Figure 5.14 Typical Curves of Tension Forces on Anchors versus Applied Load on Multiple-Anchor Connections

5.4.2 Results of Series 4-2

Table 5.9 is a summary of the test results of this series, in which multiple-anchor connections were tested in uncracked concrete. "Maximum load" is the maximum load achieved during the entire loading history in both directions.

Table 5.9 Test Results of Series 4-2

Test	Maximum Load		Failure Mode of Anchor Failing First	Load at Failure of Anchor		Tension on Failed Anchor	
	kips	kN		kips	kN	kips	kN
4203	51.3	228	Tension	51.3	228	31.7	141
4204	33.3	148	Tension	33.3	148	19.2	85.4
4205	52.7	233	Tension	43.7	194	23.4	104
4206	38.9	173	Tension	25.0	111	31.3	139

A typical load-displacement curve and typical curves of tension on anchors versus external load are shown in Figures 5.15 and 5.16.

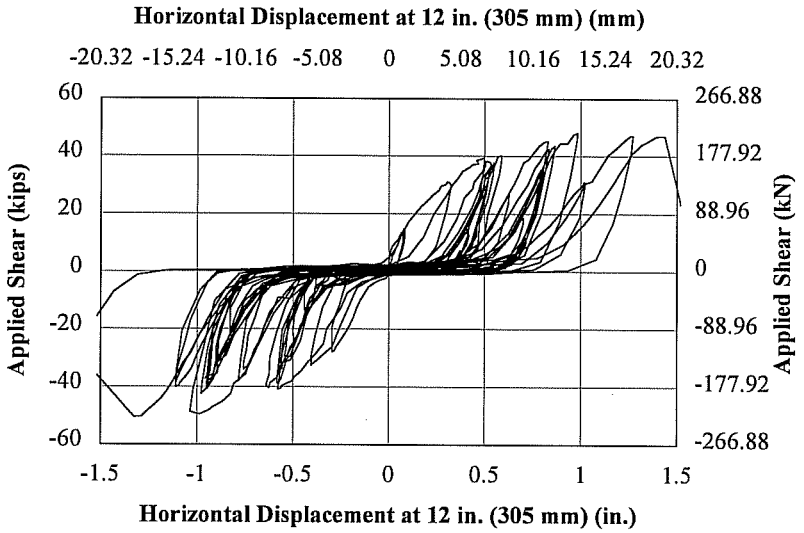

Figure 5.15 Typical Load-Displacement Curves of Connection under Dynamic Reversed Load

In the test with a flexible baseplate (Test 4203), only a slight permanent plastic deformation was observed on both sides of the attached member (Figure 5.16).

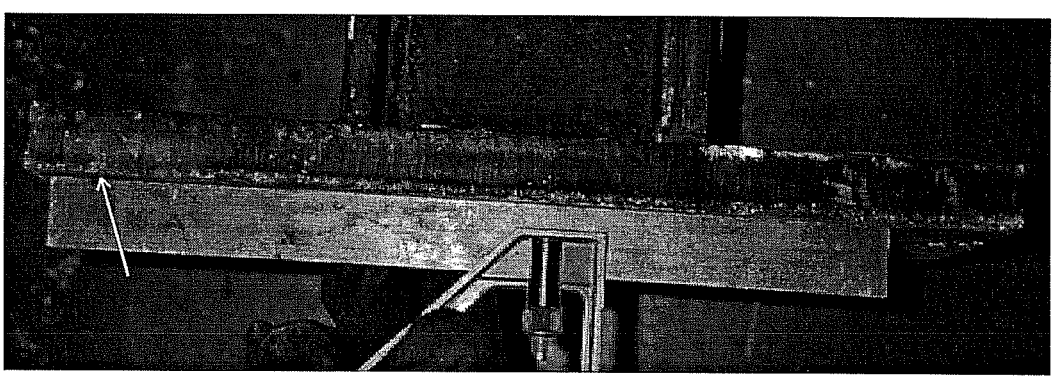

Figure 5.16 Deformation of Flexible Baseplate after Testing

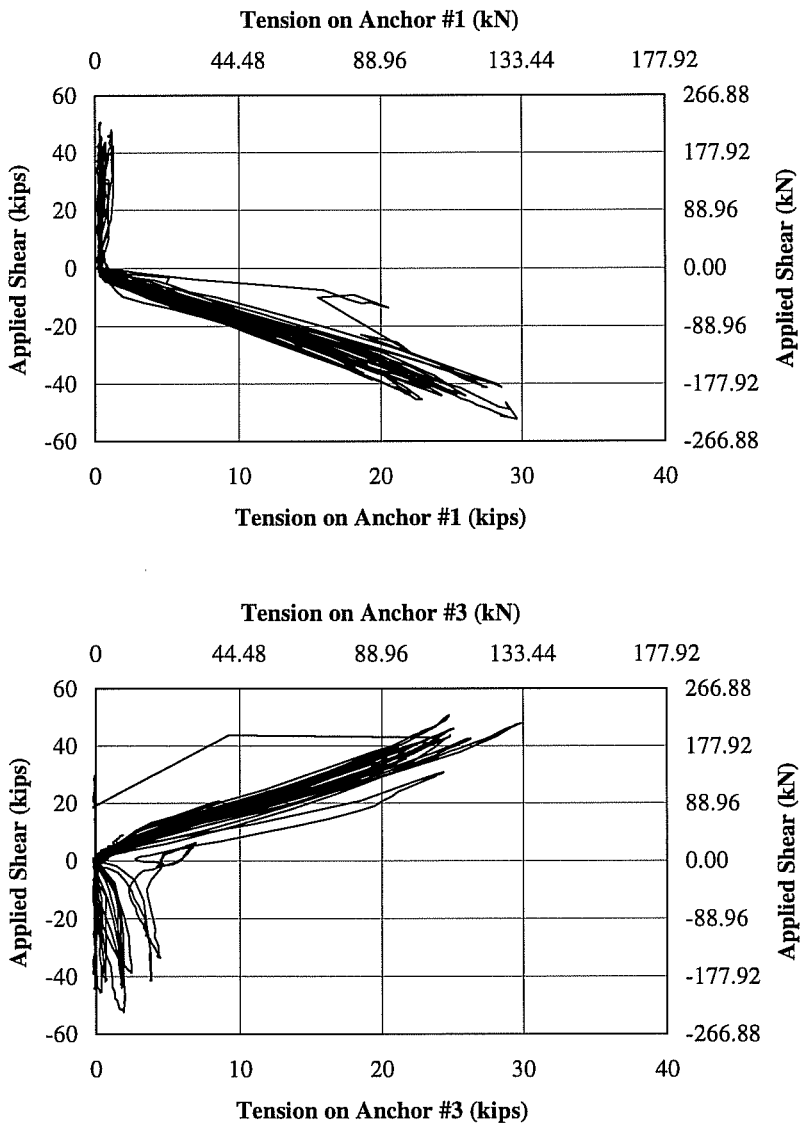

Figure 5.17 Typical Curves of Tension on Anchors versus External Load

In all four tests, severe shell-shaped concrete spalling was observed in the concrete in front of the anchors between these two rows of anchors. However, little or no concrete

spalling was visible in the concrete on the other side of the anchors. Figure 5.18 shows typical concrete spalling after a test.

Figure 5.18 Typical Concrete Spalling after Reversed Loading

5.4.3 Results of Series 4-3

The tests of Series 4-3 were conducted in cracked concrete specimen. Table 5.10 gives a summary of this test series.

Table 5.10 Summary of Test Results of Series 4-3

Test	Maximum Load		Failure Mode of Anchor Failing First	Load at Failure		Tension on the Failed Anchor	
	kips	kN		kips	kN	kips	kN
4307	28.9	129	Tension	28.9	129	20.2	90.0
4308	51.2	228	Shear	51.2	228	N/A	N/A
4309	38.7	172	Tension	31.9	142	26.6	118
4310	21.0	93.4	Pull-Out	N/A	N/A	N/A	N/A

The test on the connection with Expansion Anchor II at an 18-inch (457-mm) eccentricity (Test 4310) experienced a pullout failure, in which all anchors pulled out

grossly (Figure 5.19). Figure 5.20 shows the load-displacement curve of that test. Test 4307 was also conducted on Expansion Anchor II, the concrete in front of the anchors had deeper spalling at both directions than that of the tests on Undercut Anchor 1.

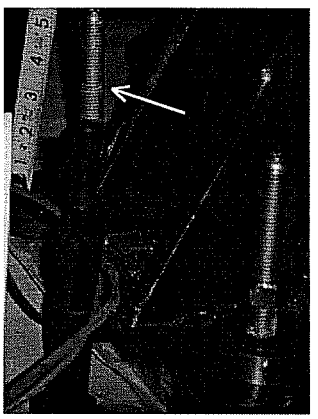

Figure 5.19 Pulled-Out Anchors

(Mark on upper anchor was flush with concrete surface at installation)

A pattern of concrete spalling in front of anchors similar to that in Series 4-2 was

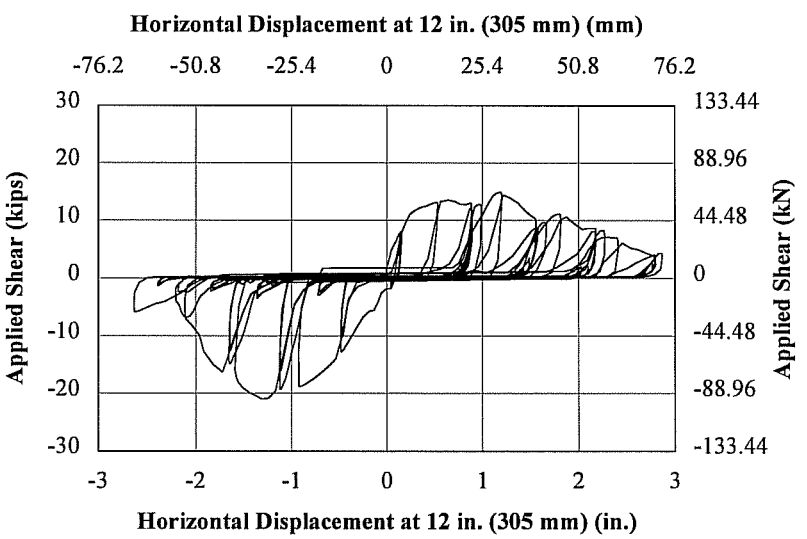

Figure 5.20 Load-Displacement Curve of Attachment with Expansion Anchors Failing by Pull-Out

observed.

5.4.4 Results of Series 4-4

Results of these two tests are shown in Table 5.11. Both tests showed concrete edge breakout failure under shear load by the two near-edge anchors, followed by steel tension failure of the back anchors. The load at the failure of the edge concrete is estimated from the load-displacement curves of these tests, when the load reached its first peak. The concrete breakout region was wide and deep, as shown in Figure 5.21. The compression edge of the baseplate on the compression side made a clearly visible mark on the top of the fractured concrete.

Table 5.11 Test Results of Series 4-4

Test	Load at Failure of Concrete Edge		Load at Failure of Back Anchor	
	kips	kN	kips	kN
4411	29.5	131	35.8	159
4412	29.9	133	31.1	138

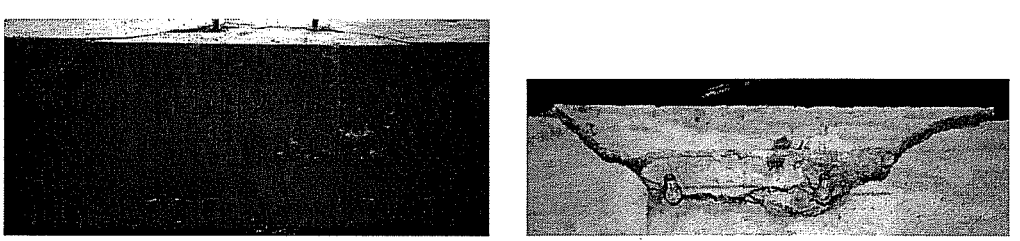

Figure 5.21 Concrete Edge Fracture in Test 4412 (Left: Side View; Right: Top View)

Figure 5.22 is a typical load-displacement curve, reflecting the effect of edge breakout on multiple-anchor connections loaded statically towards the edge.

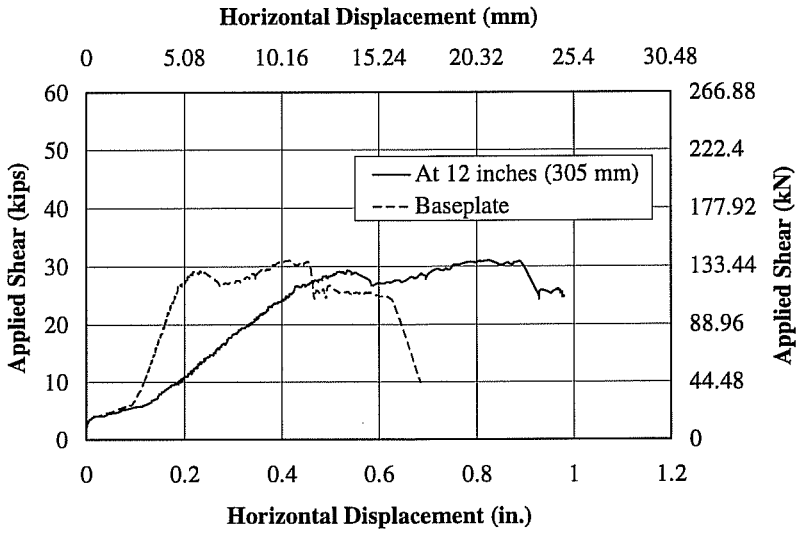

Figure 5.22 Typical Load-Displacement Curves of Near-Edge Multiple-Anchor Connection Under Static Loading toward the Edge

5.4.5 Results of Series 4-5

In these two tests, the initial failure mode was concrete edge breakout under shear. After that, the tensile capacity of the near-edge anchors was gradually lost, due to lateral concrete blowout at the heads of these anchors. This observation was made by examining load-displacement curves and the loading history curves of these tests. Table 5.12 lists the load at concrete edge breakout and the maximum loads achieved at the loading direction towards the center of specimen, which usually occurred just before concrete edge breakout.

Table 5.12 Test Results of Series 4-5

Test	Load at Failure of Edge Concrete		Max. Load Achieved at the Other Direction	
	kips	kN	kips	kN
4513	29.1	129	28.7	128
4514	30.2	134	32.7	145

Figure 5.23 shows a typical load-displacement curve, with the occurrence of concrete edge breakout noted.

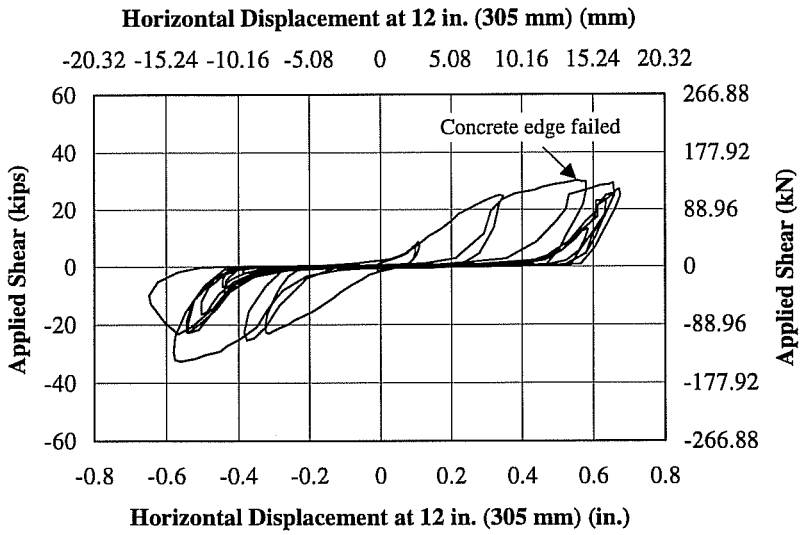

Figure 5.23 Typical Load-Displacement Curve of Near-Edge Multiple-Anchor Connection without Hairpins Under Dynamic Reversed Cyclic Loading

The shape of the cracked concrete edge was similar to that of Series 4-3.

5.4.6 Results of Series 4-6

Multiple-anchor connections with hairpins were tested in Series 4-6. A static test was conducted as a baseline test. However, because of improper bracing of the test specimen, the concrete block cracked prematurely before the back anchor failed. This resulted in a much greater horizontal displacement of the attachment when the steel failure of the back anchors occurred. Nonetheless, the load at which concrete edge breakout occurred was still readable from the load-displacement curves. The other two tests failed by lateral blowout at the heads of the near-edge anchors, after concrete edge breakout under the shear force of the anchors and the force of the baseplate.

The cracked concrete volume was much smaller for anchors with hairpins, than without. Figure 5.24 shows a typical cracked concrete edge after testing.

Figure 5.24 Concrete Edge Breakout with Hairpins after Testing

Table 5.13 shows the results of Test 4615. Figure 5.26 shows a typical load-displacement curve of the test under static loading with hairpins.

Table 5.13 Results of Test 4615

Load at Failure of Concrete Edge		Maximum Load	
kips	kN	kips	kN
28.0	125	42.3	188

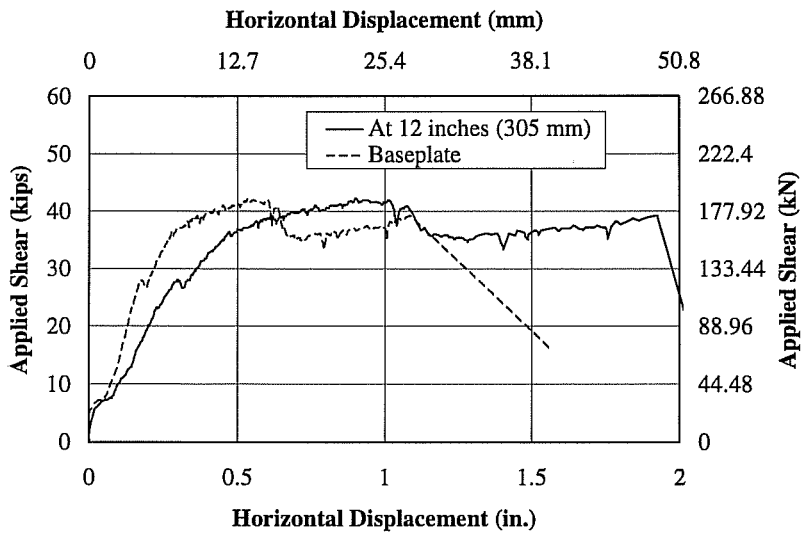

Figure 5.25 Typical Horizontal Load-Displacement Curves of Near-Edge Multiple-Anchor Connection with Hairpins under Static Loading

Table 5.14 lists the load at which the concrete edge broke out, the maximum load reached at the loading direction towards the member edge, and the maximum load at the direction towards the center of concrete specimens, of the two remaining tests of Series 4-6.

Table 5.14 Tests Results for Multiple-Anchor Connections with Hairpins under Dynamic Reversed Cyclic Loading

Test	Load at Failure of Edge Concrete		Max. Load at Direction toward Specimen Edge		Max. Load at Direction towards Specimen Center	
	kips	kN	kips	kN	kips	kN
4616	27.8	124	45.2	201	46.1	205
4617	30.0	133	30.0	133	31.2	139

Figure 5.26 presents a typical load-displacement curve of a multiple-anchor connection with hairpins under reversed cyclic loading.

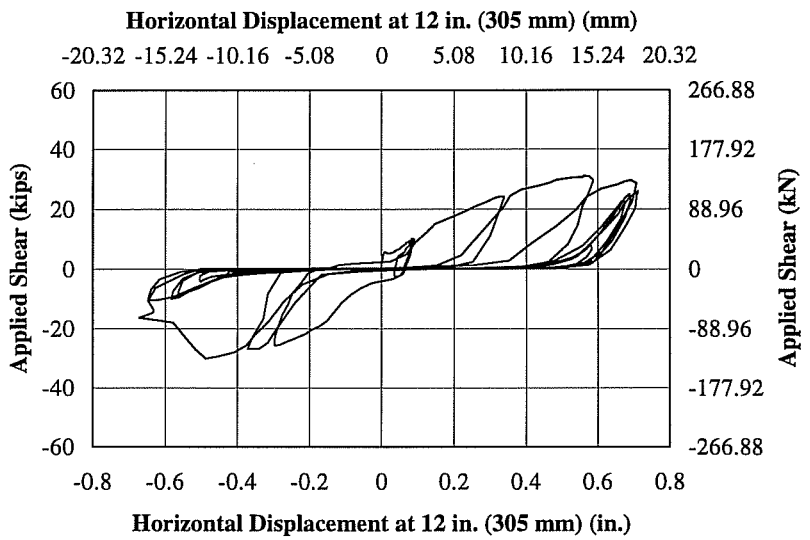

Figure 5.26 Typical Load-Displacement Curve of Near-Edge Multiple-Anchor Connection with Hairpins under Dynamic Reversed Cyclic Loading

CHAPTER 6

DISCUSSION OF TEST RESULTS

6.1 Introduction

The test results presented in Chapter 5 are discussed in this chapter.

For single-anchor tests with concrete breakout failure, results are presented in terms of the tensile normalization factor "k" (Equation 2-5), which were derived based on the average tensile capacity of five replicates in each case, to facilitate comparison among different anchors, embedment depths, and concrete strengths:

$$k = \frac{T}{\sqrt{f_c} h_{ef}^{1.5}}$$

where: k = normalization factor for tensile capacity;

T = measured tensile capacity;

h_{ef} = effective embedment; and

f_c = tested concrete cylinder compressive strength.

The displacement is read directly from the test results.

For tests failing by steel fracture, measured loads and displacements are compared directly. In tests where the concrete failure loads were influenced by the forces in the other steel elements of the connection, the measured loads are also used directly.

6.2 Behavior of Single Anchors under Dynamic Tension Loading in Cracked Concrete

In Series 1-7 and 1-8, five different types of anchors commonly used in existing nuclear plants were tested. The results are compared with the tests reported by Rodriguez (1995).

6.2.1 Effect of Cracks and Dynamic Loading on Wedge-Type Expansion Anchors

Figure 6.1 shows the comparison of the maximum loads, and of the displacements at the maximum load, of Expansion Anchor II.

Compared to the corresponding tests in uncracked concrete, the maximum capacity under static loading in cracked concrete decreased by 19%, and the captivity under dynamic loading decreased by 26%. While the displacement at maximum load decreased 28% under static loading, the displacement under dynamic loading increased by 89%. Comparing in the tests in cracked concrete only, the dynamic capacity is 5% smaller than the static capacity.

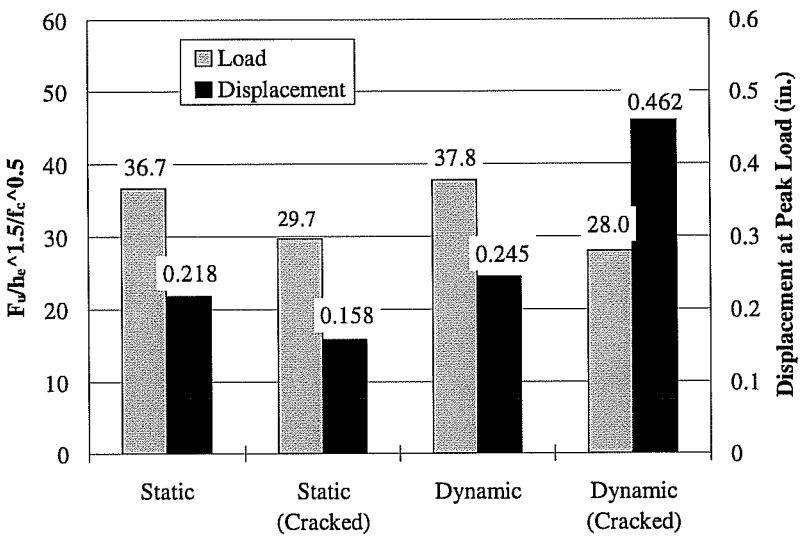

Figure 6.1 Comparison of Maximum Load and Displacements at Maximum Load of EA II Anchors

Comparing the load-displacement curves in cracked and uncracked concrete, the elastic range of the load-displacement curves of the tests in cracked concrete is dramatically smaller under both static and dynamic loading. Crack opening increases the gap between the anchor mandrel and the surrounding concrete, which was minimized by torquing during the installation of the anchor. As a result, the prestressing force on the anchor is reduced. Under tension, when the prestressing force in an anchor is overcome, the anchor will exhibit increased displacement. Therefore, the load-displacement curve of an expansion anchor in cracked concrete is flatter than that of the same anchor in uncracked concrete.

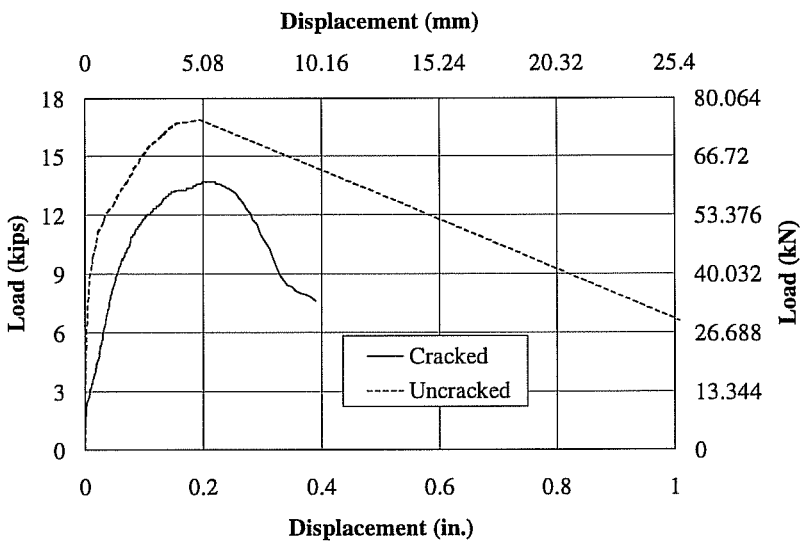

Figure 6.2 Effect of Cracking on Load-Displacement Behavior of Expansion Anchor II

Dynamic loading worsens the condition of load transfer at the heads of anchors, probably due to reduction in the coefficient of friction between mandrel and clip, and between clip and concrete (Rabinowicz 1995). Under static loading, the friction between the clip and the surrounding concrete is large enough to keep the clips in position, while the mandrel is pulled through the clips to further expand them. Under dynamic loading,

however, due to reduced friction between the concrete and the clips, the clips are first pulled out with the anchor, then re-engage the concrete at a smaller embedment, and therefore break the concrete out at a smaller load, resulting in a very long, flat portion of the load-displacement curve and a smaller load capacity. Furthermore, the increased gap between the anchor mandrel and the surrounding concrete by the crack opening reduces the maximum clamping force, which will be developed as the anchor mandrel expands the clips. As a result, the dynamic tests in cracked concrete had the largest displacement with the smallest maximum load. Figure 6.3 shows the position of cones inside the expansion sleeves after both static and dynamic tests in cracked concrete. The anchor mandrel was pulled farther into the expansion sleeve in the static test than in the dynamic test.

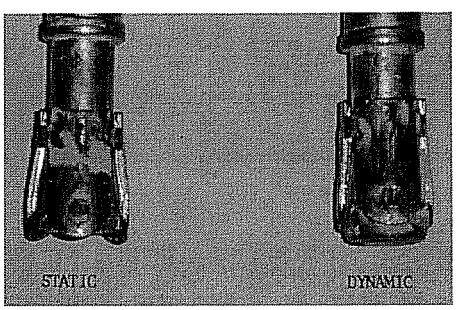

Figure 6.3 Positions of Clips of Expansion Anchors II After Tests

6.2.2 Effect of Cracks and Dynamic Loading on Sleeve Anchors

Figure 6.4 shows the comparison of the maximum loads and of the displacements at maximum load of 10-mm Sleeve Anchors. Figure 6.5 shows the same information for 20-mm Sleeve Anchors.

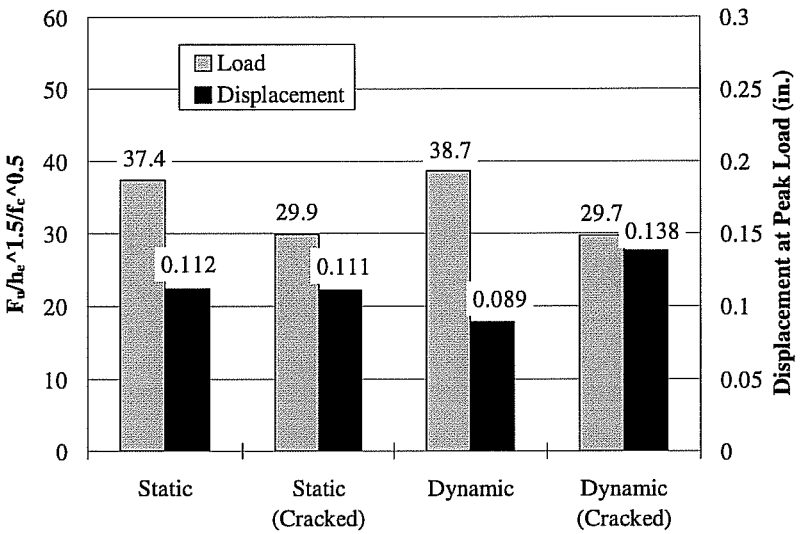

Figure 6.4 Comparison of Maximum Load and Displacements at Maximum Load of 10-mm Sleeve Anchors

In the tests on 10-mm anchors, the maximum capacity in cracked concrete is almost identical under both static and dynamic loading. The decrease in maximum load capacity compared to anchors in uncracked concrete is about 20% under static loading, and about 23% under dynamic loading. Unlike the curves of the other tests on 10-mm diameter Sleeve Anchors, the load-displacement curves of the dynamic tests in uncracked concrete near the maximum load are very flat, with a flat range extending for about 0.1 inch (2.54 mm). In the dynamic tests in cracked concrete, one of the load-displacement curves showed much more slip than the others. Excluding that amount of slip, the average displacement at maximum load is 0.112 inch (2.84 mm), almost identical to those of static tests in both uncracked and cracked concrete. The shape of the load-displacement curves of the tests in cracked concrete under both dynamic and static loading are very similar. However, compared to the curves of static tests in uncracked concrete, both of them have much smaller elastic range (only up to about 2 kips (8.9 kN) compared to up to 5 kips (22.2 kN) in the tests in uncracked concrete), because the crack released most of the prestressing

force. The releasing of prestressing force also reduced the flat portions of the load-displacement curves of tests under dynamic loading in cracked concrete.

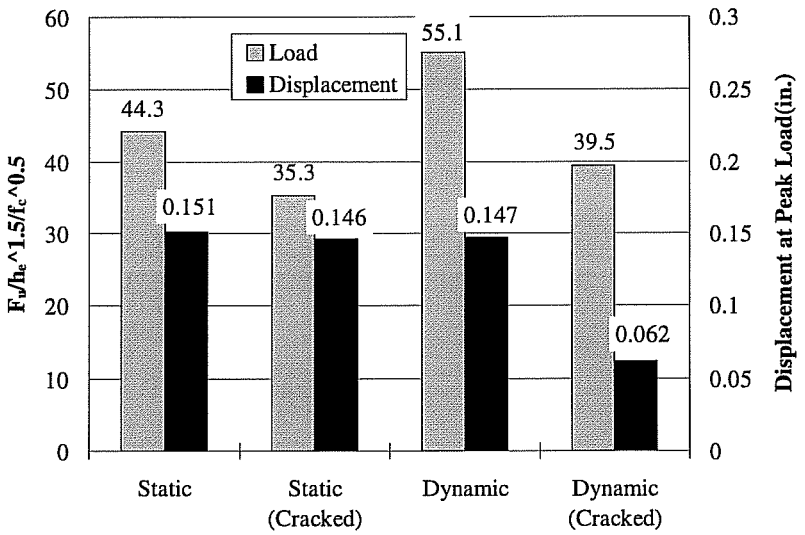

Figure 6.5 Comparison of Maximum Load and Displacements at Maximum Load of 20-mm Sleeve Anchors

For the 20-mm Sleeve Anchor, the maximum load capacity for tests in cracked concrete decreased by about 20% under static loading and by about 28% under dynamic loading, compared to tests in uncracked concrete. When comparing tests in cracked concrete only, dynamic loading increased the maximum capacity by only 12%, much less than the 24% experienced in the tests in uncracked concrete, due to more tests experienced with the pullout failure in cracked concrete under dynamic loading.

As mentioned in Section 4.3.2, the expansion sleeve of Sleeve Anchors of 20-mm diameter has an inside step, designed to limit the expansion force of the anchor on the surrounding concrete. The behavior of Sleeve Anchor was significantly affected by this design aspect.

The slope of the load-displacement curves of most static tests in cracked concrete just begins to flatten out and then increases abruptly . This happens when the expansion cone contacts the step inside the sleeve, after being pulled farther into the sleeve. At this time, relative movement between the cone and the sleeve completely stops, and large frictional forces develop between the sleeve and the surrounding concrete. In most dynamic tests in cracked concrete, after the cone stopped against the step, the expansion sleeve also slipped along the wall of the hole due to the smaller coefficient of friction, which resulted in a horizontal, saw-toothed load-displacement curve over a 1-inch (25.4-mm) displacement. As a result, the maximum load in most dynamic tests was achieved just when the expansion cone reached the step inside the sleeve; the average displacement at maximum load was only about one-third of that of the other cases.

In tests on 20-mm Sleeve Anchors in cracked concrete, the elastic range of load-displacement curves was very small or not even observable, due to the relaxation of the prestressing force. In the load-displacement curves, if the expansion sleeve did not slip along the concrete, the slope of the load-displacement curves did not change much up to the maximum load. However, the increase in slope is still noticeable.

6.2.3 Effect of Cracks and Dynamic Loading on Grouted Anchors

Typical test results for Grouted Anchors are compared in Figure 6.6.

In Grouted Anchors, the interface between the grout and the surrounding concrete is critical. During crack opening, the crack propagated along that interface in all but one test. As a result, the friction between the grout and the concrete was dramatically reduced, and the grout plug pulled out.

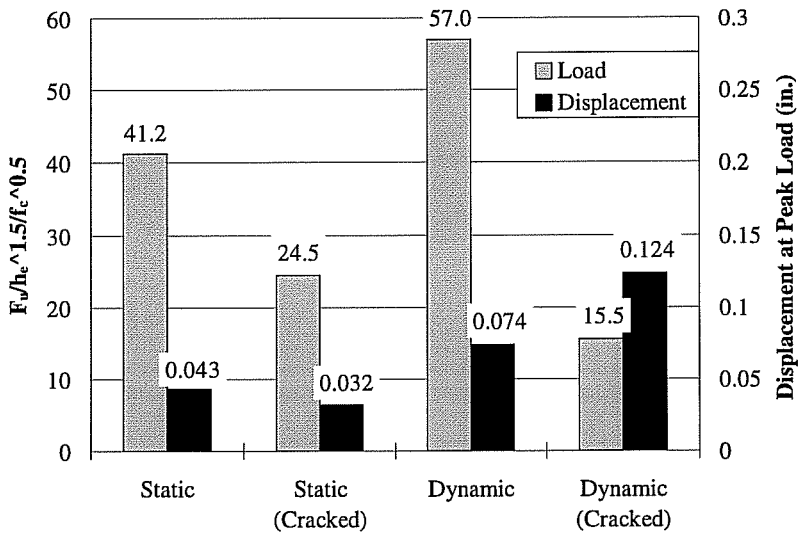

Figure 6.6 Effect of Cracking and Dynamic Loading on Maximum Load and Displacements at Maximum Load of Grouted Anchors

Under static loading in cracked concrete, the average maximum capacity decreased by about 41% compared to the tests in uncracked concrete.

Dynamic loading reduced the capacity even more due to the smaller dynamic friction coefficient between grout and concrete. In most dynamic tests, the grout plugs were completely pulled out of the cored holes, with little or even no damage to the surrounding concrete. From the load-displacement curves of these tests, it can be seen that once the initial friction was overcome, the grout slipped along the wall of the holes, which results in a horizontal saw-toothed load-displacement curves. In some case, the load increased a little during slip (Tests 8DGL5732 and 8DGL5733). Therefore, the displacement at the maximum load was very small in some tests, and very large in other tests. For this reason, the average displacement is largest in dynamic tests in cracked concrete.

6.2.4 Effect of Cracks and Dynamic Loading on Undercut Anchor 1

Figure 6.7 shows the comparison of the maximum load capacity and the displacements at the maximum load of Undercut Anchor 1 of 3/8-inch (10-mm) diameter; test results of Undercut Anchor 1 of 3/4-inch (19-mm) diameter are shown in Figure 6.8.

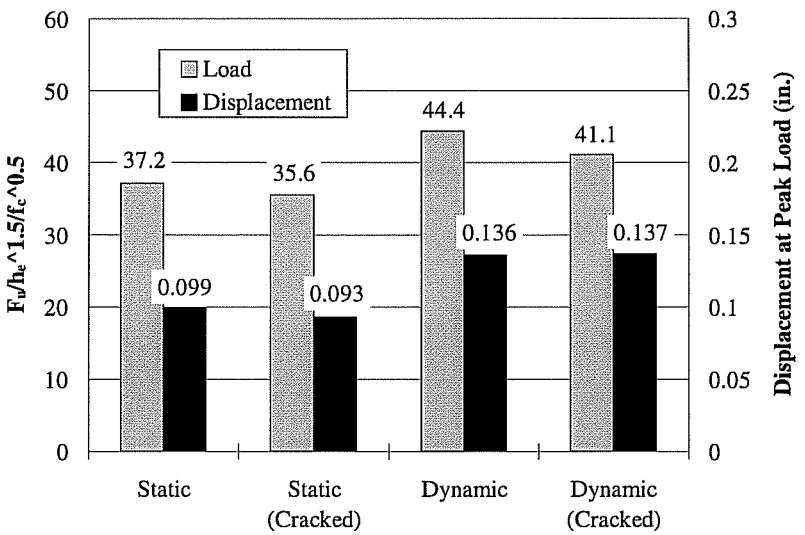

Figure 6.7 Effect of Cracking and Dynamic Loading on Maximum Load and Displacements at Maximum Load of 3/8-inch (10-mm) Undercut Anchor 1

For UC1 anchors of 3/8-inch (10-mm) diameter, the maximum load capacity in cracked concrete decreased by 4% under static loading and 7% under dynamic loading, compared to the tests in uncracked concrete. In cracked concrete, the load capacity under dynamic loading is 15% higher than under static loading. From Figure 6.7, it can be seen that the average displacement at maximum load for static tests in cracked concrete is a little smaller than in uncracked concrete. However, the displacement is almost the same for the dynamic tests in both cracked and uncracked concrete. The increase in the displacement under dynamic loading is about 47% in the tests in cracked concrete than that under static loading, which is much greater than the increase in the load capacity. This is believed due to the further expansion of the sleeve due to the larger tension load and a smaller friction coefficient between the cone and the expansion sleeve, and also due to the extra room in

which the anchor could slip and expand due to the crack. However, the load-displacement curves of all these tests were similar, except for smaller elastic range for the tests in cracked concrete.

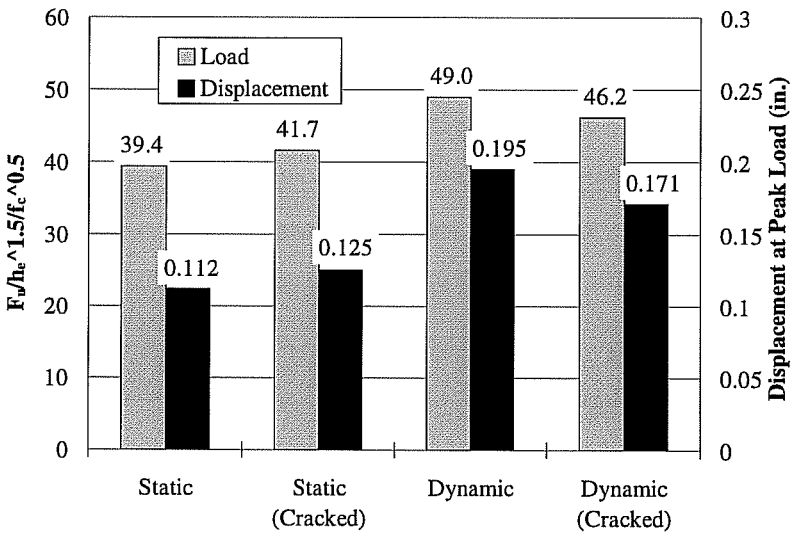

Figure 6.8 Effect of Cracking and Dynamic Loading on Maximum Load and Displacements at Maximum Load of 3/4-inch (19-mm) Undercut Anchor 1

For the tests on 3/4-inch (19-mm) diameter UC1 anchors, the maximum load increased by 6% under static loading, and decreased by 6% under dynamic loading in cracked concrete, compared with the tests in uncracked concrete. Dynamic loading increased capacity by 11% for the tests in cracked concrete, compared to that under static loading. The displacement at maximum load increased by 37% due to dynamic loading in cracked concrete, much greater than the increase in the load capacity. The load-displacement curves of the dynamic tests have much longer small-slope portions near the maximum load. The larger increase in displacement is believed also due to the further expansion of the sleeve by the larger tension force and a smaller friction coefficient between the cone and the expansion sleeve (as shown in Figure 6.9), and is also due to the larger deflection of concrete under a larger load and to the extra room provided by crack opening in which the anchor could slip and expand.

The increase in capacity of 3/4-inch (19-mm) UC1 anchors in cracked versus uncracked concrete was not expected. For the following reasons, the results are considered to be valid: First, concrete specimens from the same batch were also used in the tests on Undercut Anchor 2, which gave results similar to those obtained with UC2 in the specimens from another batch of concrete. This eliminates the possibility of incorrect concrete strength. Second, the test results were quite consistent, with a coefficient of variation of only 2.8% in the static tests in cracked concrete, and a coefficient of variation of 7.6% in static tests in uncracked concrete. Furthermore, considering the small decrease of 4% in the capacity of 3/8-inch (10-mm) anchors, it is believed that this increase might be consistent with the inherent scatter of these tests. However, the small change in capacity in cracked concrete under static load may also be related to the configuration of this type of anchors. Because of the small number of tests, further investigation might be needed.

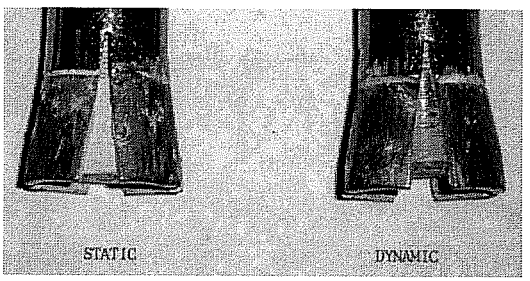

Figure 6.9 Positions of Expansion Cones of Undercut Anchor 1 after Tests

6.2.5 Effect of Cracks and Dynamic Loading on Undercut Anchor 2

Typical test results for Undercut Anchor 2 are compared in Figure 6.10.

The ultimate capacity in cracked concrete decreases by 35% under static loading, and by 16% under dynamic load, compared with the corresponding tests in uncracked concrete. The displacement at maximum load decreased by 41% and 36% respectively. The displacement was believed to be more or less directly related to the magnitude of the tension load, since the plastic deformation of the concrete at the anchor heads was mostly

eliminated during the installation of anchors. While comparing the tests in cracked concrete only, dynamic loading increased the capacity by 59%.

Undercut Anchor 2 is a unique type of anchor, whose expansion sleeve expands upward during installation, as the ends of the sleeve are pulled up against the undercut concrete hole. The bearing area is mainly the cross-sectional area of the expansion sleeve, and is therefore quite small. Furthermore, during installation, the anchor was pre-loaded to 90% of its ultimate capacity. This fully plasticized the concrete surrounding the contact area of the expansion sleeve, and much less concrete crushing would be expected to occur under loading. As a result, the displacement of this anchor is much smaller under tension than that of UC1.

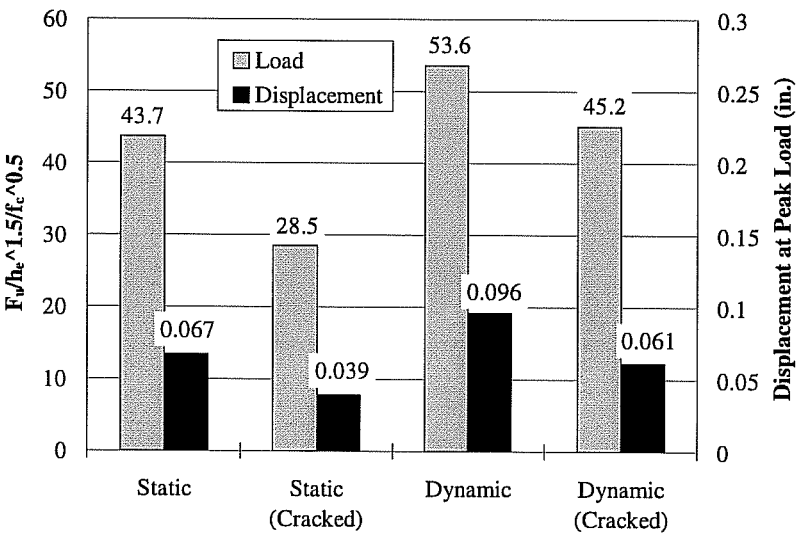

Figure 6.10 Effect of Cracking and Dynamic Loading on Maximum Load and Displacements at Maximum Load of 3/4-inch Undercut Anchor 2

Compared to Undercut Anchor 1, Undercut Anchors 2 have much lower capacity in cracked concrete under both static and dynamic loading. This could be due to the expansion mechanism of UC2, which results in a different stress distribution in the surrounding concrete than that of UC1. The larger increase in load under dynamic loading was mainly because of the higher loading rate to which it was subjected. The loading rate

of the hydraulic actuator was limited by the servo-valve flow rate. In the tests with a large peak displacement, especially at failure, the actual loading rate might be reduced due to the reduced specimen stiffness. Since the failure displacement of Undercut Anchor 2 was much smaller than that of UC1, the desired loading rate could be maintained during the entire loading time. This was verified from the loading history curves. The load-displacement curves of UC2 have almost a constant slope up to the ultimate load, while the curves of Undercut Anchor 1 have much flatter portions near the failure load.

In some tests on UC2 Anchors, the displacements acquired with a linear potentiometer changed abruptly. This might be caused by vibration of the test setup, because of the very high stiffness of the UC2 anchors.

6.2.6 Comparison of Additional Crack Opening in Single-Anchor Tension Tests

Most additional crack openings monitored during the single-anchor tests are compiled together here, to compare the effects of expansion forces for each type of anchor, including the results from the tests conducted by Hallowell (1996). The test results of the Grouted Anchor are excluded here, because of its different load-transfer mechanism and poor performance under dynamic loading. Each curve is the average of the additional crack openings of five replicates at each load level.

Generally speaking, at each load level, most anchors experienced smaller additional crack opening under dynamic than under static loading, except for the Sleeve Anchor. At very small load levels (for example, 4 kips (17.8 kN)), the additional crack opening of each type of 3/4-inch (19-mm) anchor were mostly the same under static and dynamic loading, with the exception of Expansion Anchor II, which had quite larger opening under static loading.

As shown in Figures 6.11 and 6.12, Expansion Anchor II of 3/4-inch (19-mm) diameter consistently has the highest additional crack openings under static loading. Under dynamic loading, it had only half of the additional crack opening at the same load level. The 3/4-inch (19-mm) Cast-in-Place anchor had small additional crack openings under both

static and dynamic loading, because its load-transfer mechanism -- mechanical interlock (bearing) -- produced a smaller expansion force. The 3/4-inch (19-mm) Sleeve Anchor had the least additional crack openings under static loading, but the highest under dynamic loading. The crack openings of Undercut Anchor 1 of 3/4-inch (19-mm) diameter were consistent under both static and dynamic loading. They are both the second highest among all crack openings.

If the failure mode is concrete cone breakout, the causes of additional crack opening during tests are two-fold. One is the increasing expansion force on the concrete specimens on both sides of crack produced by the increasing external load. The other is the transverse deflection of the cracked concrete cones acting as a tip-loaded cantilever beam (Figure 6.11). The former increases linearly with the external force, provided the concrete is not damaged. The latter, however, increases faster than the external load. Because the area of the concrete breakout cone also increases with external load, the stiffness of the concrete breakout cone decreases. At the ultimate load, the transverse deflection of concrete should dominate the crack opening. This can explain why all measured crack openings increased more rapidly near maximum load.

Dynamic friction coefficients between steel and steel and the friction coefficient between steel and concrete are smaller than static ones. Under dynamic load, the friction

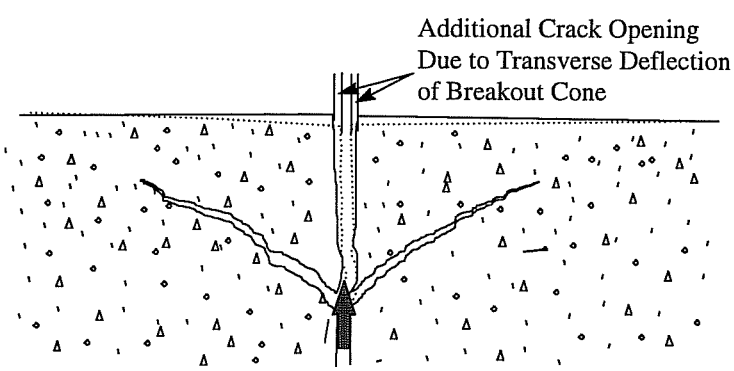

Figure 6.11 Addition Crack Opening Due to Transverse Deflection of Breakout Cone in Tension

coefficients between mandrel and expansion sleeve, and between sleeve and the surrounding concrete, might be smaller due to the rapid movement between them. In order to achieve the same load under dynamic loading, the expansion force exerted on the surrounding concrete by the anchor head could correspondingly increase.

If an anchor fails by concrete breakout, concrete starts to crack near the anchor head at about 20% of the ultimate capacity (CEB 1991). Since concrete tensile strength increases with a higher strain rate, it can be expected that at the same load level, the cracked concrete area would be smaller under dynamic than under static loading. Therefore, the crack opening at the concrete surface due to the transverse deflection of the concrete cone body would be smaller.

Since the measured crack opening was smaller under dynamic than under static loading, it can be concluded that in most of the load range, the measured crack opening is dominated by the deflection of the concrete breakout cone, and that the reinforcement in the concrete specimens was adequate to resist the expansion force of the anchor.

The additional crack opening may also be affected by other factors. In the case of Expansion Anchor II, the change of failure mode from cone breakout to pullout under dynamic load could reduce the additional concrete opening dramatically, since the deflection of concrete breakout cones did not occur.

The Sleeve Anchor's large increase in additional crack opening may be related to its unique stepped design, which might produces extremely high instantaneous expansion forces when the cone contacts the step at the inside of the sleeve.

Although the additional crack opening measured at the concrete surface during testing is subjected to several factors, comparing the cracked opening by different anchors under the same load condition may still tell the difference in the expansion forces, especially at a small load range.

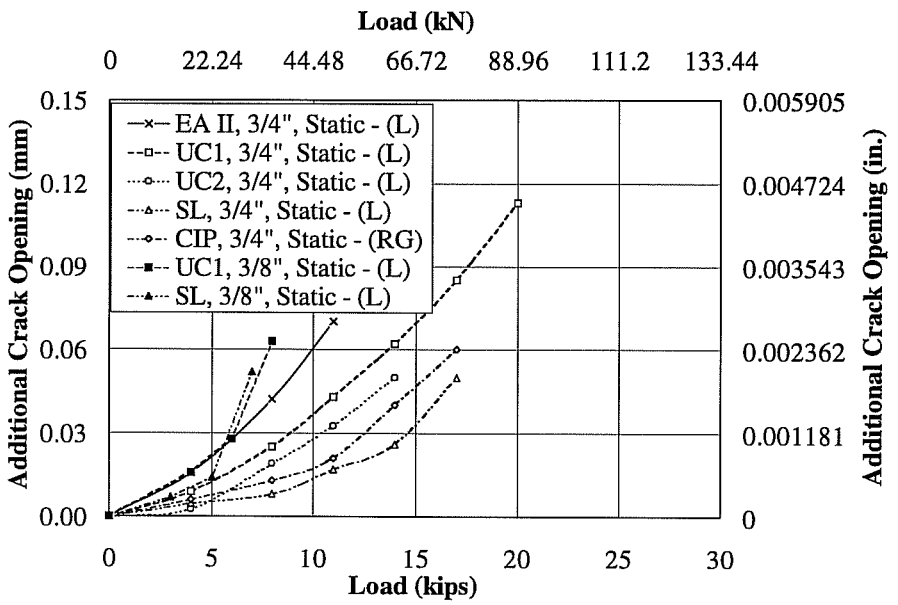

Figure 6.12 Additional Crack Opening versus Static Tensile Load

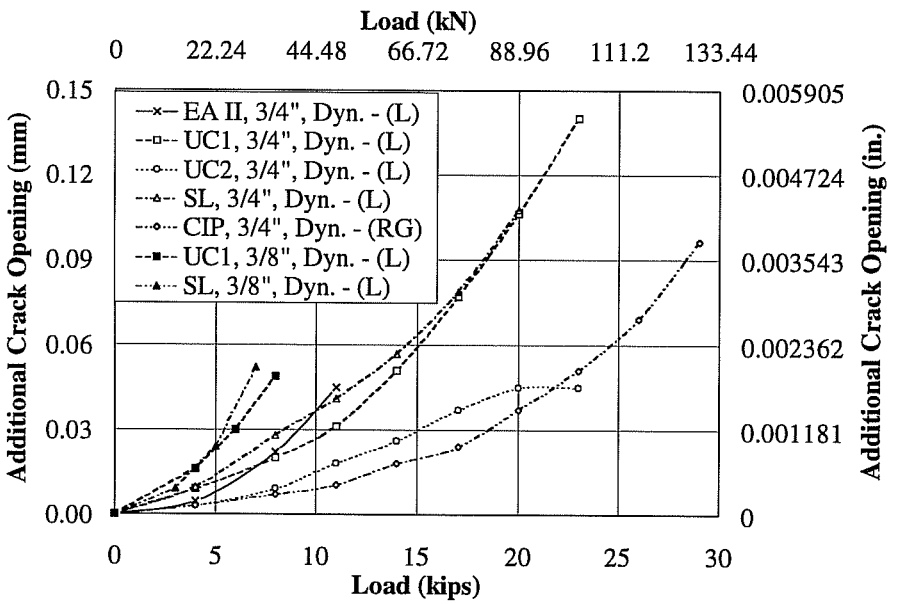

Figure 6.13 Additional Crack Opening versus Dynamic Tensile Load

6.3 Discussion of Results of Double-Anchor Shear Connection Tests under Eccentric Shear

In the following, the test results on double-anchor shear connections are discussed in detail. In addition, to better understand the basic mechanism of the change in load capacity, the shear load at the front anchor and the fracture load at the back anchor, calculated using the measured tension and bending moment at the center of the baseplate, are also discussed. However, it was sometimes very difficult to distinguish points corresponding to shear redistribution form front to back anchors. In such cases, these points were simply estimated based on all available curves.

6.3.1 Effect on Capacity of Gaps between the Baseplate and Anchor Shanks

In most tests, the gaps between the baseplate and anchor shanks were visually inspected before the test started. From the table in Appendix C, it can be seen that the conditions of gaps varied from test to test. However, there is no direct correlation between the gap and the capacity of the connection, especially for the first peak load (which is supposedly most affected by the gaps), because of the small displacement associated with concrete breakout under shear.

The amount of oversize of the holes in the inserts was controlled at 1/16 inch (1.59 mm). The drill bits are larger in diameter than the anchor sleeves by less than 1/16 inch (1.59 mm). In the worst case, the maximum gap that could occur at either anchor is the summation of the two oversizes. This is still a little smaller than the horizontal displacement of the baseplate at the first peak load (averaging 0.15 inch (3.8 mm) in most test series). For this reason, the gaps apparently had little effect on the distribution of the shear force to each anchor.

Table 6.1 Calculated Shear Loads in Front Anchors at First and Second Peak Loads

Tests	First Peak Load				Second Peak Load			
	Baseplate Tension		Shear at Front Anchor		Baseplate Tension		Shear at Front Anchor	
	kips	kN	kips	kN	kips	kN	kips	kN
Uncracked, Static	10.6	47.1	9.9	44.0	16.6	73.8	3.9	17.3
Uncracked, Dynamic	7.4	32.9	15.4	68.5	16.6	73.8	8.0	35.6
Cracked, Static	9.6	42.7	7.6	33.8	16.9	75.2	3.0	13.3
Cracked, Dynamic	10.3	45.8	8.4	37.4	14.7	65.4	9.1	40.5
Cracked, Hairpins, Static	8.1	36.0	13.5	60.0	15.2	67.6	7.8	34.7
Cracked, Hairpins, Dynamic	8.6	38.3	14.2	63.2	12.3	54.7	13.1	58.3

6.3.2 Discussion of Shear Capacity of Front Anchors

To provide more information on how the double-anchor shear connection behaved under different conditions, the shear loads on the front anchor at the first and at the second peak load, were calculated by subtracting the shear force on the back anchor and the friction between the baseplate and the concrete from the external load, assuming a friction coefficient of 0.15 and ignoring the tension force in the front anchor. The results are tabulated in Table 6.1. The shear forces in the front anchors were compared in Figures 6.14 and 6.15

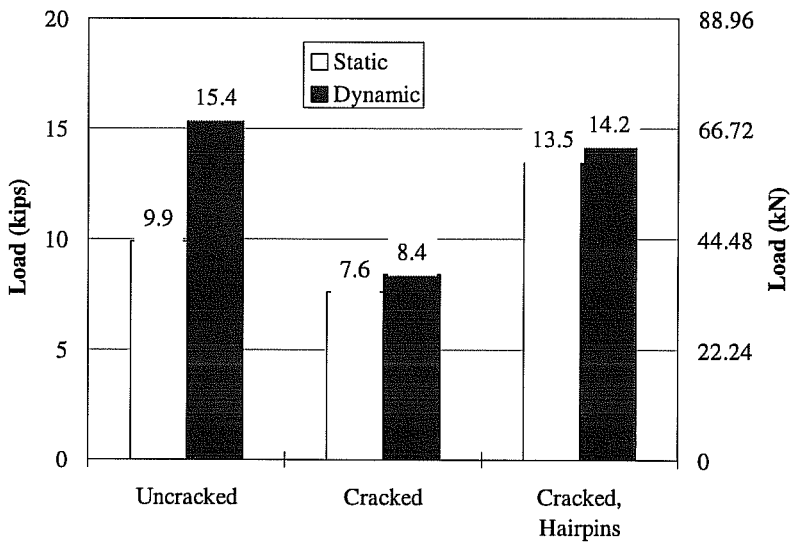

Figure 6.14 Comparison of Shear Forces on Front Anchor at Concrete Breakout of Double-Anchor Shear Connections with Cast-in-Place Anchors

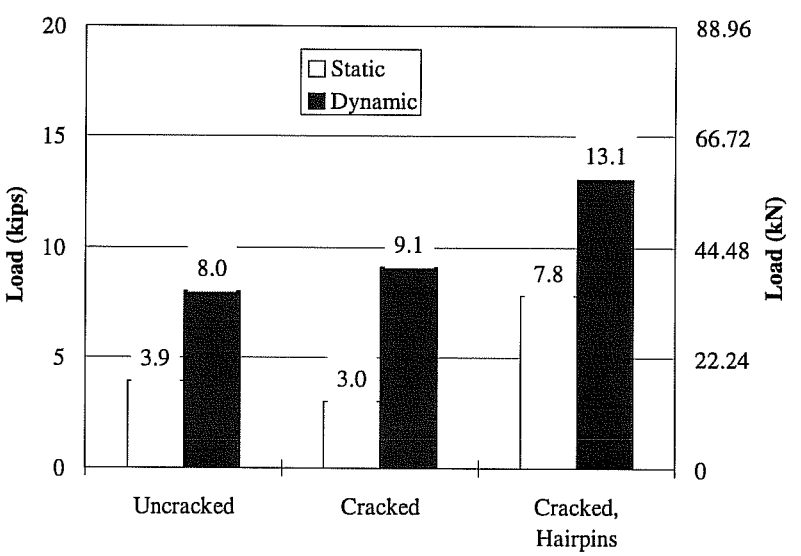

Figure 6.15 Comparison of Remaining Shear Force on Front Anchor at Failure of Back Anchor of Double-Anchor Shear Connections with Cast-in-Place Anchors

These values agree with the observations made by Hallowell (1996) on the single-anchor shear tests. The conclusions are summarized as follow:

a) Cracking in concrete decreases concrete breakout capacity of the front anchors. In these tests, the static capacity decreased by 23%, and dynamic capacity by 45%, in cracked concrete compared to those in uncracked concrete.

b) Hairpins increase the concrete breakout capacity of the front anchors. In cracked concrete, the presence of hairpins increased the capacity by 77.6% under static loading, and by 69.0% under dynamic loading. The shear breakout capacity under static loading in cracked concrete with hairpins even exceeds that in uncracked concrete without hairpins.

c) Under dynamic loading, the concrete breakout capacity is greater than the corresponding static capacity. If a hairpin is present, the percentage of increase due to dynamic loading might be smaller, because the portion of the load capacity due to hairpins is not much affected by increased loading rates in this range. In the case of uncracked concrete, the dynamic capacity increased by 54% than static one. Under dynamic loading, the concrete breakout increased by 10.5% in cracked concrete without hairpins, and by 5.2% in cracked concrete with hairpins, compared to the corresponding tests in uncracked concrete.

d) With hairpins, the shear load remaining on the front anchor after concrete breakout increases dramatically. Under static loading, the remaining load in cracked concrete with hairpins is twice as much as in uncracked concrete without hairpins, and 2.6 times that in cracked concrete without hairpins. Under dynamic loading, the remaining load in cracked concrete with hairpins is 1.6 times that in uncracked concrete without hairpins, and 1.44 times that in cracked concrete without hairpins.

6.3.3 Discussion of Steel Fracture Capacity of Back Anchors

From Figure 6.16 and Table 5.3, it can be seen that the elliptical interaction equation with an exponent of 1.8 describes quite well the steel fracture capacity of the back anchor under oblique load. In most cases, the average values are very close to 1.0, with small coefficients of variation. Only in the dynamic tests in uncracked concrete, is the average considerably higher (1.11), which might be related to the higher loading rate. Generally speaking, under the same conditions, dynamic loading increases the fracture capacity slightly (Figure 6.16).

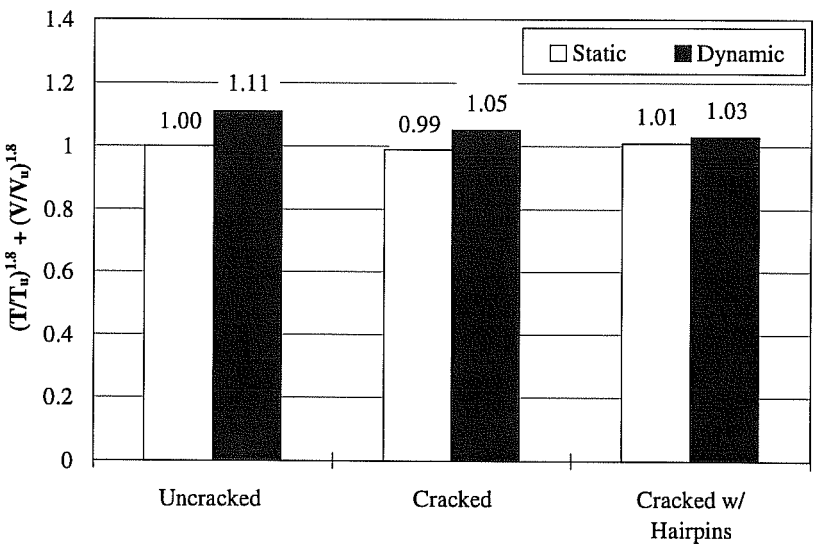

Figure 6.16 Average Value of Elliptical Interaction Calculation of an Exponent of 1.8

In Figure 6.17, the calculated forces on the back anchor are compared with an elliptical interaction curve with an exponent of 1.8 and the trilinear interaction equation. It can be seen that most test results correspond very closely to that curve. The trilinear interaction equation is conservative for all test results.

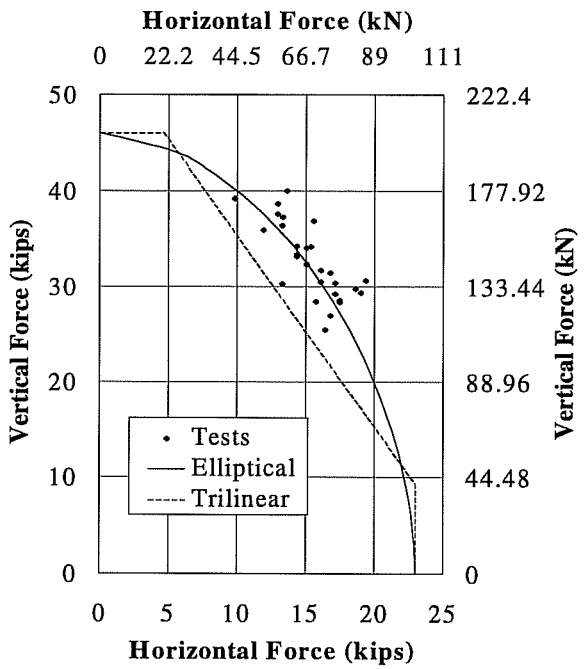

Figure 6.17 Comparison of Test Results of Back Anchors of Double-Anchor Shear Connections with Elliptical Interactive Equation with Exponent of 1.8 and Trilinear Interaction Equation

6.3.4 Discussion of Results of Test Series 3-9

As the baseline tests, Series 3-9 was conducted under static loading in uncracked concrete without hairpins.

The eccentric shear capacity of the connection with a single back anchor was predicted to be 21.8 kips (97.0 kN) with the plastic method, using a friction coefficient of 0.15 and an exponent of 1.8 in the interaction equation. That predicted capacity was about 13% lower than the test results. The extra capacity was believed due to the remaining load on the front anchor after the concrete edge broke out under shear (5.3 kips (23.6 kN)).

The average tension force in the baseplate at front anchor broke out was 10.6 kips (47.1 kN). Assuming a friction of coefficient of 0.15, the shear capacity of the front anchor was 9.9 kips (44.0 kN). This is less than the theoretical prediction of Equation 2-10 (12.5

kips (55.6 kN)), based on concrete strength of 4300 psi (29.6 MPa). The friction between the concrete and the tip of the baseplate at the compression side might reduce this shear capacity, as a consequence of additional shear force on the concrete edge in addition to the shear force of the near-edge anchor. Additionally, the compression force from the baseplate on the concrete might also affect on this capacity. However, more study is needed on this issue.

6.3.5 Effect of Dynamic Loading on Capacity of Double-Anchor Shear Connections in Uncracked Concrete

Figure 6.18 shows that capacity of double-anchor shear connections in uncracked concrete increases under dynamic loading. The increases in the first peak load, second peak load, and overall ultimate capacity are 11%, 18%, and 16% respectively.

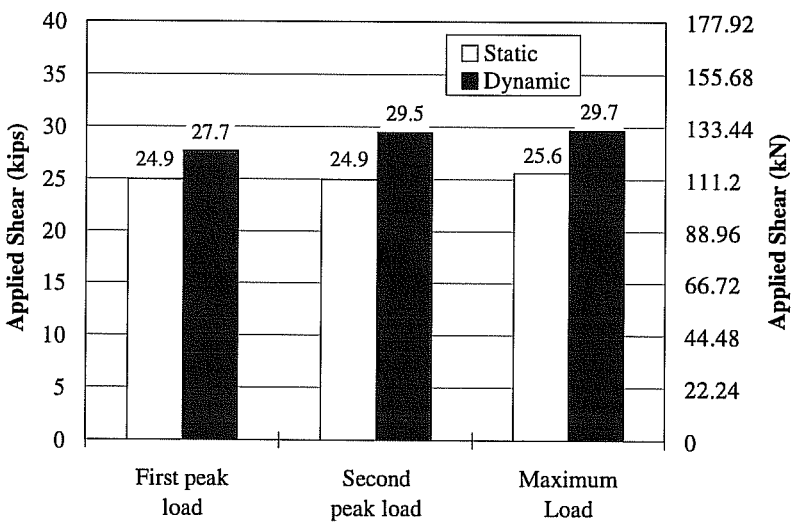

Figure 6.18 Effect of Dynamic Loading on Capacity of Double-Anchor Shear Connections with Cast-in-Place Anchors in Uncracked Concrete

As seen from Table 6.1, the reason for the increase in first peak load is an increase of 55% in the shear load capacity of the front anchor compared to that under static loading in uncracked concrete.

The increases in the second peak load and the ultimate load capacity (four out of five maximum loads occurred at the second peak load) were partially due to the increased remaining shear capacity of the front anchor at large displacements (8.6 kips (38.3 kN)), and mainly due to the increased capacity of the back anchor at a higher loading rate. According to Figure 6.16, the average fracture capacity of the back anchor of this series exceeded its average capacity in the whole test series, probably due to the higher loading rate.

6.3.6 Effect of Cracks on Static Capacity of Double-Anchor Shear Connections without Hairpins

Figure 6.19 shows the effect of cracks on the static capacity of Double-Anchor Shear Connections without hairpins. Compared to the results in uncracked concrete, the first peak load decreased by 16%, the second peak load decreased by only 2%, and the maximum load by 5%. However, the second peak load is still higher than the theoretical load capacity, 21.8 kips (97.0 kN), of a connection with only one back anchor.

Based on the measured tension force in the baseplate and a 0.15 friction coefficient, the average shear force at the front anchor was 8.2 kips (36.5 kN) at the first peak load. This is only 77% of the calculated value in the tests in uncracked concrete, and is the reason for the smaller first peak load and much smoother load-displacement curves. Since the back anchor determines the load capacity after the concrete edge breaks out, and the crack has little effect on the anchor steel fracture, the second peak load decreases only by 2%. This is due to a smaller remaining load capacity of the front anchor because of concrete cracking (3.3 kips (14.7 kN)).

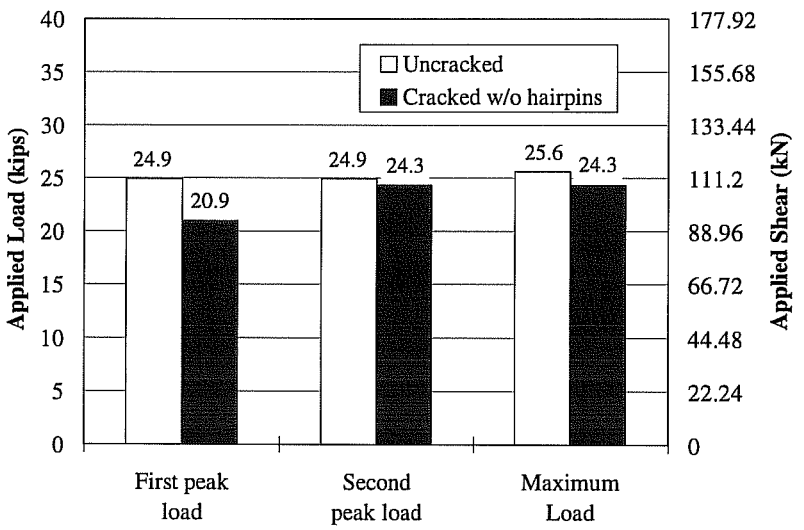

Figure 6.19 Comparison of Load in Different Concrete Specimens under Static Shear Loading

6.3.7 Effect of Hairpins on Static Capacity of Double-Anchor Shear Connections in Cracked Concrete

Figure 6.20 shows that the static capacity of double-anchor shear connections in cracked concrete increases due to hairpins.

In cracked concrete with hairpins, the first peak load increased by 8.6%, compared to the results in cracked concrete without hairpins; however, this is still smaller than that in uncracked concrete without hairpins. This is believed due to the slightly larger shear load of the front anchor at the first peak load with the help of hairpins (8.4 kips (37.4 kN)), compared to that in cracked concrete without hairpins (7.6 kips (33.8 kN)).

The increase in the second peak load and in the maximum capacity was much higher, at 19%. As observed in single-anchor shear test, after the concrete edge broke off, the anchor could still retain its load with the help of hairpins. This is exactly the reason for the greater increase in capacity. According to Table 6.1, the shear force on the front anchor at the maximum load was 9.1 kips (40.5 kN) in cracked concrete with hairpins, three times

that of cracked concrete without hairpins. For the same reason, the maximum load of connections in cracked concrete with hairpins is 13.3% higher than in uncracked concrete.

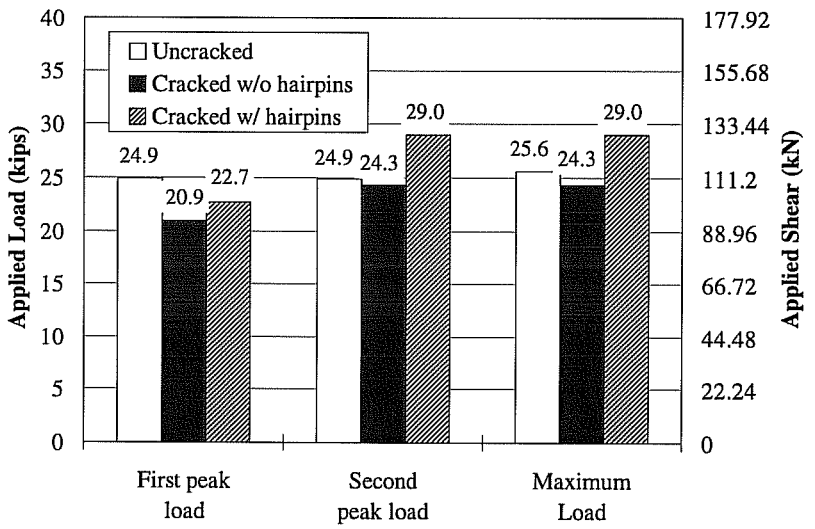

Figure 6.20 Effect of Hairpins on Static Capacity of Double-Anchor Shear Connections with Cast-in-Place Anchors

6.3.8 Effect of Cracks on Dynamic Capacity of Double-Anchor Shear Connection

Figure 6.21 shows the effect of cracks on the dynamic capacity of double-anchor shear connections.

In cracked concrete under dynamic loading, the first peak load, the second peak load, and the maximum load all decreased by 5.8%, 5.8%, and 3.4% respectively, compared to the corresponding values in uncracked concrete under dynamic loading. This was for the same reason discussed in the previous section; that is, the crack reduced the shear breakout capacity of the front anchor.

Under dynamic loading, the shear force on the front anchor at the first peak load decreased by 45% due to cracking. This decrease is much more severe than that experienced under static loading (23%). However, the decrease in the first peak load of the connection was much smaller by only 5.8%, compared to a 19% decrease in the capacity

under static load. This is attributed to the higher shear force in the back anchor, due to the relatively larger horizontal displacement at the first peak load.

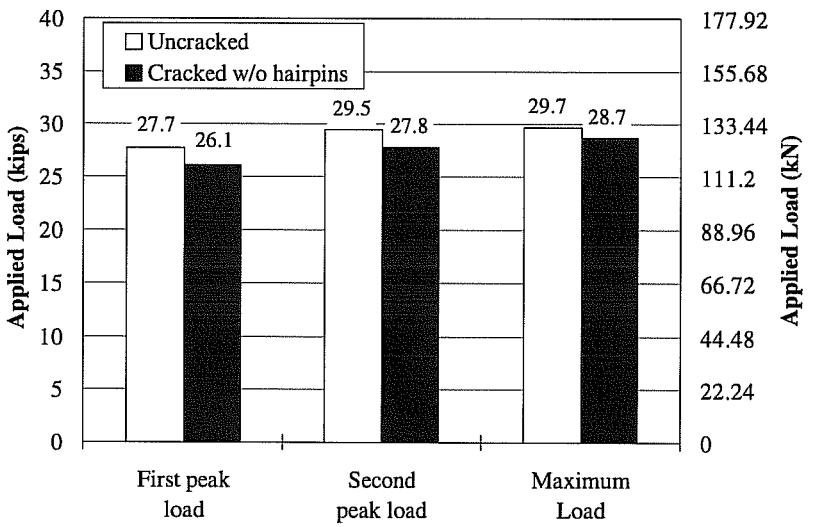

Figure 6.21 Effect of Cracks on Dynamic Capacity of Double-Anchor Shear Connections with Cast-in-Place Anchors

The reason for the decrease in the second peak load is the extremely high steel fracture load in the tests in uncracked concrete, even though the remaining shear load on the front anchor was 14% higher in this case.

6.3.9 Effect of Hairpins on Dynamic Capacity of Double-Anchor Shear Connections in Cracked Concrete

As shown in Figure 6.22, hairpins increased the dynamic load capacity of double-anchor shear connection in cracked concrete.

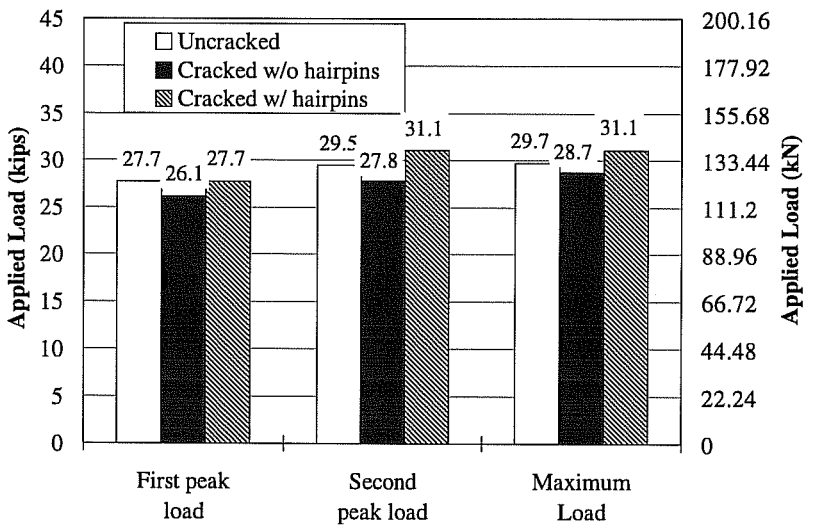

Figure 6.22 Effect of Hairpins on Dynamic Capacity of Double-Anchor Shear Connections in Cracked Concrete

Compared to the dynamic test results in cracked concrete without hairpins, the first peak load increased by 6.1%, and the second peak load and the maximum load increased by 11.9% in the dynamic tests in cracked concrete with hairpins. The second peak load and the maximum load also exceeded those in uncracked concrete without hairpins. All are owing to the increased shear capacity of the front anchor, due to the help of the hairpins.

Some load-displacement curves of dynamic tests in cracked concrete with hairpins exhibited very different characteristics. In these tests, the maximum load was reached well before the back anchors fractured. In those tests, the horizontal and vertical displacement at the maximum load are relatively small.

6.3.10 Effect of Dynamic Loading on Capacity of Double-Anchor Shear Connections in Cracked Concrete without Hairpins

Figure 6.23 shows the increase in capacity of double-anchor shear connections under dynamic loading for the tests in cracked concrete without hairpins.

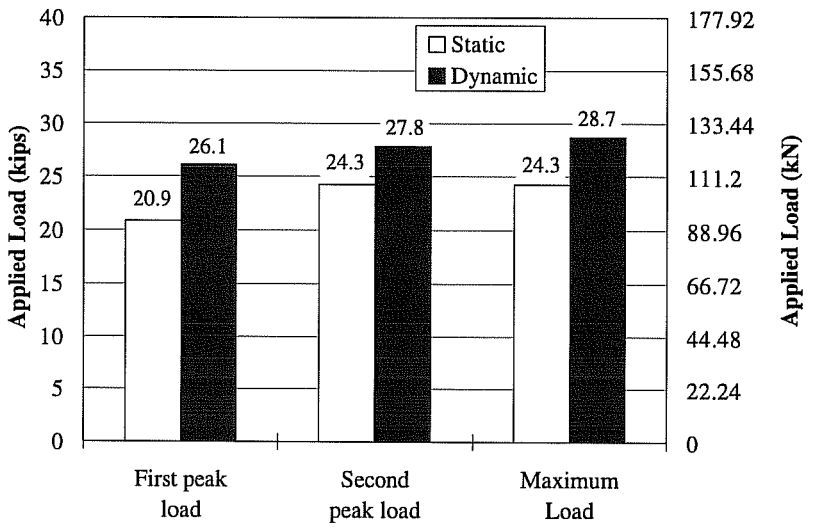

Figure 6.23 Effect of Dynamic Loading on Capacity of Double-Anchor Shear Connections in Cracked Concrete without Hairpins

The increase due to the dynamic loading in the first peak load, second peak load, and the maximum load were respectively 24.9%, 14.4%, and 18.1%. These increases were mainly due to the increase in the shear capacity of the front anchor under dynamic loading.

6.3.11 Effect of Dynamic Loading on Capacity of Double-Anchor Shear Connections in Cracked Concrete with Hairpins

Figure 6.24 illustrates all the increases in the load capacities of double-anchor shear connections under dynamic load with hairpins.

As in the other cases under dynamic loading, the dynamic loading in tests on connections in cracked concrete with hairpins also increased the first peak load, the second peak load, and the maximum load by 22%, 7%, and 7% respectively, compared to similar tests under static loading. In this case, however, the increase in the second peak load, and also in the maximum load, was much smaller than those in the other cases. This increase is also attributed to the higher shear forces on the front anchors.

The load-displacement curves show that the load capacity of the connection when the back anchors fracture is lower than the maximum load in most tests and close to that under static loading. The higher loading rate used in tests does not increase the steel strength of the back anchors much, and may not change the remaining shear force of the front anchors after the concrete cracks either. Therefore, the fracture load of the connections under dynamic loading is not expected to increase much.

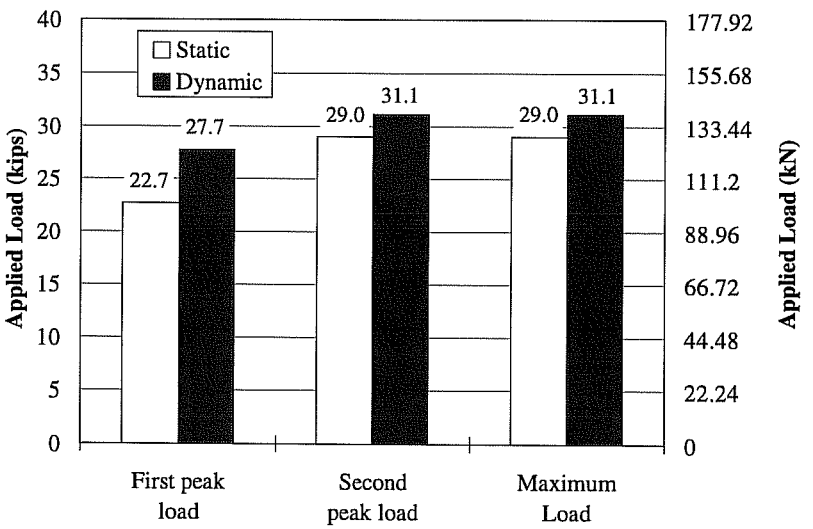

Figure 6.24 Effect of Dynamic Loading on Capacity of Double-Anchor Shear Connections in Cracked Concrete with Hairpins

6.3.12 Displacements of Double-Anchor Shear Connections at Maximum Load

Figures 6.25 and 6.26 compare the average horizontal and vertical displacements, under various conditions, at the second peak load of the double-anchor shear connection. In most tests, the second peak load is the maximum load in the test. Therefore, the average displacements at maximum load are basically discussed here . The scatter in those displacements is much greater than that of the maximum load, especially in dynamic tests

in cracked concrete with hairpins. However, they are still an indicator of the displacement behavior of double-anchor shear connections.

Generally speaking, a larger displacement is associated with a larger load. In most cases, the dynamic test had a higher load capacity than the corresponding static test, and therefore had greater average displacements in both directions.

However, the displacement at the maximum load was also controlled by the loading angle on the back anchor, as a result of the different force distribution to each anchor under various conditions. For example, in dynamic tests in cracked concrete with hairpins, a higher external load resulted from a higher tension and smaller shear on the back anchor; therefore, the average horizontal displacement of that series is much smaller than that under dynamic loading without hairpins, even with a greater load capacity.

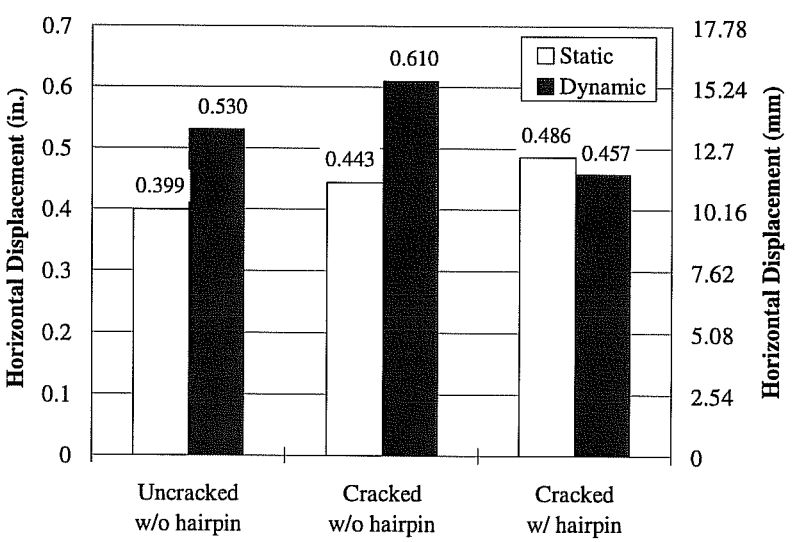

Figure 6.25 Comparison of Horizontal Displacement at Second Peak Load of Double-Anchor Shear Connections with Cast-in-Place Anchors

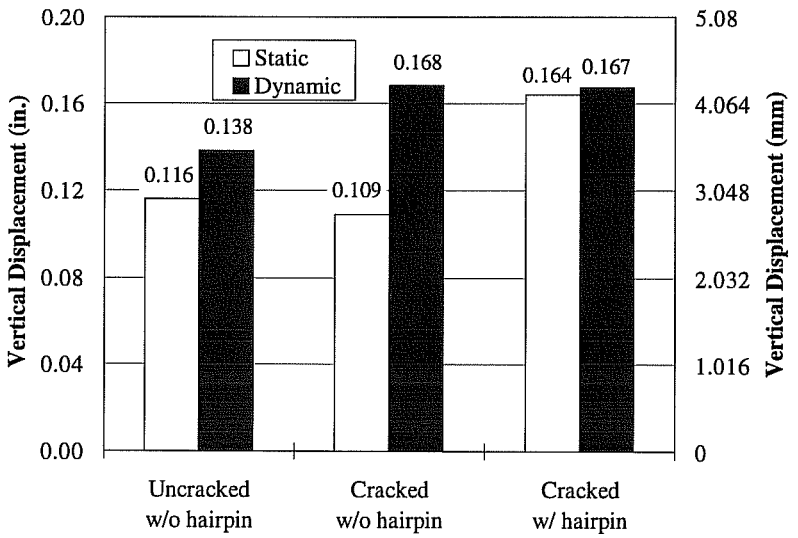

Figure 6.26 Comparison of Vertical Displacement at Second Peak Load of Double-Anchor Shear Connections with Cast-in-Place Anchors

Again, because of the particular characteristic of the load-displacement curves for dynamic tests in cracked concrete with hairpins (that is, the maximum load was achieved before the back anchors fractured), the average vertical and horizontal displacements at the maximum load were very close to those of static tests in cracked concrete with hairpins. Comparing the load-displacement curves of the tests in cracked concrete with hairpins under static and dynamic loading, it is clear that under dynamic loading, the back anchor of the connections failed at much larger displacements than under static loading.

6.4 Discussion of Test Results of Multiple-Anchor Connections

The following sections discuss the test results of the multiple-anchor connections of Task 4. Because only one test was conducted for each configuration, no solid conclusion can be drawn on the load behavior of such connections .

Furthermore, the hand-tightening of anchors after each phase of dynamic loading could have affected the tension load distribution on the tension anchors, if the anchors were not tightened equally. Also the reduced tensile deflection of anchors could also have

influenced the load distribution among all anchors, especially the distribution of shear force, because with a relatively smaller deflection, the back anchors would have greater horizontal stiffness.

If several loading sequences were performed for a single test, the displacement at 12 inches (305 mm) above the concrete was estimated by adding back the estimated amount of displacement reduced by hand-tightening anchors after each loading sequence. Therefore, the displacement behavior described here might not reflect the real situation, either.

6.4.1 Effect of Cyclic Loading on Concrete Spalling in Multiple-Anchor Connections

The concrete spalling in front of anchors was more severe in the concrete between the two rows of anchors than outside the rows, in the tests with UC1 anchors and with EA II anchors. During cyclic loading, the concrete in front of the compression anchors was confined by the baseplate, while the concrete in front the back anchor had no confinement at all. As a result, the concrete between the rows of anchor spalled worse than that outside. However, concrete spalling also depends on the anchor stiffness. An anchor with a smaller shank diameter has less flexural stiffness, resulting in a higher local stress on the concrete surface when the anchor is loaded in shear. In this case, even with confinement of the

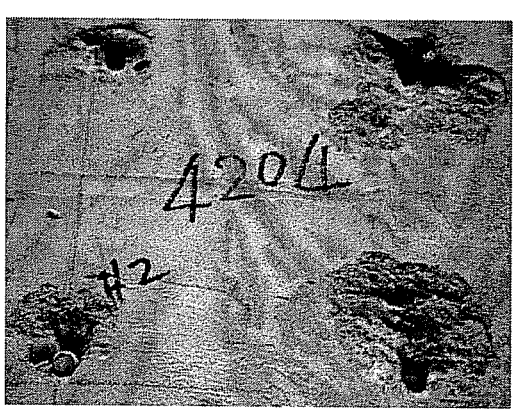

Figure 6.27 Concrete Spalling in Multiple-Anchor Connection with EAII Anchor in Dynamic Cyclic Loading

baseplate, the concrete will still have severe spalling, as happened in the test on the connection with EA II anchors (Figure 6.27).

6.4.2 Effect of Dynamic Reversed Cyclic Loading on Behavior of Multiple-Anchor Connections

In Figures 6.28 and 6.29, the load-displacement curves of dynamic tests under eccentric shear at 12 inches (305 mm) and 18 inches (457 mm) respectively, are compared with the static tests on the same configuration The following conclusions can be drawn from these figures:

1) The dynamic load-displacement curves follow the static load-displacement curves over most of the displacement range, differing only near the ultimate load.

2) The maximum load achieved in dynamic tests was close to the maximum load capacity under static loading (7% higher at a 12-inch eccentricity, 7% smaller at an 18-inch eccentricity). However, due to the small number of tests, this observation is not definitive.

3) The most significant effect of dynamic reversed loading is the increase in total displacement, measured at 12 inches above the concrete specimen. As shown in both figures, the displacement at the baseplate increased slightly (by about 0.1 inch (2.54 mm) at a 12-inch (305-mm) eccentricity) or not at all (at an 18-inch (457-mm) eccentricity, probably due to a smaller load). The increase in horizontal displacement of the baseplate was due mainly to the concrete spalling in front of the anchors, and also to some contribution from the gaps between the baseplate and the anchor and between the anchor and the concrete. The increase in the displacement measured at 12 inches (305 mm) above the concrete specimen was much greater, mainly because of the larger tensile displacement of the anchors under dynamic cyclic loading. However, the smaller displacement of anchors with the probably premature shear failure in

the static test at the 12-inch (305-mm) eccentricity might be attributed to the increase in the displacement under dynamic load.

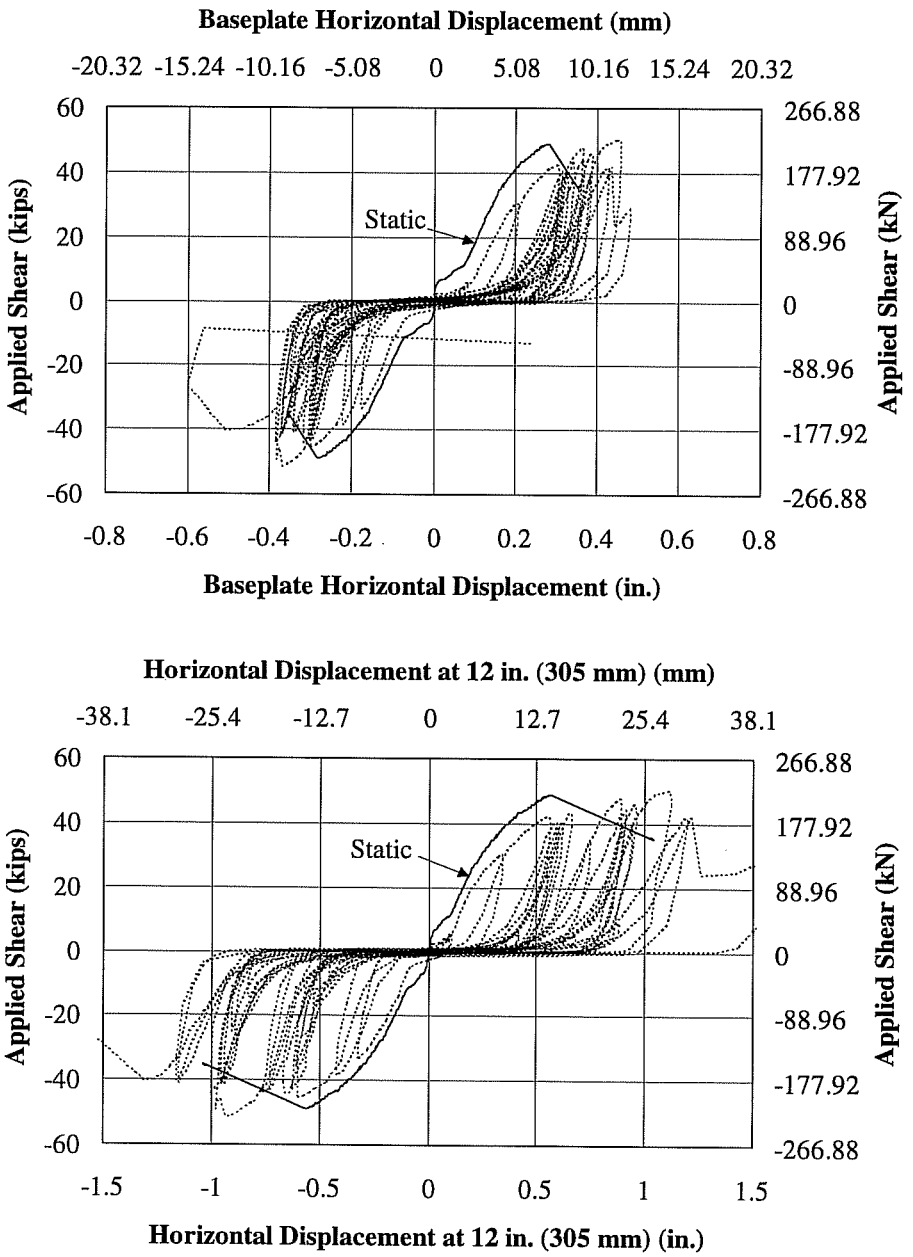

Figure 6.28 Comparison of Static and Seismic Load-Displacement Behaviors of Multiple-Anchor Connections with UC1 Anchors under Shear at 12-inch (305-mm) Eccentricity

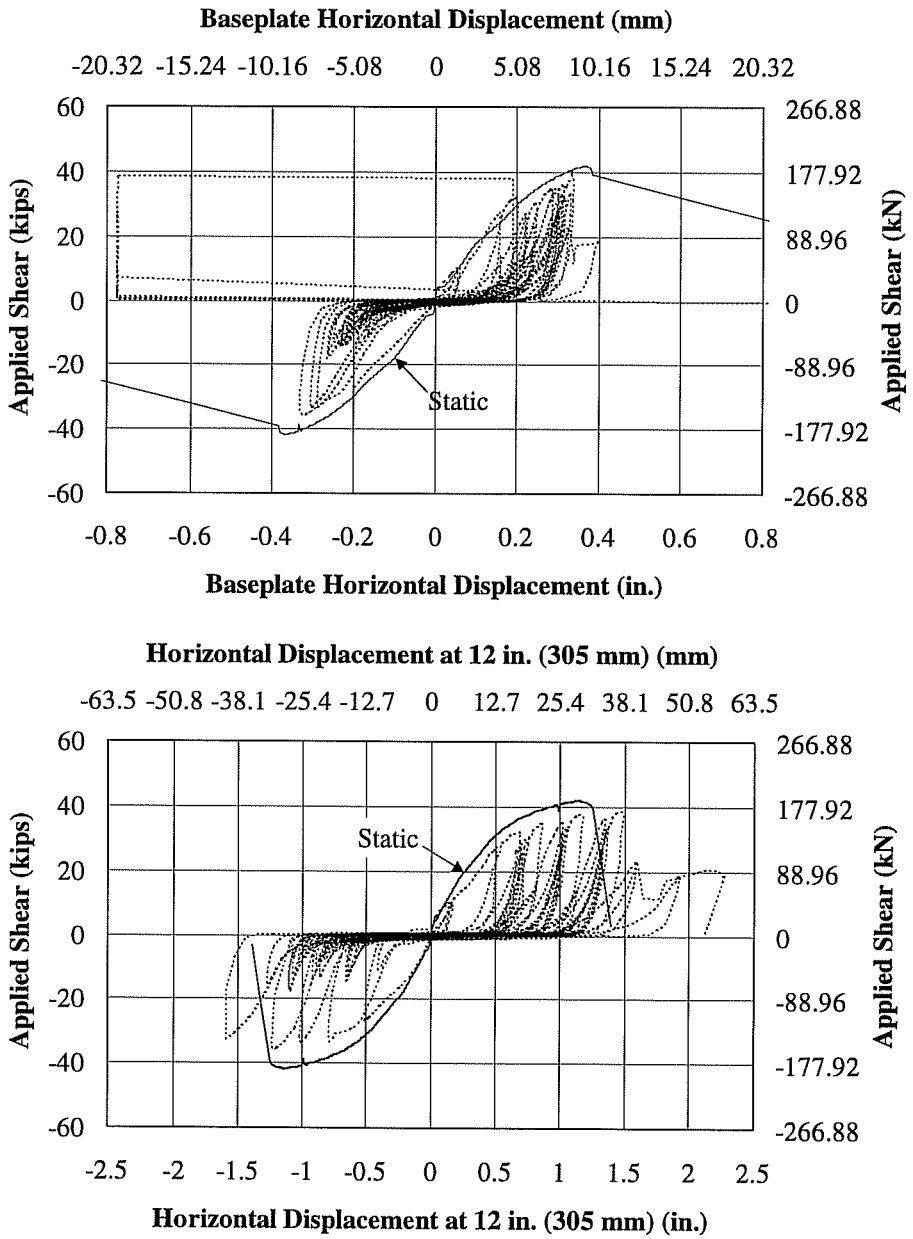

Figure 6.29 Comparison of Static and Seismic Load-Displacement Behaviors of Multiple-Anchor Connections with UC1 Anchors under Shear at 18-inch (457-mm) Eccentricity

The test on a connection with Expansion Anchor II under dynamic reversed cyclic loading also showed large displacements of about 1 inch (25.4 mm) measured at 12 inches (305 mm) above the concrete, although there is no corresponding static test with which this can be compared.

6.4.3 Effect of Baseplate Flexibility on Load-Displacement Behavior of Multiple-Anchor Connection

Test 4203 was designed to be conducted with a flexible baseplate. Based on a tension coupon test, the yield stress of the baseplate is 56.5 ksi (390 MPa). According to that value, the baseplate had a yield moment of 169.5 kip-inches (19.1 kN-m). Base on the measured maximum load of the test, the moment on the baseplate at the edge of the attached member was 205.2 kip-inches (23.2 kN-m), 21% higher than the calculated yield moment. However, only a slight yielding deformation of the baseplate was observed after

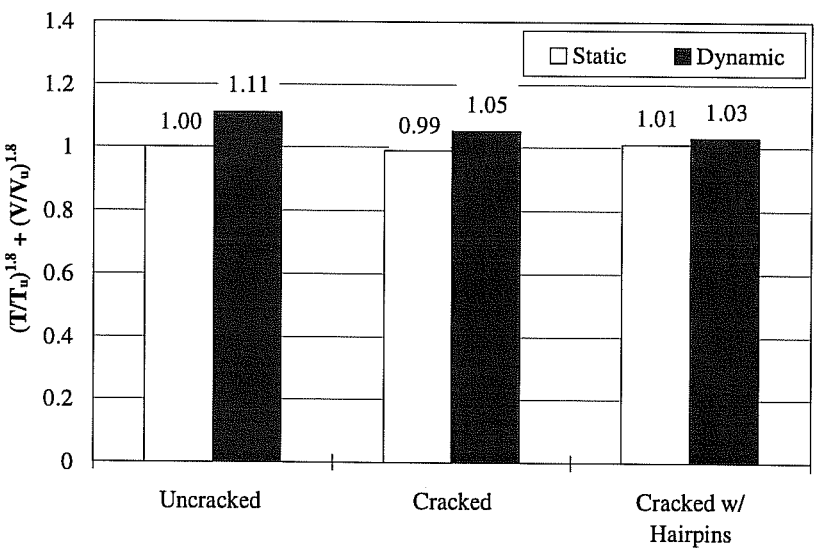

Figure 6.30 Comparison of Maximum Load and Maximum Displacement Between Multiple-Anchor Connections with Rigid and Flexible Baseplate, with UC1 Anchors, in Seismic Eccentricity Shear at 12 Inch (305 mm)

the test (Figure 5.16).

Figure 6.30 compared the maximum load and the maximum horizontal displacements reached before multiple-anchor connections connection failed, between Test 4203 with a flexible baseplate and Test 4205 with a rigid baseplate, both with UC1 anchor, loaded in dynamic eccentric shear at 12 in. (305 mm). Comparing their load-displacement behavior, the following can be noted:

1) Baseplate flexibility led to no significant change in the load capacity. The maximum load achieved in Test 4203 was only about 2.7% smaller that that of Test 4205. Since the plastic deformation was very small, there should be little effect on the distributions of tension forces to the anchors.

2) The displacement at 12 inches was a little larger in Test 4203 (with a flexible baseplate) than in Test 4205 (with a rigid baseplate). While, the test with a flexible baseplate had a smaller displacement at the baseplate. These may be attributed to the slight deformation of the baseplate observed in test, which increase the amount of rotation of the attached member, so as the measured displacement at 12 inches above the concrete.

6.4.4 Comparison of Dynamic Tests of Multiple-Anchor Connections in Cracked Concrete with Static Tests in Uncracked Concrete

In Figures 6.31 and 6.32, the load-displacement curves of the tests under dynamic loading in cracked concrete are compared with the curves from the corresponding static tests in uncracked concrete.

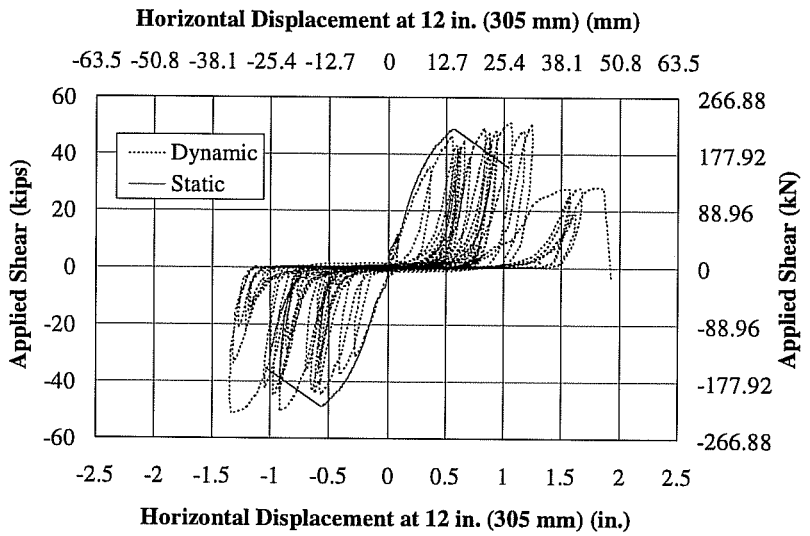

Figure 6.31 Comparison of Seismic Load-Displacement Behavior of Multiple-Anchor Connections with UC1 Anchors at 12-inch (305-mm) Eccentricity in Cracked Concrete with Static One in Uncracked Concrete

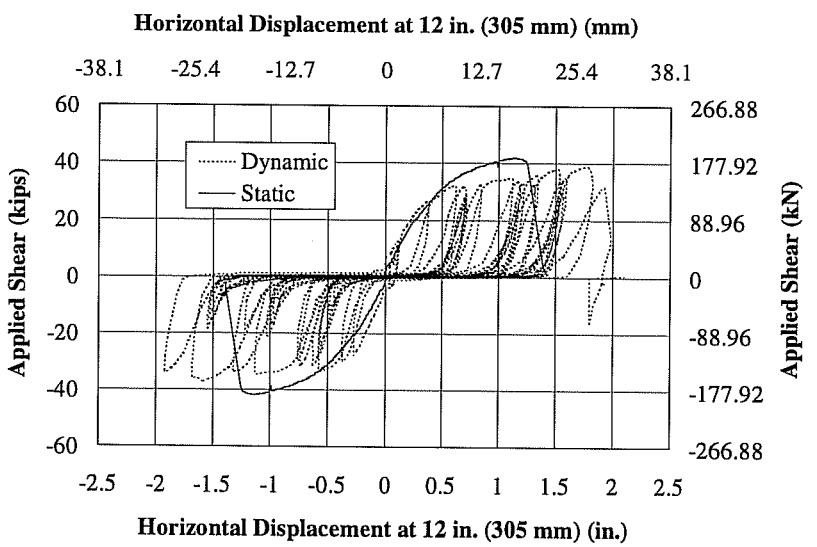

Figure 6.32 Comparison of Seismic Load-Displacement Behavior of Multiple-Anchor Connections with UC1 Anchors at 18-inch (457-mm) Eccentricity in Cracked Concrete with Static One in Uncracked Concrete

The profiles of the load-displacement curves of these tests also follow those of static tests very well, except near the ultimate load. This is similar to results of dynamic tests in uncracked concrete.

6.4.5 Effect of Cracks on Load-Displacement Behavior of Multiple-Anchor Connections under Dynamic Reversed Loading

To compared the dynamic load-displacement behavior of multiple-anchor connections in cracked and uncracked concrete, two characteristic values of connections are used, besides comparing their load-displacement curves: the maximum load capacity reached during the test, and the maximum displacement reached in the test before the connection failed, measured at 12-inch (305-mm)above concrete surface.

Figure 6.33 and 6.34 compare these values.

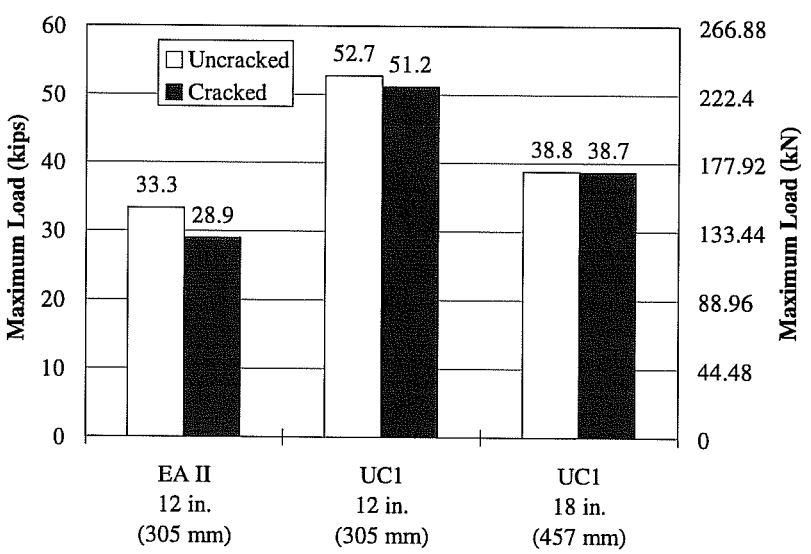

Figure 6.33 Effect of Cracks on Dynamic Load Behavior of Multiple-Anchor Connections

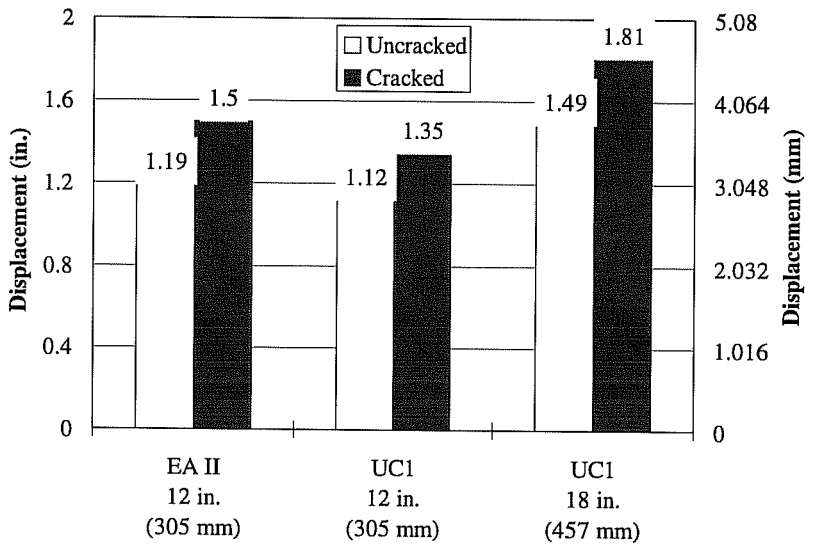

Figure 6.34 Comparison of Maximum Displacement at 12 Inch (305 mm) above Concrete Surface of Multiple-Anchor Connections under Dynamic Reversed Loading in Crack and Uncracked Concrete

Compared to the dynamic tests in uncracked concrete (Series 4-2), the maximum load achieved in dynamic tests on connections with Undercut Anchor 1 in cracked concrete did not change much (Figure 6.33). However, the displacement increased for dynamic tests at both eccentricities in cracked concrete. This is attributed to the cracked concrete specimens, which allowed the anchor heads to slip and expand further with the extra space due to additional crack opening.

Under dynamic loading in cracked concrete, the connection with Expansion Anchor II at 12-in. (305-mm) eccentricity also underwent more displacement than in uncracked concrete under dynamic loading, while the capacity decreased by 13%, although both connections failed by tensile fracture of anchor steel. Also, due to small number of tests, conclusions regarding capacity are tentative.

In the dynamic test on the connection with Expansion Anchor II at 12-in. (305-mm) eccentricity, the horizontal displacement of the baseplate was much larger than in the other

similar test in uncracked concrete, even though the external load was smaller. This correlated with the observation in the test of extensive concrete spalling at the front anchors at both directions. This is attributed to the large number of cycles of loading, and to the low stiffness of anchor shanks.

The dynamic test on a connection with Expansion Anchor II in cracked concrete at an 18-inch (457-mm) eccentricity resulted in pullout failure of anchors. All anchors pulled out by about 3 inches (76 mm) (as shown in Figure 5.19). This illustrated the deleterious effect of cracks on this kind of anchor. It confirms the observation in the single-anchor tests that Expansion Anchor II had the potential to lose its load capacity due to the change of failure mode (from cone breakout to pullout) under dynamic loading. This tendency is exacerbated in cracked concrete.

6.4.6 Effect of Concrete Edges on Multiple-Anchor Connections under Static Loading

Under static eccentric shear, near-edge connections without hairpins behaved similarly to the double-anchor shear connections without hairpins discussed in Section 6.3.4. They all exhibited a two-peak load-displacement behavior. The first peak occurred when the concrete edge broke out under shear of the front anchors. The second peak occurred at a much larger displacement, when the back anchors fractured.

The shear load at which the concrete edge broke out was almost identical at both eccentricities (Figure 6.35).

The calculated failure load when the back anchors fractured is 32.9 kips (146 kN) for the connection at a 12-inch (305-mm) eccentricity, and 27.6 kips (123 kN) for the connection at an 18-inch (457-mm) eccentricity, which are respectively 8.1% and 9.3% lower than the test results of obtained from tests of near-edge multiple-anchor connections with UC1 anchors at both eccentricities. From the curves of tension forces on anchors versus the external loading, there was a certain amount of tension force retained on these two front anchors at both eccentricities when the back anchors fractured. It is reasonable to

conclude that there was also still some remaining shear force on these anchors, which resulted in higher failure loads in tests.

6.4.7 Effect of Concrete Edges on Multiple-Anchor Connections under Dynamic Reversed Loading

In Figure 6.35, the concrete edge breakout load of the multiple-anchor connections without hairpins are compared for different loading conditions.

Compared to the static tests, there was virtually no change in the external load when the concrete edge broke out under dynamic reversed loading. This contrasts with the effect of dynamic loading on the double-anchor shear connections discussed in Section 6.3. The reason is that, in the tests under dynamic reversed loading, concrete breakout occurred almost at the maximum displacement of the pulse of the command signal, when the loading direction was about to change. Therefore, the transient loading rate was much smaller than in the ramp loading tests.

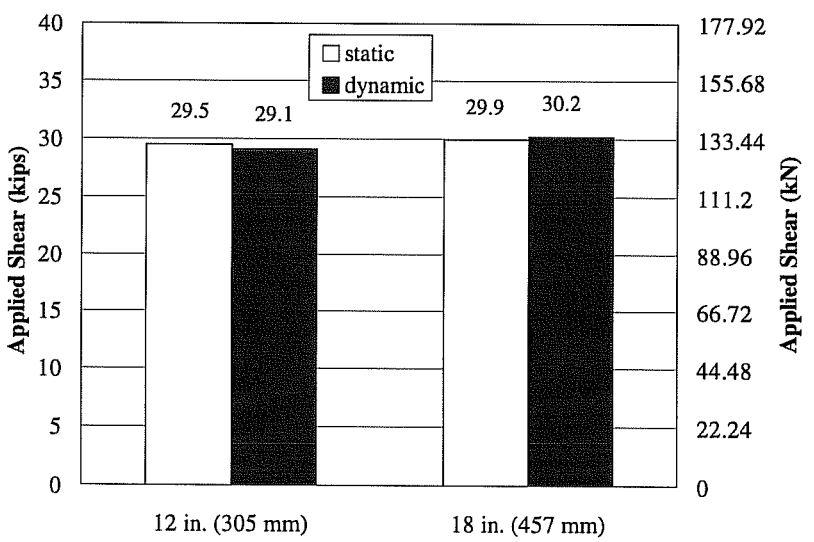

Figure 6.35 Comparison of Concrete Breakout Loads of Near-edge, Multiple-Anchor Connections with UC1 Anchors without Hairpins under Static and Dynamic Loading

After the concrete edges broke out, the capacity in the other direction deteriorated very quickly, with concrete lateral blowout failure by near-edge anchor heads. Since without hairpins, the concrete breakout volume was very large , the concrete edge cover over the near-edge anchor heads reduced dramatically. As a result, the lateral blowout of the near-edge anchors reduced significantly.

6.4.8 Effect of Hairpins on Behavior of Multiple-Anchor Connection under Static Loading

Figure 6.36 compares the concrete breakout load and the maximum load of multiple-anchor connections, with and without hairpins under static loading at a 12-inch (305-mm) eccentricity.

Since undercut anchors were installed in hardened concrete, even with a very careful placement of hairpins and a very accurate location of anchors, it was impossible to install the anchor shank directly against the hairpins. Furthermore, because the diameter of the anchor holes is larger than that of the anchor sleeve, after the anchor head was

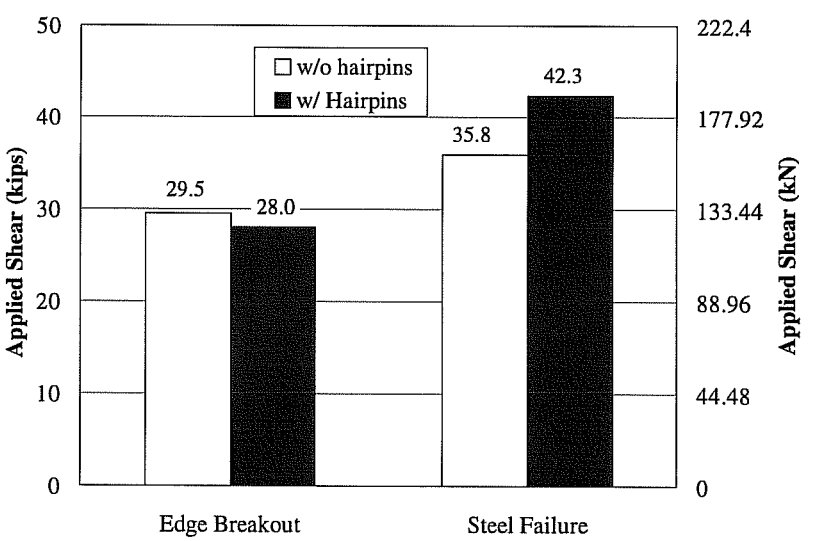

Figure 6.36 Comparison of Load Capacity of Near-Edge, Multiple-Anchor Connections with UC1 Anchors under Static Loading with and without Hairpins

expanded, the anchor would rotate about the head; under shear load, when the sleeve touches the concrete there might still be a gap between the concrete wall and the anchor at the depth of the hairpins. Therefore, the hairpins might not be as effective in immediately increasing the concrete breakout load, as they were for Cast-in-Place anchors. This may explain why there was no increase in the concrete edge breakout load in the static test with hairpins, compared to the test without hairpins.

However, when the concrete edge broke out at a relatively low load, the load-displacement curves dropped only a little, and then continued to rise, with the previous slope. With hairpins, the near-edge anchors can retain much larger shear load after the concrete breakout than those without hairpins. As a result, the ultimate load capacity of the connection with hairpins was 18% higher than that of the corresponding connection without hairpins.

6.4.9 Effect of Dynamic Reversed Loading on Near-Edge Multiple-Anchor Connections with Hairpins

Figure 6.37 compares the static and dynamic load-displacement behaviors of near-edge multiple-anchor connections with hairpins, loaded at a 12-inch (305-mm) eccentricity. It uses the portion of the static load-displacement curve just before the concrete specimen prematurely cracked under the forces of the multiple-anchor connection. The profile of the load-displacement curve under dynamic reversed loading basically follows the static curve.

In Figure 6.38, the concrete breakout load and the maximum load achieved when loading towards the specimen edges are shown, for static and reversed dynamic loading. Again, the concrete breakout load under dynamic loading was almost identical to that under static loading. The maximum load achieved in the dynamic loading, however, is about 9% higher than under static loading. Nonetheless, Figure 6.37 shows that the peak loads after the maximum load are very close to the static curve.

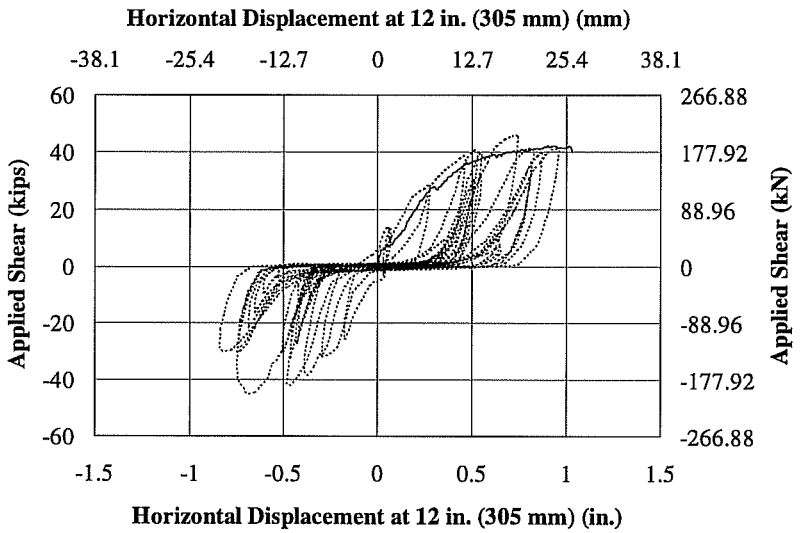

Figure 6.37 Comparison of Load-Displacement Behavior of Near-Edge, Multiple-Anchor Connections with UC1 Anchors with Hairpins, under Static and Seismic Loading

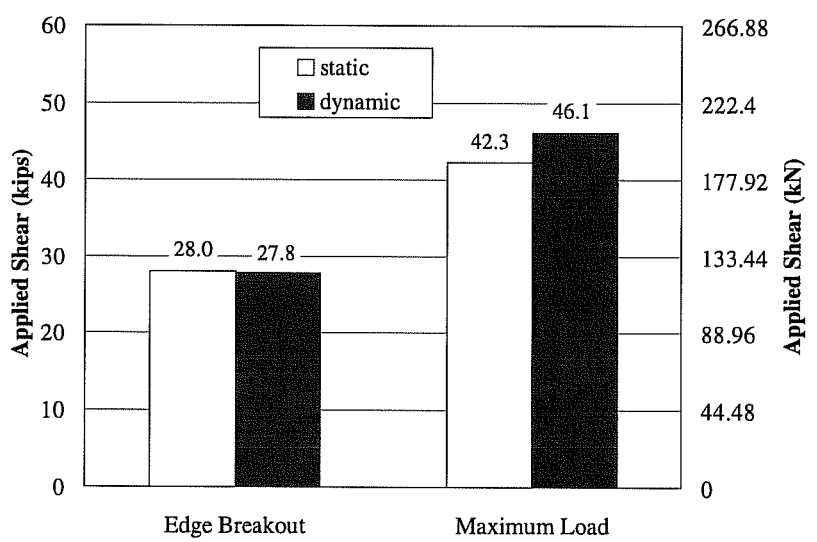

Figure 6.38 Comparison of Capacities of Near-Edge, Multiple-Anchor Connections with UC1 Anchors with Hairpins, under Static and Dynamic Loading towards Specimen Edge

6.4.10 Effect of Hairpins on the Load-Displacement Behavior of Near-Edge, Multiple-Anchor Connections under Dynamic Reversed Loading

Figure 6.39 compares the concrete edge breakout load and the maximum load achieved at both directions, with and without hairpins, of near-edge multiple-anchor connections loaded at a 12-inch (305-mm) eccentricity. Figure 6.40 shows the same comparison for connections with an 18-inch (457-mm) eccentricity.

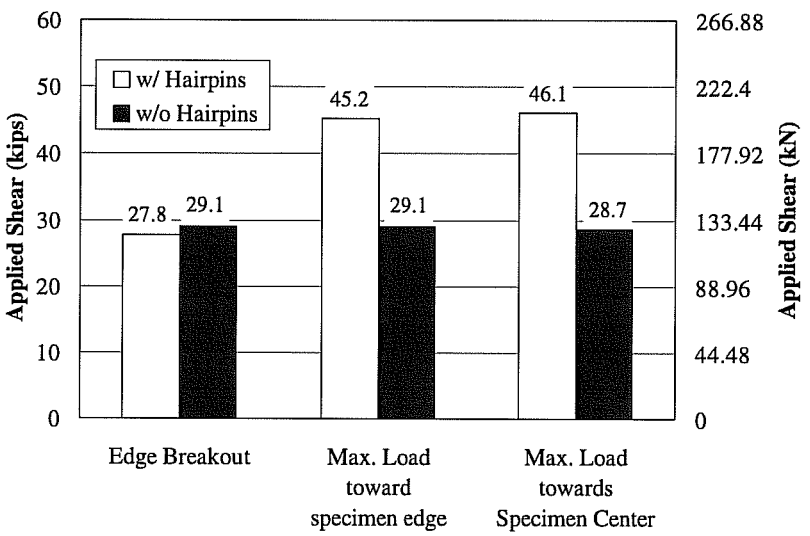

Figure 6.39 Comparison of Capacities of Near-Edge, Multiple-Anchor Connections with UC1 Anchors, with and without Hairpins, Loaded at 12-inch (305-mm) Eccentricity

Hairpins significantly increased the maximum capacity of connections with a 12-inch eccentricity, although the concrete breakout load was very close to that without hairpins. The maximum load achieved when loading towards the specimen edge was 55% higher with hairpins than without, because the hairpins increased the remaining capacity of the near-edge anchors after concrete edge broke out. In addition, the concrete lateral blowout load with hairpins is 60.6% higher with than without hairpins, because of the

smaller concrete breakout volume under shear by the near-edge anchors also due to hairpins.

Hairpins had little effect on the load behavior of the near-edge, multiple-anchor connections loaded at an 18-inch (457-mm) eccentricity. From Figure 6.40, it can be noted that the loads are almost identical in the tests with and without hairpins.

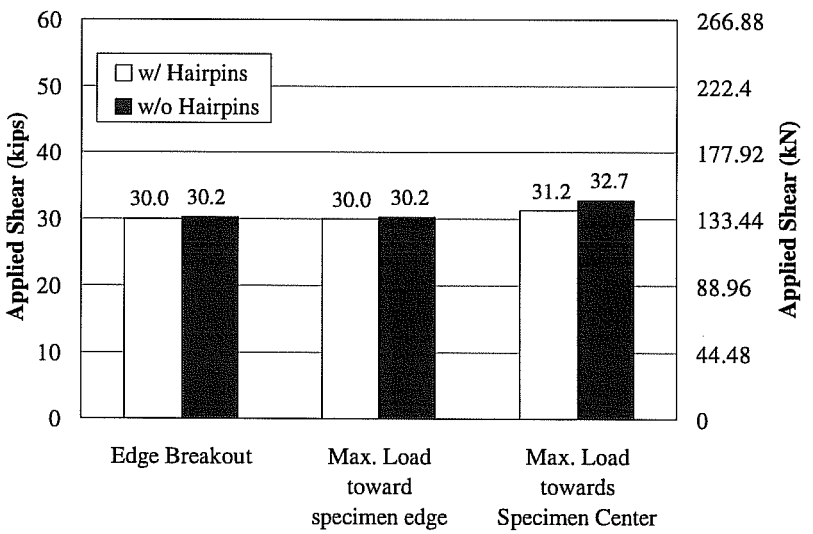

Figure 6.40 Comparison of Capacities of Near-Edge, Multiple-Anchor Connections with and without Hairpins, Loaded at 18-inch (457-mm) Eccentricity

The lateral blowout load by near-edge anchor heads of the anchor group loaded at an 18-inch (457-mm) eccentricity, which are calculated based on the maximum load achieved when loading towards the center of concrete specimens, is 46.8 kips (208 kN) with hairpins and 49.1 kips (218 kN) without. They are both slightly greater than that achieved for the connection with hairpins loaded at a 12-inch (305-mm) eccentricity. It was observed that hairpins significantly reduced the concrete breakout volume under shear of the near-edge anchors in the tests with both eccentricities. Therefore, the lateral blowout load of the connection with hairpins with an 18-inch (457-mm) eccentricity should be similar to that of the connection with hairpins loaded at a 12-inch (305-mm) eccentricity. It

was also observed that, in the test on the connection loaded at an 18-inch (457-mm) eccentricity without hairpins, the concrete breakout volume was very large, which supposedly reduced the lateral blowout capacity significantly. The only reason for the large lateral blowout load of the near-edge, multiple-anchor connection without hairpins loaded at an 18-inch (457-mm) eccentricity is that the shear load did only a little damage to the concrete edge, so the near-edge anchors could still reach a very high capacity, which occurred just after the concrete edge broke out.

CHAPTER 7

THEORETICAL STRENGTH OF CONNECTIONS TO CONCRETE

7.1 Introduction

In this chapter, for each failure mode, different design models are compared with the test results presented and discussed in Chapters 5 and 6.

A computer program, BDA5, is also discussed, and is used here to calculate the load-displacement behavior of anchor connections under eccentric shear. Its results are also compared with the experimental results of this study.

A modified plastic design method for multiple-anchor connections loaded at small eccentricities at large edge distances is proposed, to correct the overestimation of the plastic method proposed by Cook (1989) and the underestimation of the method proposed by Lotze (1997). Since enough test data are not available to resolve this issue, the calculated results from the BDA5 program are used as the basis for comparison.

The capacities of near-edge multiple-anchor connections is predicted with appropriate methods, and are compared with the test results.

7.2 Tension Capacity of Single Anchors in Cracked Concrete

Figures 7.1 and 7.2 compare the mean normalization coefficient of static tests, presented in Section 5.2, with the average coefficients used in the CC Method (Equation 2-5). The values of coefficients previously proposed for the CC Method (35 for expansion anchors and 40 for undercut and cast-in-place anchors) are generally conservative when

used to calculate the ultimate tensile capacity of anchors failing by concrete breakout. In contrast to the original CC Method, mean k values of 40 (rather than 35) have been used in recent comparisons involving the CC Method for UC anchors. They are also very close to mean normalization coefficients of most tested anchors, with only one exception of Sleeve Anchor in diameter of 3/4-inch (19-mm). The coefficient proposed for anchors in cracked concrete failing by concrete breakout, based on a reduction factor of 0.7, is also conservative for most of the tested anchor of this study. Grouted anchors had a smaller coefficient in cracked concrete. Based on test observations, behavior of Grouted Anchors in cracked concrete is considered unsatisfactory.

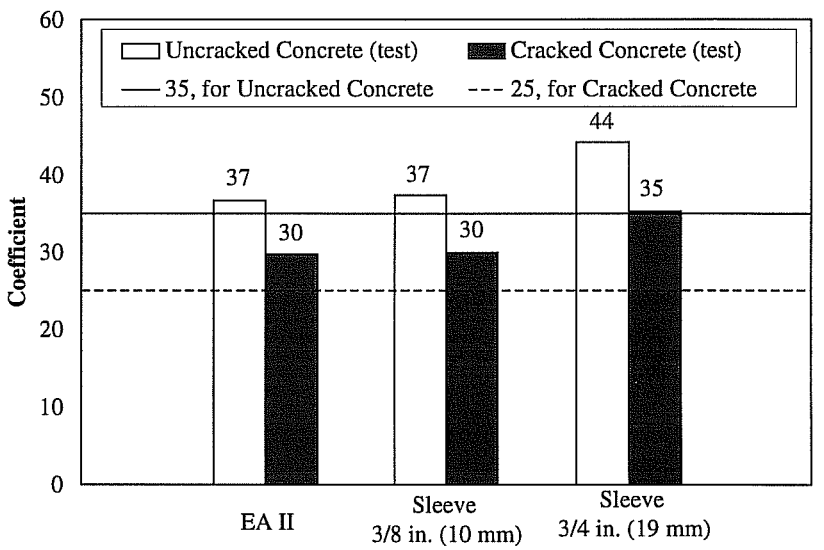

Figure 7.1 Comparison between Mean Normalization Coefficients of Static Tensile Tests on Expansion-Type Anchors and Coefficient Previously Proposed with the CC Method

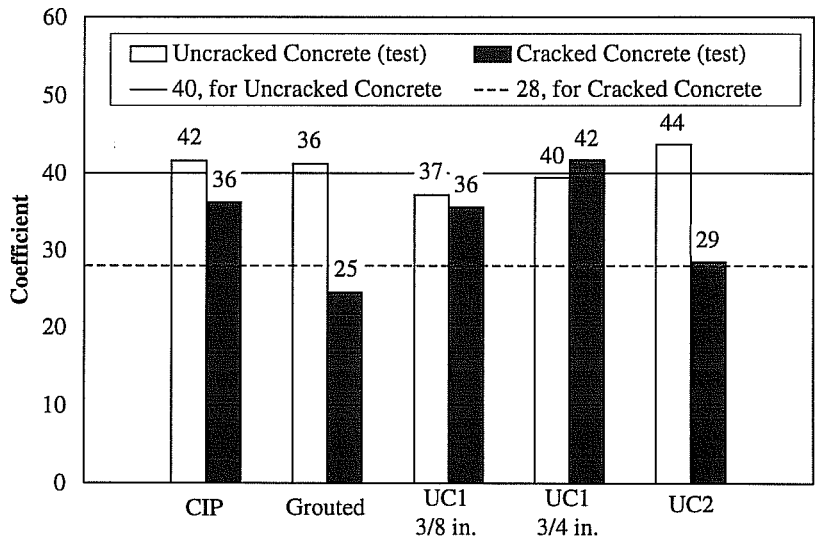

Figure 7.2 Comparison between Mean Normalization Coefficients of Static Tensile Tests on Bearing-Type Anchors and Coefficients Previously Proposed with the CC Method

Based on all the test results obtained from this testing program, which are presented and discussed in Sections 5.2 and 6.2, and on the data from the tests done by Rodriguez (1995) and Hallowell (1996), Table 7.1 proposed the normalization coefficient in terms of the CC Method of the tested anchors, using US customary units, for the predictions of tensile breakout capacity of single anchors.

These coefficients vary with anchor types and their diameters, and can only be used to calculate the concrete tensile breakout capacity of specific types of anchor of specific sizes. Since the Grouted Anchor does not behave well in cracked concrete, normalization coefficient in cracked concrete is not included for it.

Table 7.1 Proposed Normalization Coefficients (CC Method) for Single Tensile Anchors in Various Conditions

Anchor Type	Load Type and Concrete Condition			
	Static Uncracked	Dynamic Uncracked	Static, Cracked	Dynamic, Cracked
Cast-In-Place	41	50	35	50
Grouted	41	50	N/A	N/A
UC1, 3/8 in. (10 mm)	39	45	35	40
UC1, 3/4 in. (19 mm)	39	45	39	40
UC2, 3/4 in. (19 mm)	41	50	28	40
Sleeve, 10 mm	35	35	30	30
Sleeve, 20 mm	41	50	33	39
EA II	35	35	28	28

7.3 Comparison of Test Results for Multiple-Anchor Connections at Large Edge Distances with Results from BDA5 Program

7.3.1 Introduction to BDA5 Program

The BDA5 program is a macro-model program developed at the University of Stuttgart (Li 1994). It requires as input data a complete set of load-displacement curves of the anchor under oblique loading at angles from 0 to 90 degrees. In this program, the baseplate is assumed rigid, and the compressive stress distribution under the baseplate on the concrete is simplified as linear, with the maximum compressive stress of f_c'. Each row of anchors is modeled as a nonlinear spring, whose load-displacement properties are obtained by interpolating between the input load-displacement curves for the anchor. Appendix E gives an example input file for the BDA5 program. The calculated results are

given in forms of horizontal displacement and rotation of the baseplate, and the vertical displacement at the center of the baseplate.

In Task 2 of this research project, the BDA5 program was extensively examined with test results from two-anchor connections, using load-displacement curves obtained from single-anchor tests. Its accuracy and validity were demonstrated for a wide range of loading eccentricities (Lotze 1997). However, it sometimes has difficulties in convergence.

7.3.2 Calculation of Load and Displacement Behaviors of Multiple-Anchor Connections

Many multiple-anchor connections tests of this study used Undercut Anchor 1 of 5/8-inch (16-mm) diameter. Figure 7.3 shows a complete set of load-displacement curves for that anchor, obtained by Lotze (1996) in Task 2 of this research program. Those curves are used here as the input data file for the BDA5 program.

The calculated results are given in Figure 7.4 for the multiple-anchor connections tested in this study, loaded at a 12-inch (305-mm) eccentricity, and in Figure 8.5 for one loaded at an 18-inch (457-mm) eccentricity, both compared with the static test results. The starting points of some curves were adjusted to show how the curves match each other.

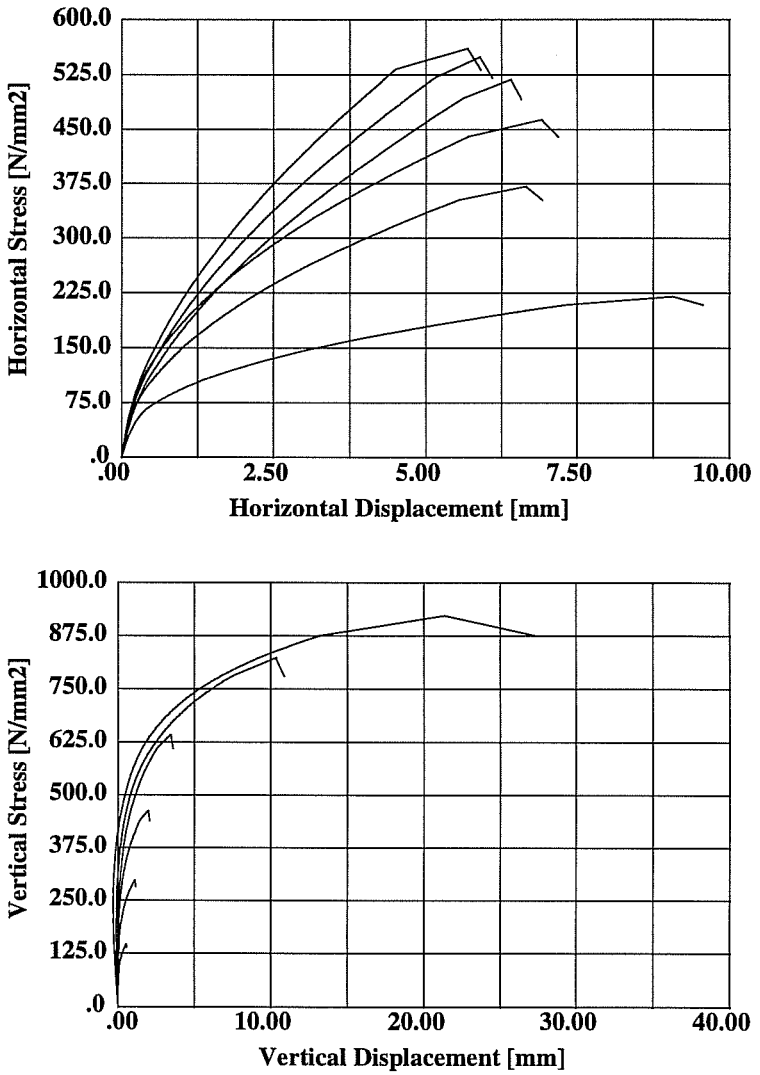

Figure 7.3 Typical Load-Displacement Curves for Single UC1 Anchor Loaded at Various Angles (Lotze 1997)

It can be seen from these figures that all the calculated load-displacement curves are initially much stiffer than those measured in tests. However, at larger loads, the predicted load-displacement behavior matches the test results well, especially for the displacement at 12 inches (305 mm) above the concrete surface. The larger measured displacements at lower loads could be attributed to several reasons: the uneven concrete surface; the uneven baseplate; and the gaps between the anchor shanks and the baseplate, and between the anchor shanks and surrounding concrete. If the rigid-body motion of the attachment had been due only to slip, the adjustment would have been the same anywhere on the attachment. The greater adjustment needed in the horizontal displacement at 12 in. (305 mm) above the concrete surface indicates that there might be some rigid-body rotation of the attachment. This could be due to imperfections on the concrete surface, or welding-induced distortion of the baseplate. However, in the input load-displacement curves of BDA5 program, the effect of gaps was completely ignored, and the concrete surface and the baseplate are assumed perfectly level. These factors might be modeled with the BDA5 program by reducing the stiffness of the load-displacement curves in the low-load range.

The ultimate capacity of the connection loaded at an 18-inch (457-mm) eccentricity was predicted accurately. However, the connection loaded at a 12-inch (305-mm) eccentricity failed at a lower load than that predicted. It was predicted to fail by shear fracture of the front anchor, just as happened in the test. The reason for the lower strength than predicted, however, might be the premature failure of one of the shear anchors due to the unevenly distributed shear force, since in the test, only one compression anchor failed.

In Figures 7.6 and 7.7, the calculated results, intentionally revised for the above departures from ideal behavior, are again compared with the static and dynamic test results. A certain amount of displacement was added to the calculated results until the curves from the BDA5 program matched closely the test results in the higher-load range to simulate the tested connection behavior of relative greater displacements in the small-load range. Compared to the curves of tests under dynamic reversed cyclic loading, they also provide a very good profile for most part of the load, except for the small-load range.

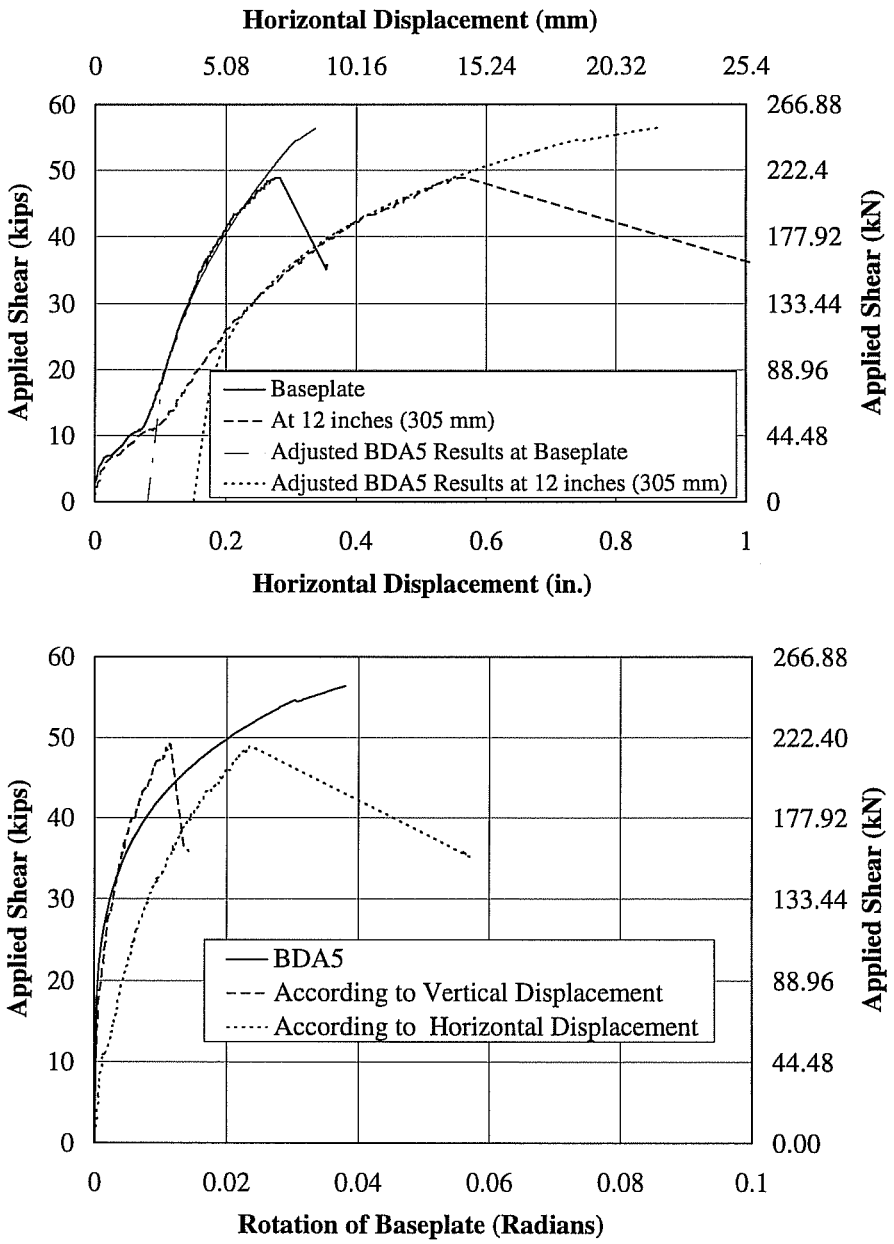

Figure 7.4 Comparison of Calculated Results from BDA5 Program with Static Test Results for Multiple-Anchor Connection with UC1 Anchors at 12-inch (305-mm) Eccentricity

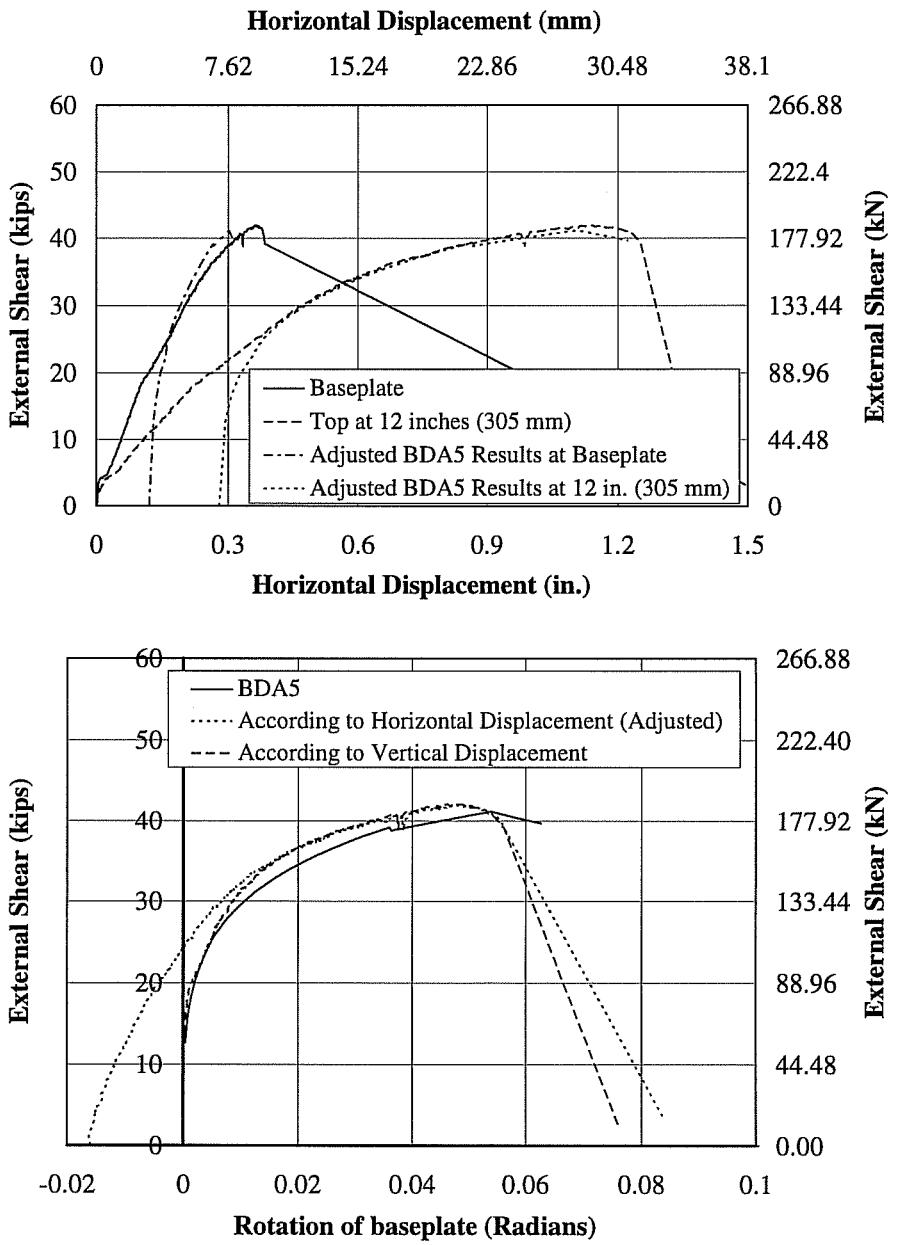

Figure 7.5 Comparison of Calculated Results from BDA5 Program with Static Test Results for Multiple-Anchor Connection with UC1 Anchors at 18-inch (457-mm) Eccentricity

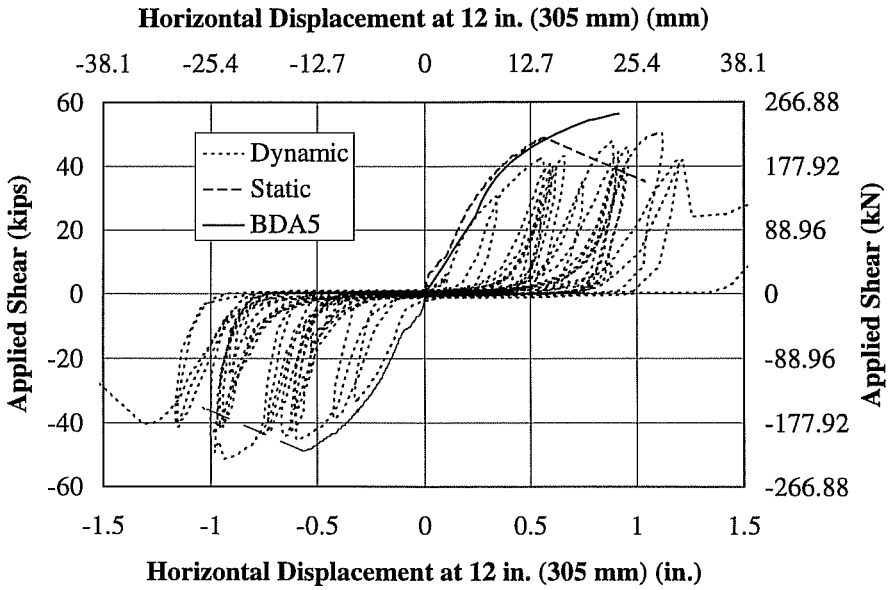

Figure 7.6 Comparison of Calculated Results from BDA5 Program with Static and Seismic Test Results of Multiple-Anchor Connection with UC1 Anchors Loaded in Eccentric Shear at 12 Inches (305 mm)

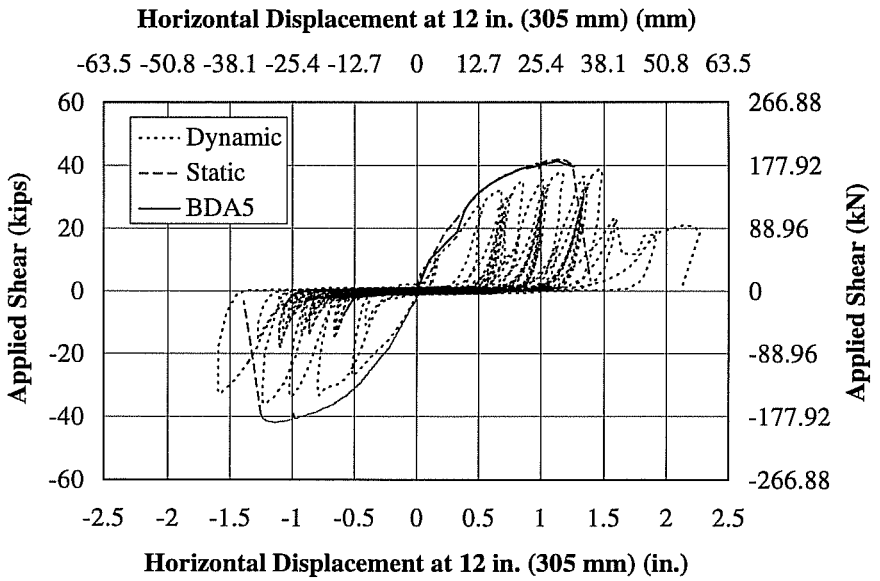

Figure 7.7 Comparison of Calculated Results from BDA5 Program with Static and Seismic Test Results of Multiple-Anchor Connection with UC1 Anchors Loaded in Eccentric Shear at 18 Inches (457 mm)

7.4 Comparison of Test Results with Plastic Method and Modified Plastic Method of Multiple-Anchor Connections at Large Edge Distances

The Plastic Method (Cook 1989) and the Modified Plastic Method (Lotze 1996) predict the capacity of multiple-anchor connections loaded in shear at large edge distances, failing by steel fracture. In the following, the test results of multiple-anchor connections with UC1 anchors, loaded in shear, obtained in this study, are compared with the calculated results from both methods and from the BDA5 program.

For the tested connections using a friction coefficient of 0.15, the critical eccentricity specified by Cook (1989) is calculated:

$$e_2 = 12/(0.15+0.6) = 16 \text{ inches } (406 \text{ mm})$$

The calculated results of connections with 5/8-inch (16-mm) Undercut Anchor 1 are compared in Figure 8.8 with the test results, based on the average of tested tensile capacity (Cook 1989) of 31.0 kips (138 kN), and the shear capacity of 18.6 kips (82.7 kN), of the anchor.

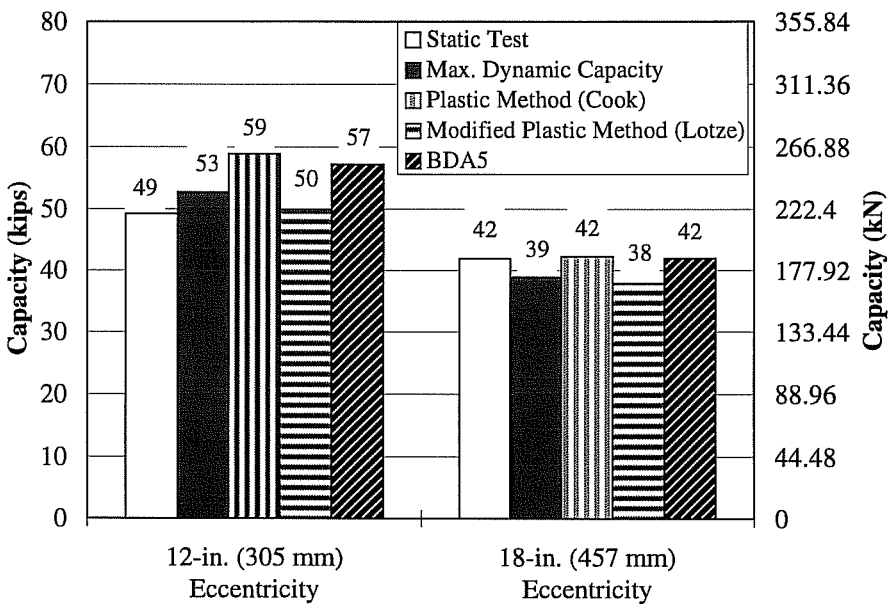

Figure 7.8 Tested versus Calculated Results of Multiple-Anchor Connections with UC1 Anchors, at Large Edge Distances, Loaded in Shear

For the connection with an eccentricity of 18 inches (457 mm), the load capacity calculated by the Plastic Method and the BDA5 program are very close to the test results. However, the Modified Plastic Method (Lotze 1996) underestimated the static load capacity by as much as 10%.

For the connection with an eccentricity of 12 inches (305 mm), the static load capacity was overestimated by both the Plastic Method and the BDA5 method. The Modified Plastic Method (Lotze 1996) is very close to the test results. However, as mentioned before, the static test of the connection with a 12-inch (305-mm) eccentricity might have failed prematurely, because of the possible unevenly distributed shear force on one of the shear anchors.

7.5 Proposal for Another Modified Plastic Design Method for Multiple-Anchor Connections at Large Edge Distance Loaded in Eccentric Shear

In Figures 7.9 and 7.10 the tested capacities of connections are compared with those predicted by the Plastic Method (Cook 1989) and the Modified Plastic Method (Lotze 1996). The Plastic Method proposed by Cook overestimates the capacity of a multiple-anchor connection loaded in shear at the eccentricities small than the critical eccentricity, e_2 (from Equation 2-18). This is due to the overestimate by the Plastic Method of the shear contribution of the tensile anchors because of the bulbous shape of the displacement interaction curves of anchors under oblique loading. The Modified Plastic Method inherits the assumption of uniform shear distribution to all anchors, used in the elastic design method. The Modified Plastic Method usually underestimate the load capacity of connections, except for cases of very large or very small eccentricities.

Based on the Plastic Method, another modified design method is proposed here, to more accurately predict the capacity of multiple-anchor connections loaded in shear.

1) For connections with an eccentricity greater than the critical eccentricity, e_2 (from Equation 2-18), the load capacity is controlled by the tension anchors, and Equation 2-20 can be used.

2) For connections with eccentricity smaller than e_2, the shear contribution of the tension anchors is somewhat limited by the restraint of the horizontal displacement of the shear anchors. The elliptical interaction equation can be modified to approximate this reduction by reducing the exponent of the shear component.

The corresponding calculation procedures are as follows:

The shear force equilibrium and the normal force equilibrium for the connection are given by:

$$V_n = \mu C + m\gamma T_o + nV \qquad (7\text{-}1)$$

and $$C = nT \tag{7-2}$$

The moment equilibrium condition for the connection is given by:

$$V_n\, e = nTd \tag{7-3}$$

Therefore the tension and shear force on the tension anchors will be:

$$V = \left(V_n - \mu C - m\gamma T_o\right) / n$$

$$T = V_n\, e / (nd)$$

Substituting them into the elliptical interaction equations gives:

$$\left[\frac{V_n\, e / (nd)}{T_o}\right]^{1.8} + \left[\frac{\left(V_n - \mu C - m\gamma\, T_o\right) / n}{V_o}\right]^{p} = 1 \tag{7-4}$$

where: V_n = maximum predicted capacity of the connection;

γ = ratio of shear strength to tension strength of an anchor;

e = eccentricity of the external shear loading;

n = number of rows of tension anchors;

m = number of rows of anchors in the compression zone;

μ = coefficient of friction between steel and concrete; and

d = distance from the compressive reaction to the centroid of the tension anchors.

The capacity of multiple-anchor connections at large edge distances can then be calculated iteratively using Equation 7-4.

An exponent p between 1 and 1.1 was found to be suitable, compared with the calculated results from the BDA5 program. Figures 7.8 and 7.9 compare the calculation results from the Plastic Method, the Modified Plastic Method of Lotze, the Modified Plastic Method proposed here with an exponent of 1.0, and the BDA5 program, with the test results reported in this study. In those calculations, coefficients of friction of 0.15 and 0.5 between steel and concrete were used, representing the cases with and without Teflon sheets between the baseplate and concrete surface. In the Plastic Methods, the tension force on the front anchors is ignored; correspondingly, calculations with the BDA5 program were also conducted with and without the tension forces on the front anchors.

Since few test results are available, the calculated results from the BDA5 program are used here as the basis for comparison of the different methods.

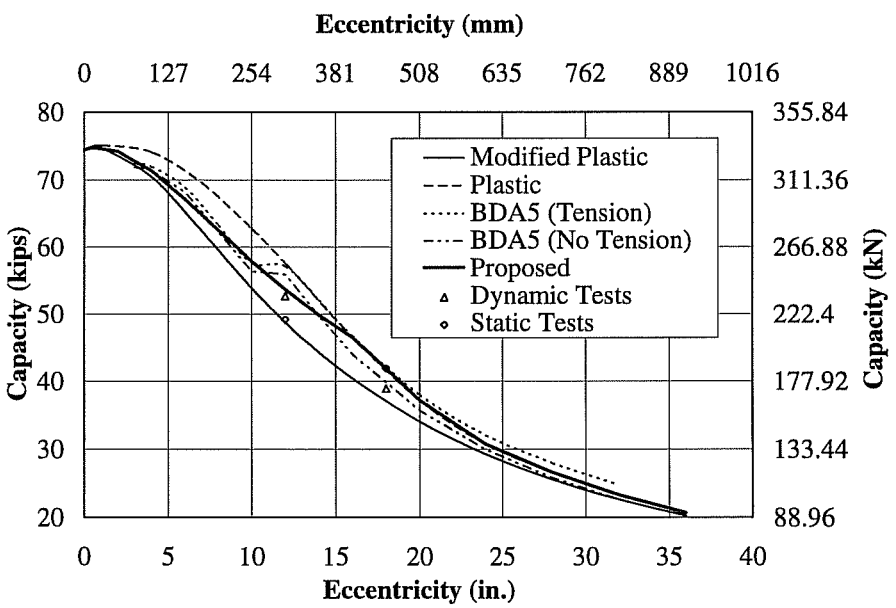

Figure 7.9 Comparison of Design Models with Test Results of Multiple-Anchor Connections with UC1 Anchors, at Large Edge Distances, Loaded in Eccentric Shear ($\mu = 0.15$)

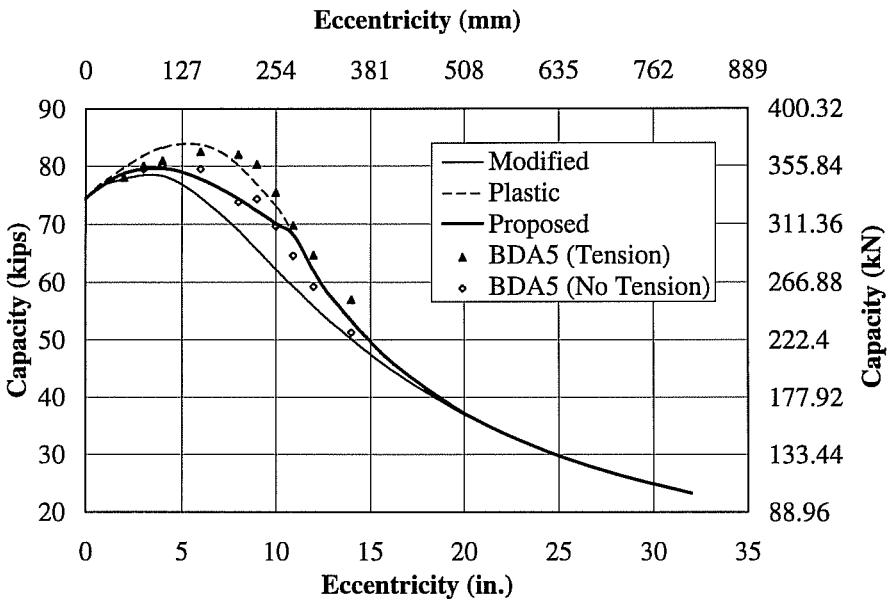

Figure 7.10 Comparison of Design Models with Test Results of Multiple-Anchor Connections with UC1 Anchors, at Large Edge Distances, Loaded in Eccentric Shear ($\mu = 0.50$)

First of all, it is noted from these figures that the results from the BDA5 program considering tension forces in the shear anchor are higher than those without. With a friction coefficient of 0.5, the results of the BDA5 program with tension forces are also higher than those calculated by the Plastic Method (Cook 1989) at eccentricities larger than 7 inches (178 mm). This is attributed to the frictional force caused by the additional compression on the concrete, due to tensile force in the shear anchor. Because of the character of the tension-shear interaction, the increase in frictional force due to the tension force in the shear anchors is greater than the loss of the shear capacity of these anchors. As a result, the shear capacity of the connection increases. This also explains why the test results of Cook (1989) exceed the calculated values of the Plastic Method with a friction coefficient of 0.5 (Cook 1989).

When the eccentricity increases so that the connection fails in the tension anchor, tensile force in the shear anchor increases the flexural capacity of the connection, and thereby the shear capacity of the connection. However, the magnitude of the tension force in the shear anchors depends on the configuration of the connection. The greater the spacing between the shear and tension anchors, the smaller the tension force will be, since the tensile deformation of the shear anchors is limited by the total elongation of the tension anchors. This tensile force also might diminish at very small eccentricities, when the tension anchors are subjected to substantial shear with very small tension force. Furthermore, the tension force will completely disappear if the baseplate is flexible (in which case there will be no prying action on the compression anchors by the baseplate), or if the connection is subjected to reversed cyclic loads (in which case the compression anchors have undergone a certain amount of tensile displacement under cyclic tensile loading). Therefore, it might be reasonable in analytical calculations to assume there is no tension force on the shear anchor at all.

The calculated results from the BDA5 program lie mostly between the results from the Plastic Method (Cook 1989) and the Modified Plastic Method (Lotze 1996) at small eccentricities. This is especially true for the BDA5 results without tension force on the shear anchors. At large eccentricities, the BDA5 results with and without tension force on the shear anchors are closer to those of the Plastic Method; those with tension forces are a little higher, and those without, a little lower. In the calculation with the BDA5 program for the case without the tension force on shear anchors, the tension anchors are subjected to a small shear force. As a results, their tensile capacity is smaller, and the capacity of the connection is smaller than that predicted by the Plastic Method, even though the physical model is exactly the same in both calculation methods.

Compared to the BDA5 results, the Modified Plastic Method of Lotze (1996) gives lower results over a very large range of eccentricities. Only at very large and extremely small eccentricities, are its results close to those BDA5 results.

In the case of a coefficient of friction of 0.15, the Modified Plastic Method proposed here gives results similar to those from the BDA5 program. With a coefficient of friction of 0.5, the Modified Plastic Method proposed here also gives results very close to the results of the BDA5 program without the tension forces on the shear anchors. It can be concluded that the Modified Plastic Method proposed here corrects the considerable overestimation of the Plastic Method proposed by Cook (1989), and also reduces the underestimation of the Modified Plastic Method proposed by Lotze (1996).

However, the Modified Plastic Method proposed here still gives predictions lying above the test results on multiple-anchor connections of this study. This might be attributed to the slight difference in the tension forces on the anchors, as observed in the tests that when one tensile anchor failed the force on the other was slightly smaller than its capacity. Further experimental study is needed to verify these different methods, especially on connections loaded at eccentricities less than the critical eccentricity, e_2.

7.6 Design Procedures for Near-Edge Multiple-Anchor Connections Loaded in Eccentric Shear

7.6.1 Load Capacity of Near-Edge Connections

In tests on double-anchor connections, the shear force distribution on both anchor was quite uniform. No correlation was observed between shear distribution and the gaps between the baseplate and the anchors. However, the shear capacity of the front anchor were much smaller than the values calculated according to Equation 2-11. The compression force and the friction of the baseplate acting on the concrete may have a significant effect on the shear capacity of the front anchor.

Neglecting the effect of the compression force of the baseplate on the concrete shear capacity, and assuming that the summation of the frictional force and the shear force on the front anchor equals the concrete shear capacity of the front anchor, gives the following:

$$V_{front} = V_{anchor} + f = V_n$$

Also assuming that the near-edge anchors take all the shear, and that the back anchors are loaded only in tension, the capacity of a near-edge connection can be calculated.

Table 7.2 compares the calculated results with the test results of this study. In the test in cracked concrete (Tests 11S11-15), a reduction factor of 0.7 was used to account for the effect of concrete cracking on the concrete edge breakout capacity.

Table 7.2 Tested versus Calculated Edge Breakout Capacity of Near-Edge Double- and Multiple-Anchor Connections Loaded in Shear

Test	Tested Capacity		Calculated Capacity	
	kips	kN	kips	kN
9S01-05	24.9	111	12.5	55.9
11S11-15	20.9	93.0	8.8	39.1
4211	29.5	131	23.1	103
4212	29.9	131	23.1	103

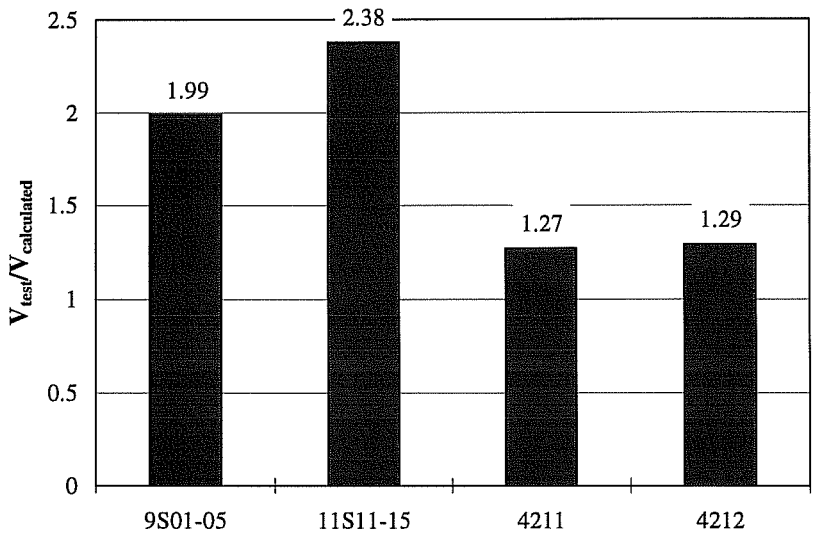

Figure 7.11 Ratio of Tested to Calculated Edge Breakout Capacities of Near-Edge, Double- and Multiple-Anchor Connections Loaded in Shear

For the double-anchor connections, the calculated values are very low, less than half the test results. However, the calculated results for multiple-anchor connections are only 30% lower than the corresponding test results. In the tests on near-edge multiple-anchor connections, the compression edge of the baseplate was located on the concrete edge breakout cone. This is in contrast to the tests on near-edge double-anchor connections, in which the location of the compression edge of the baseplate was at the edge of breakout cone, due to its special design. As a result, the forces on the baseplate might significantly decrease the concrete edge breakout capacity.

Since the effect of the forces of the baseplate on shear breakout capacity of the concrete edge is unknown, no conclusion can be drawn, and further research on this is needed.

7.6.2 Ultimate Capacity of Near-Edge Connection without Hairpins

The near-edge connection may have a greater capacity than the concrete edge breaks out load, because some shear force might remain on the front anchors even after the concrete member edge has broken out. However, the remaining shear force on the near-edge anchors should not be used for calculating the ultimate load capacity, since it may vary greatly.

The capacity can be calculated by applying the elliptical interaction equation (Equation 2- 16) to the tension anchors. In Section 6.3.3 on double-anchor test results, this was already discussed. In Table 7.3 and Figure 7.12, those results are again compared with the test results for multiple-anchor connections . The test results are both about 10% higher than calculation. This is believed to be due to the residual shear force in the front anchor.

Table 7.3 Tested versus Calculated Capacities of Near-Edge, Double- and Multiple-Anchor Connections without Hairpins at Fracture of Tension Anchors

Test	Tested Capacity		Calculated capacity	
	kips	kN	kips	kN
9S01-05	24.9	111	21.8	97.0
11S11-15	24.3	108	21.8	97.0
4411	35.8	159	33.6	149
4412	31.1	138	28.2	125

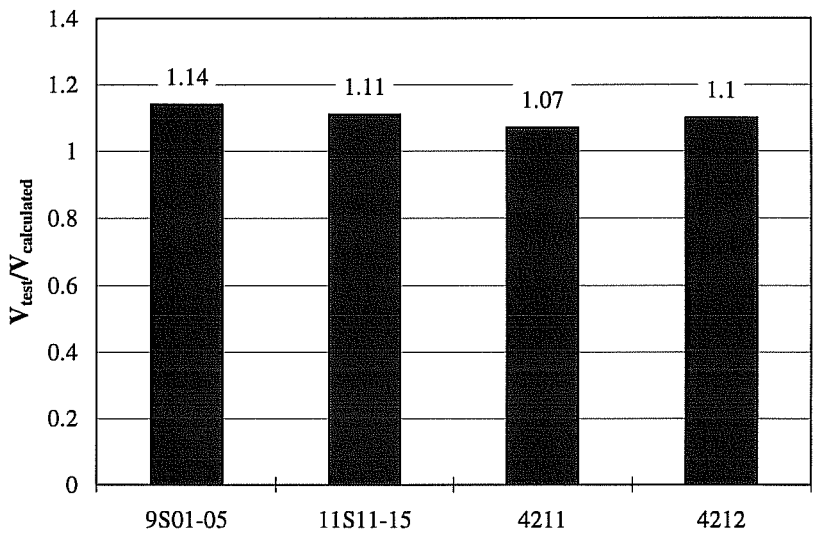

Figure 7.12 Ratio of Tested to Calculated Capacities of Near-Edge Double- and Multiple-Anchor Connections without Hairpins at Fracture of Tension Anchors

7.6.3 Ultimate Capacity of Near-Edge Connection with Hairpins

In near-edge connections with hairpins, after the concrete edge breaks out under the shear load of the front anchors, the connection may sustain a still higher load because of the residual shear capacity in the near-edge anchors. The lower bound of the sustained shear capacity of the near-edge anchors can be determined by the plastic mechanism of the anchor shanks between the baseplate and the hairpins, neglecting the effect of tension force of these anchors.

The calculation procedure involves following steps:

1) Based on the cross-sectional area of anchor shanks (including sleeves), calculate the yielding moment of the anchor shanks (Figure 7.13).

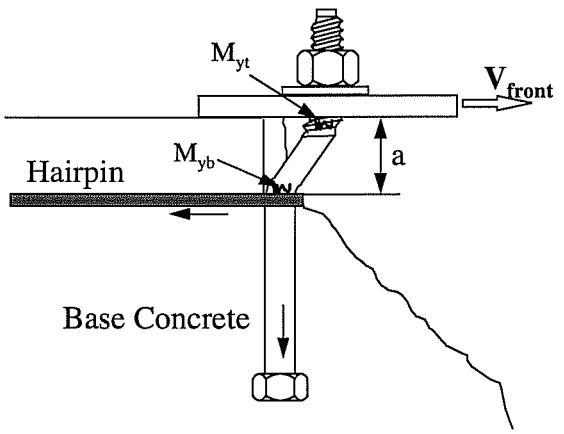

Figure 7.13 Calculation of Residual Shear Capacity Based on Plastic Mechanism

2) The sustaining shear force of the anchor can then be calculated with:

$$V_{front} = \left(M_{yt} + M_{yb}\right)/a$$

where: M_{yt} = yielding moment of anchor shank near the baseplate;

M_{yb} = yielding moment of anchor shanks near the hairpin; and

a = the concrete cover of the hairpin.

3) According to the interaction equation of anchors, calculate the capacity of the connection. In case of connections with two anchor rows (as in this project), it is calculated as:

$$V_n = V_{front} + f + V_{back}$$

$$f = \mu \cdot T_{back}$$

$$T_{back} \cdot d = V_n \cdot e$$

Substituting these into the interaction equation gives the following equation for the connection:

$$\left(\frac{V_n \frac{e}{d}}{T_o}\right)^{1.8} + \left(\frac{V_n - V_{front} - \mu V_n \frac{e}{d}}{V_o}\right)^{1.8} = 1 \qquad (7\text{-}5)$$

where: V_n = is the ultimate strength of connections;

T_o, V_o = tension and shear capacity of anchors respectively;

V_{front} = residual shear force in front anchor;

e = eccentricity of external load;

d = distance from the tension anchor to the compression reaction; and

μ = coefficient of friction.

With Equation 7-5, the ultimate strength of near-edge multiple-anchor connections with hairpins can be calculated iteratively. Table 7.4 compares the analytical results with the ultimate strength of connections from the tests reported in this study. Figure 7.14 shows the ratios of tested to calculated capacities.

Table 7.4 Tested versus Calculated Capacity of Near-Edge Double- and Multiple-Anchor Connections with Hairpins

Test	Tested Capacity		Calculated Capacity	
	kips	kN	kips	kN
11SH16-20	29.0	129	26.6	118
4415	42.3	188	44.7	199

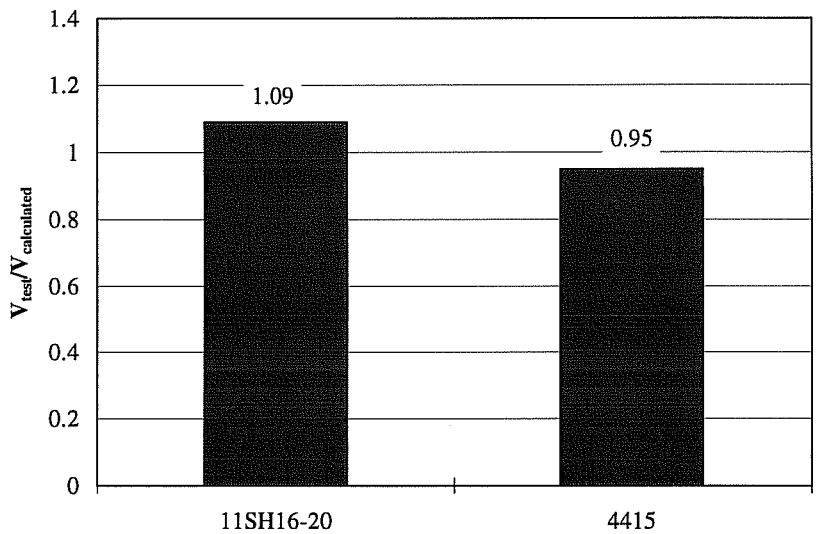

Figure 7.14 Ratio of Tested versus Calculated Capacities of Near-Edge, Double- and Multiple-Anchor Connections with Hairpins, Loaded in Shear

The calculated results match the test results quite well, with about a 10% difference.

There are two ways to increase the residual shear capacity of the near-edge anchors. One way is by reducing the distance between two yielding hinges. However, this approach might be limited by the requirement of minimum concrete cover. The other way is using a large sleeve outside the anchor shank to increase the yielding moment. With a large enough sleeve, a near-edge anchor could fail under shear without any yielding of the anchor shank. Therefore, the effect of member edges may be completely compensated for.

CHAPTER 8

FEM MODELING OF TENSILE BREAKOUT BEHAVIOR

8.1 Introduction

In the past, several attempts have been made to analyze the behavior of anchors in concrete. Different methods, such as the discrete cracking approach (Hellier et al. 1987), the smeared cracking approach (Ottosen 1981), the nonlocal microplane model (Elighausen and Ozbolt 1990), and plasticity models, have been used to model tensile breakout.

In this chapter, the fundamentals of modeling tensile breakout behavior are summarized. The method developed here and the corresponding results are discussed.

8.2 Scope

The objective of finite element approach described here is to model crack propagation in the concrete, and to model the behavior of a headed anchor failing by concrete breakout. A fixed smeared crack model based on the fictitious crack model was used. To reduce computational time, the program assigns properties of concrete cracking to only those elements on the concrete crack propagation path. No attempt is made to model the plastic deformation of concrete at the anchor head under high hydrostatic stresses.

8.3 Crack Modes

All stress systems in the vicinity of a crack tip may be derived from three modes of loading (Figure 8.1). In Mode I (opening mode), normal stresses open the crack. In Mode

II (sliding mode) and Mode III (tearing mode), shear stresses open the crack. However, what happens in the case of concrete is far from understood. Since concrete fails easily in Mode I, a crack tends to follow the maximum principal stress, and develops perpendicular to that stress. Mode I cracking is most heavily investigated and modeled.

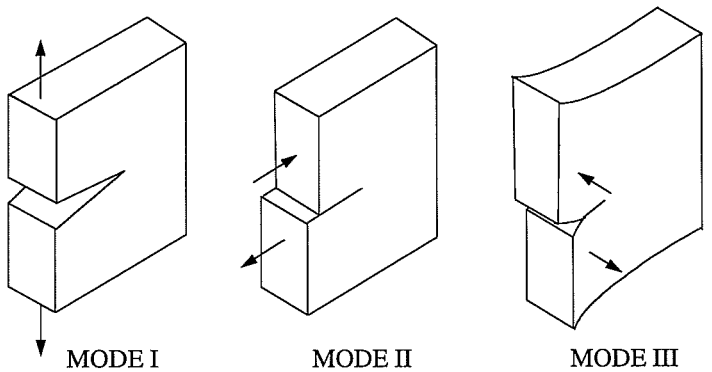

Figure 8.1 Three Modes of Loading

8.4 Fundamental Material Behavior of Concrete

Concrete is a composite material composed of three phases: mortar, coarse aggregate, and mortar-coarse aggregate interface. The mortar phase consists of cement paste and a mixture of fine aggregate particles. The nature of plain concrete gives it a very complex material behavior. It exhibits nonlinear stress-strain behavior in multiaxial state of stress; strain-softening and progressive cracking induced by tensile stress or strain; and time-dependent behavior such as creep and shrinkage.

Concrete is mainly a brittle material, whose properties are affected by a number of factors, including water-to-cement ratio, type of cement, admixtures, and the gradation, size and shape of aggregates. The failure and fracture of concrete is the propagation of flaws and microcracks, which exist within the body of the material even prior to the application of load. Its nonlinear stress-strain relation is also due to these microcracks. Many of those formed at the interfaces between the coarse aggregate and the cement paste which

constitute the weakest link in the material. Microcracks could also be generated within the paste itself by various factors, such as differential shrinkage differential thermal movements, or voids as a result of incomplete consolidation. When load is applied, additional microcracks may form at isolated tensile stress concentrations due to incompatible deformations of the aggregates and the paste. As the load increases, these microcracks propagate and eventually connect, resulting in fracture of the material (Figure 8.3). According to experimental investigations of microcracks by Yamaguchi and Chen (1991), the pre-peak concrete behavior is associated with the extension of bond cracks (cracks around aggregates), while post-peak behavior is associated with the extensive development of cracks in the paste.

In the following sections, the fundamental experimental observations of concrete regarding the short-time tensile and compressive behavior of concrete are briefly discussed. All the discussions of material properties are based at the macro level, at which concrete is treated as a continuous and homogeneous medium.

8.4.1 Behavior of Concrete in Uniaxial Compression

Concrete subjected to uniaxial compression exhibits the stress-strain relationship depicted in Figure 8.2. The stress-stain curve has a nearly linear-elastic behavior up to about 40% of its maximum compressive strength, f_c. For stresses above this point, the curve shows a gradual increase in curvature up to about 75% and 90% of f_c, whereupon it becomes clearly nonlinear and bends more sharply. Beyond the peak, the stress-strain curve has a descending branch until crushing failure occurs at a strain ε_u.

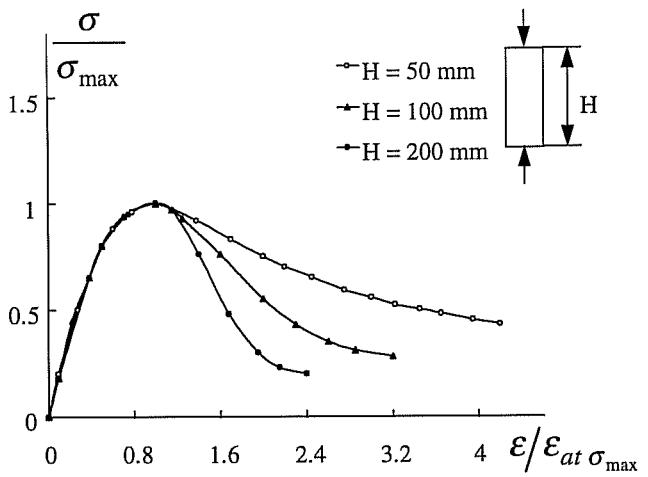

Figure 8.2 Uniaxial Compressive Stress-Strain Curve (van Mier 1984).

The nonlinear stress-strain curves are closely related to the internal mechanism of microcracking and propagation. More details are described in Chen (1982). The descending branch of the stress-strain curve is not a material property, but a characteristic associated with the specific test including loading scheme. J. van Mier (1984) noted from tests that the slope of the descending branch decreases as the length of the specimen increases (Figure 8.2). However, if post-peak displacement instead of strain is plotted against stress, the stress-displacement curves are practically identical.

The initial modulus of elasticity of concrete can be correlated to its compressive strength, f_c. The empirical formula proposed by ACI (1995) can predict the initial modulus of elasticity, defined as the slope of the line drawn from a stress of zero to a compressive stress of $0.45 f_c'$, with reasonable accuracy:

$$E_o = 33\, w^{1.5} \sqrt{f_c} \text{ psi} \tag{8-1a}$$

$$E_o = 0.043\, w^{1.5} \sqrt{f_c} \text{ MPa} \tag{8-1b}$$

where: w = unit weight of concrete in pounds per cubic foot (kg/m^3); and

f_c = the uniaxial compressive cylinder strength in psi (MPa).

For normal-weight concrete, Equation 8-1 can be approximated by the following equation with w = 150 pounds per cubic foot (2400 kg/m^3) :

$$E_o = 57000\sqrt{f_c} \text{ psi} \tag{8-2a}$$

$$E_o = 4700\sqrt{f_c} \text{ MPa} \tag{8-2b}$$

Value of Poisson's ratio v for concrete in uniaxial compression ranges from about 0.15 to 0.22. It remains constant until approximately 80 percent of f_c, at which points it begins to increase. In the unstable crushing phase, v can even exceed 0.5.

8.4.2 Behavior of Concrete in Uniaxial Tension

The tensile behavior of plain concrete play an important role in the failure of concrete structures. The most direct way to obtain the complete tensile stress-deformation relation is by deformation-controlled uniaxial tensile tests. Concrete under uniaxial tension has a stress-strain curve similar to that of concrete under uniaxial compression, as shown in Figure 8.4.

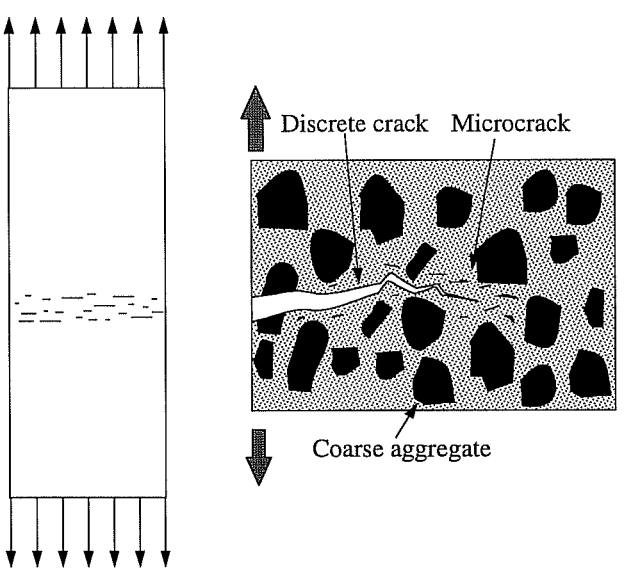

Figure 8.3 Crack Propagation of Concrete in Tension

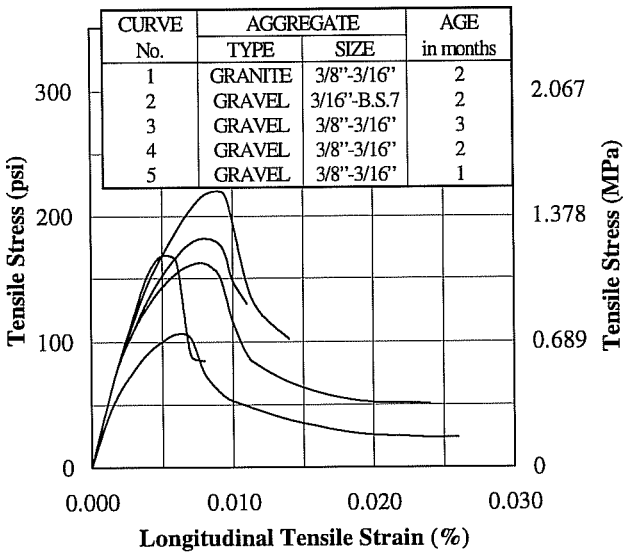

Figure 8.4 Tensile Stress-Strain Curves (Hughes and Chapman, 1966)

The tensile stress-strain curves are approximately linear up to about 75% of the tensile strength, f_t. For stress levels below about 60% of f_t, the generation of microcracks is negligible. For stresses greater than that level, interface microcracks start to grow and become visible (Evrens and Marathe 1968). Once cracks are initiated, they grow faster and lead to failure sooner than in a compression test.

If the tensile stress reaches a certain percentage of the tensile strength, all deformation due to microcracks will localize within a so-called fracture zone. As a result, concrete in tension will fail at a single critical section with a major crack in the transverse direction (Willam et al. 1985).

This crack develops soon after failure. After that, there is still post-cracking resistance caused by cohesive stresses in the microcracking region, as a result of the bridging of cracked surface by aggregates and fibrous crystals (Gopalaratnam and Shah 1985). The maximum crack opening, w_o, at which stress can no longer be transferred is

difficult to determine. Nevertheless, some values greater than 400 μm are reported (Wecharatana 1986, Guo and Zhang 1987).

The ratio of the uniaxial tensile strength to uniaxial compressive strength varies from 0.05 to 0.1. The initial elastic modulus in tension is a little larger than in compression. The tensile Poisson's ratio generally varies between 0.15 and 0.25. The stress-strain relation is almost linear up to the peak load.

The direct tensile strength of concrete can be approximated by the following equation:

$$f_t = 4\sqrt{f_c} \text{ psi} \tag{8-3a}$$

$$f_t = 0.332\sqrt{f_c} \text{ MPa} \tag{8-3b}$$

In other types of tests for determining the tensile strength of concrete, the values of strength can be different. The split-cylinder strength is estimated from Equation 8-4:

$$f_{sp} = 5 \text{ to } 6\sqrt{f_c} \text{ psi} \tag{8-4a}$$

$$f_{sp} = 0.415 \text{ to } 0.498\sqrt{f_c} \text{ MPa} \tag{8-4b}$$

8.4.3 Multiaxial Behavior of Concrete

The behavior of concrete under multiaxial stresses has been extensively, to establish concrete strength criteria and constitutive relations for computer and finite element applications.

Kupfer et al. (1969) studied the behavior of concrete under biaxial stresses. Figure 8.5 shows the envelope of concrete strength obtained from that study.

Under combined stress states, concrete behaves uniquely: its tensile strength is almost unaffected by the tensile stresses in the other directions, equal to its uniaxial tensile strength. Tensile strength decreases slowly as compressive stresses in the other directions increase.

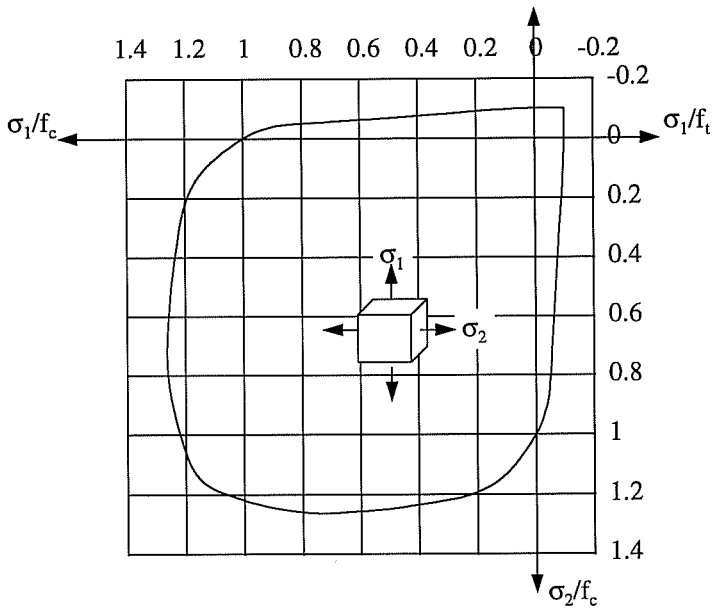

Figure 8.5 Biaxial Strength Envelope of Concrete (Kupfer et al. 1969)

Triaxial tests of Richart et al. (1928), Balmer (1949) and Wang et al. (1987), conducted at various confining stresses, indicate that depending on the confining stress, concrete acts as a quasi-brittle, plastic-softening, or plastic-hardening material. Under increasing hydrostatic stresses, the possibility of bond cracking is greatly reduced, and the failure mode shifts from fracture to crushing of the concrete paste. Consequently, axial strength increases with confining pressure; extremely high axial strengths have been recorded by Balmer (1949) and Wang et al. (1987) as shown in Figure 8.6.

Under hydrostatic compressive loading, concrete exhibits nonlinear stress-strain behavior; its hydrostatic-pressure-volumetric-strain curve, shown in Figure 8.6, shows a reversal in curvature on loading.

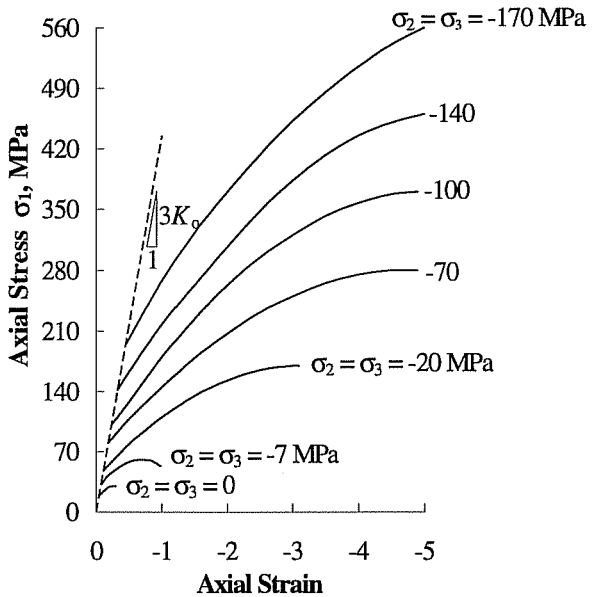

Figure 8.6 Triaxial Stress-Strain Relationship for Concrete (Balmer 1949)

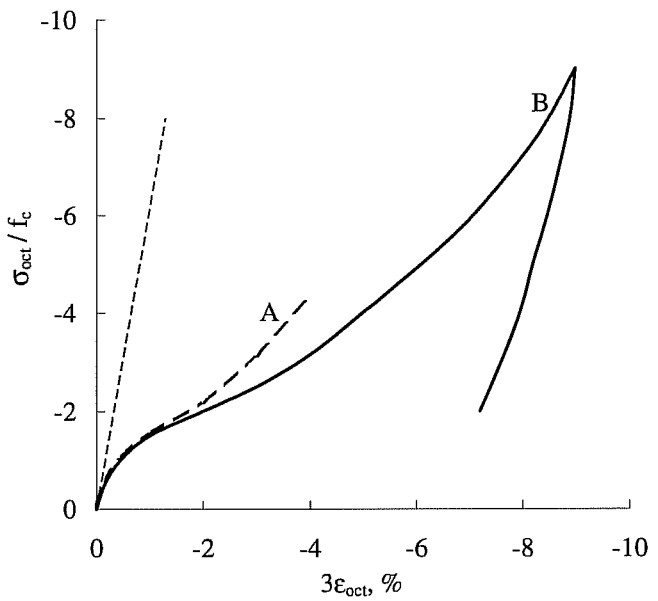

Figure 8.7 Behavior of Concrete in Hydrostatic Compression: A = Palaniswamy (1973), f_c = 22 MPa; B = Green and Swanson (1973), f_c = 48.5 MPa

8.4.4 Shear Stiffness of Concrete after Tensile Cracking

Several tests have investigated the shear stiffness of cracked concrete. Based on tests on concrete beams, Fenwick (1968) proposed that the shear stiffness across a crack due to aggregate interlock, decreases with increasing crack opening displacement :

$$\sigma_s = \left\{\left(\frac{467}{COD} - 8410\right)\left(0.0225\sqrt{f_c'} - 0.409\right)\left[CSD - 0.0436(COD)\right]\right\} \text{ psi} \qquad (8\text{-}5)$$

where: CSD = crack sliding displacement;

f_c = uniaxial compressive cylinder strength of concrete in psi; and

COD = crack opening displacement.

Tests on saw-cut specimens by Reinhardt et al. (1987) also show decreasing shear stiffness with the increasing normal displacement of the crack. Those tests also

demonstrated that the relation between normal stress on a crack and the crack opening displacement was not affected by the shear stress on the crack.

8.5 Fictitious Crack Model

The fictitious crack model was first introduced by Hillerborg et al. (1976), based on experimental observations. In this model, the crack is assumed to propagate when the principal tensile stress at its tip reaches the tensile strength, f_t. After the crack opens, the tensile stress across the crack decrease with increasing crack width, w, as shown in Figure 8.8. This model originally describes only the behavior of a crack loaded normal to its plane, and has been used in many publications to model cracking of concrete-type materials.

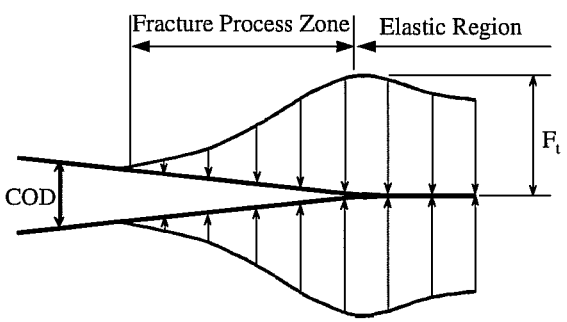

Figure 8.8 Fictitious Crack Model (Hillerborg et al. 1976)

Several empirical expressions have been proposed for the relation between tensile stress and crack opening. Cornelissen et al. (1986) proposed the following relation:

$$\sigma/f_t = \left[1+\left(c_1\frac{w}{w_0}\right)^3\right]\exp\left(-c_2\frac{w}{w_0}\right)-\frac{w}{w_0}\left(1+c_1^3\right)\exp\left(-c_2\right) \qquad (8\text{-}6)$$

For a typical normal weight concrete, $c_1 = 3$, $c_2 = 6.93$, and $w_0 = 160$ μm. Wolinski et al. (1987), comparing test results from five different mixes, asserted that a function like

Equation 8-6 is the best approximation of the stress-crack opening relation of all mixes. Figure 8-9 plots Equation 8-5.

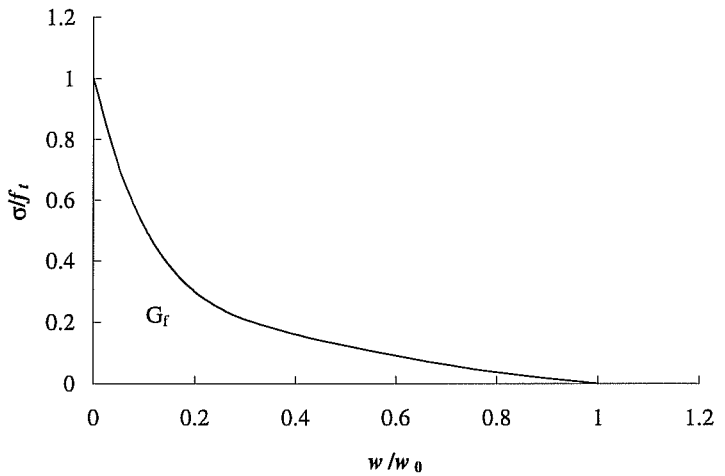

Figure 8.9 Normal Stress-Crack Opening Relation (Cornelissen et al. 1986)

The area under such a curve represents the energy absorbed within a fixed unit area when a crack sweeps through it, monotonically, to complete fracture. This is called the fracture energy, and is considered a material parameter. For normal concrete, its value is between 80 to 150 N/m, and depends on factors such as aggregate size, age of concrete, and water-cement ratio.

In numerical analysis of problems involving with concrete cracking, various simplified relations between stress and crack opening displacement have been used to model the fracture process zone. As shown in Figure 8.10, these include continuous curves, a linear model, a bilinear model (Hillerborg 1976, Petersson 1981), and a tri-linear model (Liaw et al. 1990). A model with a singular stress at the crack tip has also been proposed by Yon et al. (1991).

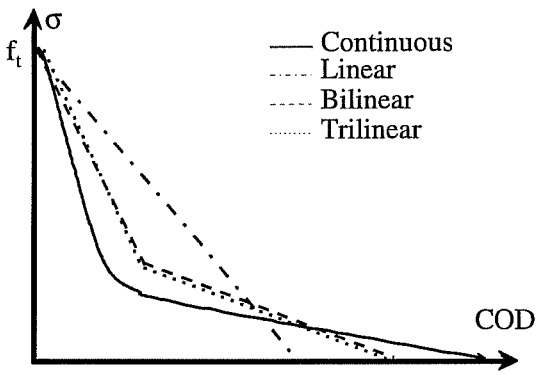

Figure 8.10 Simplified Stress-Crack Opening Relations

8.6 Methods of Modeling Concrete Cracking

8.6.1 Discrete-Crack Model

The discrete-crack model was first used by Ngo and Scordelis (1967). It is attractive physically, because it reflects the localized nature of cracking. However, its numerical implementation is hampered by the need to let the cracks follow the element boundaries, thereby requiring the introduction of additional nodal points and re-meshing of the original elements. With recent developments in the technology of interactive graphics, this model has been used in many applications. However, its implementation still places severe demands on computer hardware and software.

8.6.2 Smeared-Crack Modal

The smeared-crack model distributes local discontinuities over some tributary area within the finite element. It was pioneered by Bazant and Oh (1983), who proposed a crack band model for concrete fracture. However, the crack band model can only be used to model the crack process parallel to the element boundary. In this model, the process zone is considered to be a material property. Problems arose for the very important situation in which cracks are not parallel to the element boundaries (Rots et al. 1985). This problem was solved using the concept of an equivalent crack width (Rots et al. 1985), shown in

Figure 8.11. The ideal of the equivalent crack length is to ensure that the same amount of fracture energy along the crack path no matter what the orientation of the crack is. In this way, the lack of objectivity of the preliminary smeared model was eliminated.

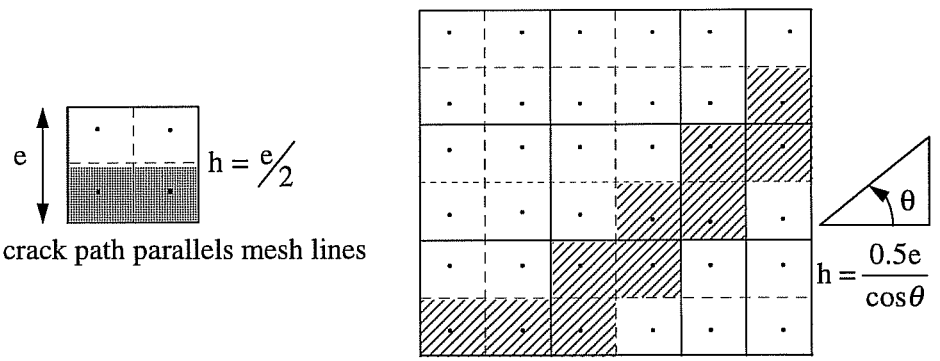

Figure 8.11 Equivalent Crack Band Width (Rots et al. 1985)

The smeared-crack model can be further categorized into fixed and rotating smeared crack models. In the fixed smeared-crack model, the orientation of each crack is determined when the cracking criterion is first exceeded, and then remains constant during the crack evolution. In this model, however, secondary cracks with the orientation different from that of the primary crack could occur. To eliminate this problem, the rotating crack model was developed, in which the current orientation of a crack always coincides with the maximum principal tensile strain.

The smeared crack model of Rots et al. (1985) is now described.

The basic assumption of the smeared crack model is the resolution of total strain increments into concrete strain increments and crack strain increments:

$$\Delta\underline{\varepsilon} = \Delta\underline{\varepsilon}^{co} + \Delta\underline{\varepsilon}^{cr} \tag{8-7}$$

where: $\Delta\underline{\varepsilon}$ = vector of total global strain increments;

$\Delta\underline{\varepsilon}^{co}$ = vector of concrete global strain increments; and

$\Delta\underline{\varepsilon}^{cr}$ = vector of crack global strain increments.

With the smeared-crack approach, the crack opening displacement is replaced by a normal local crack strain ε_{nn}^{cr}, and the crack sliding displacement is replaced by a shear local crack strain γ_{nt}^{cr}. The global crack strains are obtained by transforming the local crack strains to the global coordinate system:

$$\begin{bmatrix} \varepsilon_{xx}^{cr} \\ \varepsilon_{yy}^{cr} \\ \varepsilon_{xy}^{cr} \end{bmatrix} = \begin{bmatrix} \cos^2\theta & -\sin\theta\cos\theta \\ \sin^2\theta & \sin\theta\cos\theta \\ 2\sin\theta\cos\theta & \cos^2\theta - \sin^2\theta \end{bmatrix} \begin{bmatrix} \varepsilon_{nn}^{cr} \\ \varepsilon_{nt}^{cr} \end{bmatrix} \tag{8-8a}$$

or

$$\underline{\varepsilon}^{cr} = \underline{N}\,\underline{e}^{cr} \tag{8-8b}$$

where: $\underline{\varepsilon}^{cr}$ = vector of global strains;

$\underline{e}^{cr}$ = vector of local crack strains with respect to the crack axes;

θ = the angle between the global x-axis and the normal to the crack (Figure 8.12); and

$\underline{N}$ = crack strain transformation matrix.

For the case of plane stresses, the only stresses are a normal interface stress and a shear interface stress. The crack interface vector is related to the global stress vector:

$$\begin{bmatrix} \sigma_{nn}^{cr} \\ \sigma_{nt}^{cr} \end{bmatrix} = \begin{bmatrix} \cos^2\theta & \sin^2\theta & 2\sin\theta\cos\theta \\ -\sin\theta\cos\theta & \sin\theta\cos\theta & \cos^2\theta - \sin^2\theta \end{bmatrix} \begin{bmatrix} \sigma_{xx} \\ \sigma_{yy} \\ \sigma_{xy} \end{bmatrix} \tag{8-9a}$$

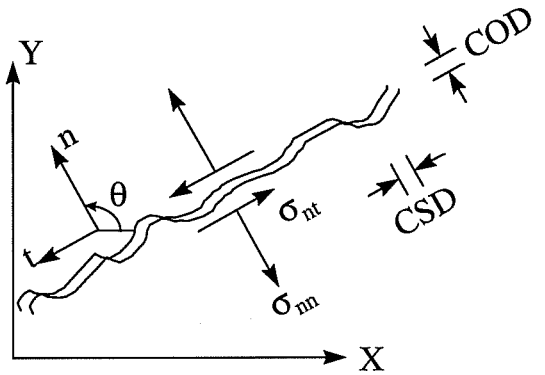

Figure 8.12 Crack Interface Stresses and Relative Displacements

or

$$\underline{s}^{cr} = \underline{N}^T \underline{\sigma} \tag{8-9b}$$

where: $\underline{s}^{cr}$ = vector of crack interface stresses;

$\underline{\sigma}$ = global stress vector; and

$\underline{N}^T$ = the crack stress transformation matrix, which is the transpose of the crack strain

transformation matrix.

The crack interface stresses are assumed to be incrementally related to the local crack strains:

$$\Delta \underline{s}^{cr} = \underline{D}^{cr} \Delta \underline{e}^{cr} \tag{8-10}$$

where: $\underline{D}^{cr}$ = the crack interface matrix.

In uncoupled form, $\underline{D}^{cr}$ can be expressed as:

$$\underline{D}^{cr} = \begin{bmatrix} D_c & 0 \\ 0 & G_c \end{bmatrix} \tag{8-11}$$

where: D_c = the tensile strain-softening modulus; and

G_c = the crack shear modulus.

Just as for the crack, a constitutive relation may be defined for the concrete:

$$\Delta\underline{\sigma} = \underline{D}^{co}\,\Delta\underline{\varepsilon}^{co} \tag{8-12}$$

where: $\underline{D}^{co}$ = linear elastic matrix according Hooke's law, defined by Young's modulus E and Poisson's ratio ν.

For cracked concrete, this relationship can be presented by subtracting the crack strains:

$$\Delta\underline{\sigma} = \underline{D}^{co}\left(\Delta\underline{\varepsilon} - N\Delta\underline{e}^{cr}\right) \tag{8-13}$$

Combining Equations 8-9 and 8-10 yields:

$$\underline{D}^{cr}\,\Delta\underline{e}^{cr} = \underline{N}^{T}\,\Delta\underline{\sigma} \tag{8-14}$$

Substituting this into Equation 8-13 gives:

$$\Delta\underline{e}^{cr} = \left[\underline{D}^{cr} + \underline{N}^{T}\,\underline{D}^{co}\,\underline{N}\right]^{-1}\underline{N}^{T}\,\underline{D}^{co}\,\Delta\underline{\varepsilon} \tag{8-15}$$

The final relation between increments of stress and increments of total strain is obtained by substituting this equation back to Equation 8-12:

$$\Delta\underline{\sigma} = \left\{\underline{D}^{co} - \underline{D}^{co}\,\underline{N}\left[\underline{D}^{cr} + \underline{N}^{T}\,\underline{D}^{co}\,\underline{N}\right]^{-1}\underline{N}^{T}\,\underline{D}^{co}\right\}\Delta\underline{\varepsilon} \tag{8-16}$$

8.6.3 Nonlocal Crack Model

A nonlocal continuum is a continuum in which at least some field variables are subjected to spatial averaging over a certain finite neighborhood of a point. In the nonlocal crack model, the strains and stresses of a crack are distributed to the integration points of adjacent finite elements, according to a certain localization limiter (Bazant et al. 1984).

8.7 Implementation of FEM

In this study, the behavior of axially-loaded headed tensile anchors was modeled with axisymmetrical, four-node elements. In the calculation, crack propagation can take place only in the r-z plane, using the fixed smeared-crack model. The orientation of the crack was determined when the maximum principal stress first exceeded the concrete tensile strength, and was fixed during the entire computational process.

8.7.1 Displacement Control Method

The displacement control method used in the program was first introduced by Ramm (1981), and is briefly described below.

In the ith iteration, the tangent load-deflection relation is rearranged so that the prescribed displacement, $\Delta U_2 = \Delta U^{ps}$, is separated from the other displacement components:

$$\begin{bmatrix} \overline{K}_{11}^i & \overline{K}_{12}^i \\ \overline{K}_{21}^i & K_{22}^i \end{bmatrix} \begin{bmatrix} \Delta \overline{U}_1^i \\ \Delta U_2 \end{bmatrix} = \Delta\lambda^i \begin{bmatrix} \overline{P}_1^s \\ P_2^s \end{bmatrix} + \begin{bmatrix} \Delta \overline{R}_1^i \\ \Delta R_2^i \end{bmatrix} \tag{8-17}$$

In this equation, the force vector consists of the applied increment force vector, $\underline{P}$, and the residual force vector, $\Delta\underline{R}$.

If the known variables are moved to the right-hand side,

$$\begin{bmatrix} \overline{K}_{11}^i & -\overline{P}_1^s \\ \overline{K}_{21}^i & -\overline{P}_2^s \end{bmatrix} \begin{bmatrix} \Delta \overline{U}_1^i \\ \Delta\lambda^i \end{bmatrix} = \begin{bmatrix} \Delta \overline{R}_1^i \\ \Delta R_2^i \end{bmatrix} - \begin{bmatrix} \overline{K}_{12}^i \\ \overline{K}_{22}^i \end{bmatrix} \Delta U_2 \tag{8-18}$$

The first equilibrium equation in Equation 8-18 is:

$$\overline{K}_{11}^i \cdot \Delta \overline{U}_1^i = \Delta\lambda^i \cdot \overline{P}_1^S + \Delta \overline{R}_1^i - \overline{K}_{12}^i \cdot \Delta U_2 \tag{8-19}$$

In this equation, the displacement vector ΔU_1^i can be divided into two parts: $\left(\Delta \overline{U}_1^i\right)^I$ for the applied force; and $\left(\Delta \overline{U}_1^i\right)^{II}$ for the residual force.

$$\Delta\overline{U}_1^i = \Delta\lambda^i \cdot \left(\Delta U_1^i\right)^I + \left(\Delta U_1^i\right)^{II} \tag{8-20}$$

The relations between the separated displacement vectors and the force vectors are

$$\overline{K}_{11}^i \cdot \left(\Delta\overline{U}_1^i\right)^I = \overline{P}_1^s \tag{8-21}$$

and

$$\overline{K}_{11}^i \cdot \left(\Delta\overline{U}_1^i\right)^{II} = \Delta\overline{R}_1^i - \overline{K}_{12}^i \cdot \Delta U_2 \tag{8-22}$$

Using the displacement vectors, the incremental parameter of the applied force vector is solved in the second equilibrium equation of Equation 8-18:

$$\Delta\lambda^i = \frac{-\Delta R_2^i + \overline{K}_{21}^i \cdot \left(\Delta\overline{U}_1^i\right)^{II} + K_{22}^i \cdot \Delta U_2}{\overline{P}_2^s - \overline{K}_{21}^i \cdot \left(\Delta\overline{U}_1^i\right)^I} \tag{8-23}$$

The total displacement increment and the total force increment are obtained by

$$\Delta\overline{U} = \sum_i \left[\Delta\lambda^i \cdot \left(\Delta\overline{U}^i\right)^I + \left(\Delta\overline{U}^i\right)^{II}\right] \tag{8-24}$$

and

$$\Delta\overline{P} = \sum_i \left[\Delta\lambda^i \cdot \overline{P}^s\right] \tag{8-25}$$

The total displacement and load vectors in each loading step are obtained by

$$\overline{U}^j = \overline{U}^{j-1} + \Delta\overline{U} \tag{8-26}$$

and

$$\overline{P}^j = \overline{P}^{j-1} + \Delta\overline{P} \tag{8-27}$$

This general method can be simplified by removing the process of stiffness modification. Instead of the modified stiffness $\overline{K}_{11}^i$, $\overline{K}^i$ is used in Equations 8-21 and 8-22:

$$\overline{K}^i \cdot \left(\Delta \overline{U}_1^i\right)^I = \overline{P}^s \tag{8-28}$$

and

$$\overline{K}^i \cdot \left(\Delta \overline{U}_1^i\right)^{II} = \Delta \overline{R} \tag{8-29}$$

where the prescribed displacement term is also removed.

Again, the incremental displacement vector is defined by the two displacement vectors obtained in Equations 8-28 and 8-29.

$$\Delta \overline{U}^i = \Delta \lambda^i \cdot \left(\Delta \overline{U}^i\right)^I + \left(\Delta U^i\right)^{II} \tag{8-30}$$

Of the incremental displacement vector components, the controlled incremental displacement should be the prescribed value:

$$\Delta U_2^i = \Delta \lambda^i \cdot \left(\Delta U_2^i\right)^I + \left(\Delta U_2^i\right)^{II} = \Delta U^{ps}. \tag{8-31}$$

In the first iteration, the incremental load parameter is obtained from Equation 8-31:

$$\Delta \lambda^1 = \frac{\Delta U^{ps} - \left(\Delta U_2^1\right)^{II}}{\left(\Delta U_2^1\right)^I} \tag{8-32}$$

After the first iteration, further incremental displacement is eliminated so that the total incremental displacement is equivalent to the prescribed value:

$$\Delta \lambda^i = -\frac{\left(\Delta U_2^i\right)^{II}}{\left(\Delta U_2^i\right)^I} \quad \text{for } (i \geq 2). \tag{8-33}$$

As shown before, since it eliminates the modification of the stiffness matrix, the simplified displacement-control method can reduce memory requirements and associated computational time (Ramm 1981, Park 1994).

8.7.2 Prediction of the Crack Path

During computation, it was found that if cracking was permitted at all integration points near the crack tip, convergence was very hard to achieve. To minimize the number of integration points with the cracked concrete properties, a scheme was developed to predict the crack path, and therefore to allow only the elements along the path to crack. Furthermore, to eliminate the unstable condition caused by the integration points in a single element, a four-node element with reduced integration points was used for modeling concrete cracking. Regular four-node elements were used for modeling uncracked concrete.

The cracking orientation is based on maximum tensile stress. The crack was prescribed to start at the tip of the anchor head; the two elements connected with that tip, just outside the anchor head, were also initially assigned as elements with concrete cracking properties. All elements are rectangular and are meshed so that each column of element has the same width and radius from the center of the anchor.

Based on the cracking orientation in the element, the crack path on the next column of element was predicted; elements intercepted by that path were changed to have only one integration point and were assigned with the properties of cracked concrete, or the possibility of cracking (Figure 8.13).

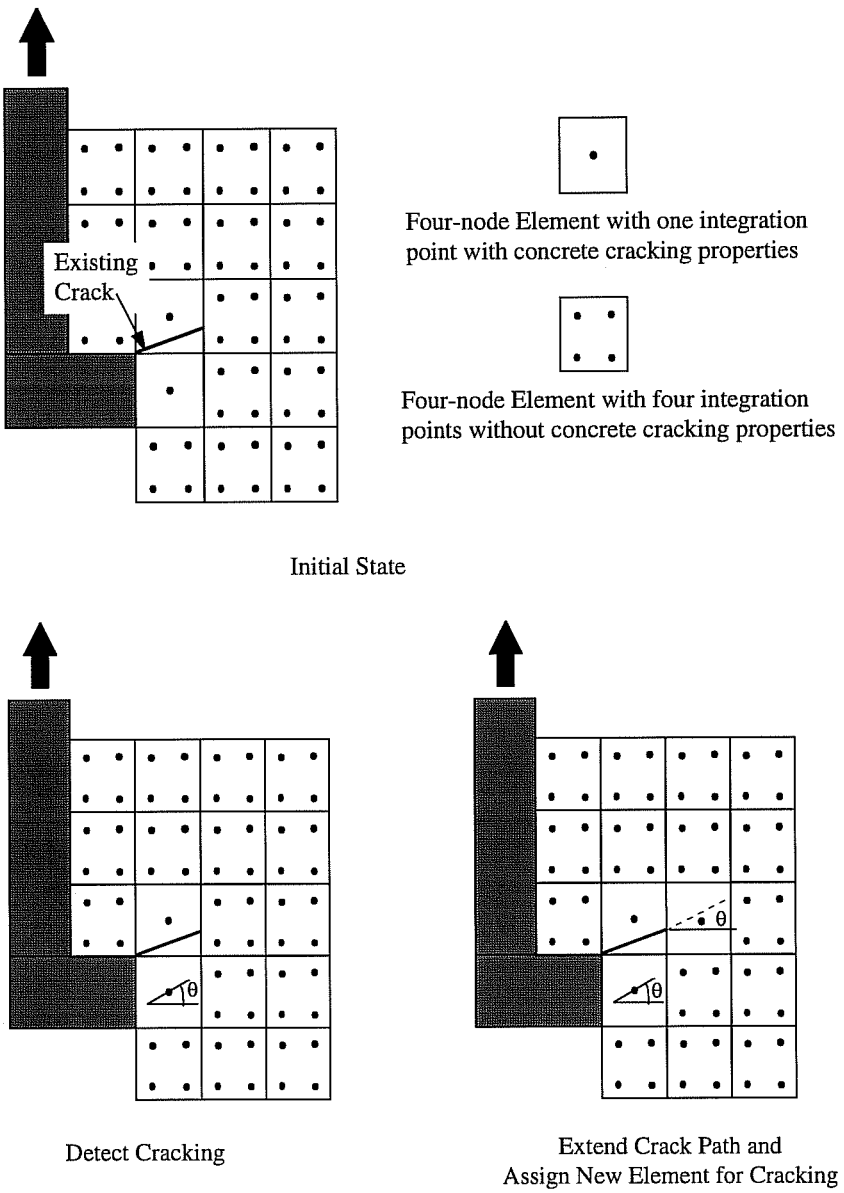

Figure 8.13 Prediction of Crack Path

8.7.3 Iteration Strategy

The incremental displacement criterion is used as the tolerance limit of convergence:

$$Tol = \left(\frac{\Delta \underline{U}^i \cdot \Delta \underline{U}^i}{\Delta \underline{U}^{tol} \cdot \Delta \underline{U}^{tol}} \right)^{1/2}$$

where: $\Delta \underline{U}^i$ = vector of the displacement increment at the ith iteration; and

$\Delta \underline{U}^{Tol}$ = vector of total displacements at the current loading step.

This criterion generally allows more residual forces than the force criterion with a given tolerance limit. In the calculation of this study, a convergence tolerance of 1% was found to give both acceptable accuracy and sufficiently rapid convergence.

Since the material behavior involves the descending branch of concrete stress-strain curve, negative terms can appear on the diagonals of the tangent stiffness matrix. When several elements having the cracked concrete proprieties, the numerical iterations may not converge. To prevent numerical difficulties, the following guidelines were used for stable and fast convergence, when the difficulties were encountered:

1) To avoid a negative or a very small stiffness element caused by elements of cracked concrete, the individual diagonal elements for cracked concrete (Equation 8.11) was changed to E/500 (de la Rovere 1990), where E is the elastic modulus of concrete.

2) When convergence is still difficult even with the strategy in 1), the initial elastic stiffness matrix is used, which was found to give the most stable convergence (de la Rovere 1990). However, such convergence requires a considerable number of iterations, and often results in a higher load than is correct at the given incremental, since the displacement criterion is used for convergence.

8.8 Case Study

A 3/4-inch (19-mm) diameter headed anchor embedded at 4 inches (102 mm) was used as a calculation example. The concrete compressive cylinder strength, f_c, was taken as 4700 psi (32.4 MPa). To avoid any boundary effects, the concrete specimens thickness

was chosen as 9.5 inches (241 mm), and its diameter was at least 9.25 inches (about 2.3 times the embedment).

8.8.1 Finite Element Meshes

The two different finite elements meshes used in this study are shown in Figures 8.14 (coarse mesh) and 8.15 (fine mesh). In the finer mesh, more elements were added in the region of the crack to investigate the effect of element size on the final results (objectivity criterion). No forces was assumed between the anchor shank and the concrete. The applied force would be transferred only through the anchor head.

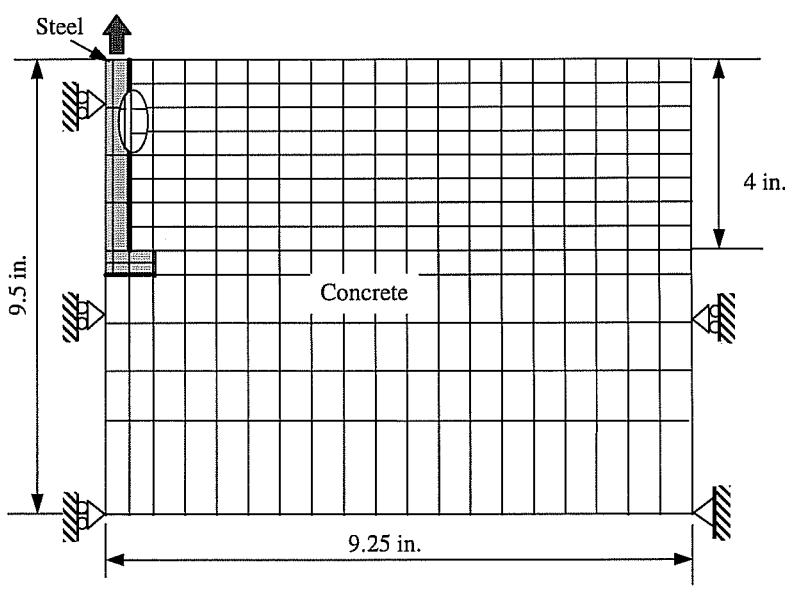

Figure 8.14 Coarse Finite Element Mesh

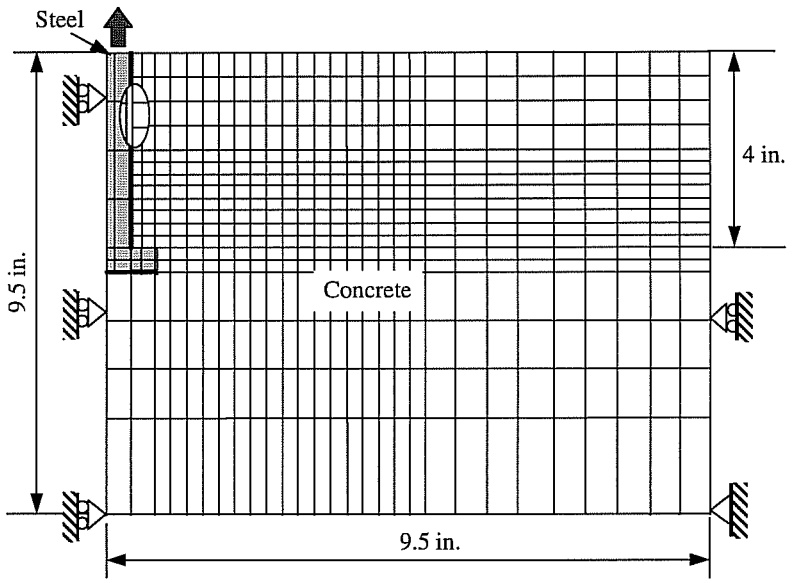

Figure 8.15 Fine Finite Element Mesh

In all FEM modeling, no effort has been made to model local concrete crushing near the anchor head. All material outside the cracked region is assumed linearly elastic.

8.8.2 Concrete Properties

Of the properties of the concrete tested in this testing program only the compressive cylinder strength was known. To make numerical analysis possible, the typical concrete properties for normal concrete from other research were used. The modulus of elasticity was assumed as 3900000 psi (26888 MPa). The Poisson' Ratio was assumed as 0.18.

8.8.2.1 Normal Stresses versus Crack Opening Displacement

The maximum tensile strength of the concrete was assumed $5\sqrt{f_c}$, with $f_c = 4700$ psi (32.4 MPa), which gives a value of 342 psi (2.36 MPa). As shown in Figure 8.16, a bilinear relation was used, which gives a fracture energy of 0.577 lb/in. (101 N/m).

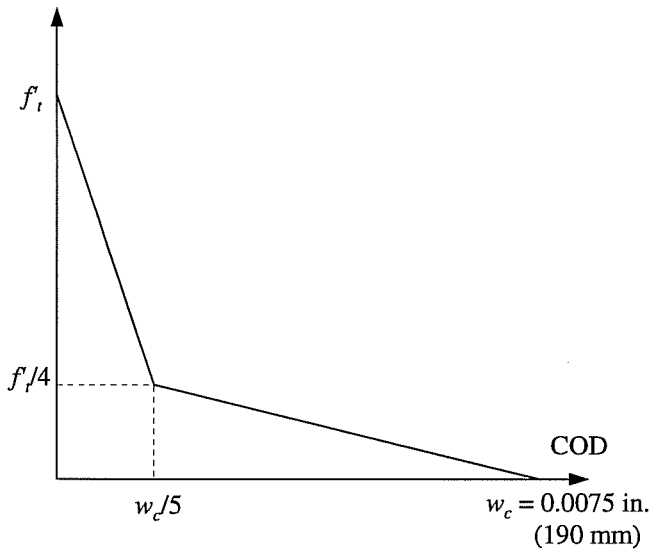

Figure 8.16 Bilinear Normal Stress versus Crack Opening Displacement Used in Calculations

8.8.2.2 Shear Stresses

The relation between shear stress and crack shear displacement expressed in Equation 8-5 (Fenwick 1968) was used. Shear stress was assumed to be negligible for COD greater than 0.02 inch (0.508 mm).

To investigate the effect of shear stress on the ultimate capacity of anchor, another approximation method using shear retention stiffness factor was also used. It assumed that the shear capacity on the crack in the cracked concrete is a certain percentage (β) of its original shear stiffness, and the shear will be ignored when the crack opening displacement is larger than a certain value (Δ). In the program, the value of Δ was set as 0.002 inch (0.051 mm); two values of β, 0.02 and 0.2, were used. This is shown in Figure 8.7.

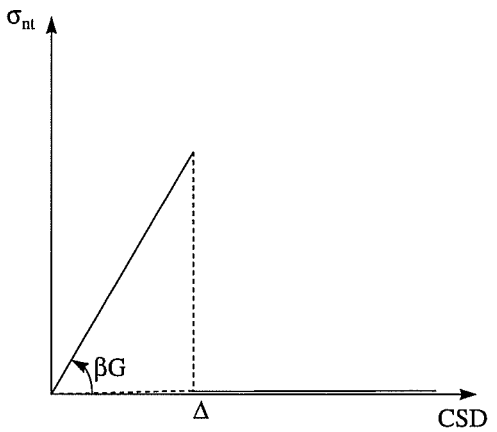

Figure 8.17 Shear Stiffness on Concrete Crack (Shear Stress v. CSD)

8.9 Calculation Results and Discussion

8.9.1 Analytical Load-Displacement Behavior

Figure 8.18 compares a typical calculated results with the test results measured at the concrete surface. The calculated capacity is very close to the tested values. However, the calculated displacement is much lower than the real behavior. In these tests, anchors were prestressed. Without this prestressing, greater displacements could be expected. In testing most displacement occurred at the anchor head, in the form of concrete plastic deformation (CEB 1991). To successfully model the load-displacement behavior of anchor in concrete, a concrete plastic deformation model is needed.

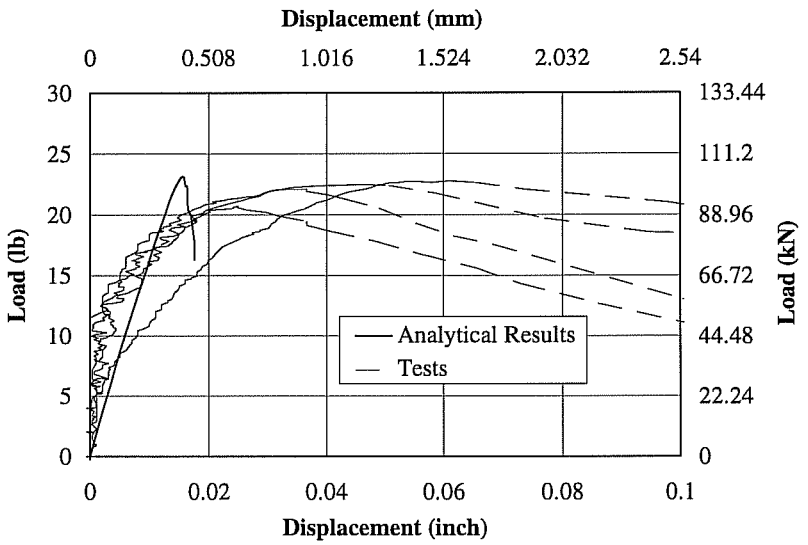

Figure 8.18 Comparison of Calculated versus Test Results

8.9.2 Effect of Element Meshes on Anchor Capacity and Crack Path

Figures 8.19 to 8.24 compare the calculated results using two different element meshes. Figure 8.21 also compares the calculated displacement at the anchor heads and at the anchor shank at the concrete surface. In the figures that compare crack paths, the cone shape measured after single-anchor tests were also noted.

In all cases, the capacities calculated using the fine element mesh were higher than those with the coarse mesh. However, the load-displacement curves have no significant difference in the small-load range. The predicted crack paths are also very close to the test data, especially within a radius smaller than 6 inches (152 mm). It can be concluded that the smeared crack approach used here is objective and that the method of equivalent crack width is effective.

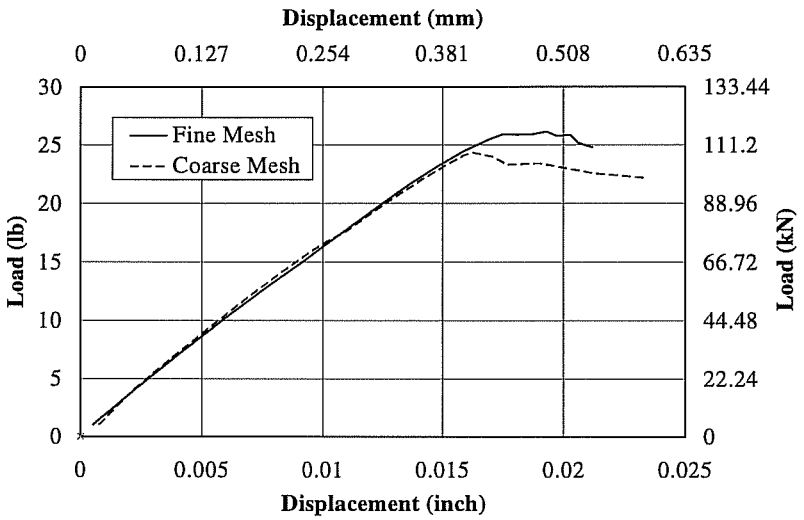

Figure 8.19 Comparison of Load-Displacement Behavior on Two Element Meshes Calculated with Crack Shear Stress Relation of Fenwick (1968)

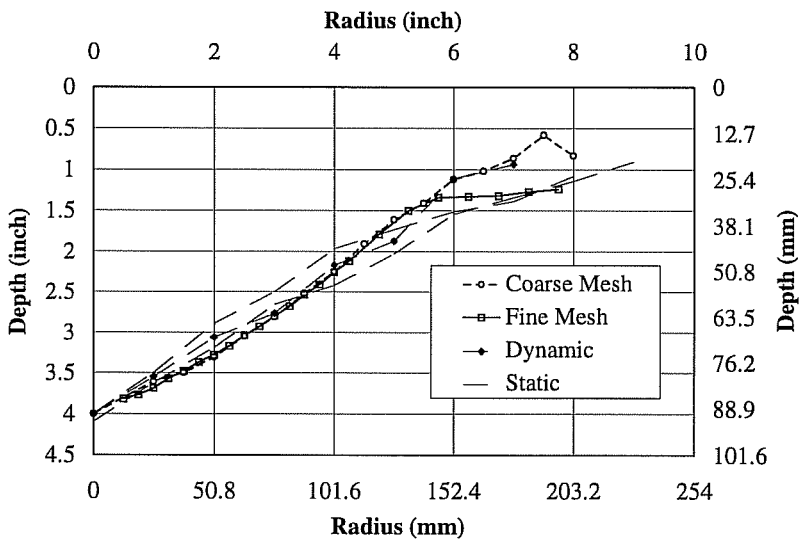

Figure 8.20 Comparison of Crack Path on Two Element Meshes Calculated with Crack Shear Stress Relation of Fenwick (1968)

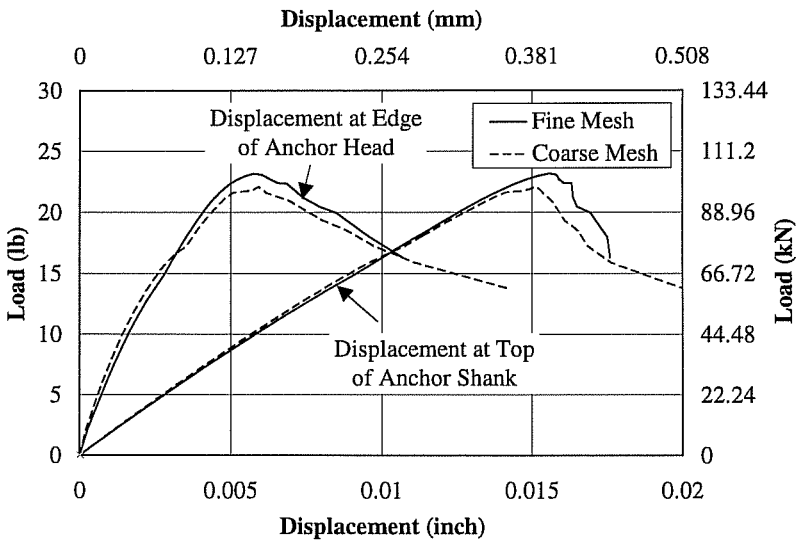

Figure 8.21 Comparison of Load-Displacement Behavior Using Two Element Meshes Calculated with Crack Shear Stress Retention of 0.02

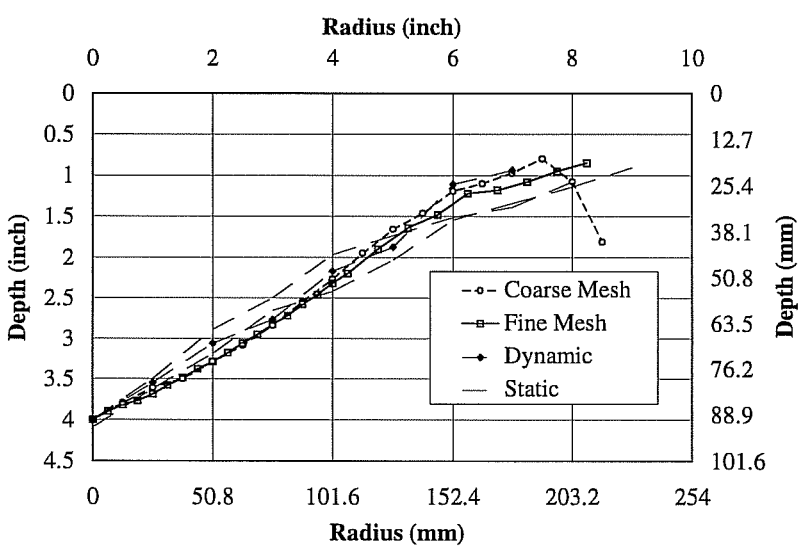

Figure 8.22 Comparison of Crack Path Using Two Element Meshes Calculated with Crack Shear Stress Retention of 0.02

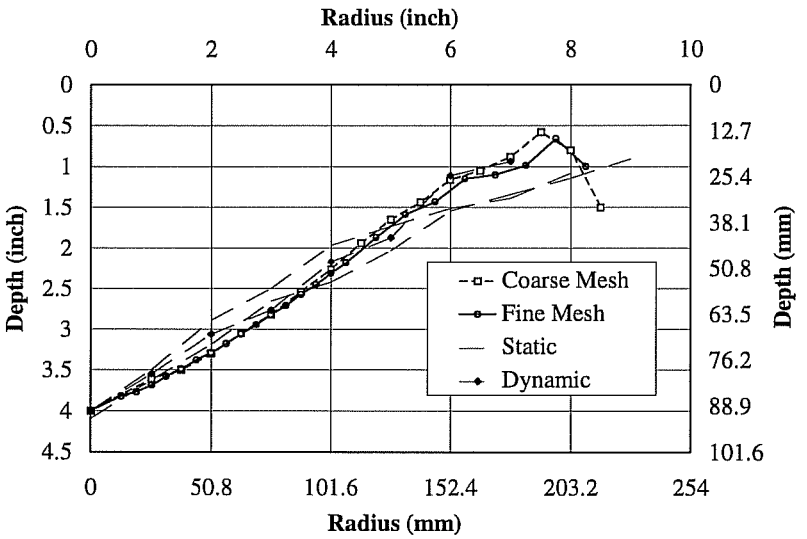

Figure 8.23 Comparison of Crack Path on Two Element Meshes Calculated with Crack Shear Stress Retention of 0.2

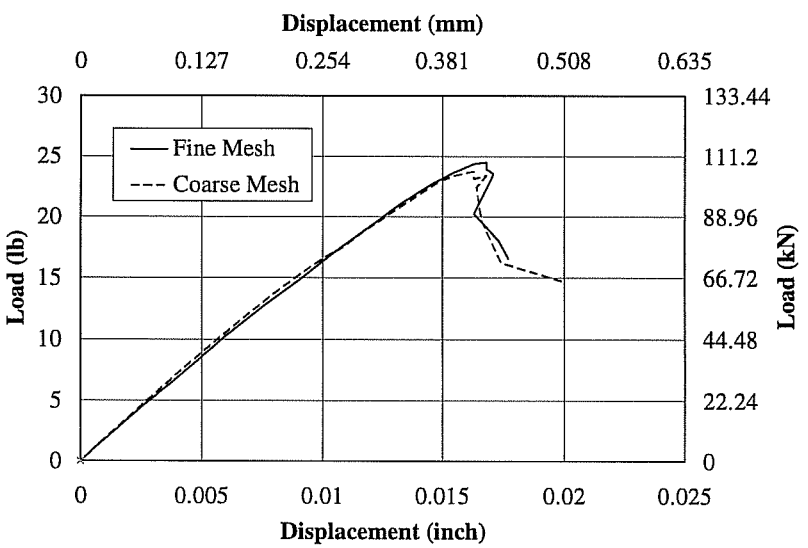

Figure 8.24 Comparison of Load-Displacement Behavior Using Two Element Meshes Calculated with Crack Shear Stress Retention of 0.2

8.9.3 Effect of Shear Stress on Crack Plane on Capacity and Crack Path

Figure 8.25 compares the calculated load-displacement behavior of anchor, using the fine mesh and different crack shear stress-CSD relations. Figure 8.26 compares the corresponding crack paths.

As seen from Figure 8.25, anchor capacity increases with the increasing shear stresses. However, calculated load-displacement behavior before the peak is not significantly affected by the shear stress on across the crack. The capacity calculated with a cutoff shear-CSD relation drops rapidly after the peak load is reached, while that calculated with a relation with residual shear capacity remains near the maximum load over a large displacement range. This is mainly owing to the component in the loading direction of the remaining shear stress along the crack after concrete cracking. In calculations with the shear-CSD relation of Fenwick (1968), the shear stress in the cracked concrete at some integration points of cracked concrete exceeded the tensile strength.

Crack paths were not significantly affected by the shear-CSD relations. They only

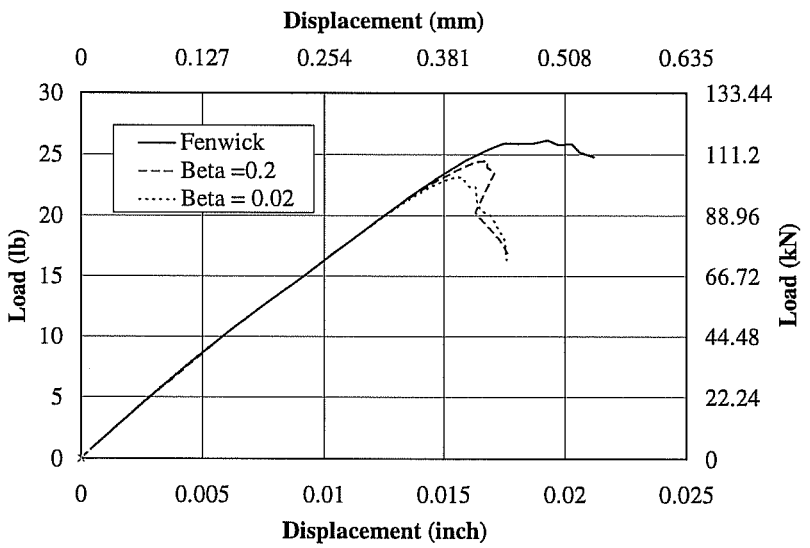

Figure 8.25 Comparison of Calculated Load-Displacement Behavior of Anchor Using Different Crack Shear Stress-CSD Relations

differed at a large radius near the concrete specimen edge, when the maximum capacity of anchor had already been reached.

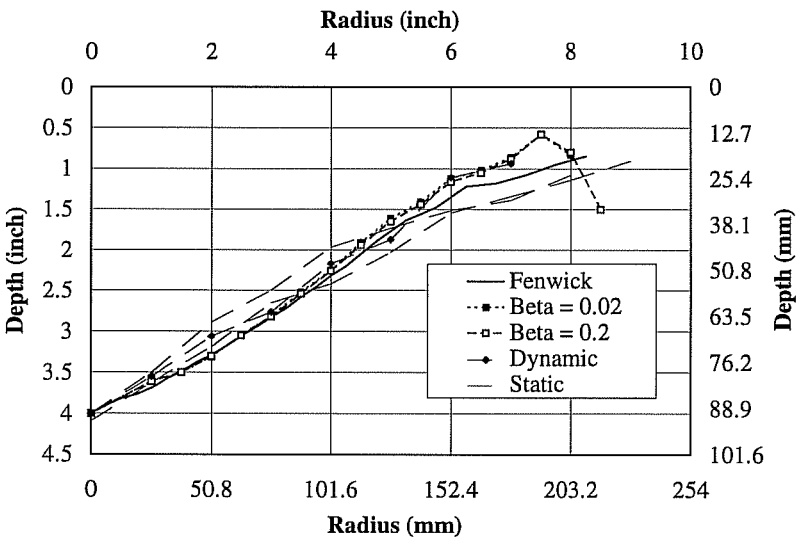

Figure 8.26 Comparison of Crack Paths Using Different Crack Shear Stress-CSD Relations

CHAPTER 9

SUMMARY, CONCLUSIONS, AND RECOMMENDATIONS

9.1 Summary

This research project, supported by the US Nuclear Regulatory Commission (NRC) at The University of Texas at Austin, is intended to assess the seismic behavior of single and multiple-anchor connections in cracked and uncracked concrete. It includes study of single anchors under tensile loading; single anchors under oblique tensile loading; double-anchor connections under tensile loading; single near-edge anchors under shear loading; near-edge double-anchor connections under eccentric shear loading; and multiple-anchor connections under shear at small eccentricities.

This dissertation addresses part of that research program. Single-anchor tensile tests in cracked concrete are presented first, and are compared to the results of Rodriguez (1995) and Hallowell (1996) in terms of normalization factors for CC Method, using average values of five replicates in each case. These tests were intended to evaluate the effect of concrete cracking on the concrete breakout capacities of various types of anchors under static and dynamic loading. For that reason, the nominal embedment depth of all anchors was chosen at 4 inches (102 mm) to ensure the anchors would fail by concrete breakout. To assess the effect of dynamic loading, all dynamic tests on single anchors were loaded with a linearly increasing ramp load with a time to failure of about 0.1 second. Results for double-anchor near-edge connections loaded in shear at a small eccentricity were also presented. For these tests, the effects of concrete cracking, hairpins, and dynamic loading were discussed in detail. In those connections, the front anchor was

designed close to the concrete edge and the back anchor had an edge distance large enough to develop its steel capacity. A small eccentricity ($e < e_2$) of applied shear was chosen, so that the back anchor would be subjected to combined tension and shear. In this way, the shear redistribution to both anchors could be investigated through testing. The pattern of dynamic loading was also a linearly increasing ramp load with a time to failure of about 0.1 second. Finally, test results for multiple-anchor connections were presented. The purpose of the multiple-anchor connection tests was to assess the effect of earthquake-type loading on the behavior of connections under various conditions, including anchor types, hairpins, concrete cracking, and vicinity to member edges. The seismic load-displacement response of a multiple-anchor connection was estimated, and subsequently used as a dynamic loading input to the connection. All anchors were installed with full embedment. Two eccentricities of shear load were used in tests, with the emphasis on the smaller eccentricity, at which the tension anchors would be subjected to both tension and shear. Based on the test results and on calculated results from the BDA5 program using the data of single-anchor in oblique tension obtained by Lotze (1997), plastic design methods were proposed for each failure mode of multiple-anchor connections. This dissertation was mainly focused on the dynamic behavior of anchors connections. Additional information regarding anchor connection design is given in Cook (1989) and Lotze (1997).

In addition, a finite element program was developed to axisymmetrically model anchor behavior in tensile loading. The smeared cracking method was used in the program to model concrete crack propagation. The analytical results were compared with test results.

9.2 Conclusions

9.2.1 Conclusions from Single-Anchor Tension Tests in Cracked Concrete

The conclusions are all based on the averages of five replicate tests, all of which were designed to fail in concrete breakout. The capacity was presented in terms of mean

normalization factors for the CC Method. In the dynamic tests, the connections were intended to fail in 0.1 second under monotonic, ramp-type dynamic loading.

1) Based on all the test results obtained from this testing program, which are presented and discussed in Sections 5.2 and 6.2, and on the data from the tests of Rodriguez (1995) and Hallowell (1996), Table 9.1 summarizes the mean normalization coefficients obtained here for the CC Method for single anchors, using US customary units. Tensile breakout capacities are well described by the CC Method.

2) Table 9.2 shows ratios of static tensile breakout capacity (cracked concrete), dynamic capacity (uncracked concrete), and dynamic capacity (cracked concrete), all divided by static capacity in uncracked concrete. For the CIP and UC1 anchors, these ratios all exceed unity. For the UC2, Sleeve, and EAII anchors, the ratios are less than unity. For the grouted anchors, they are considerably less than unity. The tests of Rodriguez (1995) and Lotze (1997) show that the effect of anchor spacing and edge distance are essentially the same for dynamic as for static loading. The implications of Table 9.2

Table 9.1 Mean Normalization Coefficients for Tensile Anchors in Various Conditions Obtained Here for CC Method

Anchor Type	Load Type and Concrete Condition			
	Static Uncracked	Dynamic Uncracked	Static Cracked	Dynamic Cracked
Cast-In-Place	41.6	53.9	36.2	52.3
Grouted	41.2	57.0	24.5	15.5
UC1, 3/8 in. (10 mm)	37.2	44.4	35.6	41.1
UC1, 3/4 in. (19 mm)	39.4	49.0	41.7	46.2
UC2, 3/4 in. (19 mm)	43.7	53.6	28.5	45.2
Sleeve, 10 mm	37.4	38.7	29.9	29.7
Sleeve, 20 mm	44.3	55.1	35.3	39.5
EA II	36.7	37.8	29.7	28.0

are clear. Anchors with capacity ratios (dynamic cracked / static uncracked) greater than 1.0, and designed for ductile behavior in uncracked concrete under static loading, will probably still behave in a ductile manner in cracked concrete under dynamic loading.

3) Based on all the test results obtained from this testing program, which are presented and discussed in Sections 5.2 and 6.2, and on the data from the tests of Rodriguez (1995) and Hallowell (1996), Table 9.3 summarizes the average displacements at maximum load of the tested single anchors.

4) As discussed in Sections 6.2.1 and 6.2.2, under dynamic loading in cracked concrete, expansion anchors (Expansion Anchors II and Sleeve Anchors of 10 mm) have a greater tendency to pull out, due to the smaller dynamic friction coefficient. As a result, combined with the effect of concrete cracking, their dynamic capacity in cracked concrete decreased more than their static capacity in cracked concrete, but with a larger

Table 9.2 Ratios of Tensile Breakout Capacities (Static, Cracked; Dynamic, Uncracked; and Dynamic, Cracked) to Static Tensile Breakout Capacities in Uncracked Concrete

Anchor Type	Load Type and Concrete Condition		
	Static Cracked / Static Uncracked	Dynamic Uncracked / Static Uncracked	Dynamic Cracked / Static Uncracked
Cast-In-Place	0.87	1.30	1.26
Grouted	0.59	1.38	0.38
UC1, 3/8 in. (10 mm)	0.96	1.19	1.10
UC1, 3/4 in. (19 mm)	1.06	1.24	1.17
UC2, 3/4 in. (19 mm)	0.65	1.23	1.03
Sleeve, 10 mm	0.80	1.03	0.79
Sleeve, 20 mm	0.80	1.23	0.89
EA II	0.81	1.03	0.76

Table 9.3 Average Displacements at Maximum Load of Single Tensile Anchors in Various Conditions

Anchor Type	Load Type and Concrete Condition							
	Static Uncracked		Dynamic Uncracked		Static Cracked		Dynamic Cracked	
	in.	mm	in.	mm	in.	mm	in.	mm
Cast-In-Place	0.047	1.19	0.069	1.75	0.051	1.30	0.105	2.67
Grouted	0.043	1.09	0.074	1.88	0.032	.081	0.124	3.15
UC1, 3/8 in. (10 mm)	0.099	2.51	0.136	3.45	0.093	2.36	0.137	3.48
UC1, 3/4 in. (19 mm)	0.112	2.84	0.195	4.95	0.125	3.18	0.171	4.34
UC2, 3/4 in. (19 mm)	0.067	1.70	0.096	2.44	0.039	0.99	0.061	1.55
Sleeve, 10 mm	0.112	28.4	0.089	2.26	0.111	2.79	0.138	3.51
Sleeve, 20 mm	0.151	3.84	0.147	3.73	0.146	3.71	0.062	1.57
EA II	0.218	5.54	0.245	6.22	0.158	4.01	0.467	11.9

displacement, compared to their corresponding capacities in uncracked concrete. Their dynamic capacity in cracked concrete was also smaller than their static capacity in cracked concrete.

5) As discussed in Section 6.2.2, in cracked concrete, the capacity of the 20-mm Sleeve Anchor decreased under both static and dynamic loading, compared to the corresponding tests in uncracked concrete. The increase in capacity due to dynamic loading is much higher in uncracked concrete than in cracked concrete. The step inside the expansion sleeve of this anchor, designed to limit its expansion force on surrounding concrete, affects its load-displacement behavior. When the cone touches the step, after being pulled farther into the expansion sleeve under tension, the friction between the expansion sleeve and the surrounding concrete determines the anchor behavior. Because of a smaller maximum clamping force between the cone and surrounding concrete due to a large gap caused by crack opening, and of a smaller dynamic friction coefficient, the friction between the expansion sleeve and surrounding

concrete is smaller in cracked concrete than in uncracked concrete, resulting in more tests with pullout failure under dynamic loading than under static loading.

6) As discussed in Section 6.2.4, compared to the corresponding tests in uncracked concrete, the capacity in cracked concrete of 3/8-inch (10-mm) Undercut Anchor 1 decreased slightly (less than 7%) under both static loading and dynamic loading. Its dynamic capacity in cracked concrete increased compared to its static capacity in cracked concrete, like its dynamic capacity in uncracked concrete.

7) As discussed in Section 6.2.4, the effect of cracks on 3/4-inch (10-mm) Undercut Anchor 1 was also very small. However, the capacity of 3/4-inch (10-mm) Undercut Anchors 1 in cracked concrete increased under static loading, and decreased under dynamic loading, compared to its corresponding tests in uncracked concrete. In cracked concrete, the dynamic capacity exceeds the static capacity. The increase in static load capacity in cracked concrete was not expected. Nonetheless, considering the relatively small increase and the small scatter in the other capacities of this type of anchor, the test results are considered valid.

8) As discussed in Section 6.2.5, compared to the corresponding tests in uncracked concrete, the capacity of Undercut Anchor 2 decreased in cracked concrete under both static and dynamic loading. Comparing the tests of UC2 in cracked concrete only, the dynamic capacity exceeds the static one. This increase is much higher than for the UC1 anchors. The installation procedure (fully pre-load of the anchor) eliminates the concrete plastic deformation under tension, and reduces the anchor displacement. As a result, the dynamic loading rate was increased at the ultimate load range, which increased the apparent dynamic capacity of UC2 more than that of UC1 anchors.

9) As discussed in Section 6.2.3, the capacity of Grouted Anchors in cracked concrete decreased the most in all tested anchors under both static and dynamic loading. Their dynamic capacity in cracked concrete dropped dramatically, compared to their dynamic capacity in uncracked concrete, because of the loss of friction at the interface between the grout and the base concrete due to cracking.

10) As discussed in Section 6.2.6, the additional crack openings measured in tests increased more rapidly than the applied load, due to the more rapid increase in the transverse deflection on the concrete surface of the breakout cones. The additional crack opening is a valid indicator of the expansion force exerted by an anchor head, especially in the low-load range

11) In terms of the CC Method, and using the US customary units, the normalization coefficients listed in Table 9.4 are appropriate for estimating the capacity of single tensile anchors in various conditions.

Table 9.4 Appropriate Normalization Coefficients (CC Method) for Single Tensile Anchors in Various Conditions

Anchor Type	Load Type and Concrete Condition			
	Static Uncracked	Dynamic Uncracked	Static, Cracked	Dynamic, Cracked
Cast-In-Place	41	50	35	50
Grouted	41	50	N/A	N/A
UC1, 3/8 in. (10 mm)	39	45	35	40
UC1, 3/4 in. (19 mm)	39	45	39	40
UC2, 3/4 in. (19 mm)	41	50	28	40
Sleeve, 10 mm	35	35	30	30
Sleeve, 20 mm	41	50	33	39
EA II	35	35	28	28

9.2.2 Conclusions from Double-Anchor Connection Shear Tests

These conclusions are based on the discussions of Sections 6.3.2 and 6.3.3, which were based on the averages of 5 replicates. The tested double-anchor connections failed by

concrete breakout under shear at the front anchor and steel fracture of the back anchors. In the dynamic tests, the connections were intended to fail in about 0.1 second under ramp-type dynamic loading.

1) The overall behavior of double-anchor shear connections is a combination of the behavior of the front (near-edge) anchor and the back anchor. The load-displacement curve is usually two-peaked, with the first peak corresponding to edge breakout of the front anchor, and the second peak corresponding to fracture of the back anchor. The maximum capacity is usually the fracture capacity of the back anchor, plus the residual capacity of the front anchor at the same displacement.

2) The maximum capacities of near-edge, two-anchor connections under ramp-type dynamic loading were higher than the corresponding static capacities. This increase is mainly attributed to the increased remaining shear force in the front anchors. The dynamic capacities at the concrete edge breakout were also higher than the corresponding static capacities, because of the increase in the concrete edge breakout capacity under dynamic loading. Reasons for these individual effects are discussed below. Their overall implication is that multiple-anchor shear connections, designed for ductile behavior in uncracked concrete under static loading, will probably still behave in a ductile manner in cracked concrete under dynamic loading.

3) The capacity of double-anchor shear connections was dominated by the behavior of the back anchor. This was essentially unaffected by concrete cracking, and was increased by about 25% to 30% by ramp-type dynamic loading.

4) The edge breakout capacity of the front anchor was about 20% less than predicted by the CC Method. Concrete cracking reduced this capacity by about 20%. Ramp-type dynamic loading increased this capacity by at least about 10%. Close hairpins increased this capacity by about 30%. The front-anchor shear necessary to produce concrete edge breakout was probably reduced by the simultaneous presence of baseplate shear and compression, on the concrete breakout body. This probably account for the over-prediction from the CC Method.

5) The most significant effect of close hairpins was to increase the sustained capacity of the front anchor after concrete edge breakout, and to permit the front anchor to form a flexural mechanism. Thereby, hairpins increased the capacity and ductility of near-edge shear connections.

6) The gap between the baseplate and anchors, and between anchors and the concrete, had little effect on the load capacities of two-anchor connections tested in this study.

9.2.3 Conclusions from Multiple-Anchor Connection Tests

In the dynamic tests on multiple-anchor connections, the connections were loaded dynamically under a simulated earthquake-type, reversed, cyclic loading. Some static tests were also conducted as baseline tests for comparison. The conclusions from these tests are:

1) Multiple-anchor connections in uncracked or cracked concrete, with or without edge effect, and with or without hairpins, loaded dynamically under reversed cyclic loading histories representative of seismic response, behaved consistently with the results of previous single- and double-anchor tests of this study. Previous observations regarding the load-displacement behavior, and failure mechanisms of single and double anchors, were applicable in predicting the behavior of complex, multiple-anchor connections under simulated seismic loading. The implications of this are clear. Multiple-anchor connections designed for ductile behavior in uncracked concrete under static loading, will probably still behave in a ductile manner in cracked concrete under dynamic loading.

2) Anchors that show relatively good performance when tested individually in cracked concrete (CIP headed anchors, UC1, and 20-mm diameter Sleeve) would also be expected to show relatively good performance when used in multiple-anchor connections subjected to seismic loading. Anchors that show relatively poor performance when tested individually in cracked concrete (Grouted Anchor, EAII, and 10-mm diameter Sleeve) would also be expected to show relatively poor performance when used in multiple-anchor connections subjected to seismic loading.

3) Cyclic load-displacement behavior of multiple-anchor connections is accurately bounded by the corresponding static load-displacement envelope, and also by the static load-displacement envelope predicted by the BDA5 program. In other words, dynamic cycling does not significantly influence the fundamental load-displacement behavior of a multiple-anchor connections.

4) Under dynamic reversed cyclic loading in both uncracked and cracked concrete, the load-displacement curves of multiple-anchor connections with the UC1 Anchor basically follow the static ones in uncracked concrete over most displacements, differing only near the ultimate load. Dynamic reversed loading did not significantly affect the maximum dynamic capacity. In uncracked concrete, the connection had larger displacements under reversed dynamic than under static loading. Under dynamic reversed loading, connections in cracked concrete had slightly larger displacements than those in uncracked concrete.

5) Under dynamic reversed cyclic loading, multiple-anchor connections with Expansion Anchor II had very large displacements. In both uncracked and cracked concrete, the connections loaded at 12-inch (305-mm) eccentricity failed by steel fracture. The test in cracked concrete had a larger displacement and smaller capacity than that in uncracked concrete. The connection loaded at an 18-inch (457-mm) eccentricity experienced pullout failure.

6) Little effect of the baseplate flexibility was observed on the load-displacement behavior of multiple-anchor connections, even though the moment applied to the baseplate at the edge of the attached member (by the compression reaction of the concrete) exceeds the tested yield moment of the baseplate by about 25%.

7) The concrete edge breakout capacity remained almost constant for near-edge, multiple-anchor connections of UC1 Anchors with both eccentricities, under static loading without or with hairpins, and under dynamic reversed cyclic loading with hairpins. Due to gaps between the anchor shanks and the hairpins, the effect of hairpins on the concrete edge breakout capacity for undercut anchors is not as great as for cast-in-place

anchors. Because of the smaller transient loading rate, the concrete edge breakout capacity did not increase as much under dynamic reversed loading as had been previously observed under dynamic ramp loading to failure.

8) As with the double-anchor shear connections, hairpins increased the ultimate capacity toward the edge, of near-edge, multiple-anchor connections. This capacity can be accurately predicted by assuming a flexural mechanism in the near-edge anchors. Hairpins also reduced the concrete edge breakout volume, and increased the lateral blowout capacity of near-edge anchors, and thereby increased the maximum capacity, for loading away from the edge, of those same connections.

9) As with the double-anchor shear connections, the forces induced by the baseplate on the edge breakout volume of near-edge, multiple-anchor connections significantly reduced the concrete edge breakout capacity.

10) The capacity of multiple-anchor connections at large edge distances was accurately predicted by the Modified Plastic Method proposed by the author. This method corrects the overestimates of capacity in the original Plastic Method of Cook (1989), and the underestimation of capacity in the Modified Plastic Method of Lotze (1997). However, this judgment was based on the calculated results from the BDA5 program, as there is insufficient test data available for comparison.

9.2.4 Conclusions Regarding Finite Element Analysis

1) The fixed smeared cracking approach used in this study can accurately predict the tensile capacity of anchors. The predicted crack path was close to the measured cone shapes. However, displacement behavior was not successfully modeled, due to the fact that concrete plastic deformation at the anchor head was ignored.

2) The maximum shear stress that can be transferred across a concrete crack has no significant effect on the load-displacement behavior of anchors in concrete, nor on the predicted crack path. Maximum predicted anchor breakout capacity increases with

increasing cracked concrete shear capacity. However, the post-peak load-displacement behavior is affected by that maximum shear stress.

3) Change in the finite element mesh had no significant effect on the calculated capacity, nor on the predicted crack path. The equivalent crack width concept is therefore objective for this problem.

4) Computational time was dramatically reduced and computational stability dramatically increased, by permitting cracking only in element on or near the projected crack path, and using a reduced number of integration points for those elements. However, this finite element approach would still be too complicated and time-consuming for use on multiple-anchor connections.

9.2.5 Conclusions Regarding BDA5 Program

The BDA5 program (Li 1994) generally predicts reasonably and very quickly the load-displacement behavior of multiple-anchor connections. However, it relies heavily on the input data file of the load-displacement behavior of single anchors. To obtain this input file, many tests must be conducted. Since load-displacement behavior varies with anchor configuration (diameter and embedment), an enormous amount of work would be required to obtain a complete set of input files for different anchor configurations.

9.3 Recommendations for Further Research

1) Tests on single grouted anchors indicated that the concrete-grout interface is critical to its capacity. In the tests of this study, no special roughening was used. To increase the load-transfer capacity along the interface, it is very important to roughen the holes. However, the roughening methods and their effectiveness need to be investigated, especially under dynamic loading.

2) For near-edge connections, the effect of the compression force of the baseplate on the bearing and shear strength of the supporting concrete was demonstrated in the near-

edge, multiple-anchor tests. However, this effect is not clearly understood, and further research is needed.

3) The effect of gaps between the baseplate and anchor shank, and between the anchor shank and the surrounding concrete, on the capacity of connections depends on the stiffness of anchor shanks, which is determined by their diameter and by the possible presence of a sleeve. Studies should be performed on connection with various diameters of anchors with different gaps to investigate the effect of gaps on shear redistribution.

4) For a near-edge, multiple-anchor connection loaded under shear towards the member edge, in which the back anchors as well as the near-edge anchors are expected to fail in concrete breakout, the concrete breakout of the front anchors may affect the breakout capacity of the back anchors. More research is needed to determine the ultimate capacity of connections with this configurations.

5) A Modified Plastic Method was proposed here to improve the prediction of multiple-anchor connections loaded at small eccentricities. However, test data on those connections were not available. Tests are needed on multiple-anchor connections at small eccentricities to verify the proposed design method in this study.

6) The tests of multiple-anchor connections and the corresponding design methods all address connections in which baseplates rested on the concrete surface. However, the position of the baseplates varies (flush with the concrete surface, or with a grout pad). Further tests are needed to investigate the strength of multiple-anchor connections with different baseplate positions.

7) Because they have no gap between the anchor shanks and the baseplate, and because the shanks are welded to the baseplate, multiple-anchor connections with headed studs would be expected to be significantly stiffer than otherwise identical connections with CIP headed or UC anchors. Tests on connections with welded headed studs are needed

to verify that it is appropriate to apply the design procedures proposed here, to such connections.

8) In the finite element analysis, the effect of shear stress on the load behavior and the crack path were investigated. However, this shear capacity along concrete cracks is not well understood. Further study on it is needed.

9) The finite element analysis developed here might be expanded into three dimensions to numerically assess the effect of cracks and concrete member edges on the load-displacement behavior of anchors. Calculated displacements were very small, due to neglecting the concrete plastic deformation near anchor heads. An appropriate model should be used to include the effect of these concrete plastic deformations under high hydrostatic stresses.

Appendix A

Calculation of Projected Area of Group Anchors in 45-Degree Cone Method and CC Method

For a anchor group loaded in tension or shear, the formulas below are used for calculating the projected area:

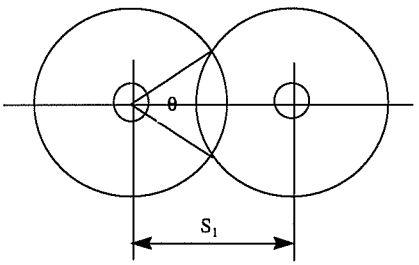

$s_1 \le 2h_{ef} + d_h$:

$$A_N = \left(2\pi - \frac{\theta}{180}\pi + \sin\theta\right)\left(h_{ef} + \frac{d_h}{2}\right)^2 - \frac{\pi}{2}d_h^2$$

$$\theta = 2\cos^{-1}\frac{s_1}{2h_{ef} + d_h}$$

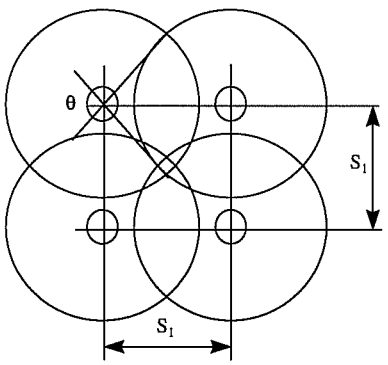

$s_1 \le \sqrt{2}\left(h_{ef} + d_h/2\right)$:

$$A_N = \left(3\pi - \frac{\theta}{90}\pi + 2\sin\theta - 2\cos\theta + 2\right)\left(h_{ef} + \frac{d_h}{2}\right)^2 - \frac{\pi}{2}d_h^2$$

$$\theta = 2\cos^{-1}\frac{s_1}{2h_{ef} + d_h}$$

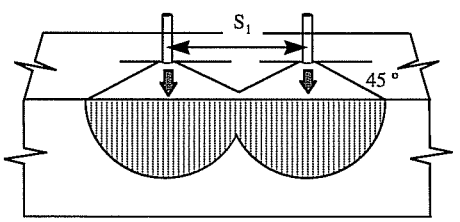

$$A_V = \left(\pi - \frac{\pi\theta/2}{180} + \sin\theta\right)c_1^2$$

$$\theta = 2\cos^{-1}\left(\frac{s_1}{2c_1}\right)$$

The following is the CC Method for calculating the projected area of an anchor group in tension and shear:

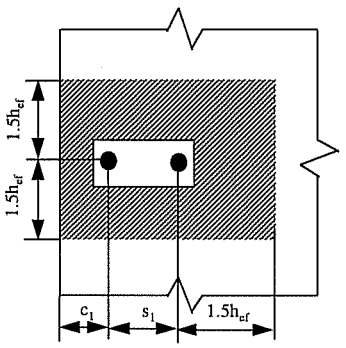

$$A_N = \left(3h_{ef} + s_1\right)\left(3h_{ef}\right)$$
$$if: s_1 \le 3h_{ef}$$

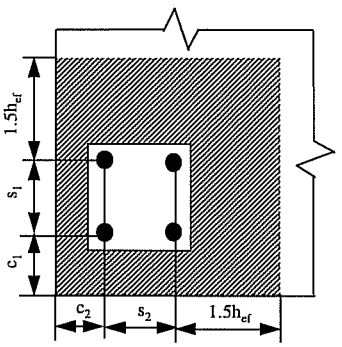

$$A_N = \left(c_1 + s_1 + 1.5h_{ef}\right)\left(c_2 + s_2 + 1.5h_{ef}\right)$$
$$if: c_1, c_2 \le 1.5h_{ef}; s_1, s_2 \le 3h_{ef}$$

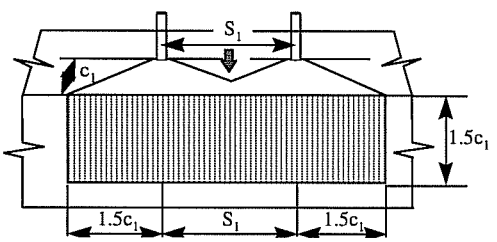

$$A_V = \left(3.0c_1 + s_1\right)\left(1.5c_1\right)$$
$$if: h \ge 1.5c_1; s_1 \le 1.5c_1$$

Appendix B

Results for Tests of Task 1

Summary of Static Tests of Single Tensile Anchor in Cracked Concrete

Anchor	Size	Embed.	Load	C-stren.	Block	Test #	F_u	Displ.	Failure	Effective	F_u/h_e^1.5
Name	[in.]	[in.]		[psi]			[lbs]	[in.]	Mode	Embed.	/f_c^0.5
										he [in.]	
EAII	0.75	4	Static	4250	S4	7skl5701	13461	0.149	cone	3.4375	30.81
		4	Static	4250	S4	7skl5702	13355	0.061	cone	3.4375	30.57
		4	Static	4250	S13	7skl5703	13668	0.202	cone	3.4375	31.28
		4	Static	4250	S13	7skl5704	11921	0.225	cone	3.4375	27.28
		4	Static	4250	S13	7skl5705	12435	0.155	cone	3.4375	28.46
						Ave.	**12968**	**0.158**		**Ave.**	**29.68**
						StDev. (%)	**5.80**	**39.83**		**StDev. (%)**	**5.80**
UC1	0.375	2.25	Static	4288	S19	7sml5406	8376	0.216	cone	2.25	36.20
		2.25	Static	4288	S19	7sml5407	8585	0.147	cone	2.25	37.10
		2.25	Static	4288	S19	7sml5408	8376	0.116	cone	2.25	36.20
		2.25	Static	4288	S19	7sml5409	7957	0.102	cone	2.25	34.39
		2.25	Static	4288	S19	7sml5410	7852	0.145	cone	2.25	33.94
						Ave.	**8229**	**0.145**		**Ave.**	**35.57**
						StDev. (%)	**3.78**	**30.29**		**StDev. (%)**	**3.78**
UC1	0.75	4	Static	4700	S1	7sml5711	23200	0.107	cone	4	42.30
		4	Static	4800	S1	7sml5712	22561	0.101	cone	4	41.14
		4	Static	4800	S1	7sml5713	21869	0.176	cone	4	39.87
		4	Static	4800	S1	7sml5714	23243	0.125	cone	4	42.38
		4	Static	4800	S1	7sml5715	23353	0.117	cone	4	42.58
						Ave.	**22845**	**0.125**		**Ave.**	**41.65**
						StDev. (%)	**2.75**	**23.84**		**StDev. (%)**	**2.75**
UC2	0.75	4	Static	4800	S1	7ssl5716	15931	0.015	cone	4	29.05
		4	Static	4800	S1	7ssl5717	16921	0.063	cone	4	30.85
		4	Static	4800	S1	7ssl5718	14051	0.054	cone	4	25.62
		4	Static	4250	S4	7ssl5719	16090	0.036	cone	4	29.34
		4	Static	4250	S4	7ssl5720	15038	0.027	cone	4	27.42
						Ave.	**15606**	**0.039**		**Ave.**	**28.45**
						StDev. (%)	**7.03**	**50.15**		**StDev. (%)**	**7.03**

Summary of Static Tests of Single Tensile Anchor in Cracked Concrete (Continued)

UC2	0.375	2.25	Static	4288	S19	7shl5421	6805	0.089	cone	2.25	29.41
		2.25	Static	4288	S19	7shl5422	7014	0.105	cone	2.25	30.31
		2.25	Static	4288	S19	7shl5423	6910	0.132	cone	2.25	29.86
		2.25	Static	4288	S19	7shl5424	7433	0.126	cone	2.25	32.12
		2.25	Static	4288	S19	7shl5425	6386	0.101	cone	2.25	27.60
						Ave.	**6910**	**0.111**		**Ave.**	**29.86**
						StDev. (%)	**5.46**	**16.21**		**StDev. (%)**	**5.46**
Sleeve	0.75	4	Static	4450	S13	7shl5726	21787	0.081	cone	4	39.72
		4	Static	4450	S13	7shl5727	17471	0.357	p. o. w/ cone	4	31.86
		4	Static	4450	S13	7shl5728	21685	0.059	cone	4	39.54
		4	Static	4450	S13	7shl5729	19115	0.094	cone	4	34.85
		4	Static	4450	S13	7shl5730	16751	0.138	p. o. w/ cone	4	30.54
						Ave.	**19362**	**0.146**		**Ave.**	**35.30**
						StDev. (%)	**12.04**	**83.36**		**StDev. (%)**	**12.04**
Grouted	0.75	4	Static	4269	S4	7sgl5731	18244	0.024	cone	4	33.26
		4	Static	4269	S4	7sgl5732	13604	0.039	cone	4	24.80
		4	Static	4269	S4	7sgl5733	9024	0.027	cone	4	16.45
		4	Static	4269	S4	7sgl5734	11332	0.036	cone	4	20.66
		4	Static	4269	S4	7sgl5735	14890	0.032	cone	4	27.15
						Ave.	**13419**	**0.032**		**Ave.**	**24.47**
						StDev. (%)	**26.12**	**19.58**		**StDev. (%)**	**26.12**

Summary of Dynamic Tests of Single Tensile Anchor in Cracked Concrete

Anchor	Size	Embed.	Load	C-stren.	Block	Test #	Fu	Displ.	Failure	Effective	$F_u/h_e^{1.5}$
Name	[in.]	[in.]		[psi]			[lbs]	[in.]	Mode	Embed.	$/f_c^{0.5}$
										he [in.]	
EAII	0.75	4	Dyn.	4250	S4	8dkl5701	11673	0.281	p. o. w/ cone	3.4375	26.72
		4	Dyn.	4450	S13	8dkl5702	11202	0.845	p. o. w/ cone	3.4375	25.64
		4	Dyn.	4450	S13	8dkl5703	12846	0.308	p. o. w/ cone	3.4375	29.40
		4	Dyn.	4450	S13	8dkl5704	14491	0.237	p. o. w/ cone	3.4375	33.17
		4	Dyn.	4450	S13	8dkl5705	10894	0.639	p. o. w/ cone	3.4375	24.93
						Ave.	**12221**	**0.462**		**Ave.**	**27.97**
						StDev. (%)	**12.03**	**57.79**		**StDev. (%)**	**12.03**
UC1	0.375	2.25	Dyn.	4288	S19	8dml5406	9737	0.166	cone	2.25	42.08
		2.25	Dyn.	4288	S19	8dml5407	9527	0.118	cone	2.25	41.17
		2.25	Dyn.	4288	S19	8dml5408	10051	0.125	cone	2.25	43.44
		2.25	Dyn.	4288	S19	8dml5409	7852	0.136	cone	2.25	33.94
		2.25	Dyn.	4288	S19	8dml5410	10365	0.142	cone	2.25	44.80
						Ave.	**9506**	**0.137**		**Ave.**	**41.09**
						StDev. (%)	**10.29**	**13.48**		**StDev. (%)**	**10.29**
UC1	0.75	4	Dyn.	4800	S1	8dml5711	26321	0.128	cone	4	47.99
		4	Dyn.	4800	S1	8dml5712	25431	0.198	cone	4	46.37
		4	Dyn.	4800	S1	8dml5713	28202	0.178	cone	4	51.42
		4	Dyn.	4800	S1	8dml5714	23650	0.131	cone	4	43.12
		4	Dyn.	4800	S1	8dml5715	23056	0.218	cone	4	42.04
						Ave.	**25332**	**0.171**		**Ave.**	**46.19**
						StDev. (%)	**8.19**	**23.51**		**StDev. (%)**	**8.19**
UC2	0.75	4	Dyn.	4800	S1	8dsl5716	28597	0.090	cone	4	52.14
		4	Dyn.	4800	S1	8dsl5717	23056	0.024	cone	4	42.04
		4	Dyn.	4800	S1	8dsl5718	21077	0.066	cone	4	38.43
		4	Dyn.	4800	S1	8dsl5719	27806	0.049	cone	4	50.70
		4	Dyn.	4250	S4	8dsl5720	23294	0.077	cone	4	42.47
						Ave.	**24766**	**0.061**		**Ave.**	**45.16**
						StDev. (%)	**13.18**	**41.94**		**StDev. (%)**	**13.18**

Summary of Dynamic Tests of Single Tensile Anchor in Cracked Concrete (Continued)

Sleeve	0.375	2.25	Dyn.	4288	S19	8dhl5421	6072	0.077	cone	2.25	26.24
		2.25	Dyn.	4288	S19	8dhl5422	7119	0.133	cone	2.25	30.77
		2.25	Dyn.	4288	S19	8dhl5423	7119	0.110	cone	2.25	30.77
		2.25	Dyn.	4288	S19	8dhl5424	6910	0.256	p. o. w/ cone	2.25	29.86
		2.25	Dyn.	4288	S19	8dhl5425	7119	0.114	cone	2.25	30.77
						Ave.	**6868**	**0.138**		**Ave.**	**29.68**
						StDev. (%)	**6.61**	**49.98**		**StDev. (%)**	**6.61**
Sleeve	0.75	4	Dyn.	4450	S13	8dhl5726	25693	0.086	p. o. w/ cone	4	46.85
		4	Dyn.	4450	S13	8dhl5727	19424	0.047	p. o. w/ cone	4	35.42
		4	Dyn.	4450	S13	8dhl5728	17056	0.037	p. o. w/ cone	4	31.10
		4	Dyn.	4450	S13	8dhl5729	19368	0.024	p. o. w/ cone	4	35.31
		4	Dyn.	4450	S13	8dhl5730	26697	0.116	p. o. w/ cone	4	48.68
						Ave.	**21648**	**0.062**		**Ave.**	**39.47**
						StDev. (%)	**19.75**	**61.34**		**StDev. (%)**	**19.75**
Grouted	0.75	4	Dyn.	4269	S4	8dgl5731	11122	0.018	p. o. w/ cone	4	20.28
		4	Dyn.	4269	S4	8dgl5732	10388	0.254	p. o. w/ cone	4	18.94
		4	Dyn.	4269	S4	8dgl5733	4302	0.197	p. o. w/ cone	4	7.84
		4	Dyn.	4269	S4	8dgl5734	9758	*	p. o. w/ cone	4	17.79
		4	Dyn.	4269	S4	8dgl5735	7030	0.028	p. o. w/ cone	4	12.82
						Ave.	**8520**	**0.124**		**Ave.**	**15.53**
						StDev. (%)	**33.10**	**96.00**		**StDev. (%)**	**33.10**

7SKL57/01-05
Expansion Anchor II, Diameter = 0.75 inch, Embedment = 4.0 inch
Static Loading

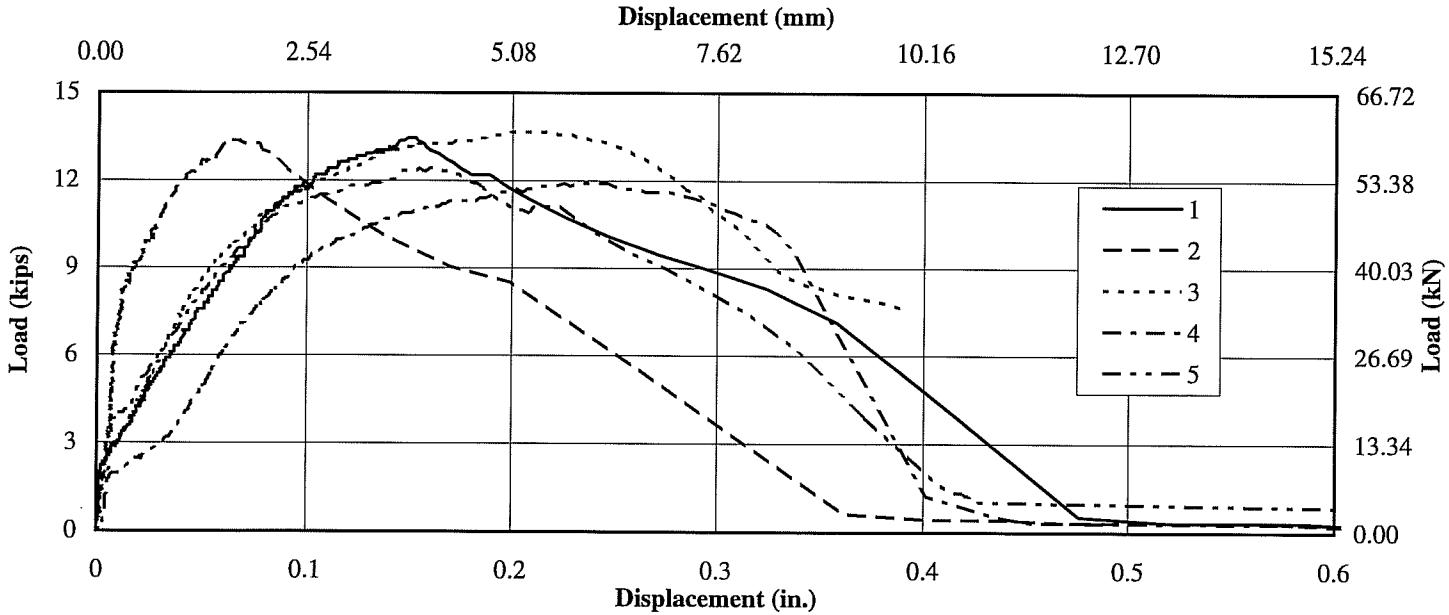

Test Number	Date	Block Number	f_c, psi	Normalized Maximum Load, kips (KN)		Displacement at Maximum Load in. (mm)		Failure Mode
7SKL5701	6/23/94	S4	4226	13.5	(60.0)	0.149	(3.78)	Cone
7SKL5702	6/23/94	S4	4226	13.4	(59.6)	0.061	(1.55)	Cone
7SKL5703	9/23/94	S13	4269	13.7	(60.9)	0.202	(5.13)	Cone
7SKL5704	9/23/94	S13	4269	11.9	(52.9)	0.225	(5.72)	Cone
7SKL5705	9/23/94	S13	4269	12.4	(55.2)	0.155	(3.94)	Cone
			Average	13.0	(57.7)	0.158	(4.02)	

7SML54/06-10
Undercut Anchor 1, Diameter = 0.375 inch, Embedment = 2.25 inch
Static Loading

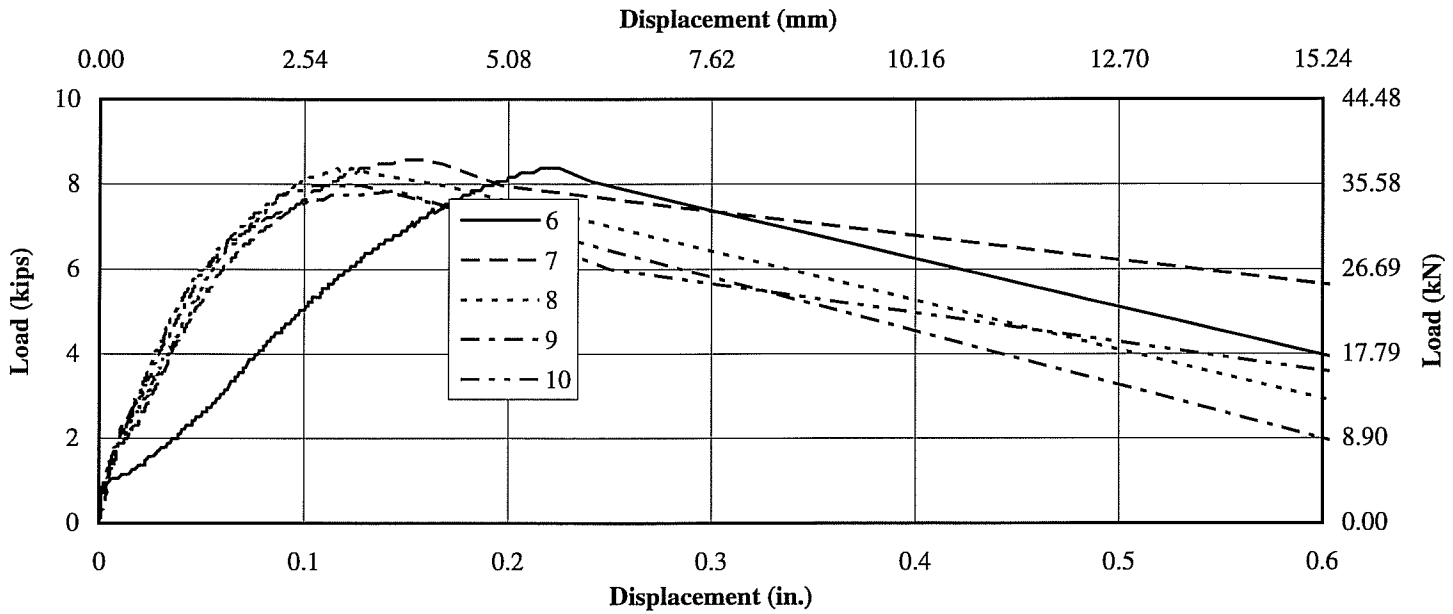

Test Number	Date	Block Number	f_c, psi	Normalized Maximum Load, kips (KN)		Displacement at Maximum Load in. (mm)		Failure Mode
7SML5406	12/16/94	S19	4288	8.38	(37.3)	0.216	(5.49)	Cone
7SML5407	12/16/94	S19	4288	8.58	(38.2)	0.147	(3.73)	Cone
7SML5408	12/16/94	S19	4288	8.38	(37.3)	0.116	(2.95)	Cone
7SML5409	12/19/94	S19	4288	7.96	(35.4)	0.102	(2.59)	Cone
7SML5410	12/19/94	S19	4288	7.85	(34.9)	0.145	(3.68)	Partial Cone
			Average	8.23	(36.6)	0.145	(3.69)	

7SML57/11-15
Undercut Anchor 1, Diameter = 0.75 inch, Embedment = 4.0 inch
Static loading

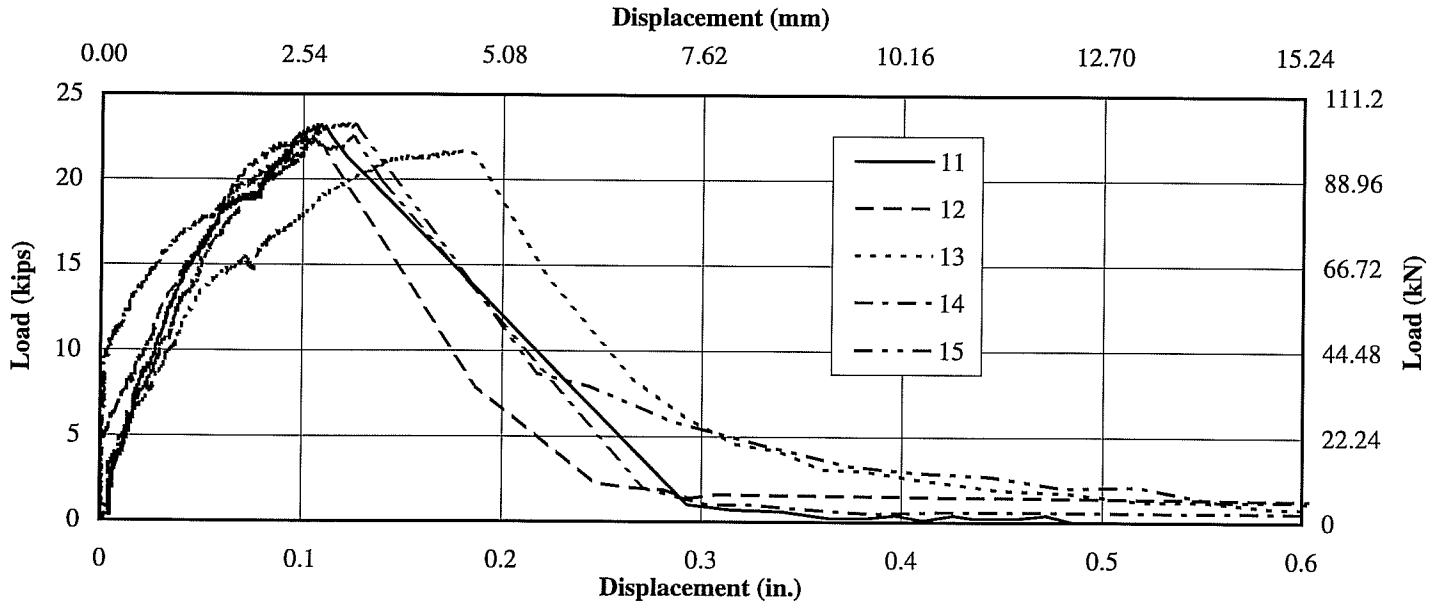

Test Number	Date	Block Number	f_c, psi	Normalized Maximum Load, kips (KN)		Displacement at Maximum Load in. (mm)		Failure Mode
7SML5711	6/3/94	S1	4700	23.2	(103.2)	0.107	(2.72)	Cone
7SML5712	6/6/94	S1	4800	22.6	(100.5)	0.101	(2.57)	Cone
7SML5713	6/6/94	S1	4800	21.9	(97.4)	0.176	(4.47)	Cone
7SML5714	6/6/94	S1	4800	22.6	(100.5)	0.125	(3.18)	Cone
7SML5715	6/6/94	S1	4800	23.4	(104.1)	0.117	(2.97)	Cone
			Average	22.7	(101.1)	0.125	(3.18)	

7SSL57/16-20
Undercut Anchor 2, Diameter = 0.75 inch, Embedment = 4.0 inch
Static Loading

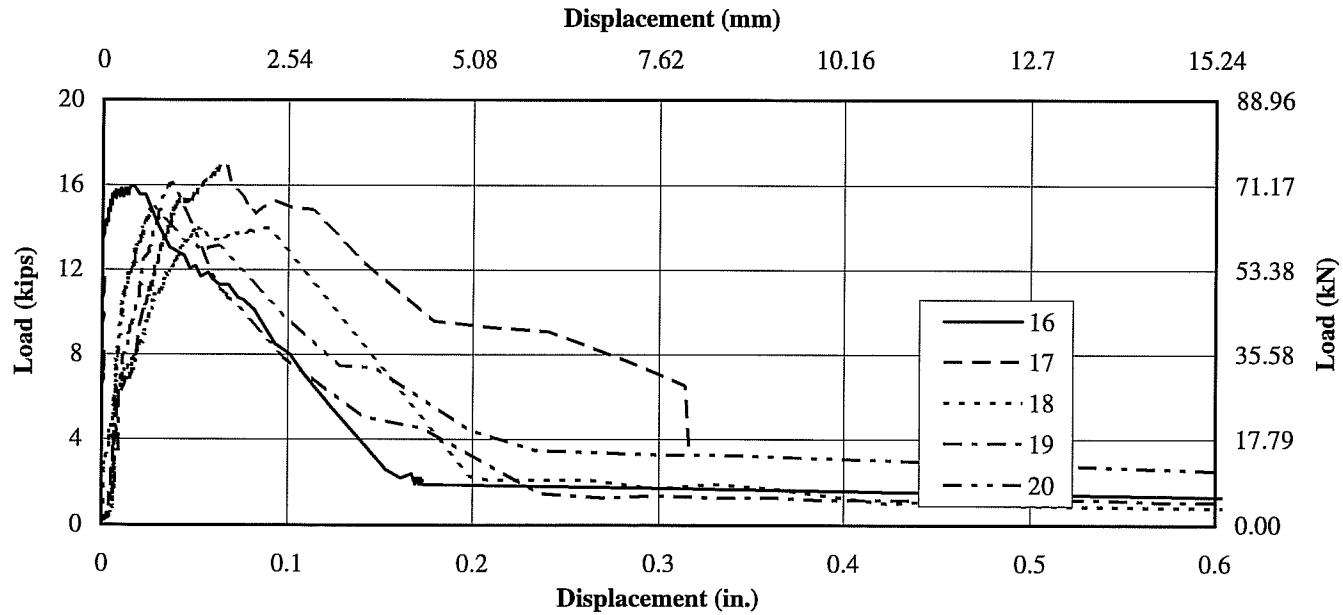

Test Number	Date	Block Number	f_c, psi	Normalized Maximum Load, kips (KN)		Displacement at Maximum Load in. (mm)		Failure Mode
7SSL5716	6/6/94	S1	4800	15.9	(70.7)	0.015	(0.38)	Cone
7SSL5717	6/9/94	S1	4800	16.9	(75.2)	0.063	(1.60)	Cone
7SSL5718	6/9/94	S1	4800	14.1	(62.7)	0.054	(1.37)	Cone
7SSL5719	6/23/94	S4	4250	16.1	(71.6)	0.036	(0.91)	Cone
7SSL5720	6/23/94	S4	4250	15.0	(66.7)	0.027	(0.69)	Cone
			Average	15.6	(69.4)	0.039	(0.99)	

7SHL54/21-25
Sleeve Anchor, Diameter = 10 mm, Embedment = 2.25 inch
Static Loading

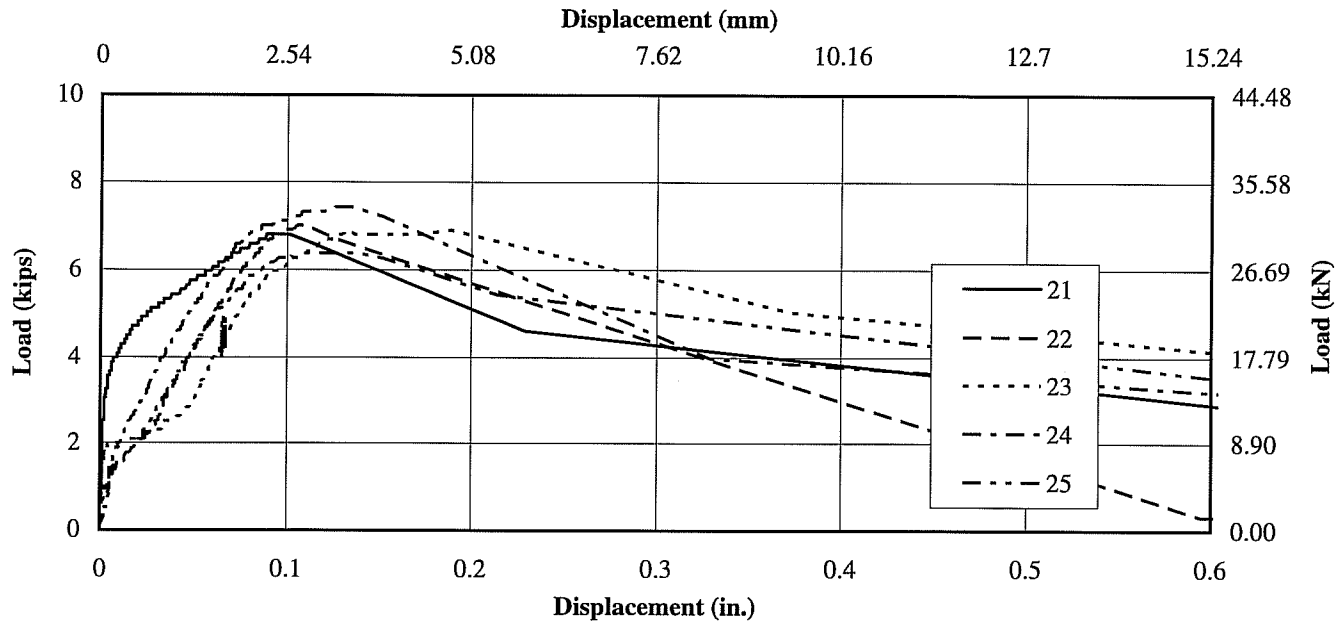

Test Number	Date	Block Number	f_c, psi	Normalized Maximum Load, kips (KN)		Displacement at Maximum Load in. (mm)		Failure Mode
7SHL5421	12/20/94	S19	4288	6.82	(30.3)	0.089	(2.26)	Cone
7SHL5422	12/20/94	S19	4288	7.01	(31.2)	0.105	(2.67)	Cone
7SHL5423	12/20/94	S19	4288	6.91	(30.7)	0.132	(3.35)	Cone
7SHL5424	12/20/94	S19	4288	7.42	(33.0)	0.126	(3.20)	Partial Cone
7SHL5425	12/20/94	S19	4288	6.39	(28.4)	0.101	(2.57)	Cone
			Average	6.91	(30.7)	0.111	(2.81)	

7SHL57/26-30
Sleeve Anchor, Diameter = 0.75 inch, Embedment = 4.0 inch
Static Loading

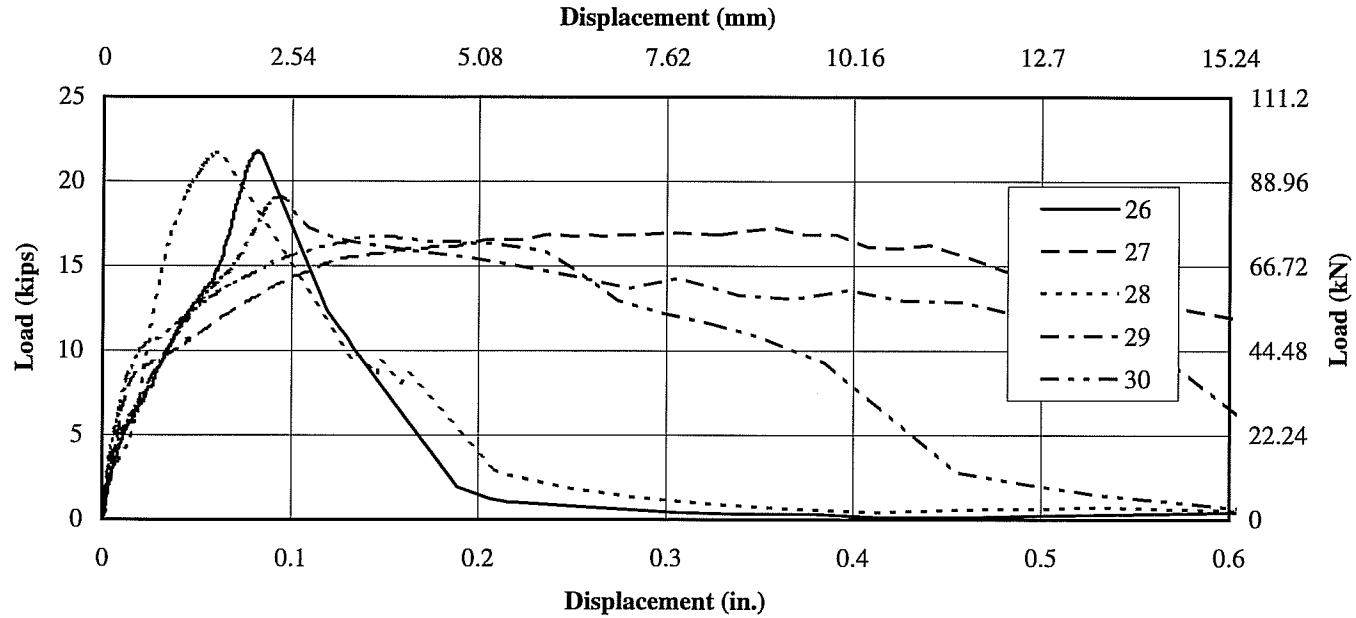

Test Number	Date	Block Number	f_c, psi	Normalized Maximum Load, kips (KN)		Displacement at Maximum Load in. (mm)		Failure Mode
7SHL5726	9/29/94	S13	4450	21.8	(97.0)	0.081	(2.06)	Cone
7SHL5727	9/29/94	S13	4450	17.3	(77.0)	0.357	(9.07)	Pullout w/ Cone
7SHL5728	9/29/94	S13	4450	21.7	(96.5)	0.059	(1.50)	Cone
7SHL5729	9/29/94	S13	4450	19.1	(85.0)	0.094	(2.39)	Pullout w/ Cone
7SHL5730	9/29/94	S13	4450	16.8	(74.7)	0.138	(3.51)	Pullout w/ Cone
			Average	19.3	(86.0)	0.146	(3.70)	

7SGL57/31-35
Grouted Anchor, Diameter = 0.75 inch, Embedment = 4.0 inch
Static Loading

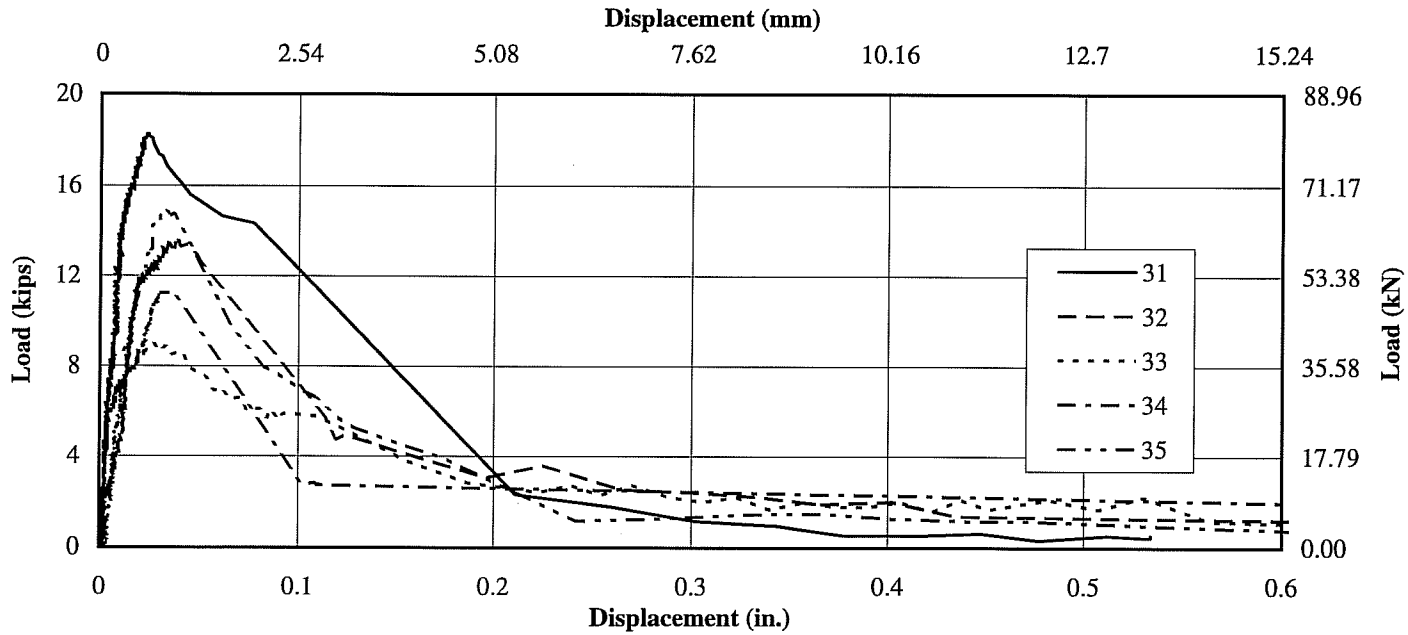

Test Number	Date	Block Number	f_c, psi	Normalized Maximum Load, kips (KN)		Displacement at Maximum Load in. (mm)		Failure Mode
7SGL5731	6/20/94	S4	4226	18.2	(81.0)	0.024	(0.61)	Cone
7SGL5732	6/20/94	S4	4226	13.6	(60.5)	0.039	(0.99)	Partial Cone
7SGL5733	6/29/94	S4	4269	9.02	(40.1)	0.027	(0.69)	Pullout w/ Cone
7SGL5734	6/29/94	S4	4269	11.3	(50.3)	0.036	(0.91)	Cone
7SGL5735	6/29/94	S4	4269	14.9	(66.3)	0.032	(0.81)	Cone
			Average	13.4	(59.6)	0.032	(0.80)	

8DKL57/01-05
Expansion Anchor II, Diameter = 0.75 inch, Embedment = 4.0 inch
Dynamic Loading

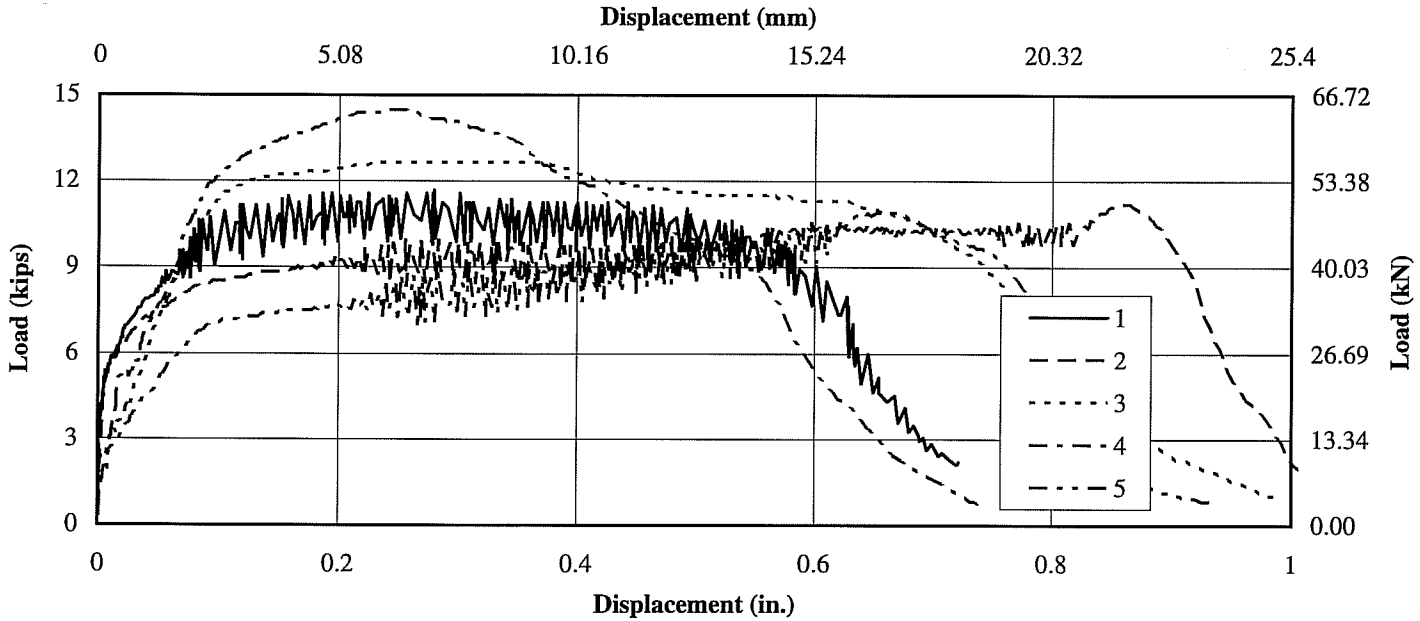

Test Number	Date	Block Number	f_c, psi	Normalized Maximum Load, kips (KN)		Displacement at Maximum Load in. (mm)		Failure Mode
8DKL5701	6/24/94	S4	4250	11.7	(52.0)	0.281	(7.14)	Pullout w/ Cone
8DKL5702	9/23/94	S13	4450	11.2	(49.8)	0.845	(21.46)	Pullout w/ Cone
8DKL5703	9/27/94	S13	4450	12.8	(57.1)	0.308	(7.82)	Pullout w/ Cone
8DKL5704	9/27/94	S13	4450	14.5	(64.5)	0.237	(6.02)	Pullout w/ Cone
8DKL5705	9/27/94	S13	4450	10.9	(48.5)	0.639	(16.23)	Pullout w/ Cone
			Average	12.2	(54.4)	0.462	(11.73)	

8DML54/06-10
Undecut Anchor 1, diameter = 0.375 inch, Embedment = 2.25 inch
Dynamic Loading

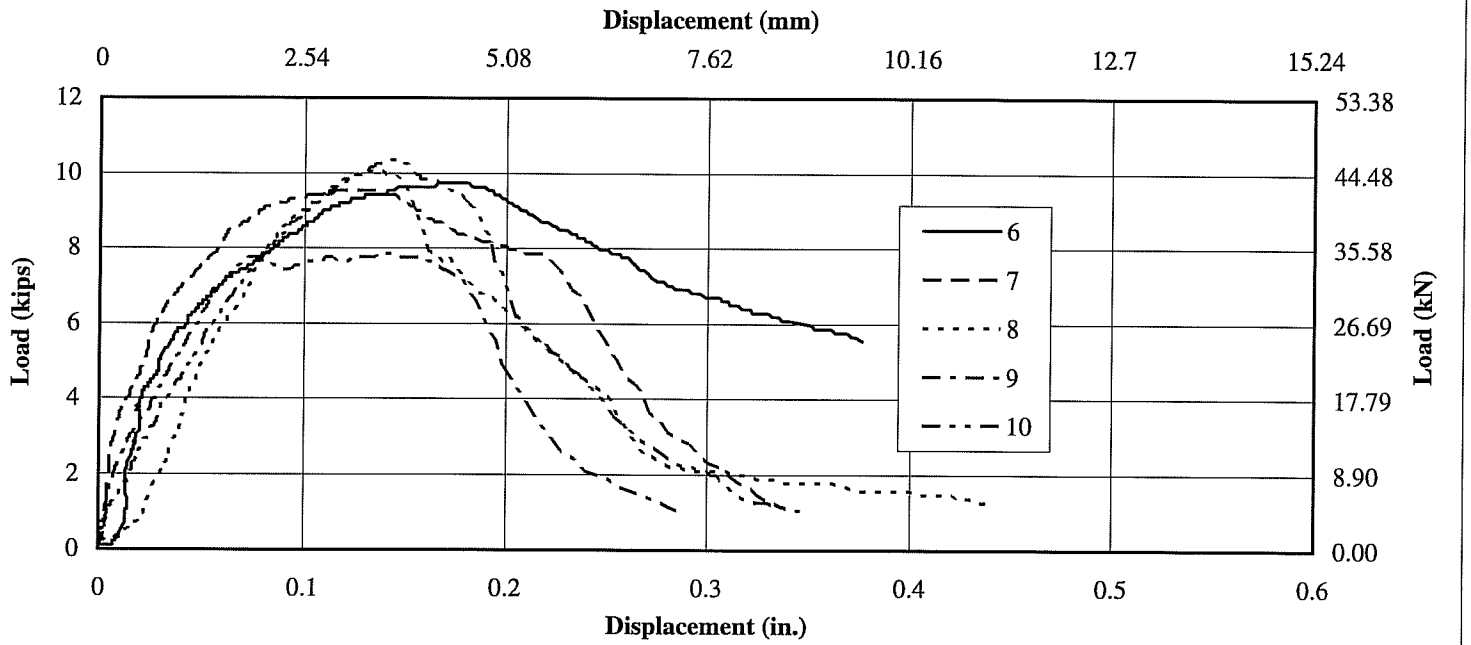

Test Number	Date	Block Number	f_c, psi	Normalized Maximum Load, kips (KN)		Displacement at Maximum Load in. (mm)		Failure Mode
8DML5406	12/19/94	S19	4288	9.74	(43.3)	0.166	(4.22)	Cone
8DML5407	12/19/94	S19	4288	9.53	(42.4)	0.118	(3.00)	Cone
8DML5408	12/19/94	S19	4288	10.1	(44.7)	0.125	(3.18)	Partial Cone
8DML5409	12/19/94	S19	4288	7.85	(34.9)	0.136	(3.45)	Partial Cone
8DML5410	12/19/94	S19	4288	10.4	(46.1)	0.142	(3.61)	Partial Cone
			Average	9.51	(42.3)	0.137	(3.49)	

8DML57/11-15
Undercut Anchor 1, Diameter = 0.75 inch, Embedment = 4.0 inch
Dynamic Loading

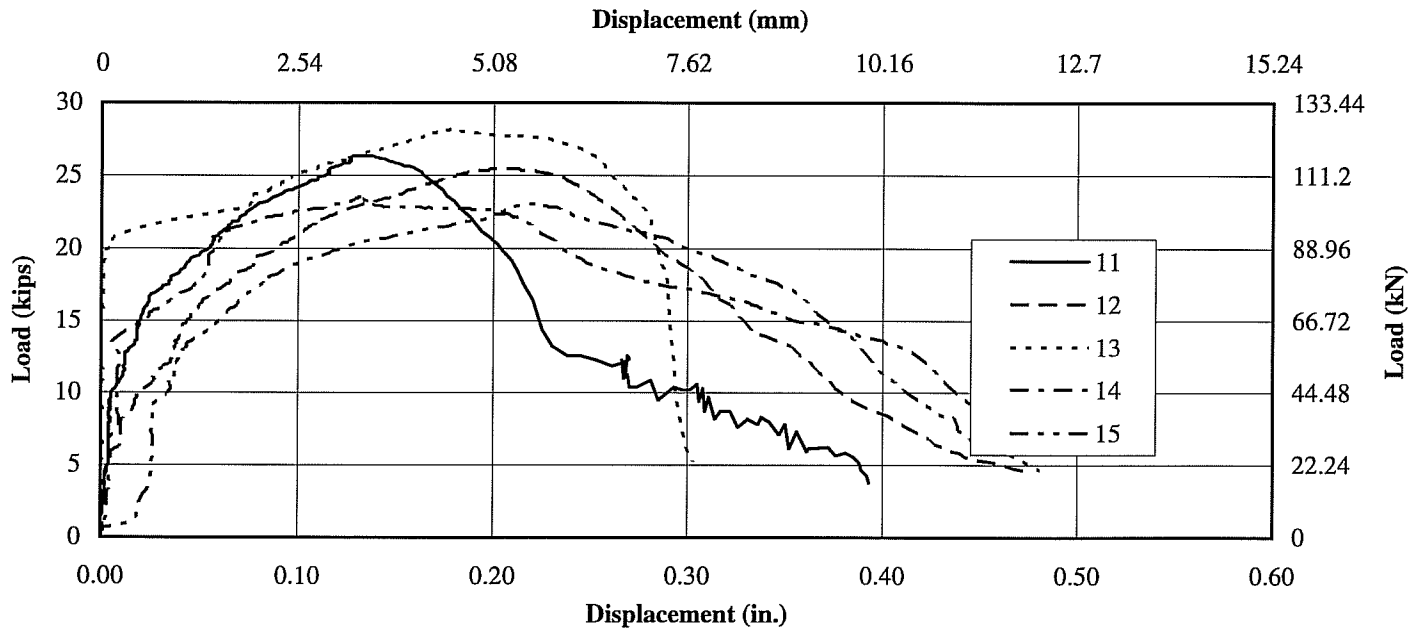

Test Number	Date	Block Number	f_c, psi	Normalized Maximum Load, kips (KN)		Displacement at Maximum Load in. (mm)		Failure Mode
8DML5711	6/7/94	S1	4800	26.3	(117)	0.128	(3.25)	Cone
8DML5712	6/7/94	S1	4800	25.4	(113)	0.198	(5.03)	Cone
8DML5713	6/8/94	S1	4800	28.2	(125)	0.178	(4.52)	Cone
8DML5714	6/8/94	S1	4800	23.7	(105)	0.131	(3.33)	Cone
8DML5715	6/9/94	S1	4800	23.1	(103)	0.218	(5.54)	Cone
			Average	25.3	(113)	0.171	(4.33)	

8DSL57/16-20
Undercut Anchor 2, Diameter = 0.75 inch, Embedment = 4.0 inch
Dynamic Loading

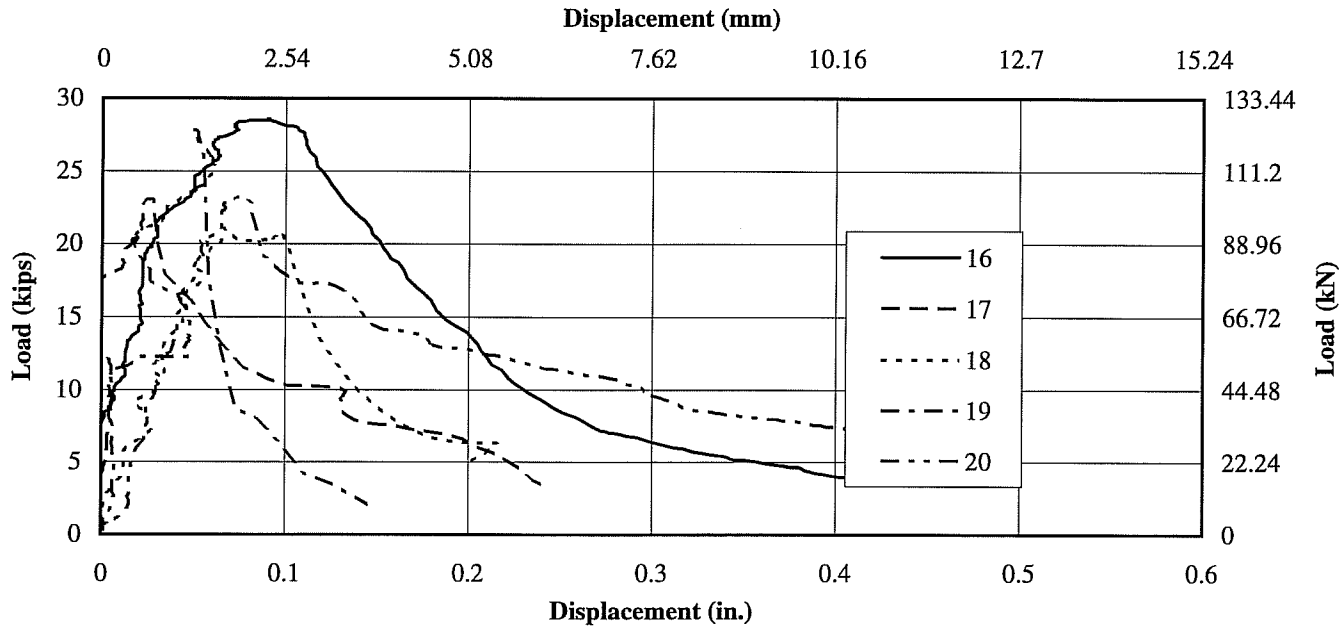

Test Number	Date	Block Number	f_c, psi	Normalized Maximum Load, kips (KN)		Displacement at Maximum Load in. (mm)		Failure Mode
8DSL5716	6/8/94	S1	4800	28.6	(127)	0.090	(2.29)	Cone
8DSL5717	6/9/94	S1	4800	23.1	(103)	0.024	(0.61)	Cone
8DSL5718	6/9/94	S1	4800	21.1	(94)	0.066	(1.68)	Cone
8DSL5719	6/9/94	S1	4800	27.8	(124)	0.049	(1.24)	Cone
8DSL5720	6/28/94	S4	4269	23.3	(104)	0.077	(1.96)	Cone
			Average	24.8	(110)	0.061	(1.55)	

8DHL54/21-25
Sleeve Anchor, Diameter = 10 mm, Embedment = 2.25 inch
Dynamic Loading

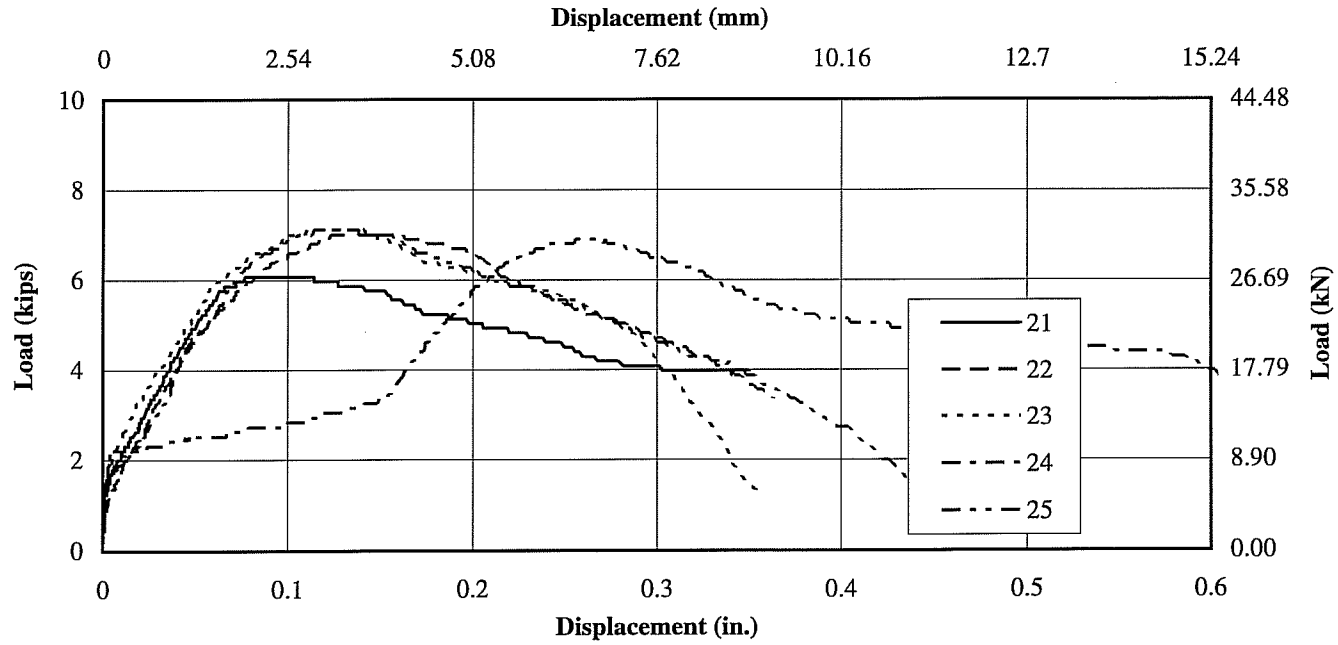

Test Number	Date	Block Number	f_c, psi	Normalized Maximum Load, kips (KN)		Displacement at Maximum Load in. (mm)		Failure Mode
8DHL5421	12/20/94	S19	4288	6.07	(27.0)	0.077	(1.96)	Cone
8DHL5422	12/20/94	S19	4288	7.12	(31.7)	0.133	(3.38)	Partial Cone
8DHL5423	12/20/94	S19	4288	7.12	(31.7)	0.110	(2.79)	Cone
8DHL5424	12/20/94	S19	4288	6.91	(30.7)	0.256	(6.50)	Pullout w/ Cone
8DHL5425	12/20/94	S19	4288	7.12	(31.7)	0.114	(2.90)	Cone
			Average	6.87	(30.5)	0.138	(3.51)	

8DHL57/26-30
Sleeve Anchor, Diameter = 20 mm, Embedment = 4.0 inch
Dynamic Loading

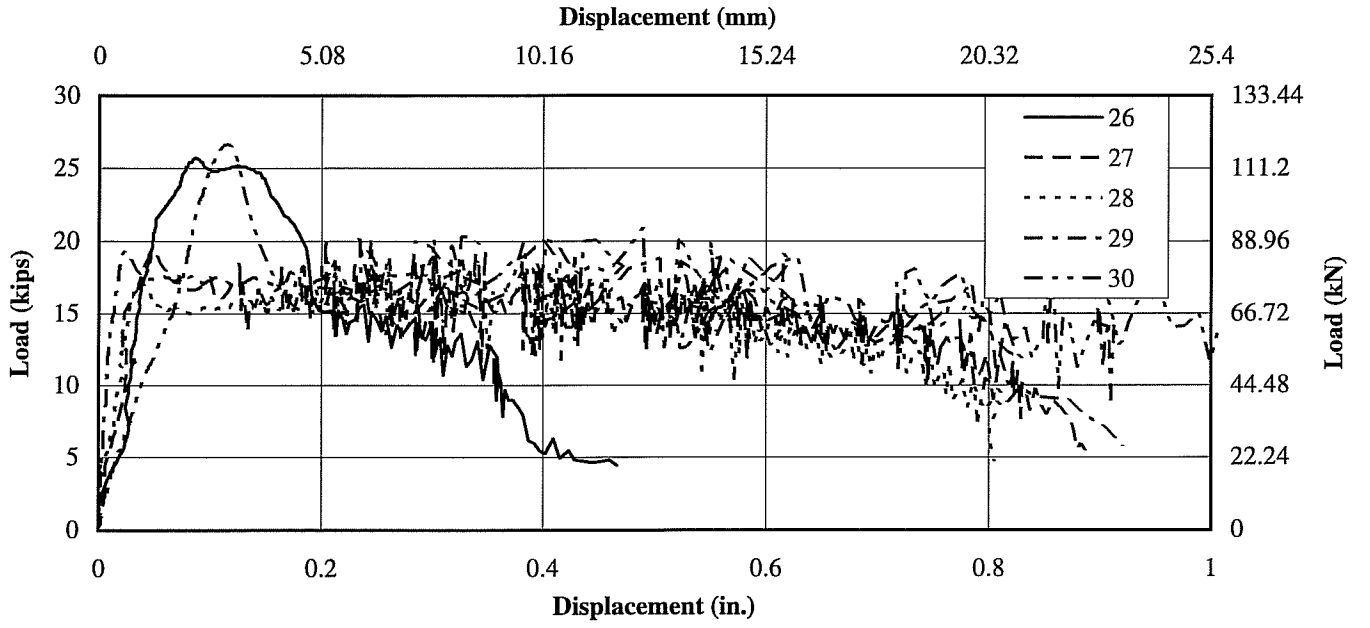

Test Number	Date	Block Number	f_c, psi	Normalized Maximum Load, kips (KN)		Displacement at Maximum Load in. (mm)		Failure Mode
8DHL5726	9/27/94	S13	4450	25.7	(114.3)	0.086	(2.18)	Cone
8DHL5727	9/27/94	S13	4450	19.4	(86.4)	0.047	(1.19)	Pullout w/ Cone
8DHL5728	9/27/94	S13	4450	17.1	(75.9)	0.037	(0.94)	Pullout w/ Cone
8DHL5729	12/21/94	S19	4288	19.4	(86.1)	0.024	(0.61)	Pullout w/ Cone
8DHL5730	12/21/94	S19	4288	26.7	(118.7)	0.116	(2.95)	Pullout w/ Cone
			Average	21.6	(96.3)	0.062	(1.57)	

8DGL57/31-35
Grouted Anchor, Diameter = 0.75 inch, Embedment = 4.0 inch
Dynamic Loading

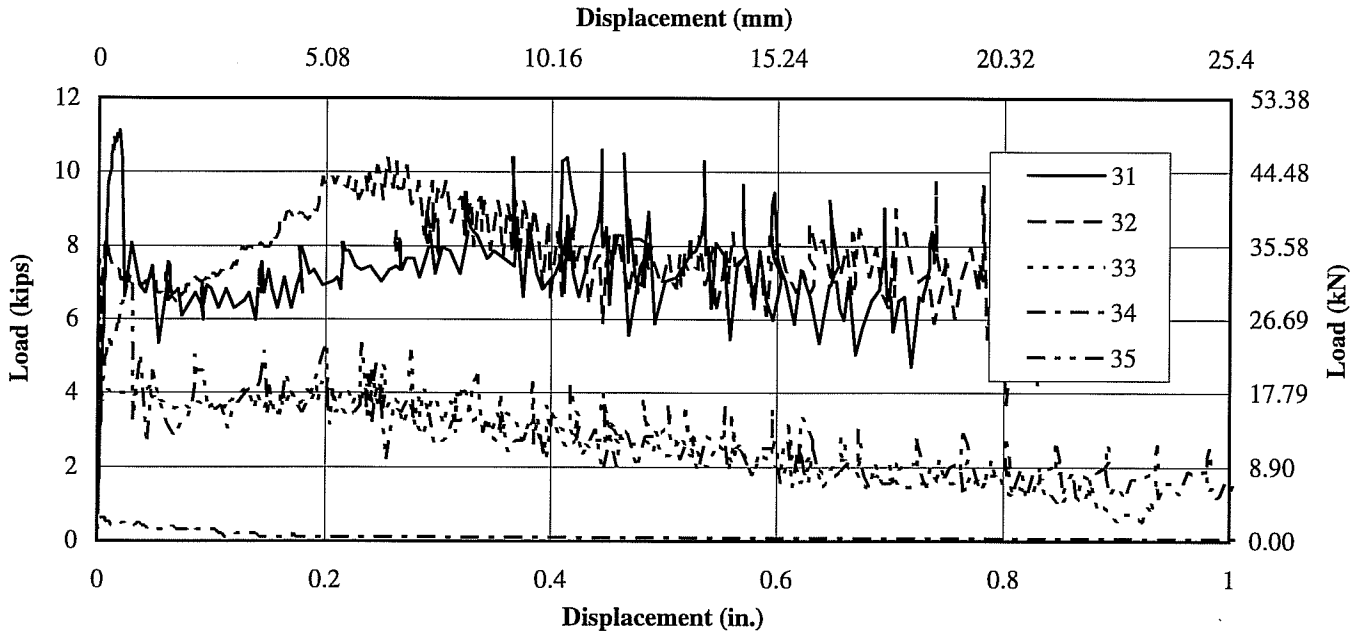

Test Number	Date	Block Number	f_c, psi	Normalized Maximum Load, kips (KN)		Displacement at Maximum Load in. (mm)		Failure Mode
8DGL5731	6/27/94	S4	4269	11.1	(49.5)	0.018	(0.46)	Pullout w/ Cone
8DGL5732	6/27/94	S4	4269	10.4	(46.2)	0.254	(6.45)	Pullout w/ Cone
8DGL5733	6/29/94	S4	4269	4.30	(19.1)	0.197	(5.00)	Pullout w/ Cone
8DGL5734	6/29/94	S4	4269	9.76	(43.4)	0.000	(0.00)	Pullout w/ Cone
8DGL5735	6/29/94	S4	4269	7.03	(31.3)	0.028	(0.71)	Pullout w/ Cone
			Average	8.52	(37.9)	0.099	(2.52)	

Crack Opening in Tests 7SKL57/01-05

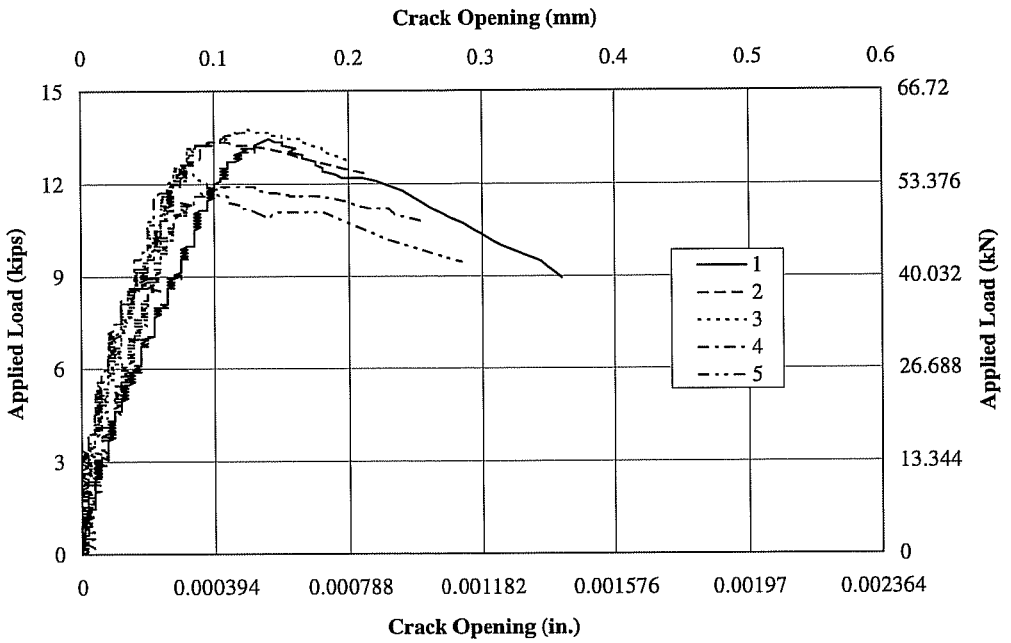

Crack Opening in Tests 7SML57/06-10

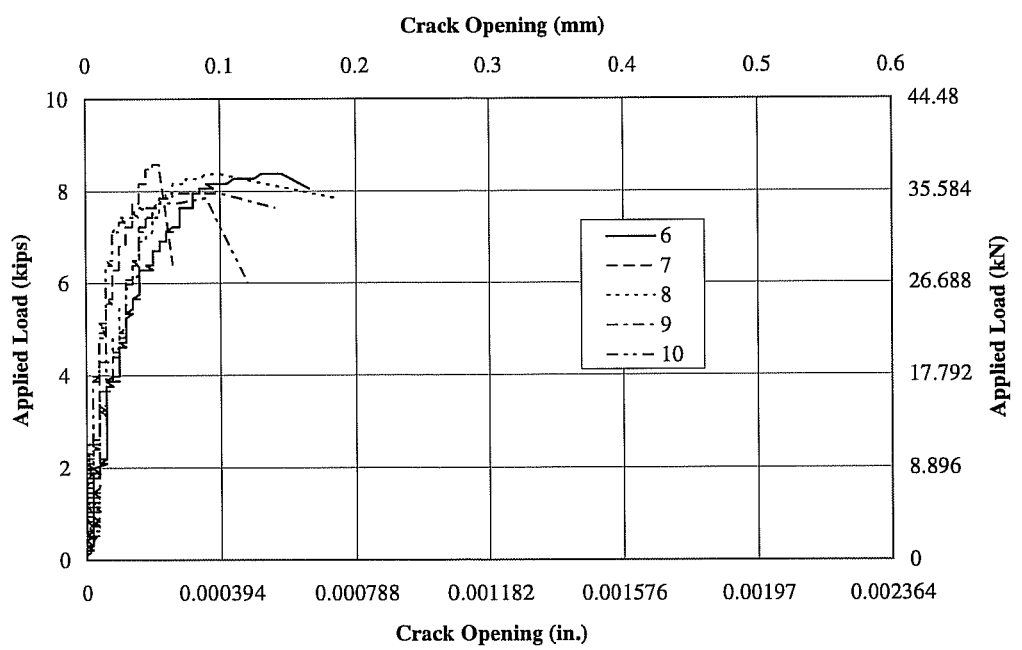

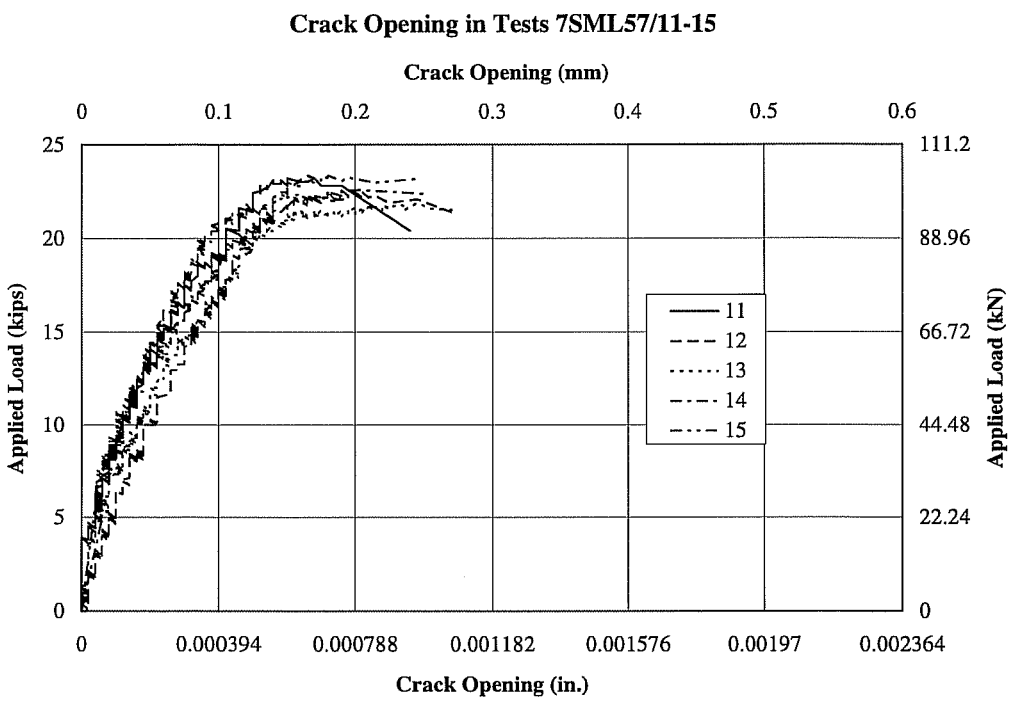
Crack Opening in Tests 7SML57/11-15
Crack Opening (mm)
0
0.1
0.2
0.3
0.4
0.5
0.6
25
20
15
10
5
0
111.2
88.96
66.72
44.48
22.24
0
Applied Load (kips)
Applied Load (kN)
11
12
13
14
15
0
0.000394
0.000788
0.001182
0.001576
0.00197
0.002364
Crack Opening (in.)

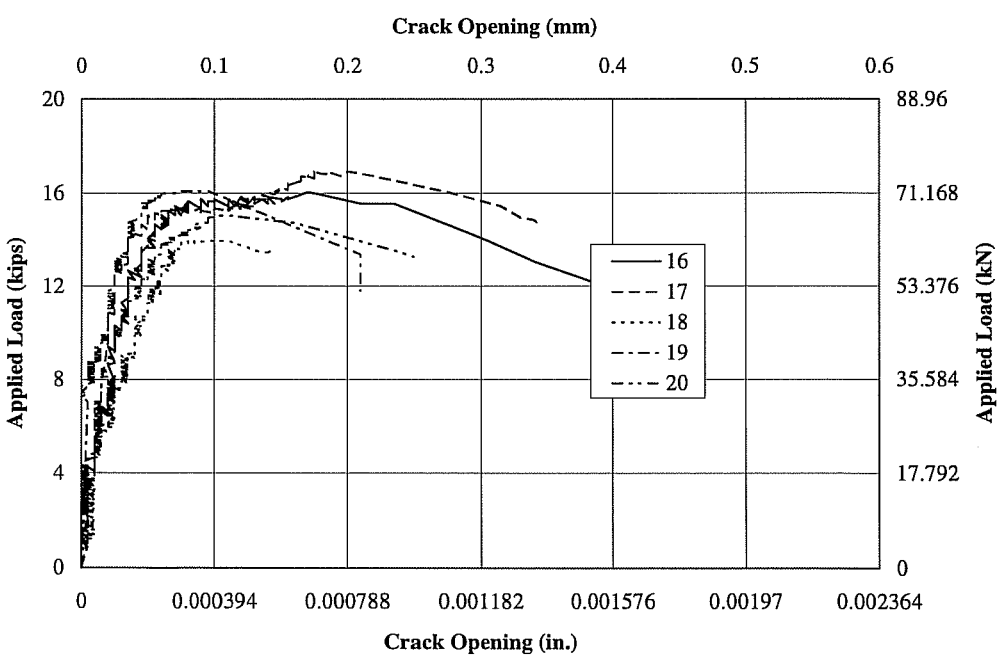
Crack Opening in Tests 7SSL57/16-20
Crack Opening (mm)
0
0.1
0.2
0.3
0.4
0.5
0.6
20
16
12
8
4
0
88.96
71.168
53.376
35.584
17.792
0
Applied Load (kips)
Applied Load (kN)
16
17
18
19
20
0
0.000394
0.000788
0.001182
0.001576
0.00197
0.002364
Crack Opening (in.)

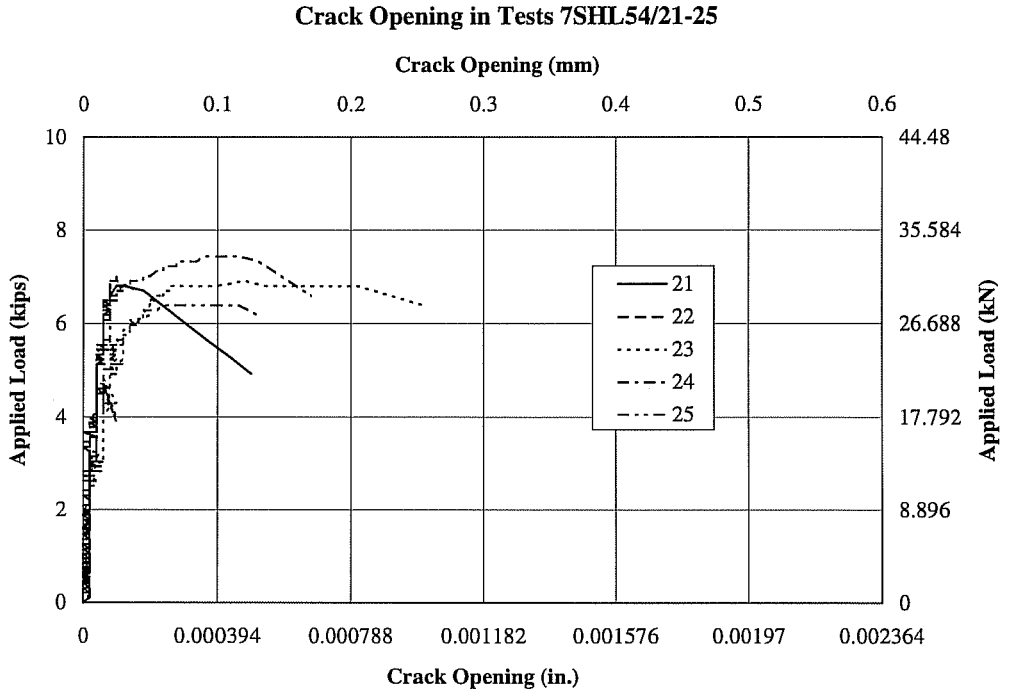
Crack Opening in Tests 7SHL54/21-25
Crack Opening (mm)
0
0.1
0.2
0.3
0.4
0.5
0.6
10
8
6
4
2
0
44.48
35.584
26.688
17.792
8.896
0
21
22
23
24
25
Applied Load (kips)
Applied Load (kN)
0
0.000394
0.000788
0.001182
0.001576
0.00197
0.002364
Crack Opening (in.)

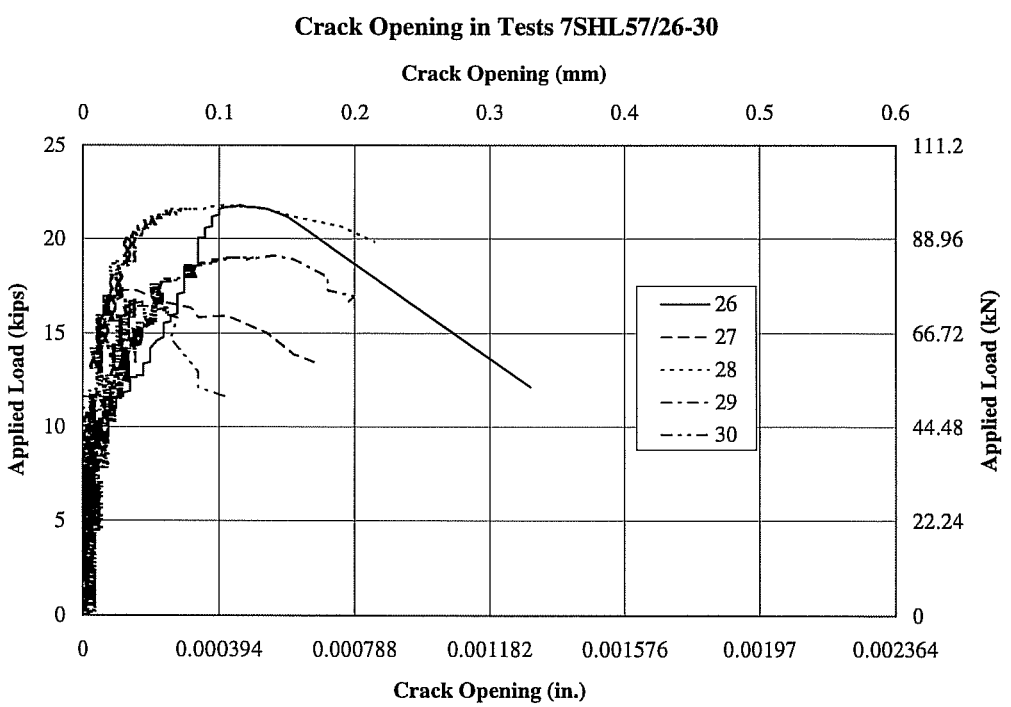
Crack Opening in Tests 7SHL57/26-30
Crack Opening (mm)
0
0.1
0.2
0.3
0.4
0.5
0.6
25
20
15
10
5
0
111.2
88.96
66.72
44.48
22.24
0
26
27
28
29
30
Applied Load (kips)
Applied Load (kN)
0
0.000394
0.000788
0.001182
0.001576
0.00197
0.002364
Crack Opening (in.)

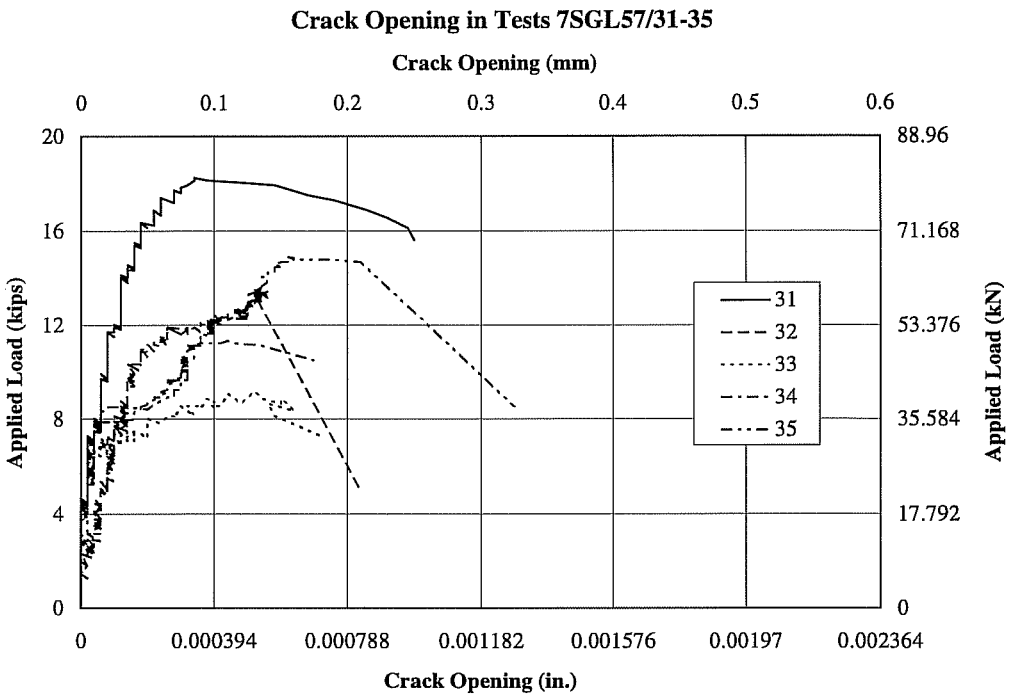
Crack Opening in Tests 7SGL57/31-35
Crack Opening (mm)
0
0.1
0.2
0.3
0.4
0.5
0.6
20
16
12
8
4
0
88.96
71.168
53.376
35.584
17.792
0
Applied Load (kips)
Applied Load (kN)
31
32
33
34
35
0
0.000394
0.000788
0.001182
0.001576
0.00197
0.002364
Crack Opening (in.)

Crack Opening in Tests 8DKL57/01-05

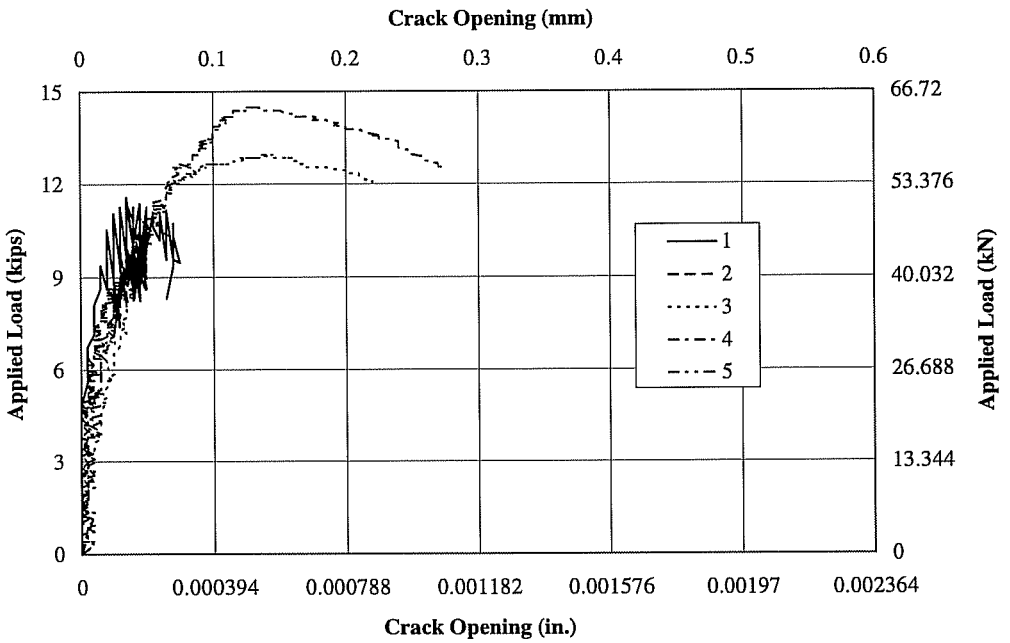

Crack Opening in Tests 8DML54/06-10

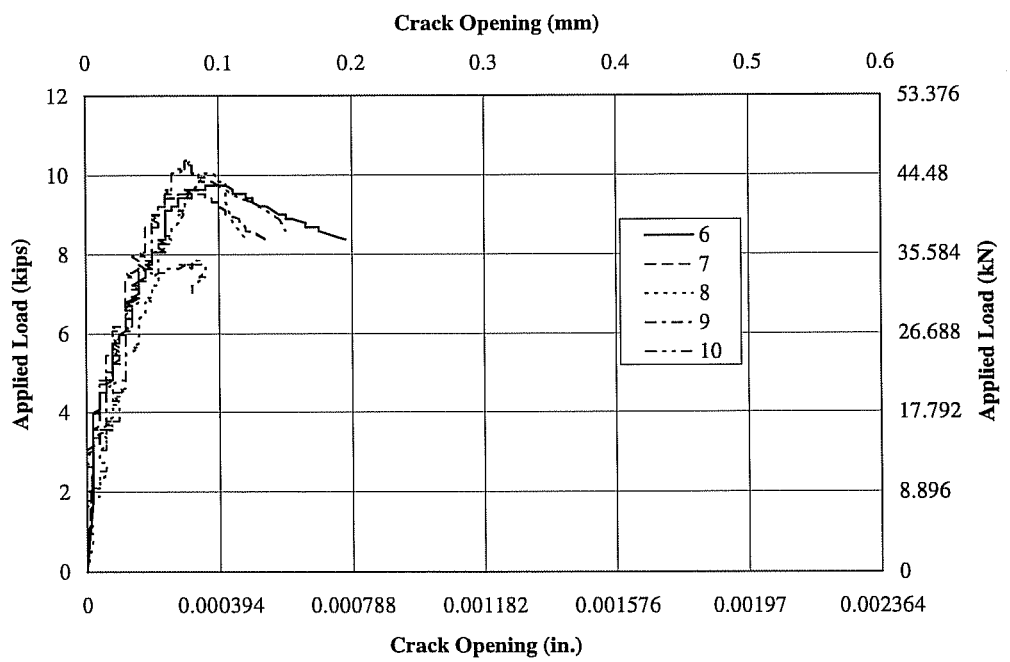

Crack Opening in Tests 8DML57/11-15

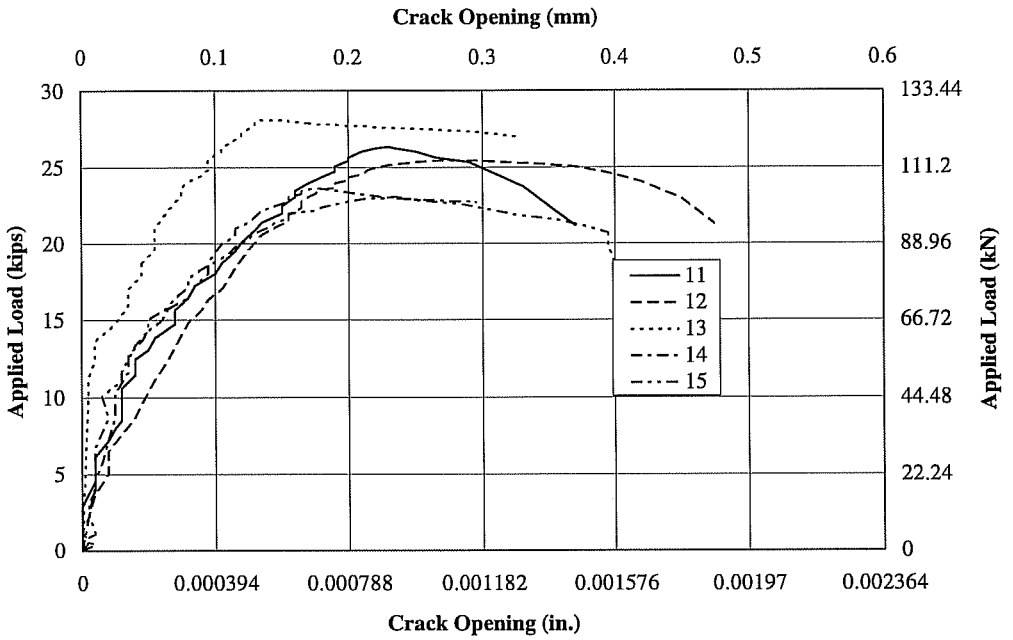

Crack Opeing in Tests 8DSL57/16-20

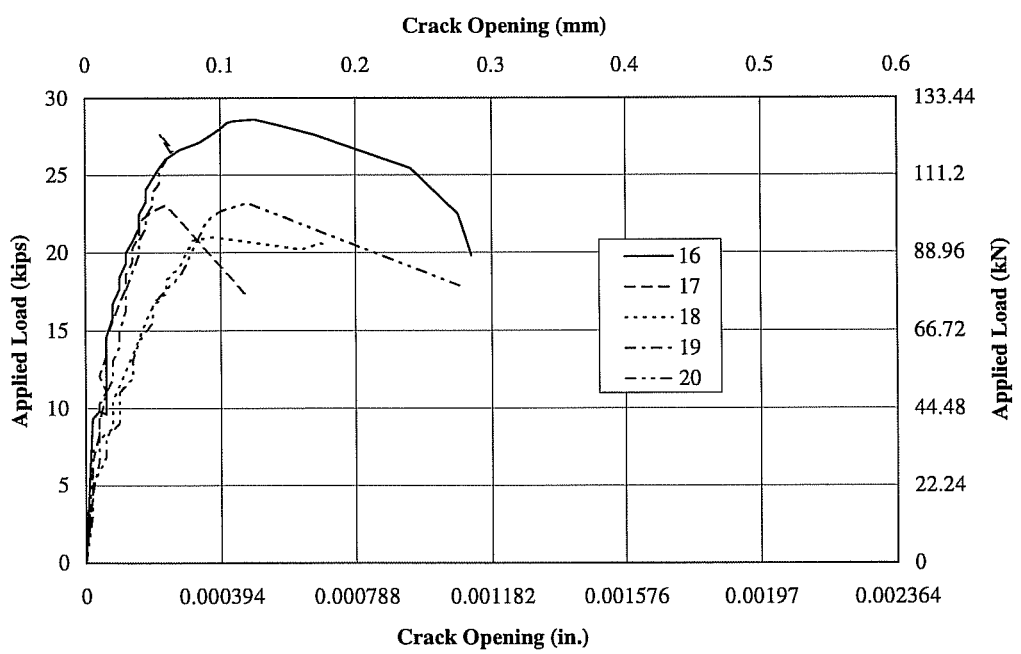

Crack Opening in Tests 8DHL54/21-25

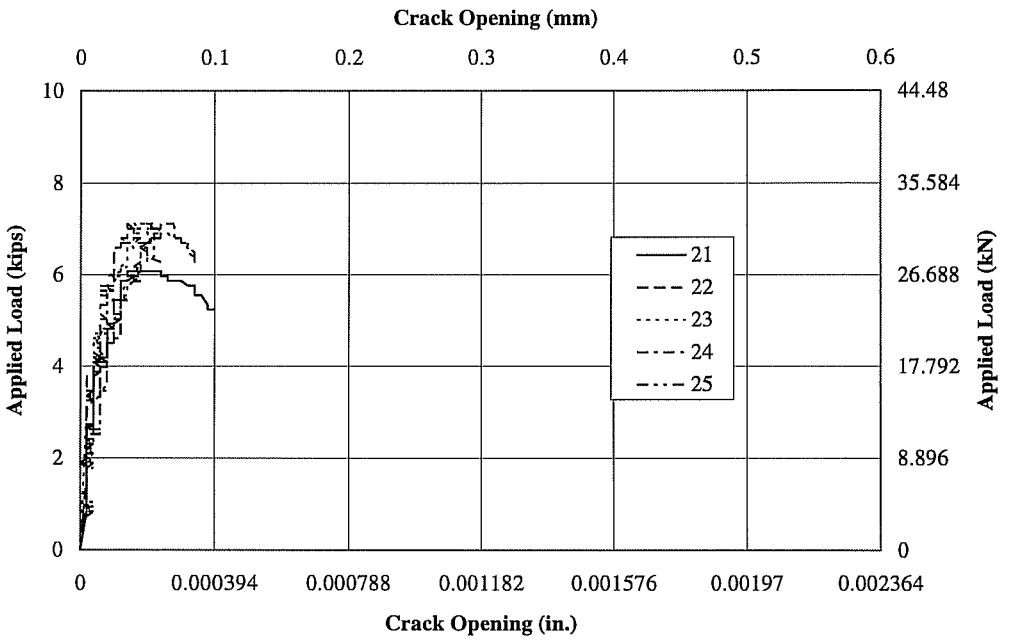

Crack Opening in Tests 8DHL57/26-30

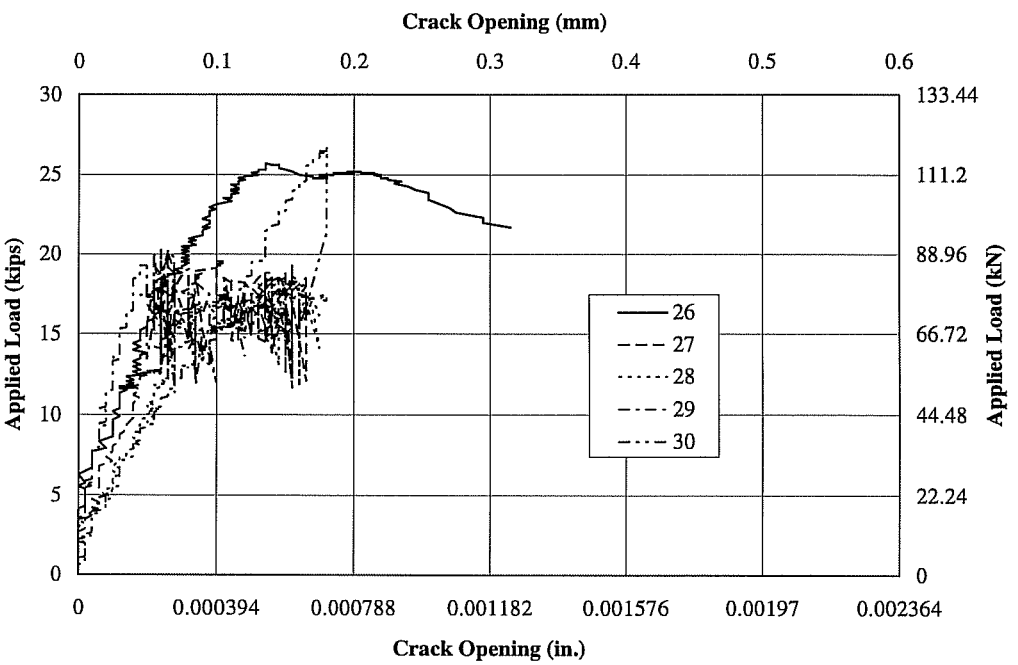

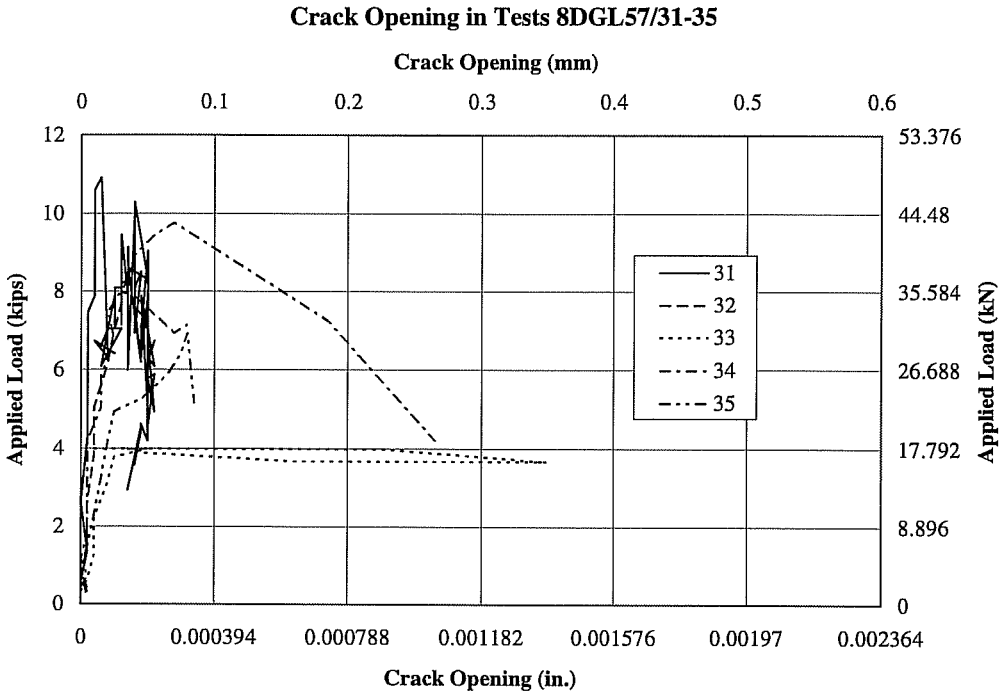
Crack Opening in Tests 8DGL57/31-35
Crack Opening (mm)
0
0.1
0.2
0.3
0.4
0.5
0.6
12
10
8
6
4
2
0
53.376
44.48
35.584
26.688
17.792
8.896
0
Applied Load (kips)
Applied Load (kN)
31
32
33
34
35
0
0.000394
0.000788
0.001182
0.001576
0.00197
0.002364
Crack Opening (in.)

Time History of Loading in Tests 8DKL57/01-05

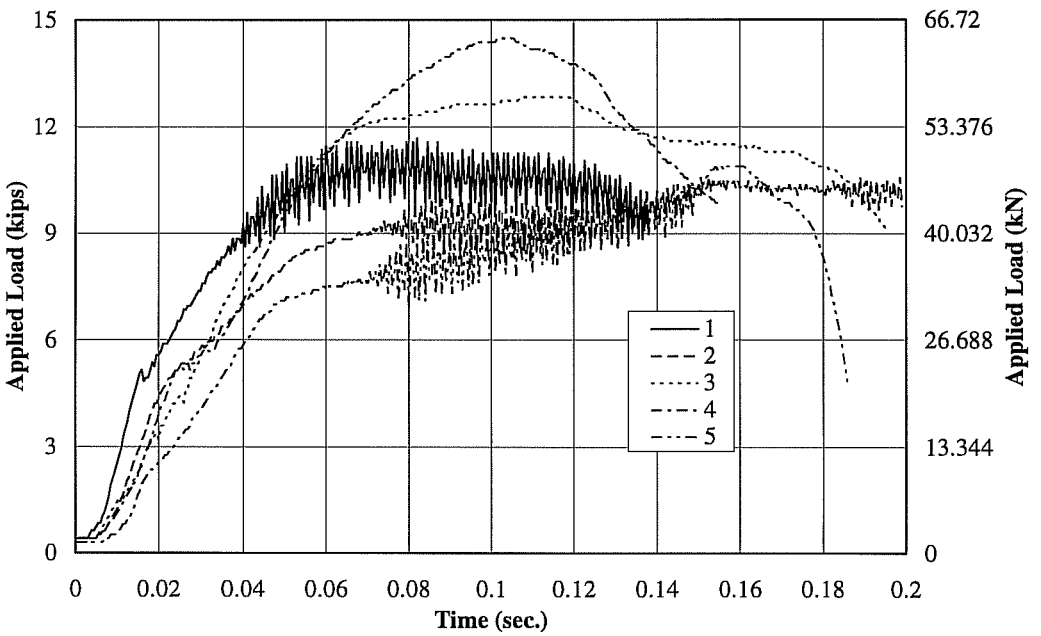

Time History of Loading in Tests 8DML54/06-10

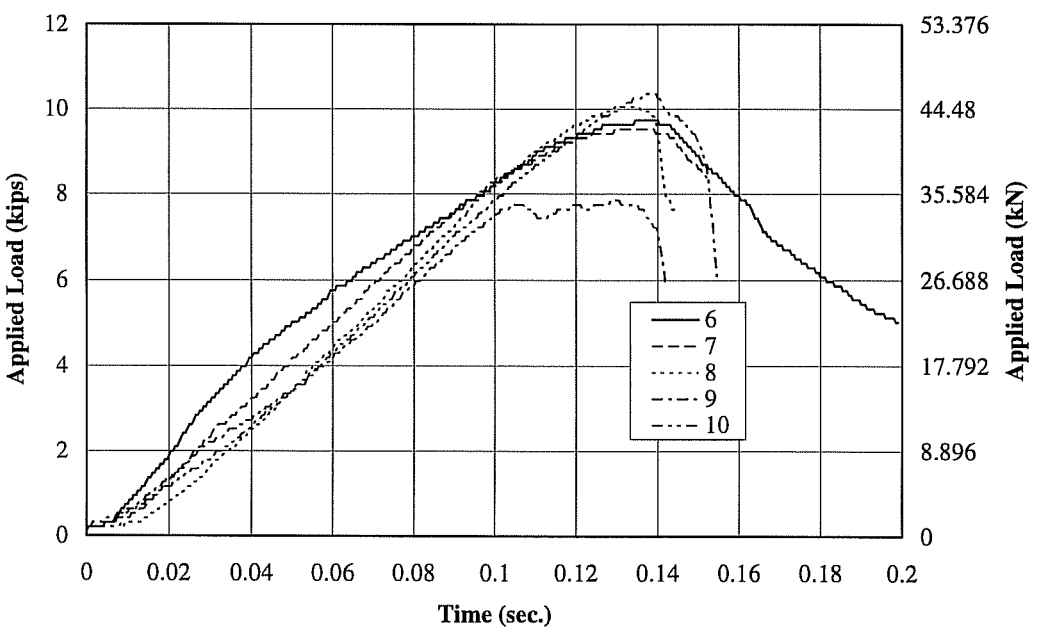

Time History of Loading in Tests 8DML57/11-15

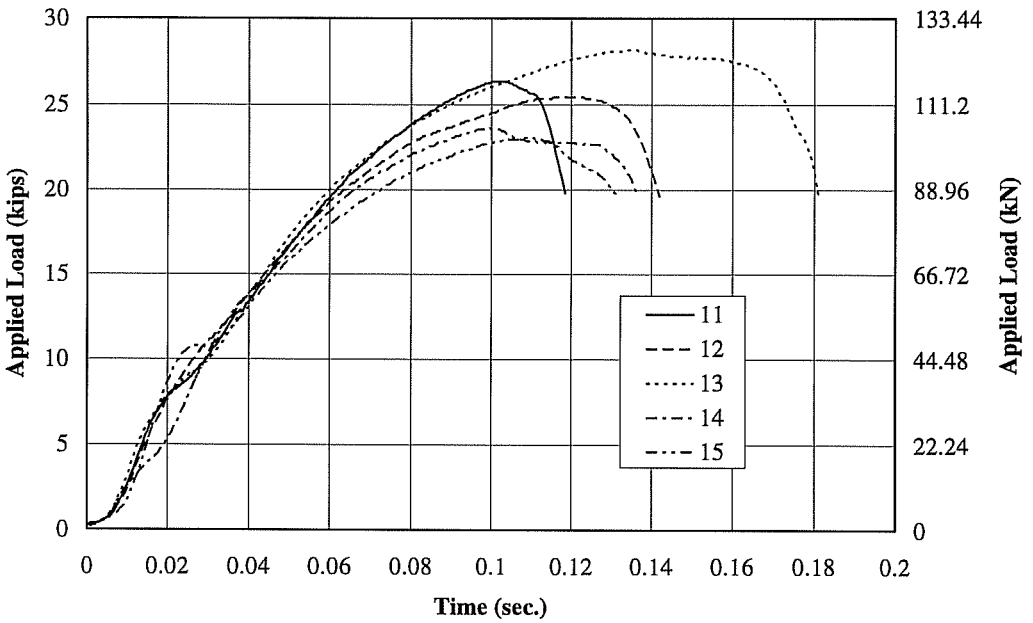

Time History of Loading in Tests 8DSL57/16-20

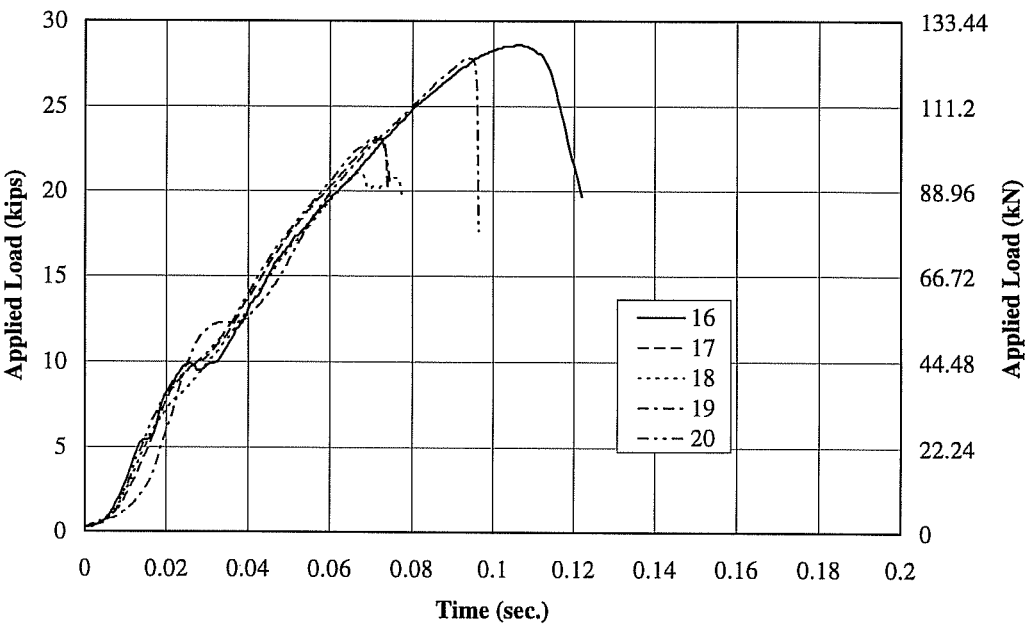

Time History of Loading in Tests 8DHL54/21-25

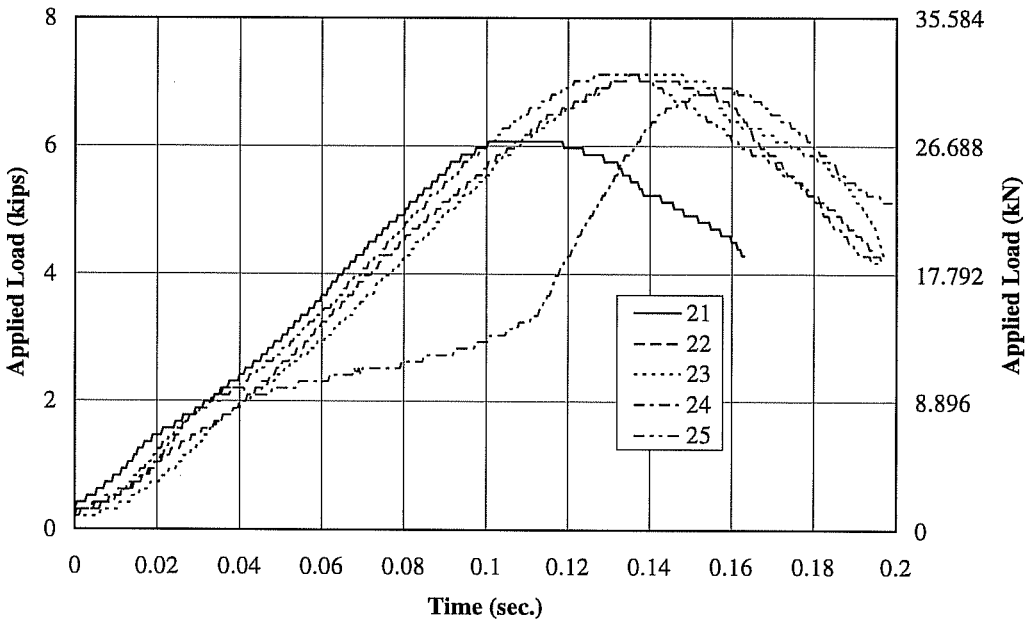

Time History of Loading in Tests 8DHL57/26-30

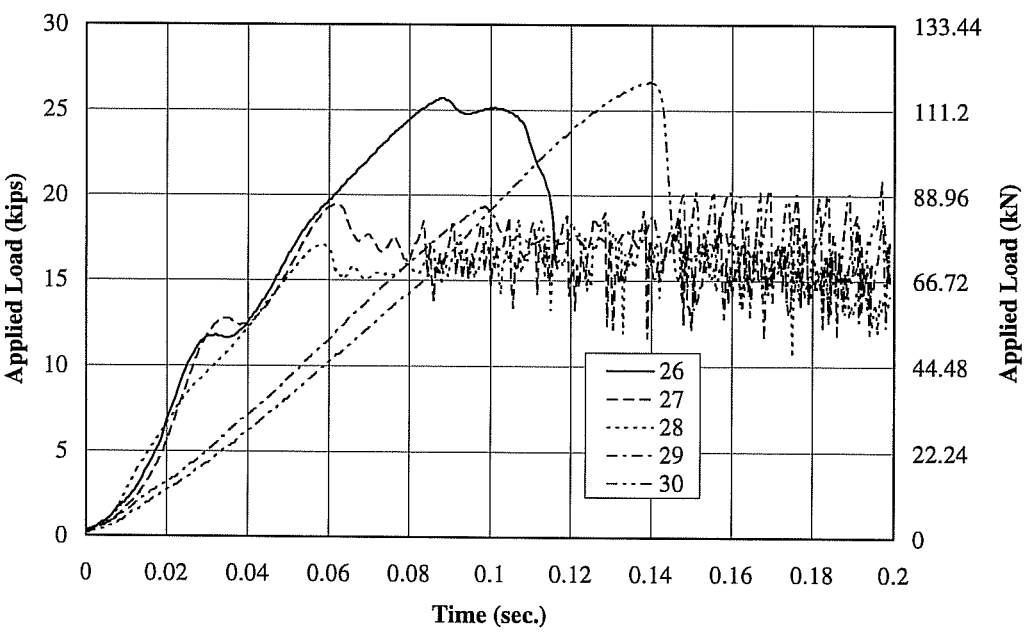

Time History of Loading in Tests 8DGL57/31-35

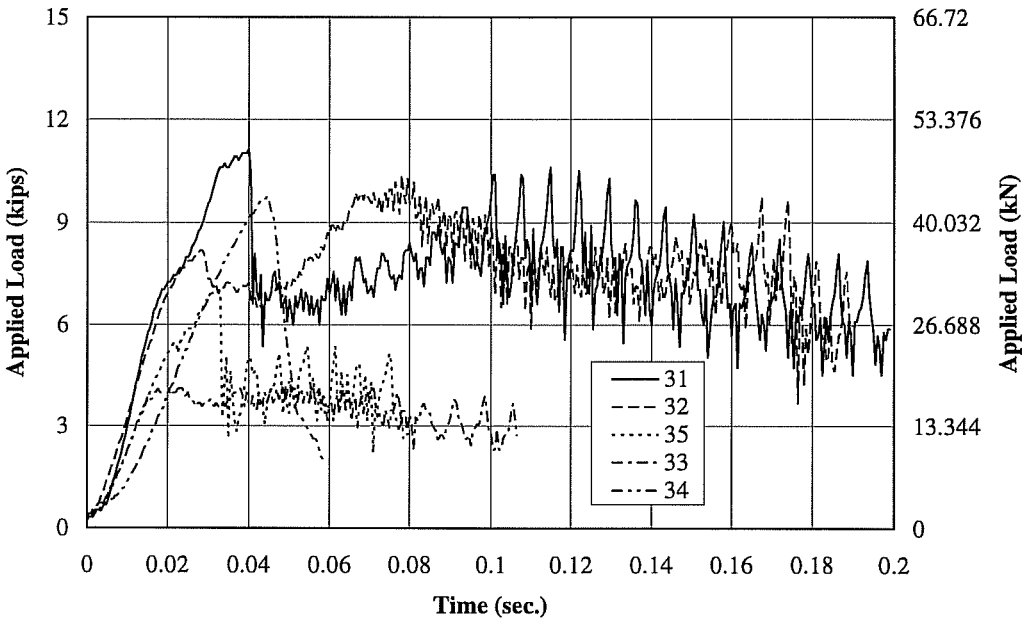

Appendix C

Results for Tests of Task 3

Summary of Double-Anchor Connections Tests

Test #	Concrete	Cncr. Strngth	Loading	Spalling Depth	Gap	Hairpin
		psi		inch		
9S01	Uncracked	2nd	Static	0.2500	large @ front	no
9S02	Uncracked	2nd	Static	0.6250	no gap	no
9S03	Uncracked	2nd	Static	0.3750	no gap	no
9S04	Uncracked	1st	Static	0.3750	very small @ back	no
9S05	Uncracked	1st	Static	0.6250	large @ front	no
			Ave.	**0.45**		
10D06	Uncracked	2nd	Dynamic	0.500	small @ back	no
10D07	Uncracked	2nd	Dynamic	0.500	no gap	no
10D08	Uncracked	2nd	Dynamic	0.250	very large @ front	no
10D09	Uncracked	2nd	Dynamic	0.250	small @ front	no
10D10	Uncracked	1st	Dynamic	0.625	no gap	no
			Ave.	**0.425**		
11S11	Cracked	2nd	Static	0.250	N/A	no
11S12	Cracked	2nd	Static	0.375	N/A	no
11S13	Cracked	2nd	Static	0.250	very large @ back	no
11S14	Cracked	2nd	Static	0.5	small @ back	no
11S15	Cracked	2nd	Static		small @ back	no
			Ave.	**0.344**		
11SH16	Cracked	1st	Static	1.000	N/A	yes
11SH17	Cracked	1st	Static	0.500	N/A	yes
11SH18	Cracked	1st	Static	0.688	N/A	yes
11SH19	Cracked	1st	Static	0.500	Very large @ back	yes
11SH20	Cracked	1st	Static	0.625	Very large @ back	yes
			Ave.	**0.663**		
12D21	Cracked	1st	Dynamic	0.625	no gap	no
12D22	Cracked	1st	Dynamic	0.375	large gap @ back	no
12D23	Cracked	1st	Dynamic	0.375	very large @ front	no
12D24	Cracked	1st	Dynamic	0.500	small @ back	no
12D25	Cracked	1st	Dynamic	0.500	small @ back	no
			Ave.	**0.475**		
12DH26	Cracked		Dynamic	0.250	no gap	yes
12DH27	Cracked		Dynamic	0.250	no gap	yes
12DH28	Cracked		Dynamic	0.500	large @ back	yes
12DH29	Cracked		Dynamic	0.500	small @ front	yes
12DH30	Cracked		Dynamic	0.750	very small @ back	yes
			Ave.	**0.450**		

Summary of Double-Anchor Connections Tests (Continued)

Test #	1st Peak Load	Hor. Dspl	Ver. Dspl	2nd Peak Load	Hor. Dspl	Ver. Dspl	Max. Load	Frac. Load	Mom.	Ver. Load	Hor. Load	Inter.
	kips	inch	inch	kips	inch	inch	kips	kips	k-ins	kips	kips	
9S01	25.75	0.13	0.05	26.04	0.32	0.10	26.04	26.04	-4.59	30.33	17.15	1.06
9S02	27.61	0.18	0.07	25.42	0.31	0.10	27.61	25.42	-6.63	29.18	17.15	1.03
9S03	21.27	0.12	0.03	24.56	0.48	0.13	24.56	24.56	11.2	31.71	16.12	1.04
9S04	23.98	0.11	0.05	23.89	0.35	0.11	23.98	23.89	-8.67	26.93	16.81	0.95
9S05	25.84	0.20	0.09	24.65	0.54	0.15	25.84	24.65	-5.76	28.43	15.75	0.93
Ave.	**24.89**	**0.15**	**0.06**	**24.91**	**0.40**	**0.12**	**25.61**			**29.32**	**16.60**	**1.00**
COV	**9.63**	**25.81**	**37.02**	**3.34**	**26.28**	**18.39**	**5.52**					**5.95**
10D06	28.52	0.14	0.05	28.80	0.53	0.12	28.80	28.80	-26.0	29.36	19.00	1.15
10D07	25.03	0.15	0.03	28.42	0.48	0.12	28.42	28.42	-8.89	32.33	15.07	1.00
10D08	25.61	0.11	0.05	30.32	0.66	0.17	30.32	30.32	-28.8	30.62	19.37	1.21
10D09	29.94	0.16	0.06	28.70	0.49	0.13	29.94	28.70	-15.2	31.41	16.83	1.07
10D10	29.47	0.20	0.07	31.09	0.49	0.15	31.09	31.09	6.56	38.62	12.95	1.09
Ave.	**27.71**	**0.15**	**0.05**	**29.47**	**0.53**	**0.14**	**29.71**			**32.47**	**16.64**	**1.11**
COV	**8.13**	**20.83**	**27.19**	**3.98**	**14.15**	**15.14**	**3.69**					**7.51**
11S11	20.50	0.13	0.04	26.08	0.45	0.13	26.08	26.08	-4.08	30.48	16.10	1.00
11S12	18.51	0.16	0.03	20.94	0.51	0.10	20.94	20.94	1.60	25.45	16.44	0.89
11S13	24.22	0.16	0.05	24.27	0.40	0.10	24.27	24.27	-3.06	28.51	17.49	1.03
11S14	21.03	0.15	0.03	25.13	0.48	0.11	25.13	25.13	-9.18	28.32	17.50	1.03
11S15	20.08	0.14	0.03	25.03	0.38	0.12	25.03					
Ave.	**20.87**	**0.15**	**0.04**	**24.29**	**0.44**	**0.11**	**24.29**			**28.19**	**16.88**	**0.99**
COV	**10.05**	**10.66**	**19.68**	**8.15**	**12.02**	**11.09**	**8.15**					**6.76**
11SH16	21.32	0.12	0.05	28.52	0.55	0.21	28.52	28.52	15.0	37.22	13.33	1.06
11SH17	22.22	0.13	0.04	27.75	0.38	0.14	27.75	27.75	3.57	34.01	15.05	1.05
11SH18	22.13	0.12	0.04	28.80	0.53	0.17	28.80	28.80	-6.12	33.34	14.35	0.99
11SH19	25.27	0.16	0.06	32.42	0.43	0.16	32.42	32.42	-10.4	36.82	15.59	1.17
11SH20	22.31	0.18	0.05	27.51	0.54	0.14	27.51	27.51	-3.57	32.30	15.05	1.00
Ave.	**22.65**	**0.14**	**0.05**	**29.00**	**0.49**	**0.16**	**29.00**			**34.74**	**14.67**	**1.05**
COV	**6.70**	**19.40**	**16.31**	**6.84**	**15.84**	**17.90**	**6.84**					**6.81**
12D21	22.70	0.18	0.05	26.37	0.66	0.17	26.37	26.37	7.51	33.15	14.35	0.98
12D22	23.65	0.13	0.04	28.85	0.64	0.16	28.85	28.85	-24.4	29.74	18.64	1.14
12D23	24.46	0.15	0.04	28.28	0.65	0.19	28.28	28.28	1.09	34.15	15.39	1.07
12D24	28.37	0.25	0.09	26.56	0.53	0.14	28.37	26.56	-8.02	30.27	13.30	0.84
12D25	31.56	0.23	0.10	28.99	0.57	0.18	31.56	28.99	-2.84	34.22	14.34	1.01
Ave.	**26.15**	**0.19**	**0.06**	**27.81**	**0.61**	**0.17**	**28.69**			**32.31**	**15.20**	**1.01**
COV	**14.21**	**27.90**	**44.80**	**4.52**	**9.29**	**12.55**	**6.50**					**10.98**

Summary of Double-Anchor Connections Tests (Continued)

Test #	1st Peak Load	Hor. Dspl	Ver. Dspl	2nd Peak Load	Hor. Dspl	Ver. Dspl	Max. Load	Frac. Load	Mom.	Ver. Load	Hor. Load	Inter.
	kips	inch	inch	kips	inch	inch	kips	kips	k-ins	kips	kips	
12DH26	30.14	0.22	0.07	30.71	0.26	0.09	30.71	30.71	3.57	37.57	12.95	1.05
12DH27	30.00	0.20	0.08	31.48	0.29	0.11	31.48	31.48	10.9	39.96	13.67	1.17
12DH28	20.31	0.11	0.04	29.04	0.71	0.27	29.04	29.04	7.44	36.34	13.30	1.03
12DH29	30.95	0.27	0.08	33.00	0.58	0.21	33.00	33.00	-2.04	39.19	9.80	0.96
12DH30	27.04	0.19	0.05	31.18	0.45	0.16	31.18	31.18	-7.51	35.91	11.90	0.95
Ave.	**27.69**	**0.20**	**0.07**	**31.08**	**0.46**	**0.17**	**31.08**			**37.79**	**12.32**	**1.03**
COV	**15.83**	**29.20**	**30.82**	**4.59**	**41.94**	**44.42**	**4.59**					**8.51**

9S/01-05
Static Load, Uncracked Concrete without Hairpin
Load vs. Horizontal Displacement

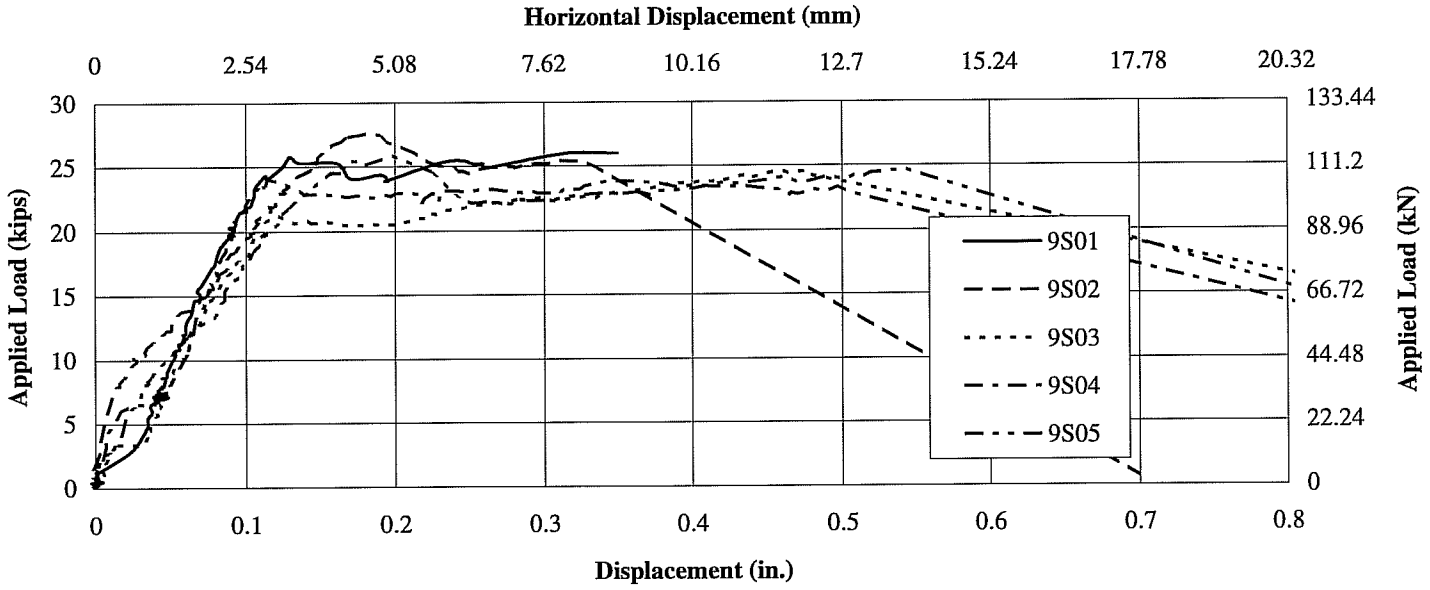

Test Number	Date	Block Number	f_c, psi	First Peak Load, kips (KN)		Displ. at First Peak Load in. (mm)		Second Peak Load, kips (KN)		Displ. at Sec. Peak Load in. (mm)		Failure Mode
9S01	7/16/96	B4	4457	25.8	(114.8)	0.129	(3.28)	26.0	(115.8)	0.319	(8.10)	Steel
9S02	7/19/96	B4	4457	27.6	(122.8)	0.182	(4.62)	25.5	(113.5)	0.310	(7.87)	Steel
9S03	7/26/96	B4	4457	21.3	(94.7)	0.121	(3.07)	24.6	(109.2)	0.476	(12.09)	Steel
9S04	8/19/19	B1	4200	24.0	(106.8)	0.114	(2.90)	23.9	(106.3)	0.345	(8.76)	Steel
9S05	8/19/96	B1	4200	25.8	(114.8)	0.198	(5.03)	24.7	(109.6)	0.543	(13.79)	Steel
			Average	24.9	(110.8)	0.149	(3.78)	24.9	(110.9)	0.399	(10.12)	

9S/01-05
Static Load, Uncracked Concrete without Hairpin
Load vs. Vertical Displacement

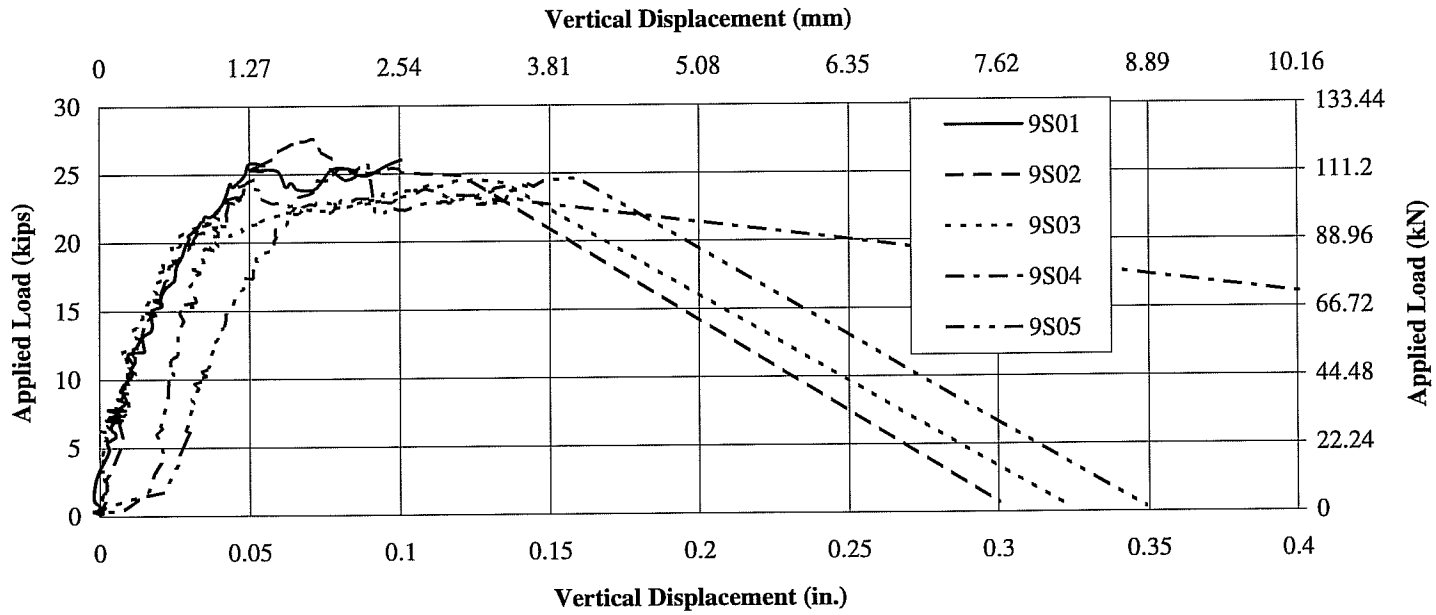

Test Number	Date	Block Number	f_c, psi	First Peak Load, kips (KN)		Displ. at First Peak Load in. (mm)		Second Peak Load, kips (KN)		Displ. at Sec. Peak Load in. (mm)		Failure Mode
9S01	7/16/96	B4	4457	25.8	(114.8)	0.050	(1.27)	26.0	(115.8)	0.101	(2.57)	Steel
9S02	7/19/96	B4	4457	27.6	(122.8)	0.071	(1.80)	25.5	(113.5)	0.097	(2.46)	Steel
9S03	7/26/96	B4	4457	21.3	(94.7)	0.034	(0.86)	24.6	(109.2)	0.125	(3.18)	Steel
9S04	8/19/19	B1	4200	24.0	(106.8)	0.048	(1.22)	23.9	(106.3)	0.108	(2.74)	Steel
9S05	8/19/96	B1	4200	25.8	(114.8)	0.089	(2.26)	24.7	(109.6)	0.149	(3.78)	Steel
			Average	24.9	(110.8)	0.058	(1.48)	24.9	(110.9)	0.116	(2.95)	

10D/06-10
Dynamic Load, Uncracked Concrete wihtout Hairpin
Load vs. Horizontal Displacement

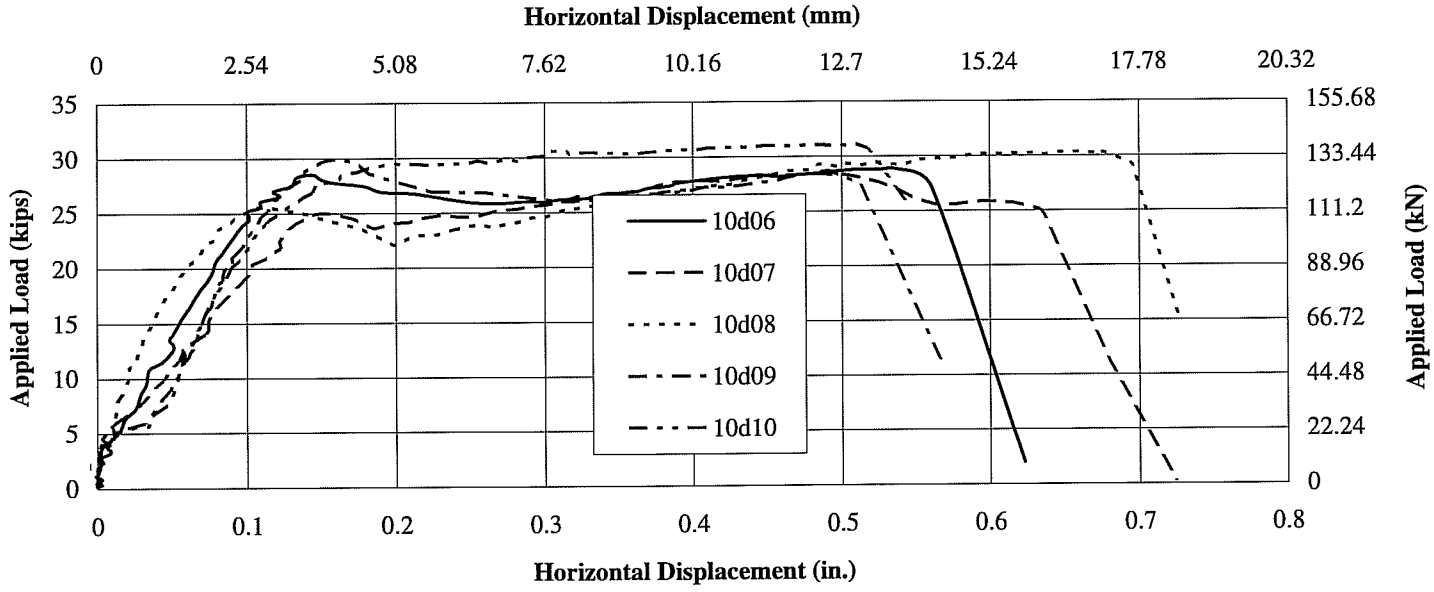

Test Number	Date	Block Number	f_c, psi	First Peak Load, kips (KN)		Displ. at First Peak Load in. (mm)		Second Peak Load, kips (KN)		Displ. at Sec. Peak Load in. (mm)		Failure Mode
10D06	8/20/96	B1	4200	28.5	(126.9)	0.140	(3.56)	28.8	(128.1)	0.526	(13.4)	Steel
10D07	8/22/96	B1	4200	25.0	(111.3)	0.150	(3.81)	28.4	(126.4)	0.483	(12.3)	Steel
10D08	8/23/96	B1	4200	25.6	(113.9)	0.113	(2.87)	30.3	(134.9)	0.661	(16.8)	Steel
10D09	8/23/96	B1	4200	29.9	(133.2)	0.161	(4.09)	28.7	(127.7)	0.491	(12.5)	Steel
10D10	8/27/96	B1	4200	29.5	(131.1)	0.200	(5.08)	31.1	(138.3)	0.490	(12.4)	Steel
			Average	27.7	(123.3)	0.153	(3.88)	29.5	(131.1)	0.530	(13.5)	

10D/06-10
Dynamic Load, Uncracked Concrete wihtout Hairpin
Load vs. Vertical Displacement

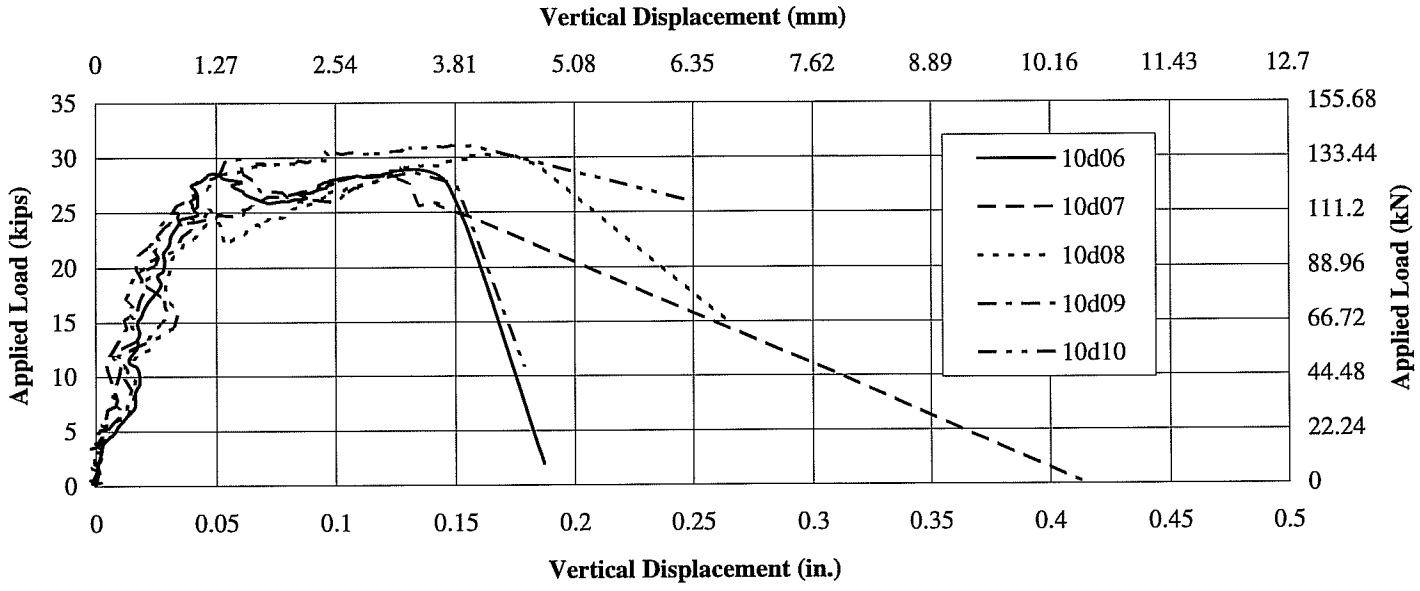

Test Number	Date	Block Number	f_c, psi	First Peak Load, kips (KN)		Displ. at First Peak Load in. (mm)		Second Peak Load, kips (KN)		Displ. at Sec. Peak Load in. (mm)		Failure Mode
10D06	8/20/96	B1	4200	28.5	(126.9)	0.047	(1.19)	28.8	(128.1)	0.124	(3.15)	Steel
10D07	8/22/96	B1	4200	25.0	(111.3)	0.032	(0.81)	28.4	(126.4)	0.118	(3.00)	Steel
10D08	8/23/96	B1	4200	25.6	(113.9)	0.046	(1.17)	30.3	(134.9)	0.170	(4.32)	Steel
10D09	8/23/96	B1	4200	29.9	(133.2)	0.061	(1.55)	28.7	(127.7)	0.132	(3.35)	Steel
10D10	8/27/96	B1	4200	29.5	(131.1)	0.067	(1.70)	31.1	(138.3)	0.148	(3.76)	Steel
			Average	27.7	(123.3)	0.051	(1.29)	29.5	(131.1)	0.138	(3.52)	

11S/11-15
Static Load, Cracked Concrete without Hairpin
Load vs. Horizontal Displacement

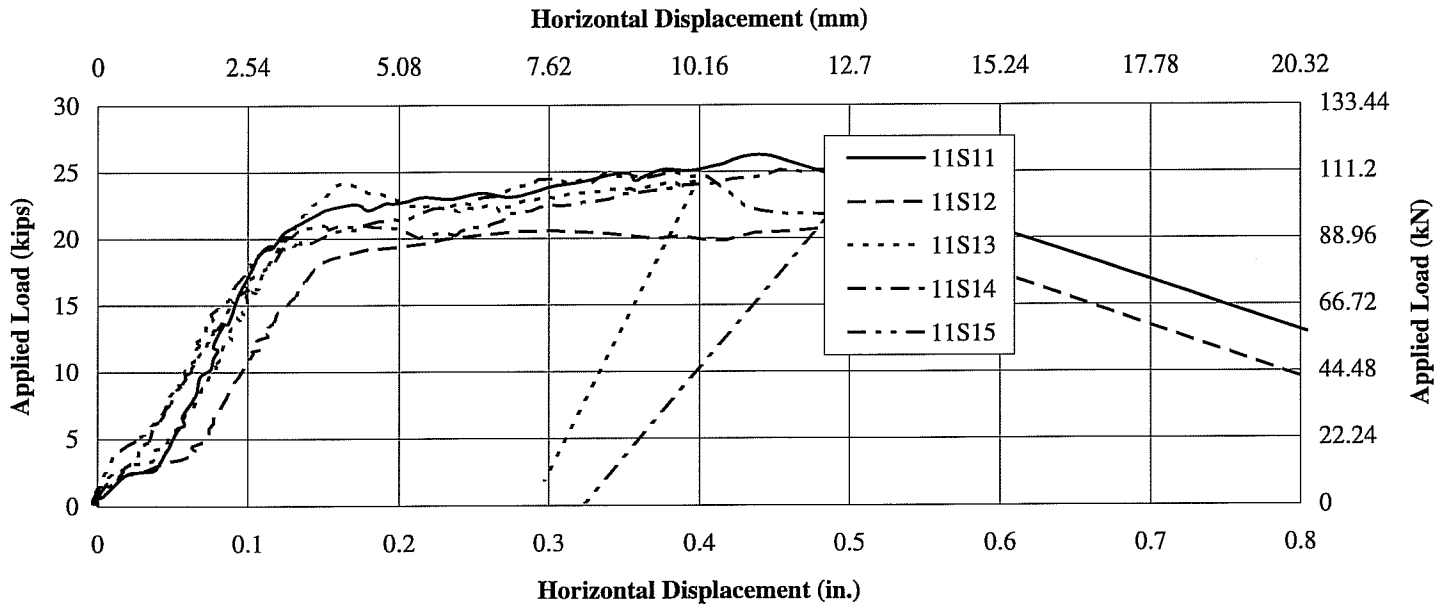

Test Number	Date	Block Number	f_c, psi	First Peak Load, kips (KN)		Displ. at First Peak Load in. (mm)		Second Peak Load, kips (KN)		Displ. at Sec. Peak Load in. (mm)		Failure Mode
11S11	7/16/96	B4	4457	20.5	(91.2)	0.125	(3.18)	26.1	(116.0)	0.450	(11.4)	Steel
11S12	7/18/96	B4	4457	18.5	(82.3)	0.155	(3.94)	20.9	(93.1)	0.507	(12.9)	Steel
11S13	7/19/96	B4	4457	24.2	(107.7)	0.164	(4.17)	24.3	(108.0)	0.397	(10.1)	Steel
11S14	7/29/96	B4	4467	21.0	(93.5)	0.151	(3.84)	25.1	(111.8)	0.480	(12.2)	Steel
11S15	8/28/96	B1	4200	20.1	(89.3)	0.136	(3.45)	25.0	(111.3)	0.382	(9.7)	Concrete
			Average	20.9	(92.8)	0.146	(3.71)	24.3	(108.0)	0.443	(11.3)	

11S/11-15
Static Load, Cracked Concrete without Hairpin
Load vs. Vertical Displacement

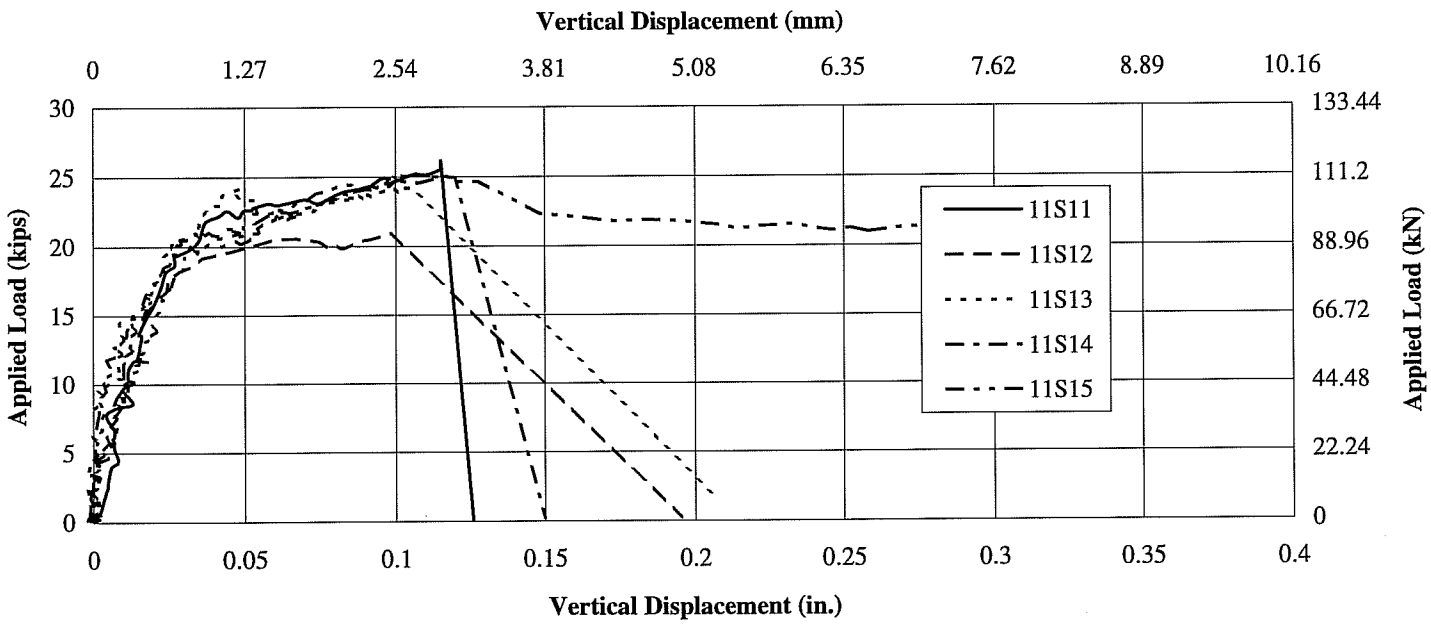

Test Number	Date	Block Number	f_c, psi	First Peak Load, kips (KN)		Displ. at First Peak Load in. (mm)		Second Peak Load, kips (KN)		Displ. at Sec. Peak Load in. (mm)		Failure Mode
11S11	7/16/96	B4	4457	20.5	(91.2)	0.035	(0.89)	26.1	(116.0)	0.126	(3.20)	Steel
11S12	7/18/96	B4	4457	18.5	(82.3)	0.032	(0.81)	20.9	(93.1)	0.096	(2.44)	Steel
11S13	7/19/96	B4	4457	24.2	(107.7)	0.049	(1.24)	24.3	(108.0)	0.101	(2.57)	Steel
11S14	7/29/96	B4	4467	21.0	(93.5)	0.034	(0.86)	25.1	(111.8)	0.107	(2.72)	Steel
11S15	8/28/96	B1	4200	20.1	(89.3)	0.032	(0.81)	25.0	(111.3)	0.117	(2.97)	Concrete
			Average	20.9	(92.8)	0.036	(0.92)	24.3	(108.0)	0.109	(2.78)	

11SH16_20
Static Load, Cracked Concrete with Hairpin
Load vs. Horizontal Displacement

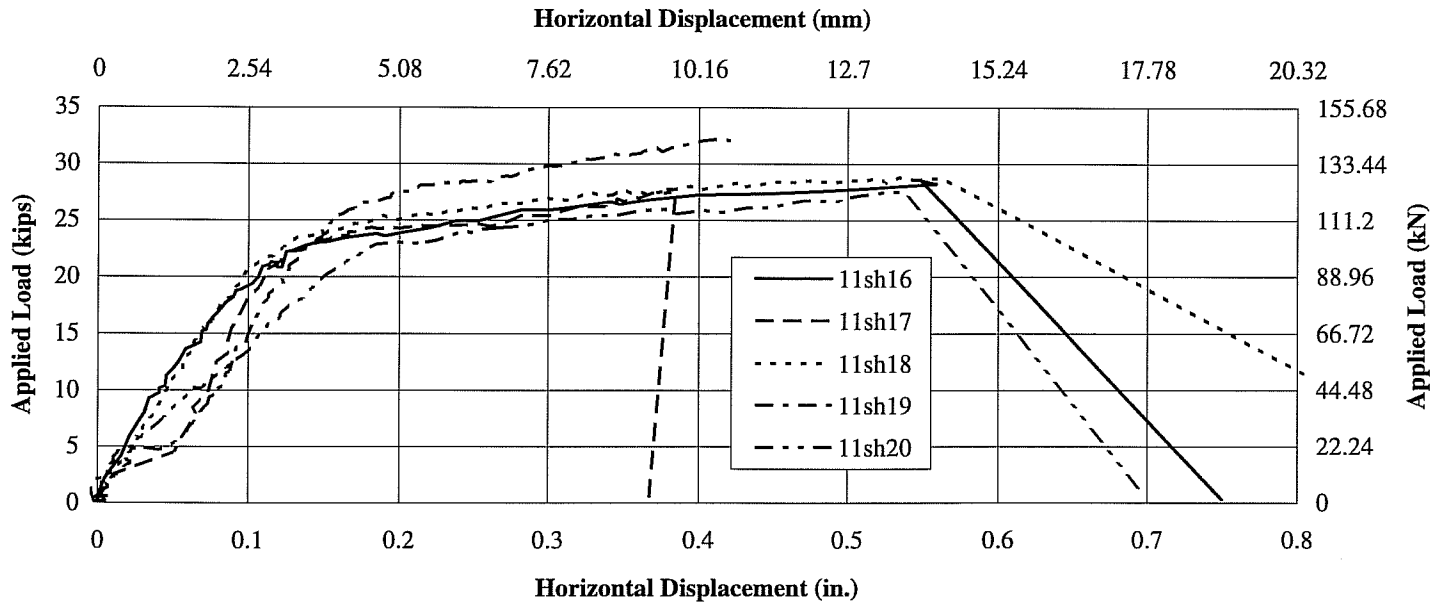

Test Number	Date	Block Number	f_c, psi	First Peak Load, kips (KN)		Displ. at First Peak Load in. (mm)		Second Peak Load, kips (KN)		Displ. at Sec. Peak Load in. (mm)		Failure Mode
11SH16	7/18/96	B4	4457	21.3	(94.8)	0.115	(2.92)	28.5	(127)	0.549	(13.9)	Steel
11SH17	7/18/96	B4	4457	22.2	(98.8)	0.125	(3.18)	27.8	(123)	0.379	(9.6)	Steel
11SH18	7/19/96	B4	4457	22.1	(98.4)	0.118	(3.00)	28.8	(128)	0.534	(13.6)	Steel
11SH19	7/25/96	B4	4457	25.3	(112.4)	0.156	(3.96)	32.4	(144)	0.429	(10.9)	Steel
11SH20	7/25/96	B4	4457	22.3	(99.2)	0.176	(4.47)	27.5	(122)	0.538	(13.7)	Steel
			Average	22.7	(100.7)	0.138	(3.51)	29.0	(129)	0.486	(12.3)	

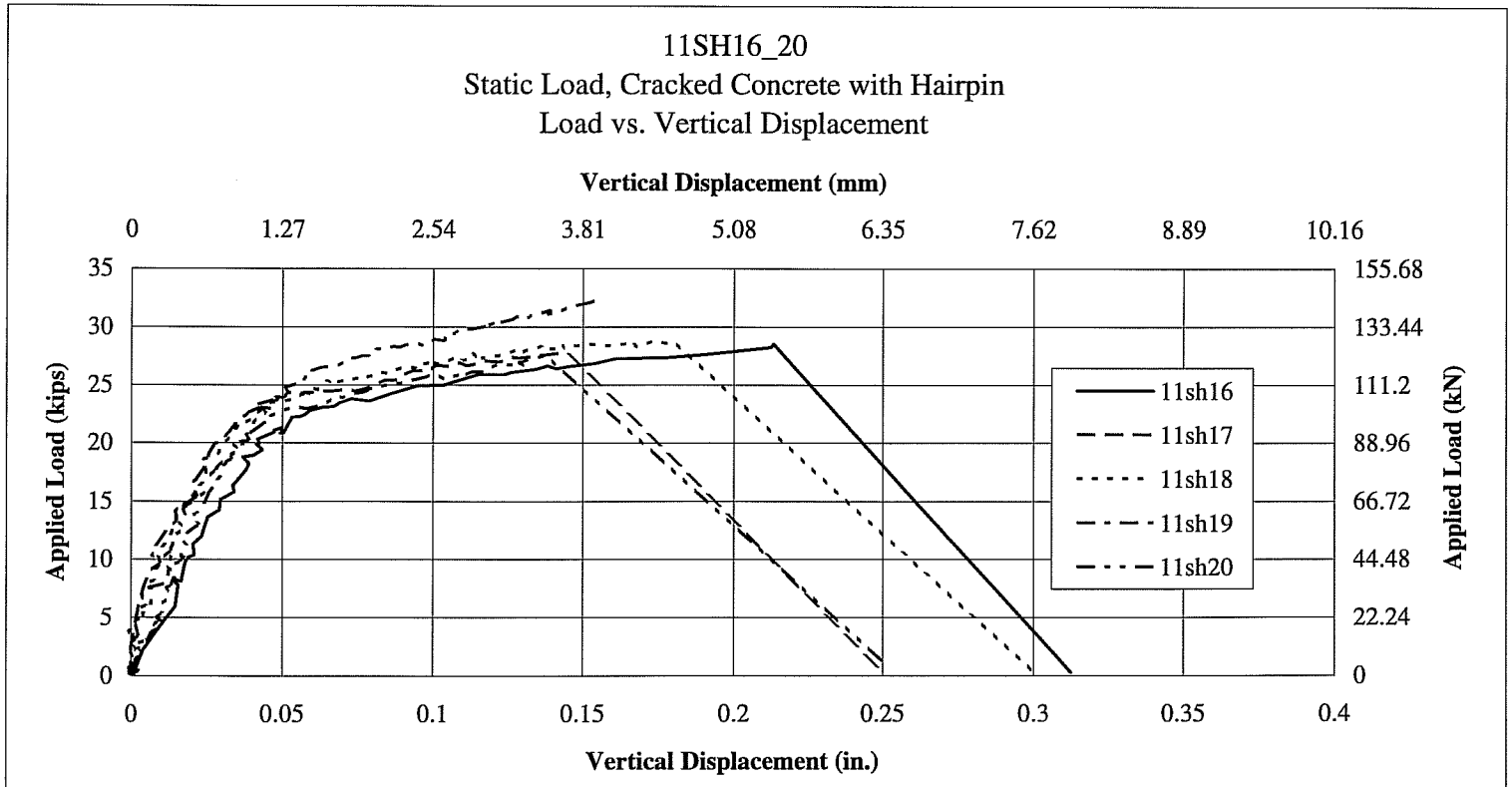

Test Number	Date	Block Number	f_c, psi	First Peak Load, kips (KN)		Displ. at First Peak Load in. (mm)		Second Peak Load, kips (KN)		Displ. at Sec. Peak Load in. (mm)		Failure Mode
11SH16	7/18/96	B4	4457	21.3	(94.8)	0.050	(1.27)	28.5	(127)	0.212	(5.38)	Steel
11SH17	7/18/96	B4	4457	22.2	(98.8)	0.036	(0.91)	27.8	(123)	0.143	(3.63)	Steel
11SH18	7/19/96	B4	4457	22.1	(98.4)	0.041	(1.04)	28.8	(128)	0.167	(4.24)	Steel
11SH19	7/25/96	B4	4457	25.3	(112.4)	0.055	(1.40)	32.4	(144)	0.160	(4.06)	Steel
11SH20	7/25/96	B4	4457	22.3	(99.2)	0.046	(1.17)	27.5	(122)	0.138	(3.51)	Steel
			Average	22.7	(100.7)	0.046	(1.16)	29.0	(129)	0.164	(4.17)	

12D/21-25
Dynamic Load, Cracked Concrete without Hairpin
Load vs. Horizontal Displacement

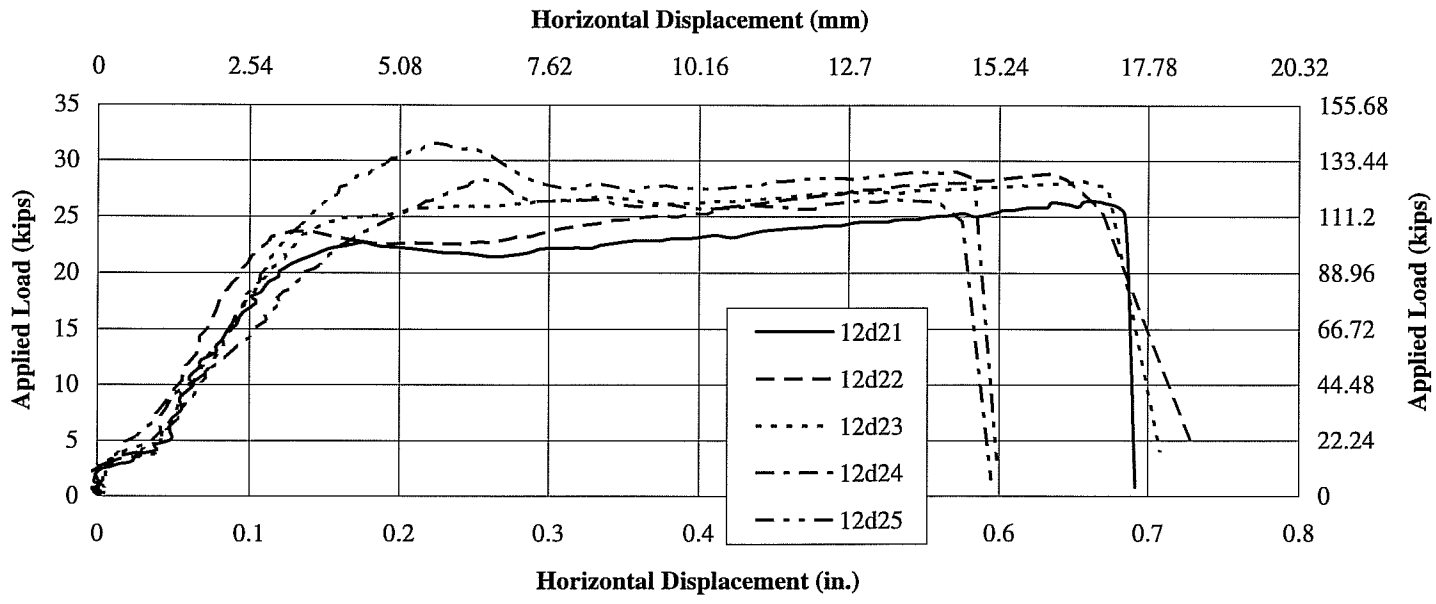

Test Number	Date	Block Number	f_c, psi	First Peak Load, kips (KN)		Displ. at First Peak Load in. (mm)		Second Peak Load, kips (KN)		Displ. at Sec. Peak Load in. (mm)		Failure Mode
12D21	8/21/96	B1	4200	22.7	(101)	0.176	(4.47)	26.4	(117)	0.658	(16.7)	Steel
12D22	8/22/96	B1	4200	23.7	(105)	0.127	(3.23)	28.9	(128)	0.636	(16.2)	Steel
12D23	8/26/96	B1	4200	24.5	(109)	0.151	(3.84)	28.3	(126)	0.654	(16.6)	Steel
12D24	8/23/96	B1	4200	28.4	(126)	0.253	(6.43)	26.6	(118)	0.530	(13.5)	Steel
12D25	8/28/96	B1	4200	31.6	(140)	0.225	(5.72)	29.0	(129)	0.571	(14.5)	Steel
			Average	26.1	(116)	0.186	(4.73)	27.8	(124)	0.610	(15.5)	

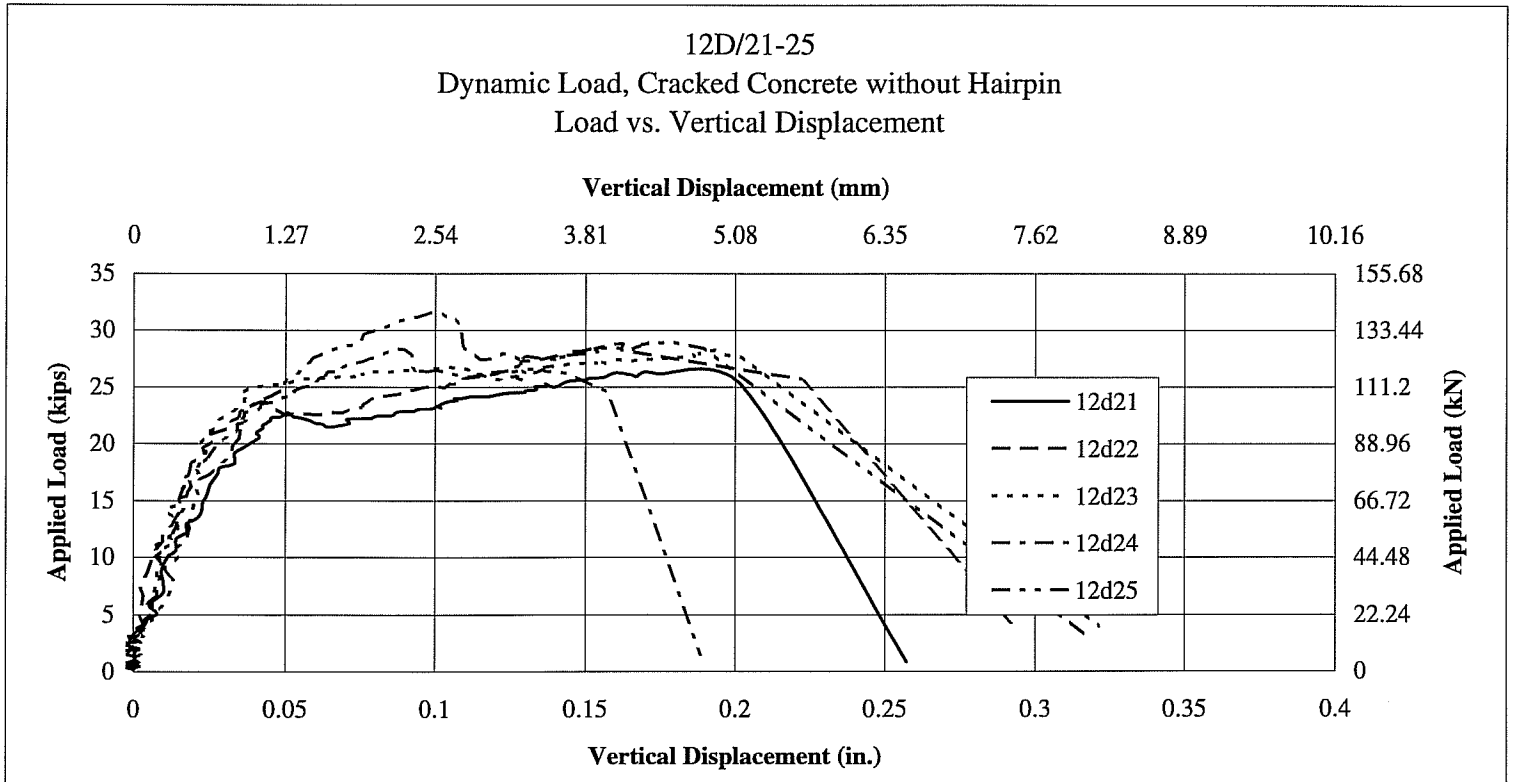

Test Number	Date	Block Number	f_c, psi	First Peak Load, kips (KN)		Displ. at First Peak Load in. (mm)		Second Peak Load, kips (KN)		Displ. at Sec. Peak Load in. (mm)		Failure Mode
12D21	8/21/96	B1	4200	22.7	(101)	0.051	(1.30)	26.4	(117)	0.169	(4.29)	Steel
12D22	8/22/96	B1	4200	23.7	(105)	0.042	(1.07)	28.9	(128)	0.163	(4.14)	Steel
12D23	8/26/96	B1	4200	24.5	(109)	0.036	(0.91)	28.3	(126)	0.193	(4.90)	Steel
12D24	8/23/96	B1	4200	28.4	(126)	0.087	(2.21)	26.6	(118)	0.136	(3.45)	Steel
12D25	8/28/96	B1	4200	31.6	(140)	0.099	(2.51)	29.0	(129)	0.178	(4.52)	Steel
			Average	26.1	(116)	0.063	(1.60)	27.8	(124)	0.168	(4.26)	

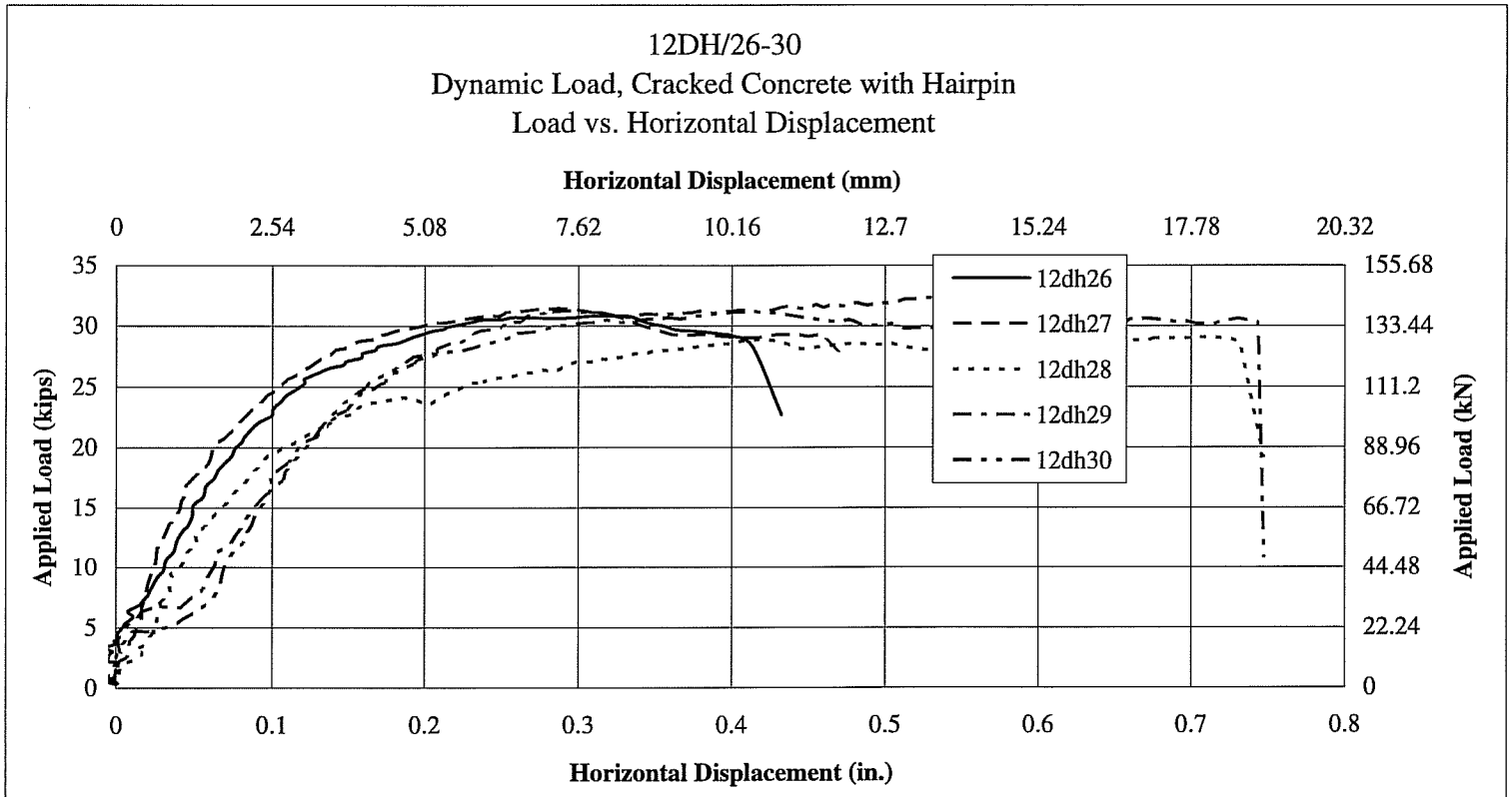

Test Number	Date	Block Number	f_c, psi	First Peak Load, kips (KN)		Displ. at First Peak Load in. (mm)		Second Peak Load, kips (KN)		Displ. at Sec. Peak Load in. (mm)		Failure Mode
12DH26	7/30/96	B4	4457	30.1	(134)	0.224	(5.69)	30.7	(137)	0.258	(6.6)	Steel
12DH27	7/30/96	B4	4457	30.0	(133)	0.197	(5.00)	31.5	(140)	0.287	(7.3)	Steel
12DH28	8/21/96	B1	4200	20.3	(90)	0.113	(2.87)	29.0	(129)	0.707	(18.0)	Steel
12DH29	8/26/96	B1	4200	31.0	(138)	0.272	(6.91)	33.0	(147)	0.583	(14.8)	Steel
12DH30	8/28/96	B1	4200	27.0	(120)	0.188	(4.78)	31.2	(139)	0.450	(11.4)	Steel
			Average	27.7	(123)	0.199	(5.05)	31.1	(138)	0.457	(11.6)	

12DH/26-30
Dynamic Load, Cracked Concrete with Hairpin
Load vs. Vertical Displacement

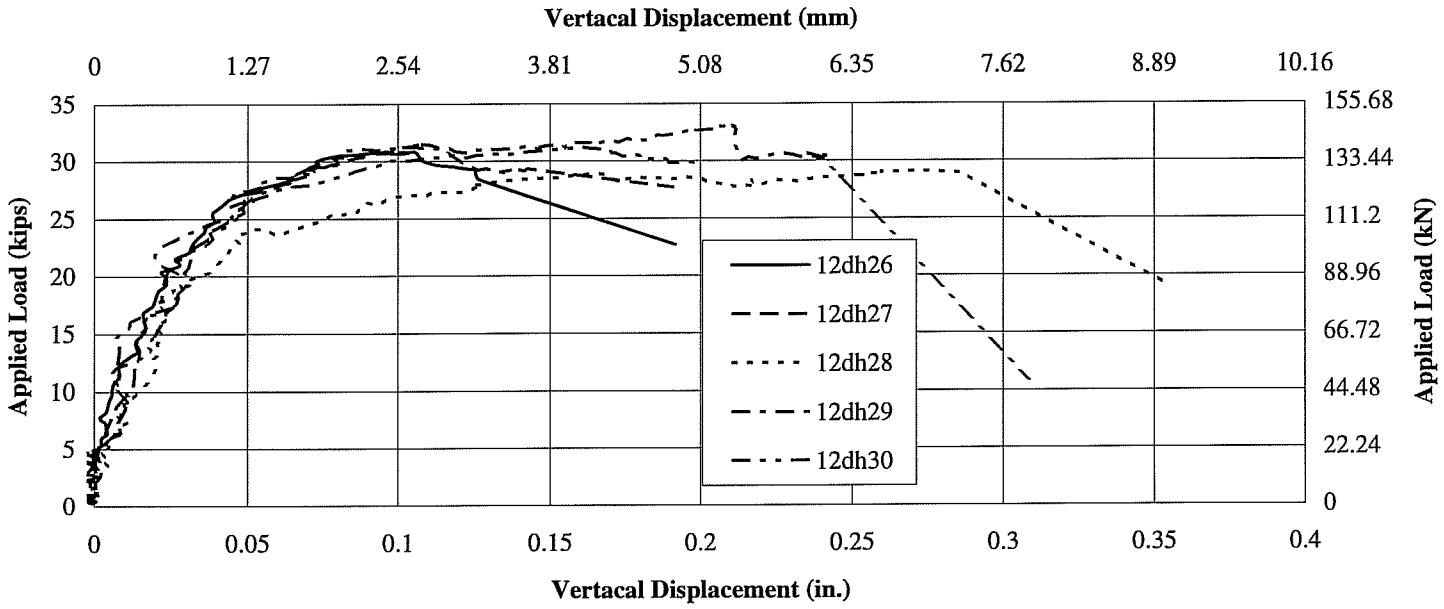

Test Number	Date	Block Number	f_c, psi	First Peak Load, kips (KN)		Displ. at First Peak Load in. (mm)		Second Peak Load, kips (KN)		Displ. at Sec. Peak Load in. (mm)		Failure Mode
12DH26	7/30/96	B4	4457	30.1	(134)	0.074	(1.88)	30.7	(137)	0.091	(2.31)	Steel
12DH27	7/30/96	B4	4457	30.0	(133)	0.081	(2.06)	31.5	(140)	0.105	(2.67)	Steel
12DH28	8/21/96	B1	4200	20.3	(90)	0.038	(0.97)	29.0	(129)	0.270	(6.86)	Steel
12DH29	8/26/96	B1	4200	31.0	(138)	0.083	(2.11)	33.0	(147)	0.210	(5.33)	Steel
12DH30	8/28/96	B1	4200	27.0	(120)	0.050	(1.27)	31.2	(139)	0.161	(4.09)	Steel
			Average	27.7	(123)	0.065	(1.66)	31.1	(138)	0.167	(4.25)	

Test 9S01

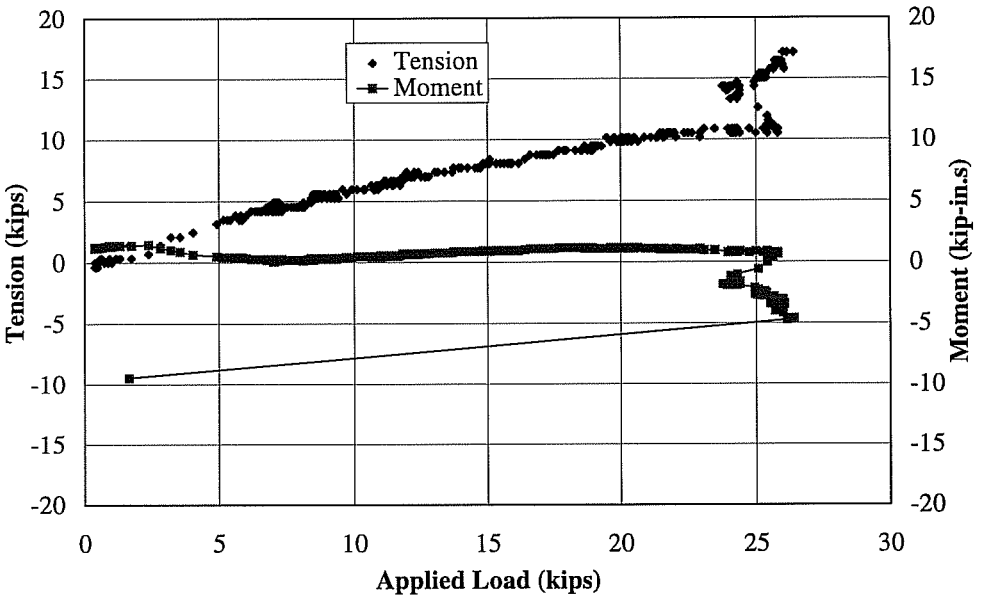

Test 9S02

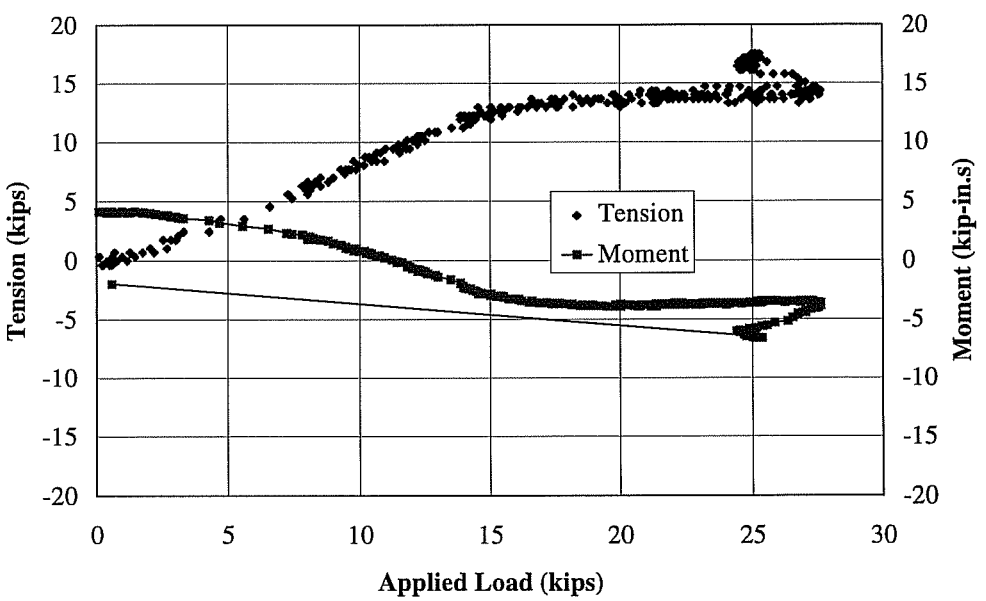

Test 9S03

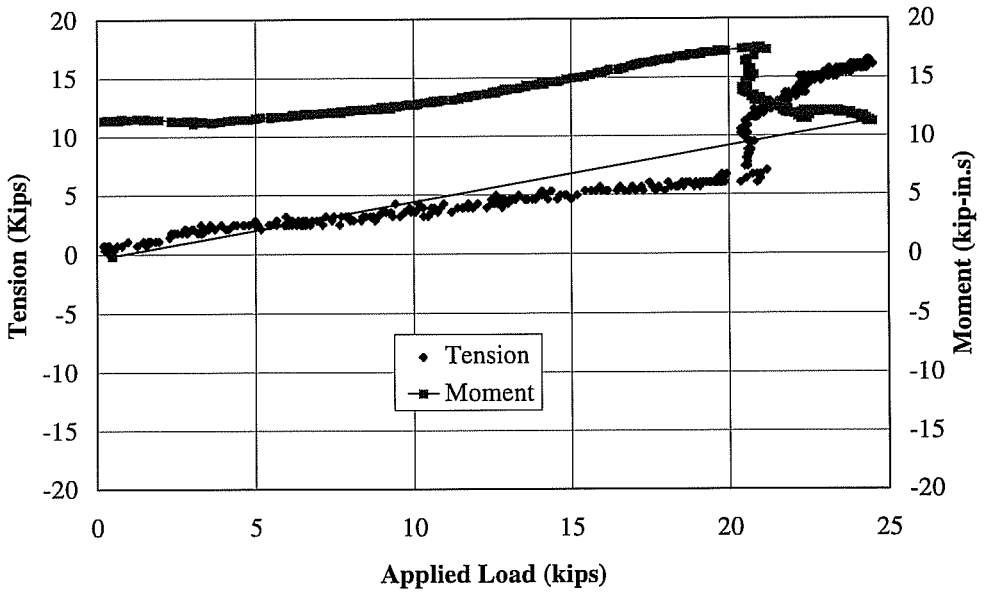

Test 9S04

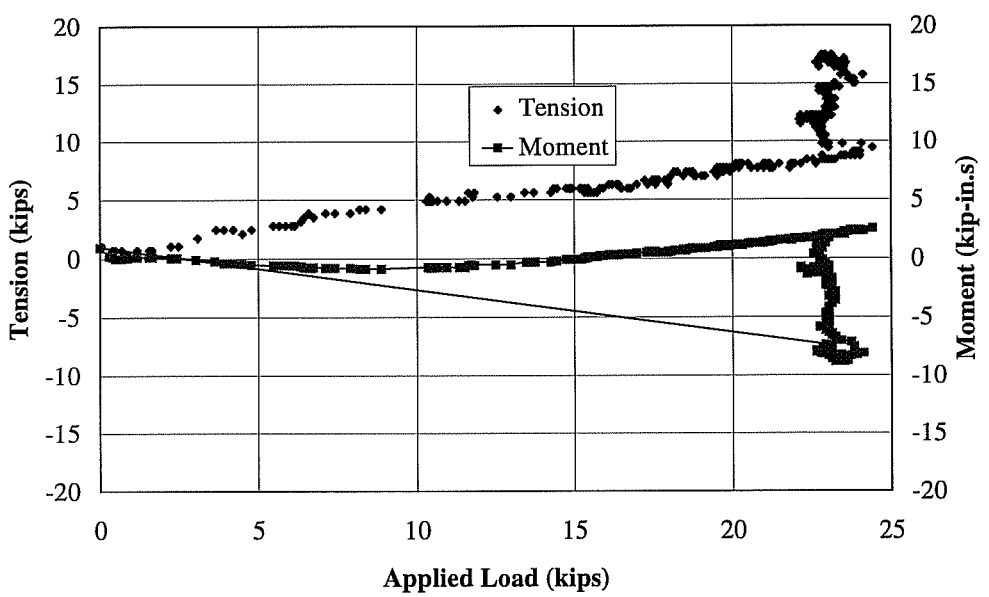

Test 9S05

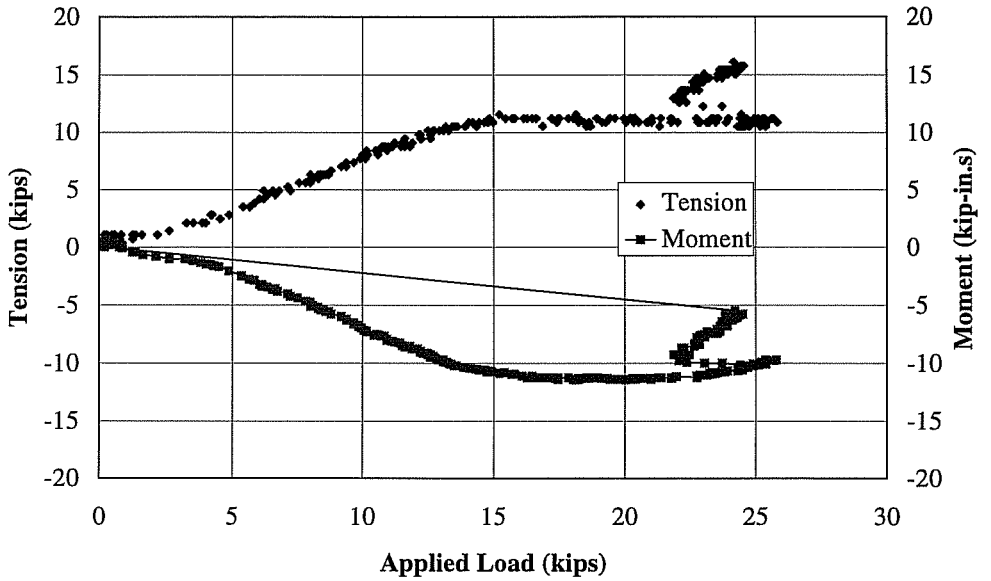

Test 10D06

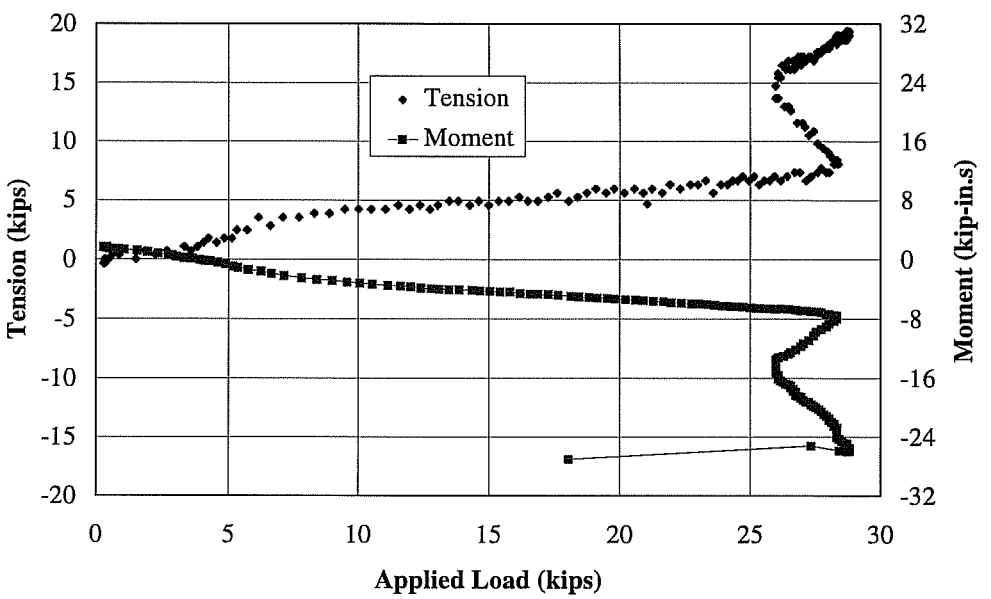

Test 10D07

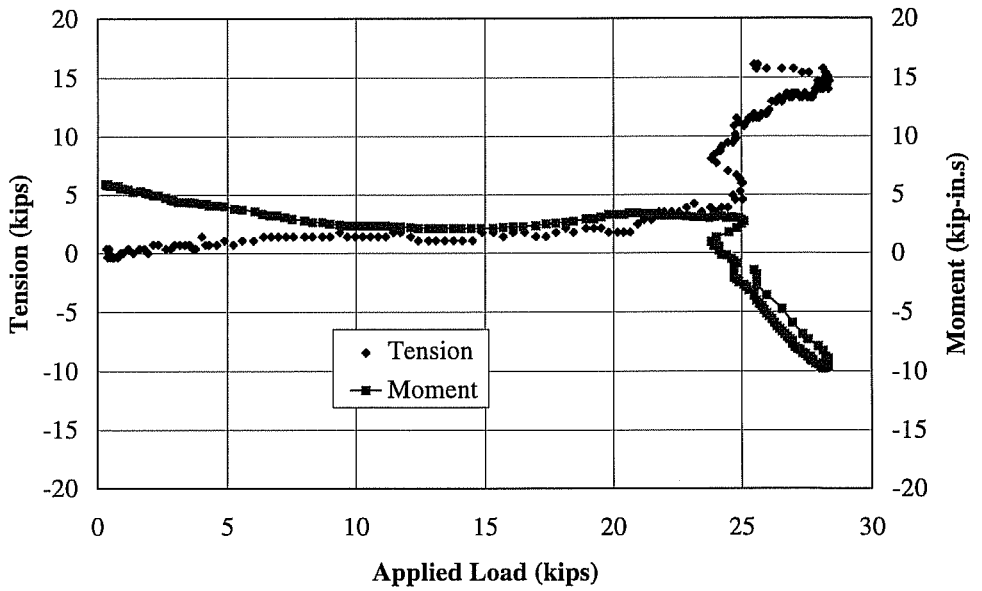

Test 10D08

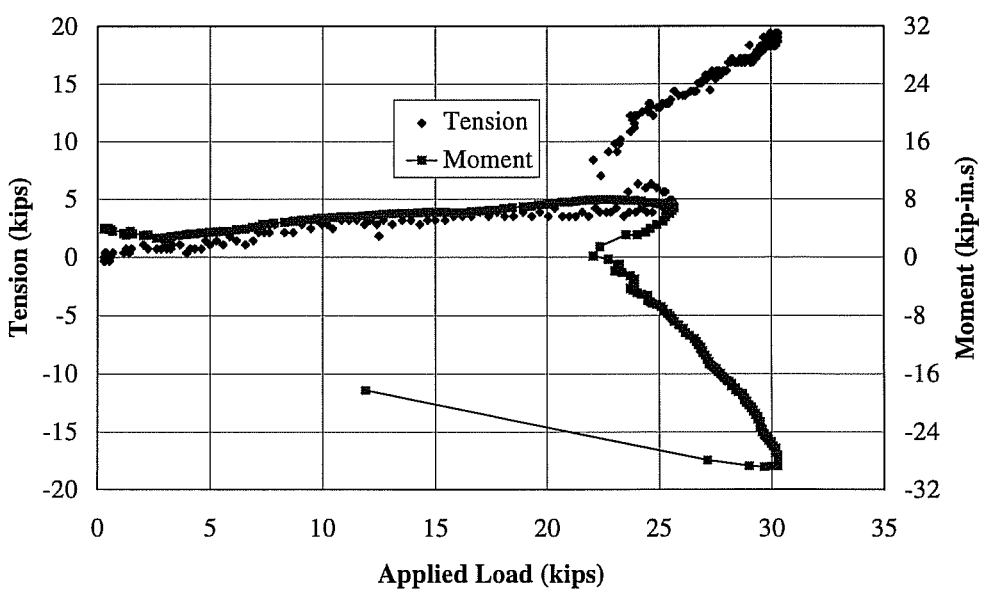

Test 10D09

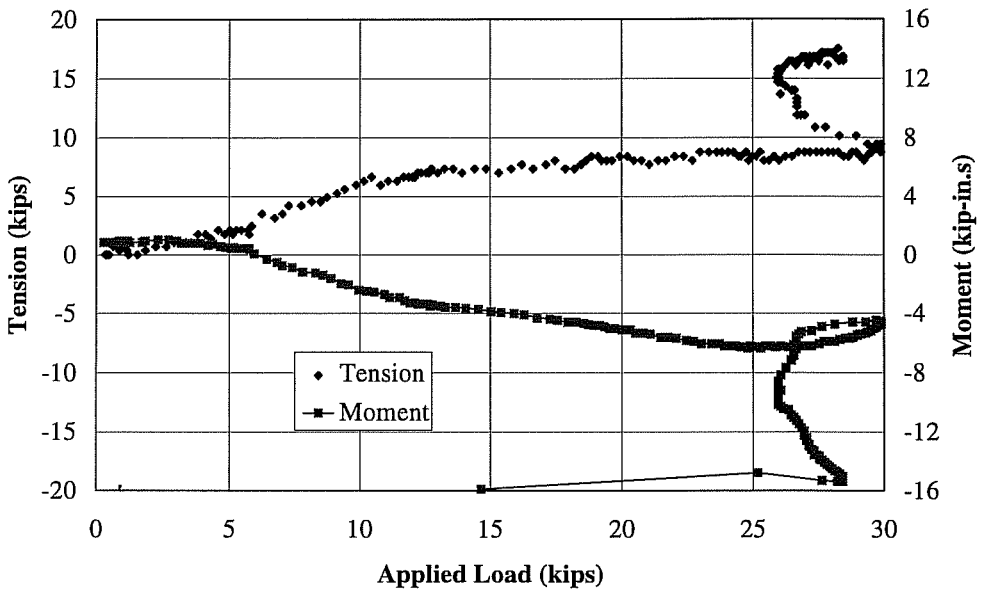

Test 10D10

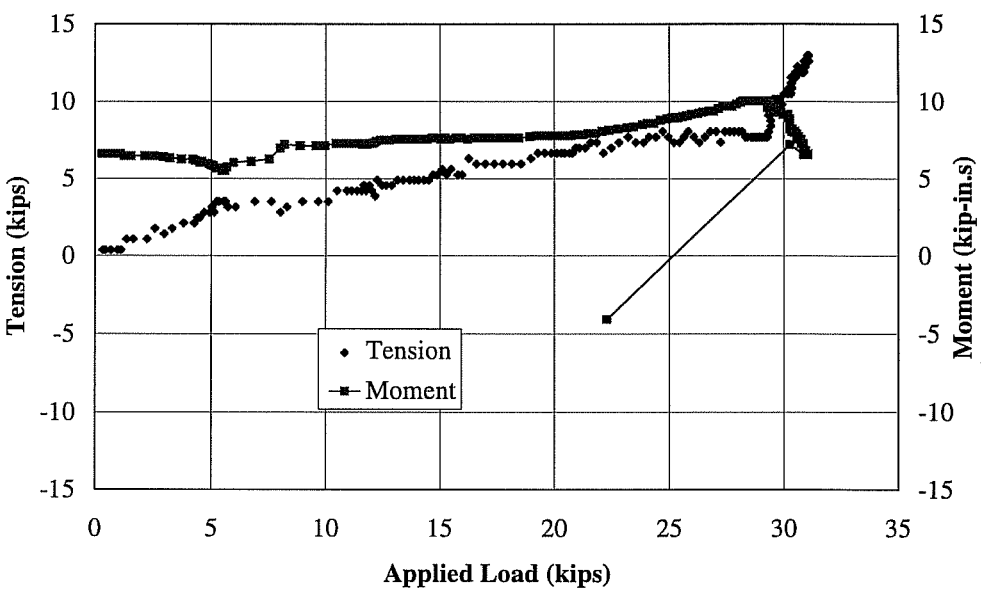

Test 11S11

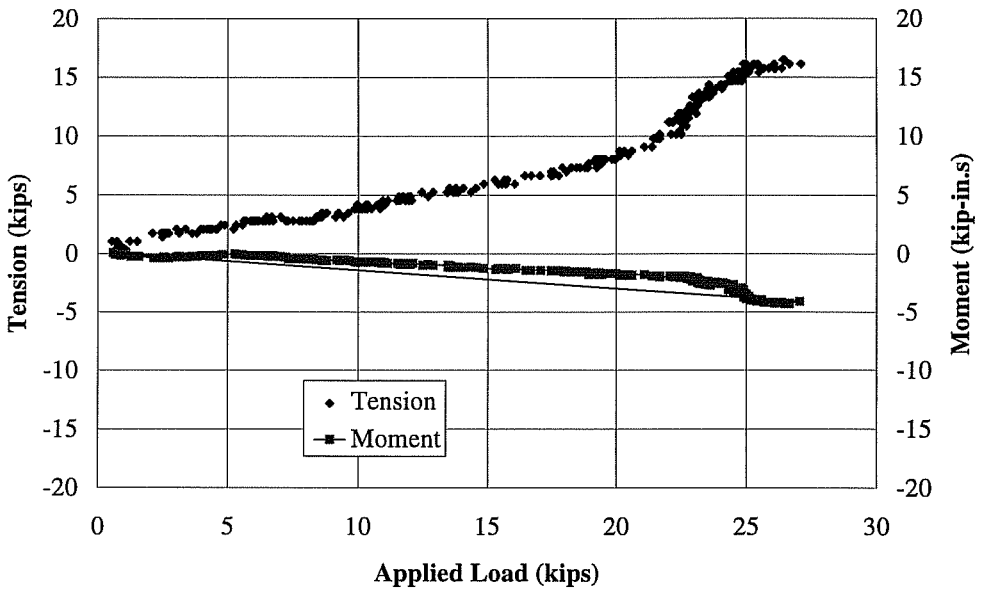

Test 11S12

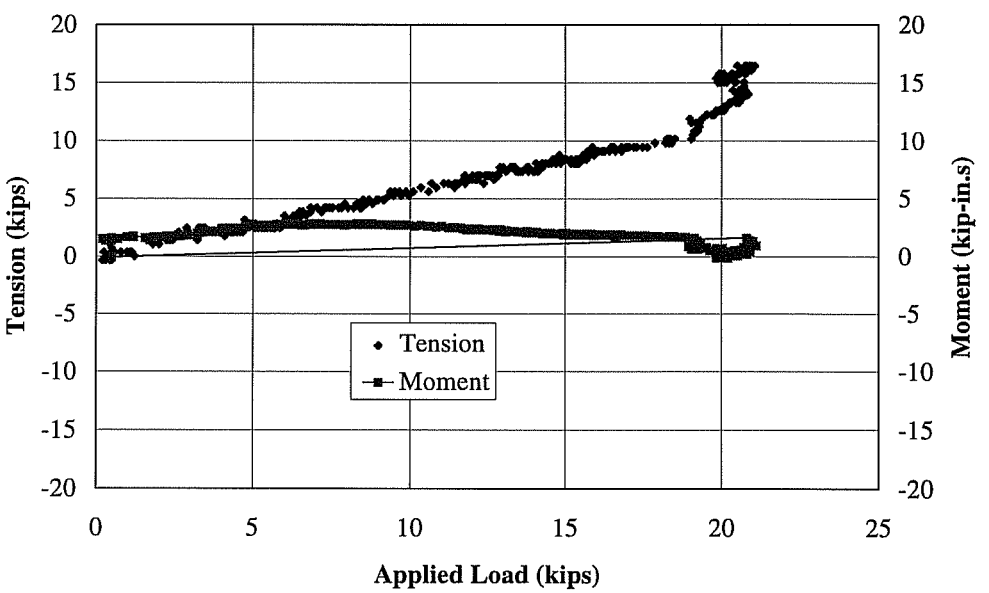

Test 11S13

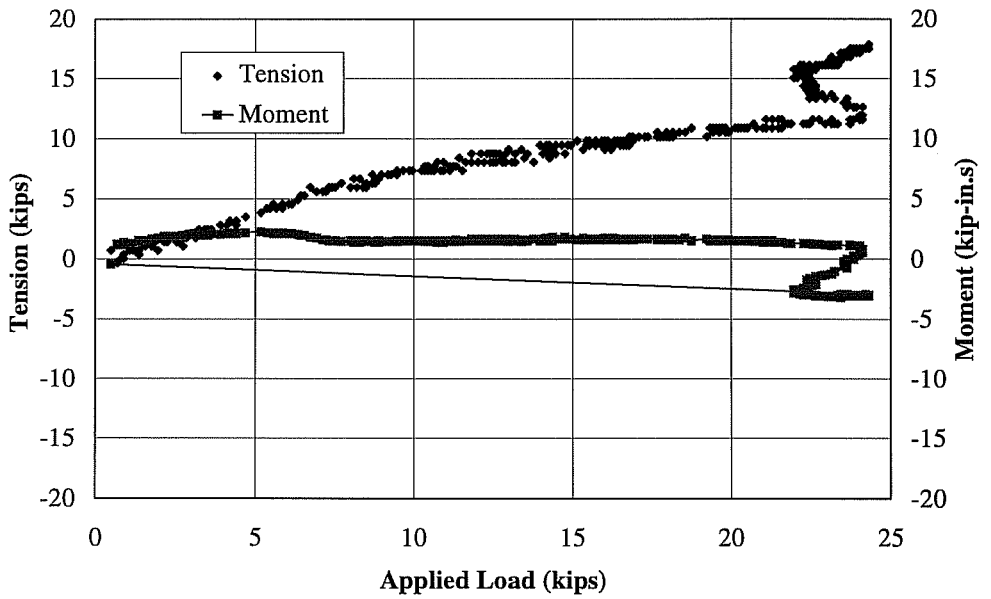

Test 11S114

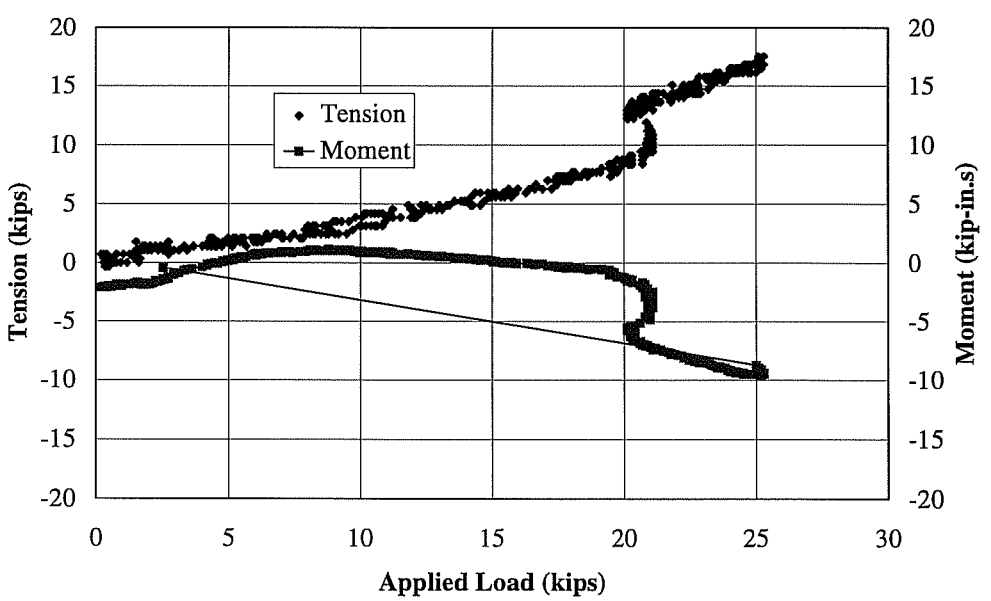

Test 11S15

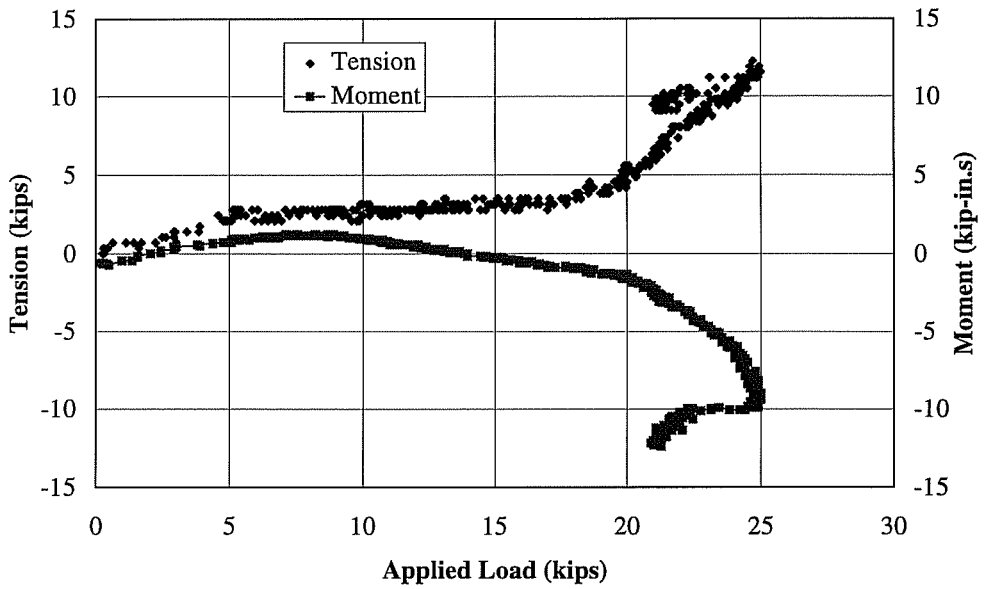

Test 11SH16

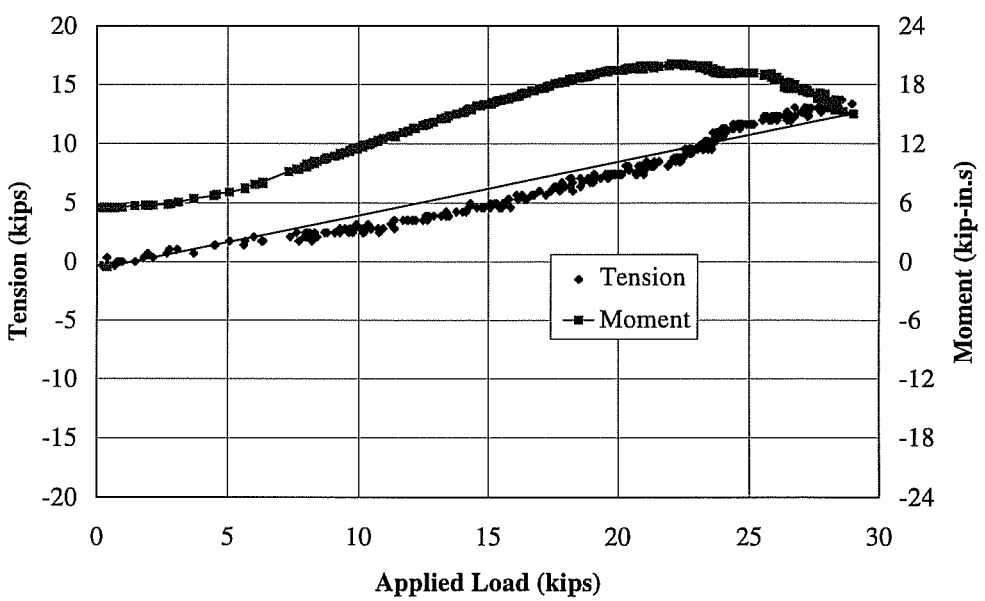

Test 11SH17

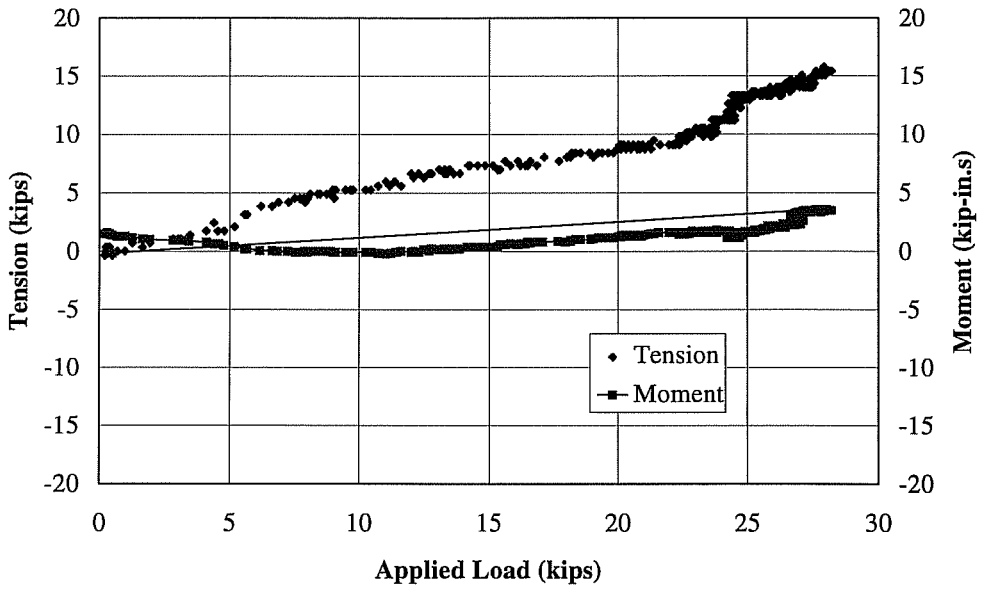

Test 11SH18

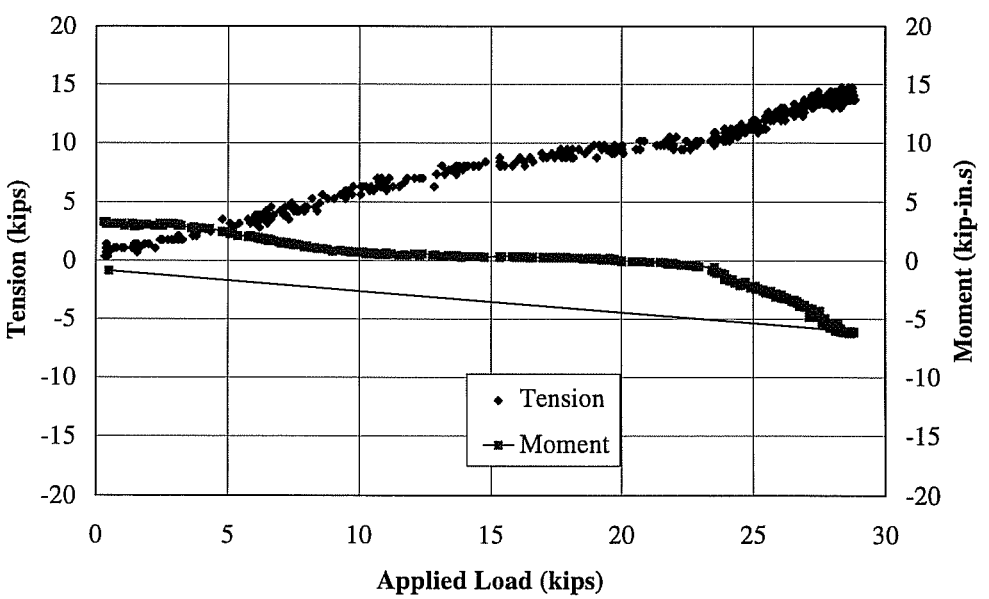

Test 11SH19

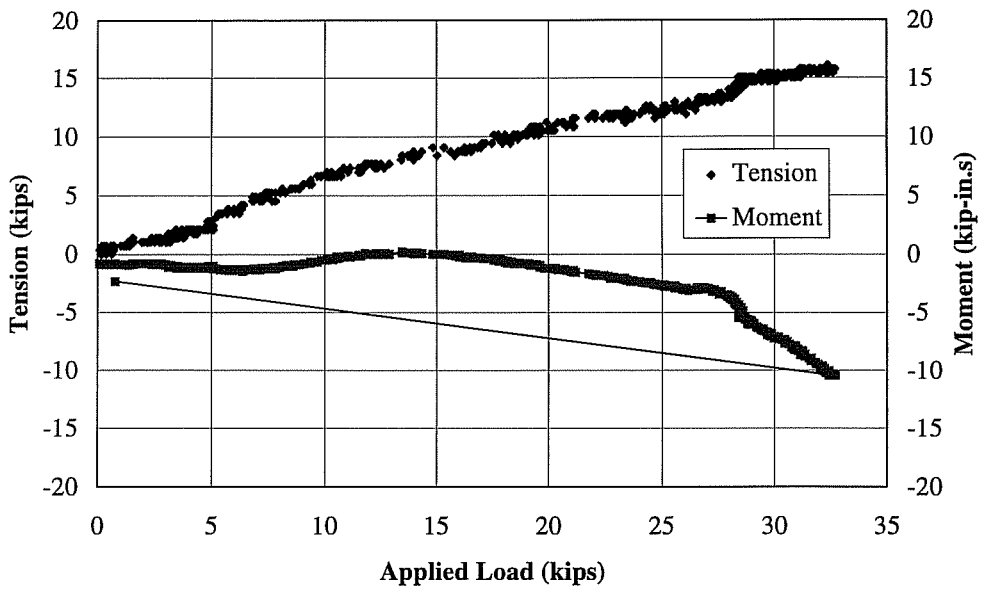

Test 12SH20

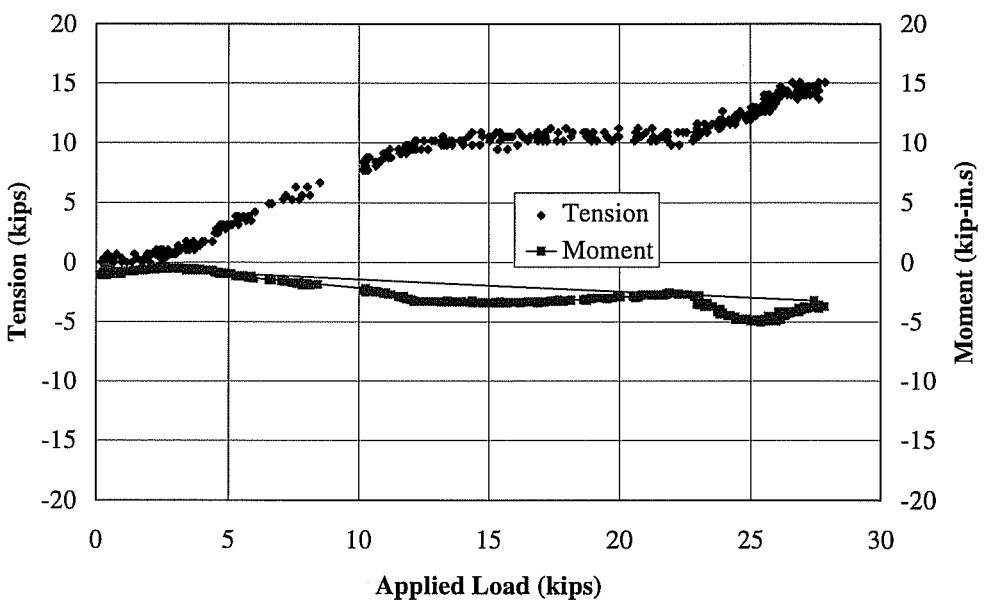

Test 12D21

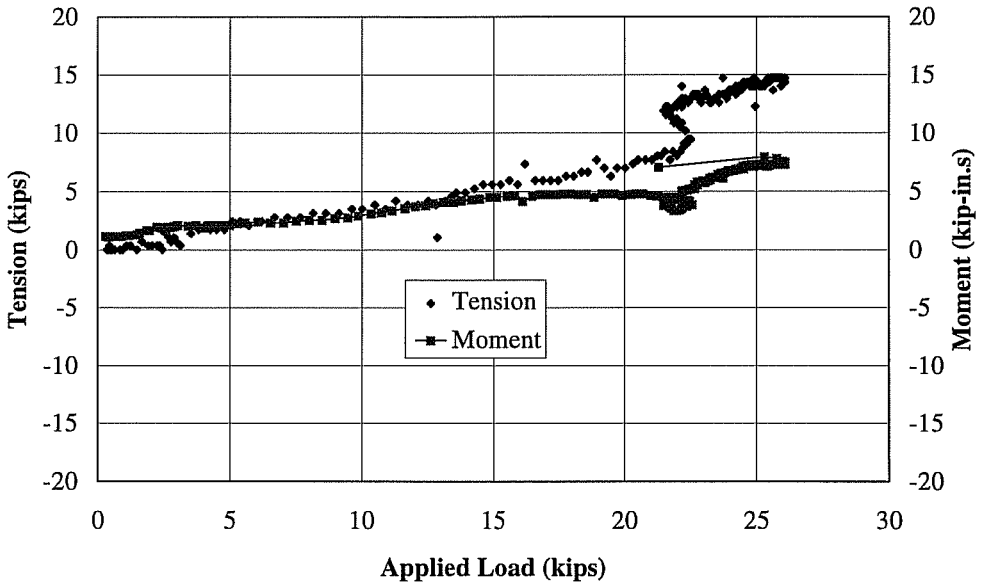

Test 12D22

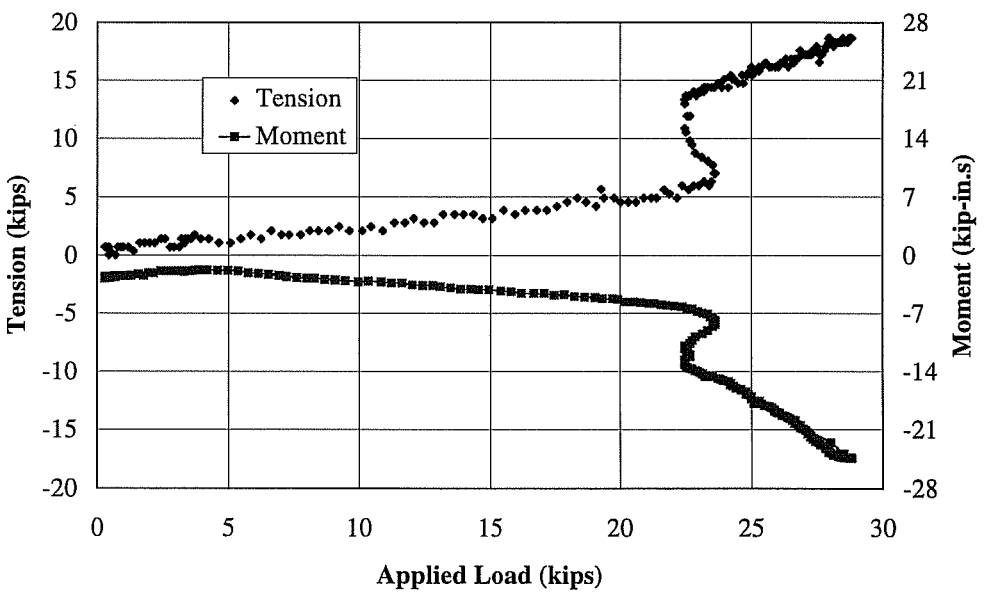

Test 12D23

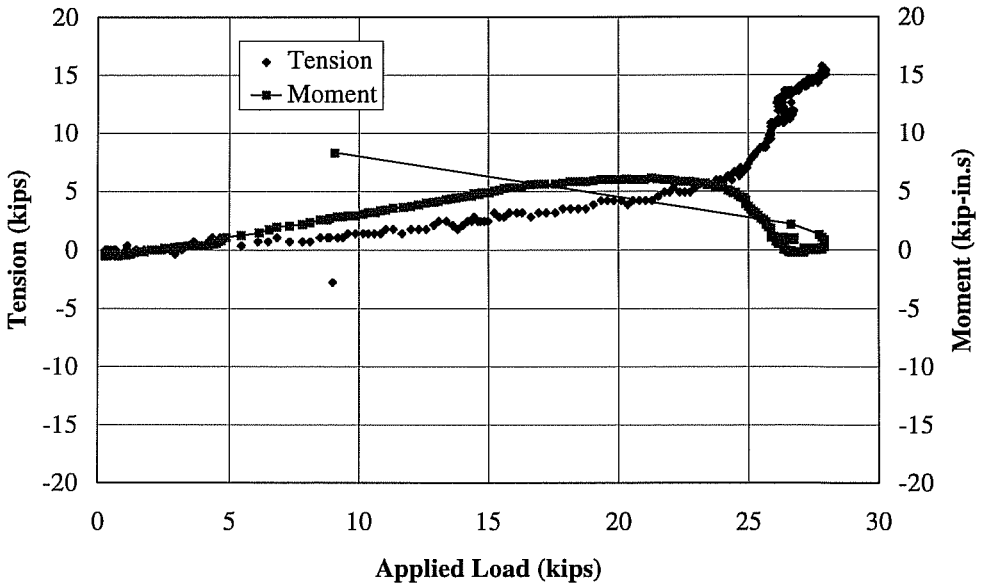

Test 12D24

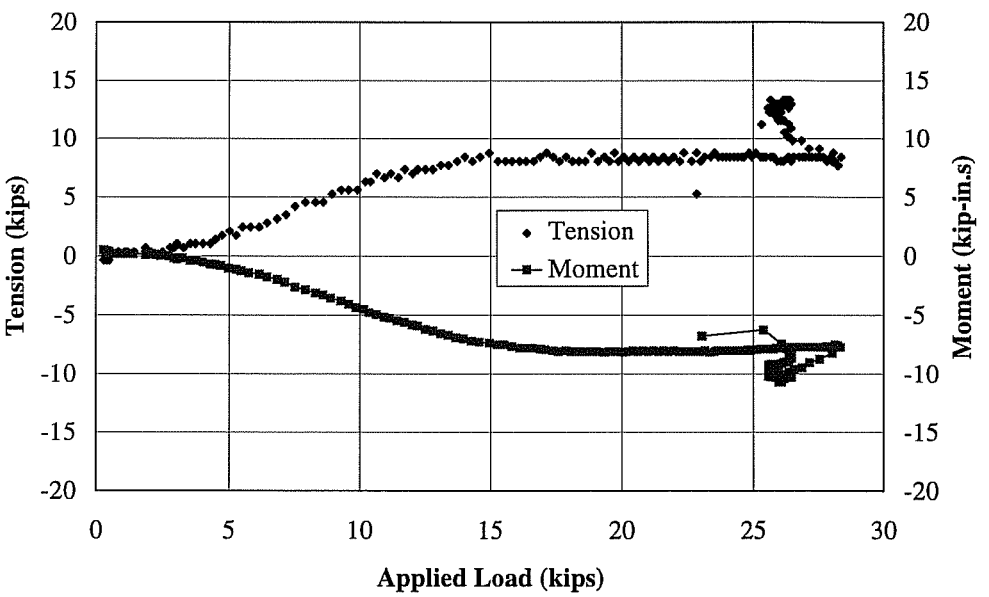

Test 12D25

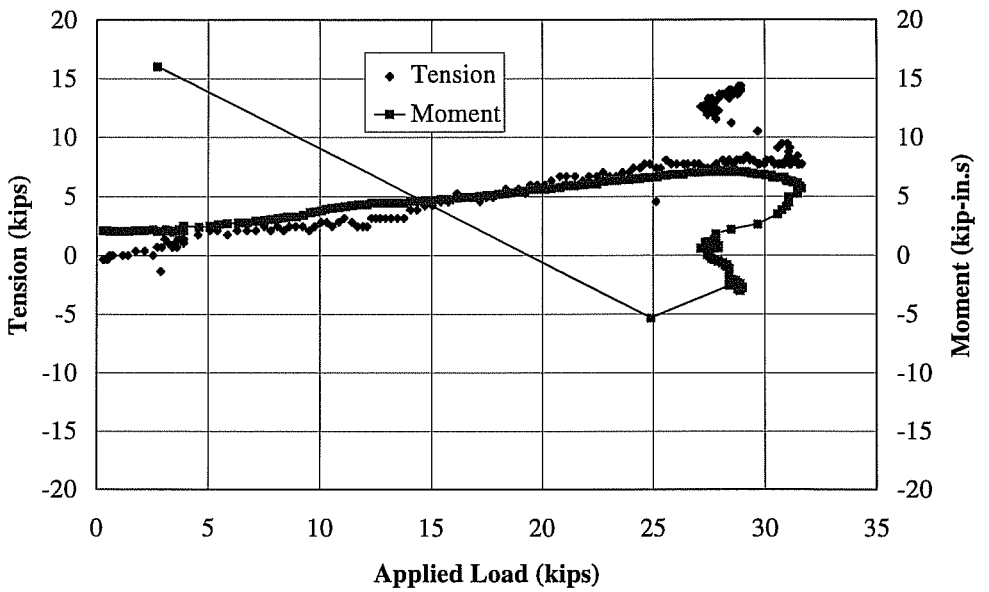

Test 12DH26

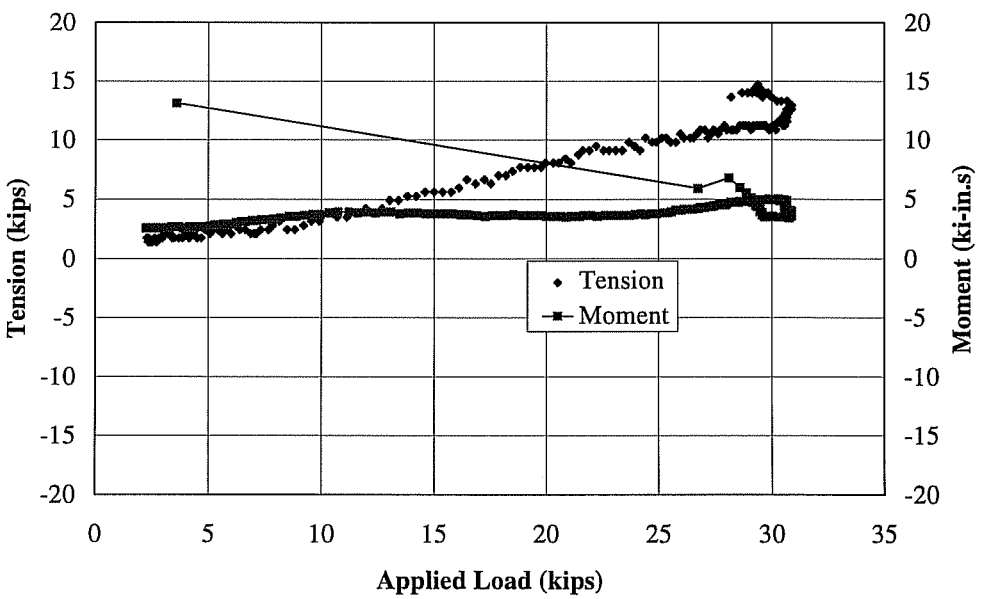

Test 12DH27

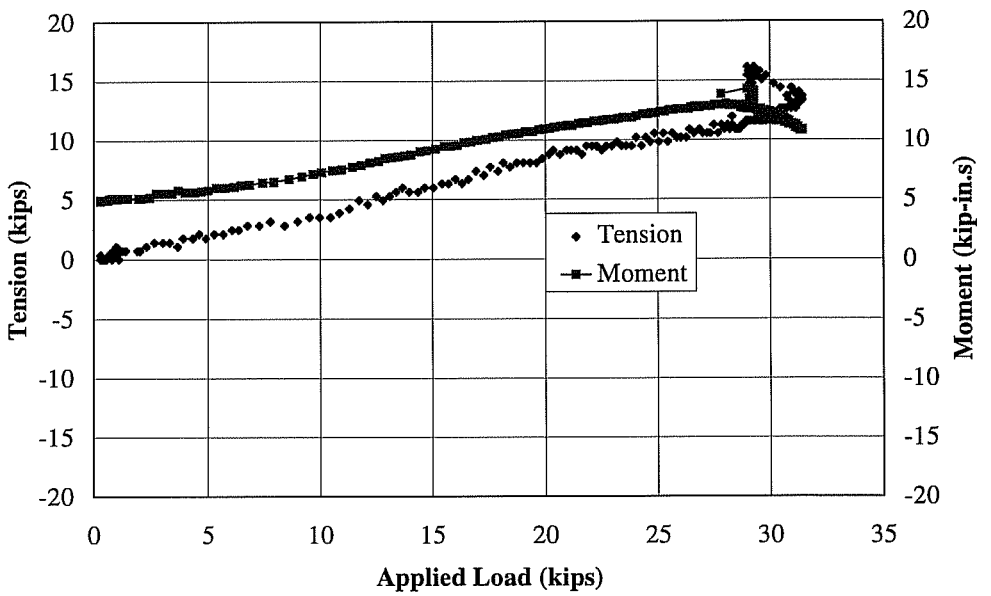

Test 12DH28

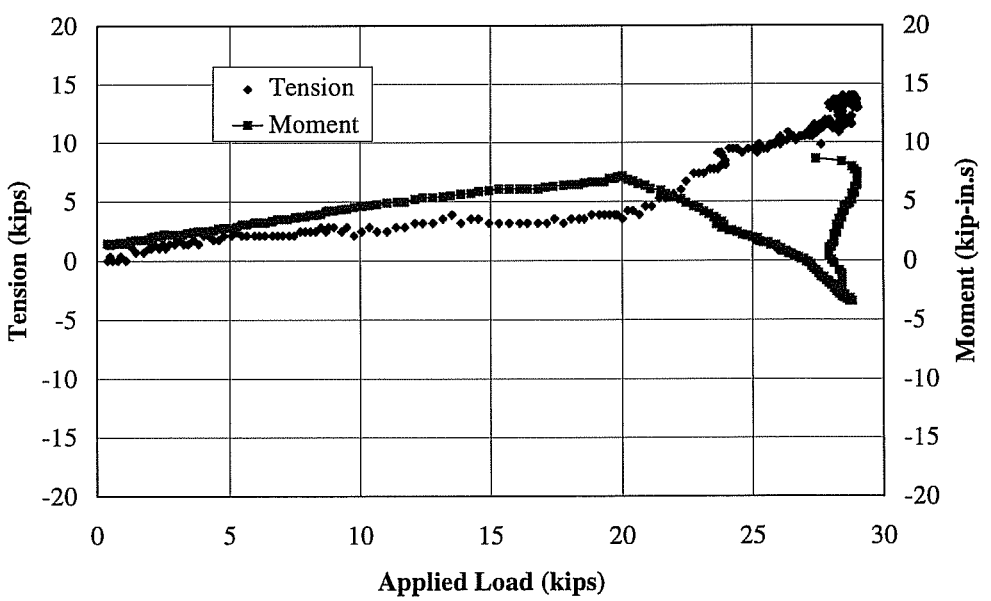

Test 12DH29

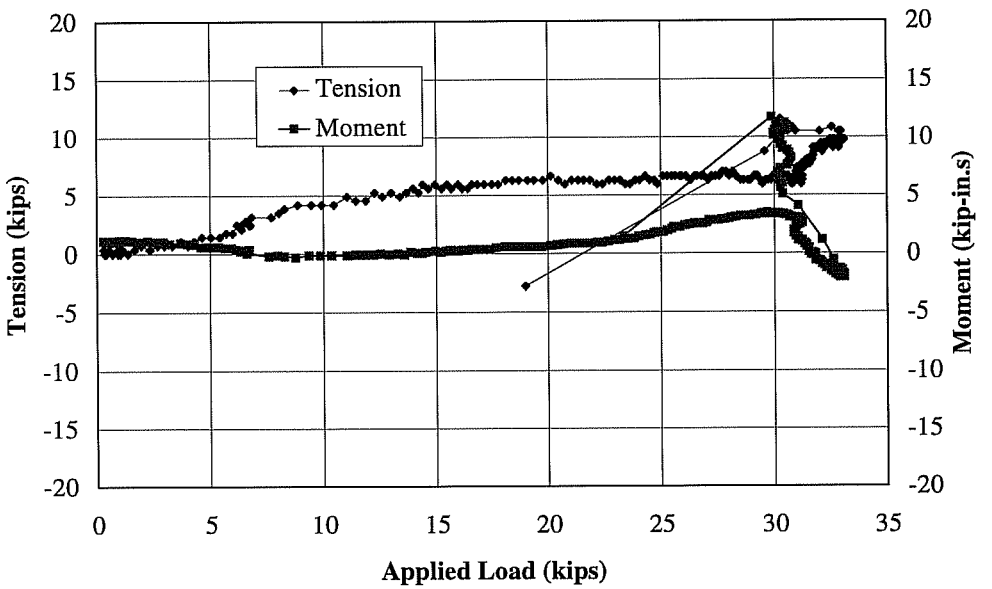

Test 12DH30

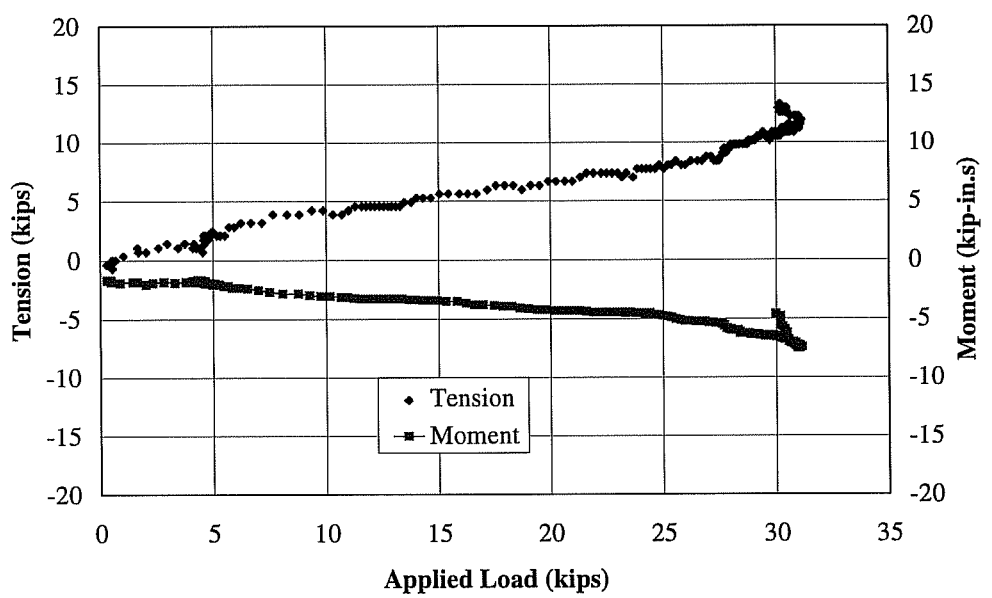

Time History of Loading in Tests 10D/06-10

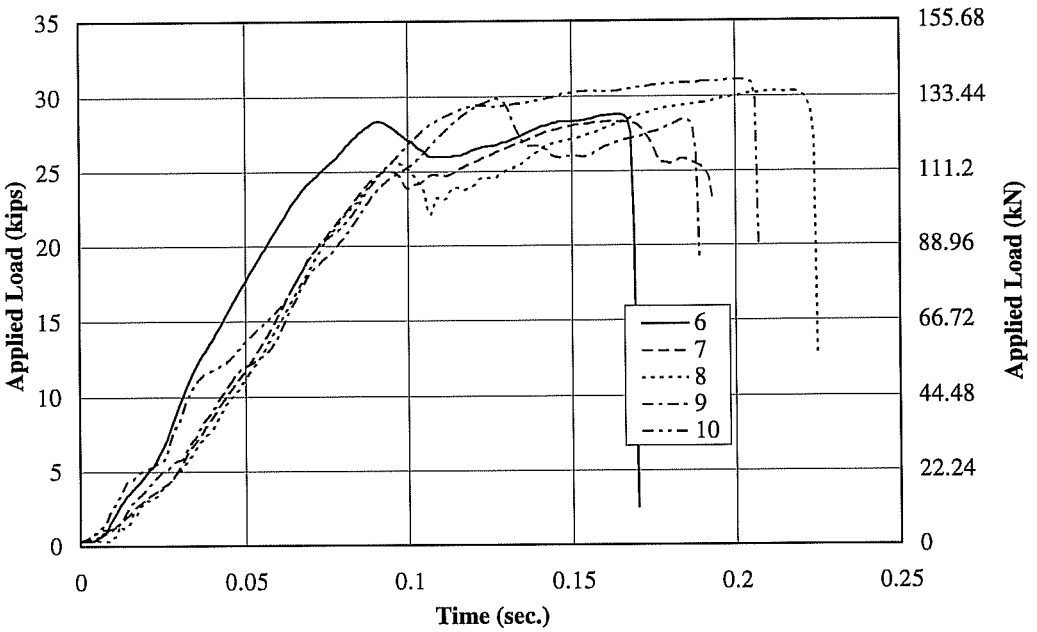

Time History of Loading in Tests 12D/21-25

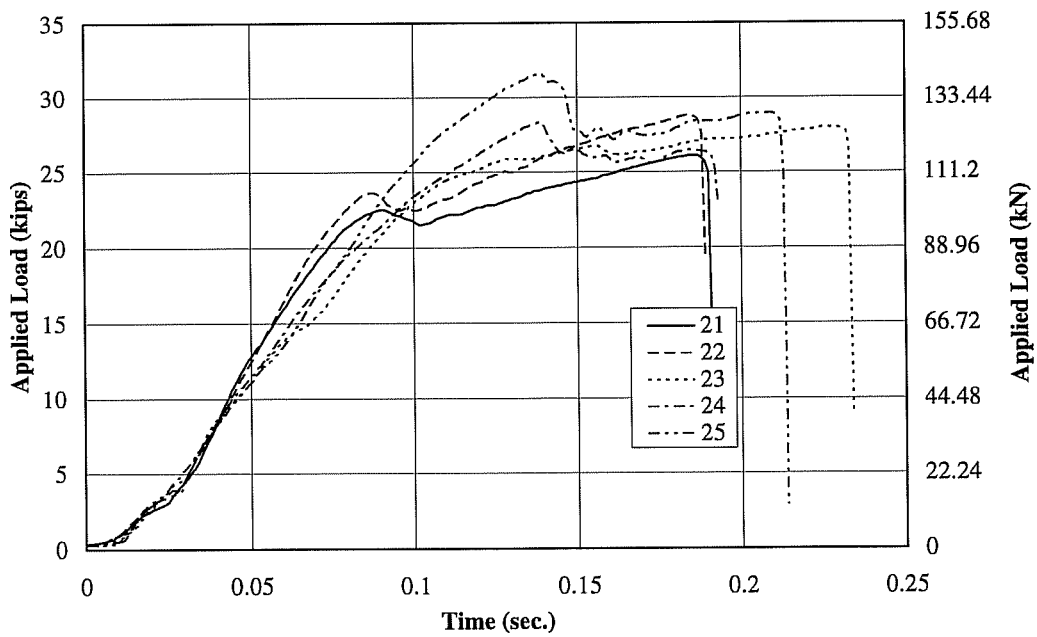

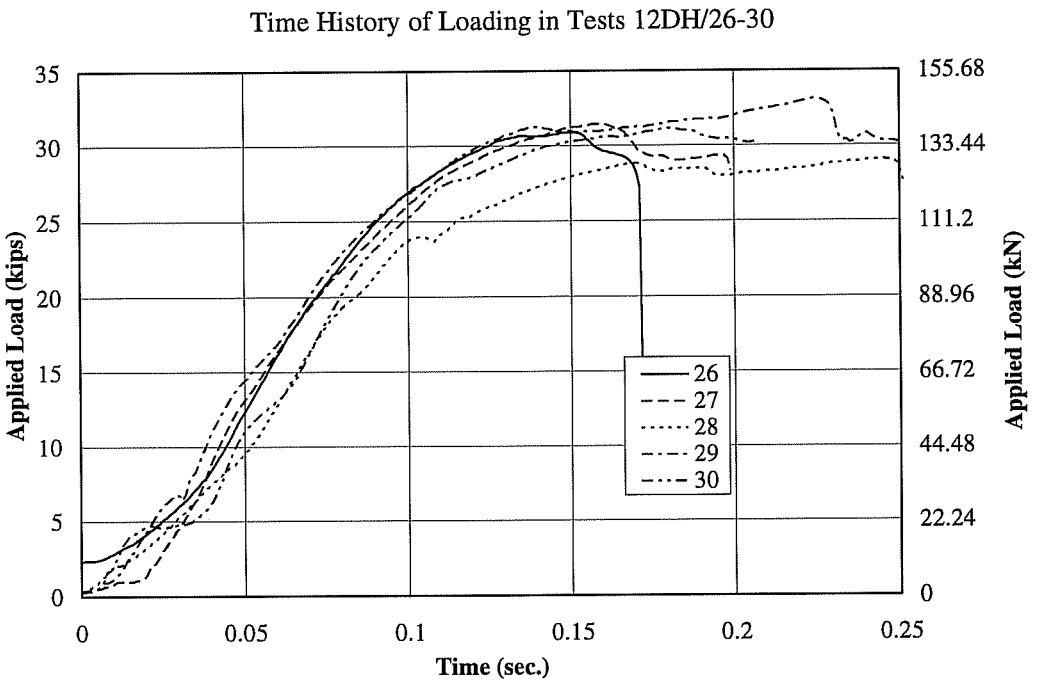
Time History of Loading in Tests 12DH/26-30
Applied Load (kips)
35
30
25
20
15
10
5
0
155.68
133.44
111.2
88.96
66.72
44.48
22.24
0
Applied Load (kN)
0
0.05
0.1
0.15
0.2
0.25
Time (sec.)
26
27
28
29
30

Appendix D

Results for Tests of Task 4

Test 4101

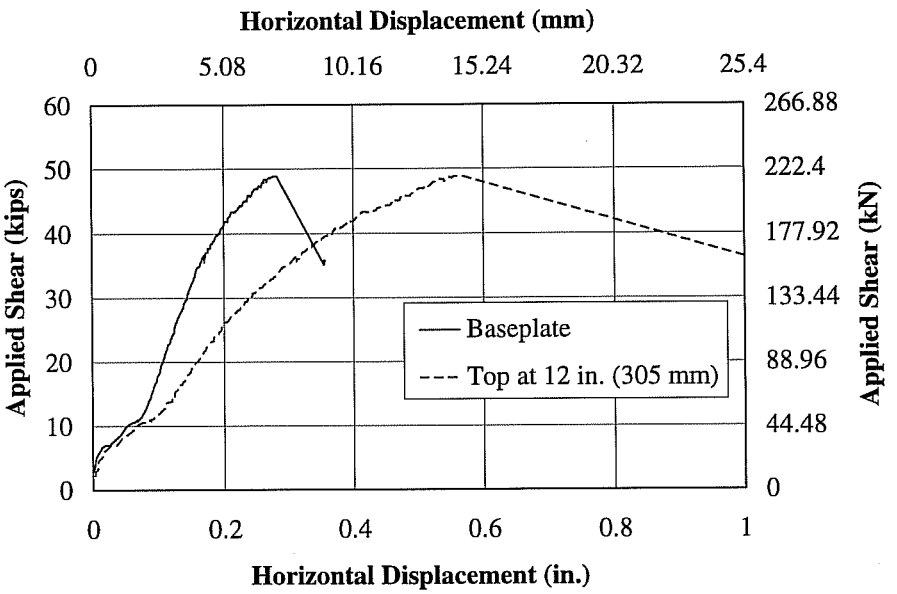
Horizontal Displacement (mm)
0
5.08
10.16
15.24
20.32
25.4
Applied Shear (kips)
60
50
40
30
20
10
0
266.88
222.4
177.92
133.44
88.96
44.48
0
Applied Shear (kN)
Baseplate
Top at 12 in. (305 mm)
0
0.2
0.4
0.6
0.8
1
Horizontal Displacement (in.)

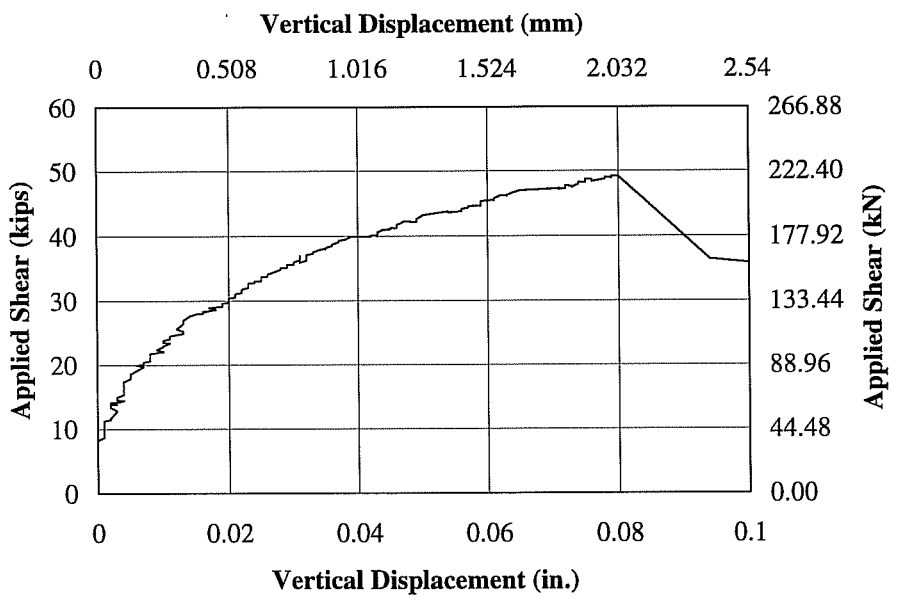
Vertical Displacement (mm)
0
0.508
1.016
1.524
2.032
2.54
Applied Shear (kips)
60
50
40
30
20
10
0
266.88
222.40
177.92
133.44
88.96
44.48
0.00
Applied Shear (kN)
0
0.02
0.04
0.06
0.08
0.1
Vertical Displacement (in.)

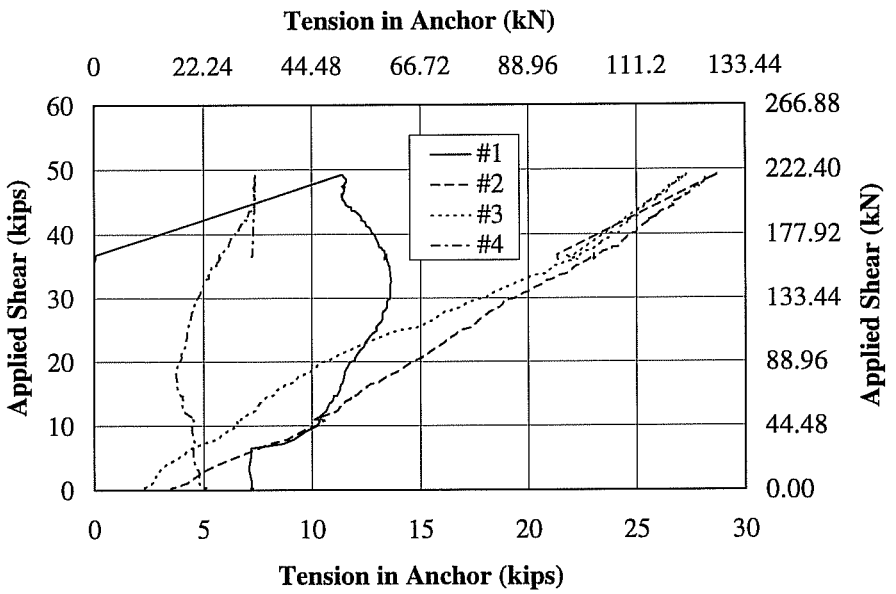
Tension in Anchor (kN)
0
22.24
44.48
66.72
88.96
111.2
133.44
60
50
40
30
20
10
0
266.88
222.40
177.92
133.44
88.96
44.48
0.00
Applied Shear (kips)
Applied Shear (kN)
#1
#2
#3
#4
0
5
10
15
20
25
30
Tension in Anchor (kips)

Test 4102

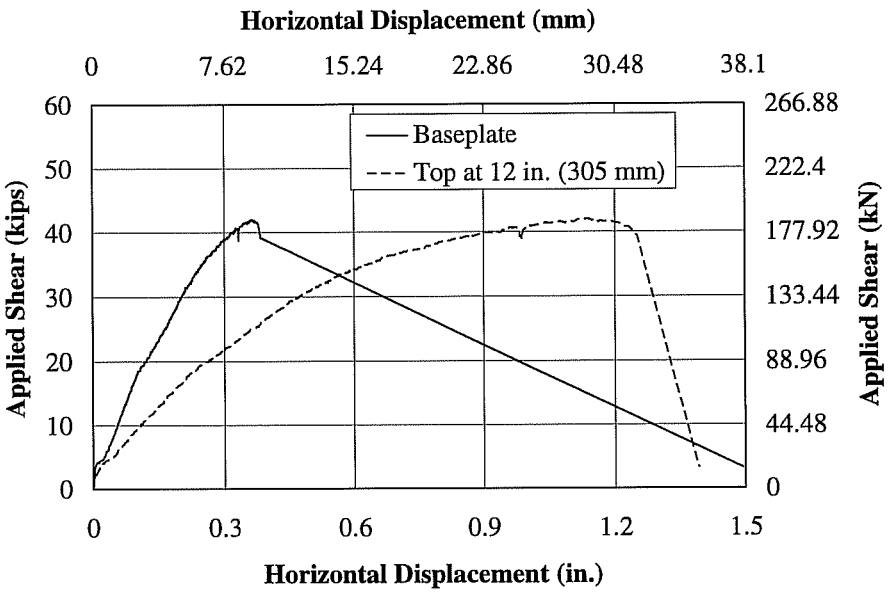
Horizontal Displacement (mm)
0
7.62
15.24
22.86
30.48
38.1
60
50
40
30
20
10
0
266.88
222.4
177.92
133.44
88.96
44.48
0
Baseplate
Top at 12 in. (305 mm)
Applied Shear (kips)
Applied Shear (kN)
0
0.3
0.6
0.9
1.2
1.5
Horizontal Displacement (in.)

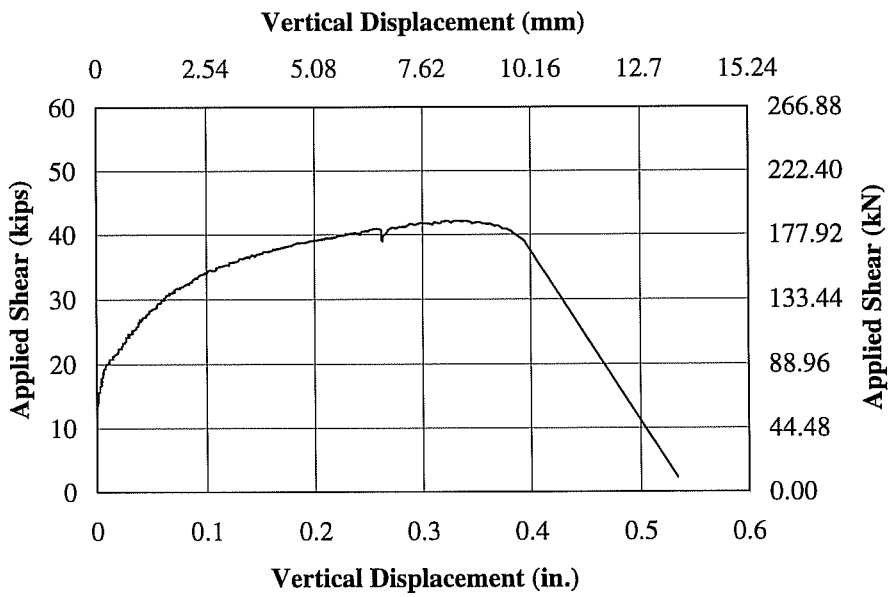
Vertical Displacement (mm)
0
2.54
5.08
7.62
10.16
12.7
15.24
60
50
40
30
20
10
0
266.88
222.40
177.92
133.44
88.96
44.48
0.00
Applied Shear (kips)
Applied Shear (kN)
0
0.1
0.2
0.3
0.4
0.5
0.6
Vertical Displacement (in.)

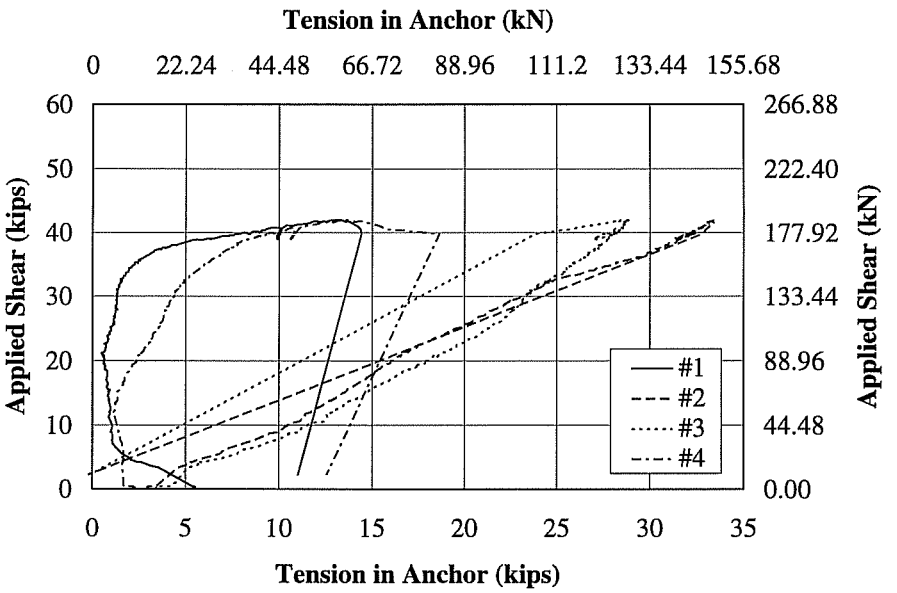
Tension in Anchor (kN)
0
22.24
44.48
66.72
88.96
111.2
133.44
155.68
60
50
40
30
20
10
0
266.88
222.40
177.92
133.44
88.96
44.48
0.00
Applied Shear (kips)
Applied Shear (kN)
#1
#2
#3
#4
0
5
10
15
20
25
30
35
Tension in Anchor (kips)

Test 4203

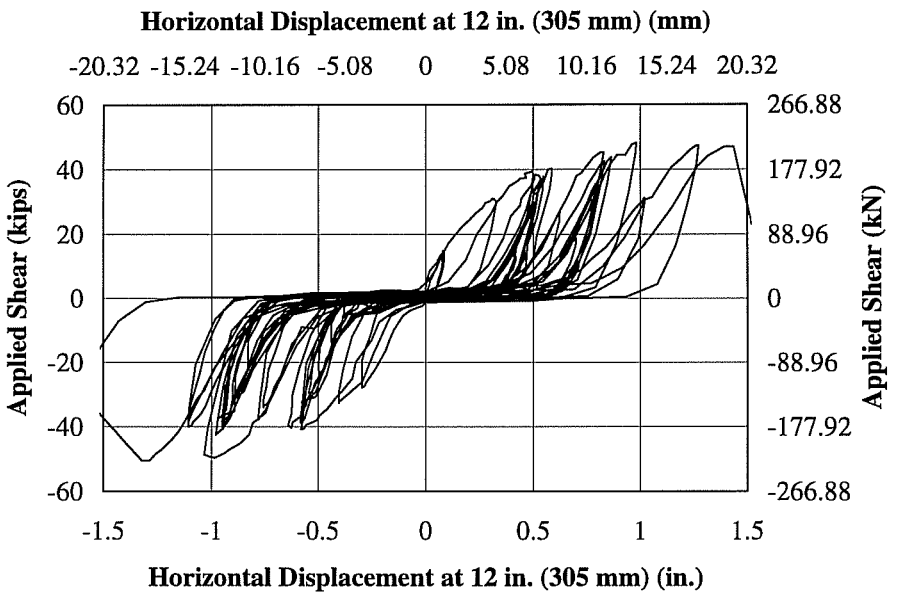
Horizontal Displacement at 12 in. (305 mm) (mm)
-20.32 -15.24 -10.16 -5.08 0 5.08 10.16 15.24 20.32
60
40
20
0
-20
-40
-60
266.88
177.92
88.96
0
-88.96
-177.92
-266.88
Applied Shear (kips)
Applied Shear (kN)
-1.5 -1 -0.5 0 0.5 1 1.5
Horizontal Displacement at 12 in. (305 mm) (in.)

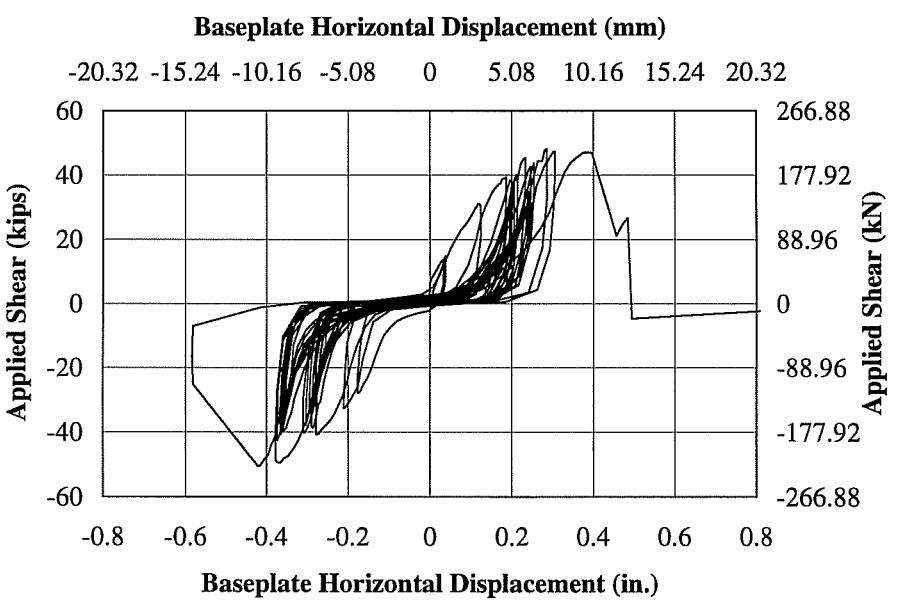
Baseplate Horizontal Displacement (mm)
-20.32 -15.24 -10.16 -5.08 0 5.08 10.16 15.24 20.32
60
40
20
0
-20
-40
-60
266.88
177.92
88.96
0
-88.96
-177.92
-266.88
Applied Shear (kips)
Applied Shear (kN)
-0.8 -0.6 -0.4 -0.2 0 0.2 0.4 0.6 0.8
Baseplate Horizontal Displacement (in.)

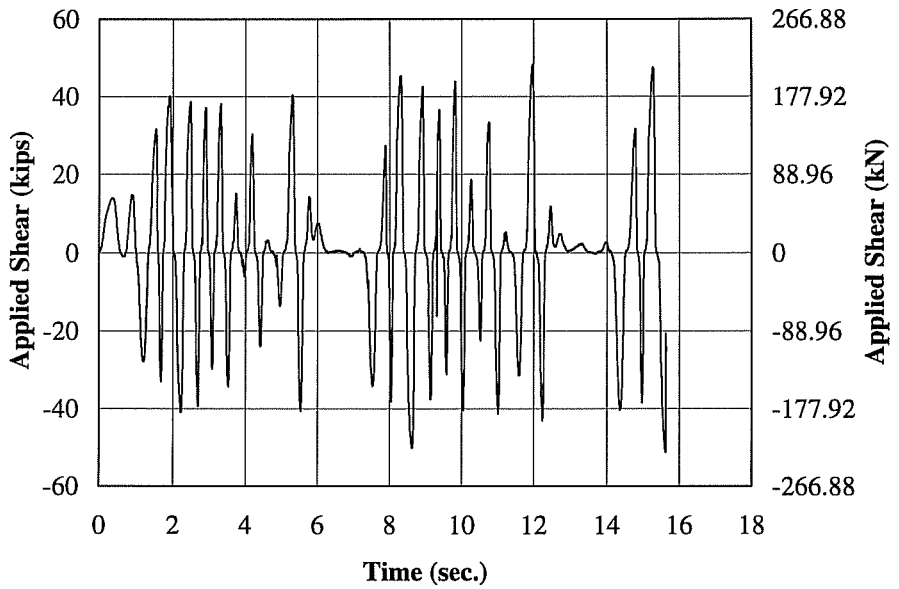
60
40
20
0
-20
-40
-60
266.88
177.92
88.96
0
-88.96
-177.92
-266.88
0 2 4 6 8 10 12 14 16 18
Applied Shear (kips)
Applied Shear (kN)
Time (sec.)

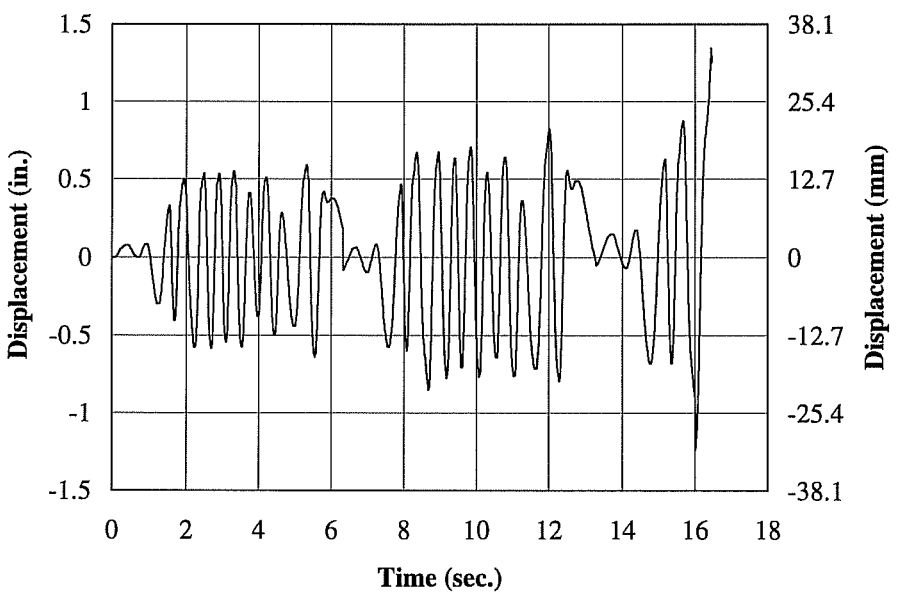
1.5
1
0.5
0
-0.5
-1
-1.5
38.1
25.4
12.7
0
-12.7
-25.4
-38.1
0 2 4 6 8 10 12 14 16 18
Displacement (in.)
Displacement (mm)
Time (sec.)

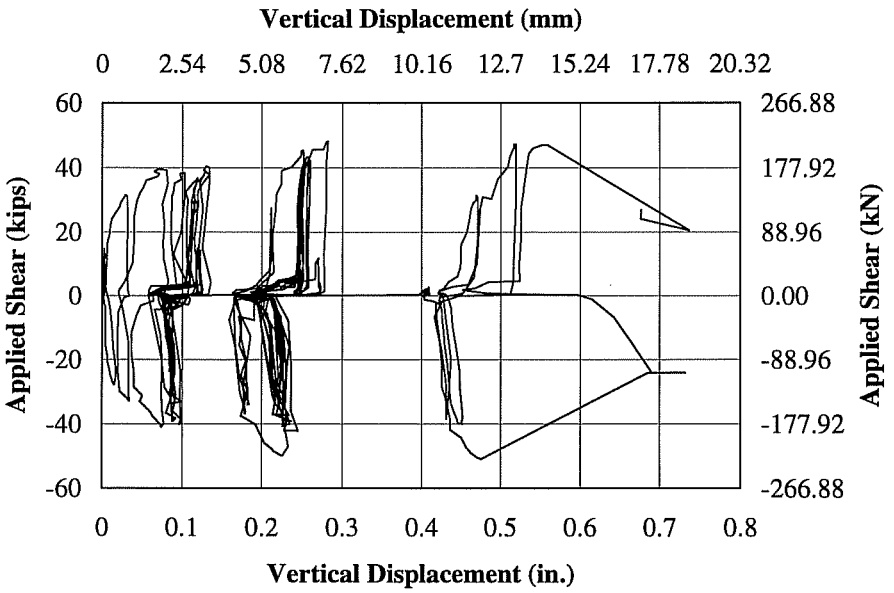
Vertical Displacement (mm)
0
2.54
5.08
7.62
10.16
12.7
15.24
17.78
20.32
60
40
20
0
-20
-40
-60
266.88
177.92
88.96
0.00
-88.96
-177.92
-266.88
Applied Shear (kips)
Applied Shear (kN)
0
0.1
0.2
0.3
0.4
0.5
0.6
0.7
0.8
Vertical Displacement (in.)

Test 4203

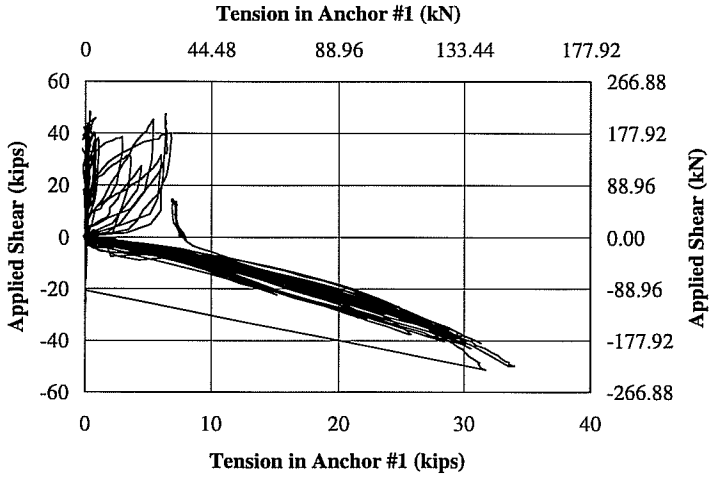
Tension in Anchor #1 (kN)
0
44.48
88.96
133.44
177.92
60
40
20
0
-20
-40
-60
266.88
177.92
88.96
0.00
-88.96
-177.92
-266.88
Applied Shear (kips)
Applied Shear (kN)
0
10
20
30
40
Tension in Anchor #1 (kips)

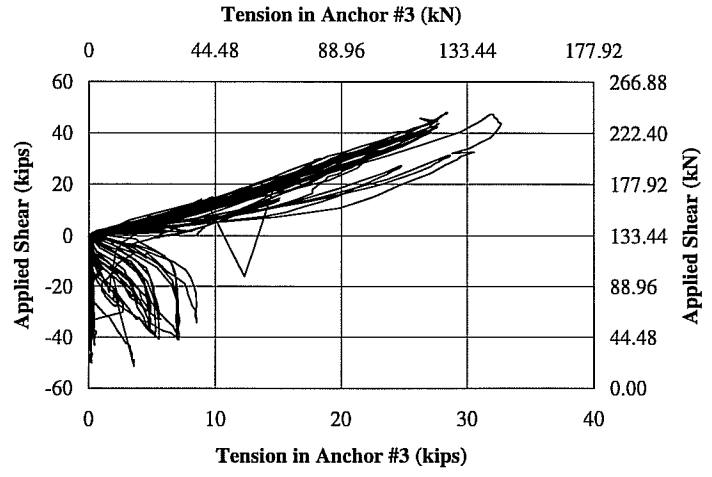
Tension in Anchor #3 (kN)
0
44.48
88.96
133.44
177.92
60
40
20
0
-20
-40
-60
266.88
222.40
177.92
133.44
88.96
44.48
0.00
Applied Shear (kips)
Applied Shear (kN)
0
10
20
30
40
Tension in Anchor #3 (kips)

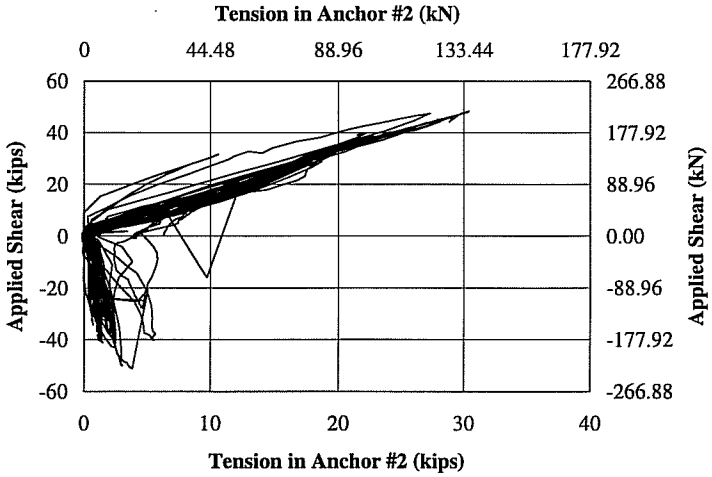
Tension in Anchor #2 (kN)
0
44.48
88.96
133.44
177.92
60
40
20
0
-20
-40
-60
266.88
177.92
88.96
0.00
-88.96
-177.92
-266.88
Applied Shear (kips)
Applied Shear (kN)
0
10
20
30
40
Tension in Anchor #2 (kips)

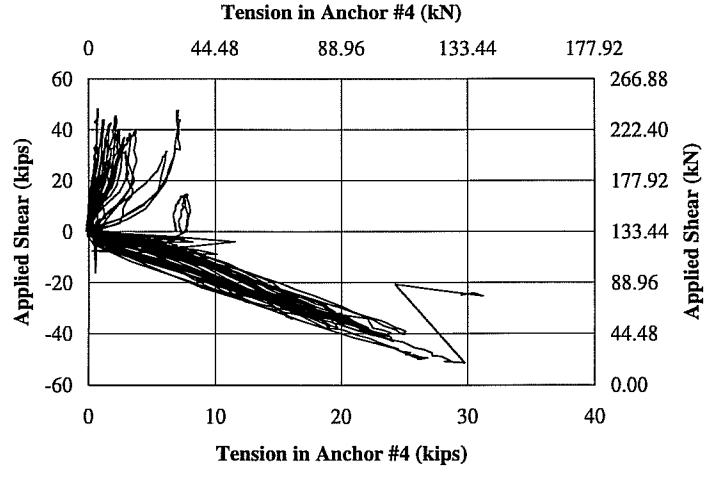
Tension in Anchor #4 (kN)
0
44.48
88.96
133.44
177.92
60
40
20
0
-20
-40
-60
266.88
222.40
177.92
133.44
88.96
44.48
0.00
Applied Shear (kips)
Applied Shear (kN)
0
10
20
30
40
Tension in Anchor #4 (kips)

Test 4204

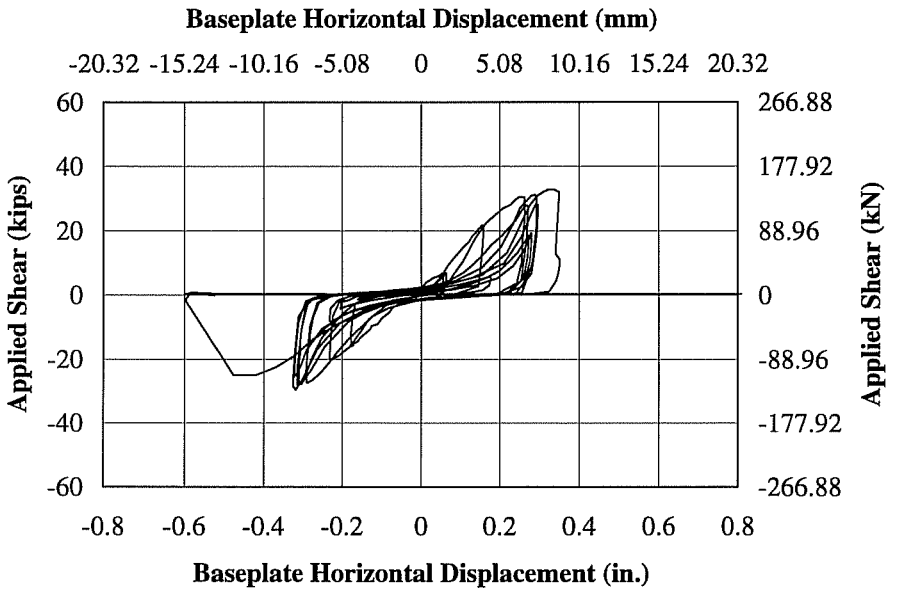
Baseplate Horizontal Displacement (mm)
-20.32 -15.24 -10.16 -5.08 0 5.08 10.16 15.24 20.32
60
40
20
0
-20
-40
-60
266.88
177.92
88.96
0
-88.96
-177.92
-266.88
Applied Shear (kips)
Applied Shear (kN)
-0.8 -0.6 -0.4 -0.2 0 0.2 0.4 0.6 0.8
Baseplate Horizontal Displacement (in.)

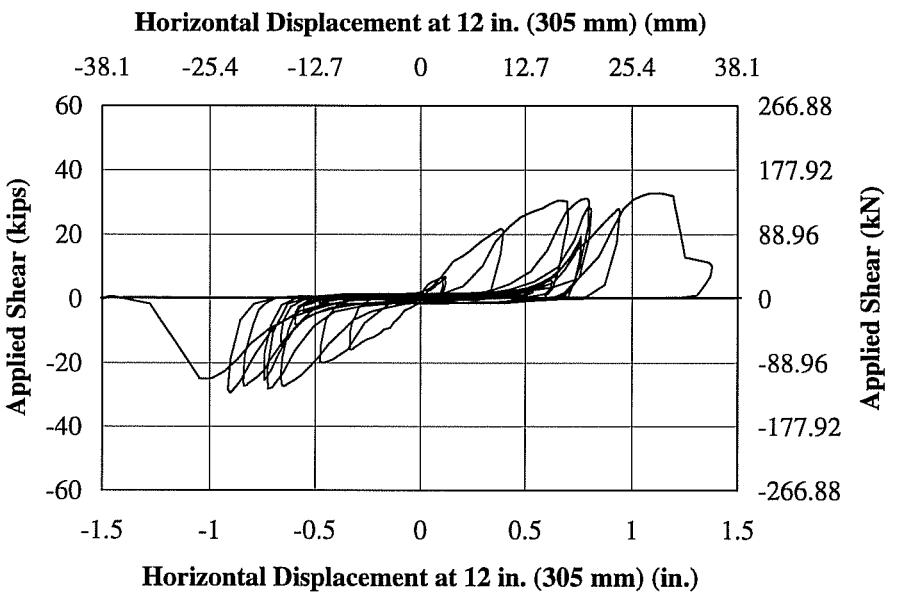
Horizontal Displacement at 12 in. (305 mm) (mm)
-38.1 -25.4 -12.7 0 12.7 25.4 38.1
60
40
20
0
-20
-40
-60
266.88
177.92
88.96
0
-88.96
-177.92
-266.88
Applied Shear (kips)
Applied Shear (kN)
-1.5 -1 -0.5 0 0.5 1 1.5
Horizontal Displacement at 12 in. (305 mm) (in.)

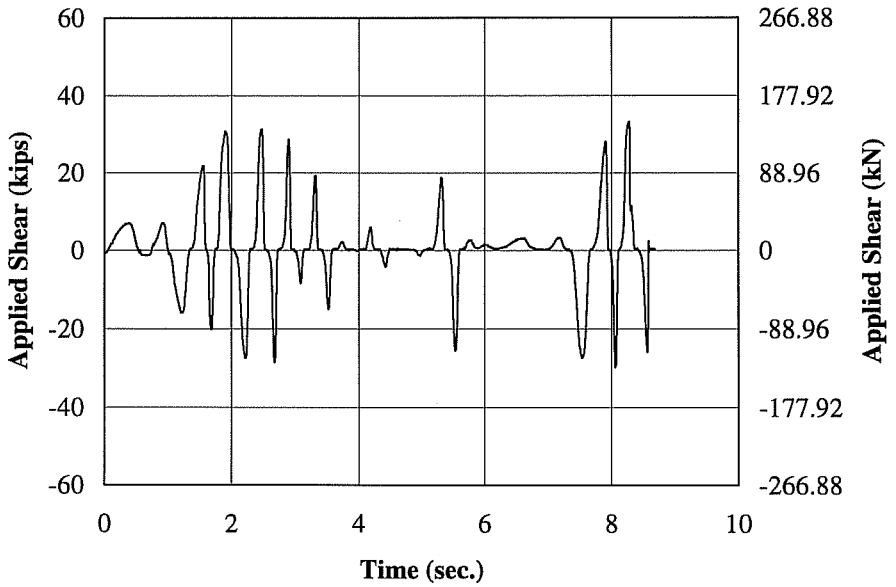
60
40
20
0
-20
-40
-60
266.88
177.92
88.96
0
-88.96
-177.92
-266.88
0
2
4
6
8
10
Applied Shear (kips)
Applied Shear (kN)
Time (sec.)

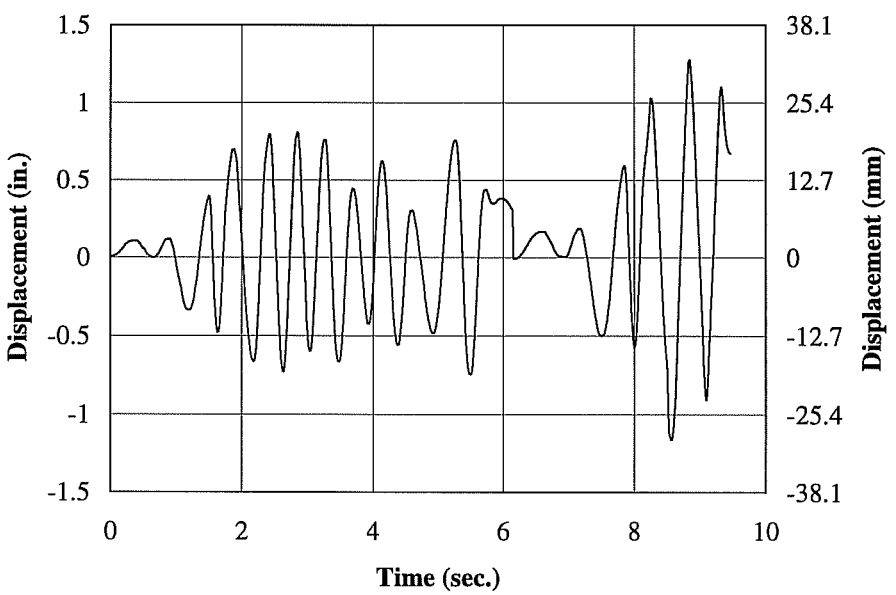
1.5
1
0.5
0
-0.5
-1
-1.5
38.1
25.4
12.7
0
-12.7
-25.4
-38.1
0
2
4
6
8
10
Displacement (in.)
Displacement (mm)
Time (sec.)

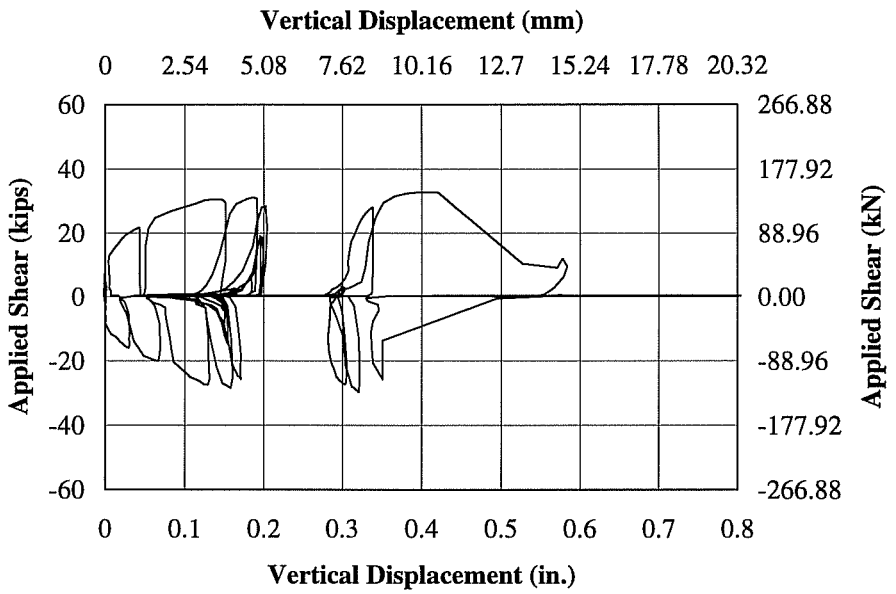
Vertical Displacement (mm)
0
2.54
5.08
7.62
10.16
12.7
15.24
17.78
20.32
60
40
20
0
-20
-40
-60
266.88
177.92
88.96
0.00
-88.96
-177.92
-266.88
Applied Shear (kips)
Applied Shear (kN)
0
0.1
0.2
0.3
0.4
0.5
0.6
0.7
0.8
Vertical Displacement (in.)

Test 4204

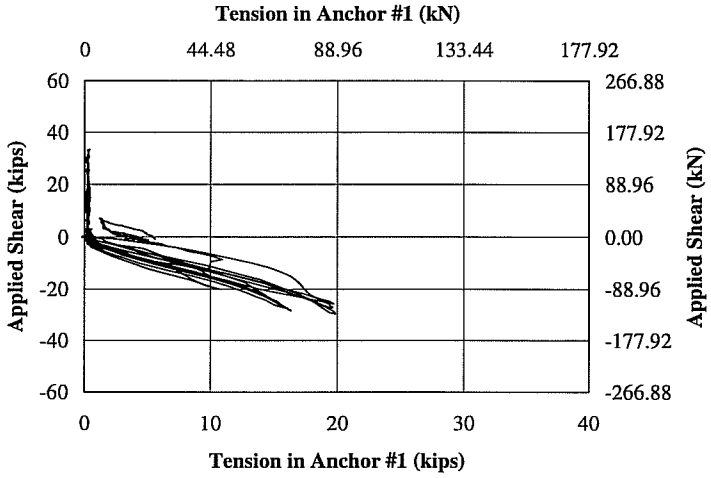
Tension in Anchor #1 (kN)
0
44.48
88.96
133.44
177.92
60
40
20
0
-20
-40
-60
266.88
177.92
88.96
0.00
-88.96
-177.92
-266.88
Applied Shear (kips)
Applied Shear (kN)
0
10
20
30
40
Tension in Anchor #1 (kips)

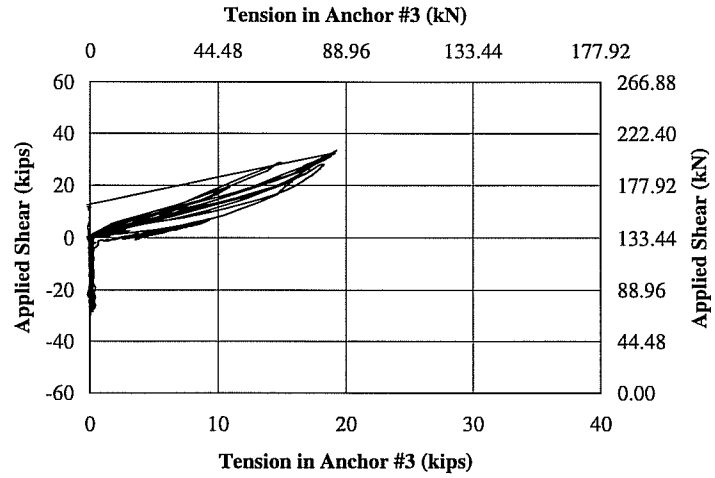
Tension in Anchor #3 (kN)
0
44.48
88.96
133.44
177.92
60
40
20
0
-20
-40
-60
266.88
222.40
177.92
133.44
88.96
44.48
0.00
Applied Shear (kips)
Applied Shear (kN)
0
10
20
30
40
Tension in Anchor #3 (kips)

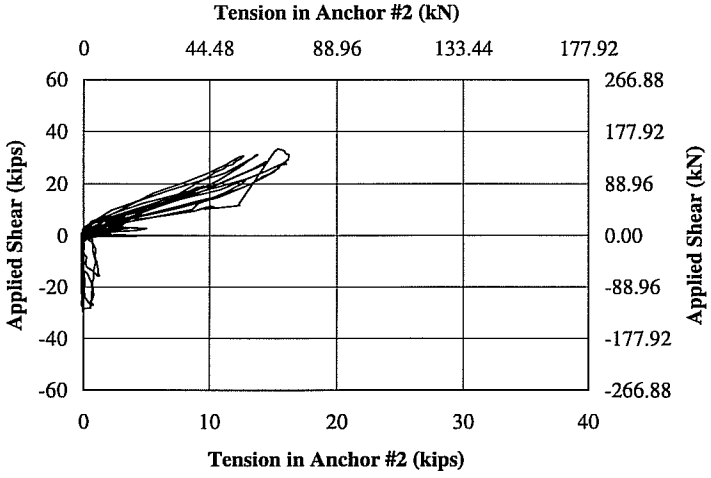
Tension in Anchor #2 (kN)
0
44.48
88.96
133.44
177.92
60
40
20
0
-20
-40
-60
266.88
177.92
88.96
0.00
-88.96
-177.92
-266.88
Applied Shear (kips)
Applied Shear (kN)
0
10
20
30
40
Tension in Anchor #2 (kips)

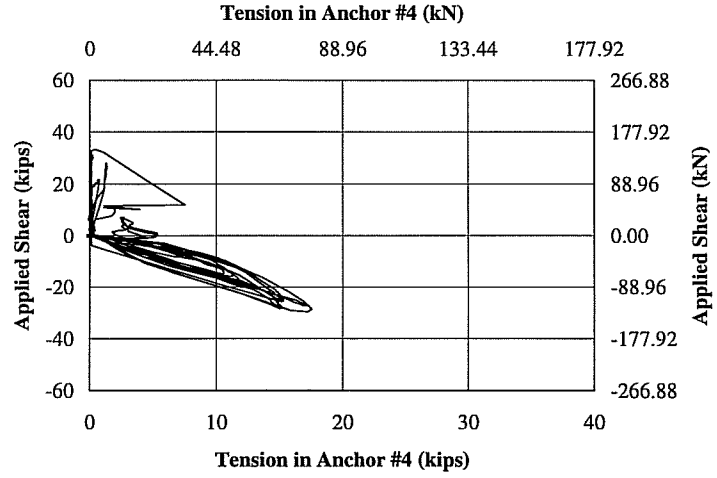
Tension in Anchor #4 (kN)
0
44.48
88.96
133.44
177.92
60
40
20
0
-20
-40
-60
266.88
177.92
88.96
0.00
-88.96
-177.92
-266.88
Applied Shear (kips)
Applied Shear (kN)
0
10
20
30
40
Tension in Anchor #4 (kips)

Test 4205

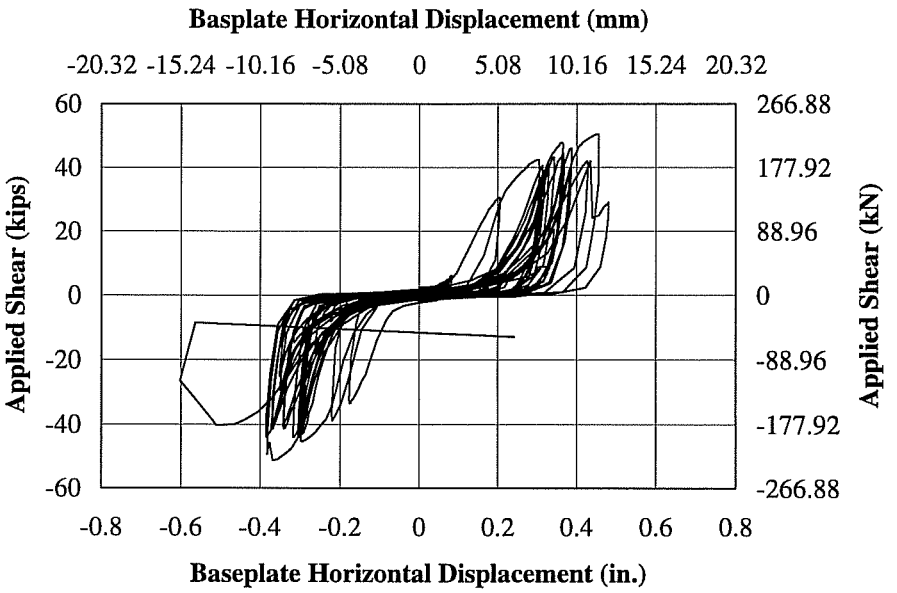
Basplate Horizontal Displacement (mm)
-20.32 -15.24 -10.16 -5.08 0 5.08 10.16 15.24 20.32
60
40
20
0
-20
-40
-60
266.88
177.92
88.96
0
-88.96
-177.92
-266.88
Applied Shear (kips)
Applied Shear (kN)
-0.8 -0.6 -0.4 -0.2 0 0.2 0.4 0.6 0.8
Baseplate Horizontal Displacement (in.)

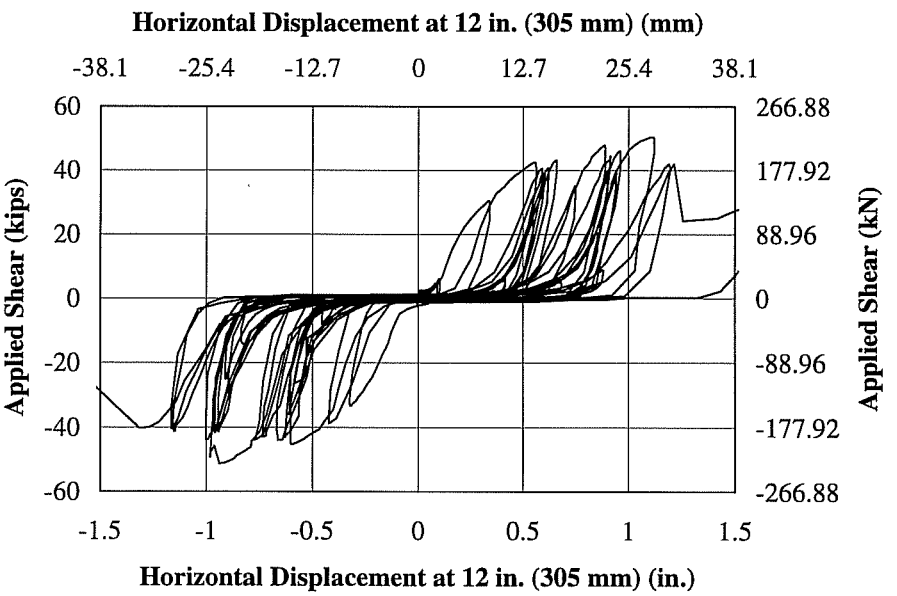
Horizontal Displacement at 12 in. (305 mm) (mm)
-38.1 -25.4 -12.7 0 12.7 25.4 38.1
60
40
20
0
-20
-40
-60
266.88
177.92
88.96
0
-88.96
-177.92
-266.88
Applied Shear (kips)
Applied Shear (kN)
-1.5 -1 -0.5 0 0.5 1 1.5
Horizontal Displacement at 12 in. (305 mm) (in.)

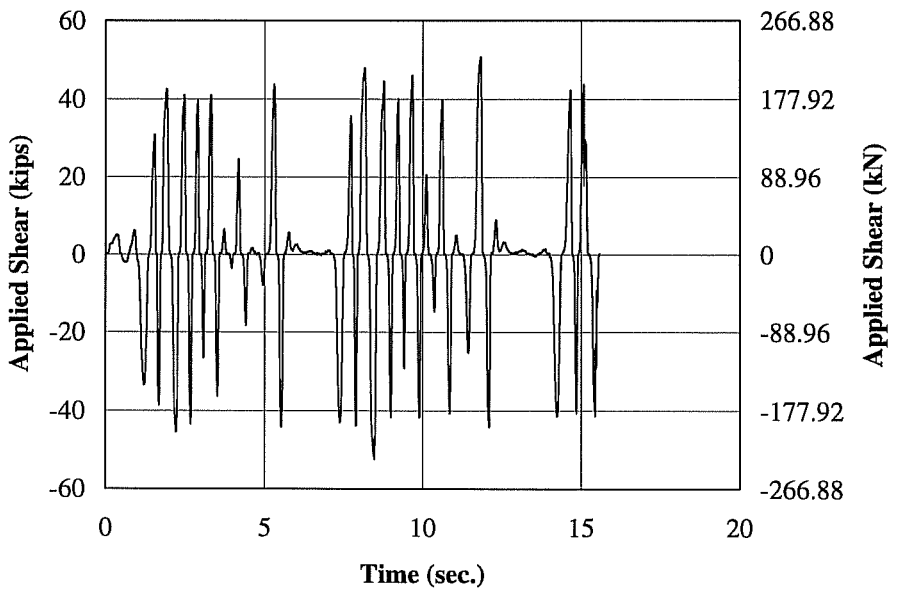
60
40
20
0
-20
-40
-60
266.88
177.92
88.96
0
-88.96
-177.92
-266.88
0
5
10
15
20
Applied Shear (kips)
Applied Shear (kN)
Time (sec.)

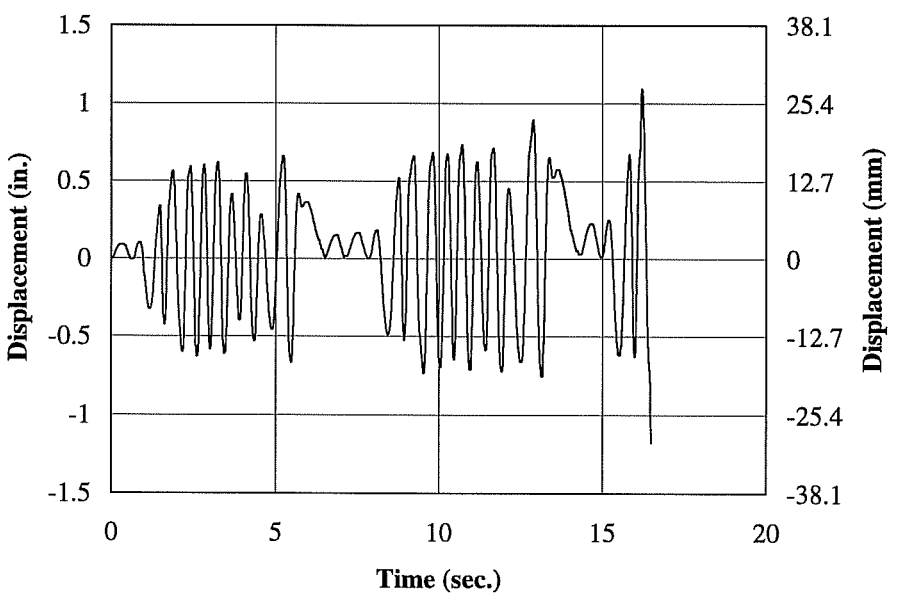
1.5
1
0.5
0
-0.5
-1
-1.5
38.1
25.4
12.7
0
-12.7
-25.4
-38.1
0
5
10
15
20
Displacement (in.)
Displacement (mm)
Time (sec.)

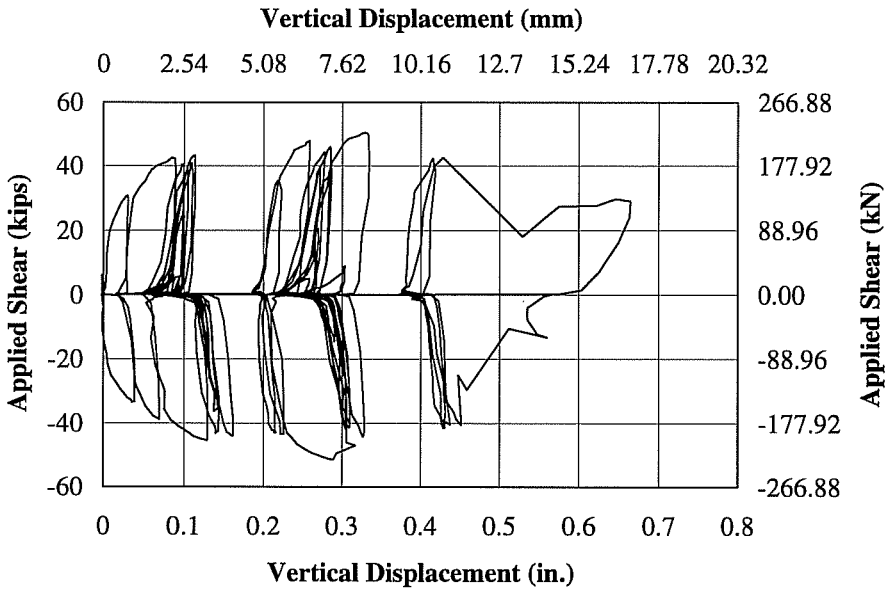
Vertical Displacement (mm)
0
2.54
5.08
7.62
10.16
12.7
15.24
17.78
20.32
60
40
20
0
-20
-40
-60
266.88
177.92
88.96
0.00
-88.96
-177.92
-266.88
Applied Shear (kips)
Applied Shear (kN)
0
0.1
0.2
0.3
0.4
0.5
0.6
0.7
0.8
Vertical Displacement (in.)

Test 4205

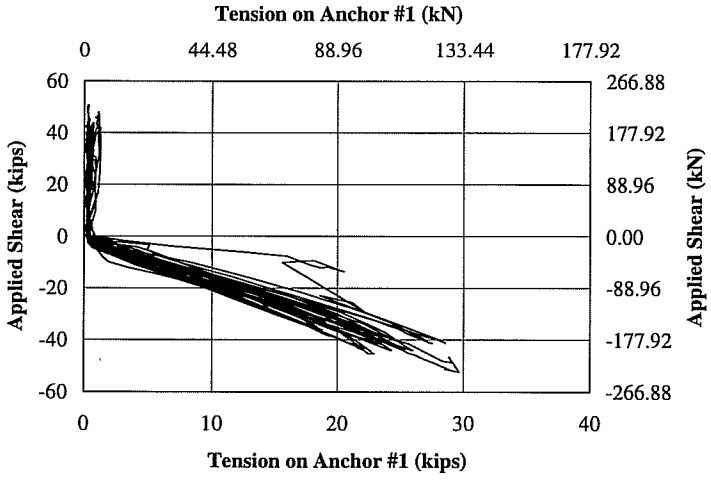
Tension on Anchor #1 (kN)
0
44.48
88.96
133.44
177.92
60
40
20
0
-20
-40
-60
266.88
177.92
88.96
0.00
-88.96
-177.92
-266.88
Applied Shear (kips)
Applied Shear (kN)
0
10
20
30
40
Tension on Anchor #1 (kips)

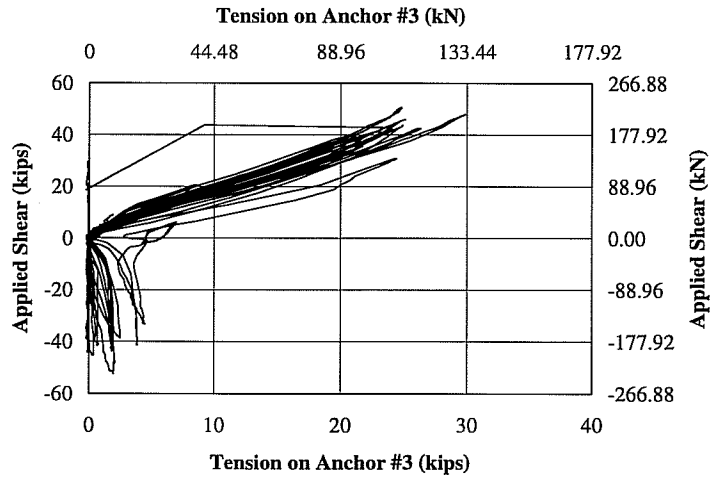
Tension on Anchor #3 (kN)
0
44.48
88.96
133.44
177.92
60
40
20
0
-20
-40
-60
266.88
177.92
88.96
0.00
-88.96
-177.92
-266.88
Applied Shear (kips)
Applied Shear (kN)
0
10
20
30
40
Tension on Anchor #3 (kips)

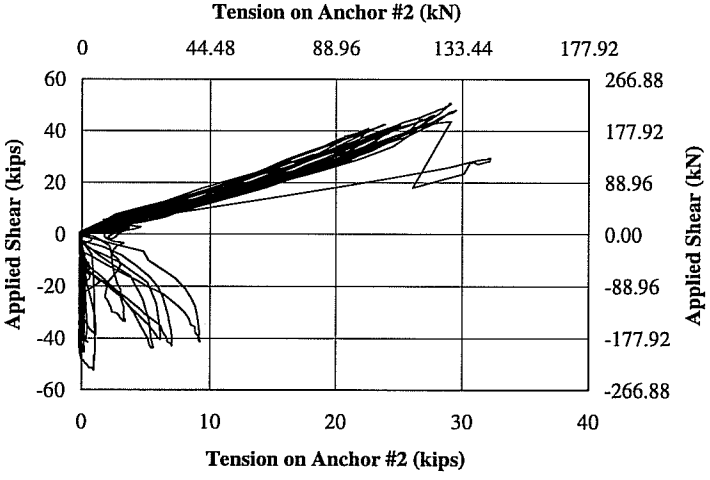
Tension on Anchor #2 (kN)
0
44.48
88.96
133.44
177.92
60
40
20
0
-20
-40
-60
266.88
177.92
88.96
0.00
-88.96
-177.92
-266.88
Applied Shear (kips)
Applied Shear (kN)
0
10
20
30
40
Tension on Anchor #2 (kips)

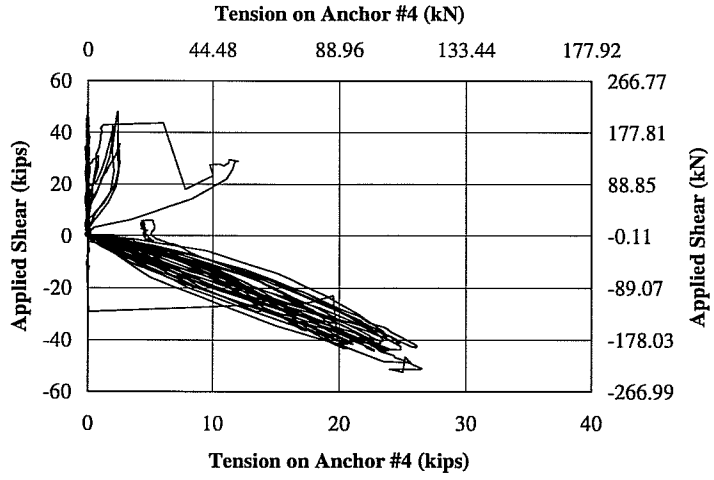
Tension on Anchor #4 (kN)
0
44.48
88.96
133.44
177.92
60
40
20
0
-20
-40
-60
266.77
177.81
88.85
-0.11
-89.07
-178.03
-266.99
Applied Shear (kips)
Applied Shear (kN)
0
10
20
30
40
Tension on Anchor #4 (kips)

Test 4206

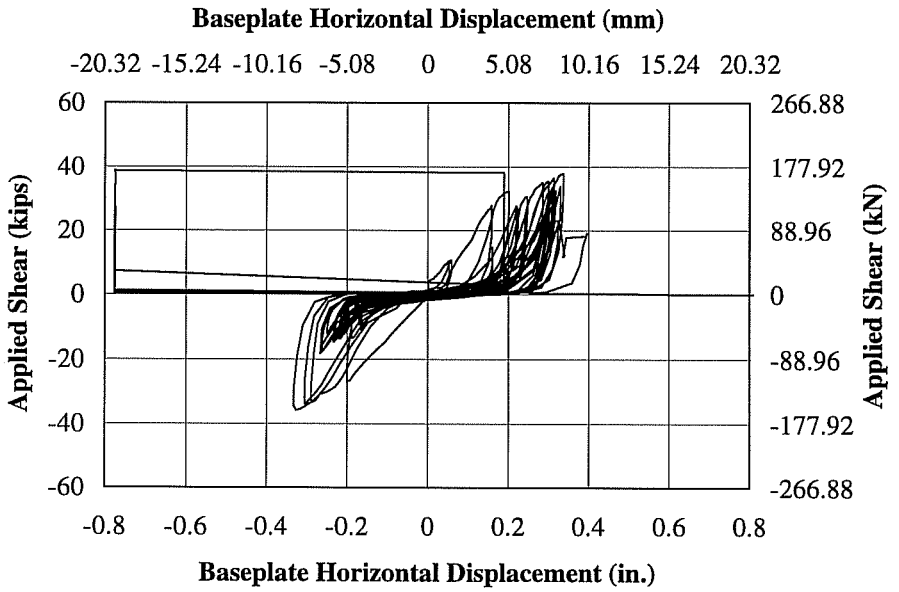
Baseplate Horizontal Displacement (mm)
-20.32 -15.24 -10.16 -5.08 0 5.08 10.16 15.24 20.32
60
40
20
0
-20
-40
-60
266.88
177.92
88.96
0
-88.96
-177.92
-266.88
Applied Shear (kips)
Applied Shear (kN)
-0.8 -0.6 -0.4 -0.2 0 0.2 0.4 0.6 0.8
Baseplate Horizontal Displacement (in.)

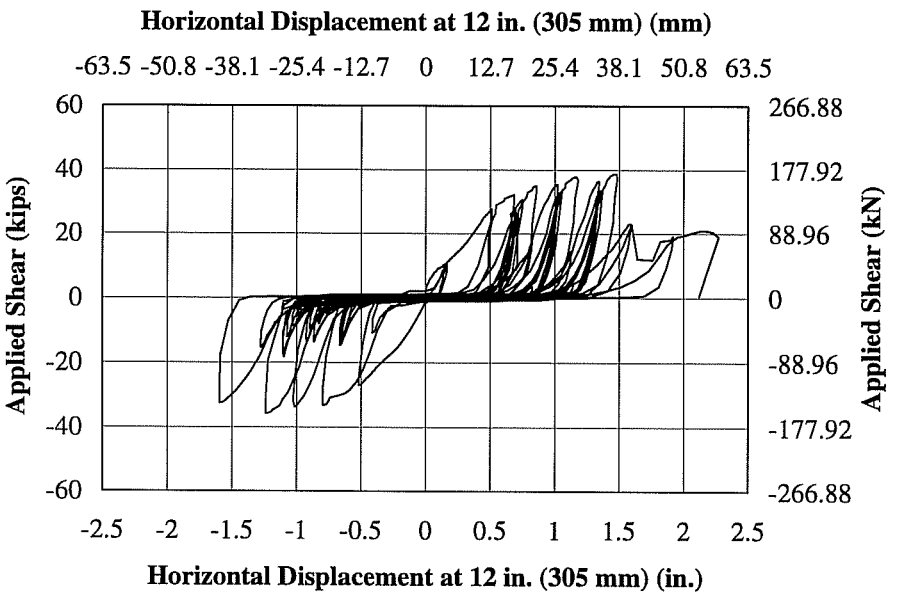
Horizontal Displacement at 12 in. (305 mm) (mm)
-63.5 -50.8 -38.1 -25.4 -12.7 0 12.7 25.4 38.1 50.8 63.5
60
40
20
0
-20
-40
-60
266.88
177.92
88.96
0
-88.96
-177.92
-266.88
Applied Shear (kips)
Applied Shear (kN)
-2.5 -2 -1.5 -1 -0.5 0 0.5 1 1.5 2 2.5
Horizontal Displacement at 12 in. (305 mm) (in.)

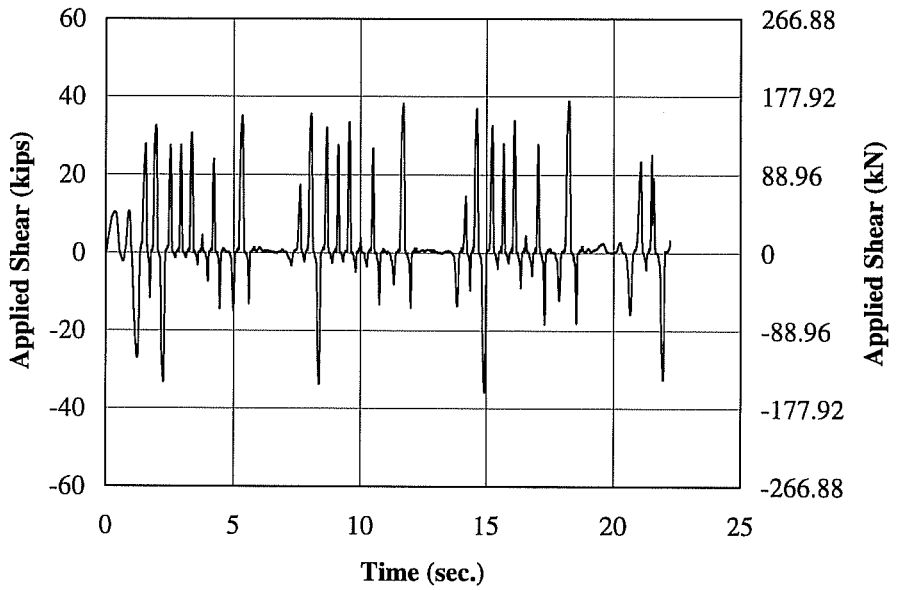
60
40
20
0
-20
-40
-60
266.88
177.92
88.96
0
-88.96
-177.92
-266.88
0
5
10
15
20
25
Applied Shear (kips)
Applied Shear (kN)
Time (sec.)

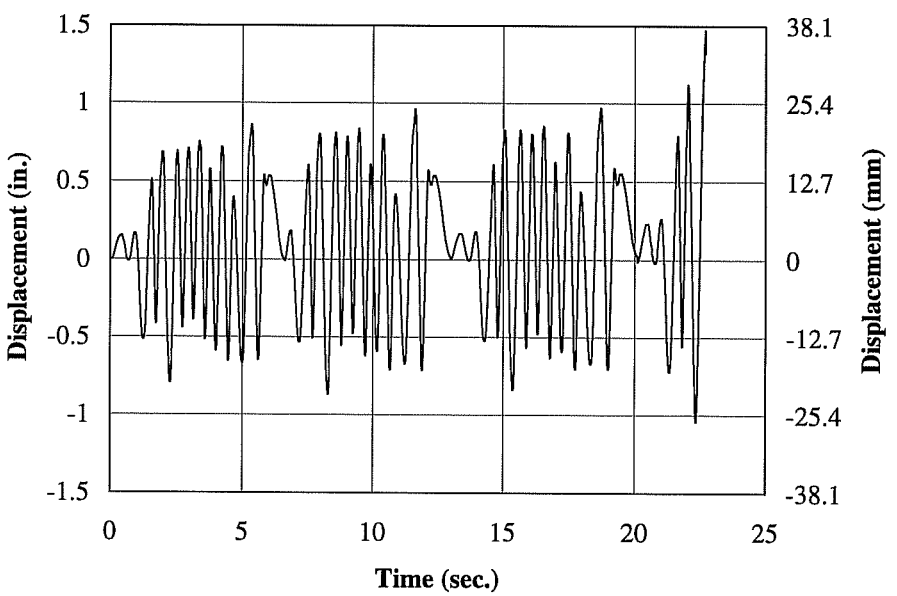
1.5
1
0.5
0
-0.5
-1
-1.5
38.1
25.4
12.7
0
-12.7
-25.4
-38.1
0
5
10
15
20
25
Displacement (in.)
Displacement (mm)
Time (sec.)

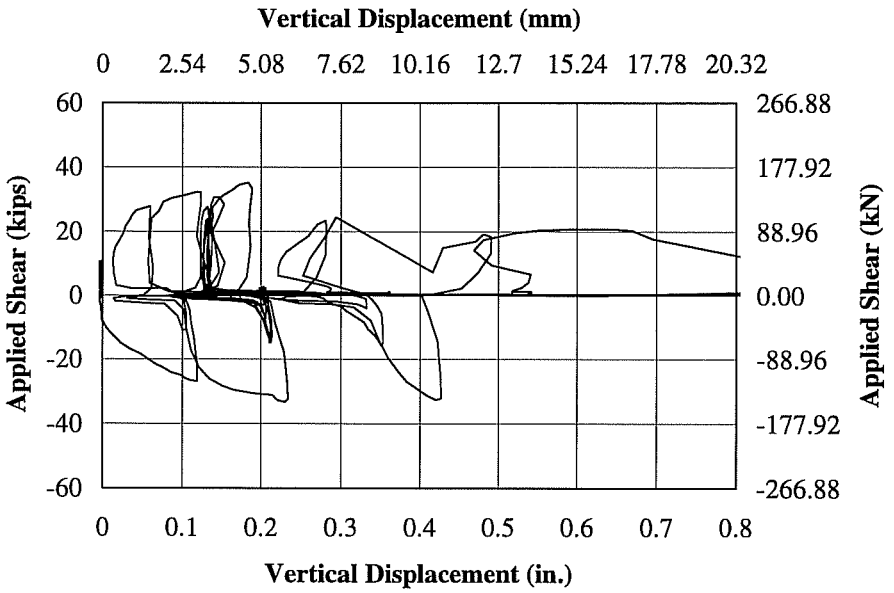
Vertical Displacement (mm)
0
2.54
5.08
7.62
10.16
12.7
15.24
17.78
20.32
60
40
20
0
-20
-40
-60
266.88
177.92
88.96
0.00
-88.96
-177.92
-266.88
Applied Shear (kips)
Applied Shear (kN)
0
0.1
0.2
0.3
0.4
0.5
0.6
0.7
0.8
Vertical Displacement (in.)

Test 4206

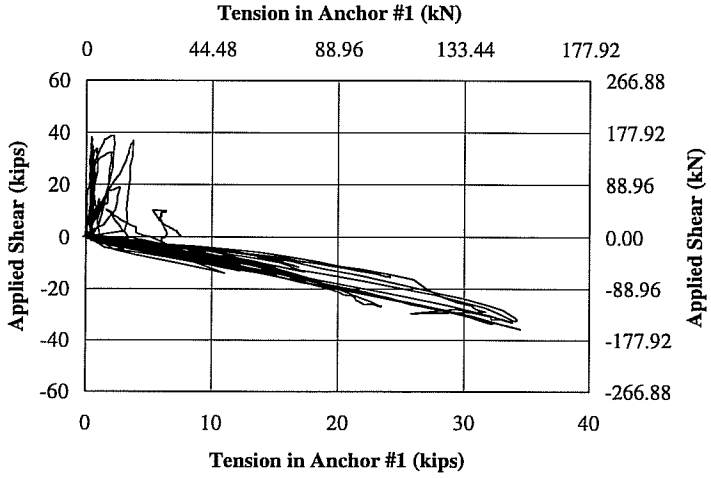
Tension in Anchor #1 (kN)
0 44.48 88.96 133.44 177.92
60 40 20 0 -20 -40 -60
266.88 177.92 88.96 0.00 -88.96 -177.92 -266.88
Applied Shear (kips)
Applied Shear (kN)
0 10 20 30 40
Tension in Anchor #1 (kips)

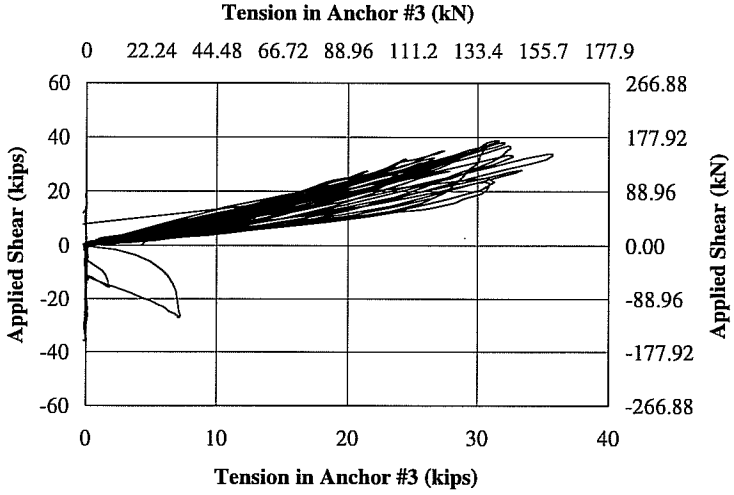
Tension in Anchor #3 (kN)
0 22.24 44.48 66.72 88.96 111.2 133.4 155.7 177.9
60 40 20 0 -20 -40 -60
266.88 177.92 88.96 0.00 -88.96 -177.92 -266.88
Applied Shear (kips)
Applied Shear (kN)
0 10 20 30 40
Tension in Anchor #3 (kips)

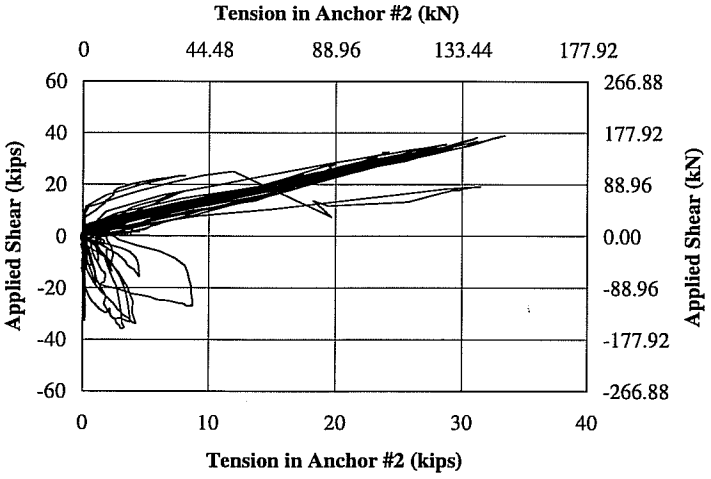
Tension in Anchor #2 (kN)
0 44.48 88.96 133.44 177.92
60 40 20 0 -20 -40 -60
266.88 177.92 88.96 0.00 -88.96 -177.92 -266.88
Applied Shear (kips)
Applied Shear (kN)
0 10 20 30 40
Tension in Anchor #2 (kips)

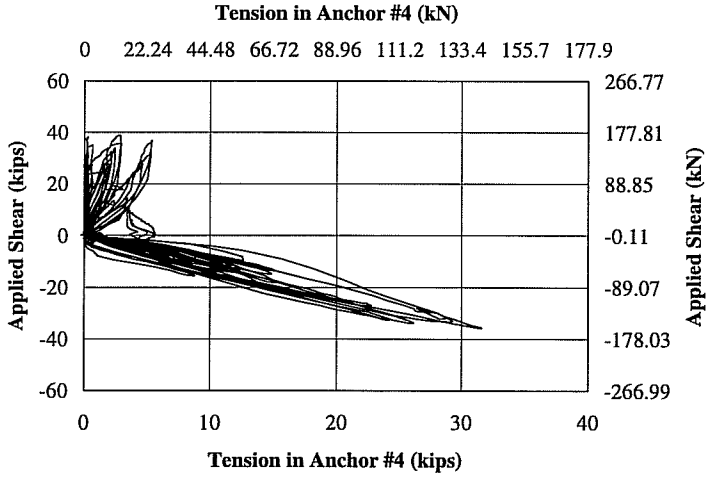
Tension in Anchor #4 (kN)
0 22.24 44.48 66.72 88.96 111.2 133.4 155.7 177.9
60 40 20 0 -20 -40 -60
266.77 177.81 88.85 -0.11 -89.07 -178.03 -266.99
Applied Shear (kips)
Applied Shear (kN)
0 10 20 30 40
Tension in Anchor #4 (kips)

Test 4307

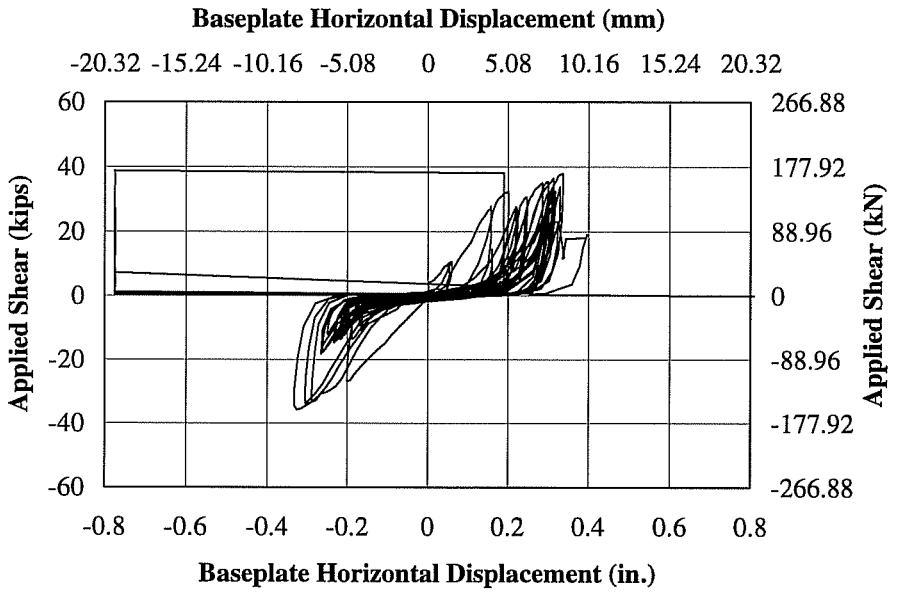
Baseplate Horizontal Displacement (mm)
-20.32 -15.24 -10.16 -5.08 0 5.08 10.16 15.24 20.32
60
40
20
0
-20
-40
-60
266.88
177.92
88.96
0
-88.96
-177.92
-266.88
Applied Shear (kips)
Applied Shear (kN)
-0.8 -0.6 -0.4 -0.2 0 0.2 0.4 0.6 0.8
Baseplate Horizontal Displacement (in.)

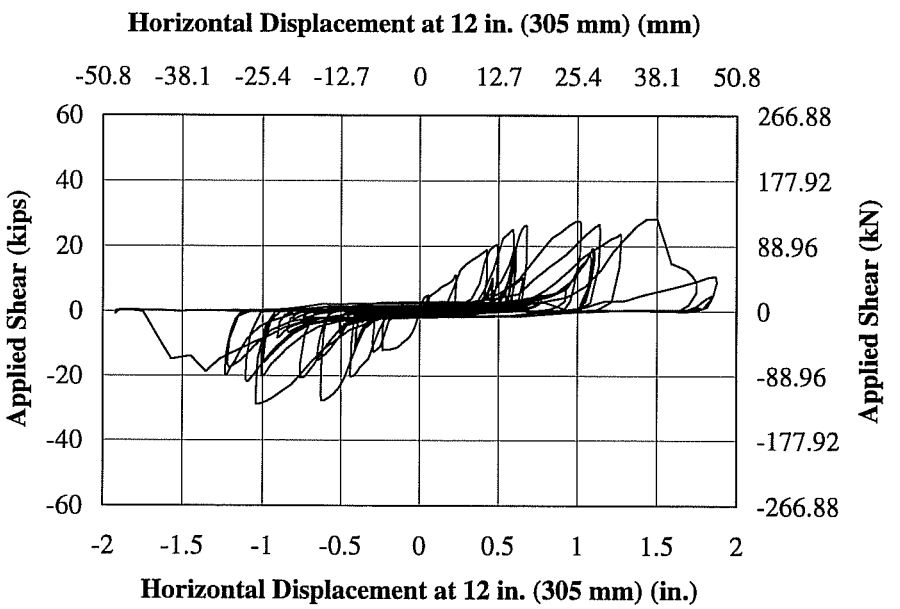
Horizontal Displacement at 12 in. (305 mm) (mm)
-50.8 -38.1 -25.4 -12.7 0 12.7 25.4 38.1 50.8
60
40
20
0
-20
-40
-60
266.88
177.92
88.96
0
-88.96
-177.92
-266.88
Applied Shear (kips)
Applied Shear (kN)
-2 -1.5 -1 -0.5 0 0.5 1 1.5 2
Horizontal Displacement at 12 in. (305 mm) (in.)

Test 4307

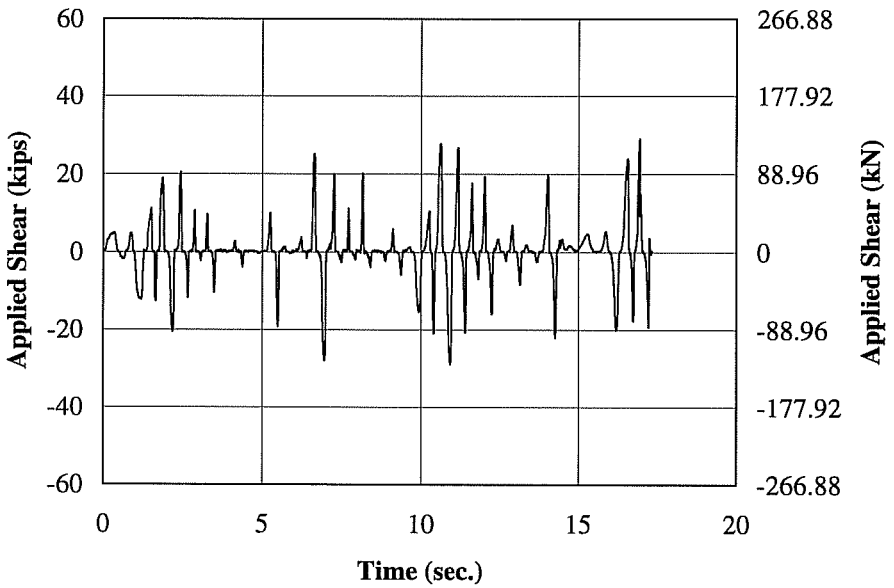
60
40
20
0
-20
-40
-60
266.88
177.92
88.96
0
-88.96
-177.92
-266.88
0
5
10
15
20
Applied Shear (kips)
Applied Shear (kN)
Time (sec.)

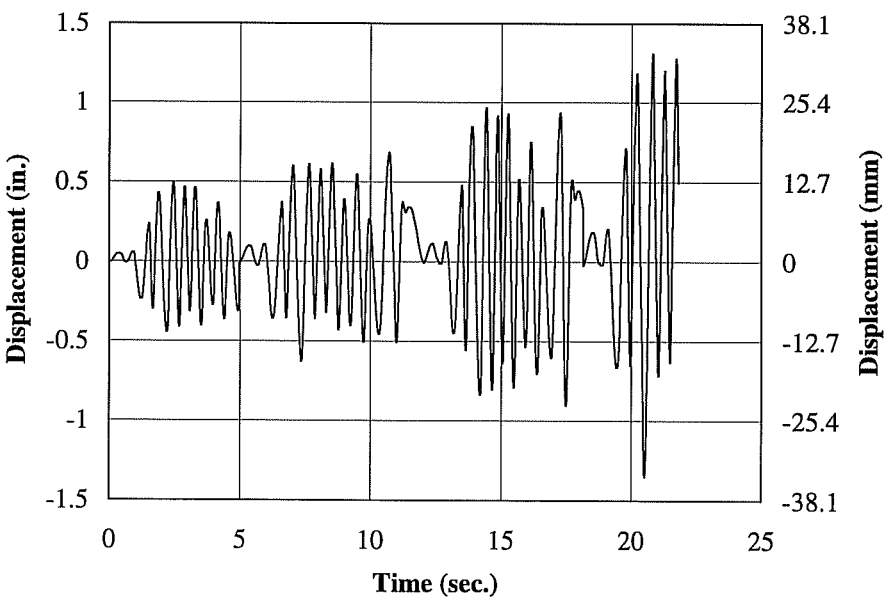
1.5
1
0.5
0
-0.5
-1
-1.5
38.1
25.4
12.7
0
-12.7
-25.4
-38.1
0
5
10
15
20
25
Displacement (in.)
Displacement (mm)
Time (sec.)

Test 4307

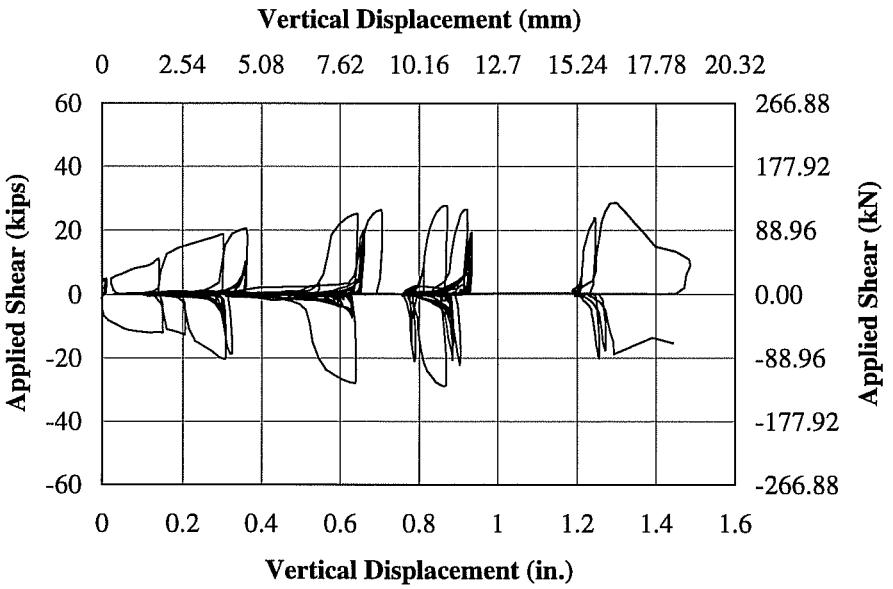
Vertical Displacement (mm)
0
2.54
5.08
7.62
10.16
12.7
15.24
17.78
20.32
60
40
20
0
-20
-40
-60
266.88
177.92
88.96
0.00
-88.96
-177.92
-266.88
Applied Shear (kips)
Applied Shear (kN)
0
0.2
0.4
0.6
0.8
1
1.2
1.4
1.6
Vertical Displacement (in.)

Test 4307

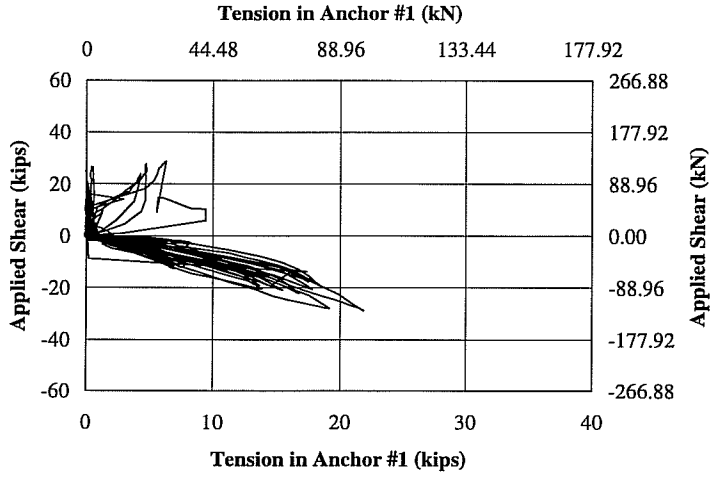
Tension in Anchor #1 (kN)
0
44.48
88.96
133.44
177.92
60
40
20
0
-20
-40
-60
266.88
177.92
88.96
0.00
-88.96
-177.92
-266.88
Applied Shear (kips)
Applied Shear (kN)
0
10
20
30
40
Tension in Anchor #1 (kips)

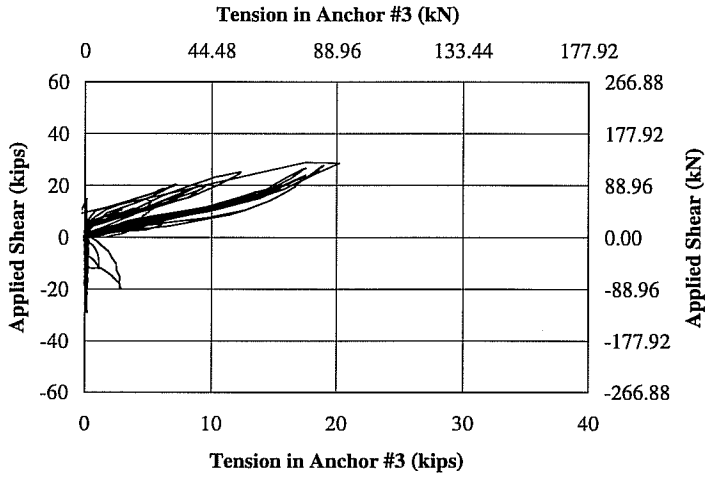
Tension in Anchor #3 (kN)
0
44.48
88.96
133.44
177.92
60
40
20
0
-20
-40
-60
266.88
177.92
88.96
0.00
-88.96
-177.92
-266.88
Applied Shear (kips)
Applied Shear (kN)
0
10
20
30
40
Tension in Anchor #3 (kips)

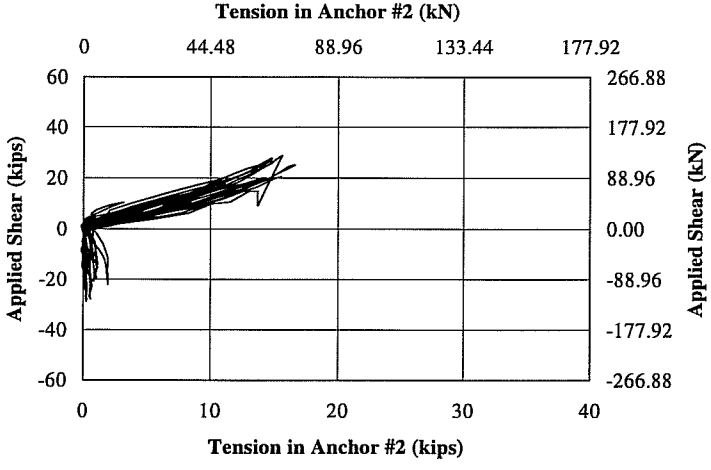
Tension in Anchor #2 (kN)
0
44.48
88.96
133.44
177.92
60
40
20
0
-20
-40
-60
266.88
177.92
88.96
0.00
-88.96
-177.92
-266.88
Applied Shear (kips)
Applied Shear (kN)
0
10
20
30
40
Tension in Anchor #2 (kips)

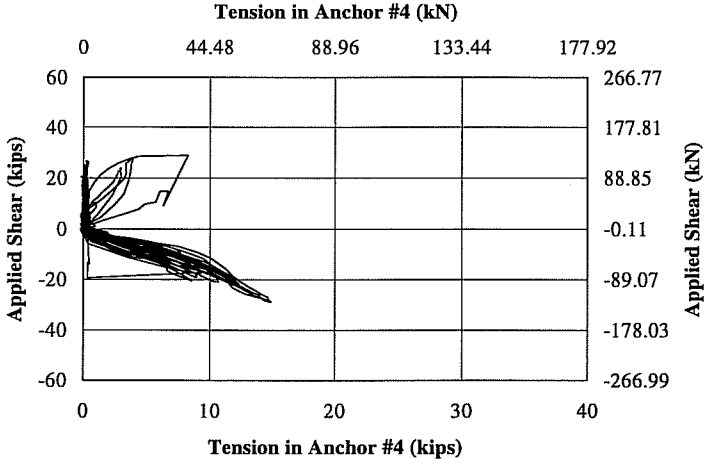
Tension in Anchor #4 (kN)
0
44.48
88.96
133.44
177.92
60
40
20
0
-20
-40
-60
266.77
177.81
88.85
-0.11
-89.07
-178.03
-266.99
Applied Shear (kips)
Applied Shear (kN)
0
10
20
30
40
Tension in Anchor #4 (kips)

Test 4308

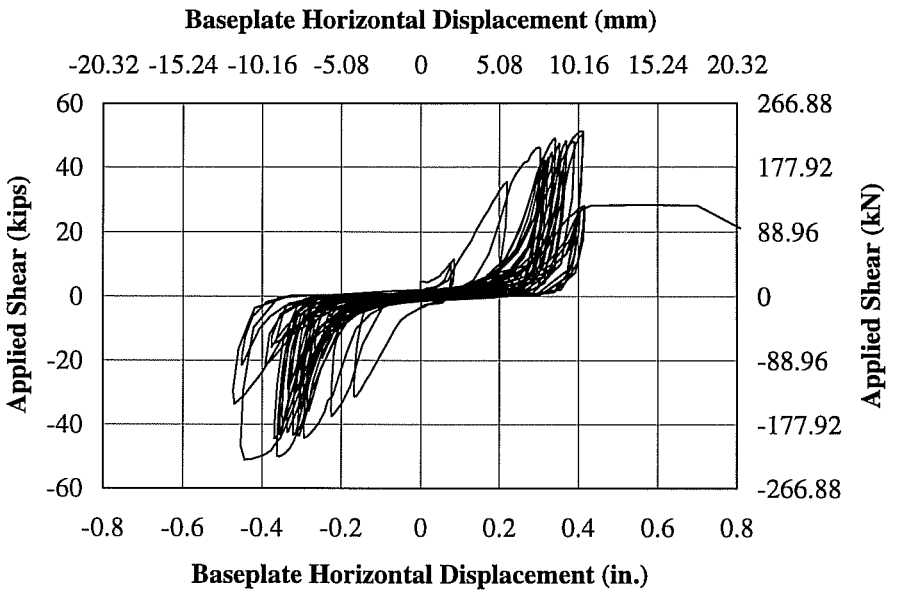
Baseplate Horizontal Displacement (mm)
-20.32 -15.24 -10.16 -5.08 0 5.08 10.16 15.24 20.32
60
40
20
0
-20
-40
-60
266.88
177.92
88.96
0
-88.96
-177.92
-266.88
Applied Shear (kips)
Applied Shear (kN)
-0.8 -0.6 -0.4 -0.2 0 0.2 0.4 0.6 0.8
Baseplate Horizontal Displacement (in.)

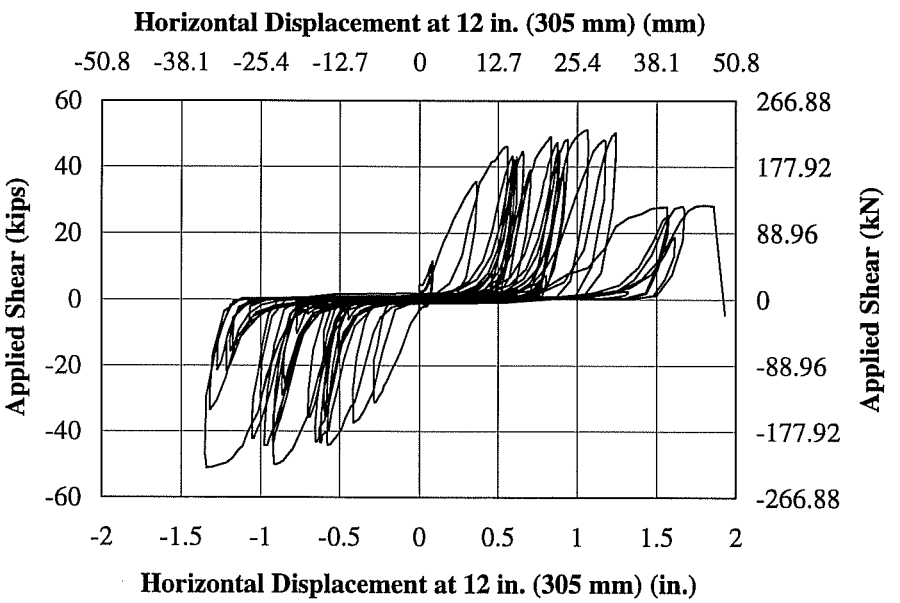
Horizontal Displacement at 12 in. (305 mm) (mm)
-50.8 -38.1 -25.4 -12.7 0 12.7 25.4 38.1 50.8
60
40
20
0
-20
-40
-60
266.88
177.92
88.96
0
-88.96
-177.92
-266.88
Applied Shear (kips)
Applied Shear (kN)
-2 -1.5 -1 -0.5 0 0.5 1 1.5 2
Horizontal Displacement at 12 in. (305 mm) (in.)

Test 4308

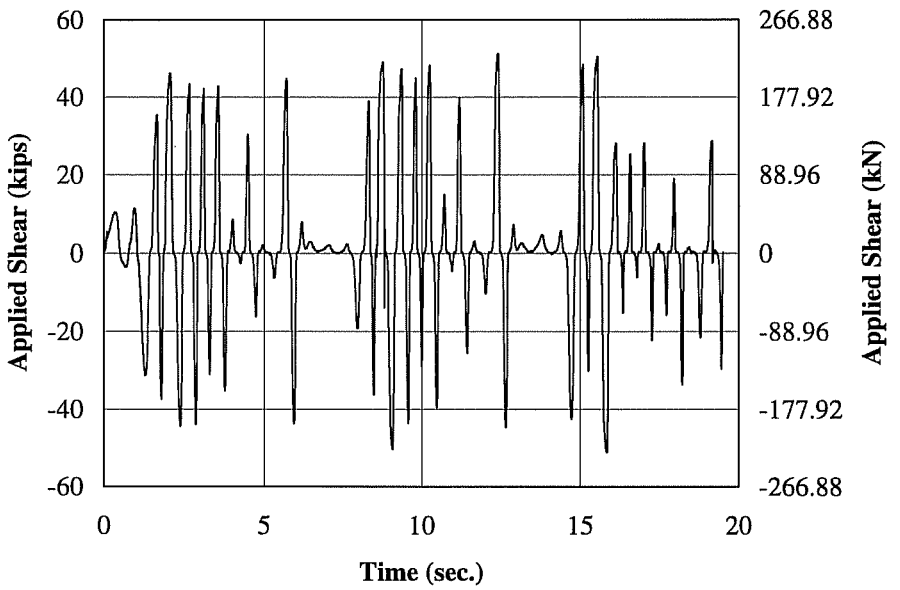
60
40
20
0
-20
-40
-60
266.88
177.92
88.96
0
-88.96
-177.92
-266.88
0
5
10
15
20
Applied Shear (kips)
Applied Shear (kN)
Time (sec.)

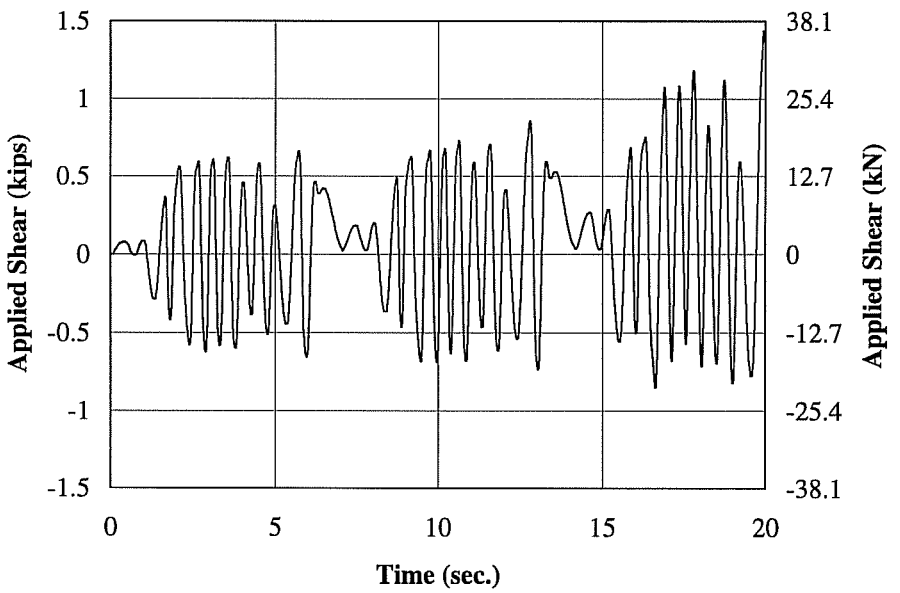
1.5
1
0.5
0
-0.5
-1
-1.5
38.1
25.4
12.7
0
-12.7
-25.4
-38.1
0
5
10
15
20
Applied Shear (kips)
Applied Shear (kN)
Time (sec.)

Test 4308

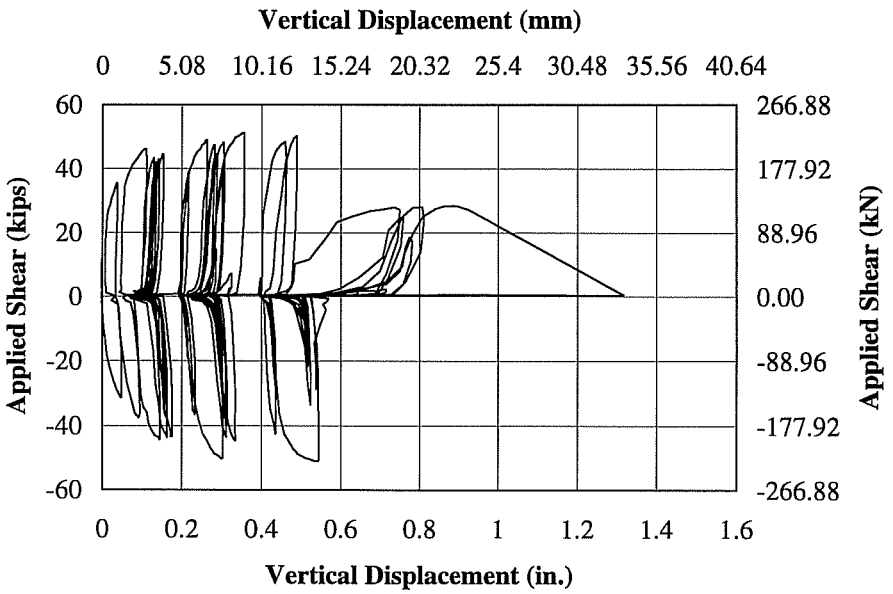
Vertical Displacement (mm)
0
5.08
10.16
15.24
20.32
25.4
30.48
35.56
40.64
60
40
20
0
-20
-40
-60
266.88
177.92
88.96
0.00
-88.96
-177.92
-266.88
Applied Shear (kips)
Applied Shear (kN)
0
0.2
0.4
0.6
0.8
1
1.2
1.4
1.6
Vertical Displacement (in.)

Test 4308

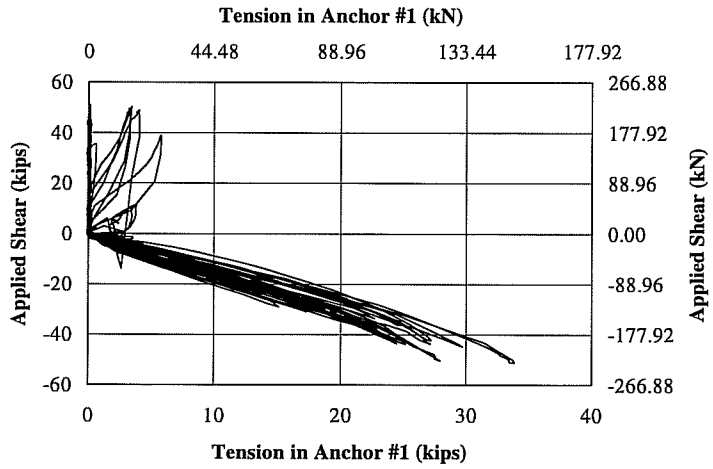
Tension in Anchor #1 (kN)
0
44.48
88.96
133.44
177.92
60
40
20
0
-20
-40
-60
266.88
177.92
88.96
0.00
-88.96
-177.92
-266.88
Applied Shear (kips)
Applied Shear (kN)
0
10
20
30
40
Tension in Anchor #1 (kips)

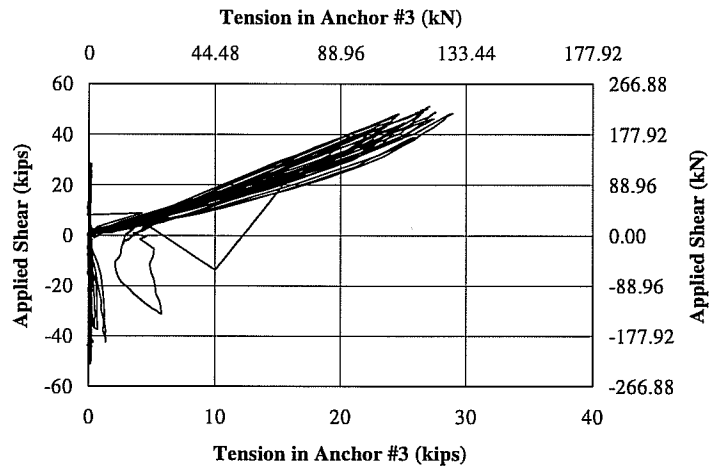
Tension in Anchor #3 (kN)
0
44.48
88.96
133.44
177.92
60
40
20
0
-20
-40
-60
266.88
177.92
88.96
0.00
-88.96
-177.92
-266.88
Applied Shear (kips)
Applied Shear (kN)
0
10
20
30
40
Tension in Anchor #3 (kips)

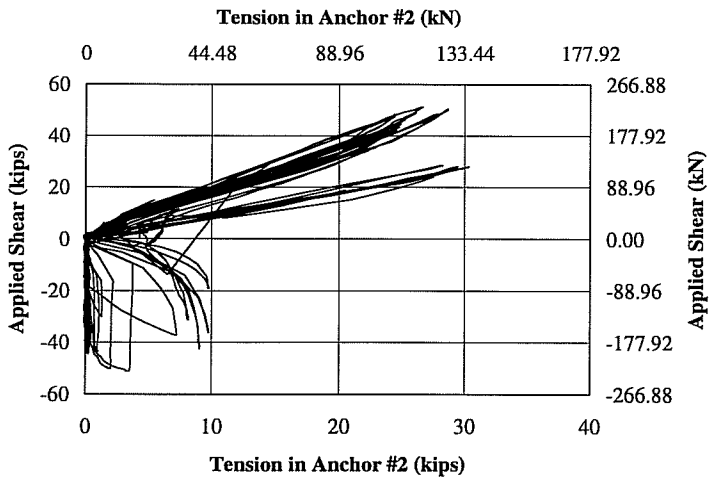
Tension in Anchor #2 (kN)
0
44.48
88.96
133.44
177.92
60
40
20
0
-20
-40
-60
266.88
177.92
88.96
0.00
-88.96
-177.92
-266.88
Applied Shear (kips)
Applied Shear (kN)
0
10
20
30
40
Tension in Anchor #2 (kips)

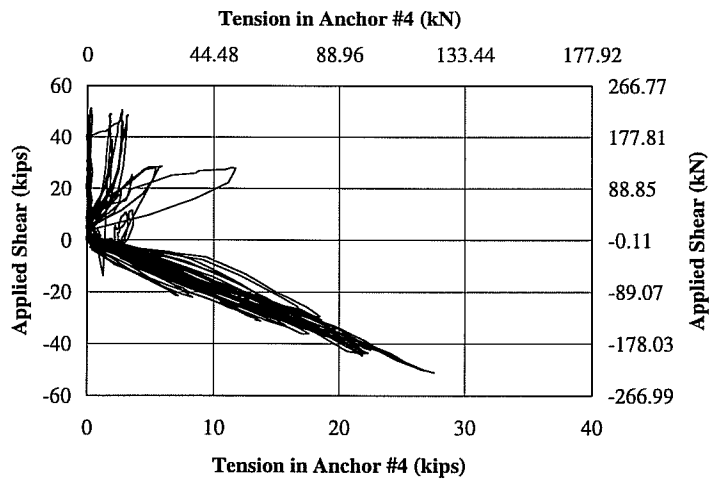
Tension in Anchor #4 (kN)
0
44.48
88.96
133.44
177.92
60
40
20
0
-20
-40
-60
266.77
177.81
88.85
-0.11
-89.07
-178.03
-266.99
Applied Shear (kips)
Applied Shear (kN)
0
10
20
30
40
Tension in Anchor #4 (kips)

Test 4309

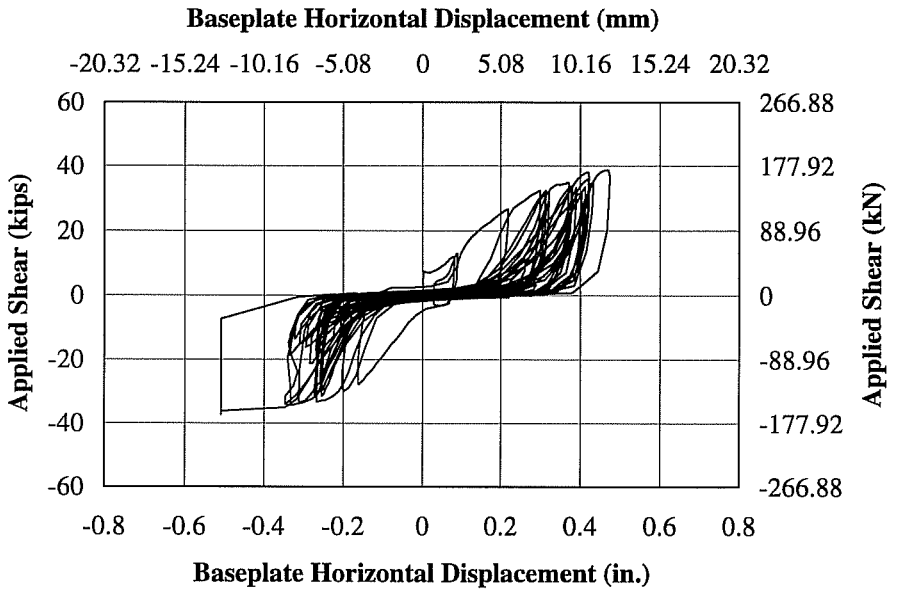
Baseplate Horizontal Displacement (mm)
-20.32 -15.24 -10.16 -5.08 0 5.08 10.16 15.24 20.32
60
40
20
0
-20
-40
-60
266.88
177.92
88.96
0
-88.96
-177.92
-266.88
Applied Shear (kips)
Applied Shear (kN)
-0.8 -0.6 -0.4 -0.2 0 0.2 0.4 0.6 0.8
Baseplate Horizontal Displacement (in.)

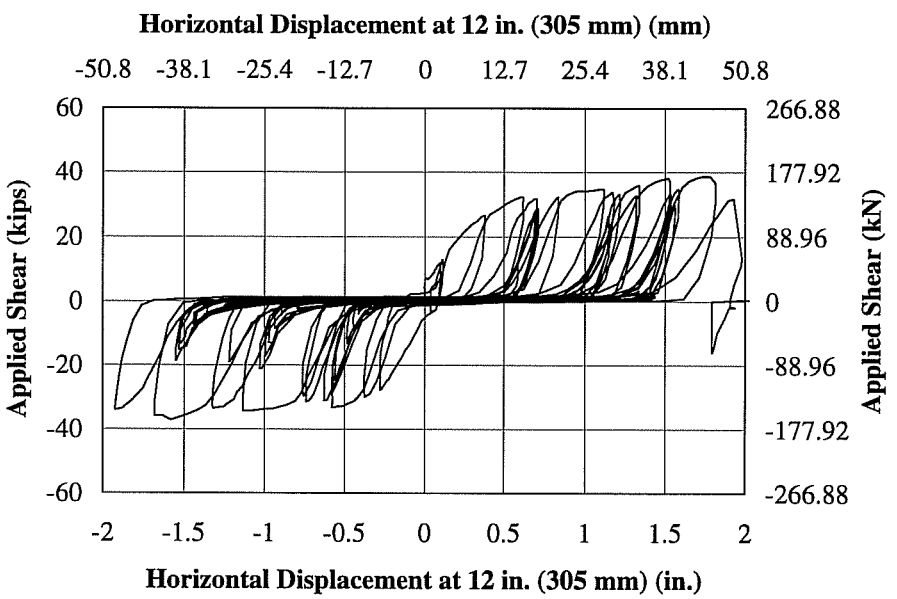
Horizontal Displacement at 12 in. (305 mm) (mm)
-50.8 -38.1 -25.4 -12.7 0 12.7 25.4 38.1 50.8
60
40
20
0
-20
-40
-60
266.88
177.92
88.96
0
-88.96
-177.92
-266.88
Applied Shear (kips)
Applied Shear (kN)
-2 -1.5 -1 -0.5 0 0.5 1 1.5 2
Horizontal Displacement at 12 in. (305 mm) (in.)

Test 4309

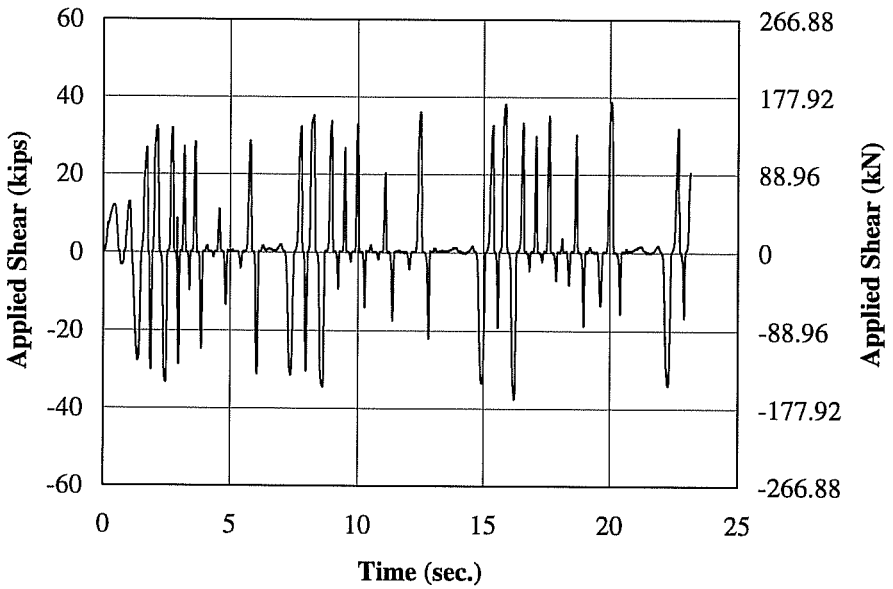
60
40
20
0
-20
-40
-60
266.88
177.92
88.96
0
-88.96
-177.92
-266.88
0
5
10
15
20
25
Applied Shear (kips)
Applied Shear (kN)
Time (sec.)

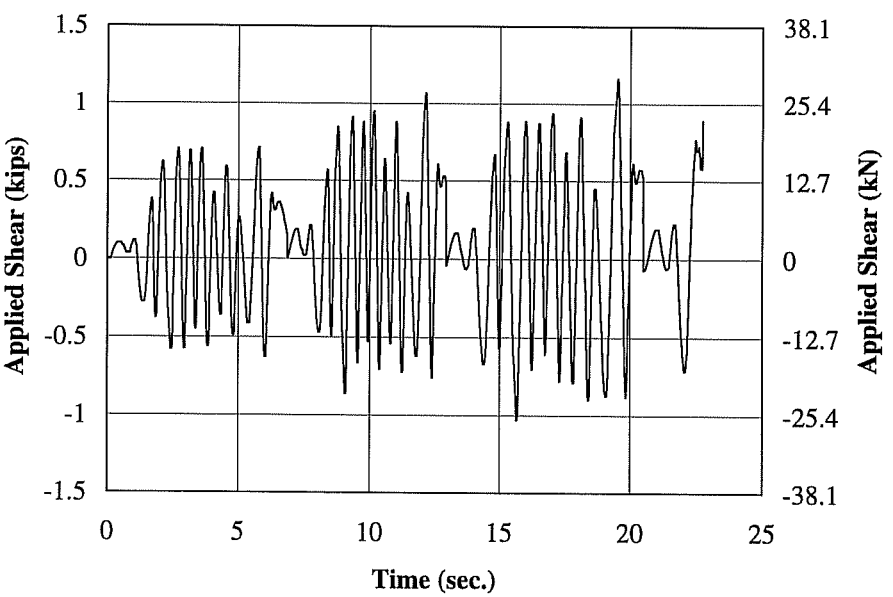
1.5
1
0.5
0
-0.5
-1
-1.5
38.1
25.4
12.7
0
-12.7
-25.4
-38.1
0
5
10
15
20
25
Applied Shear (kips)
Applied Shear (kN)
Time (sec.)

Test 4310

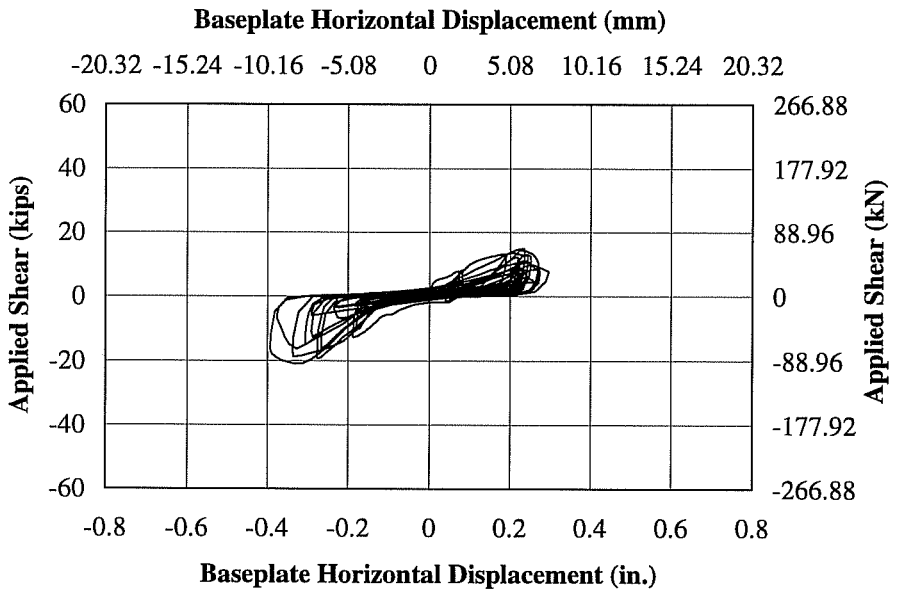
Baseplate Horizontal Displacement (mm)
-20.32 -15.24 -10.16 -5.08 0 5.08 10.16 15.24 20.32
60 40 20 0 -20 -40 -60
266.88 177.92 88.96 0 -88.96 -177.92 -266.88
Applied Shear (kips)
Applied Shear (kN)
-0.8 -0.6 -0.4 -0.2 0 0.2 0.4 0.6 0.8
Baseplate Horizontal Displacement (in.)

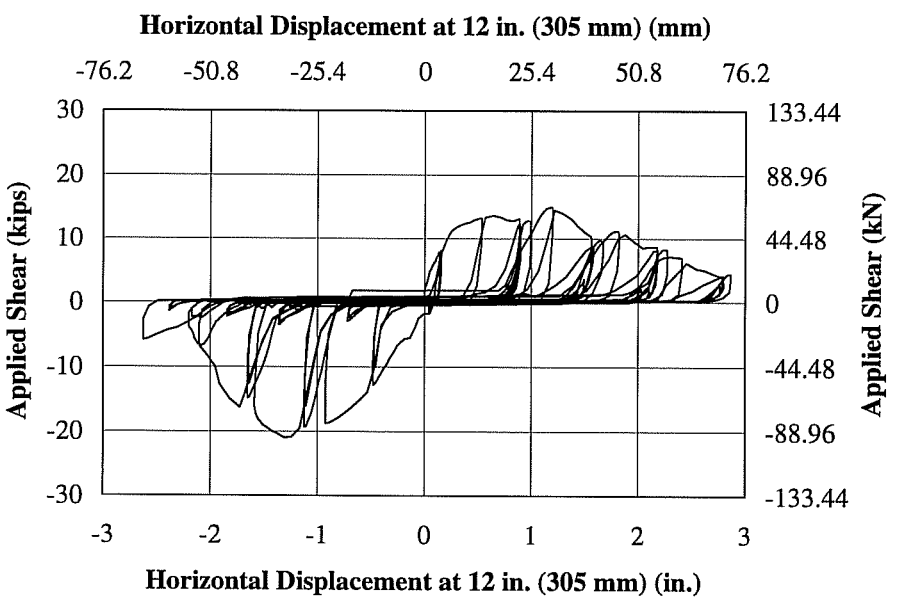
Horizontal Displacement at 12 in. (305 mm) (mm)
-76.2 -50.8 -25.4 0 25.4 50.8 76.2
30 20 10 0 -10 -20 -30
133.44 88.96 44.48 0 -44.48 -88.96 -133.44
Applied Shear (kips)
Applied Shear (kN)
-3 -2 -1 0 1 2 3
Horizontal Displacement at 12 in. (305 mm) (in.)

Test 4310

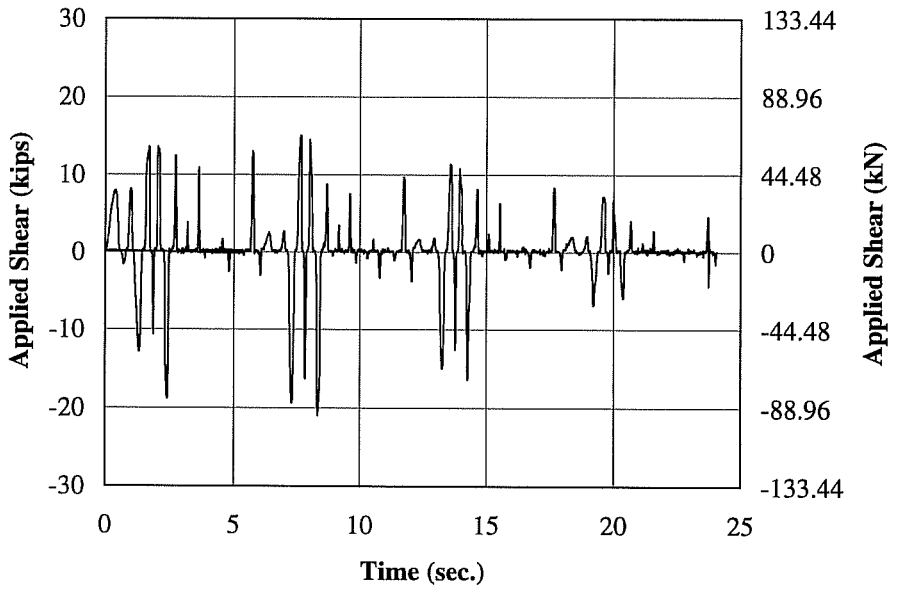
30
20
10
0
-10
-20
-30
133.44
88.96
44.48
0
-44.48
-88.96
-133.44
0
5
10
15
20
25
Applied Shear (kips)
Applied Shear (kN)
Time (sec.)

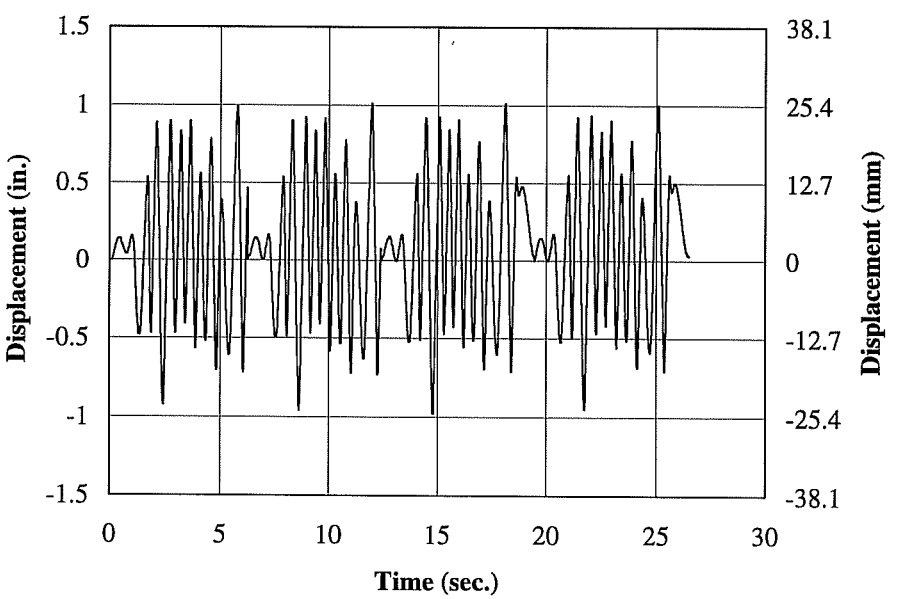
1.5
1
0.5
0
-0.5
-1
-1.5
38.1
25.4
12.7
0
-12.7
-25.4
-38.1
0
5
10
15
20
25
30
Displacement (in.)
Displacement (mm)
Time (sec.)

est 4310

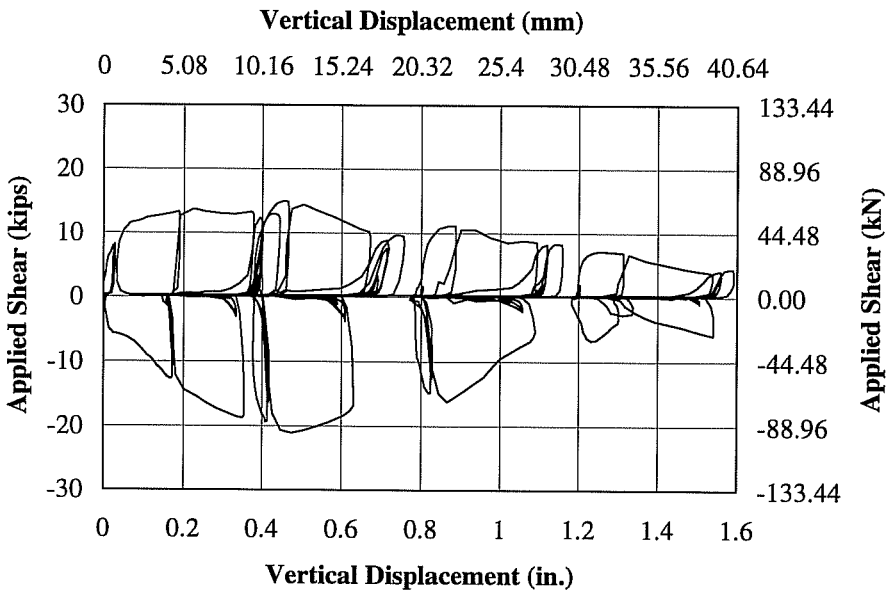
Vertical Displacement (mm)
0
5.08
10.16
15.24
20.32
25.4
30.48
35.56
40.64
30
20
10
0
-10
-20
-30
133.44
88.96
44.48
0.00
-44.48
-88.96
-133.44
Applied Shear (kips)
Applied Shear (kN)
0
0.2
0.4
0.6
0.8
1
1.2
1.4
1.6
Vertical Displacement (in.)

Test 4310

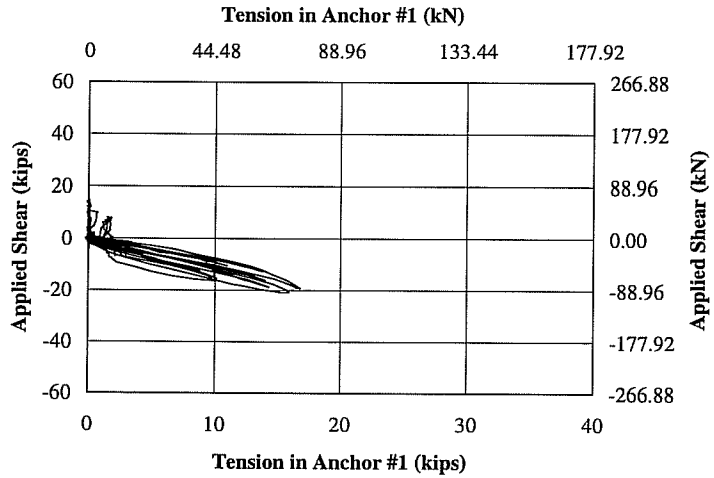
Tension in Anchor #1 (kN)
0
44.48
88.96
133.44
177.92
60
40
20
0
-20
-40
-60
266.88
177.92
88.96
0.00
-88.96
-177.92
-266.88
Applied Shear (kips)
Applied Shear (kN)
0
10
20
30
40
Tension in Anchor #1 (kips)

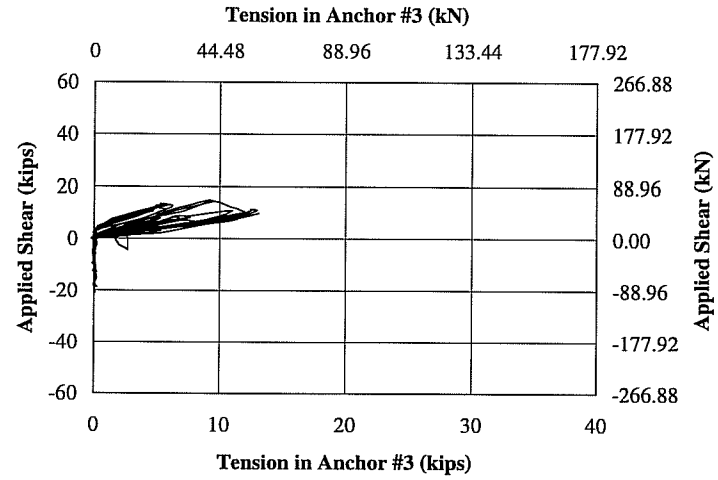
Tension in Anchor #3 (kN)
0
44.48
88.96
133.44
177.92
60
40
20
0
-20
-40
-60
266.88
177.92
88.96
0.00
-88.96
-177.92
-266.88
Applied Shear (kips)
Applied Shear (kN)
0
10
20
30
40
Tension in Anchor #3 (kips)

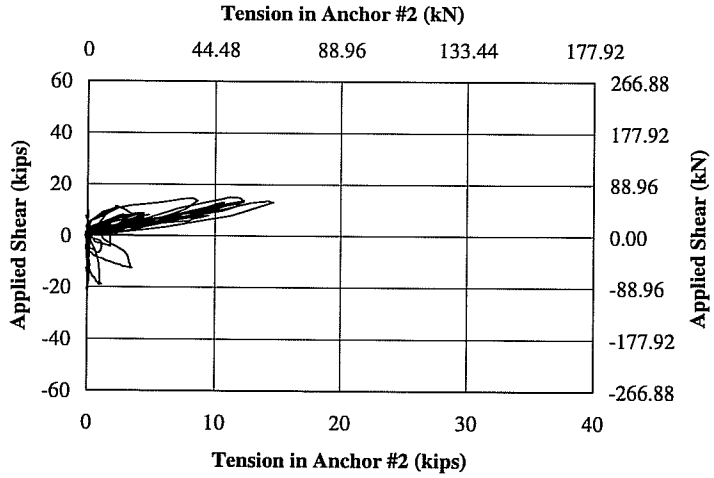
Tension in Anchor #2 (kN)
0
44.48
88.96
133.44
177.92
60
40
20
0
-20
-40
-60
266.88
177.92
88.96
0.00
-88.96
-177.92
-266.88
Applied Shear (kips)
Applied Shear (kN)
0
10
20
30
40
Tension in Anchor #2 (kips)

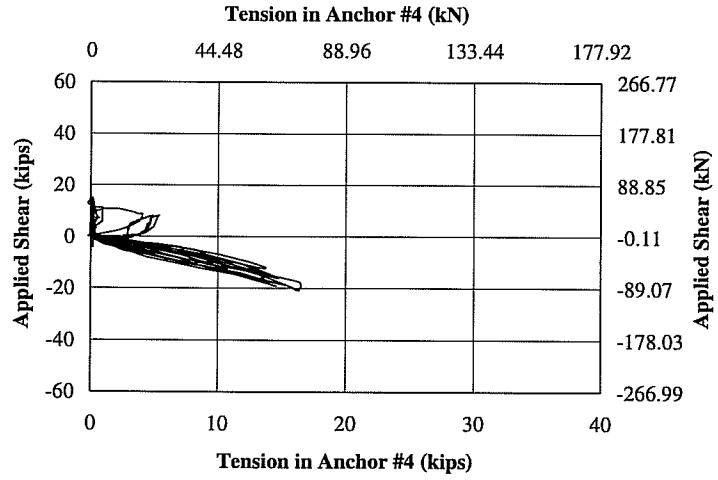
Tension in Anchor #4 (kN)
0
44.48
88.96
133.44
177.92
60
40
20
0
-20
-40
-60
266.77
177.81
88.85
-0.11
-89.07
-178.03
-266.99
Applied Shear (kips)
Applied Shear (kN)
0
10
20
30
40
Tension in Anchor #4 (kips)

Test 4411

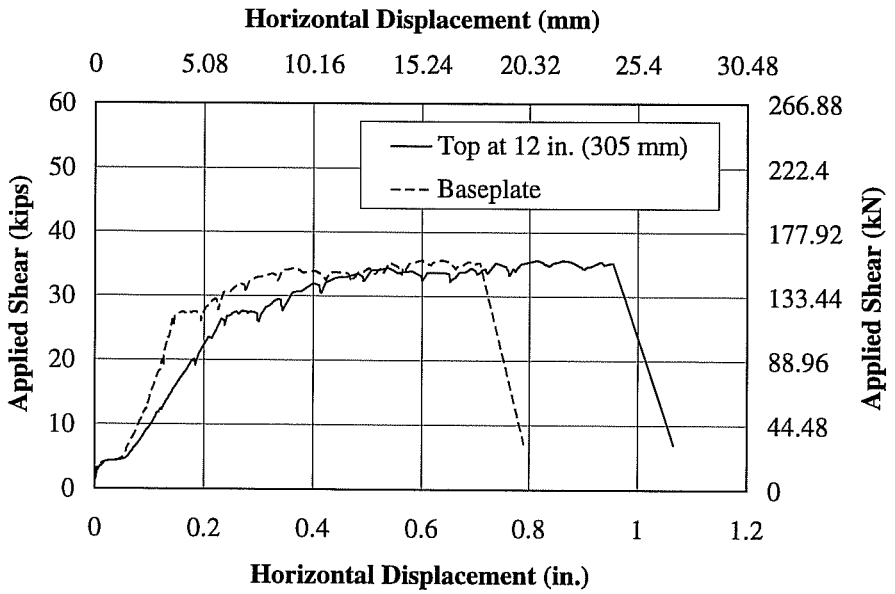
Horizontal Displacement (mm)
0
5.08
10.16
15.24
20.32
25.4
30.48
Top at 12 in. (305 mm)
Baseplate
Applied Shear (kips)
60
50
40
30
20
10
0
Applied Shear (kN)
266.88
222.4
177.92
133.44
88.96
44.48
0
0
0.2
0.4
0.6
0.8
1
1.2
Horizontal Displacement (in.)

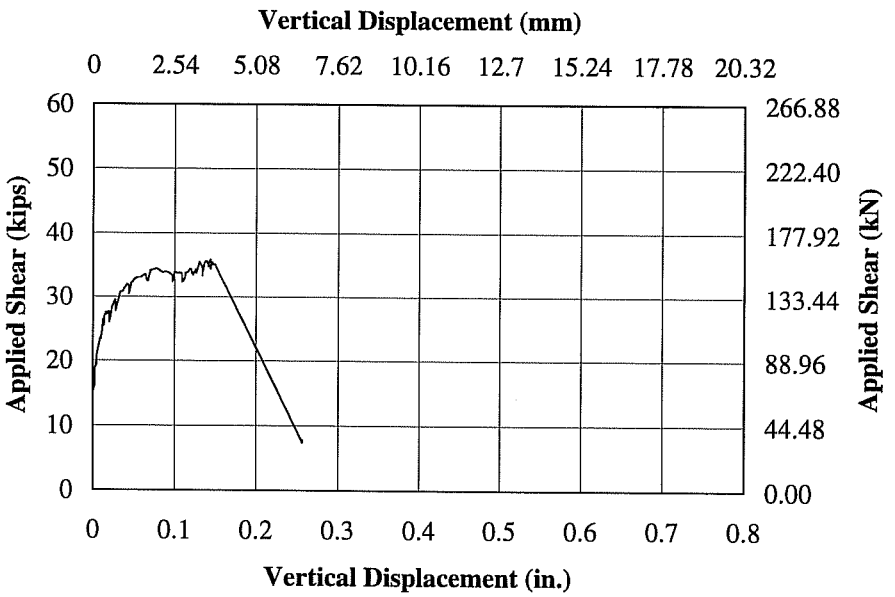
Vertical Displacement (mm)
0
2.54
5.08
7.62
10.16
12.7
15.24
17.78
20.32
Applied Shear (kips)
60
50
40
30
20
10
0
Applied Shear (kN)
266.88
222.40
177.92
133.44
88.96
44.48
0.00
0
0.1
0.2
0.3
0.4
0.5
0.6
0.7
0.8
Vertical Displacement (in.)

Test 4411

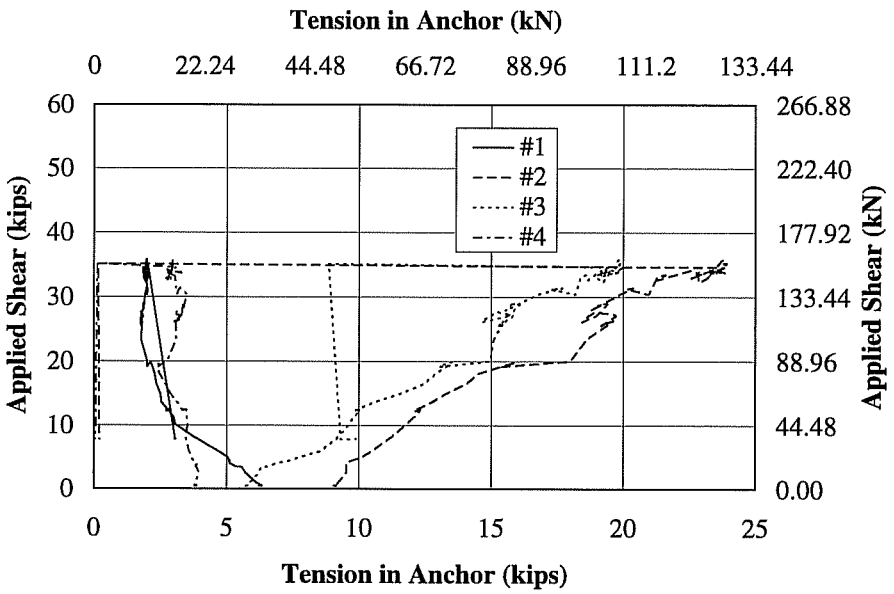
Tension in Anchor (kN)
0
22.24
44.48
66.72
88.96
111.2
133.44
60
50
40
30
20
10
0
266.88
222.40
177.92
133.44
88.96
44.48
0.00
#1
#2
#3
#4
Applied Shear (kips)
Applied Shear (kN)
0
5
10
15
20
25
Tension in Anchor (kips)

Test 4412

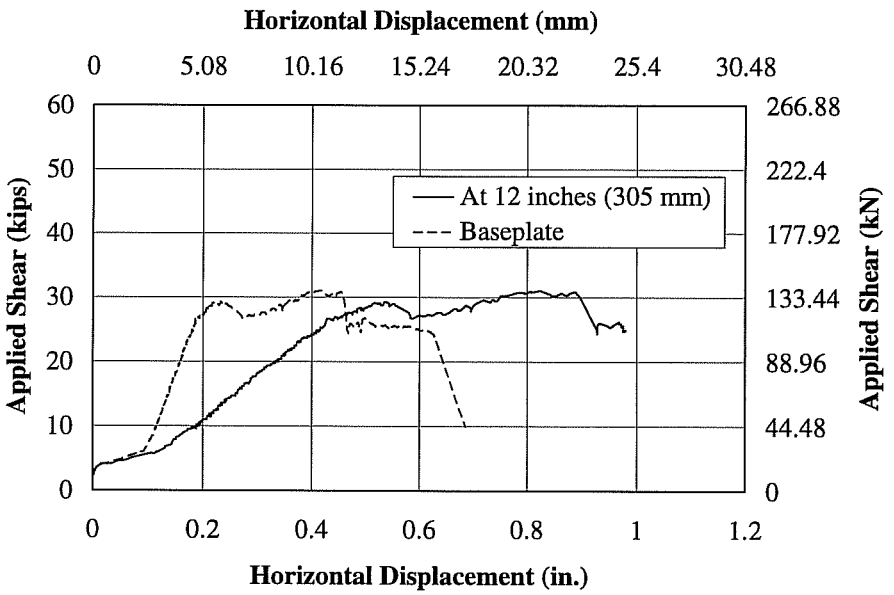
Horizontal Displacement (mm)
0
5.08
10.16
15.24
20.32
25.4
30.48
60
50
40
30
20
10
0
266.88
222.4
177.92
133.44
88.96
44.48
0
At 12 inches (305 mm)
Baseplate
Applied Shear (kips)
Applied Shear (kN)
0
0.2
0.4
0.6
0.8
1
1.2
Horizontal Displacement (in.)

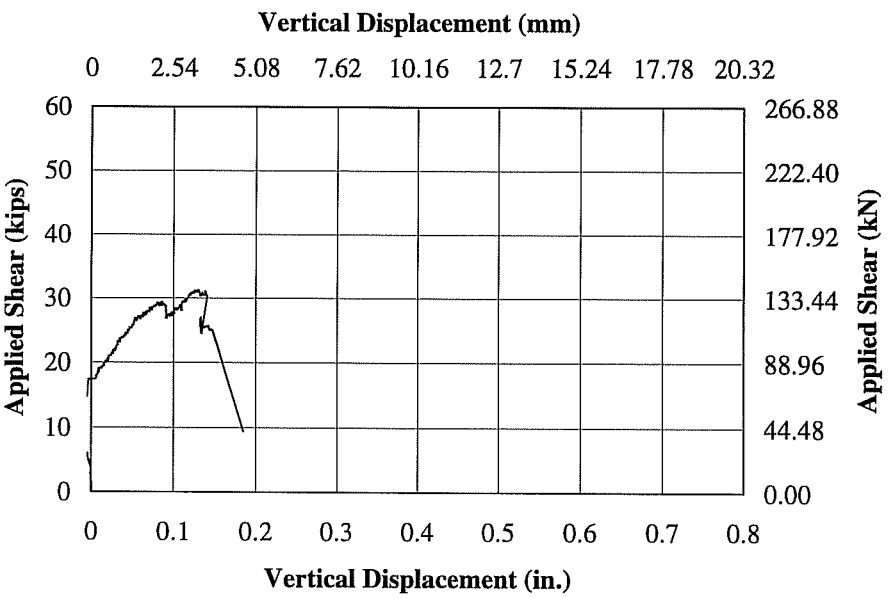
Vertical Displacement (mm)
0
2.54
5.08
7.62
10.16
12.7
15.24
17.78
20.32
60
50
40
30
20
10
0
266.88
222.40
177.92
133.44
88.96
44.48
0.00
Applied Shear (kips)
Applied Shear (kN)
0
0.1
0.2
0.3
0.4
0.5
0.6
0.7
0.8
Vertical Displacement (in.)

Test 4412

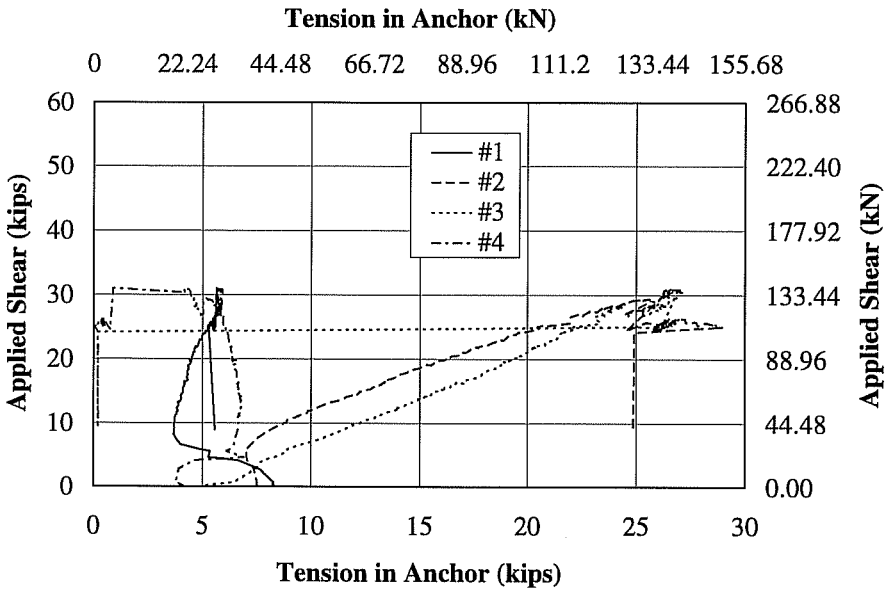
Tension in Anchor (kN)
0
22.24
44.48
66.72
88.96
111.2
133.44
155.68
60
50
40
30
20
10
0
266.88
222.40
177.92
133.44
88.96
44.48
0.00
#1
#2
#3
#4
Applied Shear (kips)
Applied Shear (kN)
0
5
10
15
20
25
30
Tension in Anchor (kips)

Test 4513

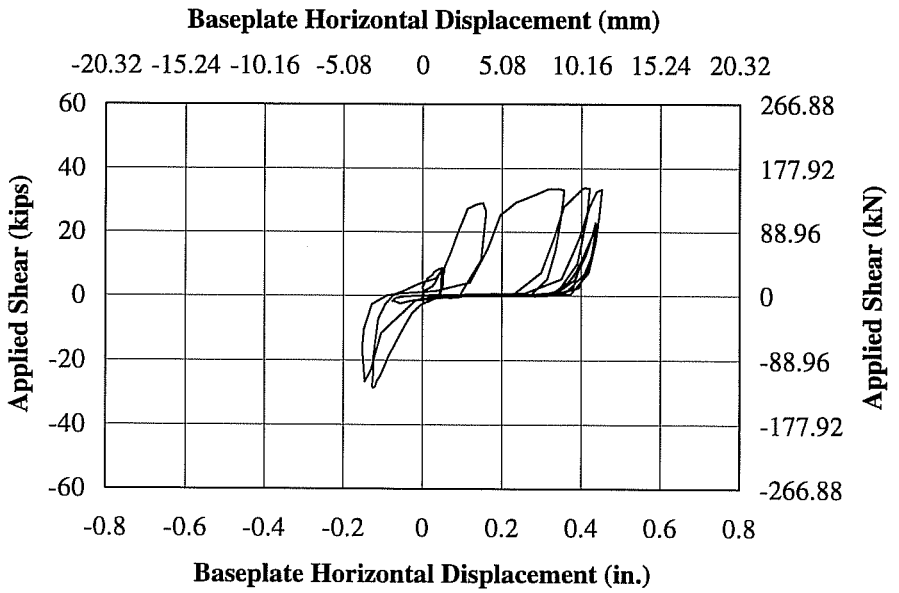
Baseplate Horizontal Displacement (mm)
-20.32 -15.24 -10.16 -5.08 0 5.08 10.16 15.24 20.32
60
40
20
0
-20
-40
-60
266.88
177.92
88.96
0
-88.96
-177.92
-266.88
Applied Shear (kips)
Applied Shear (kN)
-0.8 -0.6 -0.4 -0.2 0 0.2 0.4 0.6 0.8
Baseplate Horizontal Displacement (in.)

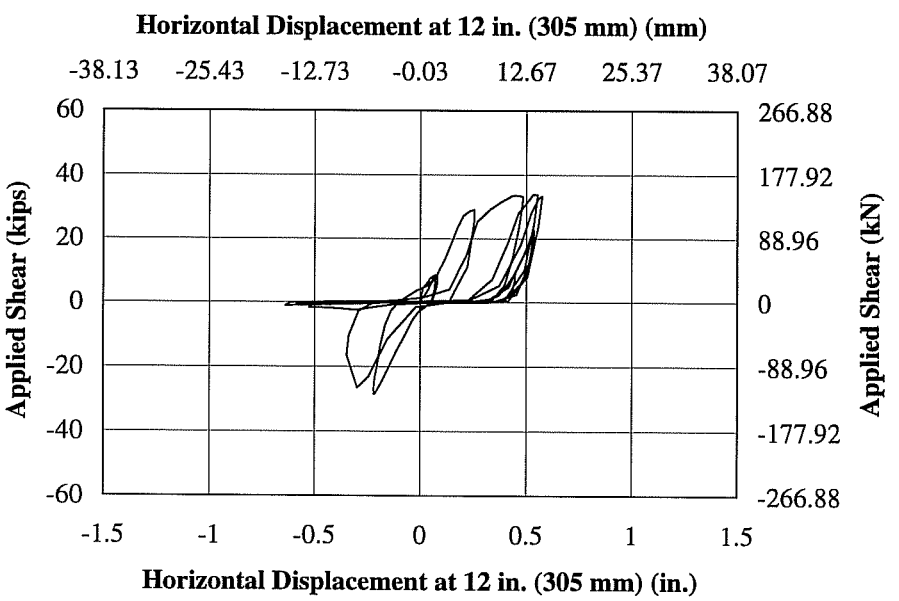
Horizontal Displacement at 12 in. (305 mm) (mm)
-38.13 -25.43 -12.73 -0.03 12.67 25.37 38.07
60
40
20
0
-20
-40
-60
266.88
177.92
88.96
0
-88.96
-177.92
-266.88
Applied Shear (kips)
Applied Shear (kN)
-1.5 -1 -0.5 0 0.5 1 1.5
Horizontal Displacement at 12 in. (305 mm) (in.)

Test 4513

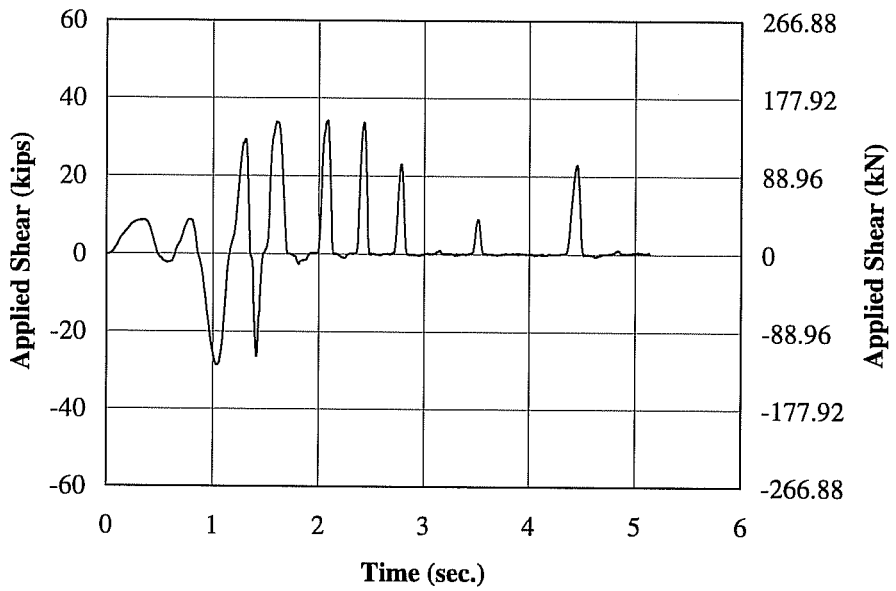
60
40
20
0
-20
-40
-60
266.88
177.92
88.96
0
-88.96
-177.92
-266.88
0
1
2
3
4
5
6
Applied Shear (kips)
Applied Shear (kN)
Time (sec.)

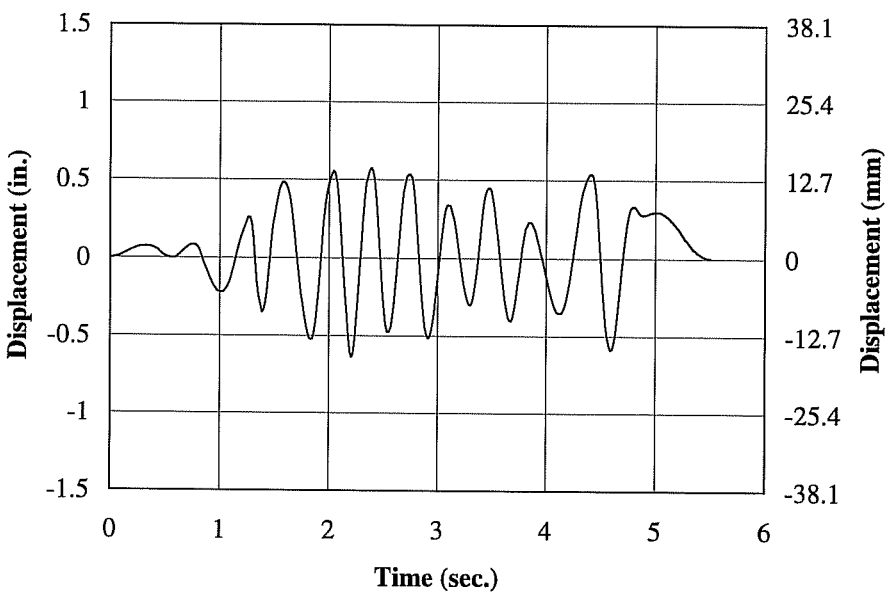
1.5
1
0.5
0
-0.5
-1
-1.5
38.1
25.4
12.7
0
-12.7
-25.4
-38.1
0
1
2
3
4
5
6
Displacement (in.)
Displacement (mm)
Time (sec.)

Test 4513

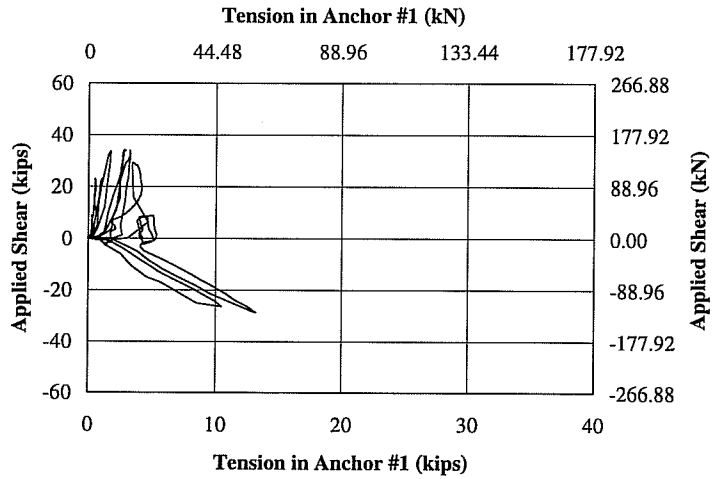
Tension in Anchor #1 (kN)
0
44.48
88.96
133.44
177.92
60
40
20
0
-20
-40
-60
266.88
177.92
88.96
0.00
-88.96
-177.92
-266.88
Applied Shear (kips)
Applied Shear (kN)
0
10
20
30
40
Tension in Anchor #1 (kips)

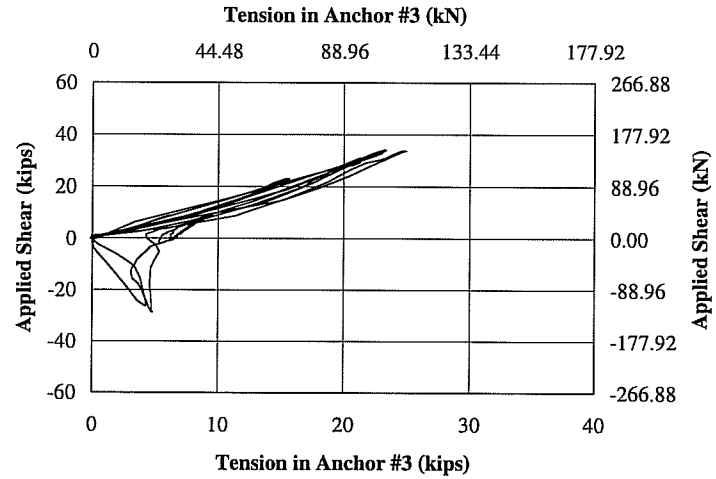
Tension in Anchor #3 (kN)
0
44.48
88.96
133.44
177.92
60
40
20
0
-20
-40
-60
266.88
177.92
88.96
0.00
-88.96
-177.92
-266.88
Applied Shear (kips)
Applied Shear (kN)
0
10
20
30
40
Tension in Anchor #3 (kips)

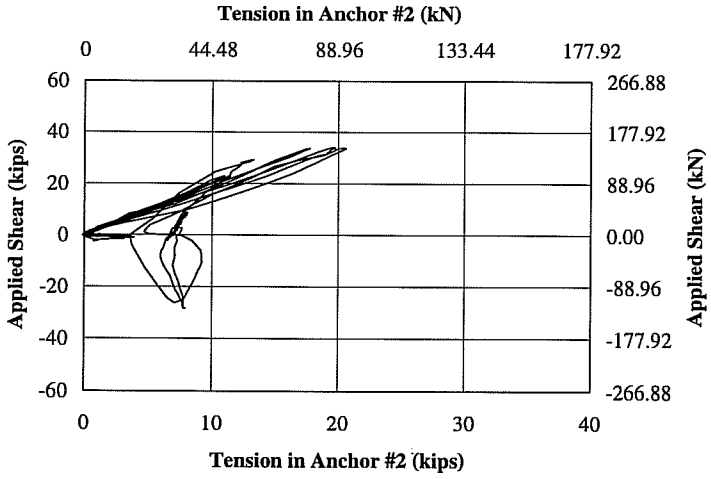
Tension in Anchor #2 (kN)
0
44.48
88.96
133.44
177.92
60
40
20
0
-20
-40
-60
266.88
177.92
88.96
0.00
-88.96
-177.92
-266.88
Applied Shear (kips)
Applied Shear (kN)
0
10
20
30
40
Tension in Anchor #2 (kips)

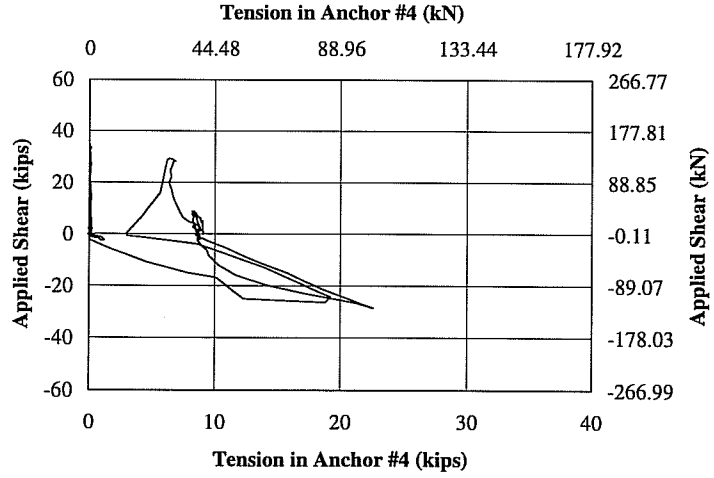
Tension in Anchor #4 (kN)
0
44.48
88.96
133.44
177.92
60
40
20
0
-20
-40
-60
266.77
177.81
88.85
-0.11
-89.07
-178.03
-266.99
Applied Shear (kips)
Applied Shear (kN)
0
10
20
30
40
Tension in Anchor #4 (kips)

Test 4514

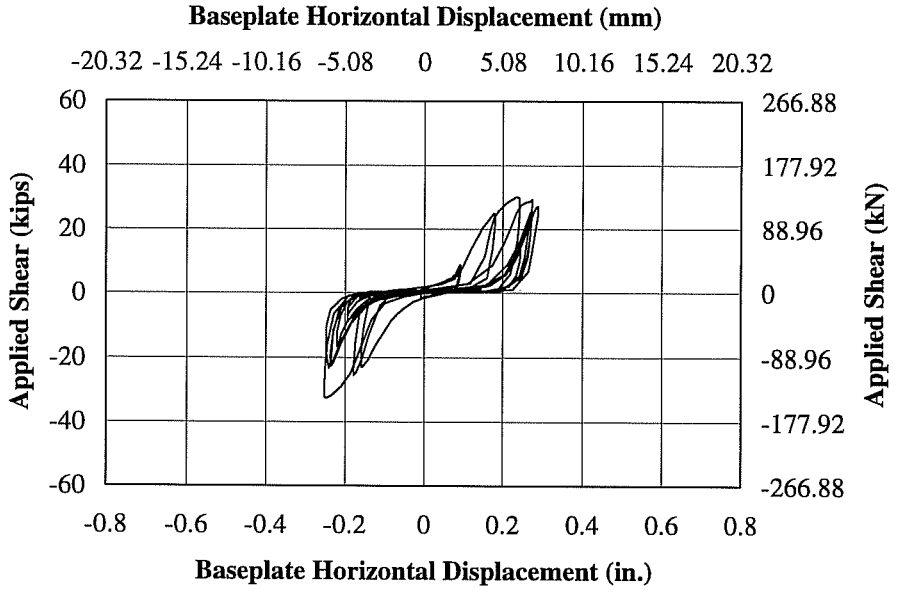
Baseplate Horizontal Displacement (mm)
-20.32 -15.24 -10.16 -5.08 0 5.08 10.16 15.24 20.32
60
40
20
0
-20
-40
-60
266.88
177.92
88.96
0
-88.96
-177.92
-266.88
Applied Shear (kips)
Applied Shear (kN)
-0.8 -0.6 -0.4 -0.2 0 0.2 0.4 0.6 0.8
Baseplate Horizontal Displacement (in.)

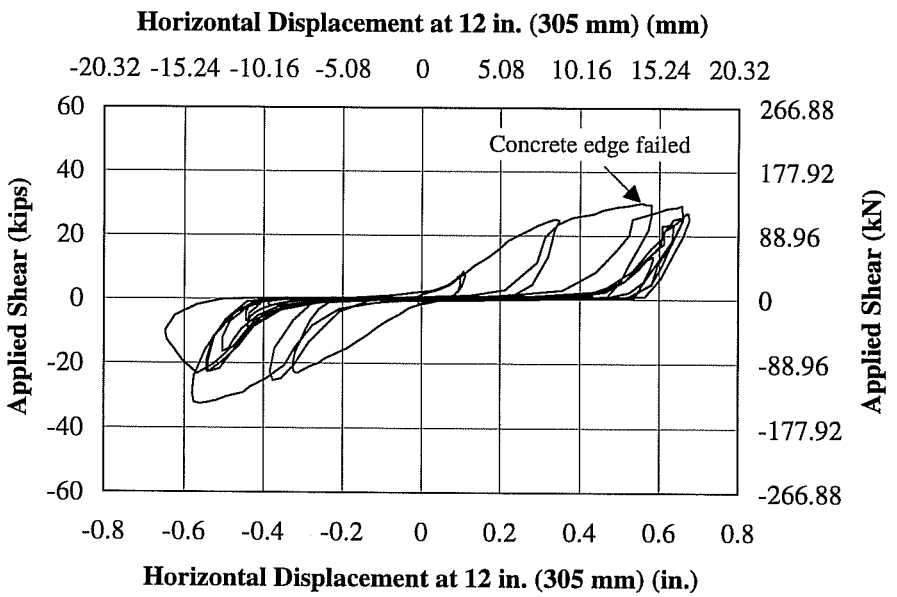
Horizontal Displacement at 12 in. (305 mm) (mm)
-20.32 -15.24 -10.16 -5.08 0 5.08 10.16 15.24 20.32
60
40
20
0
-20
-40
-60
266.88
177.92
88.96
0
-88.96
-177.92
-266.88
Concrete edge failed
Applied Shear (kips)
Applied Shear (kN)
-0.8 -0.6 -0.4 -0.2 0 0.2 0.4 0.6 0.8
Horizontal Displacement at 12 in. (305 mm) (in.)

Test 4514

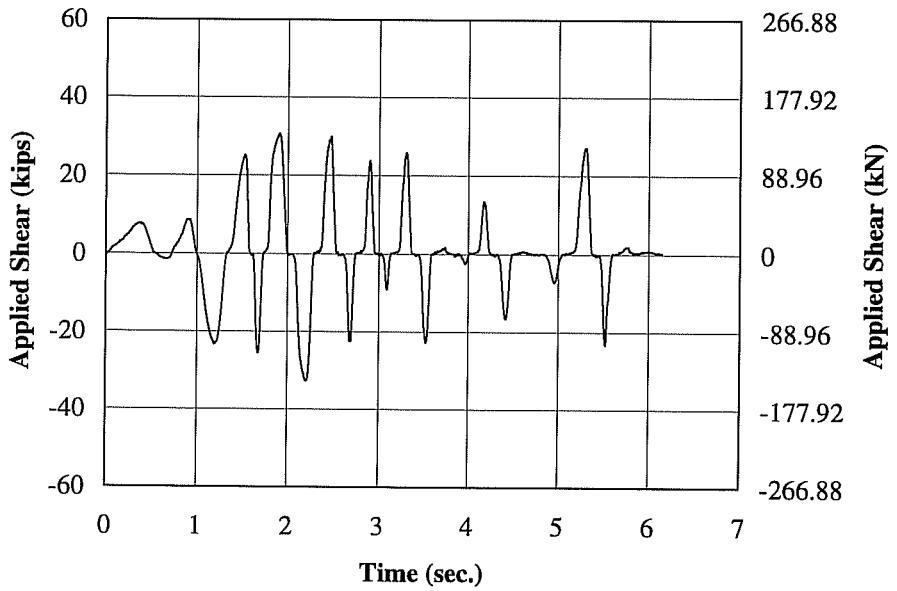
60
40
20
0
-20
-40
-60
266.88
177.92
88.96
0
-88.96
-177.92
-266.88
0 1 2 3 4 5 6 7
Applied Shear (kips)
Applied Shear (kN)
Time (sec.)

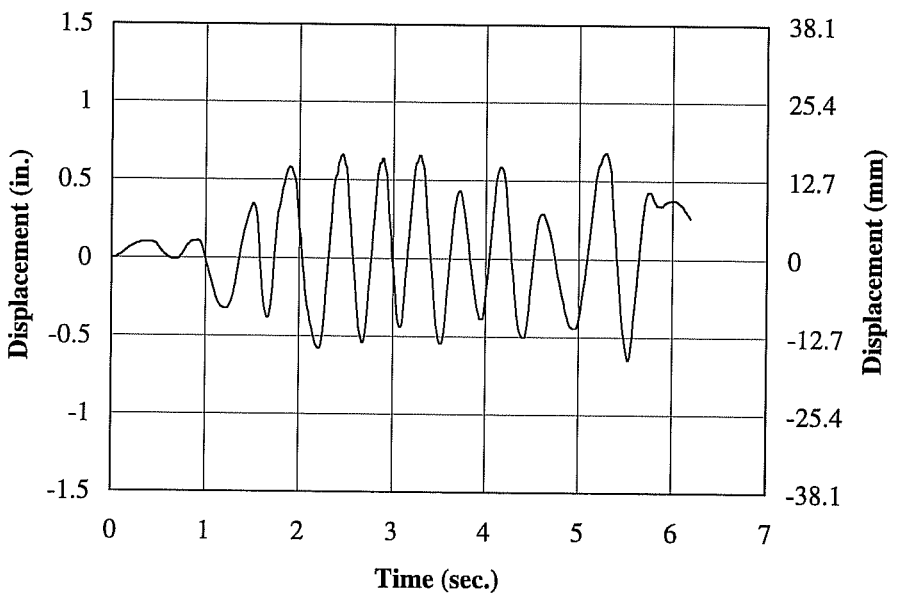
1.5
1
0.5
0
-0.5
-1
-1.5
38.1
25.4
12.7
0
-12.7
-25.4
-38.1
0 1 2 3 4 5 6 7
Displacement (in.)
Displacement (mm)
Time (sec.)

Test 4514

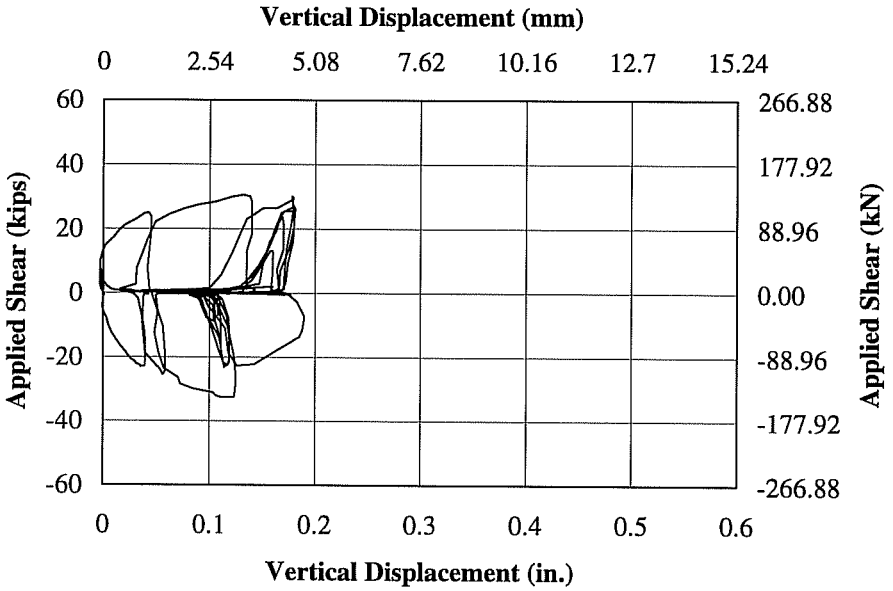
Vertical Displacement (mm)
0
2.54
5.08
7.62
10.16
12.7
15.24
60
40
20
0
-20
-40
-60
266.88
177.92
88.96
0.00
-88.96
-177.92
-266.88
Applied Shear (kips)
Applied Shear (kN)
0
0.1
0.2
0.3
0.4
0.5
0.6
Vertical Displacement (in.)

Test 4514

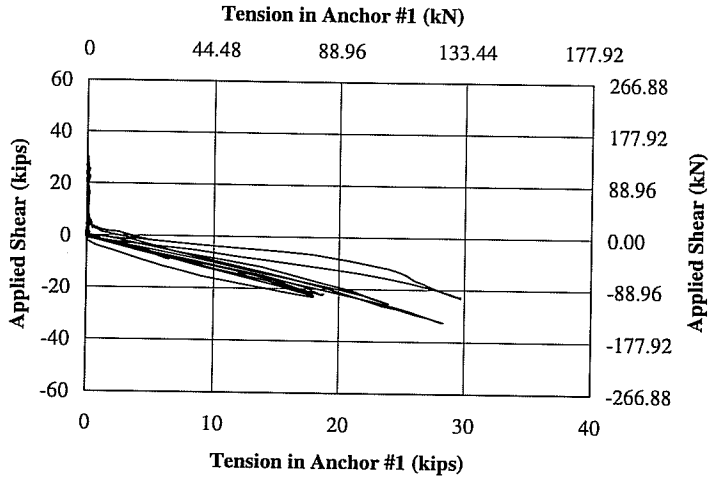
Tension in Anchor #1 (kN)
0
44.48
88.96
133.44
177.92
60
40
20
0
-20
-40
-60
266.88
177.92
88.96
0.00
-88.96
-177.92
-266.88
Applied Shear (kips)
Applied Shear (kN)
0
10
20
30
40
Tension in Anchor #1 (kips)

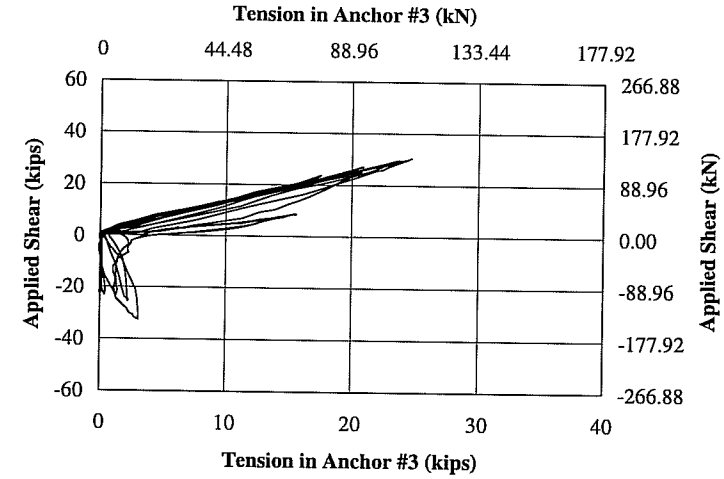
Tension in Anchor #3 (kN)
0
44.48
88.96
133.44
177.92
60
40
20
0
-20
-40
-60
266.88
177.92
88.96
0.00
-88.96
-177.92
-266.88
Applied Shear (kips)
Applied Shear (kN)
0
10
20
30
40
Tension in Anchor #3 (kips)

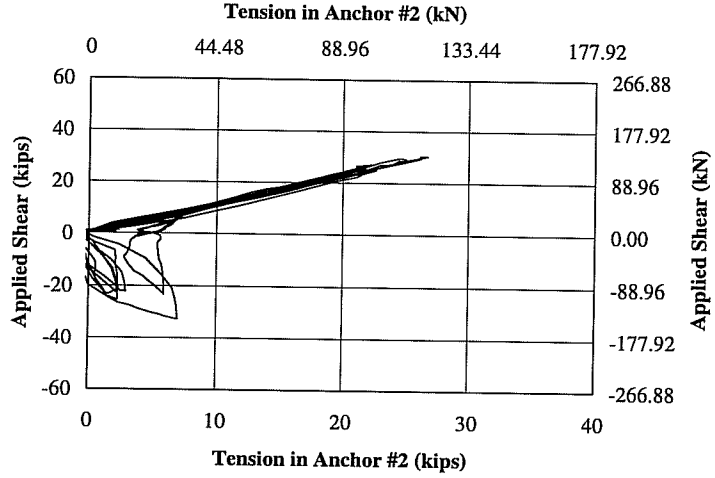
Tension in Anchor #2 (kN)
0
44.48
88.96
133.44
177.92
60
40
20
0
-20
-40
-60
266.88
177.92
88.96
0.00
-88.96
-177.92
-266.88
Applied Shear (kips)
Applied Shear (kN)
0
10
20
30
40
Tension in Anchor #2 (kips)

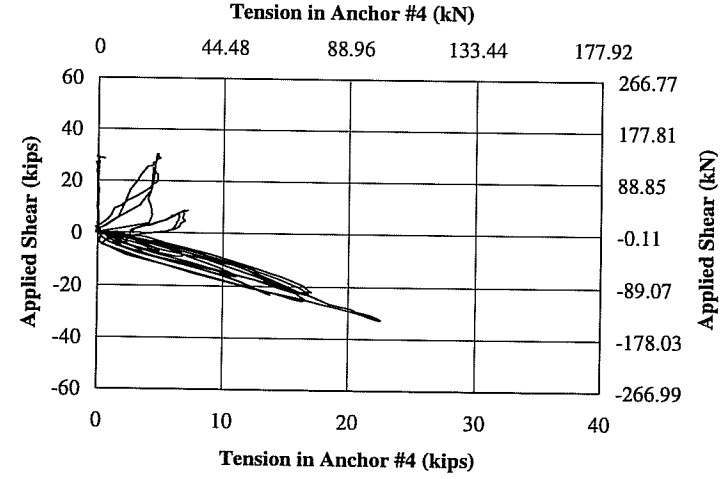
Tension in Anchor #4 (kN)
0
44.48
88.96
133.44
177.92
60
40
20
0
-20
-40
-60
266.77
177.81
88.85
-0.11
-89.07
-178.03
-266.99
Applied Shear (kips)
Applied Shear (kN)
0
10
20
30
40
Tension in Anchor #4 (kips)

Test 4615

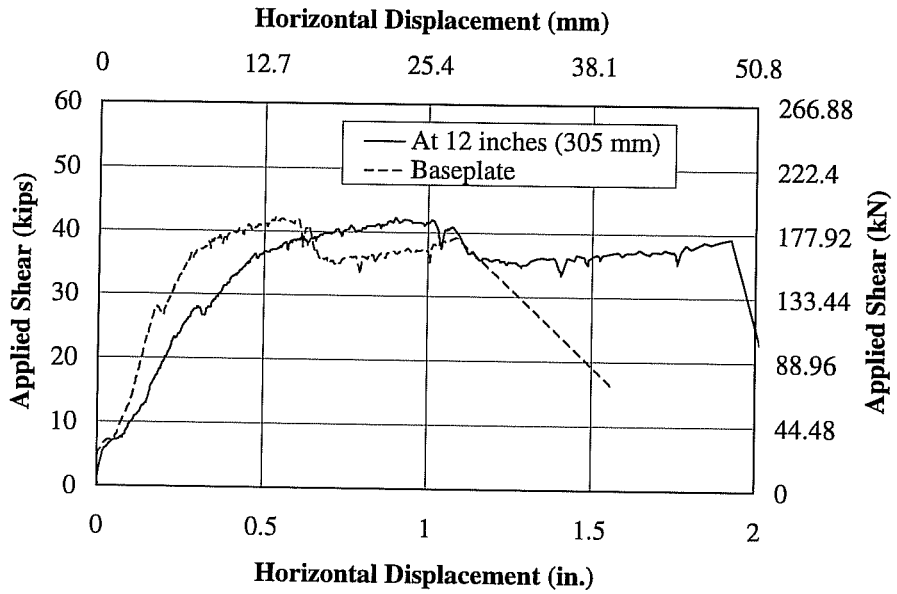
Horizontal Displacement (mm)
0
12.7
25.4
38.1
50.8
60
50
40
30
20
10
0
266.88
222.4
177.92
133.44
88.96
44.48
0
At 12 inches (305 mm)
Baseplate
Applied Shear (kips)
Applied Shear (kN)
0
0.5
1
1.5
2
Horizontal Displacement (in.)

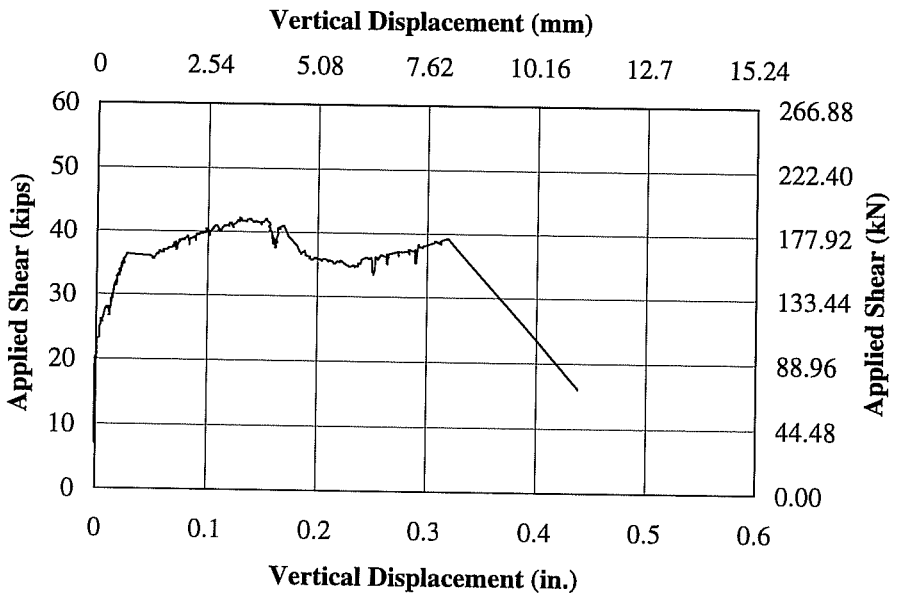
Vertical Displacement (mm)
0
2.54
5.08
7.62
10.16
12.7
15.24
60
50
40
30
20
10
0
266.88
222.40
177.92
133.44
88.96
44.48
0.00
Applied Shear (kips)
Applied Shear (kN)
0
0.1
0.2
0.3
0.4
0.5
0.6
Vertical Displacement (in.)

Test 4615

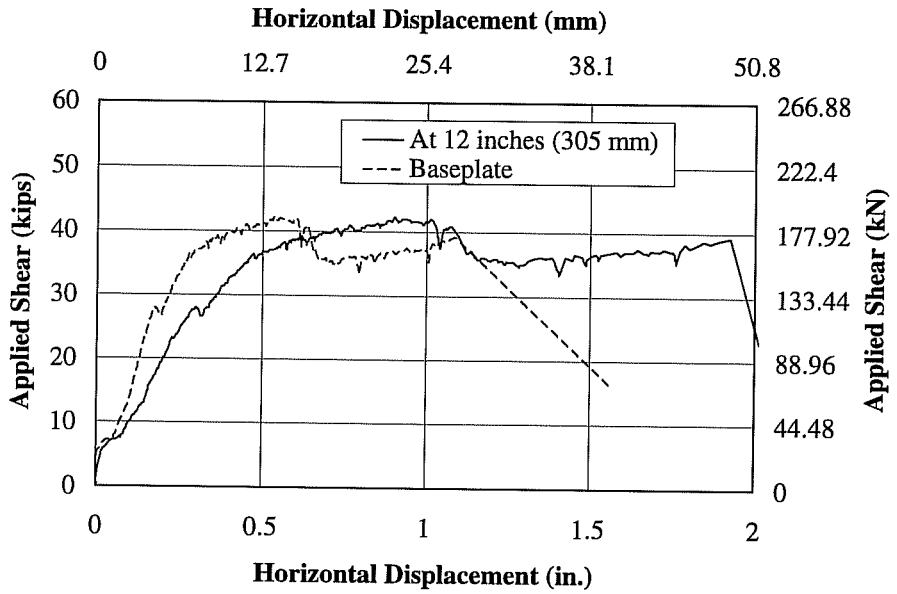
Horizontal Displacement (mm)
0
12.7
25.4
38.1
50.8
60
50
40
30
20
10
0
266.88
222.4
177.92
133.44
88.96
44.48
0
At 12 inches (305 mm)
Baseplate
Applied Shear (kips)
Applied Shear (kN)
0
0.5
1
1.5
2
Horizontal Displacement (in.)

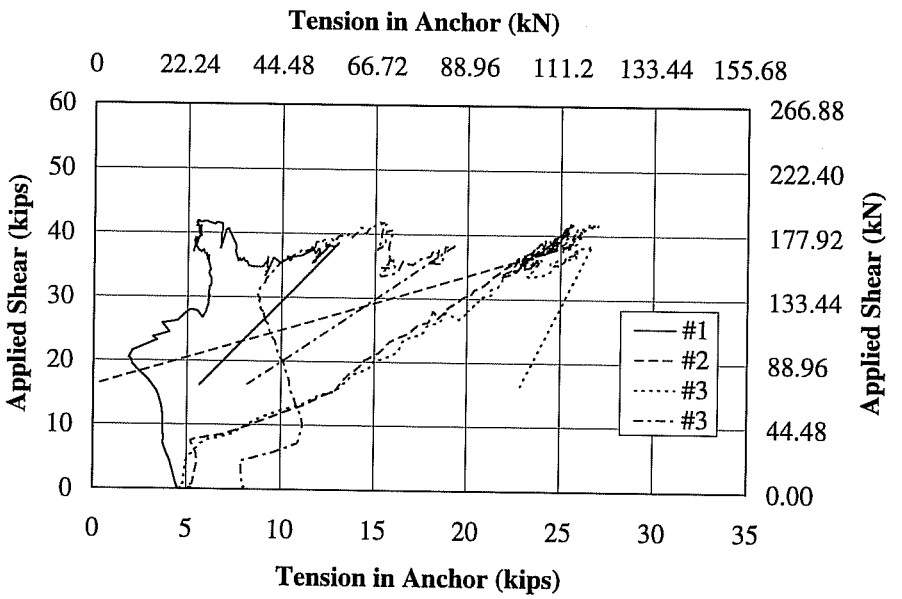
Tension in Anchor (kN)
0
22.24
44.48
66.72
88.96
111.2
133.44
155.68
60
50
40
30
20
10
0
266.88
222.40
177.92
133.44
88.96
44.48
0.00
#1
#2
#3
#3
Applied Shear (kips)
Applied Shear (kN)
0
5
10
15
20
25
30
35
Tension in Anchor (kips)

Test 4616

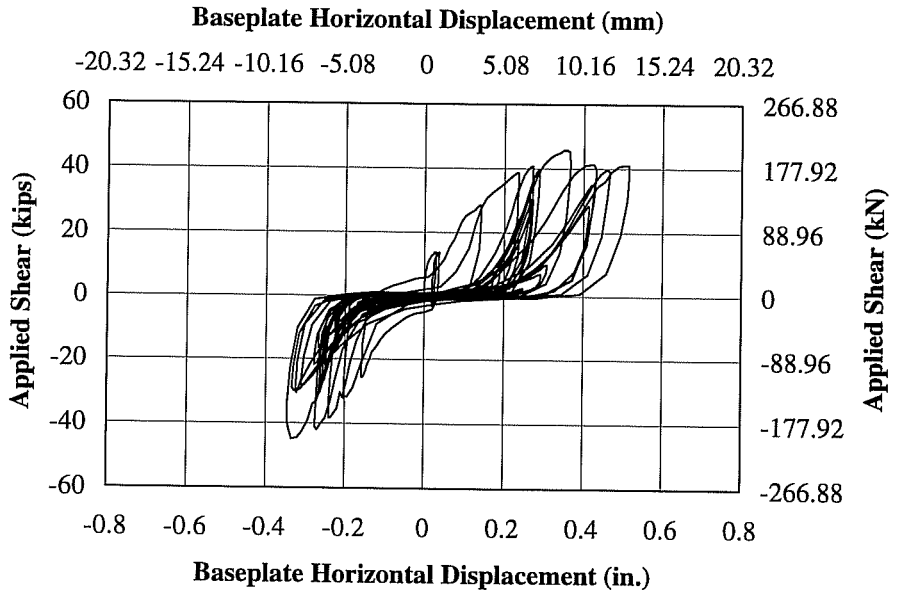
Baseplate Horizontal Displacement (mm)
-20.32 -15.24 -10.16 -5.08 0 5.08 10.16 15.24 20.32
60
40
20
0
-20
-40
-60
266.88
177.92
88.96
0
-88.96
-177.92
-266.88
Applied Shear (kips)
Applied Shear (kN)
-0.8 -0.6 -0.4 -0.2 0 0.2 0.4 0.6 0.8
Baseplate Horizontal Displacement (in.)

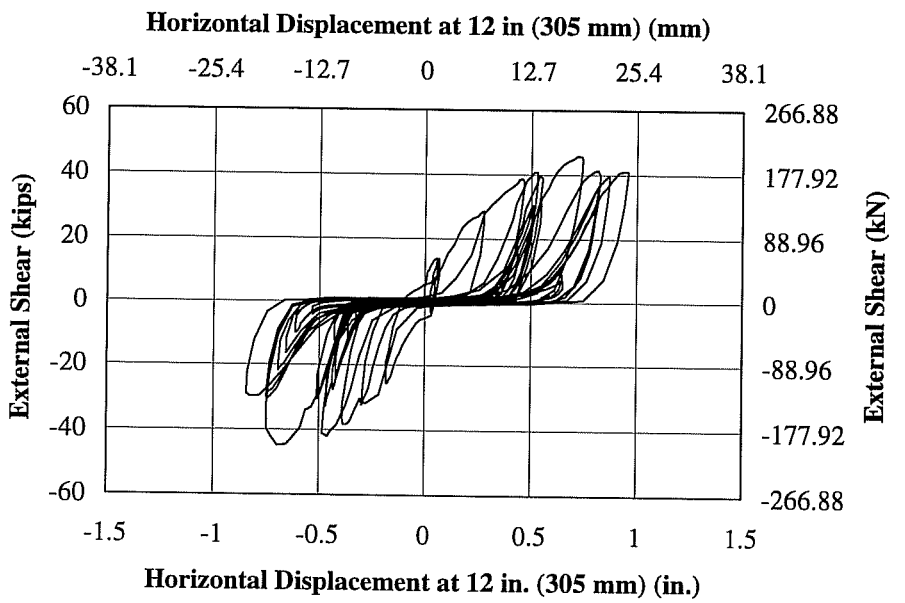
Horizontal Displacement at 12 in (305 mm) (mm)
-38.1 -25.4 -12.7 0 12.7 25.4 38.1
60
40
20
0
-20
-40
-60
266.88
177.92
88.96
0
-88.96
-177.92
-266.88
External Shear (kips)
External Shear (kN)
-1.5 -1 -0.5 0 0.5 1 1.5
Horizontal Displacement at 12 in. (305 mm) (in.)

Test 4616

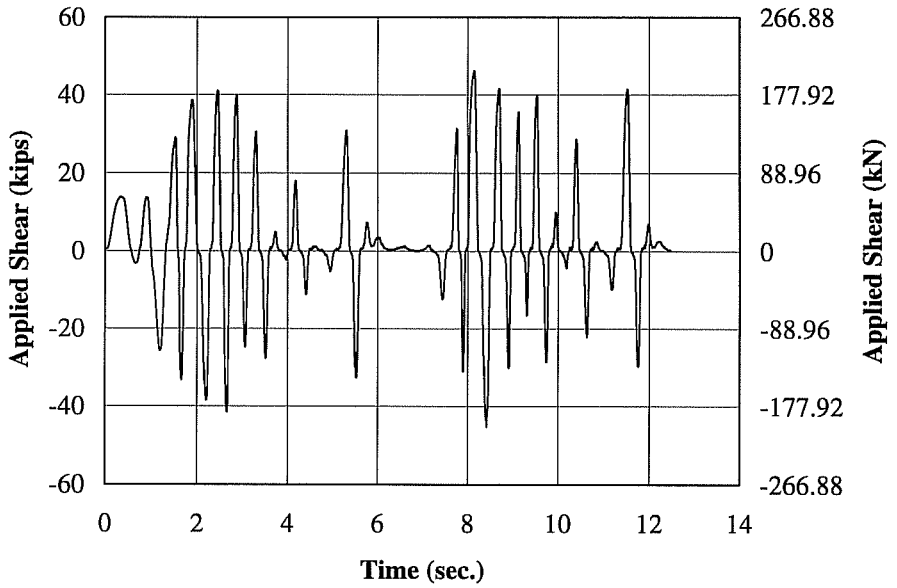
60
40
20
0
-20
-40
-60
266.88
177.92
88.96
0
-88.96
-177.92
-266.88
0
2
4
6
8
10
12
14
Applied Shear (kips)
Applied Shear (kN)
Time (sec.)

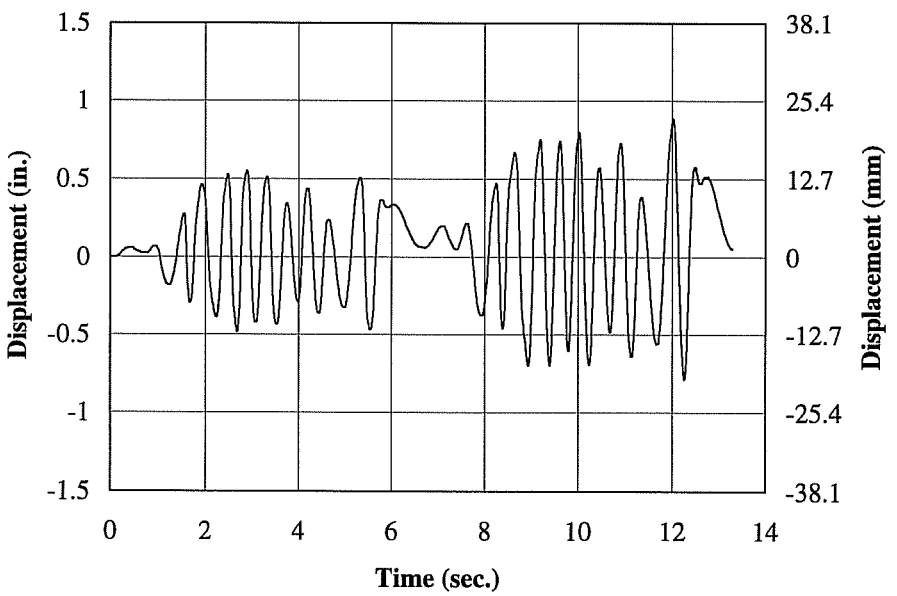
1.5
1
0.5
0
-0.5
-1
-1.5
38.1
25.4
12.7
0
-12.7
-25.4
-38.1
0
2
4
6
8
10
12
14
Displacement (in.)
Displacement (mm)
Time (sec.)

Test 4616

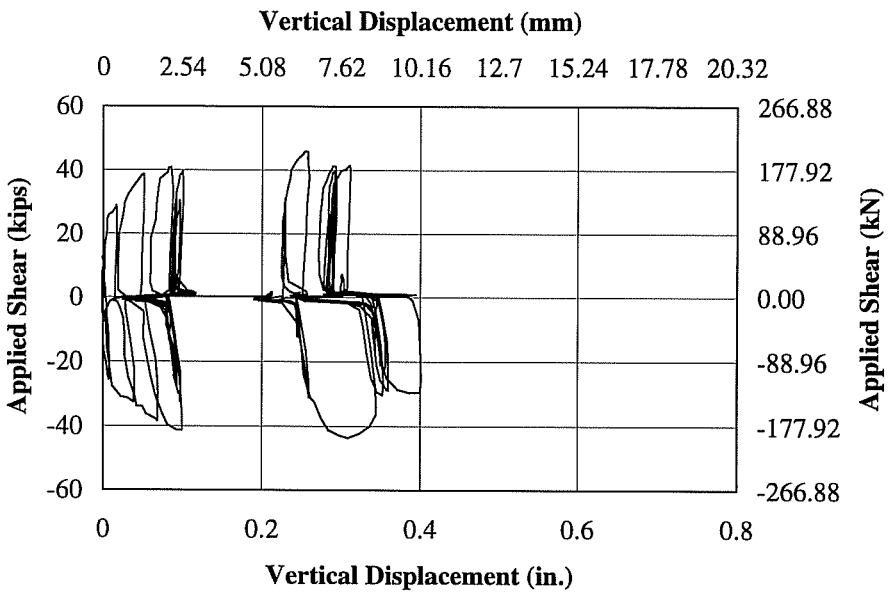
Vertical Displacement (mm)
0
2.54
5.08
7.62
10.16
12.7
15.24
17.78
20.32
60
40
20
0
-20
-40
-60
266.88
177.92
88.96
0.00
-88.96
-177.92
-266.88
Applied Shear (kips)
Applied Shear (kN)
0
0.2
0.4
0.6
0.8
Vertical Displacement (in.)

Test 4616

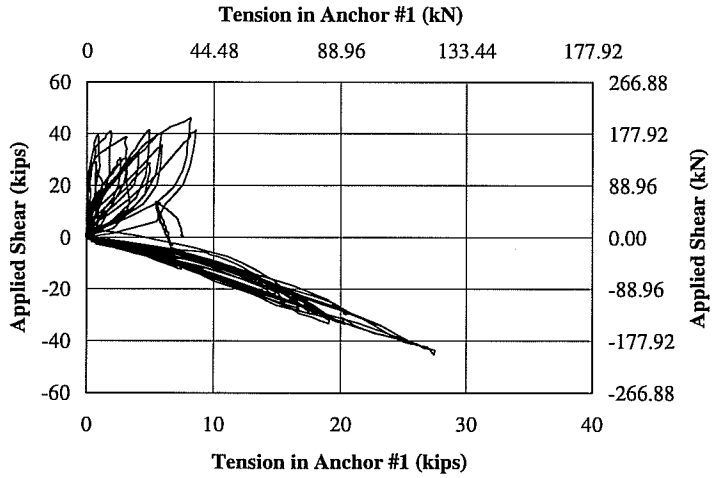
Tension in Anchor #1 (kN)
0 44.48 88.96 133.44 177.92
60 40 20 0 -20 -40 -60
266.88 177.92 88.96 0.00 -88.96 -177.92 -266.88
Applied Shear (kips)
Applied Shear (kN)
0 10 20 30 40
Tension in Anchor #1 (kips)

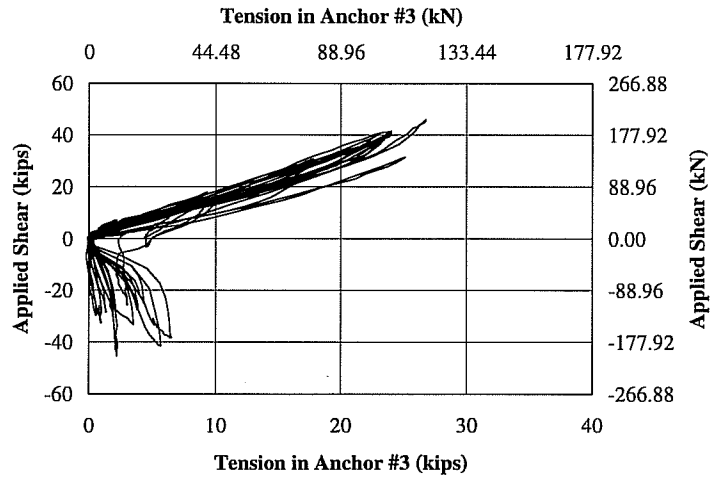
Tension in Anchor #3 (kN)
0 44.48 88.96 133.44 177.92
60 40 20 0 -20 -40 -60
266.88 177.92 88.96 0.00 -88.96 -177.92 -266.88
Applied Shear (kips)
Applied Shear (kN)
0 10 20 30 40
Tension in Anchor #3 (kips)

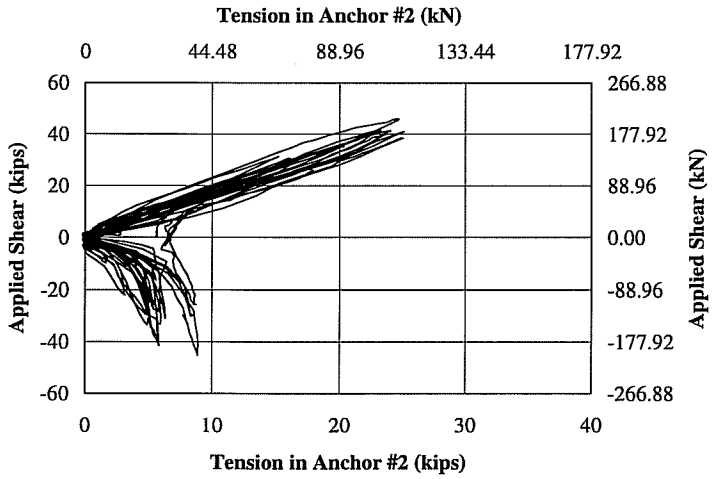
Tension in Anchor #2 (kN)
0 44.48 88.96 133.44 177.92
60 40 20 0 -20 -40 -60
266.88 177.92 88.96 0.00 -88.96 -177.92 -266.88
Applied Shear (kips)
Applied Shear (kN)
0 10 20 30 40
Tension in Anchor #2 (kips)

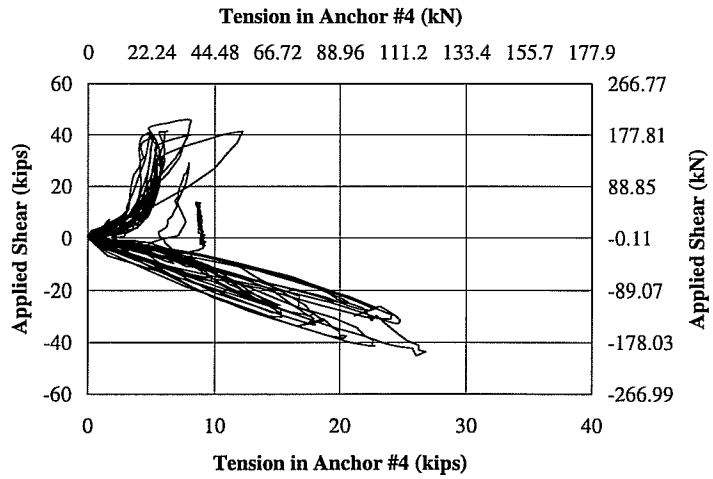
Tension in Anchor #4 (kN)
0 22.24 44.48 66.72 88.96 111.2 133.4 155.7 177.9
60 40 20 0 -20 -40 -60
266.77 177.81 88.85 -0.11 -89.07 -178.03 -266.99
Applied Shear (kips)
Applied Shear (kN)
0 10 20 30 40
Tension in Anchor #4 (kips)

Test 4617

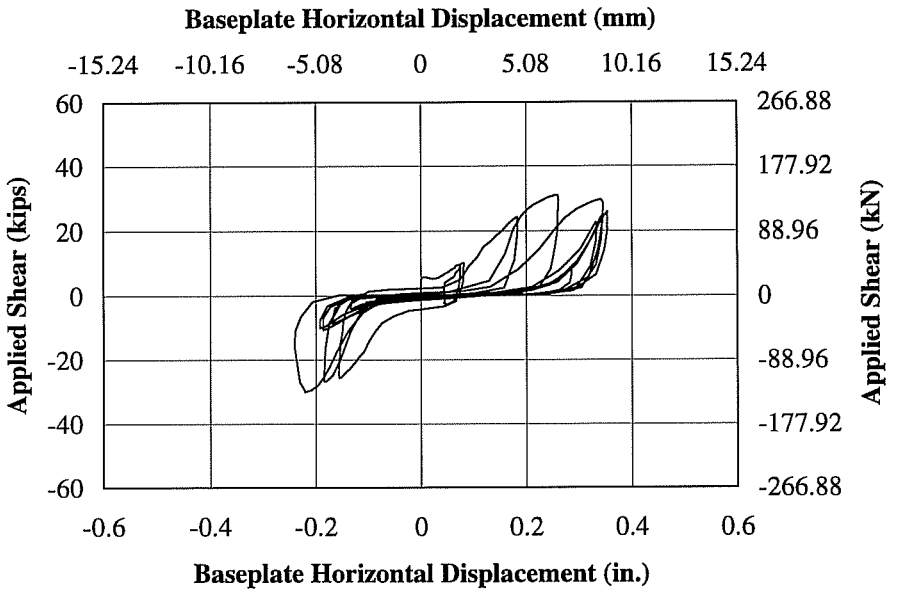
Baseplate Horizontal Displacement (mm)
-15.24 -10.16 -5.08 0 5.08 10.16 15.24
60 40 20 0 -20 -40 -60
Applied Shear (kips)
266.88 177.92 88.96 0 -88.96 -177.92 -266.88
Applied Shear (kN)
-0.6 -0.4 -0.2 0 0.2 0.4 0.6
Baseplate Horizontal Displacement (in.)

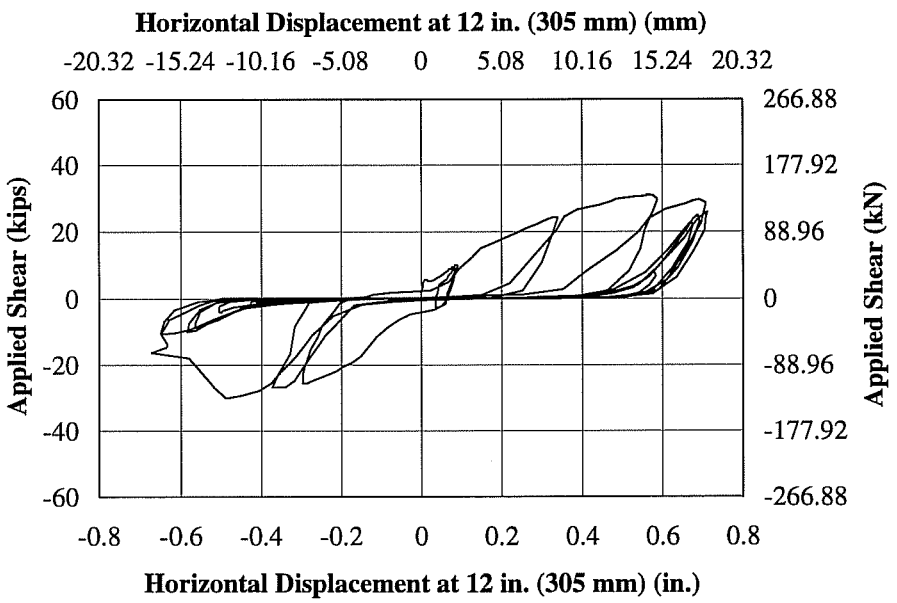
Horizontal Displacement at 12 in. (305 mm) (mm)
-20.32 -15.24 -10.16 -5.08 0 5.08 10.16 15.24 20.32
60 40 20 0 -20 -40 -60
Applied Shear (kips)
266.88 177.92 88.96 0 -88.96 -177.92 -266.88
Applied Shear (kN)
-0.8 -0.6 -0.4 -0.2 0 0.2 0.4 0.6 0.8
Horizontal Displacement at 12 in. (305 mm) (in.)

Test 4617

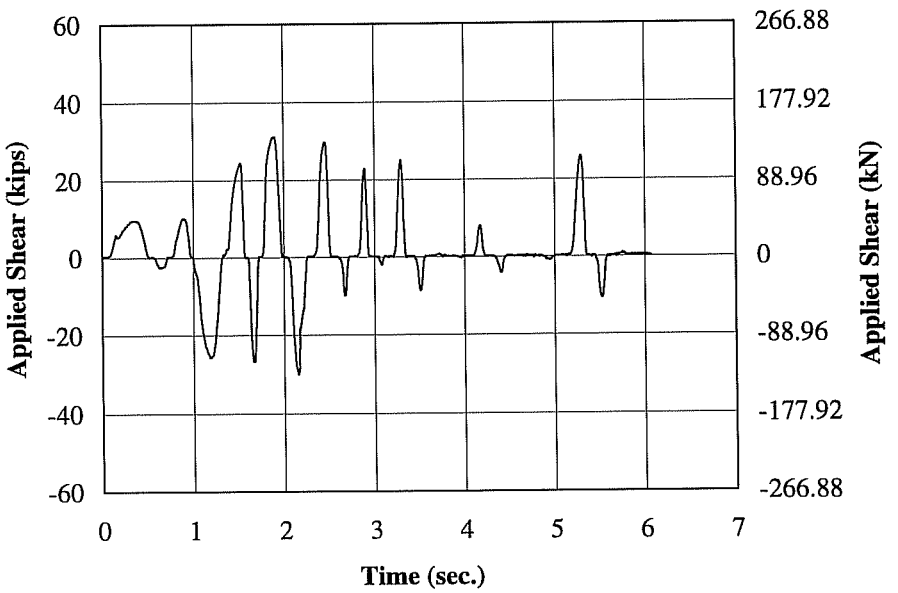
60
40
20
0
-20
-40
-60
266.88
177.92
88.96
0
-88.96
-177.92
-266.88
Applied Shear (kips)
Applied Shear (kN)
0 1 2 3 4 5 6 7
Time (sec.)

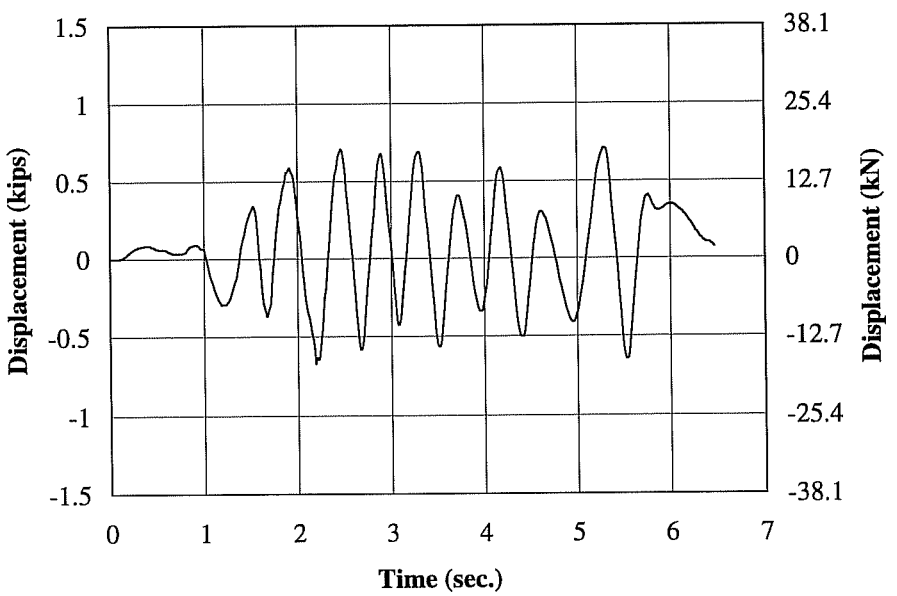
1.5
1
0.5
0
-0.5
-1
-1.5
38.1
25.4
12.7
0
-12.7
-25.4
-38.1
Displacement (kips)
Displacement (kN)
0 1 2 3 4 5 6 7
Time (sec.)

Test 4617

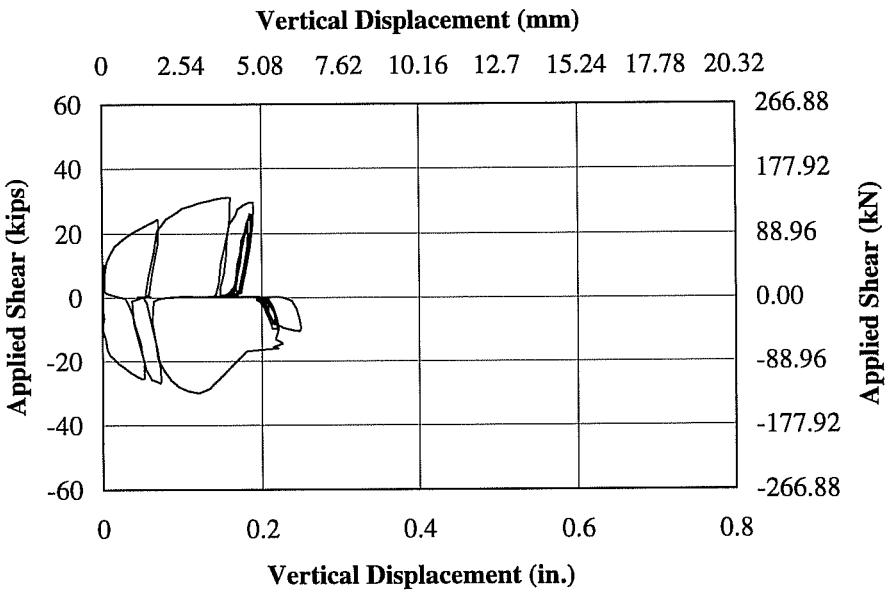
Vertical Displacement (mm)
0
2.54
5.08
7.62
10.16
12.7
15.24
17.78
20.32
60
40
20
0
-20
-40
-60
266.88
177.92
88.96
0.00
-88.96
-177.92
-266.88
Applied Shear (kips)
Applied Shear (kN)
0
0.2
0.4
0.6
0.8
Vertical Displacement (in.)

Test 4617

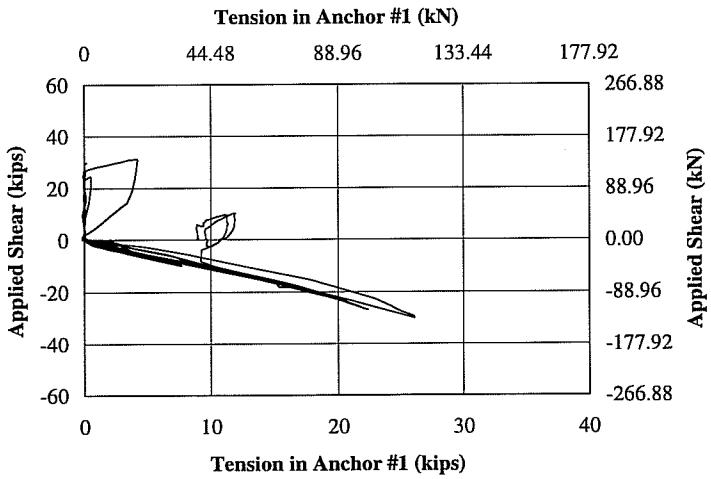
Tension in Anchor #1 (kN)
0
44.48
88.96
133.44
177.92
60
40
20
0
-20
-40
-60
266.88
177.92
88.96
0.00
-88.96
-177.92
-266.88
Applied Shear (kips)
Applied Shear (kN)
0
10
20
30
40
Tension in Anchor #1 (kips)

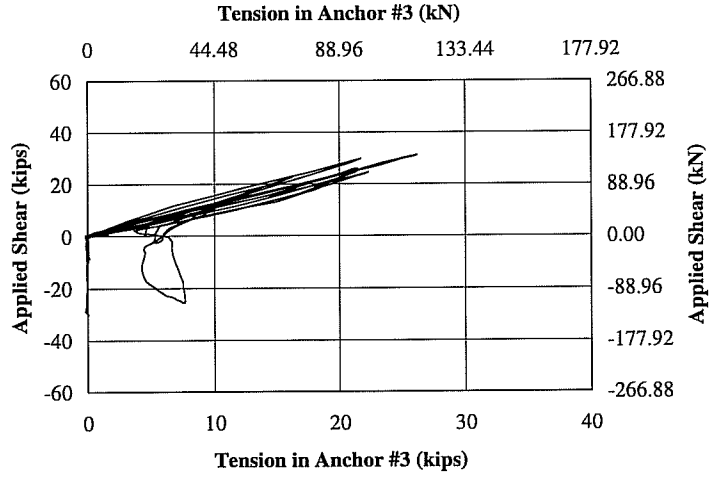
Tension in Anchor #3 (kN)
0
44.48
88.96
133.44
177.92
60
40
20
0
-20
-40
-60
266.88
177.92
88.96
0.00
-88.96
-177.92
-266.88
Applied Shear (kips)
Applied Shear (kN)
0
10
20
30
40
Tension in Anchor #3 (kips)

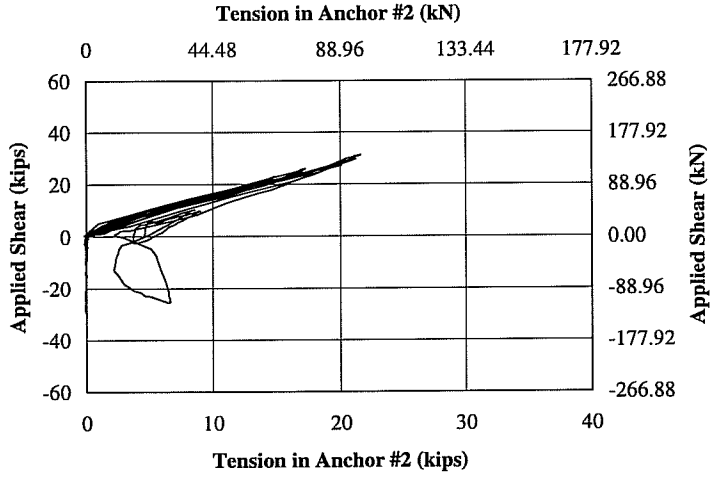
Tension in Anchor #2 (kN)
0
44.48
88.96
133.44
177.92
60
40
20
0
-20
-40
-60
266.88
177.92
88.96
0.00
-88.96
-177.92
-266.88
Applied Shear (kips)
Applied Shear (kN)
0
10
20
30
40
Tension in Anchor #2 (kips)

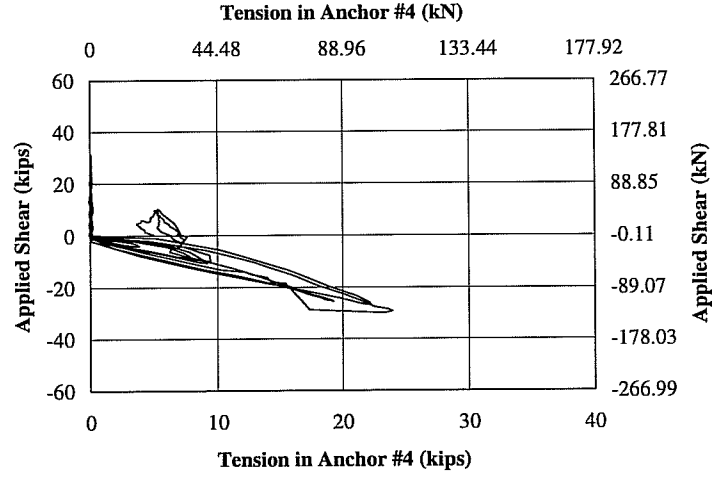
Tension in Anchor #4 (kN)
0
44.48
88.96
133.44
177.92
60
40
20
0
-20
-40
-60
266.77
177.81
88.85
-0.11
-89.07
-178.03
-266.99
Applied Shear (kips)
Applied Shear (kN)
0
10
20
30
40
Tension in Anchor #4 (kips)

Appendix E

Example of Input File for the BDA5 Program

Plastic Analysis of Anchor Group	Documentation of the input data file
90.0 304.8 0.0	load angle, eccentricity, and weight of anchor group
1,1,	Type of the baseplate, integration thickness for compression stresses in mm
355.6,304.8,	Dimensions of baseplate
2,	Number of anchor rows
50.8,291.6,0.,	first anchor row location, cross-sectional area, and gap
304.8,291.6,0.,	second anchor row location, cross-sectional area, and gap
2	Number of the load-displacement curve groups
1	1 = oblique load generated by program
1.80000 875.900 532.500	Exponent k1 of stress interaction, vertical, horizontal stress
1.80000 922.000 560.500	Exponent kM of stress interaction, vertical, horizontal stress
1.80000 875.900 532.500	Exponent kR of stress interaction, vertical, horizontal stress
7	Number of curves
0	load angle, load-displacement curve defined in following line
13.34 21.34 27.26 0.17	vertical displacements, and exponent
15.000	load angle, load-displacement curve defined in following two lines
7.370 9.070 9.550 0.4	horizontal displacements, exponent
7.533 10.33 10.88 0.2	vertical displacements, exponent
30.000	same
5.550 6.650 6.920 0.5	same
2.560 3.460 3.600 0.25	
45.000	
5.710 6.910 7.180 0.5	
1.450 2.000 2.060 0.25	
60.000	
5.600 6.400 6.570 0.60	
0.900 1.110 1.150 0.25	
75.000	
5.155 5.890 6.090 0.6	
0.450 0.550 0.570 0.25	
90.000	
4.500 5.690 5.900 0.6	
1	input for another anchor row
1.80000 875.900 532.500	
1.80000 922.000 560.500	
1.80000 875.900 532.500	

7				
0				
13.34	21.34	27.26	0.17	
15.000				
7.370	9.070	9.550	0.4	
7.533	10.33	10.88	0.2	
30.000				
5.550	6.650	6.920	0.5	
2.560	3.460	3.600	0.25	
45.000				
5.710	6.910	7.180	0.5	
1.450	2.000	2.060	0.25	
60.000				
5.600	6.400	6.570	0.6	
0.900	1.110	1.150	0.25	
75.000				
5.155	5.890	6.090	0.6	
0.450	0.550	0.570	0.25	
90.000				
4.500	5.690	5.900	0.6	
33.100	0.15			concrete compressive strength, friction coefficient
0.15E-4	1.00			relative displacement s/d, relative stress s/f_c
0.1E-8	1.00	1.00		allowable tolerance of the displacement at iterative determination of the point A and B in displacement-zone I, iteration-constant w^i (with i= 1, 2, and $0< w^i \leq 1.0$)
1.0E1	1.0E1	1.0E1		allowable tolerance of vertical, horizontal forces and balance of moment
0.60	0.50	0.60		iteration-constants of modified Newton's iteration procedure w_i (with i= 1, 2, 3 and $0 < w_i \leq 1.0$)
1.0E-3	1.0E-3	1.0E3		Step increment Δx_i for calculation
3	5.			3= calculation is controlled by baseplate rotation in radian, the maximum decrease in load to stop calculation
2				number of sets of load or displacement steps
0.6E-1	80			Load or displacement step, number of steps
8.E-2	30			same

Appendix F

Finite Element Program

```
      program sa0
      implicit real*8 (a-h,o-z)
      dimension a(30000),ia(25000)
      character*12 in,out
      logical yesno
      common /cntl/ isym,numel,iresol,nrhs,ntapeb,ntapeu,ntapel,
     *              ma,iwrt,iprint,ierr,nnegp,nposp,nrhsf,
     *              ib,iu,il,ifb,ifu,ifl,mbuf,mw,mkf,
     *              melem,mfwr,mb,mdof,mfw,mldest
      common /inds/ indr(30),indi(30)
      common /dims/ mncm,mndofn,mnip,mnsp,mnne,ndim,nmat,nn
      common /consts/ zero,one,two
      common /cycle/ icycle,iswitch,istep
      common /concrete/ ft,delta
      common /crack/ xx1,yy1,xx2,yy2,theta1,iie1
      common strmax
      data nra/30000/
      data nia/25000/
    1 write(*,110)
  110 format(1x,'enter input file name:')
      read(*,2) in
    2 format(a12)
      inquire(file=in,exist=yesno)
      if(yesno) go to 3
      write(*,200)
  200 format(1x,'input file does not exist.')
      go to 1
    3 write(*,300)
  300 format(1x,'enter output file name:')
      read(*,2) out
      inquire(file=out,exist=yesno)
      if(yesno) then
      write(*,400)
  400 format(1x,'output file already exists.')
      write(*,500)
  500 format(1x,'warning: unless you specify a different name, ',
     *          'the file will be overwritten.')
      write(*,600)
  600 format(1x,'enter output file name:')
      read(*,2) out
      endif
      open (unit=5,file=in,status='old')
      open (unit=50,file=out,status='unknown')
      open (unit=27,status='scratch',form='unformatted')
      open (unit=28,status='scratch',form='unformatted')
      open (unit=29,status='scratch',form='unformatted')
      read(5,*) irs
```

```
      if(irs.eq.0) then
      read(5,*) ndim
      write(50,10) ndim
   10 format(1x,'number of dimensions:',1x,i1,/)
      read(5,*) nn,numel,nmat,mndofn,mnne,mncm,mnip,mnsp
      write(50,20) nn,numel,nmat,mndofn,mnne,mncm,mnip,mnsp
   20 format(1x,'number of nodes:',1x,i4,/,
     *       1x,'number of elements:',1x,i3,/,
     *       1x,'number of materials:',1x,i3,/,
     *       1x,'max. number of degrees of freedom per
node:',1x,i3,/,
     *       1x,'max. number of nodes per element:',1x,i3,/,
     *       1x,'max. number of constants per material:',1x,i3,/,
     *       1x,'max. number of integration points:',1x,i3,/,
     *       1x,'max. number of state parameters:',1x,i3,/)
      open(unit=10,access='direct',status='scratch',
     *    form='unformatted',recl=8*mnip*mnsp)
      open(unit=13,file='stress',access='direct',status='unknown',
     *     form='unformatted',recl=8*mnip*mnsp)
c
c.....real storage allocation
c
      indr(1)=1
c
c.....x
c
      indr(2)=indr(1)+nn*ndim
c
c.....array to store the solution (displacement/rotation vector)
c
      indr(3)=indr(2)+nn*mndofn
c
c.....sm
c
      indr(4)=indr(3)+(mnne*mndofn)**2
c
c.....elrhs
c
      indr(5)=indr(4)+mnne*mndofn
c
c.....constm
c
      indr(6)=indr(5)+nmat*mncm
c
c.....working copy of p
c
      indr(7)=indr(6)+nn*mndofn
```

```
c
c.....y
c
      indr(8)=indr(7)+mnne*ndim
c
c.....u displacement at the last step
c
      indr(9)=indr(8)+nn*mndofn
c
c.....rhs
c
      indr(10)=indr(9)+nn*mndofn
c
c.....u
c
      indr(11)=indr(10)+nn*mndofn
c
c.....v
c
      indr(12)=indr(11)+mnne*mndofn
c
c.....state
c
      indr(13)=indr(12)+mnip*mnsp
c
c.....permament load vectors
c
      indr(14)=indr(13)+nn*mndofn
c
c.....du1
c
      indr(15)=indr(14)+nn*mndofn
c
c.....du
c
      indr(16)=indr(15)+nn*mndofn
      indr(17)=indr(16)
      indr(18)=indr(17)
      indr(19)=indr(18)
      indr(20)=indr(19)
      indr(21)=indr(20)
      indr(22)=indr(21)
      indr(23)=indr(22)
      indr(24)=indr(23)
      indr(25)=indr(24)
      indr(26)=indr(25)
      indr(27)=indr(26)
```

```
      indr(28)=indr(27)
      indr(29)=indr(28)
c
c.....array for subroutine solve
c
      indr(30)=indr(29)
      maxra=indr(30)-1
c
c.....integer storage allocation
c
      indi(1)=1
c
c.....ndofn
c
      indi(2)=indi(1)+nn
c
c.....is
c
      indi(3)=indi(2)+nn*mndofn
c
c.....iconn
c
      indi(4)=indi(3)+numel*mnne
c
c.....ielt
c
      indi(5)=indi(4)+numel
c
c.....nne
c
      indi(6)=indi(5)+numel
c
c.....integer array used in subroutine prefnt
c
      indi(7)=indi(6)+numel
c
c.....another integer array used in subroutine prefnt
c
      indi(8)=indi(7)+2*(numel*mnne+mnne)
c
c.....idest
c
      indi(9)=indi(8)+numel*mnne
c
c.....ndofe
c
      indi(10)=indi(9)+numel
```

```
c
c.....ielm
c
      indi(11)=indi(10)+numel
c
c.....main copy of ielt
c
      indi(12)=indi(11)+numel
      indi(13)=indi(12)
      indi(14)=indi(13)
      indi(15)=indi(14)
      indi(16)=indi(15)
      indi(17)=indi(16)
      indi(18)=indi(17)
      indi(19)=indi(18)
      indi(20)=indi(19)
      indi(21)=indi(20)
      indi(22)=indi(21)
      indi(23)=indi(22)
      indi(24)=indi(23)
      indi(25)=indi(24)
      indi(26)=indi(25)
      indi(27)=indi(26)
      indi(28)=indi(27)
      indi(29)=indi(28)
      indi(30)=indi(29)
      maxia=indi(30)-1
      if(maxra.gt.nra) then
      write(50,30) maxra
   30 format(1x,'insufficient real memory locations',/,
     *       1x,'required length of array a:',1x,i7)
      stop
      else
c     write(50,40) nra-maxra
c  40 format(1x,'number of unused real memory words:',1x,i7)
      endif
      if(maxia.gt.nia) then
      write(50,50) maxia
   50 format(1x,'insufficient integer memory locations',/,
     *       1x,'required length of integer array a:',1x,i7)
      stop
      else
      write(50,60) nia-maxia
   60 format(1x,'number of unused integer memory words:',1x,i7)
      endif
      call inmat(a(indr(5)),nmat,mncm)
      call innod(a(indr(1)),ia(indi(1)),ia(indi(2)),
```

```
     *           ndim,nn,mndofn)
      call inel(ia(indi(4)),ia(indi(10)),ia(indi(5)),ia(indi(3)),
     *          ia(indi(1)),ia(indi(9)),nn,numel,mnne)
      call load(a(indr(13)),ia(indi(1)),nn,mndofn)
c
c.....clear total displacements
c
      call clear(a(indr(8)),nn*mndofn)
c
c.....initiate state parameters
c
      call aeb(ia(indr(11)),ia(indr(4)),numel)
      call init(mnip,numel)
      else
      open(unit=10,access='direct',status='scratch',
     *     form='unformatted',recl=8*mnsp*mnip)
      open(unit=13,file='stress',access='direct',status='unknown',
     *     form='unformatted',recl=8*mnip*mnsp)
      call copyfile(13,10,a(indr(12)),numel,nn*mndofn)
      call load(a(indr(13)),ia(indi(1)),nn,mndofn)
      endif
c
c.....prepare for assembly and solution
c
      call prep(ia(indi(6)),ia(indi(7)),
     *          ia(indi(5)),ia(indi(1)),ia(indi(3)),
     *          numel,nn,mnne)
      isym=1
      iresol=0
      nrhs=1
      ntapeb=27
      ntapeu=28
      ntapel=29
      iprint=1
      call prefnt(ia(1),ia(indi(6)),ia(indi(7)),ms,mu,mr)
      if(irs.eq.0) then
      mamin=(mdof*(mdof+1))/2+mdof*nrhs+
     *      (mfw*(mfw+1))/2+mfw*nrhs+
     *      numel+mldest+2*mdof+mfw+nrhs
      write(50,70) mamin
   70 format(1x,'minimum memory (required) by the solver:',1x,i7)
      ma=nra-maxra
      write(50,80) ma
   80 format(1x,'memory available to the solver:',1x,i7)
      if(mamin.gt.ma) then
      write(50,90) maxra+mamin
   90 format(1x,'length of real array a must be at least:',1x,i7)
```

```
      stop
      endif
      endif
      smld=0.
      ssmld=0.
      theta1=-1.
      strmax=0.
      iswitch=0
      read(5,*) nodeps,ndimps
      read(5,*) nstep,mcycle,tol
      read(*,*) xx1,yy1,xx2,yy2
      do 1000 istep=1,nstep
      icycle=1
      write(*,*) istep
c
c.....reset displacements up to the last step
c
      call aeb(a(indr(10)),a(indr(8)),nn*mndofn)
      call clear(a(indr(15)),nn*mndofn)
c
c.....check for too many iterations
c
  100 if(iswitch.eq.2) then
      if(icycle.gt.10*mcycle.or.iconv.gt.2) goto 1010
      else
      if(icycle.gt.mcycle.or.iconv.eq.2) then
        iswitch=iswitch+1
        smld=ssmld
        icycle=1
        xx1=xxx1
        yy1=yyy1
        xx2=xxx2
        yy2=yyy2
        call aeb(ia(indi(4)),ia(indi(11)),numel)
        call aeb(a(indr(10)),a(indr(8)),nn*mndofn)
        call clear(a(indr(15)),nn*mndofn)
        call copyfile(13,10,a(indr(12)),numel,mnip*mnsp)
      endif
      endif
c
c.....reset current load vectors
c
      call clear(a(indr(6)),nn*mndofn)
      call aebb(a(indr(6)),a(indr(13)),nn*mndofn,smld)
c
c.....reset rhs
c
```

```
      call clear(a(indr(9)),nn*mndofn)
c
c.....(assemble and) solve
c
      call solve(a(1),ia(1),a(indr(29)))
      call aeb(a(indr(14)),a(indr(2)),nn*mndofn)
      u22=a(indr(14)+mndofn*(nodeps-1)+ndimps)
c
c.....reset load vectors
c
      iresol=1
      call aeb(a(indr(6)),a(indr(13)),nn*mndofn)
      call solve(a(1),ia(1),a(indr(29)))
      iresol=0
      u21=a(indr(2)+mndofn*(nodeps-1)+ndimps)
      if(istep.eq.1.and.icycle.eq.1) ups=u21
      if(icycle.eq.1) then
      dld=(ups-u22)/u21
      else
      dld=-u22/u21
      endif
      smld=smld+dld
      call aebb(a(indr(14)),a(indr(2)),nn*mndofn,dld)
      call apbb(a(indr(14)),a(indr(10)),nn*mndofn)
      call apbb(a(indr(14)),a(indr(15)),nn*mndofn)
      strmax=0.
      call stress1(a(indr(1)),a(indr(7)),a(indr(10)),a(indr(11)),
     *            a(indr(12)),
     *            ia(indi(3)),ia(indi(5)),ia(indi(1)),
     *            ia(indi(4)),ia(indi(10)),a(indr(5)),
     *            ndim,nn,numel,nmat,mndofn,mnne,mncm,mnip,mnsp)
       if(strmax.lt.ft) then
       call
converg(a(indr(14)),a(indr(15)),tol,nn*mndofn,iconv,criti)
       else
       call
converg(a(indr(14)),a(indr(15)),tol,nn*mndofn,iconv,criti)
       if(icycle.eq.1) icycle=2
       goto 100
       endif
       if(iconv.ne.0) then
       icycle=icycle+1
       goto 100
       endif
c
c.....processing after convergencing, update the displacements
c
```

```
      iswitch=0
  102 call aeb(a(indr(8)),a(indr(10)),nn*mndofn)
      call copyfile(10,13,a(indr(12)),numel,mnsp*mnip)
      ssmld=smld
      xxx1=xx1
      yyy1=yy1
      xxx2=xx2
      yyy2=yy2
      call aeb(ia(indi(11)),ia(indi(4)),numel)
c
c.....compute and print member loads
c
      call stress(a(indr(1)),a(indr(7)),a(indr(8)),a(indr(11)),
     *            a(indr(12)),
     *            ia(indi(3)),ia(indi(5)),ia(indi(1)),
     *            ia(indi(4)),ia(indi(10)),a(indr(5)),
     *            ndim,nn,numel,nmat,mndofn,mnne,mncm,mnip,mnsp)
c
c.....print results (displacements/rotations)
c
      write(50,900) istep,icycle,smld
  900 format(1x,//,1x,'results for step no.   :',i3,//
     *       1x,'number of cycle is    :',i3,//
     *       1x,'current load is       :',f10.4,// )
      call prnt(a(indr(10)),ia(indi(1)),mndofn,nn)
 1000 continue
      stop
 1010 write(50,1020)
 1020 format(1x,'maximun number of cycle exceeded')
      stop
      end
c
      subroutine aeb(a,b,n)
      implicit real*8 (a-h,o-z)
      dimension a(n),b(n)
      do 10 i=1,n
      a(i)=b(i)
   10 continue
      return
      end
c
      subroutine aebb(a,b,n,c)
      implicit real*8 (a-h,o-z)
      dimension a(n),b(n)
      do 10 i=1,n
      a(i)=a(i)+b(i)*c
   10 continue
```

```
      return
      end
c
      subroutine apbb(a,b,n)
      implicit real*8 (a-h,o-z)
      dimension a(n),b(n)
      do 10 i=1,n
      b(i)=b(i)+a(i)
   10 continue
      return
      end
c
      subroutine asbb(a,b,n)
      implicit real*8 (a-h,o-z)
      dimension a(n),b(n)
      do 10 i=1,n
      a(i)=a(i)-b(i)
   10 continue
      return
      end
c
      block data
      implicit real*8 (a-h,o-z)
      common /consts/ zero,one,two
      common /concrete/ ft,delta
      data zero,one,two/0.d0,1.d0,2.d0/
      data ft,delta/342,0.0075/
      end
c
      subroutine clear(a,na)
      implicit real*8 (a-h,o-z)
      dimension a(na)
      common /consts/ zero,one,two
      do 10 i=1,na
      a(i)=zero
   10 continue
      return
      end
c
      subroutine init(mnip,numel)
      implicit real*8 (a-h,o-z)
      common /consts/ zero,one,two
      common /concrete/ ft,delta
      do 210 i=1,numel
  210 write(10,rec=i) (-one,ft,zero,zero,j=1,mnip)
      return
      end
```

```
c
      subroutine copyfile(n1,n2,c,numel,n)
      implicit real*8 (a-h,o-z)
      dimension c(1)
      do 10 i=1,numel
      read(n1,rec=i) (c(j),j=1,n)
      write(n2,rec=i) (c(j),j=1,n)
   10 continue
      return
      end
c
      subroutine converg(du1,du,tol,n,iconv,criti)
      implicit real*8 (a-h,o-z)
      dimension du1(1),du(1)
      common /consts/ zero,one,two
      common /cycle/ icycle,iswitch,istep
      e1=zero
      e2=zero
      do 10 i=1,n
      e1=e1+du1(i)*du1(i)
      e2=e2+du(i)*du(i)
   10 continue
      write(*,*) e1,e2
      if(icycle.eq.1) criti=10*sqrt(dabs(e1))
      if(sqrt(dabs(e1)).lt.tol*sqrt(dabs(e2))) then
      iconv=0
      else
      iconv=1
      endif
      if(sqrt(dabs(e1)).gt.criti) iconv=2
      return
      end
c
      subroutine
inel(ielt,ielm,nne,iconn,ndofn,ndofe,nn,numel,mnne)
      implicit real*8 (a-h,o-z)
      dimension
ielt(numel),ielm(numel),nne(numel),iconn(mnne,numel)
      dimension ndofn(nn),ndofe(numel)
      do 20 iel=1,numel
      read(5,*) k,ielt(k),ielm(k),nne(k),(iconn(j,k),j=1,nne(k))
      ndofe(k)=0
      do 20 j=1,nne(k)
      ndofe(k)=ndofe(k)+ndofn(iconn(j,k))
   20 continue
      return
      end
```

```
c
      subroutine inmat(constm,nmat,mncm)
      implicit real*8 (a-h,o-z)
      dimension constm(mncm,nmat)
      do 10 imat=1,nmat
      read(5,*) ncm,(constm(icm,imat),icm=1,ncm)
   10 continue
      return
      end
c
      subroutine innod(x,ndofn,is,ndim,nn,mndofn)
      implicit real*8 (a-h,o-z)
      dimension x(ndim,nn)
      dimension ndofn(nn),is(mndofn,nn)
      do 10 i=1,nn
      read(5,*) k,(x(j,k),j=1,ndim),
     *          ndofn(k),(is(j,k),j=1,ndofn(k))
   10 continue
      return
      end
c
      subroutine load(p,ndofn,nn,mndofn)
      implicit real*8 (a-h,o-z)
      dimension ndofn(nn)
      dimension p(1)
      call clear(p,mndofn*nn)
   10 read(5,*) node
      if(node.ne.-999999) then
      i1=(node-1)*mndofn+1
      i2=i1+ndofn(node)-1
      read(5,*) (p(i),i=i1,i2)
      go to 10
      endif
      return
      end
c
      subroutine modif(sm,rhs,elrhs,elem,p,is,ndofn,iconn,
     *                 nne,ndof,nn,mndofn)
      implicit real*8 (a-h,o-z)
      dimension sm(ndof,ndof),rhs(mndofn,nn),elrhs(ndof)
      dimension p(mndofn,nn)
      dimension is(mndofn,nn),iconn(nne),ndofn(nn)
      dimension elem(1)
      common /cntl/ isym,numel,iresol,nrhs,ntapeb,ntapeu,ntapel,
     *              ma,iwrt,iprint,ierr,nnegp,nposp,nrhsf,
     *              ib,iu,il,ifb,ifu,ifl,mbuf,mw,mkf,
     *              melem,mfwr,mb,mdof,mfw,mldest
```

```
      common /consts/ zero,one,two
      common /cycle/ icycle,iswitch,istep
      if(iresol.eq.0) then
      k=0
      do 30 i=1,nne
      node=iconn(i)
      do 30 j=1,ndofn(node)
      k=k+1
      if(is(j,node).eq.0) then
      elrhs(k)=elrhs(k)+p(j,node)
      p(j,node)=zero
      else
      disp=p(j,node)
      if(icycle.ne.1) disp=zero
      do 10 l=1,k
      elrhs(l)=elrhs(l)-sm(l,k)*disp
      sm(l,k)=zero
   10 continue
      do 20 l=k,ndof
      elrhs(l)=elrhs(l)-sm(k,l)*disp
      sm(k,l)=zero
   20 continue
      sm(k,k)=one
      elrhs(k)=disp
      endif
   30 continue
      k=0
      do 40 j=1,ndof
      do 40 i=1,j
      k=k+1
      elem(k)=sm(i,j)
   40 continue
      do 50 i=1,ndof
      k=k+1
      elem(k)=elrhs(i)
   50 continue
      else
      k=0
      do 60 i=1,nne
      node=iconn(i)
      do 60 j=1,ndofn(node)
      k=k+1
      if(is(j,node).eq.0) then
      elrhs(k)=elrhs(k)+p(j,node)
      p(j,node)=zero
      else
      elrhs(k)=zero
```

```
      endif
   60 continue
      k=0
      do 70 i=1,ndof
      k=k+1
      elem(k)=elrhs(i)
   70 continue
      endif
      k=0
      do 80 i=1,nne
      node=iconn(i)
      do 80 j=1,ndofn(node)
      k=k+1
      if(is(j,node).eq.0) then
      rhs(j,node)=rhs(j,node)+elrhs(k)
      endif
   80 continue
      return
      end
c
      subroutine pick(x,y,iconn,nne,ndim,nn)
      implicit real*8 (a-h,o-z)
      dimension x(ndim,nn)
      dimension y(ndim,nne)
      dimension iconn(nne)
      do 10 j=1,nne
      node=iconn(j)
      do 10 i=1,ndim
      y(i,j)=x(i,node)
   10 continue
      return
      end
c
      subroutine preout(inta,iel,n,ib)
      implicit real*8 (a-h,o-z)
      dimension inta(1)
      dimension ib(1)
      common /inds/ indr(30),indi(30)
      common /dims/ mncm,mndofn,mnip,mnsp,mnne,ndim,nmat,nn
      j=indi(8)+mnne*(iel-1)-1
      do 10 i=1,n
      j=j+1
      inta(j)=ib(i)
   10 continue
      return
      end
c
```

```
      subroutine prep(in,ia,nne,ndofn,iconn,numel,nn,mnne)
      implicit real*8 (a-h,o-z)
      dimension in(1),ia(1)
      dimension nne(numel),ndofn(nn),iconn(mnne,numel)
      k=0
      l=0
      do 10 i=1,numel
      k=k+1
      in(k)=nne(i)
      do 10 j=1,nne(i)
      l=l+1
      node=iconn(j,i)
      ia(l)=10*node+ndofn(node)
   10 continue
      return
      end
c
      subroutine prnt(u,ndofn,mndofn,nn)
      implicit real*8 (a-h,o-z)
      dimension u(mndofn,nn),ndofn(nn)
      do 20 j=1,nn
      if(j.eq.
     * 1.or.j.eq.8.or.j.eq.21)
     *  then
      write(50,10) j,(u(i,j),i=1,ndofn(j))
   10 format(2x,i4,7x,d13.6,2x,d13.6,2x,d13.6,
     *             2x,d13.6,2x,d13.6,2x,d13.6)
      endif
   20 continue
      return
      end
c
      subroutine solin(a,ia,iel,ifg,numdes,ldest,elem)
      implicit real*8 (a-h,o-z)
      dimension a(1),ia(1)
      dimension ldest(1),elem(1)
      common /inds/ indr(30),indi(30)
      common /dims/ mncm,mndofn,mnip,mnsp,mnne,ndim,nmat,nn
      numdes=ia(indi(5)+iel-1)
      j=indi(8)+mnne*(iel-1)-1
      do 10 i=1,numdes
      j=j+1
      ldest(i)=ia(j)
   10 continue
      if(ifg.eq.1) return
      call stiff(a(indr(1)),a(indr(7)),a(indr(10)),a(indr(11)),
     *           ia(indi(3)),ia(indi(5)),
```

```
     *            ia(indi(9)),ia(indi(1)),ia(indi(2)),ia(indi(4)),
     *            ia(indi(10)),a(indr(5)),a(indr(3)),a(indr(9)),
     *            a(indr(4)),a(indr(6)),a(indr(12)),
     *            elem,ndim,nn,nmat,mndofn,mnne,mncm,mnip,mnsp,iel)
      return
      end
c
      subroutine solout(a,ia,iel,elem)
      implicit real*8 (a-h,o-z)
      dimension elem(1)
      dimension a(1),ia(1)
      common /inds/ indr(30),indi(30)
      common /dims/ mncm,mndofn,mnip,mnsp,mnne,ndim,nmat,nn
      j=indi(3)+mnne*(iel-1)-1
      nne=ia(indi(5)+iel-1)
      m=0
      do 20 i=1,nne
      node=ia(j+i)
      ndofn=ia(indi(1)+node-1)
      k=indr(2)+mndofn*(node-1)-1
      do 10 l=1,ndofn
      a(k+l)=elem(m+l)
   10 continue
      m=m+ndofn
   20 continue
      return
      end
c
      subroutine stiff(x,y,u,v,iconn,nne,ndofe,ndofn,is,ielt,ielm,
     *                 constm,sm,rhs,elrhs,p,state,elem,
     *                 ndim,nn,nmat,mndofn,mnne,mncm,mnip,mnsp,iel)
      implicit real*8 (a-h,o-z)
      dimension x(ndim,nn),u(mndofn,nn),v(1)
      dimension is(mndofn,nn),ndofn(nn)
      dimension y(ndim,mnne)
      dimension iconn(mnne,1),nne(1),ndofe(1)
      dimension ielt(1),ielm(1)
      dimension constm(mncm,nmat)
      dimension sm(1),rhs(1),elrhs(1),elem(1),p(1),state(1)
      call pick(x,y,iconn(1,iel),nne(iel),ndim,nn)
      k=0
      do 10 i=1,nne(iel)
      node=iconn(i,iel)
      do 10 j=1,ndofn(node)
      k=k+1
      v(k)=u(j,node)
   10 continue
```

```
      if(ielt(iel).eq.1) then
c
c.....no element available
c
      else if (ielt(iel).eq.2) then
c
c.....eight-node isoparametric element for steel
c
      call sf2(y,v,constm(1,ielm(iel)),sm,elrhs,ndim,ndofe(iel))
      else if (ielt(iel).eq.3) then
c
c.....four-node isoparametric element for concrete
c
      read(10,rec=iel) (state(i),i=1,mnsp*mnip)
      call sf3(y,v,constm(1,ielm(iel)),sm,elrhs,state,mnsp,iel)
      write(10,rec=iel) (state(i),i=1,mnsp*mnip)
      else if (ielt(iel).eq.4) then
c
c.....four-node isoparametric element for steel
c
      call sf4(y,v,constm(1,ielm(iel)),sm,elrhs,ndim,ndofe(iel))
      else
      write(*,100)
  100 format(1x,i3,'no such element available')
      stop
      endif
c
c.....modify element stiffness matrix for support conditions
c
      call modif(sm,rhs,elrhs,elem,p,is,ndofn,
     *           iconn(1,iel),nne(iel),ndofe(iel),nn,mndofn)
      return
      end
c
      subroutine stress(x,y,u,v,state,
     *                  iconn,nne,ndofn,ielt,ielm,
     *                  constm,ndim,nn,numel,nmat,mndofn,mnne,mncm,
     *                  mnip,mnsp)
      implicit real*8 (a-h,o-z)
      dimension x(ndim,nn),u(mndofn,nn)
      dimension ndofn(nn)
      dimension y(ndim,mnne),v(1)
      dimension iconn(mnne,numel),nne(numel)
      dimension ielt(numel),ielm(numel)
      dimension constm(mncm,nmat),state(1)
      do 20 iel=1,numel
      call pick(x,y,iconn(1,iel),nne(iel),ndim,nn)
```

```
      k=0
      do 10 i=1,nne(iel)
      node=iconn(i,iel)
      do 10 j=1,ndofn(node)
      k=k+1
      v(k)=u(j,node)
   10 continue
      if(ielt(iel).eq.1) then
c
c.....no element available
c
      else if (ielt(iel).eq.2) then
c
c.....eight-node isoparametric elelment for steel
c
      call ss2(y,v,constm(1,ielm(iel)),ndim)
      else if (ielt(iel).eq.3) then
c
c.....four-node isoparametric concrete element
c
      read(10,rec=iel) (state(i),i=1,mnip*mnsp)
      call ss3(y,v,constm(1,ielm(iel)),state,mnsp)
      write(10,rec=iel) (state(i),i=1,mnip*mnsp)
      else if (ielt(iel).eq.4) then
c
c.....four-node isoparametric elelment for steel
c
      call ss4(y,v,constm(1,ielm(iel)),ndim)
      else
      write(*,*) 'no such element available'
      stop
      endif
   20 continue
      return
      end
c
      subroutine stress1(x,y,u,v,state,
     *                   iconn,nne,ndofn,ielt,ielm,
     *                   constm,ndim,nn,numel,nmat,mndofn,mnne,mncm,
     *                   mnip,mnsp)
      implicit real*8 (a-h,o-z)
      dimension x(ndim,nn),u(mndofn,nn)
      dimension ndofn(nn)
      dimension y(ndim,mnne),v(1)
      dimension iconn(mnne,numel),nne(numel)
      dimension ielt(numel),ielm(numel)
      dimension constm(mncm,nmat),state(1)
```

```
      common /crack/ xx1,yy1,xx2,yy2,theta1,iiel
      iiel=0
      do 20 iel=1,numel
      call pick(x,y,iconn(1,iel),nne(iel),ndim,nn)
      k=0
      do 10 i=1,nne(iel)
      node=iconn(i,iel)
      do 10 j=1,ndofn(node)
      k=k+1
      v(k)=u(j,node)
   10 continue
      if(ielt(iel).eq.1) then
c
c.....no element available
c
      else if (ielt(iel).eq.3) then
c
c.....four-node isoparametric concrete element
c
      read(10,rec=iel) (state(i),i=1,mnip*mnsp)
      call ss3s(y,v,constm(1,ielm(iel)),state,mnsp,iel)
      endif
  20  continue
      if(iiel.gt.0) then
        call pick(x,y,iconn(1,iiel),nne(iiel),ndim,nn)
        do 25 i=1,4
          if((y(1,i)-xx1+0.01)*(y(1,i)-xx2-0.01).gt.0.) then
          theta1=-1.
          return
          endif
   25   continue
      endif
      if(theta1.ge.0) then
      do 30 iel=1,numel
      call pick(x,y,iconn(1,iel),nne(iel),ndim,nn)
      do 35 i=1,4
      if(xx2-y(1,i).gt.0.01) goto 30
   35 continue
      do 36 i=1,4
      if(abs(y(1,i)-xx2).lt.0.01) then
      xx1=xx2
      yy1=yy2
      xx2=dmax1(y(1,1),y(1,2),y(1,3),y(1,4))
      yy2=yy1+tan(theta1-1.5707963)*(xx2-xx1)
      write(50,*) xx2,yy2
        goto 39
      endif
```

```
   36 continue
   30 continue
   39 do 40 iel=1,numel
      if(ielt(iel).eq.2.or.ielt(iel).eq.4) then
      call pick(x,y,iconn(1,iel),nne(iel),ndim,nn)
      do 45 i=1,4
      if(y(1,i)-xx1.lt.-0.01.or.y(1,i)-xx2.gt.0.01) goto 40
   45   continue
      do 46 i=1,3
      if(((y(2,i)-yy1)*(y(2,i)-yy2).le.0).or.
     *   ((y(2,i)-yy1)*(y(2,i+1)-yy1).le.0)) then
        if(ielt(iel).eq.2) ielt(iel)=1
        if(ielt(iel).eq.4) ielt(iel)=3
        goto 40
      endif
   46   continue
      endif
   40 continue
      theta1=-1
      endif
      return
      end

c
      subroutine stst(dstr,constm,d,strs,state,x1,x2,mnsp,iel)
      implicit real*8 (a-h,o-z)
      dimension dstr(4),strs(4),constm(2),d(4,4),tt(2,4),t(4,2)
      dimension ttd(2,4),tdt(2,2),tdtin(2,2),state(mnsp)
      dimension dcr(2,2),dt(4,2),dtt(4,2),dtt1(4,4),dd(4,4)
      common /consts/ zero,one,two
      common /concrete/ ft,delta
      common /cycle/ icycle,iswitch,istep
      common strmax
      call clear(d,16)
      call clear(dcr,4)
c
c.....uncracked concrete sttiffness
c
      e1=constm(1)*(1.-constm(2))/(1.-2.*constm(2))/(1.+constm(2))
      e2=e1*constm(2)/(1.-constm(2))
      d(1,1)=e1
      d(1,2)=e2
      d(1,3)=e2
      d(2,1)=e2
      d(2,2)=e1
      d(2,3)=e2
      d(3,1)=e2
```

```
      d(3,2)=e2
      d(3,3)=e1
      d(4,4)=e1*(1.-2.*constm(2))/2./(1.-constm(2))
      if(nint(state(4)).gt.0) goto 110
c
c.....maximum principal stresses and direction
c
      do 10 i=1,4
   10 strs(i)=d(i,1)*dstr(1)+d(i,2)*dstr(2)+d(i,3)*dstr(3)
     *       +d(i,4)*dstr(4)
      stmax=(strs(1)+strs(2))/2.+sqrt(strs(4)**2
     *      +(strs(1)-strs(2))**2/4.)
      if(stmax.lt.strmax) return
      if(strmax.lt.ft) return
      write(*,*) iel
      call angle(strs,theta)
      state(1)=theta
      state(4)=1.
  110 sn=sin(state(1))
      cs=cos(state(1))
c
c.....element characteristic lenfth
c
      h=min(x2/sn,x1/abs(cs))
      call trans(tt,t,state(1))
c
c.....strains in the principal stress direction
c
      prsann=cs**2*dstr(1)+sn**2*dstr(2)+sn*cs*dstr(4)
      prsant=-2.*sn*cs*(dstr(1)-dstr(2))+(cs**2-sn**2)*dstr(4)
      prsatt=sn**2*dstr(1)+cs**2*dstr(2)-sn*cs*dstr(4)
      iturn=0
      goto(125,126,130,145) nint(state(4))
  125 cosann=(ft*(1.-h*prsann/delta*5.)-e2*(prsatt+dstr(3)))/
     *       (e1-ft*h/delta*5.)
      cod=(prsann-cosann)*h
      dcr(1,1)=-ft/delta*5.*h
      if(iswitch.ge.1) dcr(1,1)=constm(1)/500.
      if(cod.lt.delta*0.15) goto 140
      state(4)=2.
  126 cosann=(ft*(5./17.-h*prsann/delta/3.4)-e2*(prsatt+dstr(3)))/
     *       (e1-ft*h/delta/3.4)
      cod=(prsann-cosann)*h
      dcr(1,1)=-ft/delta/3.4*h
      if(iswitch.ge.1) dcr(1,1)=constm(1)/500.
      if(cod.lt.delta) goto 140
      state(4)=3.
```

```
      state(2)=zero
  130 cosann=-e2/e1*(prsatt+dstr(3))
      cod=(prsann-cosann)*h
      dcr(1,1)=constm(1)/10000.
  140 cong=abs(467/cod-8410)
      if(cod.gt.0.02) cong=0.001
      cosant=cong*h*prsant/(d(4,4)+cong*h)
      csd=h*(prsant-cosant)
      prsenn=e1*cosann+e2*(prsatt+dstr(3))
      if(prsenn.gt.ft) prsenn=ft
      prsett=e1*prsatt+e2*(cosann+dstr(3))
      prsent=cong*csd
      if(nint(state(4)).eq.2.or.state(3).eq.zero) goto 150
      if(prsenn.gt.state(2).and.icycle.ge.2) then
      state(4)=4.
      dcr(1,1)=state(3)
      iturn=iturn+1
      if(iturn.eq.1) goto 145
      endif
      goto 150
  145 cosann=(prsann*state(3)-e2*(prsatt+dstr(3)))/(e1+state(3))
      cod=(prsann-cosann)*h
      cong=abs(467/cod-8410)
      if(cod.gt.0.02) cong=0.001
      dcr(1,1)=state(3)
      cosant=cong*h*prsant/(d(4,4)+cong*h)
      csd=(prsant-cosant)*h
      prsenn=e1*cosann+e2*(prsatt+dstr(3))
      prsett=e1*prsatt+e2*(cosann+dstr(3))
      prsent=cong*csd
      if(prsenn.gt.state(2).and.icycle.ge.2) then
      state(4)=1
      dcr(1,1)=-ft/delta*h
      if(iswitch.ge.2) dcr(1,1)=constm(1)/500
      iturn=iturn+1
      if(iturn.eq.1) goto 125
      endif
c
c.....stresses in the global coordinates
c
   150 if(cod.le.zero) then
      write(*,*) h,state(1),iel
      endif
      if(istep.eq.119) write(50,*) state(1),prsenn,prsett, prsent
      strs(1)=cs**2*prsenn+sn**2*prsett-2.*sn*cs*prsent
      strs(2)=sn**2*prsenn+cs**2*prsett+2.*sn*cs*prsent
      strs(3)=e2*(cosann+prsatt)+e1*dstr(3)
```

```
      strs(4)=sn*cs*(prsenn-prsett)+(cs**2-sn**2)*prsent
      dcr(2,2)=cong/h
      strs(2)=sn**2*prsenn+cs**2*prsett*(state(2)/ft)**1.2
     &+2.*sn*cs*prsent
      strs(4)=sn*cs*(prsenn-prsett*(state(2)/ft)**1.2)
     &+(cs**2-sn**2)*prsent
  300 if(iswitch.eq.2.and.nint(state(4)).gt.2) return
      if(iswitch.eq.2.and.icycle.ge.2) return
      call multip(tt,d,ttd,2,4,4)
      call multip(ttd,t,tdt,2,4,2)
      call apbb(dcr,tdt,4)
      det=tdt(1,1)*tdt(2,2)-tdt(1,2)*tdt(2,1)
      tdtin(1,1)=tdt(2,2)/det
      tdtin(2,2)=tdt(1,1)/det
      tdtin(1,2)=-tdt(1,2)/det
      tdtin(2,1)=-tdt(2,1)/det
      call multip(d,t,dt,4,4,2)
      call multip(dt,tdtin,dtt,4,2,2)
      call multip(dtt,tt,dtt1,4,2,4)
      call multip(dtt1,d,dd,4,4,4)
      call asbb(d,dd,16)
      return
      end
c
      subroutine angle(strs,theta)
      implicit real*8 (a-h,o-z)
      dimension strs(4)
      common /consts/ zero,one,two
      a=strs(1)-strs(2)
      if(a.eq.0) then
      if(strs(4).ne.0.) then
      theta=0.78539815*sign(one,strs(4))
      else
      theta=0.
      endif
      return
      elseif(strs(4).eq.0.) then
      if(a.gt.0.) then
      theta=0.
      else
      theta=1.5707963
      endif
      return
      endif
      theta=atan(2.*strs(4)/a)/2.
      if(a.lt.0.) theta=theta+1.5707963
      if(theta.lt.0.) theta=3.1415926+theta
```

```
      return
      end
c
      subroutine trans(tt,t,state)
      implicit real*8 (a-h,o-z)
      dimension tt(2,4),t(4,2)
      call clear(tt,8)
      call clear(t,8)
      t(1,1)=cos(state)**2
      tt(1,1)=t(1,1)
      t(1,2)=-sin(state)*cos(state)
      tt(2,1)=t(1,2)
      t(2,1)=sin(state)**2
      tt(1,2)=t(2,1)
      t(2,2)=-t(1,2)
      tt(2,2)=t(2,2)
      t(4,1)=2*t(2,2)
      tt(1,4)=t(4,1)
      t(4,2)=t(1,1)-t(2,1)
      tt(2,4)=t(4,2)
      return
      end
c
      subroutine sf2(x,u,constm,sm,elrhs,ndim,ndof)
      implicit real*8 (a-h,o-z)
      dimension x(ndim,8),sm(ndof,ndof),elrhs(ndof),u(ndim,8)
      dimension constm(2)
      dimension b(4,16),bt(16,4),d(4,4)
      dimension dstr(4),strs(4)
      dimension f(8),fxi(8),fet(8)
      dimension c(16,4),cc(16,16)
      dimension xi(8),eta(8),xg(3),r(3)
      common /cntl/ isym,numel,iresol,nrhs,ntapeb,ntapeu,ntapel,
     *              ma,iwrt,iprint,ierr,nnegp,nposp,nrhsf,
     *              ib,iu,il,ifb,ifu,ifl,mbuf,mw,mkf,
     *              melem,mfwr,mb,mdof,mfw,mldest
      data xg/-0.7745966692,0.,0.7745966692/
      data r/0.5555555556,0.8888888889,0.5555555556/
      data xi/-1,1,1,-1,0,1,0,-1/,eta/-1,-1,1,1,-1,0,1,0/
      call clear(elrhs,16)
      if(iresol.ne.0) return
      e1=constm(1)*(1.-constm(2))/(1.-2.*constm(2))/(1.+constm(2))
      e2=e1*constm(2)/(1.-constm(2))
      call clear(d,16)
      d(1,1)=e1
      d(1,2)=e2
      d(1,3)=e2
```

```
      d(2,1)=e2
      d(2,2)=e1
      d(2,3)=e2
      d(3,1)=e2
      d(3,2)=e2
      d(3,3)=e1
      d(4,4)=e1*(1.-2.*constm(2))/2./(1.-constm(2))
      call clear(sm,256)
      do 100 l=1,3
      do 100 m=1,3
      co=r(l)*r(m)
      do 10 i=1,4
      f(i)=(1+xg(l)*xi(i))*(1+xg(m)*eta(i))
     &     *(xg(l)*xi(i)+xg(m)*eta(i)-1.)/4.

fxi(i)=xi(i)*(1+xg(m)*eta(i))*(2.*xg(l)*xi(i)+xg(m)*eta(i))/4.
 10
fet(i)=eta(i)*(1+xg(l)*xi(i))*(xg(l)*xi(i)+2.*xg(m)*eta(i))/4.
      do 13 i=5,7,2
      f(i)=(1.-xg(l)*xg(l))*(1.+eta(i)*xg(m))/2.
      fxi(i)=(-1)*xg(l)*(1.+eta(i)*xg(m))
 13   fet(i)=eta(i)*(1.-xg(l)*xg(l))/2.
      do 12 i=6,8,2
      f(i)=(1.-xg(m)*xg(m))*(1.+xi(i)*xg(l))/2.
      fxi(i)=xi(i)*(1.-xg(m)*xg(m))/2.
 12   fet(i)=(-1)*xg(m)*(1.+xg(l)*xi(i))
      rad=0.
      do 35 i=1,8
   35 rad=rad+f(i)*x(1,i)
      aj11=0.
      aj12=0.
      aj21=0.
      aj22=0.
      do 11 i=1,8
      aj11=aj11+x(1,i)*fxi(i)
      aj12=aj12+x(2,i)*fxi(i)
      aj21=aj21+x(1,i)*fet(i)
 11   aj22=aj22+x(2,i)*fet(i)
      det=aj11*aj22-aj21*aj12
      o11=aj22/det
      o12=-aj12/det
      o21=-aj21/det
      o22=aj11/det
      call clear(dstr,4)
      do 20 j=1,8
      j1=2*j-1
      j2=j1+1
```

```
      b(1,j1)=fxi(j)*o11+fet(j)*o12
      b(1,j2)=0.
      b(2,j1)=0.
      b(2,j2)=fxi(j)*o21+fet(j)*o22
      b(3,j1)=f(j)/rad
      b(3,j2)=0.
      b(4,j1)=b(2,j2)
      b(4,j2)=b(1,j1)
      dstr(1)=dstr(1)+b(1,j1)*u(1,j)
      dstr(2)=dstr(2)+b(2,j2)*u(2,j)
      dstr(3)=dstr(3)+b(3,j1)*u(1,j)
   20 dstr(4)=dstr(4)+b(4,j1)*u(1,j)+b(4,j2)*u(2,j)
      call multip(d,dstr,strs,4,4,1)
      do 40 i=1,16
   40 elrhs(i)=elrhs(i)-co*det*6.2831852*rad*
     *        (b(1,i)*strs(1)+b(2,i)*strs(2)+
     *         b(3,i)*strs(3)+b(4,i)*strs(4))
      do 21 i=1,4
      do 21 j=1,16
 21   bt(j,i)=b(i,j)
      call multip(bt,d,c,16,4,4)
      call multip(c,b,cc,16,4,16)
      do 30 i=1,16
      do 30 j=1,16
 30   sm(i,j)=sm(i,j)+co*det*6.2831852*rad*cc(i,j)
 100  continue
      return
      end
c
      subroutine multip(x,y,z,j,k,l)
      implicit real*8 (a-h,o-z)
      dimension x(j,k),y(k,l),z(j,l)
      do 10 i=1,j
      do 10 m=1,l
      z(i,m)=0.
      do 20 n=1,k
   20 z(i,m)=z(i,m)+x(i,n)*y(n,m)
   10 continue
      return
      end
c
      subroutine sf3(x,u,constm,sm,elrhs,state,mnsp,iel)
      implicit real*8 (a-h,o-z)
      dimension x(2,4),sm(8,8),elrhs(8)
      dimension constm(2),u(2,4),dstr(4),strs(4)
      dimension b(4,8),bt(8,4),d(4,4),state(mnsp,1)
      dimension f(4),fxi(4),fet(4)
```

```
      dimension c(8,4),cc(8,8)
      dimension xi(4),eta(4)
      common /cntl/ isym,numel,iresol,nrhs,ntapeb,ntapeu,ntapel,
     *              ma,iwrt,iprint,ierr,nnegp,nposp,nrhsf,
     *              ib,iu,il,ifb,ifu,ifl,mbuf,mw,mkf,
     *              melem,mfwr,mb,mdof,mfw,mldest
      data xi/-1,1,1,-1/,eta/-1,-1,1,1/
      call clear(elrhs,8)
      if(iresol.ne.0) return
      call clear(sm,64)
c
c.....characteristic length
c
      x1=dmax1(dabs(x(1,2)-x(1,1)),dabs(x(1,3)-x(1,1)))
      x2=dmax1(dabs(x(2,2)-x(2,1)),dabs(x(2,3)-x(2,1)))
c
      do 10 i=1,4
      f(i)=0.25
      fxi(i)=xi(i)/4.
   10 fet(i)=eta(i)/4.
      rad=(x(1,1)+x(1,2)+x(1,3)+x(1,4))/4.
      aj11=0.
      aj12=0.
      aj21=0.
      aj22=0.
      do 11 i=1,4
      aj11=aj11+x(1,i)*fxi(i)
      aj12=aj12+x(2,i)*fxi(i)
      aj21=aj21+x(1,i)*fet(i)
 11   aj22=aj22+x(2,i)*fet(i)
      det=aj11*aj22-aj21*aj12
      o11=aj22/det
      o12=-aj12/det
      o21=-aj21/det
      o22=aj11/det
      call clear(dstr,4)
      do 25 j=1,4
      j1=2*j-1
      j2=j1+1
      b(1,j1)=fxi(j)*o11+fet(j)*o12
      b(1,j2)=0.
      b(2,j1)=0.
      b(2,j2)=fxi(j)*o21+fet(j)*o22
      b(3,j1)=f(j)/rad
      b(3,j2)=0.
      b(4,j1)=b(2,j2)
      b(4,j2)=b(1,j1)
```

```
c
c.....strains up to the last iteration
c
      dstr(1)=dstr(1)+b(1,j1)*u(1,j)
      dstr(2)=dstr(2)+b(2,j2)*u(2,j)
      dstr(3)=dstr(3)+b(3,j1)*u(1,j)
   25 dstr(4)=dstr(4)+b(4,j1)*u(1,j)+b(4,j2)*u(2,j)
      do 21 i=1,4
      do 21 j=1,8
  21  bt(j,i)=b(i,j)
      call stst(dstr,constm,d,strs,state(1,1),x1,x2,mnsp,iel)
c
c.....equivalent nodal forces
c
      do 40 i=1,8
   40 elrhs(i)=-4.*det*6.2831852*rad*
     *       (b(1,i)*strs(1)+b(2,i)*strs(2)+
     *        b(3,i)*strs(3)+b(4,i)*strs(4))
      call multip(bt,d,c,8,4,4)
      call multip(c,b,cc,8,4,8)
      do 50 i=1,8
      do 50 j=1,8
   50 sm(i,j)=4.*det*6.2831852*rad*cc(i,j)
      return
      end
c
      subroutine sf4(x,u,constm,sm,elrhs,ndim,ndof)
      implicit real*8 (a-h,o-z)
      dimension x(ndim,4),sm(ndof,ndof),elrhs(ndof),u(ndim,4)
      dimension constm(2)
      dimension b(4,8),bt(8,4),d(4,4)
      dimension dstr(4),strs(4)
      dimension f(4),fxi(4),fet(4)
      dimension c(8,4),cc(8,8)
      dimension xi(4),eta(4),xg(2),r(2)
      common /cntl/ isym,numel,iresol,nrhs,ntapeb,ntapeu,ntapel,
     *              ma,iwrt,iprint,ierr,nnegp,nposp,nrhsf,
     *              ib,iu,il,ifb,ifu,ifl,mbuf,mw,mkf,
     *              melem,mfwr,mb,mdof,mfw,mldest
      data xg/-0.57735,0.57735/,r/1,1/
      data xi/-1,1,1,-1/,eta/-1,-1,1,1/
      call clear(elrhs,8)
      if(iresol.ne.0) return
      e1=constm(1)*(1.-constm(2))/(1.-2.*constm(2))/(1.+constm(2))
      e2=e1*constm(2)/(1.-constm(2))
      call clear(d,16)
      d(1,1)=e1
```

```
      d(1,2)=e2
      d(1,3)=e2
      d(2,1)=e2
      d(2,2)=e1
      d(2,3)=e2
      d(3,1)=e2
      d(3,2)=e2
      d(3,3)=e1
      d(4,4)=e1*(1.-2.*constm(2))/2./(1.-constm(2))
      call clear(sm,64)
      do 100 l=1,2
      do 100 m=1,2
      co=r(l)*r(m)
      do 10 i=1,4
      f(i)=(1+xg(l)*xi(i))*(1+xg(m)*eta(i))/4.
      fxi(i)=xi(i)*(1+xg(m)*eta(i))/4.
10    fet(i)=eta(i)*(1+xg(l)*xi(i))/4.
      rad=0.
      do 35 i=1,4
  35  rad=rad+f(i)*x(1,i)
      aj11=0.
      aj12=0.
      aj21=0.
      aj22=0.
      do 11 i=1,4
      aj11=aj11+x(1,i)*fxi(i)
      aj12=aj12+x(2,i)*fxi(i)
      aj21=aj21+x(1,i)*fet(i)
11    aj22=aj22+x(2,i)*fet(i)
      det=aj11*aj22-aj21*aj12
      o11=aj22/det
      o12=-aj12/det
      o21=-aj21/det
      o22=aj11/det
      call clear(dstr,4)
      do 20 j=1,4
      j1=2*j-1
      j2=j1+1
      b(1,j1)=fxi(j)*o11+fet(j)*o12
      b(1,j2)=0.
      b(2,j1)=0.
      b(2,j2)=fxi(j)*o21+fet(j)*o22
      b(3,j1)=f(j)/rad
      b(3,j2)=0.
      b(4,j1)=b(2,j2)
      b(4,j2)=b(1,j1)
      dstr(1)=dstr(1)+b(1,j1)*u(1,j)
```

```
      dstr(2)=dstr(2)+b(2,j2)*u(2,j)
      dstr(3)=dstr(3)+b(3,j1)*u(1,j)
   20 dstr(4)=dstr(4)+b(4,j1)*u(1,j)+b(4,j2)*u(2,j)
      call multip(d,dstr,strs,4,4,1)
      do 40 i=1,8
   40 elrhs(i)=elrhs(i)-co*det*6.2831852*rad*
     *       (b(1,i)*strs(1)+b(2,i)*strs(2)+
     *        b(3,i)*strs(3)+b(4,i)*strs(4))
      do 21 i=1,4
      do 21 j=1,8
 21   bt(j,i)=b(i,j)
      call multip(bt,d,c,8,4,4)
      call multip(c,b,cc,8,4,8)
      do 30 i=1,8
      do 30 j=1,8
 30   sm(i,j)=sm(i,j)+co*det*6.2831852*rad*cc(i,j)
 100  continue
      return
      end
c
      subroutine stst1(dstr,constm,strs,state,x1,x2,mnsp,istep)
      implicit real*8 (a-h,o-z)
      dimension dstr(4),strs(4),constm(2),d(4,4)
      dimension state(mnsp)
      common /consts/ zero,one,two
      common /concrete/ ft,delta
      call clear(d,16)
c
c.....uncracked concrete sttiffness
c
      e1=constm(1)*(1.-constm(2))/(1.-2.*constm(2))/(1.+constm(2))
      e2=e1*constm(2)/(1.-constm(2))
      d(1,1)=e1
      d(1,2)=e2
      d(1,3)=e2
      d(2,1)=e2
      d(2,2)=e1
      d(2,3)=e2
      d(3,1)=e2
      d(3,2)=e2
      d(3,3)=e1
      d(4,4)=e1*(1.-2.*constm(2))/2./(1.-constm(2))
      if(state(1).gt.0) goto 110
c
c.....stresses of uncracked concrete
c
      do 100 i=1,4
```

```
  100 strs(i)=d(i,1)*dstr(1)+d(i,2)*dstr(2)+d(i,3)*dstr(3)
     *        +d(i,4)*dstr(4)
      return
  110 sn=sin(state(1))
      cs=cos(state(1))
c
c.....element characteristic length
c
      h=min(x2/sn,x1/abs(cs))
c
c.....strains in the principal stress direction
c
      prsann=cs**2*dstr(1)+sn**2*dstr(2)+sn*cs*dstr(4)
      prsant=-2.*sn*cs*(dstr(1)-dstr(2))+(cs**2-sn**2)*dstr(4)
      prsatt=sn**2*dstr(1)+cs**2*dstr(2)-sn*cs*dstr(4)
      goto(115,116,120,130) nint(state(4))
  115 cosann=(ft*(1.-h*prsann/delta*5.)-e2*(prsatt+dstr(3)))/
     *       (e1-ft*h/delta*5.)
      goto 140
  116 cosann=(ft*(5./17.-h*prsann/delta/3.4)-e2*(prsatt+dstr(3)))/
     *       (e1-ft*h/delta/3.4)
      goto 140
  120 cosann=-e2/e1*(prsatt+dstr(3))
      goto 140
  130 cosann=(prsann*state(3)-e2*(prsatt+dstr(3)))/(e1+state(3))
  140 cod=h*(prsann-cosann)
      cong=abs(467/cod-8410)
      if(cod.gt.0.02) cong=0.001
      cosant=cong*h*prsant/(d(4,4)+cong*h)
      csd=h*(prsant-cosant)
      prsenn=e1*cosann+e2*(prsatt+dstr(3))
      prsett=e1*prsatt+e2*(cosann+dstr(3))
      prsent=cong*csd
c
c.....stresses in the global coordinates
c
      if(istep.eq.119) write(50,*) state(1), prsenn, prsent
      strs(1)=cs**2*prsenn+sn**2*prsett-2.*sn*cs*prsent
      strs(2)=sn**2*prsenn+cs**2*prsett+2.*sn*cs*prsent
      strs(3)=e2*(cosann+prsatt)+e1*dstr(3)
      strs(4)=sn*cs*(prsenn-prsett)+(cs**2-sn**2)*prsent
      if(nint(state(4)).eq.1.or.nint(state(4)).eq.2) then
      if(state(2).gt.prsenn) then
      state(2)=prsenn
      state(3)=prsenn/(prsann-cosann)
      if(state(3).lt.1.d-5) state(3)=1.d-5
      endif
```

```
      endif
      return
      end
c
      subroutine ss2(x,u,constm,ndim)
      implicit real*8 (a-h,o-z)
      dimension x(ndim,8),u(ndim,8)
      dimension constm(2),strs(4)
      dimension f(8),fxi(8),fet(8)
      dimension b(4,16),d(4,4),db(4,16)
      dimension uu(16),xx(3,3),yy(3,3)
      dimension xi(8),eta(8),xg(3),r(3)
      data xg/-0.7745966692,0.,0.7745966692/
      data r/0.5555555556,0.8888888889,0.5555555556/
      data xi/-1,1,1,-1,0,1,0,-1/,eta/-1,-1,1,1,-1,0,1,0/
      call clear(elrhs,16)
      e1=constm(1)*(1.-constm(2))/(1.-2.*constm(2))/(1.+constm(2))
      e2=e1*constm(2)/(1.-constm(2))
      d(1,1)=e1
      d(1,2)=e2
      d(1,3)=e2
      d(2,1)=e2
      d(2,2)=e1
      d(2,3)=e2
      d(3,1)=e2
      d(3,2)=e2
      d(3,3)=e1
      d(4,4)=e1*(1.-2.*constm(2))/2./(1.-constm(2))
      do 5 i=1,8
      uu(2*i-1)=u(1,i)
 5    uu(2*i)=u(2,i)
      do 100 l=1,3
      do 100 m=1,3
      co=r(l)*r(m)
      do 10 i=1,4
      f(i)=(1+xg(l)*xi(i))*(1+xg(m)*eta(i))
     &     *(xg(l)*xi(i)+xg(m)*eta(i)-1.)/4.

fxi(i)=xi(i)*(1+xg(m)*eta(i))*(2.*xg(l)*xi(i)+xg(m)*eta(i))/4.
 10
fet(i)=eta(i)*(1+xg(l)*xi(i))*(xg(l)*xi(i)+2.*xg(m)*eta(i))/4.
      do 13 i=5,7,2
      f(i)=(1.-xg(l)*xg(l))*(1.+eta(i)*xg(m))/2.
      fxi(i)=(-1)*xg(l)*(1.+eta(i)*xg(m))
 13   fet(i)=eta(i)*(1.-xg(l)*xg(l))/2.
      do 12 i=6,8,2
      f(i)=(1.-xg(m)*xg(m))*(1.+xi(i)*xg(l))/2.
```

```
      fxi(i)=xi(i)*(1.-xg(m)*xg(m))/2.
 12   fet(i)=(-1)*xg(m)*(1.+xg(l)*xi(i))
      rad=0.
      do 35 i=1,8
   35 rad=rad+x(1,i)*f(i)
      aj11=0.
      aj12=0.
      aj21=0.
      aj22=0.
      do 11 i=1,8
      aj11=aj11+x(1,i)*fxi(i)
      aj12=aj12+x(2,i)*fxi(i)
      aj21=aj21+x(1,i)*fet(i)
 11   aj22=aj22+x(2,i)*fet(i)
      det=aj11*aj22-aj21*aj12
      o11=aj22/det
      o12=-aj12/det
      o21=-aj21/det
      o22=aj11/det
      do 20 j=1,8
      j1=2*j-1
      j2=j1+1
      b(1,j1)=fxi(j)*o11+fet(j)*o12
      b(1,j2)=0.
      b(2,j1)=0.
      b(2,j2)=fxi(j)*o21+fet(j)*o22
      b(3,j1)=f(j)/rad
      b(3,j2)=0.
      b(4,j1)=b(2,j2)
   20 b(4,j2)=b(1,j1)
      xx(l,m)=0.
      yy(l,m)=0.
      do 60 i=1,8
      xx(l,m)=xx(l,m)+x(1,i)*f(i)
   60 yy(l,m)=yy(l,m)+x(2,i)*f(i)
      call multip(d,b,db,4,4,16)
      call multip(db,uu,strs,4,16,1)
  100 continue
      return
      end
c
      subroutine stst1s(dstr,constm,iel)
      implicit real*8 (a-h,o-z)
      dimension dstr(4),strs(4),constm(2),d(4,4)
      common /concrete/ ft,delta
      common /crack/ xx1,yy1,xx2,yy2,theta1,iiel
      common strmax
```

```
      call clear(d,16)
c
c.....uncracked concrete sttiffness
c
      e1=constm(1)*(1.-constm(2))/(1.-2.*constm(2))/(1.+constm(2))
      e2=e1*constm(2)/(1.-constm(2))
      d(1,1)=e1
      d(1,2)=e2
      d(1,3)=e2
      d(2,1)=e2
      d(2,2)=e1
      d(2,3)=e2
      d(3,1)=e2
      d(3,2)=e2
      d(3,3)=e1
      d(4,4)=e1*(1.-2.*constm(2))/2./(1.-constm(2))
c
c.....stresses of uncracked concrete
c
      do 100 i=1,4
  100 strs(i)=d(i,1)*dstr(1)+d(i,2)*dstr(2)+d(i,3)*dstr(3)
     *        +d(i,4)*dstr(4)
      stmax=(strs(1)+strs(2))/2.+sqrt(strs(4)**2
     *      +(strs(1)-strs(2))**2/4.)
      if(strmax.le.stmax.and.stmax.gt.ft) then
      strmax=stmax
      iiel=iel
      call angle(strs,theta)
      theta1=theta
      endif
      return
      end
c
      subroutine ss3s(x,u,constm,state,mnsp,iel)
      implicit real*8 (a-h,o-z)
      dimension x(2,4)
      dimension constm(2),u(2,4),dstr(4)
      dimension b(4,16),state(mnsp,1)
      dimension f(4),fxi(4),fet(4)
      dimension xi(4),eta(4)
      data xi/-1,1,1,-1/,eta/-1,-1,1,1/
      if(nint(state(4,1)).ne.0) return
      do 10 i=1,4
      f(i)=0.25
      fxi(i)=xi(i)/4.
   10 fet(i)=eta(i)/4.
      rad=(x(1,1)+x(1,2)+x(1,3)+x(1,4))/4.
```

```
      aj11=0.
      aj12=0.
      aj21=0.
      aj22=0.
      do 11 i=1,4
      aj11=aj11+x(1,i)*fxi(i)
      aj12=aj12+x(2,i)*fxi(i)
      aj21=aj21+x(1,i)*fet(i)
 11   aj22=aj22+x(2,i)*fet(i)
      det=aj11*aj22-aj21*aj12
      o11=aj22/det
      o12=-aj12/det
      o21=-aj21/det
      o22=aj11/det
      call clear(dstr,4)
      do 25 j=1,4
      j1=2*j-1
      j2=j1+1
      b(1,j1)=fxi(j)*o11+fet(j)*o12
      b(1,j2)=0.
      b(2,j1)=0.
      b(2,j2)=fxi(j)*o21+fet(j)*o22
      b(3,j1)=f(j)/rad
      b(3,j2)=0.
      b(4,j1)=b(2,j2)
      b(4,j2)=b(1,j1)
c
c.....strains up to the last iteration
c
      dstr(1)=dstr(1)+b(1,j1)*u(1,j)
      dstr(2)=dstr(2)+b(2,j2)*u(2,j)
      dstr(3)=dstr(3)+b(3,j1)*u(1,j)
   25 dstr(4)=dstr(4)+b(4,j1)*u(1,j)+b(4,j2)*u(2,j)
      call stst1s(dstr,constm,iel)
      return
      end
c
      subroutine ss3(x,u,constm,state,mnsp)
      implicit real*8 (a-h,o-z)
      dimension x(2,4)
      dimension constm(2),u(2,4),dstr(4),strs(4)
      dimension b(4,8),state(mnsp,1)
      dimension f(4),fxi(4),fet(4)
      dimension xi(4),eta(4)
      common /cycle/ icycle,iswitch,istep
      data xi/-1,1,1,-1/,eta/-1,-1,1,1/
c
```

```
      x1=dmax1(dabs(x(1,2)-x(1,1)),dabs(x(1,3)-x(1,1)))
      x2=dmax1(dabs(x(2,2)-x(2,1)),dabs(x(2,3)-x(2,1)))
c
      do 10 i=1,4
      f(i)=0.25
      fxi(i)=xi(i)/4.
   10 fet(i)=eta(i)/4.
      rad=(x(1,1)+x(1,2)+x(1,3)+x(1,4))/4.
      aj11=0.
      aj12=0.
      aj21=0.
      aj22=0.
      do 11 i=1,4
      aj11=aj11+x(1,i)*fxi(i)
      aj12=aj12+x(2,i)*fxi(i)
      aj21=aj21+x(1,i)*fet(i)
 11   aj22=aj22+x(2,i)*fet(i)
      det=aj11*aj22-aj21*aj12
      o11=aj22/det
      o12=-aj12/det
      o21=-aj21/det
      o22=aj11/det
      call clear(dstr,4)
      do 25 j=1,4
      j1=2*j-1
      j2=j1+1
      b(1,j1)=fxi(j)*o11+fet(j)*o12
      b(1,j2)=0.
      b(2,j1)=0.
      b(2,j2)=fxi(j)*o21+fet(j)*o22
      b(3,j1)=f(j)/rad
      b(3,j2)=0.
      b(4,j1)=b(2,j2)
      b(4,j2)=b(1,j1)
c
c.....strains up to the last iteration
c
      dstr(1)=dstr(1)+b(1,j1)*u(1,j)
      dstr(2)=dstr(2)+b(2,j2)*u(2,j)
      dstr(3)=dstr(3)+b(3,j1)*u(1,j)
   25 dstr(4)=dstr(4)+b(4,j1)*u(1,j)+b(4,j2)*u(2,j)
      xx=0.
      yy=0.
      do 60 i=1,4
      xx=xx+x(1,i)*f(i)
   60 yy=yy+x(2,i)*f(i)
      call stst1(dstr,constm,strs,state(1,1),x1,x2,mnsp,istep)
```

```
      if(istep.eq.119) write(50,*) xx,yy
      return
      end
c
      subroutine ss4(x,u,constm,ndim)
      implicit real*8 (a-h,o-z)
      dimension x(ndim,4),u(ndim,4)
      dimension constm(2),strs(4)
      dimension f(4),fxi(4),fet(4)
      dimension b(4,8),d(4,4),db(4,8)
      dimension uu(8),xx(2,2),yy(2,2)
      dimension xi(4),eta(4),xg(2),r(2)
      data xg/-0.57735,0.57735/,r/1,1/
      data xi/-1,1,1,-1/,eta/-1,-1,1,1/
      call clear(elrhs,8)
      e1=constm(1)*(1.-constm(2))/(1.-2.*constm(2))/(1.+constm(2))
      e2=e1*constm(2)/(1.-constm(2))
      d(1,1)=e1
      d(1,2)=e2
      d(1,3)=e2
      d(2,1)=e2
      d(2,2)=e1
      d(2,3)=e2
      d(3,1)=e2
      d(3,2)=e2
      d(3,3)=e1
      d(4,4)=e1*(1.-2.*constm(2))/2./(1.-constm(2))
      do 5 i=1,4
      uu(2*i-1)=u(1,i)
 5    uu(2*i)=u(2,i)
      do 100 l=1,2
      do 100 m=1,2
      co=r(l)*r(m)
      do 10 i=1,4
      f(i)=(1+xg(l)*xi(i))*(1+xg(m)*eta(i))/4.
      fxi(i)=xi(i)*(1+xg(m)*eta(i))/4.
10    fet(i)=eta(i)*(1+xg(l)*xi(i))/4.
      rad=0.
      do 35 i=1,4
35    rad=rad+x(1,i)*f(i)
      aj11=0.
      aj12=0.
      aj21=0.
      aj22=0.
      do 11 i=1,4
      aj11=aj11+x(1,i)*fxi(i)
      aj12=aj12+x(2,i)*fxi(i)
```

```
      aj21=aj21+x(1,i)*fet(i)
11    aj22=aj22+x(2,i)*fet(i)
      det=aj11*aj22-aj21*aj12
      o11=aj22/det
      o12=-aj12/det
      o21=-aj21/det
      o22=aj11/det
      do 20 j=1,4
      j1=2*j-1
      j2=j1+1
      b(1,j1)=fxi(j)*o11+fet(j)*o12
      b(1,j2)=0.
      b(2,j1)=0.
      b(2,j2)=fxi(j)*o21+fet(j)*o22
      b(3,j1)=f(j)/rad
      b(3,j2)=0.
      b(4,j1)=b(2,j2)
   20 b(4,j2)=b(1,j1)
      xx(l,m)=0.
      yy(l,m)=0.
      do 60 i=1,4
      xx(l,m)=xx(l,m)+x(1,i)*f(i)
   60 yy(l,m)=yy(l,m)+x(2,i)*f(i)
      call multip(d,b,db,4,4,8)
      call multip(db,uu,strs,4,8,1)
  100 continue
      return
      end
```

REFERENCES

ACI 318 1995: Committee 318, "Building Code Requirements for Structural Concrete," American Concrete Institute, Detroit, 1995

ACI 349 1990: Committee 349, "Code Requirements for Nuclear Safety Related Concrete Structures," American Concrete Institute, Detroit, 1990.

Ahmud and Shah 1982: Ahmud, S. H. and Shah, S. P., "Complete Triaxial Stress-Strain Curves for Concrete," *Journal of the Structural Division*, Proceedings, ASCE, Vol. 108, No. ST4, April, 1982, pp. 728-742.

AISC LRFD Specifications 1986: AISC, *Manual of Steel Construction, Load and Resistance Factor Design*, 1st Edition, American Institute of Steel Construction, Chicago, Illinois, 1986.

AISC LRFD Specifications 1994: AISC, *Manual of Steel Construction, Load and Resistance Factor Design*, 2nd Edition, American Institute of Steel Construction, Chicago, Illinois, 1994.

Armstrong et al. 1985: Armstrong, K. S., Klingner, R. E. and Steves, M. A., "Response of Highway Barriers to Repeated Impact Loads: Steel Post Barriers," *Research Report 382-1*, Center for Transportation Research, The University of Texas at Austin, November, 1985.

ASTM C39-86 1986: "Standard Test Method for Compressive Strength of Cylindrical Concrete Specimens," ASTM, Philadelphia, 1986.

Balmer 1949: Balmer, G. G., "Shearing Strength of Concrete under High Triaxial Stress-Computation of Mohr's Envelope as a Curve," *Structural Research Laboratory Report, SP-23*, Denver, Colorado, October, 1949.

Bashandy 1996: Bashandy, T. R., "Application of Headed bars in Concrete Members," Ph.D. Dissertation, The University of Texas at Austin, December, 1996.

Bazant et al. 1984: Bazant, Z. P., Belytschko, T. B. and Chang, T. P., "Continuum Model for Strain Softening," *Journal of Engineering Mechanics*, ASCE, Vol. 110, 1984, pp. 1666-1692.

Bode and Roik 1987: Bode, H. and Roik, K., "Headed Studs-Embedded in Concrete and Loaded in Tension," *Anchorage to Concrete*, SP-103, American concrete Institute, Detroit, 1987, pp. 61-88.

Cannon 1981: Cannon, R. W., "Expansion Anchor Performance in Cracked Concrete," *ACI Journal, Proceedings*, V. 78, No. 6, November-December, 1981, pp. 471-479.

Carrato 1991: Carrato, P., "Testing and Analysis of Base Plate Connections," *Anchors in Concrete: Design and Behavior*, SP-130, American Concrete Institute, Detroit, 1991, pp. 253-277.

CEB 1991: CEB, "Fastenings to Reinforced Concrete and Masonry Structures: State-of-Art Report, Part 1", Euro-International-Concrete Committee (CEB), August, 1991.

Cedolin et al. 1977: Cedolin, L., Crutzen, R. J. and Poli, S. D., "Triaxial Stress-Strain Relationship for Concrete," *Journal of The Engineering Mechanics Division*, Proceedings, ASCE, Vol. 103, No. EM3, June, 1977, pp. 423-439.

Chen 1982: Chen, W. F., *Plasticity in Reinforced Concrete*, McGraw-Hill, Inc., New York, 1982.

Clough and Penzien 1975: Clough, R W. and Penzien, J., *Dynamics of Structure*, McGraw-Hill, Inc., 1975.

Collins et al. 1989: Collins, D., Klingner, R., E. and Polyzois, D., "Load-Deflection Behavior of Cast-in Place and Retrofit Concrete Anchors Subjected to Static, Fatigue, and Impact Tensile Loads," *Research Report CTR 1126-1*, Center for Transportation Research, The University of Texas at Austin, February, 1989.

Copley and Burdette 1985: Copley, J. D. and Burdette, E. G., "Behavior of Steel-to-Concrete Anchorage in High Moment Regions," *ACI Journal, Proceedings*, V. 82, No. 2, March-April, 1985, pp. 180-187.

Cook 1989: Cook, R. A., "Behavior and Design of Ductile Multiple-Anchor Steel-to-Concrete Connections ," Ph.D. Dissertation, The University of Texas at Austin, May, 1989.

Cook and Klingner 1992: Cook, R. A. and Klingner, R. E., "Ductile Multiple-Anchor Steel-to-Concrete Connections," *Journal of Structural Engineering*, Vol. 118, No. 6, June, 1992, pp. 1645-1665.

Cornelissen et al. 1986: Cornelissen, H. A. W., Hordijk, D. A. and Reinhardt, H. W., "Experiment and Theory for the Application of Fracture Mechanics to Normal and Lightweight Concrete," *Fracture Toughness and Fracture Energy of Concrete: Proceedings of the International Conference on Fracture Mechanics of Concrete*, Editor Wittmann, F. H., Elsevier, 1986.

DeWolf and Sarisley 1980: DeWolf, J. T. and Sarisley, E. F., "Column Base Plates with Axial Loads And Moments," *Journal of the Structural Division*, ASCE, Vol. 106, No. ST11, November 1980, 1980, pp. 2167-2184.

Eligehausen and Balogh 1995: Eligehausen, R. and Balogh, T., "Behavior of Fasteners Loaded in Tension in Cracked Reinforced Concrete," ACI Structural Journal, Vol. 92, No. 3, May-June, 1995, pp. 365-379.

Eligehausen et al. 1987, 1988: Eligehausen, R., Fuchs, W. and Mayer, B., "Bearing Behavior of Anchor Fastenings under Tension," *Betonwerk und Fertigteil-Technik*, No. 12, 1987, pp. 826-832; and No. 1, 1988, pp. 29-35.

Eligehausen and Fuchs 1988: Eligehausen, R. and Fuchs, W., "Loadbearing Behavior of Anchor Fastenings under Shear, Combined Tension and Shear or Flexural Loading," *Betonwerk und Fertigteil-Technik*, No. 2, 1988,pp. 44-56.

Eligehausen and Ozbolt 1990: Eligehausen, R. and Ozbolt, J., "Size effect in Anchorage Behavior," *Proceedings, ECF8, Fracture Behavior and Design of Materials and Structures*, Turin, October, 1990.

Eligehausen and Ozbolt 1992: Eligehausen, R. and Ozbolt, J., "Influence of Crack Width on the Concrete Cone Failure Load," *Fracture Mechanics of Concrete Structures*, Z. P. Bazant, ed., Elsevier Applied Science, 1992, pp. 876-881.

Eligehausen and Sawade1989: Eligehausen, R., and Sawade, G., "Fracture Mechanics Based Description of the Pull-Out Behavior of Headed Bolts Embedded in Concrete," *Fracture Mechanics of Concrete Structures: From Theory to Applications*, L. Elfgren, Ed., Chapman & Hall, London, 1989, pp. 263-281.

Evans and Marathe 1968: Evans, R. H. and Marathe, M. S., "Microcracking and Stress-Strain Curves for Concrete in Tension," *Materials and Structures* (RILEM, London), Vol. 1, No. 1, January-February, 1968, pp. 61-64.

Farrow 1992: Farrow, C. B., "Tensile Capacity of Anchors with Partial or Overlapping Failure Surface: Evaluation of Existing Formulas on an LRFD Basis," M.S. Thesis, The University of Texas at Austin, August, 1992.

Fenwick and Paulay 1968: Fenwick, R. C. and Paulay, T., "Mechanisms of Shear Resistance of Concrete Beams," *Journal of the Structural Division*, ASCE, Vol. 94, No. 10, October, 1968, pp. 2325-2350.

Frigui 1992: Frigui, I., "Tensile Capacity of Single Anchors in Concrete: Evaluation of Existing Formulas on an LRFD Basis," M.S. Thesis, The University of Texas at Austin, August, 1992.

Fuchs et al. 1995: Fuchs, W., Eligehausen and R. and Breen, J. E., "Concrete Capacity Design (CCD) Approach for Fastening to Concrete", *ACI Structural Journal*, Vol. 92, No. 1, January-February, 1995, pp. 73-94.

Furche and Eligehausen 1991: Furche, J. and Eligehausen, R., "Lateral Blow-Out Failure of Headed Studs Near a Free Edge," *Anchors in Concrete: Design and Behavior*, SP-130, American Concrete Institute, Detroit, 1991, pp. 235-252.

Gopalaratnam and Shah 1985: Gopalaratnam, V. S. and Shah, S. P., "Softening Response of Plain Concrete in Direct Tension," *ACI Journal*, Vol. 82, No. 3, May-June, 1985, pp. 310-323.

Green and Swanson 1973: Green, S. J. and Swanson, S. R., "Static Constitutive Relations for Concrete," *Air Force Weapons Laboratory Technical Report,* AFWL-TR-72-244, Kirtland Air Force Base, Albuquerque, New Mexico, 1973.

Guo and Zhang 1987: Guo, Z. and Zhang, X., "Investigation of Complete Stress-Deformation Curves for Concrete in Tension," *ACI Material Journal*, Vol. 84, No. 4, July-August, 1987, pp. 278-285.

Hallowell 1996: Hallowell, J. M., "Tensile and Shear Behavior of Anchors in Uncracked and Cracked Concrete under Static and Dynamic Loading," M.S. Thesis, The University of Texas at Austin, August, 1996.

Hawkins et al. 1980: Hawkins, N. M., Mitchell, D. and Roeder, C. W., "Moment Resisting Connections for Mixed Construction," *Engineering Journal*, AISC, Vol. 17, No. 1, January, 1980, pp. 1-10.

Hellier et l. 1987: Hellier, A. K., Sansalon, M., Carino, N. J., Stone, W. C. And Ingratffea, A. R., "Finite-Element Analysis of the Pullout Test Using a Nonlinear Discrete Cracking Approach," *Cement, Concrete and Aggregates*, ASTM, Vol. 9, No. 1, 1987, pp. 20-29.

Hughes and Chapman 1966: Hughes, B. P. and Chapman, G. P., "The Complete Stress-Stain Curve for Concrete in Direct Tension," *RILEM Bulletin*, No. 30, March, 1966, pp. 95-97.

Klingner and Mendonca 1982a: Klingner, R. E. and Mendonca J. A., "Tensile Capacity of Short Anchor Bolts and Welded Studs: A Literature Review," *ACI Journal, Proceedings*, Vol. 79, No. 4, July-August, 1982, pp. 270-279.

Klingner and Mendonca 1982b: Klingner, R. E. and Mendonca J. A., "Shear Capacity of Short Anchor Bolts and Welded Studs: A Literature Review," *ACI Journal, Proceedings*, Vol. 79, No. 5, September-October, 1982, pp. 339-349.

Kupfer et al. 1969: Kupfer, H., Hilsdorf, H. K. and Rusch, H, "Behavior of Concrete Under Biaxial Stresses," *ACI Journal, Proceedings*, Vol. 66, No. 8, August, 1969, pp. 656-666.

Li 1994: Li, L., BDA: *Programm zur Berechnung des Trag- und Verformungsverhaltens von Gruppenbefestigungen unter kombinierter Schragzug- und Momentenbeanspruchung (Programmbeschreibung)*, The University of Stuttgart, June, 1994.

Liaw et al. 1990: Liaw, B. M., Jeang, F. L., Du, J. J., Hawkins, N. M. and Kobayashi, A. S., "Improved Nonlinear Model for Concrete Fracture," *Journal of Engineering Mechanics*, Vol. 116, No. 2, February, 1990, pp. 429-445.

Lotze 1997: Lotze, D. and Klingner, R. E., "Behavior of Multiple-Anchor Connections to Concrete From the Perspective of Plastic Theory," *PMFSEL Report No. 96-4*, The University of Texas at Austin, March 1997.

Maitra 1978: Maitra, N., "Graphical Aid for Design of Base Plate Subjected to Moment," *Engineering Journal*, AISC, Vol. 12, No. 2, April, 1978, pp. 50-53.

Malik 1980: Malik, J. B., "Shear Resistance of Anchor Bolts under Monotonic and Reversed Cyclic Loading," M.S. Thesis, The University of Texas at Austin, May, 1980.

McMackin et al. 1973: McMackin, P. J., Slutter, R. G. and Fishere, J. W., "Headed Steel Anchor under Combined Loading," *Engineering Journal*, AISC, Vol. 10, No. 2, April, 1973.

Metha et al. 1984: Metha, N. K., Hangorani, N. V. and Longlais, T. G., "Simplified Design of Flexible Expansion Anchored Plates for Nuclear Structures," *Structural Engineering in Nuclear Facilities, Proceedings*, J. J. Ucciferro, Ed., North Carolina State University, Raleigh, 1984, pp. 1013-1036.

McGuire 1986: McGuire, W., *Steel Structures*, Prentice-Hall, Inc., Englewood Cliffs, N. J., 1986, pp. 987-1004.

van Mier 1984: Mier, van J. G. M., "Complete Stress-Strain Behavior and Damaging Status of Concrete under Multiaxial Conditions," *RILEM-CEB-CNRS, International Conference on Concrete under Multiaxial Conditions*. Presses de l'Universite paul Sabatier, Toulouse, France. Vol. 1, 1984, pp. 75-85.

Ngo and Scordelis 1967: Ngo, D and Scordelis, A. C., "Finite Element Analysis of Reinforce Concrete Beams," *ACI Journal, Proceedings*, Vol. 64, No. 3, March 1967, pp. 152-163.

Ottosen 1981: Ottosen, N. S., "Nonlinear Finite-Element Analysis of Pull-out-tests," *Journal of the Structural Division*, ASCE, Vol. 107, No. ST4, April, 1981, pp. 591-603.

Palaniswanmy 1973: Palaniswanmy, R. G., "Fracture and Stress-Strain Law of Concrete under Triaxial Compressive Stresses," Ph.D. Dissertation, University of Illinois at Chicago Circle, 1973.

Park 1994: Park, H., "Nonlinear Finite Element Analysis of Reinforced Concrete Planar Structures," Ph.D. Dissertation, The University of Texas at Austin, May, 1994.

PCI Design Handbook 1985: PCI Design Handbook - *Precast and Prestressed Concrete*, 3rd Edition, Prestressed Concrete Institute, Chicago, 1985.

PCI Design Handbook 1992: PCI Design Handbook - *Precast and Prestressed Concrete*, 4th Edition, Prestressed Concrete Institute, Chicago, 1992.

Picard and Beaulieu 1985: Picard, A. and Beaulieu, D., "Behavior of a simple Column Base Connection," *Canadian Journal of Civil Engineering*, Vol. 12 No. 1, March, 1985, pp. 126-136.

PMFSEL 1992: Phil M. Ferguson Structural Engineering Laboratory, "Catalog of Earthquake Records (Preliminary)," The University of Texas at Austin, June, 1992.

Rabinowicz 1995: Rabinowicz, E., *Friction and Wear of Materials*, 2nd Edition, John Wiley & Sons, Inc., 1995.

Ramm 1981: Ramm, E., "Strategies for Tracing the Nonlinear Response Near Limit Points," *Nonlinear Finite Element Analysis in Structural Mechanics*, Wundelich, W., Stein, E., and Bathe, K. J., Ed., Springer-Verlag, Berlin, 1981, pp. 63-89.

Reinhardt et al. 1987: Reinhardt, H. W., Cornelissen, H. A. W. and Hordjjk, D. A., "Mixed Mode Fracture Tests on Concrete," *Fracture of Concrete and Rock, SEM-RILEM International Conference,* Shad, S. P., and Swartz, S. E. Ed., 1987, pp. 324-337.

Rodriguez 1995: Rodriguez, M., "Behavior of Anchors in Uncracked Concrete under Static and Dynamic Loading," M.S. Thesis, The University of Texas at Austin, August, 1995.

Rots et al. 1985: Rots, J. G., Nauta, P., Kusters, G. M. A. and Blaauwendraad, J., "Smeared Crack Approach and Fracture Localization in Concrete," *Heron*, Vol. 30, No. 1, 1985, pp. 5-48.

de la Rovere 1990: de la Rovere, H. L., "Nonlinear Analysis of Reinforced Concrete Masonry Walls under Simulated Seismic Loading," Ph.D. Dissertation, The University of California at San Diego, 1990.

Salmon 1955: Salmon, C. G., Schenker, L. and Johnston, B. G., "Moment-Rotation Characteristics of Column Anchorages," *Transactions*, ASCE, April, 1955, pp. 132-154.

Shipp and Haninger 1983: Shipp, J. G. and Haninger, E. R., "Design of Headed Anchor Bolts," *Engineering Journal*, AISC, Vol. 20, No. 2, April, 1983, pp. 58-69.

Sutton and Meinheit 1991: Sutton, R. W. and Meinheit, D., "Evaluation of Expansion Anchor Ultimate Tensile Capacity Prediction Equations", *Anchors in Concrete: Design and Behavior*, SP-130, American Concrete Institute, Detroit, 1991, pp. 19-46.

Takiguchi and Hotta 1995: Takiguchi, K. and Hotta H., "Pull-out Strength of a Headed Stud in Cracked Concrete," *Transactions of the 13th International Conference on Structural Mechanics in Reactor Technology*, R. C. Ramos de Menezes Ed., Brazil, August 13-18, 1995, pp. 51-56.

Task Group on Steel Embedment 1984: Task Group on Steel Embedment, "State of Art Report on Steel Embedment," *Structural Engineering in Nuclear Facilities, Proceedings*, J. J. Ucciferro, Ed., North Carolina State University, Raleigh, 1984, pp. 1080-1218.

TVA CEB Report No. 79-18 1978: "Anchorage Tests of Load Transfer Through Flexible Plate: Interin Report," *TVA CEB Report No. 79-18*, Tennessee Valley Authority, Knoxville, TN, 1978.

TVA Civil Design Standard No. DS-C1.7.1 1984: TVA Civil Design Standard No. DS-C1.7.1, "General Anchorage to Concrete,", Tennessee Valley Authority, Knoxville, TN, 1984.

Wang et al. 1987: Wang, C., Guo, Z., and Zhang, X., "Experimental Investigation of Biaxial and Triaxial Compressive Concrete Strength," *ACI Materials Journal*, March-April, 1987, pp. 92-100.

Wecharatana 1986: Wecharatana, M., "Specimen Size Effects on Non-linear Fracture Parameters in Concrete," *Fracture Toughness and Fracture Energy of Concrete: Proceedings of the International Conference on Fracture Mechanics of Concrete*, Editor Wittmann, F. H., Elsevier, 1986.

Willam et al. 1985: Willam, K., Hurlburt, B. and Sture, S., "Experimental, Constitutive and Computational Aspects of Concrete Failure," *Proceedings, U.S.-Japan Seminar on Finite Element Analysis of Reinforced Concrete Structures*, Tokyo, May 21-24, 1985, pp. 149-171.

Wolinski 1987: Wolinski, S., Hordijk, D. K., Reinhardt, H. W. and Cornelissen, H. A. W., "Influence of Aggregate Size on Fracture Mechanics Parameters of Concrete," *International Cement Composites and Lightweight Concrete*, Vol. 9, No. 2, 1987, pp. 95-103.

Yamaguchi and Chen 1991: Yamaguchi, E. and Chen, W. F., "Microcrack Propagation Study of Concrete Under Compression," *Journal of Engineer Mechanics*, ASCE, Vol. 117, No. 3, March, 1991, pp. 653-673.

Yon et al. 1991: Yon, J., Hawkins, N. M. and Kobayashi, A. S., "Numerical Simulation of Model 1 Dynamic Fracture of Concrete," *Journal of Engineering Mechanics*, Vol. 117, No. 7, July, 1991, pp. 1595-1610.

VITA

Yonggang Zhang, son of Bin-duo Zhang and Shu-fen Zheng, was born on February 16, 1966 in Shanghai, P. R. China. After graduating in July 1984 with highest honors from Yang-pu Middle School, Shanghai, he entered Shanghai Jiao Tong University (Shanghai, P. R. China), majoring in naval and ocean engineering. At that University, he was the recipient of several scholarships and prizes. He completed his B.S. in July 1988, and entered the graduate program in the Department of Naval and Ocean Engineering at Shanghai Jiao Tong University (Shanghai, P. R. China), majoring in structural mechanics. In September 1990, he began graduate study at Utah State University, majoring in Civil Engineering. In August 1991, he entered the Graduate School at The University of Texas at Austin.

Permanent Address: Tong-Ji Xincun, # 705/9
Shanghai, P. R. China
200092

This dissertation was typed by the author.